APRIL 1985

# analytical chemistry

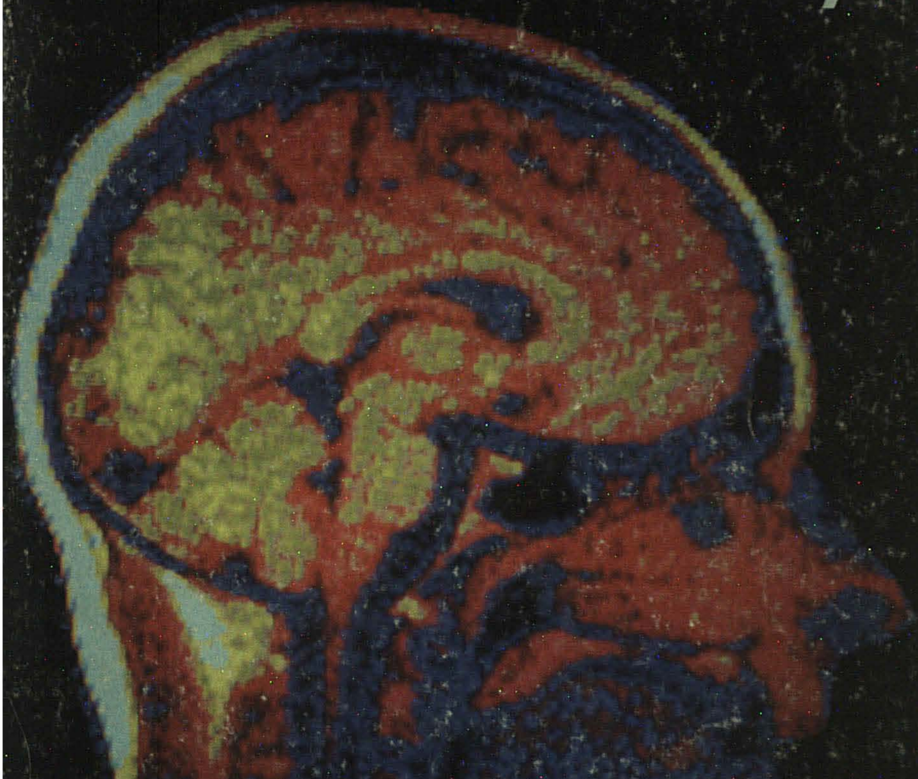

## Nuclear Magnetic Resonance Imaging

595 A

Automatic

C,H,N Analyzer

Introducing the CHN-O Rapid for Automatic Carbon, Hydrogen, Nitrogen Analysis

The CHN-O Rapid is the latest design in automated C,H,N analyzers. Heraeus has utilized its years of experience in combustion techniques to produce an elemental analyzer which encompasses both extreme sensitivity with an unprecedentedly large dynamic range, minimizing errors due to sample inhomogeneity.

Pre-weighed samples are automatically introduced from the 49 position sample carousel into the analyzer. There, they are combusted in an oxygen stream at temperatures up to 1050°C (1922°F). Efficient reduction, absorption and desorption systems allow measurements with an accuracy of ±0.15% absolute.

An H-P 150 Touchscreen® computer handles all data manipulations from sample weight introduction from the microbalance, to calibration, calculations and report generation.

An optional oxygen kit modifies the analyzer for automated oxygen analysis.

**Features Include:**

- 49 position sample carousel for solids or liquids
- Direct input microbalance
- Simple Touchscreen® operation
- Automatic calibration
- Prompting of time to regenerate catalyst
- Flexible, hard copy report formats of results and calibration curves
- Large sample size . . . up to 300mg
- Large dynamic range:
  - **C**: $5\times10^{-4}$ to 15 mg absolute
  - **H**: $1\times10^{-4}$ to 1.5 mg absolute
  - **N**: $1\times10^{-3}$ to 7.0 mg absolute
- On-site installation and start-up assistance
- Full one year warranty

Call 815-727-5431

UIC Inc.

P.O. BOX 863 JOLIET, ILLINOIS 60434 TELEX 723421 UAR JOL

CIRCLE 211 ON READER SERVICE CARD

*YOUR ACCESS TO EXCELLENCE IN GAS CHROMATOGRAPHY.*

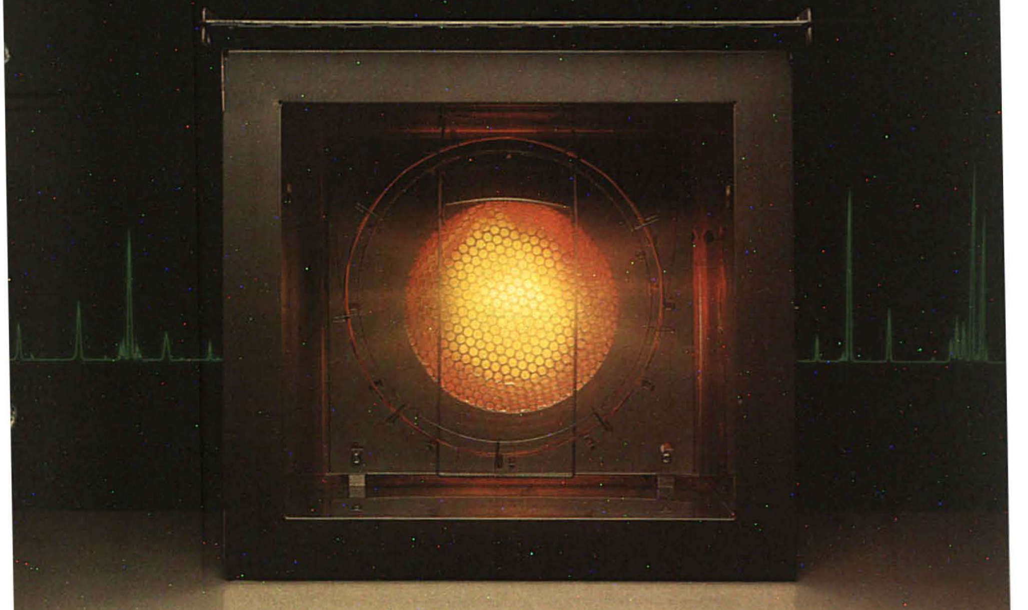

# Two ways to use what may be the best GC oven ever built.

We build two variations of this oven. Both deliver the same superlative *performance*. Each is part of a GC with its own special *capabilities*.

**The team player. Our HP 5890 GC.** The HP 5890 has been designed to meet the needs of two different kinds of users: the small lab with steady but predictable work; the large lab that relies heavily on lab automation with many instruments operating together using the same data base. In both cases, the HP 5890 is ideal. It delivers the necessary basic chromatographic data with high precision, repeatability, and reliability (99% guaranteed uptime is available*). All at the very economic price of just $6650.**

**The sophisticate. Our HP 5880 GC.** The HP 5880, a proven performer, has been designed to be a fully stand-alone system. It not only acquires the data, it processes it on the spot. Handy if you're involved in methods development, research… In automated test applications, it has the on-board intelligence not only to monitor its own results but also to change the test parameters based on those results. The HP 5880's extraordinary capabilities make it an excellent investment.

One, or perhaps both of these systems is just right for the work going on today in your laboratory.

To find out more about either system or to discuss which might be the optimum choice for your application, call the HP office listed in your telephone directory white pages and ask for the Analytical representative. Or, write: Hewlett-Packard, Analytical Group, 1820 Embarcadero Road, Palo Alto, CA 94303.

*Customers may purchase a Guaranteed Uptime Maintenance agreement. If an instrument fails to meet the guarantee, the agreement will be extended at no extra charge.

**U.S. domestic price only, single FID packed column, temperature programmable configuration.

HEWLETT PACKARD

AG04409

Circle 96 for literature. Circle 97 to have an HP representative contact you.

analytical
chemistry®

**APRIL 1985**

**COVER FEATURE**

**REPORT**

**How good are the standard atomic weights?** H. Steffen Peiser addresses his answer to analytical chemists, who are perhaps apt to place too much confidence in the accuracy of atomic weight values

511 A

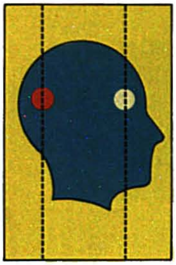

**INSTRUMENTATION**

**Nuclear magnetic resonance imaging.** The basic principles, current techniques, instrumentation, and possible chemical applications of NMR imaging are discussed by Stanford Smith of the University of Kentucky

595 A

**FOCUS**

**Academic vs. industrial careers**—what are the trade-offs? ▶ **Paternity testing** has benefited from recent improvements in analytical technology. ▶ **Office testing lab newsletter debuts**

526 A

Volume 57, No. 4
April 1985
ANCHAM
57(4) 489A–614A
785–960 (1985)
ISSN 0003 2700

**Registered in U.S. Patent and Trademark Office; Copyright 1985 by the American Chemical Society**

ANALYTICAL CHEMISTRY (ISSN 0003-2700) is published monthly except semimonthly in April and August by the American Chemical Society at 1155 16th St., N.W., Washington, D.C. 20036. Editorial offices are located at the same ACS address (202-872-4600; TDD 202-872-8733). Second-class postage paid at Washington, D.C., and additional mailing offices. Postmaster: Send address changes to Membership & Subscription Services, P.O. Box 3337, Columbus, Ohio 43210.

**Claims for missing numbers** will not be allowed if loss was due to failure of notice of change of address to be received in the time specified; if claim is dated (a) North America: more than 90 days beyond issue date, (b) all other foreign: more than one year beyond issue date, or if the reason given is "missing from files."

**Copyright Permission:** An individual may make a single reprographic copy of an article in this publication for personal use. Reprographic copying beyond that permitted by Section 107 or 108 of the U.S. Copyright Law is allowed, provided that the appropriate per-copy fee is paid through the Copyright Clearance Center, Inc., 21 Congress St., Salem, Mass. 01970. For reprint permission, write Copyright Administrator, B&J Division, ACS, 1155 16th St., N.W., Washington, D.C. 20036.

**Registered names and trademarks,** etc., used in this publication, even without specific indication thereof, are not to be considered unprotected by law.

**Advertising Management:** Centcom, Ltd., 25 Sylvan Road South, Westport, Conn. 06881 (203) 226-7131

**Technical Contents/Briefs** .................. **494 A**
**Letters** .................................. **506 A**
**Call for Papers** .......................... **550 A**
**Meetings** ................................. **552 A**
**For Your Information** ..................... **552 A**
**New Products** ............................. **562 A**
**Chemicals** ................................ **566 A**
**Software** ................................. **566 A**
**Manufacturers' Literature** ................ **570 A**
**Advertising Index** ........................ **612 A**
**Author Index, Future Articles** ........... **inside back cover**

## NEWS

**Surface Characterization of Catalytic and Electronic Materials** is the topic of this year's Summer Symposium of the ACS Division of Analytical Chemistry, to be held June 18–20 at Clarkson University, Potsdam, N.Y.

543 A

## THE ANALYTICAL APPROACH

**Snow peas and acephate.** Routine FDA monitoring of some California snow peas revealed that they contained the pesticide acephate. Thomas Cairns and co-workers describe their efforts to confirm the illegal residues

572 A

## BOOKS

**Critical reviews.** Books on electroanalytical chemistry, small-bore LC, and regulatory compliance monitoring are reviewed by F. C. Anson, R. A. Hartwick, and T. D. Martin

583 A

## EDITORIAL

**Editors of ACS publications** meet periodically to discuss their operations and their common problems. One result of these meetings is "Ethical Guidelines to Publication of Chemical Research," to be published shortly

785

**1985 subscription rates include air delivery outside the U.S., Canada, and Mexico**

|  | 1 yr | 2 yr |
|---|---|---|
| **Members** |  |  |
| Domestic | 20 | 34 |
| Canada and Mexico | 40 | 74 |
| Europe | 57 | 108 |
| All Other Countries | 80 | 154 |
| **Nonmembers** |  |  |
| Domestic | 30 | 51 |
| Canada and Mexico | 50 | 91 |
| Europe | 99 | 179 |
| All Other Countries | 122 | 225 |

Three-year and other rates contact: Membership & Subscription Services, ACS, P.O. Box 3337, Columbus, Ohio 43210, (614) 421-3776.

**Subscription orders by phone** may be charged to Visa, MasterCard, Barclay card, Access, or American Express. Call toll free at (800) 424-6747 from anywhere in the continental U.S.; from Washington, D.C., call 872-8065. Mail orders for new and renewal subscriptions should be sent with payment to the Treasurer's Office at the Washington address.

**Subscription service inquiries and changes of address** (include both old and new addresses with ZIP code and *recent mailing label*) should be directed to the ACS Columbus address noted above. Please allow six weeks for change of address to become effective.

**ACS membership information:** Ann Donahue, Washington address.

**Single issues,** current year, $7.50 except review issue and LabGuide, $8.50; **back issues and volumes and microform editions available by single volume or back issue collection.** For information or to order, call (800) 424-6747 or write the Sales Department at the Washington address.

**Nonmember rates in Japan:** Rates at left do not apply to nonmember subscribers in Japan, who must enter subscription orders with Maruzen Company Ltd., 3–10 Nihonbashi 2-chome, Chuo-ku, Tokyo 103, Japan. Tel (03) 272-7211.

ห้องสมุดกรมวิทยาศาสตร์บริการ
15 เม.ย. 2528

# More Membranes

GELMAN
ACRODISC
GELMAN
ACRODISC
ACRO LC13
0.45
FLOW
GELMAN
ACRO 50

# And More Resources to Serve

Nobody gives you more in laboratory filtration products than Gelman. Products that increase efficiency along with your confidence.

Like our Acro® disposable filter devices, allowing you to spend more time evaluating data... not waste time obtaining it. And the largest selection of membranes in the world. Membranes proven lowest in extractables for HPLC. Low protein-binding membranes for tissue culture study. The broadest family of membranes for air, water, and beverage analysis.

We also think of the little things. Like a magnetic filter funnel that works without clamps or frustrating threads. Microbiological broths free of worrisome particulates. And a petri dish that opens easily and seals tight... with one hand.

Of course, what good are great ideas you can't get your hands on. So we've established the broadest

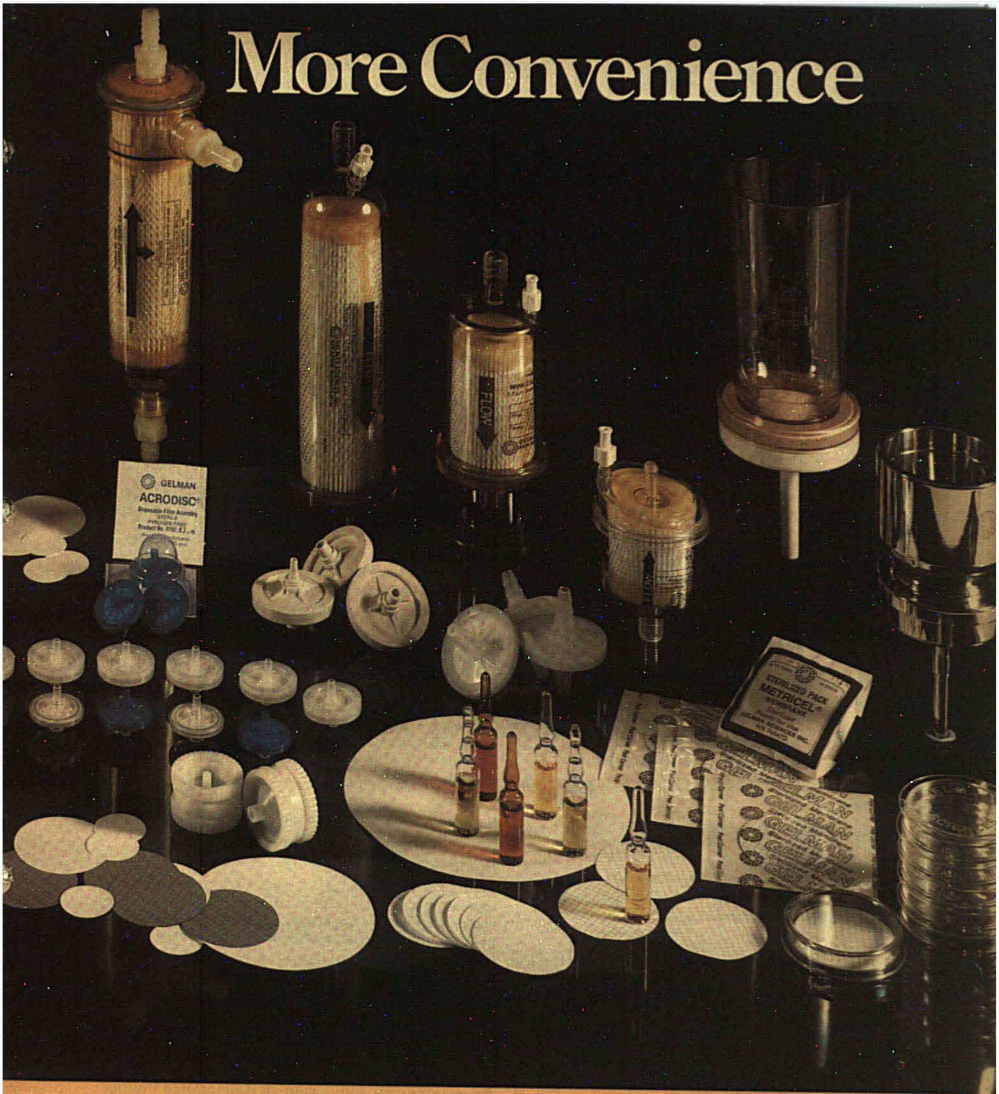
More Convenience
GELMAN
ACRODISC
FLOW
STERILIZED PACK
METRICEL
GELMAN

# Your Lab in the Way You Want

network of distributors in the industry: nearly 1500 professional service representatives. Or, if you choose, you'll find us in the filtration section of your favorite dealer catalogue. We let *you* decide what you want in service.

Selection. Confidence. Convenience. Nobody's working harder to help you than Gelman.

**Gelman Sciences**
600 South Wagner Road • Ann Arbor, Michigan 48106

**Circle our reader service number for the *new,* Second Edition of The Filter Book… your personal guide to the finest selection of microfiltration membranes and laboratory products. *Free!***

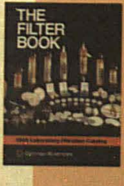
THE
FILTER
BOOK

CIRCLE 56 ON READER SERVICE CARD

# Briefs

### Neutral Reactions in Gas Chromatography/Chemical Ionization Mass Spectrometry 786

Schiff base derivatives of aldehydes and ketones are formed on a GC column using $NH_3$ as carrier gas and detected using CIMS. Postcolumn addition of $NH_3$ or $CH_3NH_2$ also produces neutral products that can be detected by CIMS.

**Patrick Rudewicz and Burnaby Munson***, Department of Chemistry, University of Delaware, Newark, Del. 19716
*Anal. Chem.*, *57* (*1985*)

### Gas Chromatography/Mass Spectrometry Determination of Water-Soluble Primary Amines as Their Pentafluorobenzaldehyde Imines 790

A 10-ppb detection limit is achieved for seven primary alkyl amines in 0.5-mL samples of tap, river, and oil shale process waters.

**Michael J. Avery* and Gregor A. Junk**, U.S. Department of Energy, Ames Laboratory, Ames, Iowa 50011
*Anal. Chem.*, *57* (*1985*)

### Rapid and Precise Method for the Measurement of Vapor/Liquid Equilibria by Headspace Gas Chromatography 793

An automated headspace GC is described for the determination of vapor/liquid equilibria, including vapor pressure and infinite-dilution activity coefficients. Precision of measurement is often better than 0.5%.

**Abul Hussam and Peter W. Carr***, Department of Chemistry, Smith and Kolthoff Hall, University of Minnesota, Minneapolis, Minn. 55455
*Anal. Chem.*, *57* (*1985*)

### Determination of Chlorinated Benzenes in Bottom Sediment Samples by WCOT Column Gas Chromatography 801

Extraction efficiencies of steam distillation, ultrasonication, and soxhlet extraction are compared. An integrated analytical procedure for quantitation by high-resolution GC is presented.

**F. I. Onuska* and K. A. Terry**, National Water Research Institute, Canada Centre for Inland Waters, Burlington, Ontario, Canada L7R 4A6
*Anal. Chem.*, *57* (*1985*)

### Industrial Wastewater Analysis by Liquid Chromatography with Precolumn Technology and Diode-Array Detection 806

Precolumns packed with $C_{18}$, $PRP_1$, and cation exchange resin are used for on-line group separation and trace enrichment of complex samples. Multisignal plots are used to obtain preliminary compound identification.

**M.W.F. Nielen, U.A.Th. Brinkman, and R. W. Frei***, Department of Analytical Chemistry, Free University, De Boelelaan 1083, 1081 HV Amsterdam, The Netherlands
*Anal. Chem.*, *57* (*1985*)

### Computer-Based Numerical Integration for the Calculation of Retention Times in Gradient High-Performance Liquid Chromatography 811

The programs can be used for solvent composition vs. either solute capacity factor or time. Accuracies average better than 5% for complex gradients using microbore HPLC.

**Sterling A. Tomellini and Richard A. Hartwick***, Department of Chemistry, Rutgers University, P.O. Box 939, Piscataway, N.J. 08854, and **Hugh B. Woodruff**, Merck Sharp & Dohme Research Laboratories, P.O. Box 2000, Rahway, N.J. 07065
*Anal. Chem.*, *57* (*1985*)

### Polarity of Chemically Modified Silica Surfaces and Its Dependence on Mobile-Phase Composition by Fluorescence Spectrometry 817

Polarity of RP-18 and RP-2 surfaces decreases with increasing methanol concentration in the solvent, whereas acetonitrile has a more complex influence on surface polarity. A molecular model based on these results is discussed.

**Jan Ståhlberg***, Astra Pharmaceutical Production AB, Quality Control, S-151 85 Södertälje, Sweden, and **Mats Almgren**, Institute of Physical Chemistry, P.O. Box 532, S-751 21 Uppsala, Sweden
*Anal. Chem.*, *57* (*1985*)

### Interface of a Microbore High-Performance Liquid Chromatograph with a Diffuse Reflectance Fourier Transform Infrared Spectrometer 822

Detection limits of 10 ng of injected material are obtained. Several different microbore columns are studied, and the relative advantages and disadvantages of each with respect to the interface are discussed.

**Christine M. Conroy and Peter R. Griffiths***, Department of Chemistry, University of California, Riverside, Calif. 92521, and **Kiyokatsu Jinno**, School of Materials Science, Toyohashi University of Technology, Toyohashi 440, Japan
*Anal. Chem.*, *57* (*1985*)

* Corresponding author

# SAVE 53%

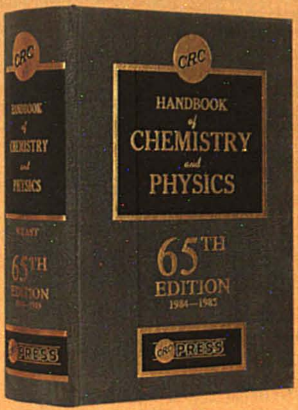

*" . . . it packs more important and reliable data between two covers than any other publication of its kind."*

*Clinical Chemistry*

*"This classic work is a 'must' for scientists and engineers in most fields."*

*Environmental Science and Technology*

The most recent edition of the *CRC Handbook of Chemistry and Physics* is being offered for a limited time only at less than half price — that's $35.00 off the regular price of $64.95.

Each year *The Handbook* is reviewed and revised by an international panel of authorities, placing it among the most complete and up-to-date references available to scientists worldwide.

You'll quickly find what you're looking for in this comprehensive resource of over 2300 pages of graphs, tables, formulas, and property information.

# NOW ONLY $29.95

## ORDER FORM

Rush me the 65th Edition of the *CRC Handbook of Chemistry and Physics* for only $29.95* (regularly $64.95).
To qualify for this special offer, each order should:

- be prepaid by check, money order, or charged to one of the credit cards below
- be postmarked by May 15, 1985
- specify catalog no. 465KYK

Enclosed is my check/money order for $________________

Name______________________________

Co./Inst.______________________________

Address______________________________

City____________State________Zip________

*Outside U.S., $34.95 per copy. Payable in U.S. currency or draft on a U.S. bank. Florida residents add 5% sales tax.

☐ American Express ☐ MasterCard ☐ Visa

Account # (include all digits)

☐☐☐☐☐☐☐☐☐☐☐☐☐☐☐☐☐

Expiration Date________Validation Date (AMEX)________

______________________________

Signature (required for credit card orders). Please use ink.

______________________________

Please print name appearing on credit card.

Order **TOLL FREE** 1-800-272-7737 • Monday-Friday • 8:30 a.m. to 5 p.m.
(In Florida call collect: 1-305-994-0563.)

CRC PRESS, INC. 2000 Corporate Blvd., N.W. Boca Raton, Florida 33431

## Briefs

### Pulse Residence in Short Chromatographic Columns 826

Influence of inter- and intraparticle mass transfer, input and effluent boundary conditions, and chemical reactions on mean residence time are discussed.

**Dwight W. Underhill**, Department of Industrial and Environmental Health Sciences, Graduate School of Public Health, University of Pittsburgh, Pittsburgh, Pa. 15261
*Anal. Chem.*, *57* (*1985*)

### Potassium Hydroxide Eluent for Nonsuppressed Anion Chromatography of Cyanide, Sulfide, Arsenite, and Other Weak Acids 829

Fifteen inorganic monovalent anions are determined with detection limits of 22–200 ppb.

**Tetsuo Okada* and Tooru Kuwamoto**, Department of Chemistry, Faculty of Science, Kyoto University, Sakyo-ku, Kyoto 606, Japan
*Anal. Chem.*, *57* (*1985*)

### Electrokinetic Chromatography with Micellar Solution and Open-Tubular Capillary 834

Aqueous and micellar phases are displaced differentially by electrokinetic phenomena, and solutes are distributed between the two phases by micellar solubilization.

**Shigeru Terabe*, Koji Otsuka, and Teiichi Ando**, Department of Industrial Chemistry, Faculty of Engineering, Kyoto University, Sakyo-ku, Kyoto 606, Japan
*Anal. Chem.*, *57* (*1985*)

### Rotating Arc Direct Current Plasma as an Emission Excitation Source 841

The source operates by forcing a dc arc to rotate reproducibly on the surface of a graphite anode disk. Argon gas is introduced tangentially to the anode. Detection limits are comparable to those obtained using a commercially available dc plasma.

**L. Y. Hara and M. L. Parsons***, Department of Chemistry, Arizona State University, Tempe, Ariz. 85287
*Anal. Chem.*, *57* (*1985*)

### Moderate-Power Helium Plasma as an Element-Selective Detector for Gas Chromatography of Dioxins and Other Halogenated Compounds 846

Multielement chromatograms are obtained by monitoring wavelengths corresponding to the elemental emission of specific compounds. Elemental ratios are determined using an off-line background correction scheme.

**David L. Haas and Joseph A. Caruso***, Department of Chemistry, University of Cincinnati, Cincinnati, Ohio 45221
*Anal. Chem.*, *57* (*1985*)

### Improved Detection Limits in Inductively Coupled Plasma Multichannel Spectrometry of Uranyl Nitrate Solutions by Compensation of Nonrandom Background Fluctuations 851

A 20-fold improvement in detection limits of 20 elements is achieved by monitoring the background fluctuations at several wavelengths.

**Avraham Lorber*, Michael Eldan, and Zvi Goldbart**, Nuclear Research Centre—Negev, P.O. Box 9001, Beer-Sheva 84190, Israel
*Anal. Chem.*, *57* (*1985*)

### Determination of Gallium in Sediment, Coal, Coal Fly Ash, and Botanical Samples by Graphite Furnace Atomic Absorption Spectrometry Using Nickel Matrix Modification 857

Detection limits at the ng/g level are obtained. A mechanism explaining the observed improved sensitivity in the presence of Ni and suppressed sensitivity in the presence of $HClO_4$ is discussed.

**Shan Xiao-quan, Yuan Zhi-neng, and Ni Zhe-ming***, Institute of Environmental Chemistry, Academia Sinica, P.O. Box 934, Beijing, People's Republic of China
*Anal. Chem.*, *57* (*1985*)

### Determination of Formaldehyde with the Thermal Lens Effect 861

A 20-fold improvement in sensitivity over standard absorption techniques is observed. A formaldehyde concentration of $1.5 \times 10^{-8}$ M is detected.

**Jan A. Alfheim and Cooper H. Langford***, Department of Chemistry, Concordia University, 1455 de Maisonneuve, West, Montreal, Quebec H3G 1M8, Canada
*Anal. Chem.*, *57* (*1985*)

### Determination of Structural Characteristics of Saturates from Diesel and Kerosene Fuels by Carbon-13 Nuclear Magnetic Resonance Spectrometry 864

Gated spin echo $^{13}C$ NMR data are used to derive average structure parameters for determining the extent of branching and ring structures in saturated hydrocarbon fractions.

**David J. Cookson and Brian E. Smith***, The Broken Hill Proprietary Co., Ltd., Melbourne Research Laboratories, 245 Wellington Road, Mulgrave, Victoria, Australia 3170
*Anal. Chem.*, *57* (*1985*)

### Comparison of Photoacoustic and Attenuated Total Reflectance Sampling Depths in the Infrared Region 871

Infrared analysis of multilayer organic polymers indicates that for optically transparent, thermally thick films, typical ATR sampling depths are an order of magnitude less than those for PAS.

**Daniel A. Saucy, Steven J. Simko, and Richard W. Linton***, Kenan Laboratories of Chemistry, Department of Chemistry, University of North Carolina, Chapel Hill, N.C. 27514
*Anal. Chem.*, *57* (*1985*)

### Surface Reactivities of Polynuclear Aromatic Adsorbates on Alumina and Silica Particles Using Infrared Photoacoustic Spectroscopy 876

The nature of submonolayer organic films and their reactivity on inorganic particulate adsorbents are studied. The detection limit is estimated at 0.2 monolayers of adsorbed organic compound.

**Daniel A. Saucy, George E. Cabaniss, and Richard W. Linton***, Department of Chemistry, University of North Carolina, Chapel Hill, N.C. 27514
*Anal. Chem.*, *57* (*1985*)

Universal Drive
Body
Rotor
Pre-load Assembly

VICI

**Valco Instruments Co. Inc.**
P.O. Box 55603 Houston, Texas 77255
(713) 688-9345
TWX 910-881-5500 Telex 79-0033

**Valco Switzerland**
Tannberg P.O. Box 13 CH-6214 Schenkon
(045) 216868
Telex 868342 vici ch

# ANNOUNCING

## NEW FOR GC

**NOW — FOR FUSED SILICA COLUMNS**

- **sample injection**
- **recycling**
- **backflushing**
- **concentration**
- **heartcutting**
- **stripping**

.25mm bore throughout,
350°C maximum temperature

**The first devices for direct sampling and switching of fused silica columns are now available from Valco and leading international dealers.**

## AND

## NEW FOR HPLC

**The most advanced "user friendly" HPLC sample injection and switching valves.**

- **smallest internal volume of any HPLC valve**
- **the *easiest* to turn HPLC injector**
- **sample sizes from .06 µl to 10 cc**
- **use standard syringes**
- **lowest bandspreading**
- **air or electric automation**
- **3-12 port models for flow switching**
- **simplest servicing — no tools needed for rotor replacement**

CIRCLE 218 ON READER SERVICE CARD

Fermentation Analysis in 60 seconds with Immobilized Enzymes

Determination of ethanol or specific sugars has never been so fast, easy and accurate!

The YSI Model 27 uses immobilized enzymes to provide specific, reproducible determinations of ethanol, dextrose, sucrose, lactose, lactate, fructose or starch in a wide variety of sample matrices. Sample preparation is simple and no distillation is required. Measurements are specific with readout directly in mg/dl. Analysis time is only 60 seconds. Color, turbidity and volatiles do not interfere.

The Model 27 takes the drudgery and guesswork out of ethanol or sugar determinations. It's also easy to operate and cost efficient. That's why nearly a thousand analyzers are in use worldwide.

Let us demonstrate the Model 27 in your lab and show you the easy way to determine fermentation ingredients and products.

**Call toll-free 800-343-HELP.**

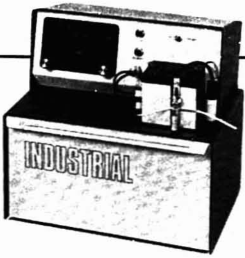

Please send information on the YSI Model 27 Industrial Analyzer to:
Name ____ Title ____
Organization ____
Address ____
City, State, ZIP ____
Phone ____

YSI SCIENTIFIC

**Scientific Division**
**Yellow Springs Instrument Co.**
**Yellow Springs, Ohio 45387 USA • 513-767-7241**

CIRCLE 242 ON READER SERVICE CARD

## Briefs

### Angular Distribution X-ray Photoelectron Spectroscopy Studies on Compacted Lead Ion Selective Membrane Powders 880

The effects of EDTA and $HClO_4$ on the subsurface distribution of corrosion and substrate species are reported. Surface topography of powder pellets is studied, as are the data used to assess the effect of roughness on XPS intensity ratios.

**Vaneica Young* and Paul C. McCaslin,** Department of Chemistry, Texas A&M University, College Station, Tex. 77843
*Anal. Chem.*, *57* (*1985*)

### Detection of Gaseous Organophosphorus Compounds Using Secondary Ion Mass Spectrometry 886

Gaseous analytes are introduced onto a polyphosphoric acid matrix under primary ion bombardment. A linear relationship is observed between the abundance of secondary analyte ions and the introduction rate.

**Gary S. Groenewold and Peter J. Todd*,** Analytical Chemistry Division, Oak Ridge National Laboratory, Oak Ridge, Tenn. 37831
*Anal. Chem.*, *57* (*1985*)

### Negative Gold Ion Gun for Liquid Secondary Ion Mass Spectrometry 890

The construction and operating characteristics of the ion gun are described. The $Au^-$ ion energy can be varied up to 20 keV using the high-voltage feedthroughs supplied with most high-performance instruments.

**Charles N. McEwen* and J. Ronald Hass,** Laboratory of Molecular Biophysics, National Institute of Environmental Health Sciences, Research Triangle Park, N.C. 27709
*Anal. Chem.*, *57* (*1985*)

### Identification of Stereoisomers of Some Hexoses by Mass Spectrometry Using Fast Atom Bombardment and Mass Ion Kinetic Energy 892

Two kinds of cationized ions, $(\text{aldohexose-cat})^+$ and $(\text{matrix-cat})^+$, are generated. The abundances of these fragment ions are characteristic of all D-aldohexose stereoisomers.

**Germain Puzo*, Jean-Jacques Fournie, and Jean-Claude Prome,** Centre de Recherche de Biochimie et de Génétique Cellulaires du C.N.R.S., 118 route de Narbonne, 31062 Toulouse Cedex, France
*Anal. Chem.*, *57* (*1985*)

### Laser Desorption Mass Spectrometry of Nonvolatiles under Shock Wave Conditions 895

High-laser-power densities and thick sample layers produce extremely soft desorption–ionization conditions leading to abundant quasimolecular peaks and low-level fragmentation.

**Buko Lindner and Ulrich Seydel*,** Forschungsinstitut Borstel, Parkallee 1-40, D-2061 Borstel, Federal Republic of Germany
*Anal. Chem.*, *57* (*1985*)

# Optimum Performance with ONE System

Pneumatic Flow Controllers
Accepts Packed Column or Capillary Column
GOW MAC
GAS CHROMATOGRAPH
Offers FID and TID Detectors
Offered with a 1 Year Firm Guarantee

## *...and the Price is $4750.**

The new GOW-MAC 740P GC SINGLE COLUMN System is priced realistically and gives an unequalled performance. It is productive and meets every laboratory or quality control need.

Here's why. The 740P offers you the choice of the standard packed column injection port or split/splitless, direct, and on-column capillary injection systems. Available detectors are FID and TID (thermionic ionization detector). Communications possibilities are standard: Integrator, recorder or CRT.

The 740P has a microprogrammer which enables you to keyboard programs or to repeat frequently used programs. This is for precision, accuracy and convenience in commanding the instrument.

Cost. Not only is the initial cost low but it is combined with a one year (no kidding) guarantee. The GOW-MAC 740P will be the least expensive GC you will ever own or operate.

All in all, the GOW-MAC new 740P system is the *most flexible, best performing* GC you can have. It has been, and is today, the standard by which other compact GC's are judged.

For prices, options, and more information, use the Reader Service Nos. or contact:

**GOW-MAC** INSTRUMENT CO.
P.O. Box 32, Bound Brook, NJ 08805, (201) 560-0600

*Price includes 69-740P single column, temperature programmed FID Gas Chromatograph with 75-650 pneumatic fuel gas system.

GOW-MAC INSTRUMENT CO.
P.O. Box 32, Bound Brook, NJ 08805

Name ____________________
Title ____________________
Company ____________________
Address ____________________
City ____________________
State ____________ Zip ________

CIRCLE 68 ON READER SERVICE CARD

ห้องสมุดกรมวิทยาศาสตร์บริการ

LABORATORY INTERFACE PERIPHERAL SUBSYSTEM
AUTOMATE SPECs, GCs, GEL SCANNERs
for less than $2000
including
computer and disk drive

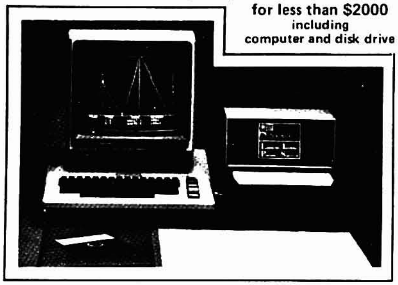

**CHROMATOGRAPHY SOFTWARE** — Auto or manual peak detection and integration. Store and retrieve scan on floppy.

**16 BIT ADCs** — Four independent channels of 16 bit ADCs giving 1 part in 65000 resolution throughout ADC span. (Other mfgrs. use 12 bit ADCs resolving to only 1 part in 4096.) Differential inputs with dedicated integrator for each channel for optimum noise rejection. Full-scale sensitivities of 10 mv to 10 volts available.

**DIGITAL I/O** — 24 lines of digital input/output included.

**DAC CHANNELS** — Optional analog output with full-scale voltages of 1 to 15 volts for controlling devices or data output.

**HIGH RESOLUTION – VERSATILE**
**COMPLETE** — 4 channels of ADC with digital I/O and chromatography software for only **$1185.**

205 Weaver Street / Carrboro, N.C. 27510
(919) 929-5001 for more information

SPECTROFUGE
CORPORATION OF NORTH CAROLINA, INC.

CIRCLE 189 ON READER SERVICE CARD

Safe,
Effective
Ethyl Ether

B&J Brand™ High Purity Methyl t-Butyl Ether, when used as a replacement for ethyl ether, minimizes peroxide hazards and interferences for high performance applications. Yet, it performs as effectively, or better, than solvents with similar physical properties. For complete information on B&J Brand Methyl t-Butyl Ether—or other high purity solvents—contact American Burdick & Jackson, 1953 South Harvey Street, Muskegon, MI USA 49442. Phone: 616 726 3171.

American Burdick & Jackson Subsidiary of American Hospital Supply Corporation

©1985 American Hospital Supply Corporation

CIRCLE 6 ON READER SERVICE CARD

## Briefs

### Reliability Ranking and Scaling Improvements to the Probability Based Matching System for Unknown Mass Spectra 899

A weighted combination of matching parameters that predicts directly the probability that a retrieved answer is correct, along with quadratic scaling of abundance values, significantly improves matching performance.

**Barbara L. Atwater, Douglas B. Stauffer, and Fred W. McLafferty***, Chemistry Department, Cornell University, Ithaca, N.Y. 14853, and **David W. Peterson**, Scientific Instrument Division, Hewlett-Packard, 1501 California Avenue, Palo Alto, Calif. 94304 *Anal. Chem., 57 (1985)*

### Multicomponent Mixture Analysis Using Room-Temperature Phosphorimetry 904

Four phosphorescent toxic compounds are determined by RTP without prior separation. The method of calibration and subtraction is used to determine two spectroscopically overlapping compounds in mixtures.

**Ebenezer B. Asafu-Adjaye, Jung Im Yun, and Syang Y. Su***, Department of Chemistry, Virginia Commonwealth University, Richmond, Va. 23284 *Anal. Chem., 57 (1985)*

### Background Detection and Correction in Multicomponent Analysis 908

A method to test for the presence of background interferents during the quantitation step of a multicomponent analysis is reported. Two distinct quantitation methods, the perpendicular projection and the extreme vertex projection techniques, are proposed.

**D. W. Osten and B. R. Kowalski***, Laboratory for Chemometrics, Department of Chemistry, University of Washington, Seattle, Wash. 98195 *Anal. Chem., 57 (1985)*

### Automated Fluorometric Method for Hydrogen Peroxide in Atmospheric Precipitation 917

Hydrogen peroxide is reacted with horseradish peroxidase and *p*-hydroxyphenylacetic acid (POPHA) to form a fluorescent dimer of POPHA. A detection limit of $1.2 \times 10^{-8}$ M with a RSD of 0.7% is obtained for a 1.5-mL aqueous sample.

**Allan L. Lazrus*, Gregory L. Kok, Sonia N. Gitlin, and John A. Lind**, National Center for Atmospheric Research, P.O. Box 3000, Boulder, Colo. 80307, and **Scott E. McLaren**, Atmospheric Science Research Center, 1400 Washington Avenue, Albany, N.Y. 12222 *Anal. Chem., 57 (1985)*

### Determination of Acidity Constants by Solvent Extraction/Flow Injection Analysis Using a Dual-Membrane Phase Separator 922

Absorbances of both the aqueous and organic phases are simultaneously monitored. Acidity constants are determined from straight-line plots relating the ratio of peak areas in the aqueous and organic phases to the $H^+$ activity of the aqueous phase.

**Lynette Fossey and Frederick F. Cantwell***, Department of Chemistry, University of Alberta, Edmonton, Alberta, Canada T6G 2G2 *Anal. Chem., 57 (1985)*

# Specialty gases have never been compressed like this before.

Our new 16-page capabilities brochure is the closest we've ever come to squeezing our world between two covers.

In it, you'll find out how to judge a gas by looking at the cylinder.

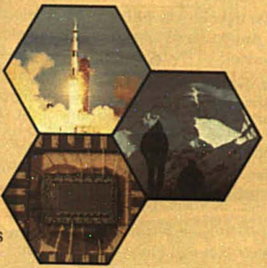

How our quality equipment can actually make an inferior gas perform better.

How our designers work with their ears.

Why everyone—including our competitors—comes to Matheson for information.

And why Matheson participated in the Apollo space program, a scientific expedition to Mount Everest, and the development of the semiconductor chip.

**Just the highlights.**

But try as we might, there's simply no way for 16 pages to tell the entire Matheson story.

For that you'll want to look through our 208-page catalog of gases and gas mixtures.

You'll want to look over our selection of more than 2,000 equipment items from regulators, flowmeters, and hand trucks, to custom engineered gas handling systems.

And you'll want to consult our "Gas Data Book," and our other technical and safety publications.

**Call or write, today.**

Our new brochure may be condensed, but it's still a great mind expander. For your free copy, or to contact a Matheson representative for a complete analysis of how our products, services, and information can help *your* unique process or experiment, just call 1-201-867-4100. Or write: Matheson Gas Products, Inc., P.O. Box 1587, Secaucus, NJ 07094.

MATHESON
World Leader in Specialty Gases and Equipment

**Matheson®**
**Gas Products**
**World Leader in Specialty Gases & Equipment**

CIRCLE 138 ON READER SERVICE CARD

Capture an entire UV-visible spectrum
...in less than 20 ms

OMA III

The OMA III family is the culmination of over ten years experience in building and using optical multichannel analyzers.

The Model 1460 OMA III is our own 68000 based system processor designed specifically for extremely rapid parallel spectral data acquisition, analysis and presentation.

Our Model 1461 Detector Interface is designed to connect any of our solid state multichannel detectors to virtually any computer. The Model 1461 is easily programmed using high level mnemonic commands over RS232 or IEEE.

M1461
M1460

- Detectors include Diode Arrays and Vidicons.
- Soft-touch screen, IEEE, RS232, VME Expansion Capability.

EG&G
PRINCETON APPLIED RESEARCH
P.O. BOX 2565 • PRINCETON, NJ 08540, U.S.A. • 609/452-2111 • TELEX 843409

682

CIRCLE 48 ON READER SERVICE CARD

## Briefs

### Electrochemistry and Reverse Pulse Polarographic Determination of 1,2-Dibromo-2,4-dicyanobutane 927

Reverse-pulse voltammetry of the two-electron reduction of DBDCB at mercury electrodes in acetonitrile requires liberation of two $Br^-$ and an organic product, $C_6N_2H_6$, per mole of reactant.

**Marek Wojciechowski and Janet Osteryoung***, Department of Chemistry, State University of New York at Buffalo, Buffalo, N.Y. 14214 *Anal. Chem.*, *57* (*1985*)

### Distribution of Electrochemical Activity on Graphite–Epoxy Surfaces 933

Iontophoresis is used to determine that electrochemical activity is concentrated in 80–130-μm irregularly shaped regions of aggregated graphite.

**Royce C. Engstrom*, Michael Weber, and Jane Werth,** Department of Chemistry, University of South Dakota, Vermillion, S.D. 57069 *Anal. Chem.*, *57* (*1985*)

### Flow Injection and Liquid Chromatography Detector for Amino Acids Based on a Postcolumn Reaction with Luminol 936

The detector is based on suppression of chemiluminescence in the copper(II)–luminol–peroxide system. Detection limits depend on the magnitude of the complex formation constants and range from 0.004–20.0 nmol in the FIA mode.

**Allan MacDonald and Timothy A. Nieman***, Department of Chemistry, University of Illinois, 1209 West California Street, Urbana, Ill. 61801 *Anal. Chem.*, *57* (*1985*)

### Laser-Induced Fluorescence Spectrometry of Aromatic Hydrocarbon Derivatives in Vapor-Deposited Parent Molecule Matrices 940

Chloronaphthalenes are detected at low-nanogram levels from two-photon excitation spectra. Advantages of a low-temperature parent molecule matrix and of sample preparation by vapor deposition are discussed.

**Charles F. Pace and Jon R. Maple***, Department of Chemistry, University of New Mexico, Albuquerque, N.M. 87131 *Anal. Chem.*, *57* (*1985*)

LECO RA-100
LECO RAC-100
NEW!

# RA-100 Rapid Acid Soluble Aluminum Determinator

- **Allows control of the aluminum content during the steel making process.**
- **Fast . . .Acid soluble aluminum content is obtained while there is still time to adjust the chemistry of the melt.**
- **Easy sample preparation using the LECO® Diskpin® sampler.**
- **One step analysis.**

Using an innovative technique, the RA-100 removes a known quantity of metal from the sample disc by electrolytic reaction. There is no longer a need for time consuming, tedious, wet chemical methods of sample preparation. Furthermore, the sample is not destroyed in the process. After light grinding, it can be reused for additional or different analyses.

The two-cabinet instrument includes a corrosion-resistant solutions unit, the RA-100, and a control unit, the RAC-100.

The simplicity of the design leads to economical, reliable performance. All reagents necessary are readily available, and the only laboratory facilities required are 115 or 230 VAC power, nitrogen or argon gas for the pneumatic system, and drainage. Minimal operator training is required since procedures are microprocessor controlled. The instrument is fully self-monitoring. System variables are repeatedly checked by the microprocessor throughout the analysis.

***To learn more about this new LECO® instrument, call or write today!***

**LECO CORPORATION**
3000 Lakeview Avenue
St. Joseph, MI 49085-2396
(616) 983-5531
Cable: LECO
Telex: 72 9411

CIRCLE 128 ON READER SERVICE CARD

ULTRA PURE ACIDS

- Double sub-boiling distilled in Quartz.
- Produced under CLASS 100 clean room conditions.
- Certificate of Analysis.
- The world's highest purity acids available commercially.
- Ultra cleaned TEFLON acid containers are returnable. Low cost refills.

Seastar
SEASTAR CHEMICALS
(A Division of Seastar Instruments)
MANUFACTURERS OF ULTRA PURE ACIDS
2045 MILLS ROAD
SIDNEY, B.C., CANADA V8L 3S1
(604) 656-0891 • TELEX 049-7526

CIRCLE 187 ON READER SERVICE CARD

GUARANTEED!

C18 HPLC COLUMN PROVIDES EFFICIENT SEPARATIONS.

American Burdick and Jackson's model OD5 LC Column delivers guaranteed quality and performance for Reverse Phase Liquid Chromatography. Developed to meet B&J internal quality control requirements, it features:
- Fully endcapped monomeric C18 bonded phase 5 μM spherical silica
- Fingertight endfittings included
- Rigorous quality control testing
- Choice of two column sizes for specific applications.

For a free technical bulletin complete with typical applications—contact American Burdick & Jackson. 1953 South Harvey Street, Muskegon, MI USA 49442. Phone: 616 726-3171

American Burdick & Jackson Subsidiary of American Hospital Supply Corporation

©1985 American Hospital Supply Corporation

CIRCLE 5 ON READER SERVICE CARD

## Briefs

### Correspondence

**Optimized Field-Flow Fractionation System Based on Dual Stream Splitters** 945

**J. Calvin Giddings**, Department of Chemistry, University of Utah, Salt Lake City, Utah 84112 *Anal. Chem.*, 57 (1985)

**Pulsed Semiconductor Laser Fluorometry for Lifetime Measurements** 947

**Totaro Imasaka, Akinori Yoshitake, Kaoru Hirata, Yuji Kawabata, and Nobuhiko Ishibashi***, Faculty of Engineering, Kyushu University, Hakozaki, Fukuoka 812, Japan *Anal. Chem.*, 57 (1985)

**Laser Photodissociation/Tandem Mass Spectrometry of Synthetic Porphyrins: A Structural Probe** 949

**Elaine K. Fukuda and Joseph E. Campana***, Naval Research Laboratory, Chemistry Division, Washington, D.C. 20375-5000 *Anal. Chem.*, 57 (1985)

**Unbiased Generalized Standard Addition Method** 952

**Avraham Lorber**, Nuclear Research Centre—Negev, P.O. Box 9001, Beer-Sheva 84190, Israel *Anal. Chem.*, 57 (1985)

**Square Wave Voltammetry at Electrodes Having a Small Dimension** 954

**John O'Dea, Marek Wojciechowski, and Janet Osteryoung***, Department of Chemistry, State University of New York at Buffalo, Buffalo, N.Y. 14214, and **Koichi Aoki**, Department of Electronic Chemistry, Tokyo Institute of Technology, Nagatsuta, Midori-ku, Yokahama 227, Japan *Anal. Chem.*, 57 (1985)

### Aids for Analytical Chemists

**Constrained Calibration Curves: A Novel Application of Lagrange Multipliers in Analytical Chemistry** 956

**J. J. Leary* and E. B. Messick**, Department of Chemistry, James Madison University, Harrisonburg, Va. 22807 *Anal. Chem.*, 57 (1985)

**Microdetermination of Nitrogen in Organic Compounds by the Sodium Fusion-Spectrophotometric Method** 958

**Ernest J. Breda**, E. I. du Pont de Nemours & Company, Inc., Beaumont Works, P.O. Box 3269, Beaumont, Tex. 77704 *Anal. Chem.*, 57 (1985)

**Vacuum Actuated High-Vacuum Glass Valve** 960

**C.A.M. Brenninkmeijer* and M.L. Louwers**, Louwers Hapert, Hapert, The Netherlands *Anal. Chem.*, 57 (1985)

**BOMEM** INC

# elegant FTIR

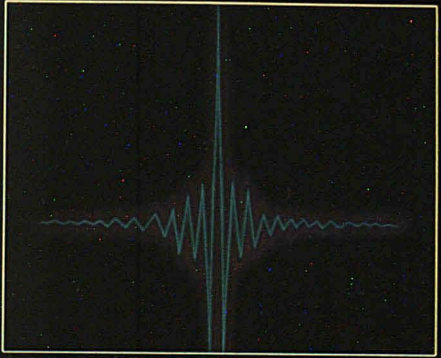

*Interferogram of a crystal taken through a 12 micron pinhole, no beam condensing, 300-400 nm.*

**the DA3.10 – THE BEST ALTERNATIVE**
From the FAR IR to the UV, the DA3.10 gives you the power of FT techniques for your analyses.

**AQUEOUS SAMPLES** long a problem for IR, are now routine when you use commercial accessories in the DA3.10.

**MICROSAMPLES** as small as 10 microns can be analysed without delicate beam condensers.

**POWDERS** are easily analysed by reflectance, pellets, or other techniques.

**POLYMERS** and other samples requiring time resolved and/or temperature controlled studies are swiftly examined with the DA3.10's Vacuum or purge modes.

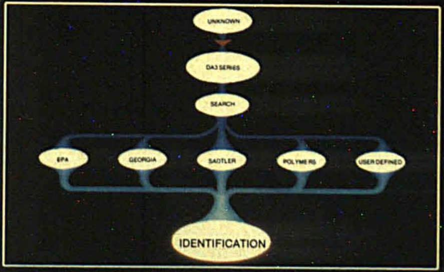
UNKNOWN
DA3 SERIES
SEARCH
EPA
GEORGIA
SADTLER
POLYMERS
USER DEFINED
IDENTIFICATION

*Powerful Library Search Routines for last identification*

**Bomem Inc., 625, Marais, Vanier, Québec G1M 2Y2 (418) 683-1707 Telex: 051-3438**

CIRCLE 17 ON READER SERVICE CARD

If you haven't looked at
LEEMAN
you haven't looked at
ICP

In three short years, we've brought a state-of-the-art ICP spectrometer from our imaginations to some of the most prestigious analytical chemistry benches in the field.

We did it through innovative design, technical craftsmanship, hard work, and commitment to our customers.

PLASMA SPEC features high resolution, benchtop size, versatility and ease of operation. Performance, reliability, service, price, and customer satisfaction are the elements in our success.

Let us demonstrate it to you. Call or write for information on our free, hands-on, local seminars.

LEEMAN LABS INC.
600 Suffolk St., Lowell, MA 01854, (617) 454-4442
Circle 125 for ICP Seminar Information. Circle 126 for Product Information.

# Letters

## Column efficiency measurement

**Sir:** The authors of "Column Efficiency Measurement" (Bidlingmeyer, Brian A.; Warren, F. Vincent, Jr. *Anal. Chem.* **1984,** *56,* 1583–96 A) made a serious omission in their Table II, "Calculation methods for column efficiency used by LC column suppliers."

Brownlee (now a Division of Applied Biosystems) was not mentioned, and although Brownlee is not currently a major LC column supplier, it has been using the moments method for calculating column efficiency on its columns since 1977. In fact, Jerry Higgins of Brownlee has been a strong proponent of the moments method. He has given seminars and Pittsburgh Conference talks and has written application notes explaining the method.

The same table points out that none of the other column manufacturers provide accurate column efficiencies. This is surprising, because data systems that will automatically perform these calculations are available for relatively low cost from Nelson Analytical.

**Glenn I. Ouchi**
Nelson Analytical
10061 Bubb Rd.
Cupertino, Calif. 95014

**Reply:** As the text indicated, Table II was intended to list methods of various suppliers to give the readers a feel for the range of methods used. Presently there are over 65 suppliers of LC columns, and we apologize for not listing a favorite of any of the readers.

We are not under the impression that "none of the other column manufacturers provide accurate column efficiencies," as Dr. Ouchi writes. The situation is that a variety of calculation methods are used and that some of these are potentially less accurate when used under adverse conditions. As stated in the text, "If the test peak is truly Gaussian, each of the calculation methods will give the same [efficiency] results." In this sense, every method is "correct" for calculating plate counts. However, each has particular strengths and weaknesses, and it is important that a user recognize this and use each method appropriately.

**Brian A. Bidlingmeyer**
**F. Vincent Warren**
Waters Chromatography Division
of Millipore
Maple St.
Milford, Mass. 01757

# The Reflective Vision

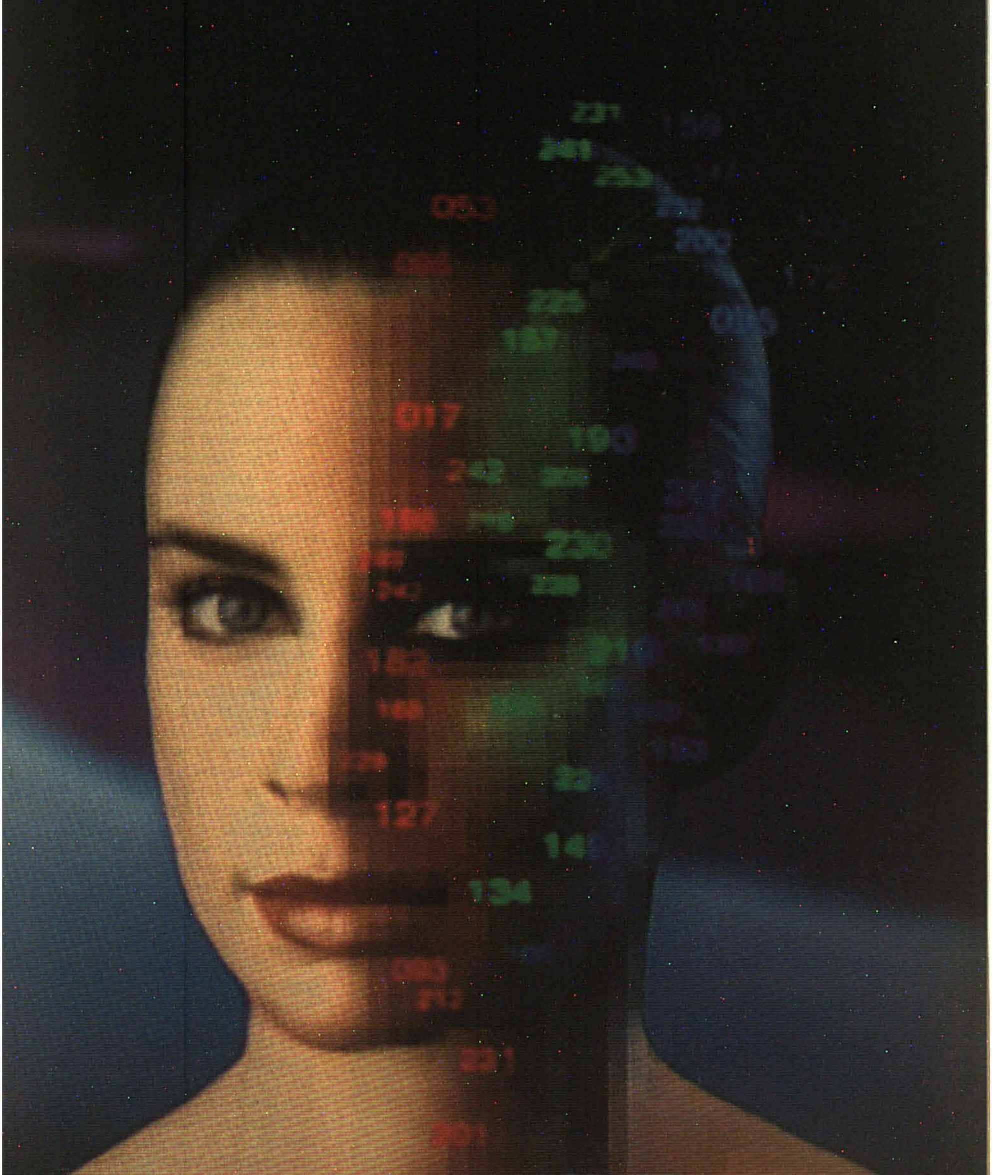

# The Reflective Vision

*A highly advanced design tool developed at the General Motors Research Laboratories uses computers to generate visual images from mathematical data with such accuracy that, soon, in-depth aesthetic evaluations of new concepts may be made prior to creating a costly physical model.*

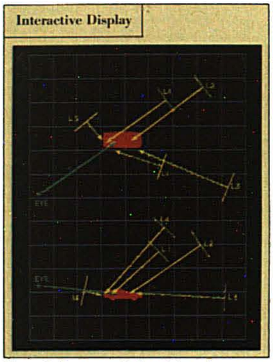

*Figure 1: Computer display of plan view (upper) and side elevation (lower), indicating automobile location (red), lighting selections (L1-L5), and viewing position (EYE).*

*Figure 2: Four Autocolor images, showing the same view of an automobile as background and lighting change.*

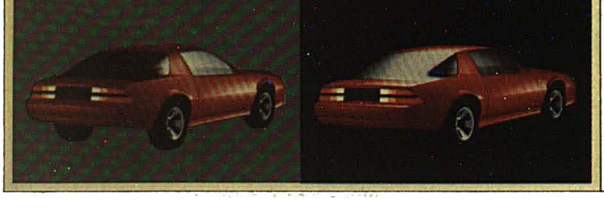

WITH AUTOCOLOR, users can synthesize three-dimensional, shaded images of design concepts on a color display and then quickly explore how major or minor changes affect the overall aesthetic impression. The system is completely interactive. By choosing from a menu on the screen, the designer can redefine display parameters, select a viewing orientation, or mix a color. Each part of an object can be assigned a surface type with associated color and reflectance properties. Built-in lighting controls generate realistic "highlights" on simulated surfaces composed of differing materials.

Before developing the system, David Warn, a computer scientist at the General Motors Research Laboratories, observed the complex lighting effects achieved in the studio of a professional photographer. By simulating these effects, Autocolor can produce results unattainable by conventional synthetic image display systems. Previous systems used a point source model of light, which allows adjustments only in position and brightness.

The versatility of the lighting controls constitutes a major advance in Autocolor. An unlimited number of light sources can be independently aimed at an object and the light concentration adjusted to simulate spotlight and floodlight effects. The lighting model even includes the large flaps or "barndoors" found on studio lights. These comprehensive controls permit the user to view the simulation in studio lighting conditions, as well as to make revisions in color, paint type, and materials.

With real lights, direction and concentration are produced by reflectors, lenses, and housings. It would be possible to model these components directly, but that would introduce considerable overhead to the lighting computation. Instead of modeling individual causes, Autocolor models the overall effect, reducing complexity by simulating those aspects needed to produce realistic results.

Autocolor approximates the geometric shape of an object with a mesh of three or four-sided polygons. These polygons are grouped to form parts. For a car body, there might be separate parts for the door, hood, roof, fender, and so on. Each part is assigned a surface type, such as painted metal or glass, and each type of surface has associated color and reflectance properties. The entire data structure is stored in tables using an interactive relational data base developed at the GM Research Laboratories.

THE LIGHTING model determines the intensity of the reflected light that reaches the eye from a given point on the object. It takes into account the reflectance properties of the surface as well as the physics of light reflection. A hidden surface algorithm determines which point on the object is visible at each point on the display. For each of these visible points, the intensity is computed for each light source. The displayed intensity is the sum of the contributions from all the lights plus an ambient term which indicates the general level of illumination.

Using the point source lights of conventional image generation systems, highlighting a particular area of an object can be a difficult task and can result in unwanted highlights in other areas. By contrast, the light direction and concentration controls found in Autocolor make it possible to isolate the effect of a light to a particular area, and achieve a desired highlight easily and quickly (see Figure 2). This is not because Autocolor's lighting model computations are faster, but because its controlled "lights" behave in a more natural way.

Another unique feature of Autocolor is the ability to portray realistically a variety of different materials and lighting conditions. The color seen from a surface is really a combination of two colors: the color of the surface or material itself (diffuse reflection) and the color of the reflected highlights (specular reflection). The highlight color may be the color of the material, the color of the light, or a color derived from the material and the light.

A different highlight color can be used for each different surface type that is defined. This makes it possible to simulate materials such as plastic, painted metal, and chrome—each of which has different reflectance properties and requires a different highlight color.

The user can interactively adjust the blending of the surface and highlight colors, watching the image change dynamically on the screen until a desired effect is achieved.

"Autocolor will free designers to be more creative," says researcher Warn. "Our goal is to move from controls that show changes in lighting, color, and materials, to software that will let the user change the actual shape, manipulating the image on the screen like a flexible clay model."

---

**General Motors**

GM
MARK OF EXCELLENCE

## THE MAN BEHIND THE WORK

David Warn is a Senior Staff Research Scientist in the Computer Science Department at the General Motors Research Laboratories.

He received his undergraduate degree in mathematics from Carnegie-Mellon University, and his M.S. in computer science from Purdue.

He has done extensive research in relational data management systems with special emphasis on user interfaces and human factors. He also designed the prototype for the network data manager used in the GM Corporate Graphic System. His previous work on other aspects of computer-aided design include system design, file management, and simulation models.

His foremost research interests are in color synthetic image generation and interactive surface design. He joined General Motors in 1968.

# RENT OR LEASE

## Short or Long Term

# NEW ANALYTICAL INSTRUMENTS

- Gas, Liquid and Ion Chromatographs
- GC/MS Systems
- IR, FTIR, UV/VIS, Fluorescence and AA Spectrophotometers
- Thermal Analyzers
- And MORE!

## IMMEDIATE AVAILABILITY

**From Our Extensive Inventory**

**CALL US AT**
**800-437-9701**
**415-572-4115**

**United States**
**Analytical Instruments**

2988 Campus Drive
San Mateo, CA 94403

A U.S. Leasing Company

CIRCLE 213 ON READER SERVICE CARD

**Report**

**H. Steffen Peiser**
National Bureau of Standards (retired)
Washington, D.C. 20234

# How Good Are the Standard Atomic Weights?

It is now more than 20 years since Edward Wichers asked: "How Good Are the New Atomic Weights?" in the title of a REPORT in this JOURNAL (*1*). His article followed the 1961 Report of the International Commission on Atomic Weights (ICAW) of the International Union of Pure and Applied Chemistry (IUPAC) (2) in which A. E. Cameron and he had undertaken to adjust the tabulated atomic-weight values of all elements to the then-new atomic-weight scale based on the atomic mass of 12 u for the carbon isotope of mass number 12 ($A_r(^{12}C) = 12$ exactly). Among chemists, Wichers himself had been the principal proponent of the new scale. The previously used atomic-weight scale based on oxygen ($A_r(O) = 16$) had proved unsuitable since the discovery of the isotopes of minor and variable abundance in natural oxygen. To carry out the conversion to the new scale, Cameron and Wichers found it necessary to carry out an element-by-element review of the significant original literature. They recalculated most atomic weights and their uncertainties, which are reflected in the number of digits included in the IUPAC Table of Atomic Weights. This table is revised every two years; the latest is the 1983 table (*3*).

Science has not stood still since 1961. Based mostly on more searching analysis and better mass spectrometry, the 1983 table (*3*) contains a good deal of better data than the 1961 table (*2*).

It is now well recognized that atomic weights are not all constants of nature. It is thus appropriate to assign an atomic weight to a given sample. Accordingly, IUPAC feels free to define the "standard atomic weight" of an element as referring to "our best knowledge of the atomic weight of an element in (normal) natural terrestrial sources." Its uncertainty is implied by the precision of its tabulated value and arises from experimental uncertainty and variability of isotopic composition in such sources. The IUPAC table is now called the Table of the Standard Atomic Weights, as recommended by the IUPAC Commission now called Commission on Atomic Weights and Isotopic Abundances (CAWIA). A subcommittee of CAWIA has just completed another "Element by Element Review of Their Atomic Weights" (*4*). It is therefore appropriate to ask the same question Wichers asked: How good are they now? In this simplified discussion, I am chiefly addressing chemical analysts, who perhaps place too much confidence in the accuracy of these values.

## Clarke's atomic weights

To illustrate some of my points, I would like to go one step farther back in history to the limits of living memory—to 1920 when Frank W. Clarke (*5*) completed the element-by-element review prior to the one done by Cameron and Wichers (*2*). In Table I, Clarke's values are compared with current atomic weights. Clarke listed the atomic weights of the then-well-known elements on the two scales in use at that time: $A_r(H) = 1$ and $A_r(O) = 16$. For our purposes, the latter, which alone is used in Table I, offers a fair comparison, because the present value for $A_r(O)$ is very close to 16. Where differences in element names are involved, Table I uses the modern name.

Some atomic weights in the 1920 table agree well with current values, but others show unacceptable differences. Which are more nearly correct? If we could have asked Clarke: "How good are your values?" I do not know what answer we would have received. However, in 1967, on my election to ICAW, I did ask that question with respect to the then-current values. The surprising answer was: "When we give an atomic weight without an indicated uncertainty, we state it to as many significant figures of decimal as possible but none more than would allow us to remain confident that the last quoted significant decimal is better than one higher or lower (by one) in that figure." Apart from inconsistencies in interpretations with literature of the

0003-2700/85/0357-511A$01.50/0
© 1985 American Chemical Society

**Table I. Table of standard atomic weights**

| Element name | 1983 value[a] | 1920 value | Element name | 1983 value[a] | 1920 value |
|---|---|---|---|---|---|
| Aluminum | 26.98154 | 27.039 | Molybdenum | 95.94 | 96.03 |
| Antimony (stibium) | 121.75(3) | 120.06 | Neodymium | 144.24(3) | 144.24 |
| Argon | 39.948 | 39.9 | Neon | 20.179 | 20.2 |
| Arsenic | 74.9216 | 74.956 | Nickel | 58.69 | 58.676 |
| Barium | 137.33 | 137.36 | Niobium | 92.9064 | 93.277 |
| Beryllium | 9.01218 | 9.093 | Nitrogen | 14.0067 | 14.008 |
| Bismuth | 208.9804 | 208.06 | Osmium | 190.2 | 191.07 |
| Boron | 10.811(5) | 10.912 | Oxygen | 15.9994(3) | 16.000 |
| Bromine | 79.904 | 79.923 | Palladium | 106.42 | 106.66 |
| Cadmium | 112.41 | 112.38 | Phosphorus | 30.97376 | 31.011 |
| Calcium | 40.078(4) | 40.090 | Platinum | 195.08(3) | 195.21 |
| Carbon | 12.011 | 12.003 | Potassium (kalium) | 39.0983 | 39.097 |
| Cerium | 140.12 | 140.21 | Praseodymium | 140.9077 | 140.88 |
| Cesium | 132.9054 | 132.81 | Rhodium | 102.9055 | 102.93 |
| Chlorine | 35.453 | 35.460 | Rubidium | 85.4678(3) | 85.434 |
| Chromium | 51.9961(6) | 52.036 | Ruthenium | 101.07(2) | 101.65 |
| Cobalt | 58.9332 | 58.956 | Samarium | 150.36(3) | 150.40 |
| Copper | 63.546(3) | 63.561 | Scandium | 44.95591 | 45.1 |
| Dysprosium | 162.50(3) | 162.5 | Selenium | 78.96(3) | 79.168 |
| Erbium | 167.26(3) | 167.6 | Silicon | 28.0855(3) | 28.255 |
| Europium | 151.96 | 152.07 | Silver | 107.8682(3) | 107.88 |
| Fluorine | 18.998403 | 19.011 | Sodium (natrium) | 22.98977 | 23.003 |
| Gadolinium | 157.25(3) | 157.01 | Strontium | 87.62 | 87.631 |
| Gallium | 69.723(4) | 70.10 | Sulfur | 32.066(6) | 32.065 |
| Germanium | 72.59(3) | 72.50 | Tantalum | 180.9479 | 181.3 |
| Gold | 196.9665 | 197.21 | Tellurium | 127.60(3) | 127.53 |
| Helium | 4.002602(2) | 4.0 | Terbium | 158.9254 | 159.20 |
| Holmium | 164.9304 | 163.4 | Thallium | 204.383 | 204.03 |
| Hydrogen | 1.00794(7) | 1.0078 | Thorium | 232.0381 | 232.19 |
| Indium | 114.82 | 114.87 | Thulium | 168.9342 | 168.5 |
| Iodine | 126.9045 | 126.93 | Tin | 118.710(7) | 118.71 |
| Iridium | 192.22(3) | 193.04 | Titanium | 47.88(3) | 48.099 |
| Iron | 55.847(3) | 55.833 | Tungsten (wolfram) | 183.85(3) | 184.10 |
| Krypton | 83.80 | 82.9 | Uranium | 238.0289 | 238.15 |
| Lanthanum | 138.9055(3) | 138.80 | Vanadium | 50.9415 | 50.947 |
| Lead | 207.2 | 207.10 | Xenon | 131.29(3) | 130.2 |
| Lithium | 6.941(2) | 6.937 | Ytterbium | 173.04(3) | 173.0 |
| Lutetium | 174.967 | 175.0 | Yttrium | 88.9059 | 89.33 |
| Magnesium | 24.305 | 24.296 | Zinc | 65.39(2) | 65.397 |
| Manganese | 54.9380 | 54.949 | Zirconium | 91.224(2) | 91.17 |
| Mercury | 200.59(3) | 200.60 | | | |

[a] Figures in parentheses indicate uncertainties in the preceding digit when the uncertainty is other than one.

time, that policy differs from good practice never to discard completely the largest uncertain significant figures. Moreover, this 1967 IUPAC policy implies an uncertainty that can vary from 0.5 in the last decimal to near zero depending on unpublished additional digits of the "best" value and—when the uncertainty is near zero—on the rules of rounding figures.

From studying the extensive recorded discussions of Clarke's methodologies in averaging the best published atomic-weight data, I conclude that he himself would not have made such sweeping claims for the accuracy of his values. However, I am sure that it would have distressed him to know of the serious errors in some of his atomic weights, such as in $A_r$(Al).

From mass doublets compared in mass spectrometers and the Einstein energy/mass equation governing nuclear reactions, we know the nuclidic masses on a self-consistent atomic scale to better than 1 in $10^7$. With very little added uncertainty, these then give us directly the atomic-weight values of the 20 mononuclidic elements: Be, F, Na, Al, P, Sc, Mn, Co, As, Y, Nb, Rh, I, Cs, Pr, Tb, Ho, Tm, Au, and Bi. We can boldly label any difference between the significant figures quoted by Clarke and current values as errors by Clarke (Table II). These are not grounds to criticize Clarke—he was one of the most careful and knowledgeable chemists of his day. However, Clarke's values on average are mistaken by 43 units in the last quoted decimal, but almost half of that is due

TRIONE
ninhydrin reagent
MODEL 121
FLUOROMETER
AUTO ZERO
POWER
EVENT
GILSON
PICKERING LABORATORIES

# "Gilson's 121 is the best fluorometer I've used."

*Mike Pickering, Pickering Laboratories, Inc.*

Mike Pickering is a leading manufacturer of high-purity reagents for fluorescence detection of amino acids. He knows his fluorometers. So when Mike started using our 121 Fluorometer, we were anxious to hear what he thought of it. This is what he had to say:

"The Gilson 121 Fluorometer is simple, inexpensive, quiet, reliable. You unpack it, plug it in and it goes. I can turn it off in the evening, and when I turn it on again the next day it is working within a few minutes.

I used to use and recommend Gilson's Spectra/glo fluorometer. The 121 is even better—easier to use and more sensitive, with superior signal-to-noise ratio.

Because of our heavy workload, we need a detector that can be serviced easily. In most detectors, the flow cells are hidden—a nightmare when you have to clean them. The 121 flow cell is accessible from the front, and we don't have to bother with optical realignment when we put it back after cleaning. Actually, the only servicing we've ever needed to perform on either of our Gilson fluorometers consisted of cleaning the flow cell and replacing the lamp.

In short, the 121 is the best fluorometer I've used."

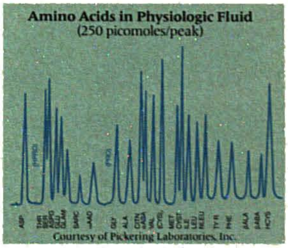
**Amino Acids in Physiologic Fluid**
(250 picomoles/peak)

Courtesy of Pickering Laboratories, Inc.

Apply your own standards to evaluating the 121 Fluorometer. Contact your local Gilson representative or call us toll-free at (800) 445-7667.

**GILSON**
INTERNATIONAL

Gilson Medical Electronics, Inc., Box 27 3000 W. Beltline, Middleton, WI 53562 USA, Tel: 608/836-1551 or 800/445-7667
Gilson Medical Electronics, (France) S.A., 72 rue Gambetta, B.P. No 45, 95400 Villiers-le-Bel, FRANCE, Tel: (3) 990.54.41, Telex: 696682

Circle 63 for literature. Circle 64 have your representative call us.

No other laboratory shaker is more accurate or provides faster results than the

# Burrell Wrist-Action® Shaker

**If you expect fast, accurate results from your laboratory shaker, there's only one shaker that duplicates true wrist-action shaking. The Burrell Wrist-Action Shaker.**

**Here's why.**

The Burrell Wrist-Action Shaker duplicates a hand mixing swirl for as long as necessary, at the speed and shaking angle you select. The swirling motion is the key . . . all the contents are in continuous motion, assuring faster, more complete mixing. The swirling motion is consistant at every speed, so you can replicate exact operations . . . every time.

**Flexible and versatile.**

Flexibility and versatility are what make the Burrell Wrist-Action Shaker so popular. We call it the Build-Up® System. With it you can add on or interchange side-arms and platforms so the capacity of your Burrell Shaker grows and changes with your needs. The Burrell Shaker can accommodate from four to twenty-four Erlenmeyer flasks, and with special clamps a Burrell platform can hold up to eight 250 ml flasks, as well as separatory funnels as large as 2000 ml.

**Who uses the Burrell Wrist-Action Shaker?**

The Burrell Shaker is working accurately in hundreds of industrial and clinical laboratories; government research departments; universities, colleges and technical schools. For more than forty years, the Burrell Shaker has been working hard in laboratories around the world. It's a proven, quality, indispensable piece of laboratory equipment.

**Get the whole story.**

We want you to know all the facts. Write or call Burrell Corporation and we'll send you our brochure describing the only true wrist-action shaker available.

BURRELL

**BURRELL** CORPORATION
SCIENTIFIC INSTRUMENTS
AND LABORATORY SUPPLIES
2223 FIFTH AVENUE, PITTSBURGH, PA 15219
Telephone 412/471-2527

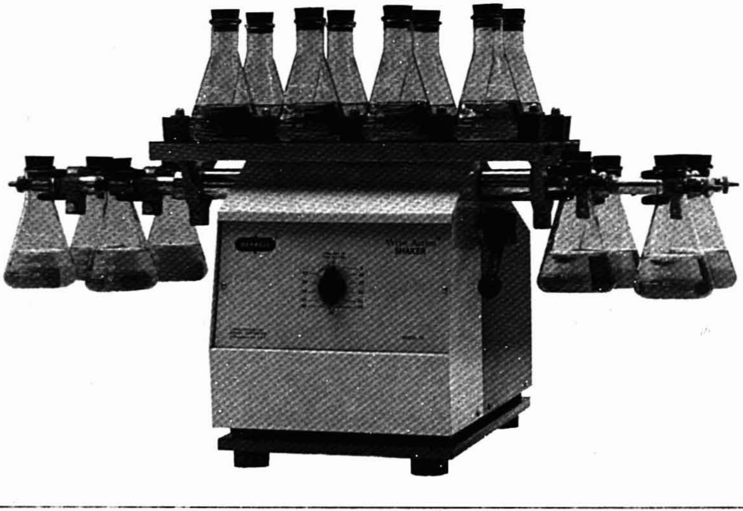

**ALL THE FEATURES OF THE BURRELL WRIST-ACTION SHAKER ADD UP TO THE MOST VERSATILE SHAKER AVAILABLE.**

CIRCLE 19 ON READER SERVICE CARD

to niobium, which Clarke himself suspected of being contaminated by tantalum. As for the current Table of Standard Atomic Weights (3), it is unlikely that even one of the mononuclidic values is in error by more than one unit in the last significant quoted figure—and all are quoted to at least six figures.

## Elements with atomic weights determined by calibrated MS

Cameron and Wichers already were fully aware of the remarkable accuracy of the atomic weights of mononuclidic elements determined by physical methods. These were indeed constants of nature, as all atomic weights were once thought to be.

The principal achievement since 1961 lies in the development of mass spectrometry. This has enabled a number of investigators to determine atomic weights of some polynuclidic elements with greatly enhanced precision by comparison with synthetic mixtures of almost pure isotopes. Of special interest here are those elements that have also been subjected to extensive mineral surveys without any appreciable credible natural variability of isotopic composition being discovered. The atomic weights of the seven qualifying elements are now confidently thought to be reliable to less than 1 part in $10^5$. These highly reliable atomic weights are compared with the 1920 and 1961 values in Table III.

**Table II. Clarke's atomic weights of elements now known to be mononuclidic**

| Element | 1920 $A_r$(E) | Error | Element | 1920 $A_r$(E) | Error |
|---|---|---|---|---|---|
| Be | 9.093 | +81 | Nb | 93.277 | +371 |
| F | 19.011 | +13 | Rh | 102.93 | + 2 |
| Na | 23.003 | +13 | I | 126.93 | + 3 |
| Al | 27.039 | +57 | Cs | 132.81 | − 10 |
| P | 31.011 | +37 | Pr | 140.88 | − 3 |
| Sc | 45.1 | + 1 | Tb | 159.20 | + 27 |
| Mn | 54.949 | +11 | Ho | 163.4 | − 15 |
| Co | 58.956 | +23 | Tm | 168.5 | − 4 |
| As | 74.956 | +34 | Au | 197.21 | + 24 |
| Y | 89.33 | +42 | Bi | 208.06 | − 92 |

Relative to one in the last given digit, the average error is 43 and the average bias is +31. Neglecting Nb, the average error becomes 25 and the average bias is +12.

**Table III. Polynuclidic elements with standard atomic weights of high precision based on calibrated mass spectrometry**

| Element | 1920 value | 1961 value | 1983 value |
|---|---|---|---|
| Si | 28.255 | 28.086(1)[a] | 28.0855(3) |
| K | 39.097 | 39.102 | 39.0983(1) |
| Cr | 52.036 | 51.996(1) | 51.9961(6) |
| Rb | 85.434 | 85.47 | 85.4678(3) |
| Ag | 107.88 | 107.870(3) | 107.8682(3) |
| Re | — | 186.2 | 186.207(1) |
| Tl | 204.03 | 204.37 | 204.383(1) |

[a] Figures in parentheses indicate uncertainties in the preceding digit.

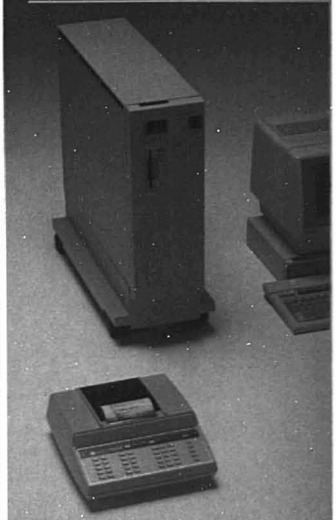

YOUR ACCESS TO EXCELLENCE
IN LAB AUTOMATION AND
INFORMATION MANAGEMENT

Minicomputer power at a workstation price.

The HP 3350X is as affordable, compact and easy to use as a workstation yet gives you real-time data acquisition from multiple instruments, data integration, instrument control and file management—all simultaneously.

It's not only multitasking but multiuser and can be upgraded with additional software, terminals, instruments, memory and computational power until you have the most powerful system available.

For more information, call your local HP Analytical representative at the HP office listed in your white pages. Or write Hewlett-Packard, Analytical Group, 1820 Embarcadero Road, Palo Alto, CA 94303.

Circle 98 for literature.
Circle 99 to have an HP Representative contact you.

HEWLETT
PACKARD

**290 B.C.**
**To cope with a need to collect information, man creates the Library at Alexandria.**

The Alexandrian Library during the Roman Empire

**Today,**
**the problem isn't how to collect information, it's how to find it.**

In ancient Egypt, an information problem was solved when the world's knowledge was organized in the Alexandrian Library.

Today, it's no longer possible to store all needed information in a single place. How do you gather the information you need from thousands of sources?

The solution is DIALOG,® the world's largest scientific and technical databank. For over a decade we've been providing online access to chemical information.

To millions of journal articles, conference papers, technical reports, and patents indexed by Chemical Abstracts Service since 1967.

Plus, over 100 additional databases covering medicine, pharmacology, energy, industry, engineering, materials, patents and trademarks. The information you need to do your job.

All available instantly, from your desktop terminal or personal computer. With no monthly minimums or initiation fees.

To learn more about this revolutionary tool for chemists, contact DIALOG Marketing, 3460 Hillview Ave., Dept. 25, Palo Alto, CA 94304. Call 800/227-1927 (800/982-5838 in Calif.).

DIALOG
INFORMATION SERVICES, INC.
A subsidiary of the Lockheed Corporation

© Dialog Information Services, Inc. 1985

**See us at ACS Conference, Booth #'s 707-709.**
CIRCLE 42 ON READER SERVICE CARD

### Effects from radioactivity and other anomalies in isotopic abundances

Unfortunately, most of the other elements with stable or quasi-stable isotopes are much more uncertain and, therefore, of greater justifiable concern to most chemists. Nuclides with half-lives greater than $4 \times 10^8$ years are called quasi-stable (*4*). Radioactive decay of these nuclides into other elements cannot cause a significant change of the atomic weight of the original element to the precision of its IUPAC tabulation in a million years. However, one has to watch the daughter elements. Because of nature's efficiency in separating elements by their properties, the radioactive daughter in the geological past is typically deposited in isolation from the parent. This daughter element is produced over geologic time in only one of its isotopes. Take the example of rubidium; the less common of its two isotopes, $^{87}$Rb, decays by the loss of a beta particle to $^{87}$Sr. Now imagine the evaporation of an ocean lagoon millions of years ago. Dissolved strontium is far less soluble than rubidium, so rubidium is concentrated in the solids of the very last evaporation process long after virtually all the strontium has been deposited. Over the eons on dry land, the rubidium now produces strontium isotope with an anomalous atomic weight. Strontium-87 that is isotopically almost pure is found only in traces as an anomaly—accorded no more than a footnote in the IUPAC table. The atomic weight of this most unusual strontium sample will be 86.91, not 87.62 as in the IUPAC table.

One cannot really be happy about this treatment of highly anomalous occurrences. After all, analysts are called upon to analyze the most unusual specimens, too; and they are apt to take the published IUPAC values for the atomic weights without a thought for the footnotes. Alternative treatments of these very unusual isotopic compositions of naturally occurring specimens seem even less desirable. For example, one surely would not favor lowering the tabulated precision of $A_r$(Sr) to 87.3(4), the (4) indicating uncertainty in the last digit. The dilemma is compounded because, as technology progresses, artificially induced anomalies in isotopic composition will become more widespread. Consequently, analysts are also facing samples with inadvertent or undisclosed changes in isotopic composition. Of course, the IUPAC table was never meant to be applicable to such altered specimens, but such samples represent a potential pitfall to analysts. Fission product palladium, if it enters the market in metallo-organic compounds, will have an atomic

In a busy laboratory, data can pile up faster than snowflakes in a blizzard. How do you organize it? How do you compile it? How do you find it weeks later when you need to formulate a report? Data base management for chromatographers is here, and only Nelson Analytical offers it to you on a desk top computer.

Think of our new data base management software as a tool to turn your microcomputer into an electronic filing cabinet for the storage, correlation and rapid retrieval of data—not only faster and easier than you do it manually, but by compiling, correlating, comparing and reporting data in a way that can only be done by powerful software.

This unique software enables you to define your own data base format, one specifically suited to your needs.

To make it as easy as possible, each format is defined by simple menu prompts so that users unfamiliar with programming can quickly master basic operations.

Call or write for the complete story on how to make your data work for you in more ways than you ever imagined possible.

10061 Bubb Road, Cupertino, CA 95014. Telephone (408) 725-1107.
East: 205 Robin Road, Paramus, NJ 07652 (201) 967-8980.

**NELSON ANALYTICAL**

# Data you can't get your hands on is like no data at all.

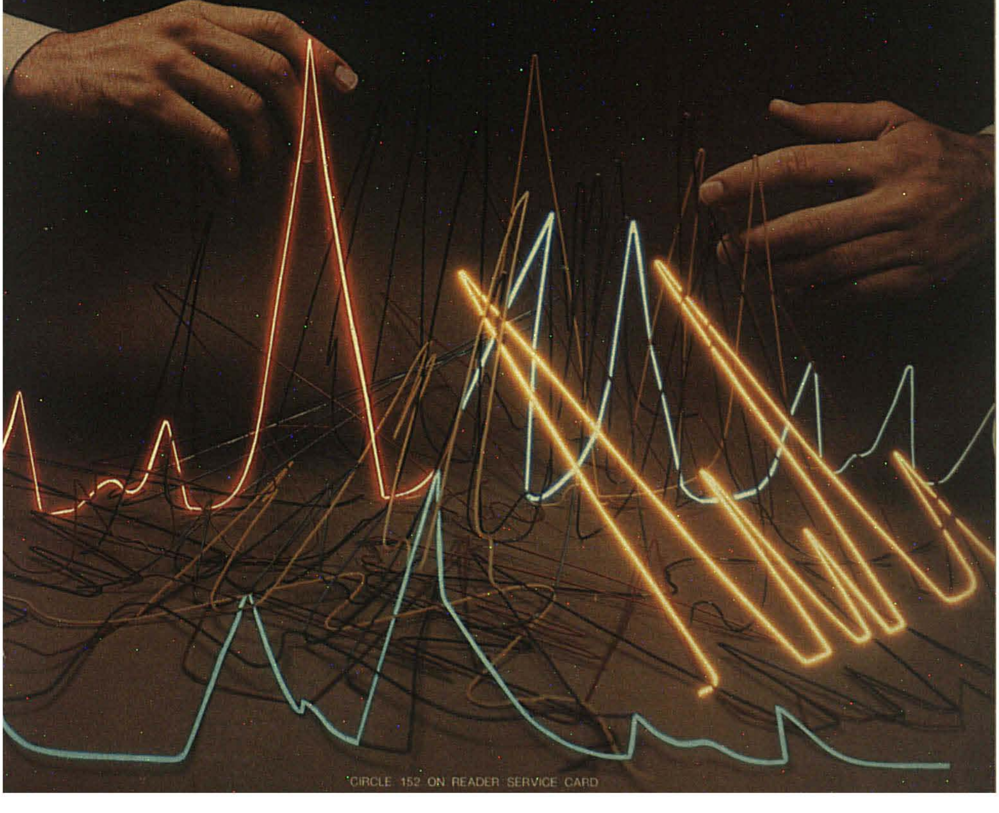

CIRCLE 152 ON READER SERVICE CARD

When You Use
ANSPEC'S Catalogs
It's Like Having . . .

CHROMATOGRAPHY
LIQUID & THIN LAYER
CHROMATOGRAPHY
ANSPEC

A Chromatography
Stockroom
On Your Shelf

☐ Columns
☐ Detectors
☐ Packings
☐ TLC Plates
☐ Solvents
☐ Tubing
☐ Fittings
☐ Pumps
☐ Valves
☐ Vials
☐ Standards
☐ Syringes

Your source for thousands of chromatography products are in Anspec's LC & TLC catalog and GC catalog.

Anspec will quickly ship the instrumentation & supplies you choose from manufacturers such as Altex, J. T. Baker, Brownlee, Hamilton, J & W, Kratos, L.D.C., S.G.E., Upchurch, Valco, Whatman...hundreds of suppliers of high quality separation products.

Contact us now for your catalogs and see for yourself all the new state-of-the-art products Anspec offers to make your work in chromatography easier than ever.

CALL TOLL FREE:
800-521-1720
800-482-3452 in Michigan
800-237-1017 in Canada

ANSPEC
company, inc.
P. O. Box 7730 ☐ Ann Arbor, MI 48107

CIRCLE 1 ON READER SERVICE CARD

weight of 105.90, instead of the tabulated 106.42. Lithium depleted of $^{6}$Li and therefore with an unduly high atomic weight is already in wide circulation commercially. Electrolytic hydrogen that is significantly depleted of deuterium is a common laboratory source of hydrogen.

### Elements with variable isotopic composition in common sources

Thus, the example of $^{87}$Sr points out one of the greatest problems of establishing standard atomic weights: All, except the mononuclidic elements, can have variable atomic weights because of natural differences in isotopic abundances. At current precisions and for most elements, this is not a serious problem. The very close similarity of properties of an element's isotopes keeps the composition almost constant over virtually all natural actions and synthetic reactions that commonly affect the elements. Uncertainties in the experimental determination of the absolute atomic-weight values tend to overshadow the differences due to range, but the most precise mass spectrometric measurements can detect the smaller differences. Such studies already have fascinating applications to cosmology, geology, biology, archeology, physical chemistry, and industrial technologies. They do not yet limit the precision with which most atomic weights are tabulated. Perhaps in another 40 years, if a REPORT of similar title is published in ANALYTICAL CHEMISTRY, more precisely tabulated standard atomic weights may have to be qualified by more widespread significant variability, some of which may await discovery from as yet inaccessible portions of the Earth's crust.

For the time being, it is possible for IUPAC to adhere to the principle that the standard atomic weights apply to all "normal" terrestrial sources of the elements and their compounds. Admittedly, 11 elements—H, He, Li, B, C, O, Si, S, Ar, Cu, and Pb—have tabulated standard atomic weights that could have been given one more significant figure (with an uncertainty of no more than nine), if it were not for such natural variability from normal sources. With an experimental measurement, the individual atomic weight of a sample can be more accurately determined than the natural range of atomic weights permits for the tabulated standard atomic weight in the IUPAC table. This measurement capability, generally derived from mass spectrometry, can be useful in overcoming the shortcomings of the IUPAC tables. For these elements, when a more precise value of the atomic weight of a sample is required than that offered by the IUPAC table, one can either measure it one's self or have it measured. For this measurement, it is helpful to use generally available standard reference materials of known isotopic composition, which result in the most accurate absolute atomic-weight determinations.

Thus, the standard atomic weights of these 11 elements cannot be tabulated nearly as precisely as those of the mononuclidics. No improvement in experimental measurements could increase appreciably the precision of the tabulated value of one of these 11 elements. A change could result only from a change in convention or in definition of the tabulated IUPAC standard atomic weights. Unlike the group of mononuclidic elements, this group of 11 is sure to grow as experimental accuracies and knowledge of isotopic compositional variability improve. Only occasionally an element might also drop out of the group of 11 elements when previously believed variability in nature is proved to be illusionary.

As mentioned above, CAWIA now allows the last tabulated standard atomic-weight figure to be uncertain to any single digit integer combining the natural variability and experimental uncertainty of published information evaluated by CAWIA. It spares no effort in trying to provide all reliable precision in atomic-weight values but, if in doubt, tends to be conservative and avoids unnecessarily frequent changes. The commission criteria of reliability might be expressed as follows:

- It is unlikely that any known normal natural source of an element will be found to have an atomic weight outside the range indicated in the IUPAC table. (My personal interpretation of "unlikely" is less than 1 in 100.)

# VG covers the elemental range.

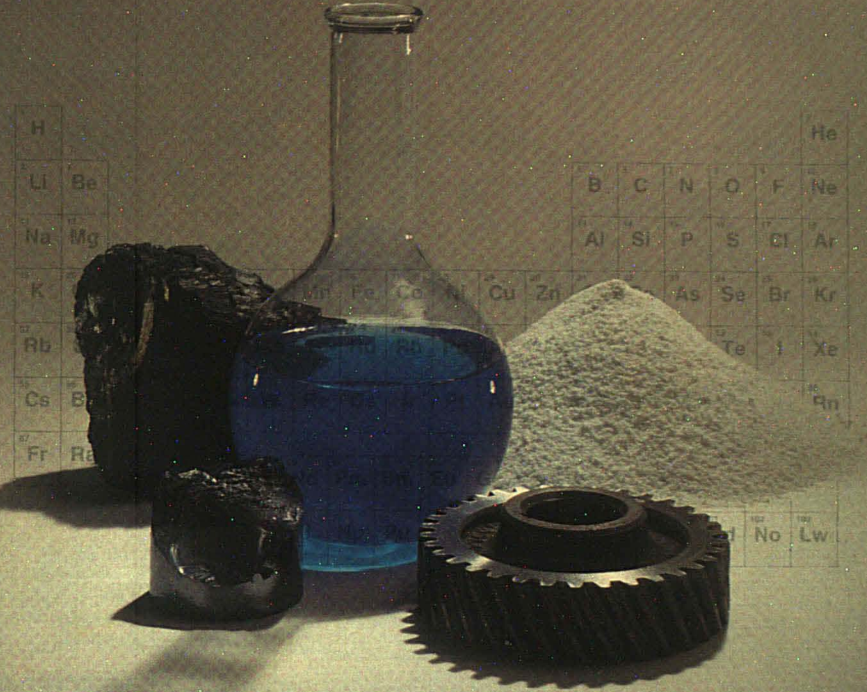

Whatever your elemental analysis requirements or problems, a VG instrument can help. VG covers the elemental range from hydrogen to uranium, regardless of sample form—liquid, solid, powder or gas—with two broad-ranging analytical techniques.

The VG PlasmaQuad ICP-MS system allows liquid samples to be processed quickly and analyzed at sub-PPB levels. With its multielement capability, the PlasmaQuad performs comprehensive, direct routine analysis simply and efficiently. Elements can be measured at major, minor, trace and ultratrace levels because of the wide dynamic range and low detection limits.

The VG 9000 Glow Discharge Mass Spectrometer provides for fast, sensitive and direct elemental analysis of solid samples. The simple spectra and highly stable ion beams ensure that accurate and consistent results are always obtained. Glow Discharge mass spectrometry is a powerful new technique with a dynamic concentration range of eight orders and limits of detection at the PPB level directly in the materials being analyzed.

For all your elemental analysis needs—when simple operation, fast throughput, direct data and high performance are priorities—VG covers the elemental range. For more information on how VG covers the elemental range, call VG or circle the reader service number.

**VG INSTRUMENTS**

VG Instruments, Inc.
300 Broad Street
Stamford, CT 06901
(203) 322-4546

Mass Spectrometers
Gas Analysis MS
Isotope Ratio MS
LC-MS • MBE • ICP-MS
Ion Beam Lithography

CIRCLE 223 ON READER SERVICE CARD

NO CHARGE?

no problem for Zetasizer II

In studies of flocculation and colloid stability, the region close to the zero point of charge is the most critical. It is in precisely this region of low mobility that other electrophoresis systems are least accurate and most difficult to use.

With its high frequency optical modulator, the Malvern Zetasizer II solves this problem, allowing you to measure mobility and zeta potential with uncompromising accuracy right across the range.

Measurements are simple, fast and operator-independent and Zetasizer II also gives you built-in submicron particle size capability.

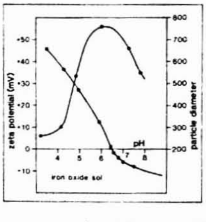

Learn more about the potential of Zetasizer II in your laboratory.

MALVERN

Malvern Instruments Inc
187 Oaks Road
Framingham
MA 01701, USA
Telephone: (617) 626 0200
Telex: 311397

CIRCLE 137 ON READER SERVICE CARD

- It is exceedingly unlikely that any randomly selected shelf sample, mineral specimen, or industrial product will have an atomic weight outside the range indicated in the IUPAC table. (My personal interpretation of "exceedingly unlikely" is less than 1 in 100,000.)

When we talk of accuracies, we refer to the difference between a measured and a "true" value. The concept of a "true" atomic weight becomes diffuse for elements with variable composition. You never know whether you have found specimens exhibiting the maximum as well as the minimum of an atomic weight range. You also wonder whether you should average the known extremes for the standard value or look for the most probable value relative to laboratory samples, or for the most widely distributed natural sources. The problems are real, for instance, for hydrogen. Hydrogen atoms on the average are lightest in the laboratory, heavier in river water, and still heavier in ocean water, which should not be allowed to weight the average. In other cases, you probably would wish to take an average for the entire Earth. Given that we cannot sample the core, the uncertainty for the overall average would become far greater than if we sought to average over all reasonably deliverable specimens. Such considerations spoil the notion of a "true" atomic weight for polynuclidic elements.

### Atomic-weight limitations from experimental uncertainties

Most annoying is the estimated uncertainty in standard atomic weights that is not caused by natural variability but by experimental uncertainty so large that it equals or overshadows the uncertainty of good chemical analytical measurements. These cases, in which the atomic-weight data limit the analytical accuracy, are shown in Table IV. Standard reference materials cannot help, and it is surprising that so little has been done to improve our knowledge. The common belief is that the IUPAC values are better than they are said to be, and chemists appear to rely on them blindly. During the five years that I was secretary of the commission, I became aware of only one challenge of a standard atomic weight (that of tin), and the basis for that challenge was questionable and has since, in the light of much more reliable measurements, been found to have been erroneous. However, there is in my view plenty of opportunity to question CAWIA and for young experimenters to generate new or better data, especially for the elements in Table IV.

In this discussion, the critical question for these 21 elements is this: Are the uncertainties of their atomic weights really as large as indicated in Table IV? Perhaps CAWIA underestimates, as Clarke did earlier, experimental errors or faces future evidence of larger natural variabilities in as yet undiscovered sources. Or perhaps CAWIA is playing it safe by overestimating the uncertainties and ranges to keep the reliability of tabulated data inviolate.

My own impression is that CAWIA

**Table IV. Elements whose standard atomic weights are estimated to be uncertain by 0.015% or more arising from experimental uncertainty**

| Element | Uncertainty |
|---|---|
| Ti | 0.063% |
| Ni | 0.017% |
| Zn | 0.031% |
| Ge | 0.041% |
| Se | 0.038% |
| Ru | 0.020% |
| Sb | 0.025% |
| Te | 0.024% |
| Xe | 0.023% |
| Nd | 0.021% |
| Sm | 0.020% |
| Gd | 0.019% |
| Dy | 0.018% |
| Er | 0.018% |
| Yb | 0.017% |
| Hf | 0.017% |
| W | 0.016% |
| Os | 0.053% |
| Ir | 0.016% |
| Pt | 0.015% |
| Hg | 0.015% |

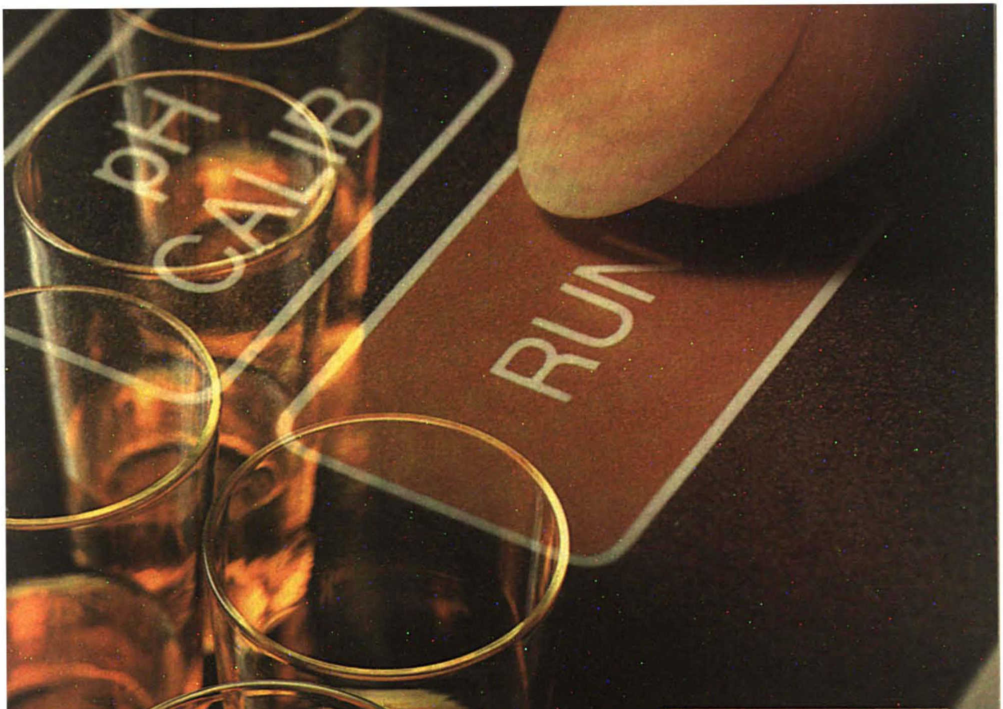

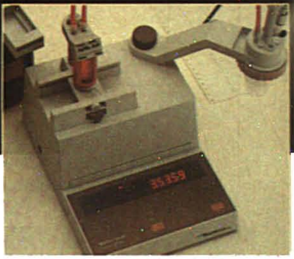

The new Mettler DL20 CompactTitrator...$4,950 complete.

### No more manual and recording titrations...

# Mettler's new DL20 titrator gets down to specifics

Designed for efficient routine analysis, the DL20 permits exact repetition of specific titrations with speed, accuracy and reliability—even after a change in operating personnel.

***Practical***

From simple acid/base to more difficult TAN/TBN in oil determinations, the DL20 CompactTitrator performs according to your specified titration method at the touch of a button. Quick sample change, rapid rinsing of the titration head, easy push-button operation and short titration time assure high productivity.

Mettler's rugged DL20 is extremely compact. It can be set up anywhere—in research or quality control labs—even out in the production area.

***Precise and economical***

Mettler burettes can dispense even the smallest increments precisely. Reproducible results are achieved with very small sample quantities and reagents can be used sparingly. With a price of $4,950, the DL20 is a good investment.

For more information on the new DL20 CompactTitrator, the DL40RC all-purpose and DL18 Karl Fischer titrators, contact Mettler today. Mettler Instrument Corporation, Box 71, Hightstown, NJ 08520. Phone (609) 448-3000.

CIRCLE 140 ON READER SERVICE CARD

***Limited Introductory TRADE-IN OFFER***

**Mettler gives you up to $500 off of the DL20 for:**

- **Autoburettes**
- **Endpoint titrators**
- **Recording titrators**

**Ask for details.**

Mettler

has recently steered well between Scylla and Charybdis, so that an overall condemnation cannot be leveled that it has either withheld reliable atomic-weight data or betrayed the chemists' trust in the reliability of the data. Anyone making a critical judgment probably needs to analyze data for one element at a time, and for that the evidence will typically be scant. It is conceivable that CAWIA may have to correct one or even several standard atomic weights beyond the presently indicated uncertainty range. This is not likely, and I hope that it will never happen. Corrections by small shifts or even extensions of the ranges for some standard atomic weights must be expected. Such a possibility already exists for palladium, a major natural source of which seems to have an anomalous atomic weight, which is under active investigation. Palladium might then join the group of 11 elements whose variability in nature prevents the tabulation of the full number of significant figures justified by experimental accuracy. This is typical of the trend to be expected in the years ahead. With existing conventions for the IUPAC Table of Standard Atomic Weights, the implied uncertainties are likely to decrease appreciably only for the elements in Table IV.

## Conclusion

Summing up then, I believe the values in the Table of Standard Atomic Weights—as long as they are applied only to materials for which they are intended—are at least as good as the precision of their entries implies. The most precise atomic weights may be somewhat better than they imply, but the worst of these values are no better than is indicated. This is not quite good enough for the best chemical analyses, which for more and more elements can be improved by determining the sample atomic weight.

## Acknowledgment

The privilege of working with colleagues on the IUPAC Commission on Atomic Weights has been a richly rewarding experience. I acknowledge my debt to all. For the preparation of this REPORT, I particularly thank I. L. Barnes, T. J. Murphy, and M. Shima. The late E. Wichers chaired the commission with great distinction during the early years of my membership when several ideas presented here gained acceptance.

## References

(1) Wichers, E. *Anal. Chem.* **1963,** *35,* 23 A.
(2) Cameron, A. E.; Wichers, E. *J. Am. Chem. Soc.* **1962,** *84,* 4175.
(3) Holden, N. E.; Martin, R. L. *Pure Appl. Chem.* **1984,** *56,* 653.
(4) Peiser, H. S. et al. *Pure Appl. Chem.* **1984,** *56,* 695.
(5) Clarke, F. W. *Memoirs of the Natl. Acad. Sci.* **1920,** *16,* Pt. 5, 5.

*H. Steffen Peiser received his chemical education at Cambridge University in England. His research in X-ray crystallography brought him to the National Bureau of Standards (NBS) in 1957, where he specialized in metrology—the practice of making measurements to the highest attainable accuracy. Now retired, he looks back with pleasure at NBS contributions in designing analytical balances and in assessing the reliability of the atomic weights.*

**Finally!**
**Routine In-Plant**
**THERMAL ANALYSIS Instrumentation**
**and Back-up Service**
**at a Low Cost.**

Basic
Model
$9,500.00
cell not included

INSTRUMENTATION

The Q.C. 25 Controller and Programmer for DSC, TGA or TMA Analysis features —

- Low cost DSC with one pen X, Y recorder and cell for $15,000.00
- Easy to use push button controls
- Linearized output and digital readout of sample temperature
- Failsafe temperature protection eliminating accidental furnace overheating
- Also available with the following options: Program Cool, Automatic Gas Switching, Step Programming and Rapid Return to Start

Prices subject to change without notice.

SERVICE

In addition to servicing the Q.C. 25 System, our service group has eight years of experience in servicing, repairing and training on DuPont 990 and 900 systems and maintains a full complement of parts and supplies for on site repairs. We also offer a comprehensive service contract designed to suit the customer's needs for preventative maintenance and/or emergency service.

OMNITHERM CORPORATION
48 EAST UNIVERSITY DRIVE • ARLINGTON HEIGHTS, IL 60004 • (312) 870-7006

CIRCLE 156 ON READER SERVICE CARD

# Buy a Waters™ Ion Chromatograph, and get more than just an instrument.

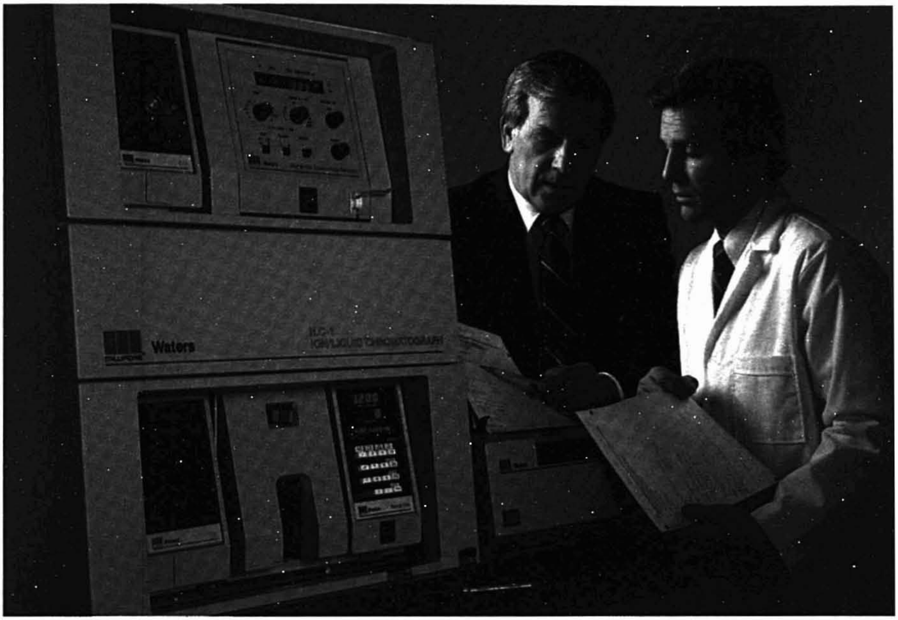

© 1984 Millipore Corporation

In-depth applications development...responsive customer support and service...20 years of chromatography expertise. The same qualities that established our world leadership in HPLC are a part of every Waters ILC Series Ion/Liquid Chromatograph.

The result of our commitment is advanced Ion Chromatography capabilities. Now you can change selectivity without switching columns—just by changing eluents. Routinely quantitate ions at sub-ppb levels. Analyze a wider range of ions without added system complexity (no expensive post-column chemistries required).

Our worldwide support network includes a dedicated group of ion chromatographers and over 300 technical, sales and field service personnel. Together, they have provided answers for a broad spectrum of application problems.

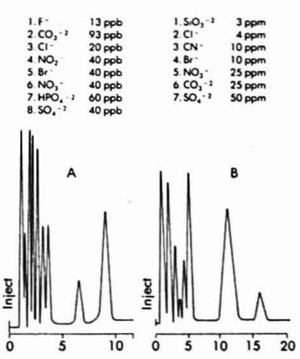

*Eight* anions determined at low ppb levels (A); by simply changing eluents on the same column, you can also determine *silicate* and *cyanide* (B).

To learn more about how Waters Ion Chromatography expertise can go to work for you, please call the Ion Chromatography Hotline at (617) 478-2000, ext. 2500. In Canada, call 1-800-268-4881. Or write to the Ion Chromatography Group, Millipore Corporation, Waters Chromatography Division, 34 Maple Street, Milford, MA 01757.

**MILLIPORE**
Waters Chromatography Division

CIRCLE 232 ON READER SERVICE CARD

ACS Meeting

# FREE ONLINE INFORMATION WORKSHOP

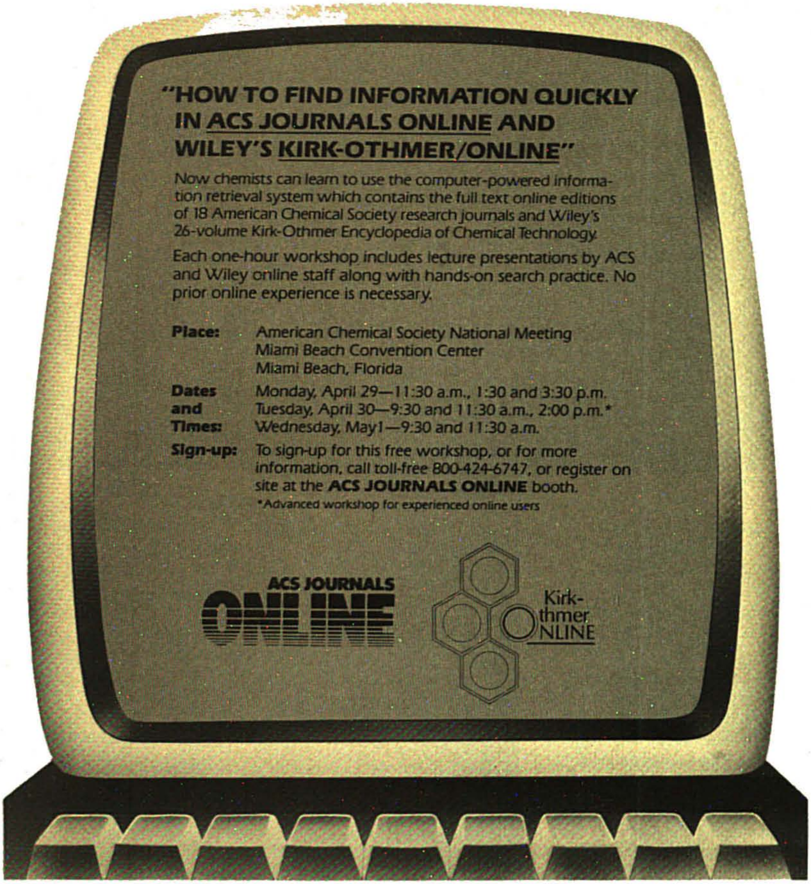

## "HOW TO FIND INFORMATION QUICKLY IN ACS JOURNALS ONLINE AND WILEY'S KIRK-OTHMER/ONLINE"

Now chemists can learn to use the computer-powered information retrieval system which contains the full text online editions of 18 American Chemical Society research journals and Wiley's 26-volume Kirk-Othmer Encyclopedia of Chemical Technology.

Each one-hour workshop includes lecture presentations by ACS and Wiley online staff along with hands-on search practice. No prior online experience is necessary.

**Place:** American Chemical Society National Meeting
Miami Beach Convention Center
Miami Beach, Florida

**Dates and Times:** Monday, April 29—11:30 a.m., 1:30 and 3:30 p.m.
Tuesday, April 30—9:30 and 11:30 a.m., 2:00 p.m.*
Wednesday, May1—9:30 and 11:30 a.m.

**Sign-up:** To sign-up for this free workshop, or for more information, call toll-free 800-424-6747, or register on site at the **ACS JOURNALS ONLINE** booth.

*Advanced workshop for experienced online users

ACS JOURNALS ONLINE

Kirk-Othmer ONLINE

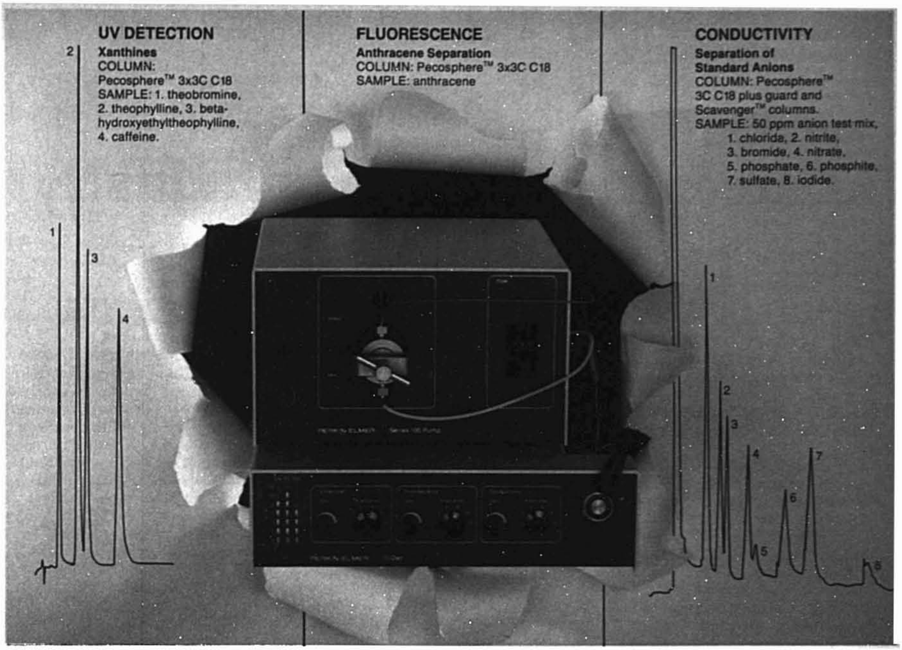
UV DETECTION
Xanthines
COLUMN:
Pecosphere™ 3x3C C18
SAMPLE: 1. theobromine, 2. theophylline, 3. beta-hydroxyethyltheophylline, 4. caffeine.
FLUORESCENCE
Anthracene Separation
COLUMN: Pecosphere™ 3x3C C18
SAMPLE: anthracene
CONDUCTIVITY
Separation of Standard Anions
COLUMN: Pecosphere™ 3C C18 plus guard and Scavenger™ columns.
SAMPLE: 50 ppm anion test mix, 1. chloride, 2. nitrite, 3. bromide, 4. nitrate, 5. phosphate, 6. phosphite, 7. sulfate, 8. iodide.
1
2
3
4
1
2
3
4
5
6
7
8
PERKIN-ELMER Series 100 Pump
PERKIN-ELMER TriDet

# For less than $5,500, our new 3D™ HPLC System is an amazing breakthrough in LC technology.

**Only from Perkin-Elmer**

A complete HPLC System—the Series 100 pump, 7010 injector, a P-E 3x3 C18 cartridge column, R-50 recorder and the new TriDet™ trifunctional detector—all for the amazingly low price of $5,460.* The 3D HPLC System is an excellent tool for teaching, quality control, screening—for any laboratory where quality technology is required on a limited budget.

**3 detectors in one**

The central focus of the new 3D HPLC System is the patented** trifunctional TriDet detector. UV, Fluorescence and Ion Conductivity detection are all built into a single compact unit. For multiple, simultaneous detection, or to have three of the most often used LC detection modes at your fingertips, the flexibility of the 3D HPLC System can't be beat. Even if your only application is Ion Chromatography or if you only require the UV function, the 3D HPLC System is still a great value.

**It's very easy to use**

The 3D HPLC System is a joy to operate. As the workhorse in a quality control lab, the mainstay of a therapeutic drug monitoring lab, or the first LC in a college chemistry lab, the 3D HPLC System sets up easily, and runs reliably, day after day.

For complete information on this highly economical new system, talk to your Perkin-Elmer representative. Or, for literature, please call 1-800-762-4000.

* F.O.B. Norwalk, CT, USA
** Patent Pending

Perkin-Elmer Corp., Main Ave. (MS-12),
Norwalk, CT 06856 U.S.A.
Tel. (203) 762-1000. Telex 965-954.

Bodenseewerk Perkin-Elmer & Co., GmbH,
Postfach 1120, 7770 Ueberlingen,
Federal Republic of Germany. Tel: (07551) 811.

Perkin-Elmer Ltd., Post Office Lane,
Beaconsfield, Bucks HP9 1QA, England.
Tel: Beaconsfield (049 46) 6161.

PERKIN-ELMER

The science and computer company.
Where solutions come first.

CIRCLE 166 ON READER SERVICE CARD

# A Career in Academia or Industry?

*A recent spate of negative tenure decisions has chemists discussing some of the trade-offs*

The trickle of analytical chemists changing careers in midstream seems to have increased lately. And the flow has been primarily in one direction—from academia to industry and government.

Many of these recent career changes stem from an unusually high number of negative tenure decisions for assistant professors of analytical chemistry. According to Henry Blount, program director for chemical analysis at the National Science Foundation, there were about 10 negative tenure decisions for analytical chemists in U.S. colleges and universities last year.

Because a majority of these negative tenure decisions involved people who entered academic careers without the usual one or two years of postdoctoral research, observers are pointing to this lack of experience as an important causative factor in many of the tenure denials. In recent years, it has become common for analytical chemistry PhDs to leave graduate school and take up academic posts immediately, but it is still very uncommon for PhDs in other fields of chemistry to accept academic posts without several years of postdoctoral work.

"It is not that people without postdoctoral experience know less about their specialties," explains Blount, "but they lack the maturation normally gained in the postdoctoral experience—what I call street smarts. They know the technical material, but they don't necessarily know how to write a grant proposal, how to write a paper, or how to respond in a variety of situations."

Gary Hieftje, professor of analytical chemistry at Indiana University, agrees with Blount that young assistant professors without postdoctoral experience are at a substantial disadvantage. "It might seem like an advantage," says Hieftje, "because you get to start on your career earlier. But you won't have time to sit back and decide what you're going to write your first few grant proposals on, and that slower start can mean the death knell when a tenure decision comes along."

Some say that department chairmen frequently expect the "wrong things" from the analytical chemists they hire and eventually become disappointed with them. "I think, in part, it's the old snobbery of pure chemistry vs. applied chemistry," says Michael Parsons of Los Alamos National Laboratory. "The organic and physical chemists who run most of the chemistry departments in this country think that the analytical chemists are doing applied research, and they don't think that's pure research. They seem to feel that analytical [chemistry] is not a viable area. But that is not borne out by the job market or by the vigorous interest of the students." Parsons himself recently switched to Los Alamos from academia, though a negative tenure decision was not involved here; Parsons had been at Arizona State University for 17 years and left with the title of full professor.

According to an analytical chemist who declined to be identified, generous funding levels for analytical chemistry research in the past few years and the attraction of graduate students into the field in large numbers have tended to engender something akin to jealousy on the part of non-analytical-chemistry professors. "I think that other people in chemistry are now less likely to go easy on analytical chemists," he said. "What that means is that people who go into academia directly from graduate school are placed at a major disadvantage."

Unfortunately, low postdoctoral salaries tend to deter graduating PhD chemists from seeking postdoctoral appointments and, hence, from seeking academic careers in general. "I think we should pay our postdocs a decent wage," says NSF's Henry Blount. "It is an absolute affront to pay a postdoc $13,000 a year. If that's the group from which our universities are drawing their faculty, then they're going to get the cream of that group, which isn't going to be very strong, with a few exceptions—people who really have a Calvinistic bent.

"Unless a person receiving his degree is committed to an academic pursuit," he continues, "or there is a specific person he wants to work with, or there is a new area he wants to learn at that time, he will likely take the industrial job offer rather than the postdoctoral position, the reasons being primarily financial reward and long-term security." According to Blount, the difference in salary between a postdoctoral position and a starting job in industry is "a factor of two minimum, and in some cases a factor of three."

Not only for postdoctoral work, but for full-time academic appointments as well, salary seems to have become an increasingly negative factor. According to Blount, a new hire at one of the top three or four U.S. institutions in chemistry can expect to earn about $30,000 in a nine-month academic year. "You look at an average," says Blount, "and you see starting salaries of 25, 26, or 27 thousand dollars for nine months, with no guarantee of summer salary. And if you look at what industry offers you with the total benefit package, you'll probably see a factor of 1.8 over the academic starting salary."

0003-2700/85/0357-526A$01.50/0
© 1985 American Chemical Society

Here's the new GC detector you've been waiting for.

It will give you positive identification faster than any mass spec detector on the market.

It will put itself to work immediately in your laboratory. You don't need to be a mass spectrometrist to use it.

It will give you high sensitivity, day in and day out.

It will work with any GC of your choice.

And it will do all this for half the cost of a competitive unit.

The Finnigan MAT Ion Trap Detector™ (ITD™).

Call or write us about the fastest, easiest to use, and lowest priced mass spec detector on the market today.

355 River Oaks Parkway, San Jose, CA 95134, USA (408) 946-4848.
Postfach 14 40 62, D-2800 Bremen 14, FRG (0421) 54-93-0.
Paradise, Hemel Hempstead, Herts HP2 4TG, UK (0442) 4 04 91.

Finnigan MAT

Circle 65 for literature. Circle 66 to have a representative contact you.

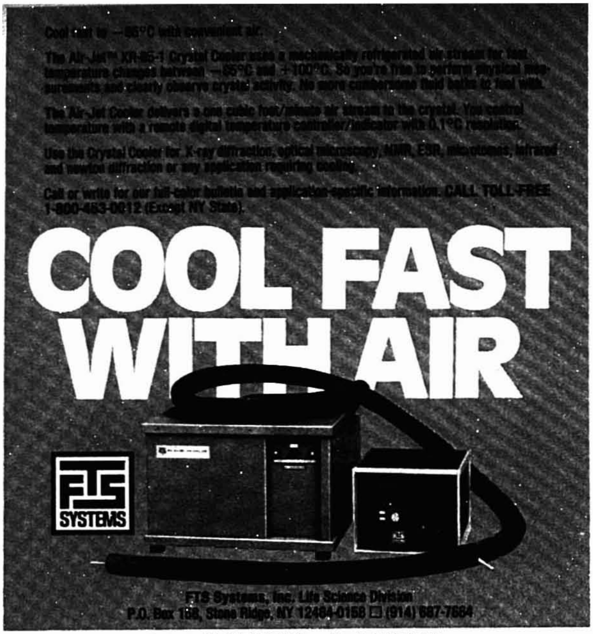

Cool fast to −85°C with convenient air.

The Air-Jet™ XR-85-1 Crystal Cooler uses a mechanically refrigerated air stream for fast temperature changes between −85°C and +100°C. So you're free to perform physical measurements and clearly observe crystal activity. No more cumbersome fluid baths to fuss with.

The Air-Jet Cooler delivers a one cubic foot/minute air stream to the crystal. You control temperature with a remote digital temperature controller/indicator with 0.1°C resolution.

Use the Crystal Cooler for X-ray diffraction, optical microscopy, NMR, ESR, microtomes, infrared and neutron diffraction or any application requiring cooling.

Call or write for our full-color bulletin and application-specific information. CALL TOLL-FREE 1-800-453-0012 (Except NY State).

COOL FAST WITH AIR

FTS SYSTEMS

FTS Systems, Inc. Life Science Division
P.O. Box 158, Stone Ridge, NY 12484-0158 ☐ (914) 687-7664

**See us at FASEB/ASBC — Booth 3303/3305**
CIRCLE 57 ON READER SERVICE CARD

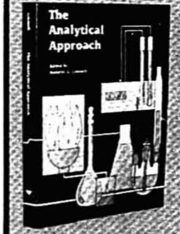

**The Analytical Approach**

**Jeanette G. Grasselli**, *Editor*

**Brings together 52 papers from *The Analytical Approach* column in ANALYTICAL CHEMISTRY. Provides unique approaches to analytical science and focuses on real-world problems. Discusses topical and interesting subjects such as the analysis of the JFK assassination bullets, Mt. St. Helens ash, flavor changes in food, and failure mechanisms in spacecraft parts. Written in a "popular" style yet is highly informative. Will serve as a teaching aid in higher education or as a guide in corporate training programs on analytical capabilities.**

**CONTENTS**

Sections include:
- Production Processes
- Products
- Environmental
- Toxicity
- Forensic
- Miscellaneous

240 pages (1983) Clothbound
LC 82-22618 ISBN 0-8412-0753-4
US & Canada $29.95 Export $35.95

240 pages (1983) Paper
LC 83-22618 ISBN 0-8412-0775-0
US & Canada $19.95 Export $23.95

**Order from:**
**American Chemical Society**
**Distribution Office — 50**
**1155 Sixteenth St., N.W.**
**Washington, DC 20036**
**or CALL TOLL FREE 800-424-6747**
**and use your credit card.**

Michael Parsons offers another startling statistic: In his 17 years at Arizona State, all but two of his PhD students who went into industry started out at a higher salary than Parsons was earning at the time.

Although the salary differential is an important factor in deciding between academia and industry, many contend that it is not the principal one. Gary Hieftje agrees with Blount that the ratio of industrial to academic starting salaries is about 1.8, but he contends that academic and industrial salaries are nearly equal after about 10 years of employment and that the salaries of senior academic researchers often exceed what they could have earned in industry. Therefore, Hieftje insists, salary is not the most important factor discouraging people from pursuing academic careers.

Another negative for those considering a career in academia is the prospect of fighting for grants. Obtaining grants simply requires more effort and more applications than it used to, and "grantsmanship" is at the heart of academic success. "If you don't have grants, you don't have the resources to perform your research, and if you don't have the resources, you don't do well," says Hieftje.

"Most universities can't fund research at the same level they used to," Hieftje adds, "because state educational funding is shrinking. Therefore, the academic researcher has to go out and scratch out funds where he can. In industry, if you do your job well and address appropriate problems, the resources are more readily obtained."

According to Henry Blount, an academic chemist "is expected to raise money, recruit graduate students, teach effectively at the undergraduate and graduate levels, publish papers, and, in his spare time, serve on a few committees. If you're trying to raise a family, you're going to have to scramble to raise money in the summer also; otherwise that $27,000 is going to be spread over 12 months, not nine. If you get all this together and things are going well at the university, they may tenure you in five years, and if not, you're on the bricks, pal. Now that's not a very inviting thing to look forward to for an analytical chemist in the job market for the first time, especially in light of the recent spate of negative tenure decisions.

"As a community," Blount continues, "we need to think seriously about ways to teach young analytical chemists the nontechnical skills that are essential to success in academia. These skills can be taught either through the traditional postdoctoral route or

# The Nonsuppressed Ion Chromatography System that adapts to *your* Ion Chromatography Application

Ion Chromatography has until now been possible only with extremely complex and expensive instrumentation. LDC/Milton Roy has developed the Series III Ion Chromatography System to provide the necessary sensitivity and reliability in a simple, economical system.

In addition, the Series III Ion Chromatography System is fully adaptable so you are never limited in the types of ion analyses you may wish to perform.

Through state-of-the-art conductivity detection, positive temperature control of the flow cell, and virtually pulseless flow, parts-per-billion sensitivity for common anions and cations is finally a reality.

Call LDC/Milton Roy today for more information on the new Series III Ion Chromatography System.

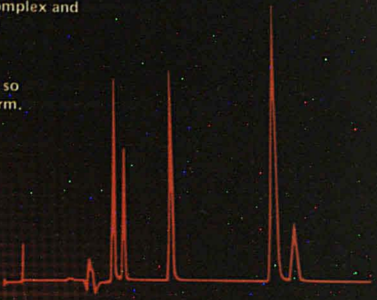

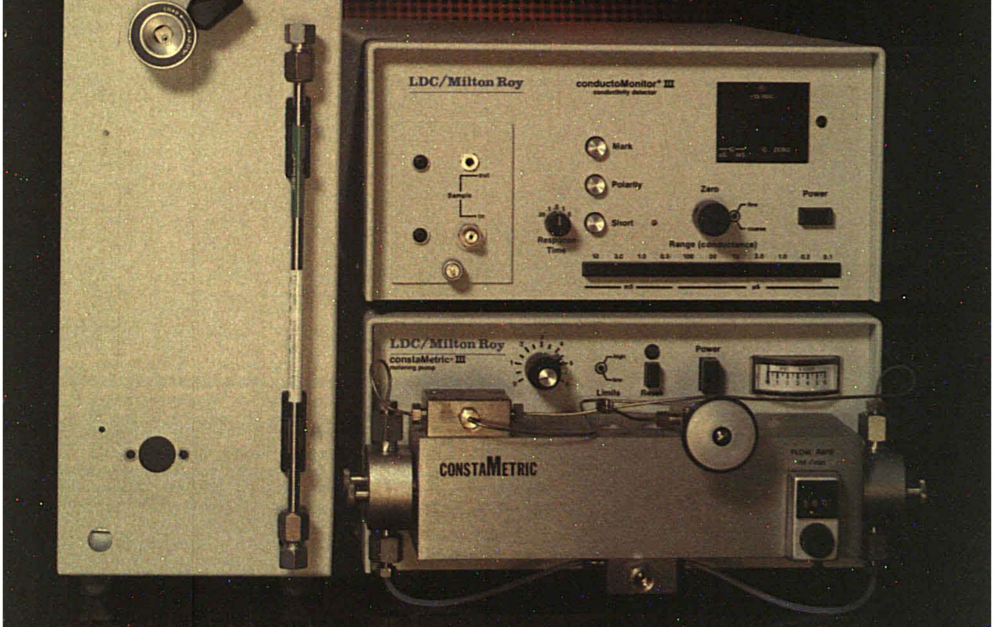

**LDC/Milton Roy**

**U.S. HEADQUARTERS,** P.O. Box 10235, Riviera Beach, FL 33404 Toll-free: 800-327-6182, In Florida: (305) 844-5241 Telex: 441098
**UNITED KINGDOM,** LDC UK, Milton Roy House, 52 High Street, Stone, Staffordshire ST15 8AR England Telephone: (0) 785-81-3542 Telex: 36623
**FRANCE,** LDC S.A., 15 rue Guyton de Morveau, Paris 75013, France Telephone: 588-2800 Telex: 205331
**WEST GERMANY,** Milton Roy (Deutschland) GMBH Jahnstrasse 22-24 6467 Hasselroth 2, West Germany Telephone: (0) 6055-3366 (2031) Telex: 4184357
**JAPAN,** Milton Roy K.K., Takanawa Dai-Ichi Building 21-41, Takanawa 2-Chome, Minato-Ku, Tokyo 108, Japan Telephone: (03) 473-3181 Telex: 242-4296

CIRCLE 131 ON READER SERVICE CARD

**Here's a fast, simple way to measure Molecular Weight**

**and**

**QC solutions and reagents, Measure Concentration of LC fractions.**

The new Wide Range CRYETTE™ from Precision Systems can be a useful, economical addition to almost any laboratory. With it you can measure freezing point of aqueous solutions — or now *any solutions with solvents having freezing points from −6 to +22°C.* Fast, accurate, reliable, the CRYETTE measures freezing point to 0.001°C at the rate of about one minute per determination.

Freezing point depression data gives you a precise determination of concentration and average molecular weight to 1% or better. With the Wide Range CRYETTE you also can get a handy check of solution and reagent quality. And . . . you will probably find it useful to check fractions without chromophores coming off an LC column.

If you haven't discovered how useful an automatic cryoscope can be, now is the time to call or write Precision Systems for complete information.

PRECISION SYSTEMS, INC.

60 Union Avenue, Sudbury, Mass. 01776 U.S.A.
Telephone: 617-443-8912

CIRCLE 168 ON READER SERVICE CARD

NEWS from the

**KRATOS HPLC APPLICATION LAB**

Ask for any of these FREE HPLC Lab Reports:

**INDOMETHACIN IN SERUM**

**CARBOHYDRATES**

Ask for details on this or other pioneering HPLC Applications from Kratos

*Call or Write:*

KRATOS ANALYTICAL
a division of SPECTROS

170 Williams Drive • Ramsey, N.J. 07446
Telephone: 201/934-9000 • Telex: 6853505

CIRCLE 121 ON READER SERVICE CARD

through other means, such as graduate courses on the professional aspects of chemistry."

Nevertheless, young people *do* continue to look forward to careers in teaching, an indication that the academic life offers many countervailing benefits and rewards. "I agree there would be a decrease in salary," admits one analytical chemist in government who is currently interviewing for an academic position and who requested anonymity. "But if you live on a college campus as part of an academic environment, the cost of living is going to be lower in most cases, so you can put up with a little bit less salary. I've heard that the academic salaries are about $3000 per month, assuming you've done a year or two of postdoctoral work. Normally, when you start out in academia, they'll pay your salary the first summer. So it's not much lower than what industry is paying starting PhDs, which is about $36,000. My feeling is that the salary is not that different—but I admit I could be in for a big surprise."

This same individual, who is probably representative of many young academic hopefuls, is not deterred by the tenure system either. "I don't think people getting out of college look at the tenure issue closely in their decision. Tenure is five or six years down the road. What people *do* look at are differences in salaries and the amount of work that has to be done. That's what I've heard most people say—you're going to take a low salary and you're going to work your tail off.

"I want to establish my own research program and work on my own ideas, the kind of research I want to see done," he adds. "Academia offers the freedom to do long-term fundamental research instead of working on short-term project- and product-related problems. I think the trade-offs are worth it. It's like starting your own business. When you start your own business, you have to work a lot harder, usually for fewer rewards at first. But if you make it, you can surpass what other people have been making all along."

In the final analysis, perhaps the most stimulating aspect of academic life is helping students to develop their talents and abilities and watching as they thrive in their chosen scientific careers—whether academic, industrial, or governmental. As Gary Hieftje puts it, "Even if academic salaries are significantly lower—which I don't believe—the opportunity to help people grow intellectually will always attract people to teaching."

*S.A.B.*

CombinationX-EL
CORNING
pH meter 145
7.00
mode

# 99.9% READING IN 5 SECONDS OR LESS. NO EXTRA CHARGE.

You get a $120 Corning® X-EL® Plastic Barrel Combination Electrode in place of our usual general purpose electrode when you buy a Corning 140 or 145 pH meter.

The X-EL electrode features an exclusive ion exchange barrier. Eliminates AgCl clogging *and* silver contamination.

- Fast: results in 5 seconds or less.
- Reliable: one year warranty.
- Stable: less than 0.002 pH drift/24 hrs.
- Precise: ±0.002 pH.

Corning 140 is totally automatic.

- Four simple function keys.
- Excellent repeatability.
- Automatic endpoint sensing.
- Sealed surface keypad.
- Automatic calibration, buffer recognition.

Corning 145 has all the features of the 140 plus full pH versatility.

- Keypad data entry.
- Alphanumeric prompting in five languages.

Each new Corning meter comes with a two year warranty.

Join us in celebrating 70 years of vision with this X-EL electrode offer. From the first low-expansion borosilicate Pyrex® beaker to space shuttle windows and heat-resistant shielding, Corning applies 70 years of vision to making labware the way you want it.

CIRCLE 30 ON READER SERVICE CARD

70 YEARS
OF VISION
1915-1985
CORNING

**FIND OUT MORE**

☐ Call to set up a demo
☐ Send a representative
☐ Send literature

Mail coupon on your letterhead with name, phone number, address. Corning Glass Works, Science Products, P.O. Box 1150, Elmira, New York 14902-9944. Offer good through November 29, 1985. AC-04-85-VP

The Most Trusted Tools Of Science

CORNING

# Electrophoresis Improves Accuracy of Paternity Testing

Recent research in electrophoresis of isoenzymes, serum proteins, and DNA fragments is making it possible for forensic scientists to more accurately evaluate paternity in cases of disputed parentage. Paternity tests are designed to determine whether a man could have fathered a child by comparing the genetic markers present in the parents' and the child's blood. If the suspected father cannot be excluded by statistical analysis of data obtained from these blood tests, he is included in a population of men who could be the biological father.

Paternity testing methods can be broadly classified into two general areas: immunochemical typing of red-cell antigens and human leukocyte antigens (HLA), and electrophoresis of red-cell isoenzymes and serum proteins. Red-cell antigen typing has been done routinely for many years, but HLA typing and electrophoresis (especially isoelectric focusing) have only recently been applied to paternity testing.

Joseph Melvin, codirector of the Paternity Testing Laboratory at the Edward W. Sparrow Hospital in Lansing, Mich., and author of a book chapter on paternity testing (*1*), points out that legal acceptance of scientific paternity evidence has been slow. In a 1946 case, Charlie Chaplin was forced to pay child support even though blood testing excluded him as the father. In 1950, however, the U.S. Supreme Court established a legal precedent by allowing blood test results to be introduced as evidence. "The contemporary legal development of genetic testing to exclude paternity," Melvin explains, "stems from introduction in 1975 of [Title IV-D] of the Social Security Act, which requires states that receive federal support for Aid for Dependent Children to attempt to prosecute suspected fathers for support. Many states rapidly amended their laws in reference to genetic testing to more expeditiously resolve these difficult cases." Today, most types of scientific paternity evidence, including electrophoretic determinations, are accepted by the courts.

Determination of paternity is based on the fact that many antigens and proteins are polymorphic, meaning that several distinct types of each can be inherited. An individual may possess one or more different types of each antigen or protein; the measurement of the different possible combinations is termed the phenotype. To assess possible paternity, the phenotypes of each parent and the child are determined by antigen typing and electrophoresis of serum proteins. The data obtained are used to statistically determine the probability of paternity based on the number of possible types of each antigen or protein, the gene frequency, and the race of the alleged father.

Separation of red-cell isoenzymes and serum proteins on various electrophoretic media is based on inherent differences in protein mobility in an electric field. Since any difference in the size, shape, or amino acid composition of a protein will cause a change in the migration rate, conventional electrophoresis can usually differentiate among the various forms of the protein of interest.

Recently, isoelectric focusing methods have been developed that significantly improve the electrophoretic resolution of different protein forms. Isoelectric focusing differs from conventional electrophoresis in that instead of a constant pH maintained by an aqueous buffer, separation occurs in a linear pH gradient established using ampholytes. Proteins focus on their isoelectric point, and any protein molecules that diffuse away are pushed back to this point. Thus, proteins on an isoelectric focusing gel show up as sharp bands even after a long run. Special narrow-range gradients can be formulated to further increase the resolving power of this technique. Because of its superior resolving power, isoelectric focusing has revealed previously unknown genetic variations in several proteins (*2*).

Melvin uses one of the polymorphic serum proteins, phosphoglucomutase (PGM), to illustrate how the ability of isoelectric focusing to subdefine genetic markers provides an advantage over conventional electrophoresis. The various forms of PGM can be resolved into three phenotypes using conventional electrophoresis on starch, agarose, or polyacrylamide. "Isoelectric focusing of this enzyme," Melvin writes, "increases the number of phenotypes observed from three to ten, thus increasing its usefulness in paternity testing."

Restriction endonucleases, enzymes that recognize unique strings of nucleotides in DNA and snip the DNA into fragments wherever these strings occur, are also being used to determine paternity, although these methods are still in the developmental stage and not yet widely used. Because of individual differences in DNA structure, the restriction enzymes will cut each person's DNA in a slightly different place. These select DNA fragments are called restriction fragment length polymorphisms (RFLPs).

A recent article (*3*) describes the efforts of two researchers at the University of Wales Institute of Science and Technology to use RFLPs to provide genetic proof of thoroughbred horses' parentage. After digestion of the horse's DNA with restriction enzymes, the fragments are mixed with short pieces of radioactive DNA, which will adhere to similar DNA pieces and show up as a dark band on an electrophoretic gel. Each individual has a different banding pattern or "genetic fingerprint." Breeders should be able to compare the banding patterns of the parents and offspring and statistically determine the chance that the two horses are related.

Marjorie Shaw of the University of Texas Institute for the Interprofessional Study of Health Law predicts that by the end of the century the application of DNA sequence polymorphisms and computer technology will make it possible to positively identify the biological father of any person unless the alleged father has an identical twin (*4*). Shaw writes, "Motherhood

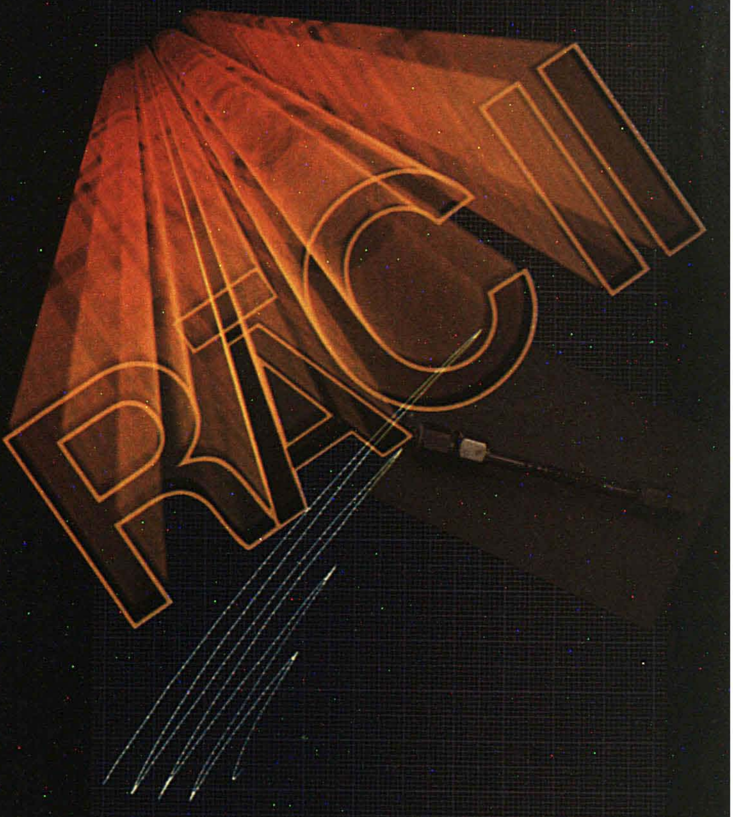

## You Can Cut Separation Time In Half… And Still Get Excellent Resolution.

Whatman RAC II—Second Generation Rapid Analysis Chromatography. The 4.6 mm x 10 cm long column prepacked with proven 5 μm Partisil media offers guaranteed performance that is simply faster and more efficient.

In fact, compared to the standard 25 cm long column used in most applications, RAC II gives you equal resolution with no change in flow rate or mobile phase composition…with one-half the solvent usage…twice the sample throughput…in one-half the time. That's productivity.

And, you may choose from six different phases to handle virtually all LC separation needs, including ODS-3, C$_8$, Silica, and the *new* PAC, SAX and SCX.

RAC II special geometry eliminates unswept corners to maximize peak symmetry and resolution. Whatman compression screw end fittings provide for uniform sample distribution to improve effectiveness and lower asymmetry values.

Get speed, get resolution, get RAC II. Call a Whatman technical representative now to discuss your applications. Toll-free 800-922-0361. (In N.J. 201-773-5800.)

RAC is a trademark of Whatman, Inc.

**Whatman**

has always been a biologic certainty; now fatherhood will be as well. We will have come one step closer to equality of the sexes."

### References

(1) Melvin, Joseph. In "Forensic Science Handbook, Part II"; Saferstein, Richard, Ed.; Prentice-Hall: Englewood Cliffs, N.J., in preparation.

(2) Sensabaugh, George F. In "Forensic Science Handbook"; Saferstein, Richard, Ed.; Prentice-Hall: Englewood Cliffs, N.J., 1982; Chapter 8.

(3) *New Scientist*, Nov. 8, 1984, *108*, 24.

(4) Shaw, Marjorie W. *J. Am. Med. Assoc.* **1983**, *250*, 2536–37.

*M.D.W.*

# Office Testing Lab Newsletter Debuts

If there is any lingering doubt that an increasing number of clinical and diagnostic tests are being performed in physicians' in-office laboratories on small, low-cost analyzers (see *Anal. Chem.* **1985,** *57,* 38–39 A), the appearance of the premier edition of "Doctor's In-Office Lab News" should dispel those notions forever. The newsletter will keep readers informed of the latest new products for the doctor's office and the private home market, government regulations affecting these tests, the relative cost-effectiveness of in-office and in-home testing vs. laboratory testing, and the latest market surveys in the field.

In the first issue of the newsletter, Ronald H. Laessig of the Wisconsin State Laboratory of Hygiene explains that reservations among physicians, laboratory professionals, and regulators about the quality of in-office test results are now misplaced. Industry vendors, aware of the fact that the success or failure of the in-office laboratory concept will hinge on the quality issue, have been expending considerable effort on the quality assurance of test results.

Laessig explains that "The technology developed and successfully marketed in 1986 and beyond will not only have to deliver quality results to the physician; it will [also] have to aid the user in meeting the regulatory (performance) criteria imposed on the doctor's office laboratory."

The key advance that has helped put the bloom on the office testing rose is the adoption of prepackaged reagent systems and instrumental devices that eliminate most of the traditional pitfalls and labor of testing. Laessig points out that demand for in-office testing is driven, in part, by demands from patients for more efficient health care delivery: "Patients are less willing to return for a second visit because the physician is awaiting a laboratory result on a specimen sent elsewhere."

Ten-issue subscriptions to "Doctor's In-Office Lab News" are available for $95 (add $10 for overseas postage) from Scientific Newsletters Inc., P.O. Box 4546, Anaheim, Calif. 92803 (714-497-3522).

*S.A.B.*

**Specialty Gases & Chemicals**

- Calibration Gas Standards
- High Purity Gases
- Electronic Gases
- Silanes
- Clinical Gases
- Emission Gases
- Fluorocarbons
- Sterilizing Gases
- Research Gases

We offer a full range of high-purity gases and mixtures. Whether you require specialty gases in small quantities for laboratory work, or in production volumes, Liquid Carbonic can meet your needs.

Liquid has established a network of specialty gas laboratories and stocking depots throughout North America. Our laboratories are equipped with sophisticated analytical instruments and staffed by chemists and engineers ready to meet your needs for specialty gases and solve your problems.

If quality and service are what you expect from a supplier, why not write to Liquid Carbonic for further information and a catalog.

Liquid®

**LIQUID CARBONIC**
SPECIALTY GAS CORPORATION
135 SOUTH LA SALLE STREET • CHICAGO, ILLINOIS 60603 4282

Send me your catalog and information on:

☐ Calibration Gases ☐ Emission Gases ☐ Equipment
☐ Electronic Gases ☐ Clinical Gases ☐ Sterilizing Gases

Name____________________
Title____________ Phone (___)________
Company____________________
Address____________________
City________ State________ Zip________
☐ Have your local representative contact me.
AL

CIRCLE 132 ON READER SERVICE CARD

# Here's where accuracy and precision begin.

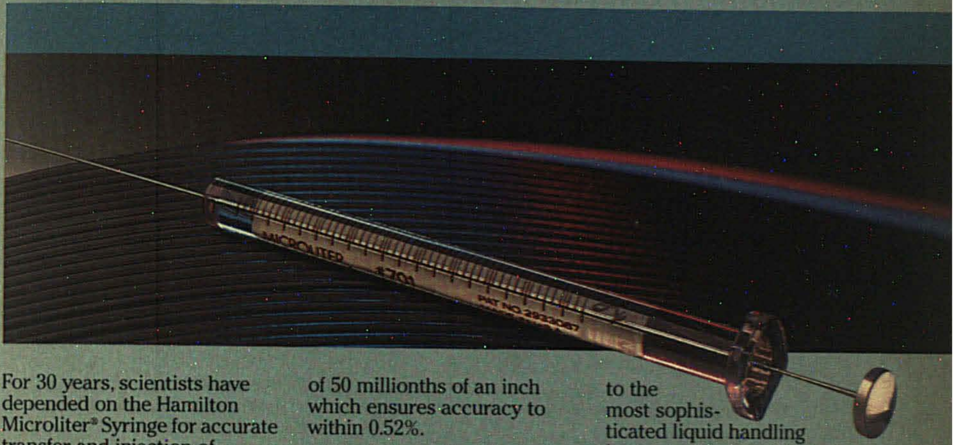

For 30 years, scientists have depended on the Hamilton Microliter® Syringe for accurate transfer and injection of precise volumes of liquids and gases.

There are good reasons why. Commitment to quality. Attention to detail. And constant improvement of our manufacturing and quality control procedures. We always keep your analytical needs in mind.

For example, our 10 μl syringes carry a stringent bore tolerance of 50 millionths of an inch which ensures accuracy to within 0.52%.

Today, our syringes are part of a comprehensive line of high quality products that includes liquid diluter/dispensers, miniature valves and fittings, chromatography columns and accessories, and advanced sample handling and analysis systems.

As our product line grows, we continue to place the same premium of quality on everything we manufacture—from the precision Microliter® Syringes to the most sophisticated liquid handling instruments.

When you demand accurate analytical results, begin with Hamilton.

For your copy of our latest catalog, call (800) 648-5950. Or write to the Hamilton Company, P.O. Box 10030, Reno, Nevada 89520.

**HAMILTON**

The measure of excellence.

CIRCLE 95 ON READER SERVICE CARD

**See Us At FASEB — Booth #'s 1703–1707.**

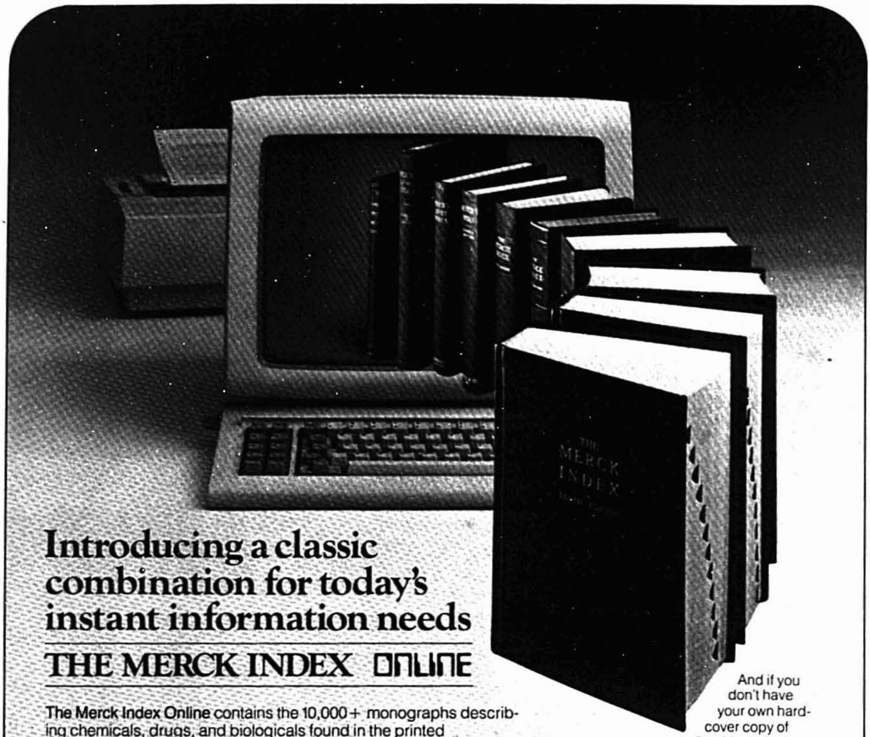

# Introducing a classic combination for today's instant information needs

## THE MERCK INDEX ONLINE

**The Merck Index Online** contains the 10,000+ monographs describing chemicals, drugs, and biologicals found in the printed 10th Edition of The Merck Index. More than 300 of these have been revised. In addition, there are 56 monographs that have been written especially for the online version.

**The Merck Index Online** will be updated every six months.

**The Merck Index Online** puts the authoritative information you have always associated with The Merck Index at your fingertips. Searches that once took hours or couldn't be done at all now require only minutes to complete.

**The Merck Index Online**, an ideal partner for your hardcover copy of The Merck Index (10th Edition), is now available through:

**Chemical Information Systems, Inc.**
**a subsidiary of Fein-Marquart Associates, Inc.**
**(800) CIS-USER,**
and
**BRS, (800) 833-4707.**

And if you don't have your own hardcover copy of The Merck Index (10th Edition), why not order it today. To order, send a check or money order for $28.50, payable to Merck & Co., P.O. Box 2000, Rahway, NJ 07065. You may ask to be billed later and be charged shipping and sales tax.

# THE MERCK INDEX ONLINE

(First Update, November 1984)

## a thoroughly modern classic

CIRCLE 142 ON READER SERVICE CARD

# A TALE OF FOUR CHEMISTS

*Not too long ago, four chemists were working in four labs.*

*All four encountered analysis problems: the first chemist's problem concerned metals, the second's had to do with organic ions, the third's involved amino acids, and the fourth's was with common inorganic anions.*

*While our chemists pondered their analysis problems, a common solution was already waiting for them...*

*Request Reader Service #41*

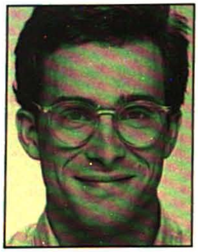

# The Metals Story

*"I had to analyze a variety of transition metals at extremely low concentration levels. Interferences were always a problem."*

"My sample load and research needs are such that AA and ICP alone aren't sufficient. We needed to increase the efficiency of our electroless nickel plating solutions for the manufacture of magnetic storage media. Of particular importance were transition metals: lead, cadmium, cobalt, copper, and nickel. However, monitoring hypophosphite and organic acid concentrations was crucial too. To my delight, I discovered that a Dionex system can analyze all of these *and* speciate metals and other ions according to their oxidation states.

"Our Dionex virtually eliminated the old interference problems and gave us the sensitivity we needed to improve our production yields. Now we even do our routine wastewater samples on our Dionex."

```
--------------------------
Sample Name:Electroless
Nickel Bath #32
--------------------------

 PEAK  RET    PEAK       CONC. in
  NUM  TIME   NAME       ug/1
--------------------------

   1    2.13  LEAD       1.216E+02
   2    2.95  COPPER     9.340E+01
   3    4.01  CADMIUM    9.554E+01
   4    6.77  COBALT     1.271E+03
   5   12.53  NICKEL     9.844E+06
--------------------------
```

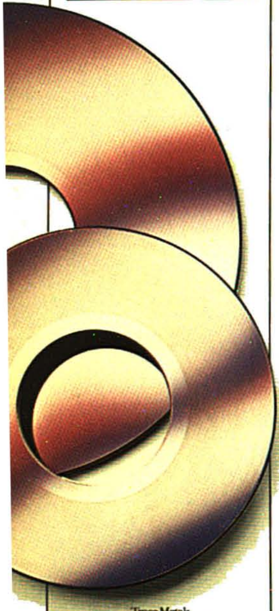

Trace Metals in Electroless Plating Bath

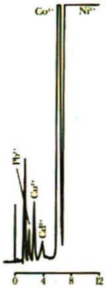

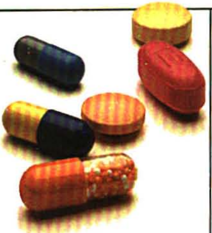

# The Organic Story

*"The ionic organics I was analyzing had no chromophores and were difficult to chromatograph. Conventional HPLC just couldn't do the job."*

Comparison of Detection Modes in the Analysis of Milk

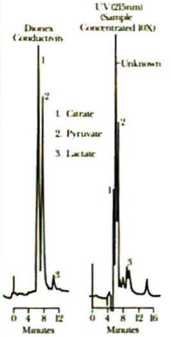

N-Methyl Pyrrolidine (NMP) in an Antibiotic

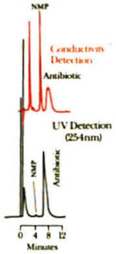

"We do a lot of work for clients in the food and pharmaceutical industries. Naturally, we depend on LC and GC. But there are cases where these techniques won't separate and detect the components we're analyzing.

"For example, many organic amines are difficult to chromatograph. We've found that a Dionex Ion Chromatograph is an easy solution to this tough problem.

"In this case, our Dionex enabled us to determine an amine impurity in an antibiotic, something we couldn't do with silica-based columns and UV detection.

"Highly complex samples, like milk, have always been a problem. Our Dionex is able to detect organics in milk with better selectivity and sensitivity."

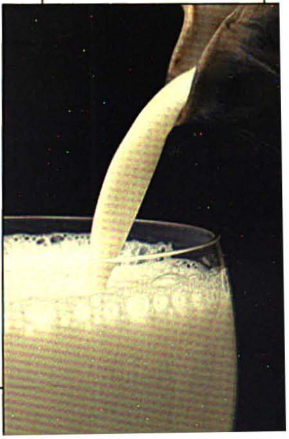

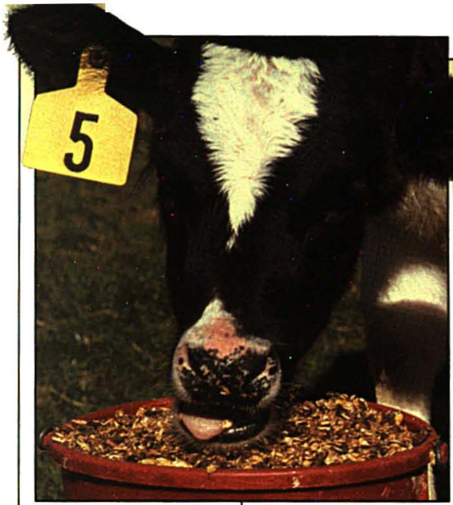

## The Amino Acid Story

*"I need to determine amino acids, carbohydrates, and anions in my samples. I got tired of running from instrument to instrument."*

"To get all three profiles, we had to run samples through a series of procedures on several different instruments. Our expensive dedicated amino acid analyzer could only do part of the job.

Hydrolyzed Feed Sample

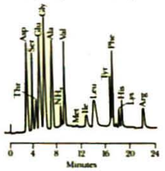

"Now I can do it all—automatically if I want—on a single instrument: a Dionex Ion Chromatograph.

"Our Dionex gives us excellent resolution of amino acids in record time, and we can switch to carbohydrates or anions at the touch of a button."

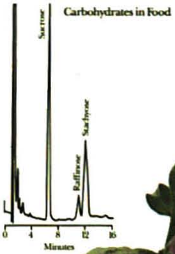
Carbohydrates in Food

## The Inorganic Story

*"In our lab we have to analyze a variety of common anions in a large number of samples, and it always has to be done yesterday."*

"My specialty is water analysis, and I've tried every method: wet chemistry, automatic titrators, ion-selective electrodes. I've even modified an HPLC with an ion exchange column and a conductivity detector. My Dionex Ion Chromatograph beats them all.

"With our high sample load, we simply couldn't cope without unattended sample preparation, analysis, and data reduction. We get all of those from our Dionex systems, with consistent accuracy—it doesn't matter whether we're analyzing sub-part-per-billion concentrations in ultra-pure water or percentage-level concentrations in turbid solutions. Our chromatograms speak for themselves."

Anions in Water

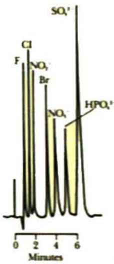

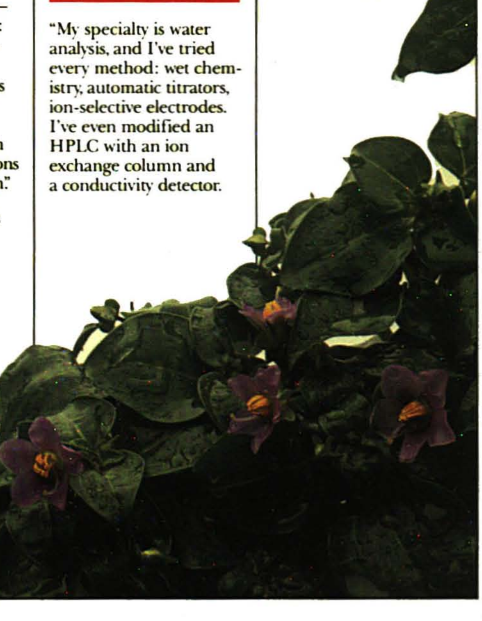

# DIONEX
# THE COMMON SOLUTION

*Dionex systems are solving tough problems in all areas of analytical chemistry. Turn your analysis problems into success stories:*

## Metals Analysis

Dionex lets you determine transition metals, metal complexes, and mono- and divalent cations at trace- and high percent-level concentrations, directly from acid or alkaline digests or brines, even in the presence of other major metal constituents. You can also speciate metal oxidation states such as $Fe^{2+}/Fe^{3+}$ and $Cr^{3+}/Cr^{6+}$. And with Dionex automatic precolumn concentration, you can analyze as many as nine metals in a single run at concentrations below parts-per-billion.

## Organic Analysis

High-efficiency Dionex ion exchange resins are revolutionizing organic ion separations. Our unique ion detection systems allow trace quantitation of amines, organic acids, sugar alcohols, carbohydrates, and chelates that have little UV absorbance. Dionex systems can solve problems that HPLC and GC can't. Of course, you can use standard HPLC columns on a Dionex for your routine HPLC work as well.

## Amino Acid Analysis

New high-speed pellicular ion exchange resins combined with metal-free instrumentation make Dionex Ion Chromatography more versatile, faster, and more reliable than other amino acid analysis systems. You get highly specific ion exchange separation with automatic post-column derivatization and your choice of anion or cation exchange modes. In addition, you can use your Dionex system to analyze inorganic ions, transition metals, and organic ions as well as amino acids—all in a single instrument.

## Inorganic Analysis

Dionex Ion Chromatography has made tedious wet chemical analysis methods obsolete. Furthermore, single-column techniques simply can't match the performance and versatility of a Dionex. Thanks to advanced membrane-based detection technologies, Dionex guarantees sub-ppb sensitivity and the highest specificity for all common anions. Dionex technology also gives you high precision analysis for assaying complex solutions such as plating baths, Kraft liquors, foods, and paints.

## Automation

Improve your lab's productivity by adding the convenience and consistent accuracy of Dionex automation. With multimode switching, you can go from organics to metals to anions at the touch of a button. Add the AutoIon 300 computer for multiple-instrument control and you can further increase your lab's productivity and sample throughput.

Dionex brings true automation to chromatography—in sample preparation, unattended analysis, and data handling.

For the complete story, or for a demonstration, contact your nearest Dionex representative or call us direct.

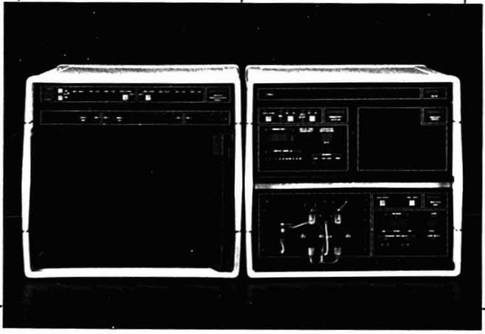

**DIONEX**
THE ION EXPERTS

Dionex Corporation
P.O. Box 3603
Sunnyvale, CA
94088-3603
(408) 737-0700

Itasca, IL
(312) 773-6850
Atlanta, GA
(404) 953-8981

Houston, TX
(713) 847-5652
Marlton, NJ
(609) 596-0600

Dionex (UK) Ltd.
Farnborough, Hants
England
(0252) 541346

Dionex GmbH
West Germany
06150-3047

Semsa, S.A.
Boulogne, France
(1) 621 66 66

Dionex S.r.l.
Roma, Italy
(06) 536130

©Dionex Corporation 1985

LPN 32555 3/85

*Request Reader Service #41*

# INTEGRATE. COMMUNICATE. ORCHESTRATE.

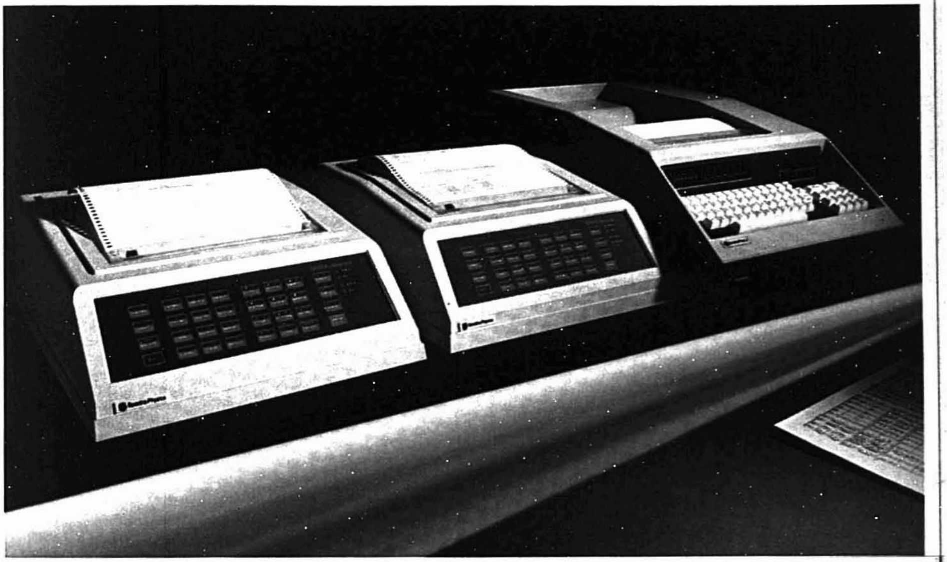

## IMPROVE YOUR PERFORMANCE WITH THE RIGHT INSTRUMENT

Spectra-Physics integrators perform solo, as multi-channel data systems, or as system controllers for LCs or GCs.

If you require an entry-level integrator, our new SP4290 can give you many of the features our leading integrators have at the lowest price yet to come from Spectra-Physics. Plus a two-year warranty.

For a little more, the SP4270 can provide you with BASIC and communication with the IBM PC XT via LABNET,™ our local area network. Or you may opt for the virtuoso performance of the SP4200, with its host of sophisticated features.

Call Spectra-Physics today and ask for the brochure describing all three integrators. In California: (408) 946-9682, in Texas: (713) 688-9886, in New Jersey: (201) 981-0390. Elsewhere: (800) 253-8324. Spectra-Physics, 3333 North First Street, San Jose, California 95134.

|  | SP 4290 | SP 4270 | SP 4200 |
|---|---|---|---|
| **INTEGRATE** |  |  |  |
| Wide Printer/Plotter | Yes | Yes | Yes |
| 50/60 Hz Data Sampling | Yes | Yes | Yes |
| Second Channel | Optional |  |  |
| Transmits Raw Data to IBM-XT | No | Yes | Yes |
| Reintegration/Replotting | No | No | Yes |
| **COMMUNICATE** |  |  |  |
| Alphanumeric Peak & Sample Names | Yes | Yes | Yes |
| Multilevel Calibration | Yes | Yes | Yes |
| Full Keyboard & LEDs | No | No | Yes |
| X-Y Graphics Program | No | No | Yes |
| **ORCHESTRATE** |  |  |  |
| BASIC | No | Yes | Yes |
| LABNET/RS-232 or Current Loop | Optional |  | Yes |
| Timed Events | Optional |  | Yes |
| GPC. Methods Optimization. UV Scan | No | No | Yes |
| Battery Backup | No | No | Yes |
| Price* | $1985 | $2490 | $4490 |

*Domestic U.S. price only.

CIRCLE 188 ON READER SERVICE CARD

**Spectra-Physics**

THE PERFORMANCE LEADER IN AUTOMATED CHROMATOGRAPHY

# THE AUTOMATIC VOLTAMMETRIC ELECTRODE!

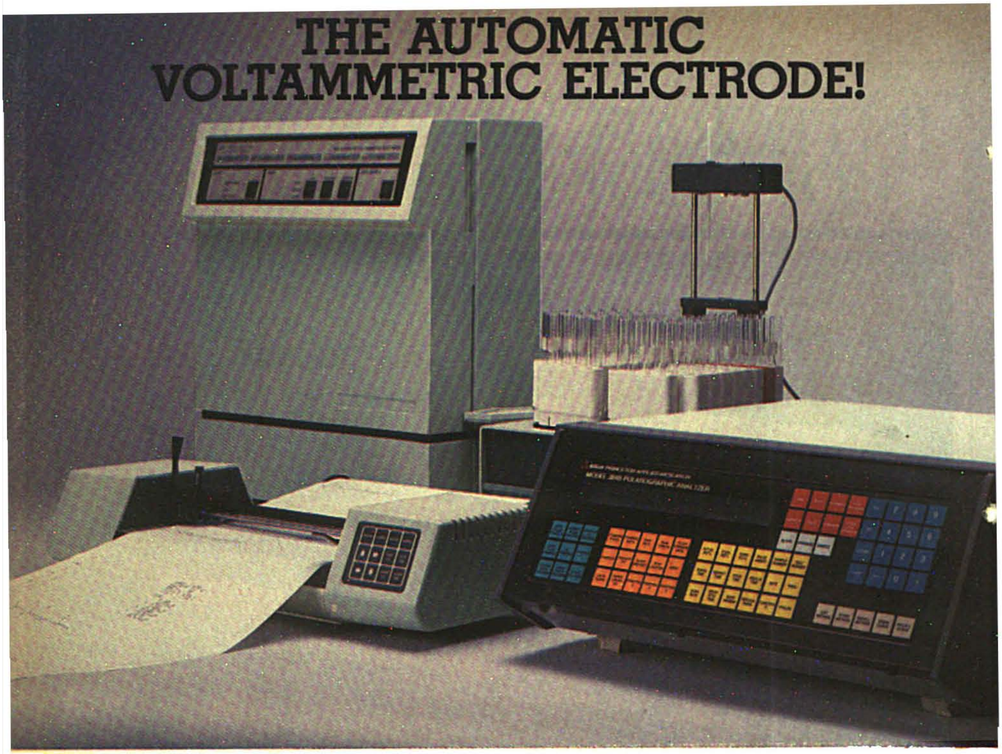

**Versatility, reliability, multi-component capability, simplicity—and now *speed*.**
The list of attributes of voltammetry is growing. Our new Model 309 Automatic Voltammetric Electrode (A.V.E.), together with the new Model 319 Sample Changer, permits rapid deaeration and unattended sample handling. The radically new A.V.E. design can be manually operated to enhance the capabilities of any of our Polarographic Analyzers—or it can be controlled by our Model 384B microprocessor-based analyzer (with the additional speed of Square Wave Voltammetry) to achieve new levels of hands-off, high through-put analytical capability.

**A unique approach to streamlining the analysis**
An ingenious nebulization technique both deaerates and transports the sample solution to the measurement chamber in a matter of seconds (conventional purging techniques require four to eight minutes!). The measurement chamber incorporates our Static Mercury Drop Electrode which has been perfected over the past six years to give reliable performance with outstanding sensitivity and reproducibility.

Find out how the latest advancement in voltammetry can be put to work in your lab. Write or call our Applications Group for more details.

***It's not magic anymore!***

**EG&G PRINCETON APPLIED RESEARCH**
P.O. BOX 2565 • PRINCETON, NJ 08540, U.S.A. • 609/452-2111 • TELEX: 843409

686

EUROPEAN HEADQUARTERS • EG&G INSTRUMENTS • KINGSWICK HOUSE, SUNNINGHILL,
ASCOT, BERKSHIRE, ENGLAND SL5 7BJ • 990-23491 • TELEX: 848980 • FAX: 0990 23141

CIRCLE 49 ON READER SERVICE CARD

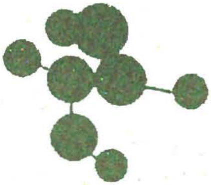

# 38th Annual Summer Symposium on Analytical Chemistry

## Surface Characterization of Catalytic and Electronic Materials

### June 18–20, 1985
### Clarkson University, Potsdam, N.Y.

"Surface Characterization of Catalytic and Electronic Materials" is the subject of the 1985 Summer Symposium of the Division of Analytical Chemistry of the ACS. The symposium will be held June 18–20, 1985, at Clarkson University in Potsdam, N.Y. The general chairman is Petr Zuman of Clarkson University, and the program chairman is Nick Winograd of Pennsylvania State University. The symposium is sponsored by the ACS Division of Analytical Chemistry and ANALYTICAL CHEMISTRY.

### About Clarkson University

Clarkson University is located in Potsdam, N.Y., halfway between the Adirondack Mountains and the Thousand Islands region of the St. Lawrence River. It has a student population of 4500, and its department of chemistry is comprised of 15 faculty members and 40 graduate students. It is also the site of the Institute of Colloid and Surface Science, which will be hosting an International Symposium of Colloid and Surface Chemistry (sponsored by the ACS Division of Colloid and Surface Chemistry) at Clarkson University following the Summer Symposium, from June 23 to 28, 1985.

### Travel

Potsdam can be reached by car or Greyhound bus, or by air to Ogdensburg, Montreal (Dorval), or Syracuse. Transportation from these airports can be arranged, provided that the Conference Center at Clarkson University is notified at least a week before arrival.

### Housing and meals

Housing is available in modern residence halls on the Clarkson University campus or at local motels. Residence hall rates are \$13 per night for a single-occupancy room and \$17 per night for a double-occupancy room. All rooms have a bath shared between two rooms. Children 10 and under may stay in the residence halls for half price. Linens, pillows, and towels are furnished. There is ample free parking adjacent to the residence hall. The Clarkson University residence hall used for this Summer Symposium is within several hundred yards of the Science Center, where all lectures will be held. Local motels are ½ to 10 miles from the university. No transportation from motels to Clarkson will be provided. Requests for housing should be made on the attached registration form and must be received by June 1.

A university room and board special package price is available, which includes housing costs plus all meals from Monday night dinner through Thursday lunch (excluding the Wednesday night banquet, which is included in the registration fee). Special package rates are \$70 per person for a single room and \$56 per person for a double room.

### Registration and special gatherings

Registration will take place in the Educational Resources Center of Clarkson University on Monday, June 17, from 4 P.M. to 8 P.M., on Tuesday, June 18, from 8 A.M. to 2 P.M., and on Wednesday, June 19, from 9 A.M. to 12 noon. A reception will be held at 7 P.M. on Monday, June 17. The registration fee of \$110 includes admission

*General Chairman Petr Zuman (top) and Program Chairman Nicholas Winograd*

to all technical sessions, symposium materials, the reception, and the Wednesday night banquet. The student registration fee of $20 includes only admission to the technical sessions, the reception, and the symposium materials. Students and guests may order banquet tickets on the attached registration form.

### Family activities

Intramural athletic facilities, swimming pool, tennis courts, canoes, paddle tennis, and racquetball courts are available to all registrants. Golf courses are in the vicinity; Lake Placid is a 70-minute drive; Remington Art Museum in Ogdensburg is a 35-minute drive. A visit to the Potsdam Museum and a magician's performance for children can be arranged provided there is sufficient interest.

For further information about any aspect of the symposium, contact Petr Zuman, Department of Chemistry, Clarkson University, Potsdam, N.Y. 13676, (315-268-2340 or 6566).

### Symposium format

The symposium is divided into five half-day sessions dealing with fundamental techniques, surface studies with lasers, surface characterization of catalytic materials, microscopy at surfaces, and surface characterization of electronic materials. The following is the complete program of the symposium.

## Program

### Tuesday Morning, June 18

#### Fundamental Techniques

E. Matijevic, *Presiding*

8:30 **Welcome and Introductory Statements**

8:45 **XPS in Combination with Other Techniques for Surface Characterization.** C. R. Brundle, IBM

9:25 **Ion Beam Spectroscopy of Surfaces and Interfaces.** P. Williams, Arizona State U

10:35 **Vibrational Spectroscopy of Monolayers.** B. Koel, U of Colorado

11:15 **Surface Science: Where We Are and Where We Are Going.** M. White, U of Texas

---

## 38th Annual Summer Symposium on Analytical Chemistry

### Surface Characterization of Catalytic and Electronic Materials

June 18–20, 1985 Clarkson University, Potsdam, N.Y.

Name (Print) ______________________

Title ____________ Phone ____________

Institution ______________________

Address ______________________

City ________ State ________ Zip ________

☐ I will arrange my own housing

☐ Please send me a motel list

☐ I request room and meals at the university from Monday to Thursday at the special package rate of:

- ☐ Single room plus meals—$70/person
- ☐ Double room plus meals—$56/person
    - ☐ Roommate ______________
    - ☐ Assign me a roommate

☐ I request room only at the university for the following nights (no meals): ______________

- ☐ Single—$13/night
- ☐ Double—$17/night

**Transportation**

☐ Car ☐ Bus ☐ Airplane

Airport ______________________

Airline and flight number______________________

Date and time of arrival______________________

☐ I will be staying for the Colloid Symposium

☐ I will be bringing: ☐ spouse
☐ family

| | |
|---|---|
| Registration fee ($110) | $ ________ |
| Student registration ($20) | $ ________ |
| Single room and meals | $ ________ |
| Double room and meals | $ ________ |
| Banquet tickets ($20)<br>(for students and guests only) | $ ________ |
| Single room—no meals | $ ________ |
| Double room—no meals | $ ________ |
| **TOTAL AMOUNT ENCLOSED** | $ ________ |

**Return this form with check made payable to"Clarkson University" for the total amount due to: Doris Frazer, Conference and Information Center, Clarkson University, Potsdam, N.Y. 13676. For further information, call 315-268-6647.**

# Now, a low-cost FT-IR *priced and designed for the first-time FT-IR user.*

## Advanced capabilities at a surprisingly modest price.

Nicolet's new 5DXB now offers you elegant ease-of-use with the same proven productivity and performance as all of Nicolet's world-leading FT-IR spectrometers *— all at a remarkably low price!*

*Standard 5DXB benefits and features:*

- **Excellent sensitivity, reliability, performance from the all-new 5DXB optical bench and high-energy air-cooled source.**

***Removable sample plates mean rapid-yet-precise interchange of accessories.***

- **Fast, accurate, versatile spectral processing from Nicolet's proven, powerful computer with sophisticated yet easy-to-use software.**
- **Superb color graphics from a high-speed high-resolution display, providing instant information and convenient user interaction.**

## Unprecedented ease-of-use for the first-time FT-IR user.

Nicolet's 5DXB eases the transition up from dispersive IR to FT-IR by providing complete spectral processing from a simple menu software system with detailed "HELP" and advice information. The 5DXB offers the most comprehensive tutorial messages of any FT-IR — plus fully versatile, streamlined programmability for the experienced FT-IR spectroscopist.

## 5DXB grows to meet your future needs.

You can select extended capabilities to tailor the 5DXB to your needs — *now or in the future.*

- **Highest sensitivity MCT detectors.**
- **Auxillary sample compartment with computer-controlled beam directly connects to main bench for dedicated special applications accessories.**
- **High-capacity Winchester disk.**
- **Advanced research-grade SX software.**
- ***And lots more!***

*New Nicolet 5DXB: The best value in FT-IR today, with versatility for your future applications. Please phone or write today for complete information.*

**NIC Nicolet**

*The FT Spectroscopy People*

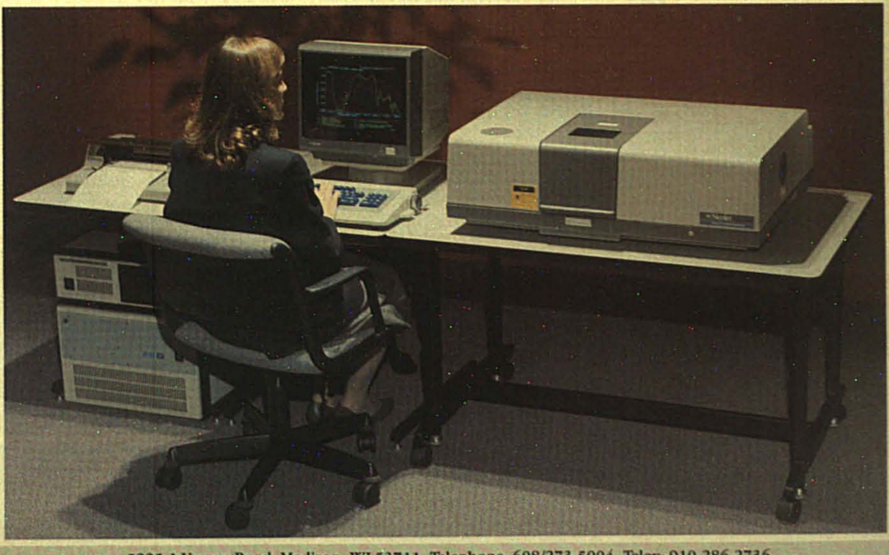

5225-1 Verona Road, Madison, WI 53711 Telephone: 608/273-5004, Telex: 910-286-2736

Required Reading

Solving Emulsion Problems

Emulsions are finely dispersed droplets of one immiscible liquid in another. They pose a problem when they are formed during liquid-liquid extractions. While centrifugation is often used to break emulsions, it is tedious and time consuming. There are ways to break emulsions.

How?

Find out in Technical Tip No. 103.

To receive a copy of Mixxor Technical Tip No. 103, call (617) 275-4480 for immediate help or circle the reader service card.

LIDEX®

LIDEX TECHNOLOGIES, INC.
4 ALFRED CIRCLE
BEDFORD, MA 01730

*Innovators In Sample Prep*

CIRCLE 133 ON READER SERVICE CARD

### Tuesday Afternoon

**Surface Studies with Lasers**

H. Helbig, *Presiding*

1:30 **Surface-Enhanced Raman Spectroscopy.** R. P. Van Duyne, Northwestern U

2:15 **Laser Microprobe Mass Analysis.** D. A. Hercules, U of Pittsburgh

3:30 **Laser-Induced Thermal Desorption Using FT-MS Detection.** J. C. Hemminger and R. I. McIver, U of California at Irvine

4:15 **Surface Analysis by Laser Ionization.** K. T. Gillen and C. H. Becker, SRI International

### Wednesday Morning, June 19

**Surface Characterization of Catalytic Materials**

E. J. Karwacki, *Presiding*

8:30 **Characterization and Adsorption Chemistry of Modified Molybdenum Surfaces.** P. Stair, Northwestern U

9:15 **Carbon–Sulfur Bond Activation on Platinum: A HREELS and NEXAFS Study.** J. Gland, Corporate Research Science Lab, Exxon Research and Engineering Co.

10:30 **Surface Science and Heterogeneous Catalysis.** D. W. Goodman, Sandia Research Lab

11:15 **Surface Science and Electrocatalysis.** Phil Ross, Lawrence Berkeley Laboratory

### Wednesday Afternoon

**Microscopy at Surfaces**

T. Fleisch, *Presiding*

1:30 **Atomic Imaging of Surfaces by High-Resolution Electron Microscopy.** L. D. Marks, Northwestern U

2:15 **Atom Probe and Field Ion Microscope Microanalysis of Surfaces.** T. T. Tsong, Pennsylvania State U

3:30 **Ion Probe Imaging Microanalysis at High Spatial Resolution.** R. Levi-Setti, U of Chicago

4:15 **Scanning Tunneling Microscopy.** R. Wilson, IBM

### Thursday Morning, June 20

**Surface Characterization of Electronic Materials**

D. Denley, *Presiding*

9:00 **Surface Science of Electronic Materials.** S. Williams, U of California at Los Angeles

9:45 **Microanalysis of Semiconductor Materials.** C. A. Evans, Evans and Associates

11:00 **Ion Beam Studies of Silicon-Based Devices.** C. Magee, RCA Labs

11:45 **Surface Characterization of Molecular and Macromolecular Structure.** J. Gardella, State U of New York at Buffalo

---

## IUPAC Nomenclature Document

A nomenclature document on the absolute electrode potential has been prepared by IUPAC. The document begins with illustrations of the most widespread misunderstandings in the literature about the physical meaning of the term. The correct expression for this quantity is then derived by a thermodynamic analysis of the components of the emf of an electrochemical cell. It is shown that, in principle, three reference levels can be chosen to measure an absolute value of the electrode potential. Only one of these possesses all the requisites for a meaningful comparison on a common energy scale between electrochemical and physical parameters. To allow such a comparison, the adoption of a correct scale for absolute electrode potentials is a prerequisite. The document ends with recommendations of critically evaluated values for the absolute potential of the standard hydrogen electrode in water and in a few other protic solvents.

Comments on these recommendations are welcome and should be sent by August 1985 to the Secretary of the IUPAC Commission on Electrochemistry: S. Trasatti, Dipartimento di Chimica Fisica ed Elettrochimica, Via Venezian 21, I-20133 Milano, Italy. Those interested in making comments can obtain a copy of the document from the American Chemical Society, P.O. Box 3330, Columbus, Ohio 43210.

## Hänsch to Receive Meggers Award

Theodor Hänsch of Stanford University is the 1985 recipient of the William F. Meggers Award. The award, established in 1970, is given for outstanding work in spectroscopy. A

# LAB TOOLS from Sargent-Welch

## High Precision Thermostatic Water Baths

Unique, efficient heat distribution system combines ± 0.01°C precision (time based and point-to-point) with the excellent visibility afforded by a single walled, glass tank. Two models-one with direct temperature dialing - both with high efficiency heating/circulating tower, PYREX® brand glass tank, constant level device, cooling coil, booster heater and separate temperature monitoring/controlling unit.

CIRCLE 194 ON READER SERVICE CARD

## Model SD Near UV-Visible-Near IR Spectrophotometer

Luminescent digital readout 0-199.9%T, 0-1.999A and 0-1999 in concentration. Wavelength range of 325-625 nm, extensible to 925 nm with low cost red phototube. Digital wavelength indicator with readability and accuracy of ± 1 nm. Excellent spectral purity - 10 nm bandpass and <0.5% stray light at 325 nm. Interchangeable test tube or rectangular cell holders. Forced draft ventilation to reduce warm-up time, extend lamp life, minimize heat transfer to sample.

CIRCLE 195 ON READER SERVICE CARD

## Model SM Near UV-Visible-Near IR Spectrophotometer

Wavelength range of 325-625 nm, extensible to 925 nm with low cost red phototube. Excellent spectral purity - 10 nm bandpass and <0.5% stray light at 325 nm. Meter readout 0-100%T and 0-2A. Interchangeable test tube or rectangular cell holders. Forced draft ventilation to reduce warm-up time, extend lamp life, minimize heat transfer to cell compartment. Digital wavelength indicator with readability and accuracy of ± 1 nm.

CIRCLE 196 ON READER SERVICE CARD

## Power Driven Cork and Stopper Boring Machine

Bores a straight, smooth, true hole in a rubber stopper or cork quickly, easily and with minimum risk of injury to the operator. Multiple, off-center and angled boring are made easy. Drill press action ensures accuracy alignment and cutting of holes through rubber stoppers rather than punching and tearing as with a hand held cork borer.

CIRCLE 197 ON READER SERVICE CARD

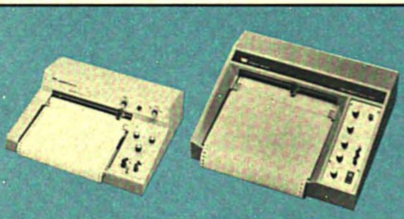

## Potentiometric Analog Data Recorders

**Model SRG-2:** Linear mode with 10 calibrated spans. Log mode with up to 3 cycles full scale. Fully guarded input and AC servo for AC common mode rejection of 5,600,000 to 1. Stepless (uncalibrated) span selection from 400 µV to 1 V. Nine chart speeds.

**Model XKR:** Excellent pen response (51 cm/sec) and a high performance chart drive (9 speed with nonslipping sprocket drum and 4-phase stepper motor) at an economical price.

CIRCLE 198 ON READER SERVICE CARD

## Heavy Duty Air Cooled Magnetic Stirrer

Large (about 8" square) sturdy case and heavy duty drive magnet (3" × ¾") handles up to 13 litres (3½ gallons) of aqueous liquid. Quiet cooling fan limits top temperature rise to only 2° C to protect thermosensitive materials. Stirring speed range, 1 -1000 rpm.

CIRCLE 199 ON READER SERVICE CARD

## Cone Drive Stirring Motor

Combines sparkless but constant speed induction motor with a simple, adjustable transmission to provide stirring speed range of 200 - 1200 rpm. Quiet operating, long lived, adjustable during operation and safe to use where sparks must be avoided.

CIRCLE 200 ON READER SERVICE CARD

SARGENT-WELCH SCIENTIFIC COMPANY
7300 NORTH LINDER AVENUE • SKOKIE, ILLINOIS 60077 • (312) 677-0600
Anaheim/Birmingham/Chicago/Cleveland/Dallas/Denver/Detroit/Springfield, N.J./Toronto/Montreal

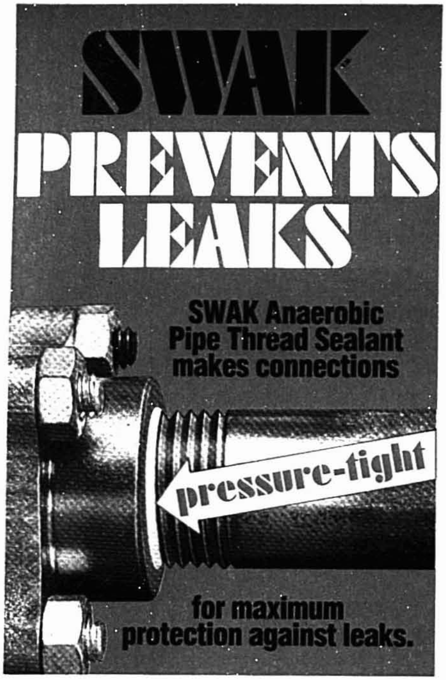

- Contains TFE to lubricate threads during make-up, preventing galling and seizing
- Seals to pipe working pressure
- Vibration and shock-proof
- Temperature range: − 65°F to 350°F (− 53°C to 180°C)
- Handy, built-in applicator
- Compatible with a wide variety of fluids and gases
- Long shelf life
- Available from your local Authorized Sales & Service Representative

*NOW available in two sizes!*

CAJON
SWAK
Patented

*You can order **SWAK** in either 50cc or NEW 250cc tubes.*

**CAJON COMPANY**
9760 Shepard Road, Macedonia, Ohio 44056
©1980-1984 Markad Service Co., all rights reserved K-44f

CIRCLE 32 ON READER SERVICE CARD

## News

prize of $1000, a silver medal, and a citation are included in the award, which Hänsch will receive at the 1985 Optical Society of America annual meeting, to be held Oct. 15–19 in Washington, D.C.

Hänsch has been named to this award for his "discoveries of powerful techniques for high-resolution laser spectroscopy, and their application to fundamental problems of physics, particularly through precision measurements on atomic hydrogen." These techniques include the first narrowline tunable dye laser and the saturation, polarization, and polinex methods for eliminating Doppler broadening.

### Dating Technique Tested

An analytical technique for dating groundwater and polar ice up to a million years old has been successfully tested by scientists at Oak Ridge National Laboratory (ORNL). The system, known as a rare gas atom counter, extends the capabilities of resonance ionization mass spectrometry to include counting single atoms of krypton-81. The counter is composed of a pulsed dye laser operated in tandem with a mass spectrometer to separate the various isotopes of krypton.

In a collaborative study, ORNL scientists recently used the method for the first time to count krypton-81 in a liter of groundwater removed from a

*Linking Value to Performance.*

# Perfect Quality LC.

**Gradient**

**Gradient LC System G-II**

- *Complete automation of binary gradient LC*

**Simple**

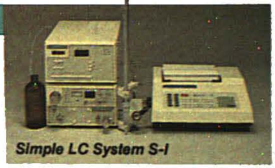

**Simple LC System S-I**

- *Simple and low cost yet high performance*

**Universal**

**Universal LC System U-I**

- *Complete automation of ternary gradient LC as well as low and high pressure valve control*

**Automated**

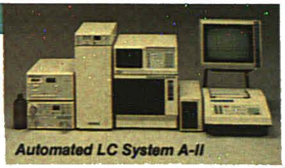

**Automated LC System A-II**

- *Complete automation of isocratic LC*

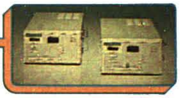

***UV Spectrophotometric Detector SPD-6A, UV-VIS Spectrophotometric Detector SPD-6AV***

- *SPD-6A has wavelength range of 195 – 350nm and SPD-6AV of 195 – 700nm*

***System Controller SCL-6A***

- *Complete control of LC module as well as external devices*
- *Menu driven control of parameters*

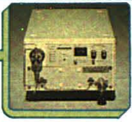

***High Performance Liquid Pump LC-6A***

- *Capable of stable flow rate between 0.01 — 9.9ml/min*

***Column Oven CTO-6A***

- *Temperature control up to 99° C*

***Auto Injector SIL-6A***

- *Capability of 100 samples*

***Data Processor C-R3A***

- *Large capacity for chromatogram memory (176 KByte)*

## Introducing Shimadzu's full spectrum of modular HPLC Systems.

For full value HPLC systems, ask for the Shimadzu LC-6A. From simple to complex LC, the new high-performance Shimadzu LC-6A Liquid Chromatograph System can meet any requirement perfectly.

The modular design provides an easy and cost-efficient way to upgrade any system. But this isn't all you get with Shimadzu.

You get competitive specifications at the lowest cost. Proven reliability, a one-year warranty at no extra cost. And applications support. Important reasons to consult Shimadzu today about the full value LC-6A.

For further information, please contact:

**Shimadzu Scientific Instruments, Inc.**
7102 Riverwood Drive, Columbia, MD 21046, U.S.A.
Phone: (301) 997-1227

**Shimadzu (Europa) GmbH**
Acker Strasse 111, 4000 Düsseldorf, F.R. Germany
Phone: (0211) 666371 Telex: 08586839

**Shimadzu Corporation, International Marketing Div.**
Shinjuku-Mitsui Building, 1-1, Nishishinjuku 2-chome,
Shinjuku-ku, Tokyo 160, Japan
Phone: Tokyo 03-346-5641
Telex: 0232-3291 SHMDT J.

SHIMADZU

CIRCLE 192 ON READER SERVICE CARD

INTERFERENCES
IN FURNACE
ATOMIC ABSORPTION

A Thing of the Past . . .

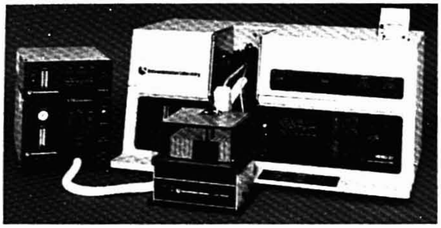

Allied Analytical Systems offers an approach to furnace atomic absorption that takes the worry out of furnace interferences. Our new system is based on the following:

- The NEW *IL755 CTF*™ Controlled-Temperature Furnace Atomizer with the Delayed Atomization Cuvette (DAC) which reduces vapor phase interferences by delaying atomization and causing atoms to be released into a hotter temperature environment.
- The IL *FASTAC*®II autosampler, a flame/furnace aerosol sampling system that not only automates sample introduction, but actually reduces solid phase interferences by eliminating the drying step associated with conventional autosamplers.
- The SMITH-HIEFTJE System. A surprisingly simple but effective background correction system for correcting broadband and structured background over the entire wavelength range of atomic absorption.
- Video graphics for visualization of uncorrected and background corrected signals.

**Send in coupon for *FREE* applications information on our total AA system.**

☐ **1** Trace Metals in Urine
☐ **2** Priority Pollutants in Drinking Water
☐ **3** Toxic Metals in Food
☐ **4** Contaminants in High Temperature Nickel Alloys
☐ **5** Delayed Atomization Techniques to Reduce Background Correction Problems

NAME ______________________
COMPANY ______________________
ADDRESS ______________________
CITY ____________ STATE ________ ZIP ________
TELEPHONE ______________________

Or contact: Allied Analytical Systems,
590 Lincoln Street, Waltham, MA 02254,
Telephone: (617) 890-4300.

ALLIED Analytical Systems

CIRCLE 3 ON READER SERVICE CARD

sandstone aquifer near Zurich. Fewer than 1000 krypton-81 atoms were isolated from the groundwater samples. According to Bernard Lehman, a collaborating geochemist at the University of Bern, this first test proved that counting the small numbers of krypton-81 atoms necessary to make an estimate of the age of water could actually be done. Among the applications of this method, Lehman says, could be improved siting of locations for the disposal of radioactive wastes.

## NBS Budget for FY 1986

A total of $120 million is allotted for the National Bureau of Standards in the fiscal year 1986 budget proposal sent by the president to Congress. This budget request is $4 million less than the bureau's fiscal year 1985 appropriation of $124 million.

Included are program increases totaling $16.4 million and cost-of-living and other built-in changes of $4.9 million. Proposed program increases are process and quality control measurements ($1.9 million), biotechnology ($3 million), advanced ceramics ($3.5 million), and cold neutron source ($8 million). The proposed budget also includes program reductions of $16.5 million and decreases of $8.8 million attributable to the Deficit Reduction Program. Proposed program reductions are building research ($3.1 million), computer sciences and technology ($5 million), fire research ($5.1 million), and equipment replacement ($3.3 million). Hearings on this budget proposal began the first week in March.

## Call for Papers

**1986 Winter Conference on Plasma Spectrochemistry**
Lahaina, Maui, Hawaii. Jan. 3–10, 1986. The conference will feature developments in atomic plasma spectrochemical analysis by inductively coupled plasma, dc plasma, and microwave plasma excitation sources. Papers describing original work in atomic plasma spectrochemistry applications, fundamentals, and instrument development are being solicited. Title and 50-word abstract are due July 1, 1985. For further information contact Ramon Barnes, 1986 Winter Conference Chairman, Department of Chemistry, GRC Towers, University of Massachusetts, Amherst, Mass. 01003-0035 (413-545-2294).

*Linking Value to Performance.*

# Perfect Quality UV-VIS.

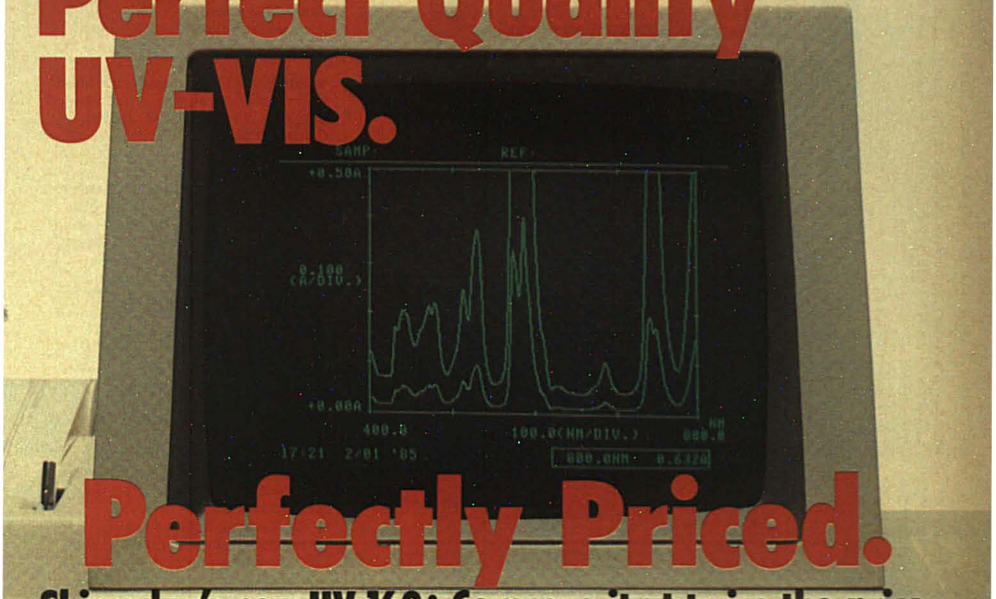

# Perfectly Priced.

## Shimadzu's new UV-160: Compare it at twice the price.

With one design, one price and no costly options, Shimadzu's UV-160 UV-VIS Recording Spectrophotometer has everything you need for rapid and accurate spectrophotometry—including flexible data processing functions, CRT and printer output. The double beam design means freedom from baseline drift. Five different multi-component analysis methods mean high-precision quantitation. And the error-free scanning speed of 2400nm/min means you can scan the full range, 1100 to 200nm and display the spectrum, in roughly 25 seconds.

Competitive features include stored and realtime spectrum manipulation. Find out more about the full value spectrophotometer.

For further information, please contact:

**Shimadzu Scientific Instruments, Inc.**
7102 Riverwood Drive, Columbia, MD 21046, U.S.A.
Phone: (301) 997-1227

**Shimadzu (Europa) GmbH**
Acker Strasse 111, 4000 Düsseldorf, F.R. Germany
Phone: (0211) 666371 Telex: 08586839

**Shimadzu Corporation, International Marketing Div.**
Shinjuku-Mitsui Building, 1-1, Nishishinjuku 2-chome,
Shinjuku-ku, Tokyo 160, Japan
Phone: Tokyo 03-346-5641
Telex: 0232-3291 SHMDT J.

SHIMADZU

CIRCLE 193 ON READER SERVICE CARD

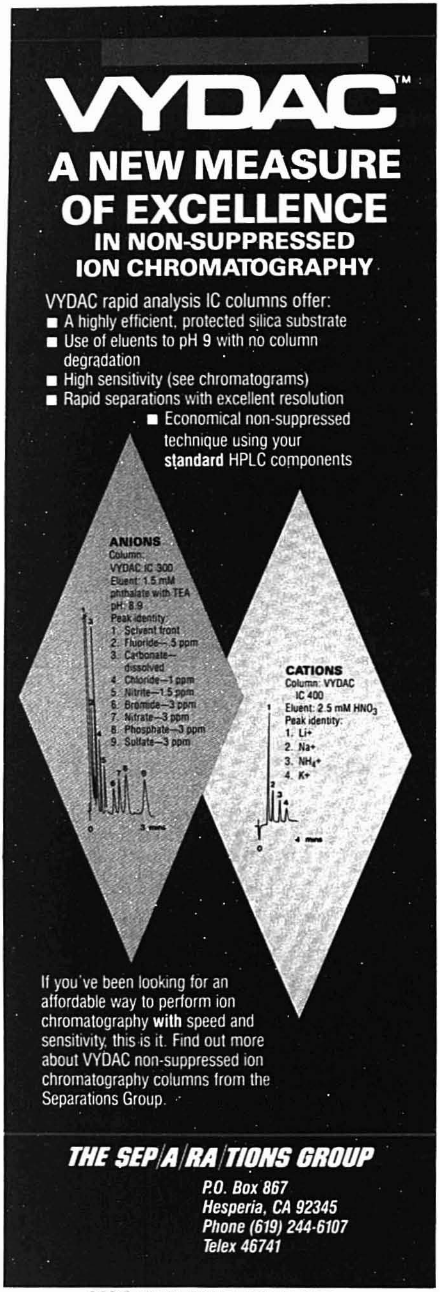
VYDAC™

A NEW MEASURE OF EXCELLENCE IN NON-SUPPRESSED ION CHROMATOGRAPHY

VYDAC rapid analysis IC columns offer:

- A highly efficient, protected silica substrate
- Use of eluents to pH 9 with no column degradation
- High sensitivity (see chromatograms)
- Rapid separations with excellent resolution
- Economical non-suppressed technique using your **standard** HPLC components

ANIONS
Column:
VYDAC IC 300
Eluent: 1.5 mM phthalate with TEA
pH: 8.9
Peak identity:
1. Solvent front
2. Fluoride—.5 ppm
3. Carbonate—dissolved
4. Chloride—1 ppm
5. Nitrite—1.5 ppm
6. Bromide—3 ppm
7. Nitrate—3 ppm
8. Phosphate—3 ppm
9. Sulfate—3 ppm
0
3 mins
CATIONS
Column: VYDAC IC 400
Eluent: 2.5 mM HNO3
Peak identity:
1. Li+
2. Na+
3. NH4+
4. K+
0
4 mins

If you've been looking for an affordable way to perform ion chromatography **with** speed and sensitivity, this is it. Find out more about VYDAC non-suppressed ion chromatography columns from the Separations Group.

THE SEP/A/RA/TIONS GROUP

P.O. Box 867
Hesperia, CA 92345
Phone (619) 244-6107
Telex 46741

CIRCLE 185 ON READER SERVICE CARD

## News

### Meetings

*The following meetings are newly listed in ANALYTICAL CHEMISTRY. Other 1985 meetings are listed in the January, February, and March issues.*

- **Analytical Techniques in Water Pollution Control.** May 2–3. Cincinnati, Ohio. *Contact: Water Pollution Control Federation, 2626 Pennsylvania Ave., N.W., Washington, D.C. 20037*
- **Chemometrics Research Conference.** May 20–22. Gaithersburg, Md. *Contact: Clifford Spiegelman, Statistical Engineering Division, or Robert Watters, Inorganic Analytical Research Division, National Bureau of Standards, Gaithersburg, Md. 20899*
- **Electron Microscopy and Analysis Group Conference.** Sept. 2–5. Newcastle upon Tyne, U.K. *Contact: Meetings Officer, Institute of Physics, 47 Belgrave Square, London SW1X 8QX U.K.*
- **Analytical Laboratory Managers Association Annual Conference.** Oct. 17–18. Argonne, Ill. *Contact: Dave Green, Argonne National Laboratory, 9700 S. Cass Ave., Bldg. 205, Argonne, Ill. 60439*
- **5th Danube Symposium on Chromatography.** Nov. 11–16. Yalta, U.S.S.R. *Contact: L. N. Kolomiets, Academy of Sciences of the U.S.S.R., Institute of Physical Chemistry, Lenin-Prospect 31, Moscow 117312, U.S.S.R.*
- **First Beijing Conference and Exhibition on Instrumental Analysis.** Nov. 15–18. Beijing, China. *Contact: Conference Secretariat, Room 912, Xi Yuan Hotel, Beijing, China*
- **1985 Water Quality Technology Conference.** Dec. 7–11. Houston, Tex. *Contact: F. W. Pontius, AWWA, 6666 West Quincy Ave., Denver, Colo. 80235*

### For Your Information

Colleges and universities that subscribe to ***Chemical Abstracts*** are now eligible for ACS grants covering 90% of the cost of searching CAS ONLINE service during off-peak hours. The grant applies to all searches performed between 5 P.M. and 8 A.M. eastern standard time on weekdays and 8 A.M. to 1 P.M. eastern standard time on Saturdays. Participants must establish a deposit account of at least $200 with CAS. Usage fees will be cal-

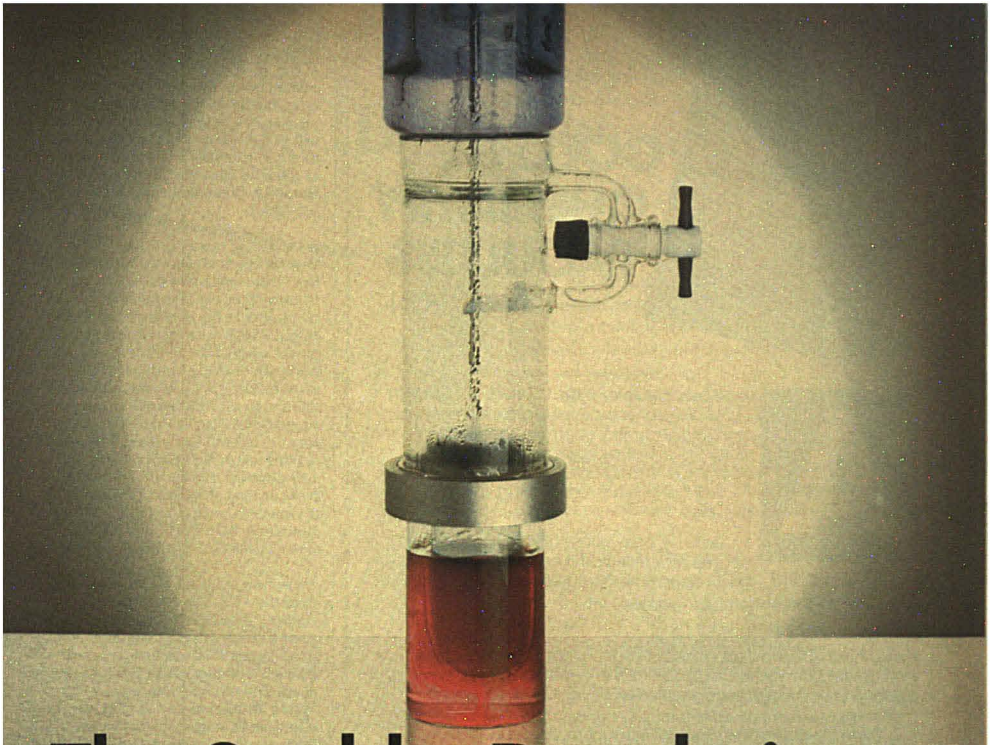

# The Soxhlet Revolution.

When Dr. F. von Soxhlet introduced his method of extraction he had no idea how far it would one day be developed. So he would be very surprised if he could see how effectively our Soxtec Systems carry out the same process today.

With Soxtec the traditional methods such as Soxhlet and Goldfisch have been improved in every essential aspect.

Soxtec is much faster. The extraction time has been reduced by 80 % when compared to that of Soxhlet.

It is much safer. There is no risk of electrical discharge in the vicinity of solvent vapours to touch off any explosions.

It is much cheaper to carry out. Faster analyses, batchwise sample handling and up to 70 % solvent recovery bring improved economies.

And this we achieved without loss of accuracy. Detailed comparisons show that Soxtec provides results equal in accuracy and reproducibility to Soxhlet and Goldfisch.

In short, Soxtec is the Soxhlet revolution. It is also a further example of the Tecator philosophy. To develop and rationalize well proven and tested methods and to convert them into modern routine analyses. Today there are more than a thousand laboratories using Soxtec. And their numbers are increasing every day.

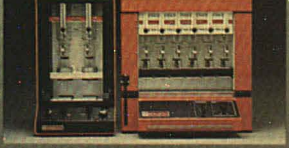

CIRCLE 292 ON READER SERVICE CARD

**tecator**

WE MAKE ROUTINE ANALYSIS SIMPLE.

Tecator AB, Box 70, S-263 01 Höganäs, Sweden. Telephone + 46 42 423 30. Telex 72695.
UK: Tecator Ltd, Bristol. Telephone (0454) 41 77 98. USA: Tecator Inc. Herndon, Virginia. Telephone (703) 435 33 00.
GERMANY: Tecator GmbH, Rodgau. Telephone (06106) 13072-73. FRANCE: Tecator S.A., Paris. Telephone (1) 260 24 24.
Representatives in more than 50 countries.

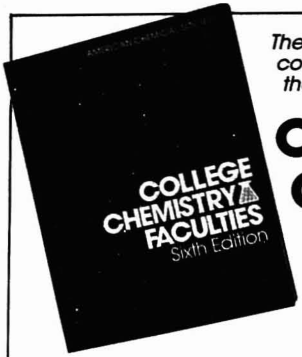

*The most complete listing of college chemistry faculties in the U.S. and Canada*

COLLEGE CHEMISTRY FACULTIES

SIXTH EDITION

A multi-purpose reference, COLLEGE CHEMISTRY FACULTIES is an important tool for researchers, recruiters, industrial chemistry labs, students and teachers as well as college and high school counselors and libraries.

For convenient researching, the directory provides:

1. State-by-state listings of institutions showing degrees offered, staff members and their major fields, department address and phone number.
2. Index of faculty members' names.
3. Index of institutions.

Covering 2,400 two-year and four-year colleges and universities in the U.S. and Canada, COLLEGE CHEMISTRY FACULTIES lists the current affiliations and major teaching fields of over 18,000 faculty members.

State-by-state listings make it easy for students and faculty to find chemistry departments in any area they choose, and for marketers to use the state listings for planning sales and service territories.

Just published, the Sixth Edition of COLLEGE CHEMISTRY FACULTIES is available in time for the fall semester. Order now and keep your information up-to-date. Soft cover, 8 1/2" x 11". 204 pages. . . $34.00

**CALL TOLL FREE 1-800-424-6747**

(for credit card orders),
write, or mail coupon below.

**American Chemical Society** Distribution Office 1155 Sixteenth Street, NW, Washington, DC 20036

Please send _______________ copies of **COLLEGE CHEMISTRY FACULTIES** @ $34.00. On prepaid orders, ACS pays shipping and handling charges.

☐ Payment enclosed (payable to American Chemical Society)
☐ Bill me ☐ Bill company

Charge my ☐ MasterCard ☐ VISA ☐ Barclay Card ☐ ACCESS

Card # ____________________ Interbank # ____________________ (MasterCard only)

Expiration Date ______________ Signature ____________________

Name ________________________________________

Company/Organization ________________________________

Address ____________________ Telephone Number ____________________

Billing Address ________________________________

City ____________________ State __________ ZIP __________

56170/2504/E710

culated at the standard subscriber rates, but an ACS grant will be applied to 90% of the fees, and only 10% will be deducted from the deposit account. For further information, write or call CAS Customer Service, P.O. Box 3012, Columbus, Ohio 43210 (800-848-6538).

A marketing report entitled **"The Bioscience Instrumentation Market"** is available that covers the rapidly growing market for research instrumentation in the biotechnology disciplines. The key categories of instruments selected for analysis in the report include HPLC systems, DNA synthesizers, UV-VIS spectrophotometers, gel electrophoresis apparatus, tissue culture incubators, and laboratory or research fermenters. The price for this report is $1100; however, a 10% discount is being offered for payment at time of ordering. For further information contact Delco Scientific Resources, 2315 Post Rd., Fairfield, Conn. 06430 (203-254-0652).

Three new publications are available from the ACS. The first, **"Less Is Better,"** discusses the waste management strategy of reducing the generation of hazardous waste at the source through laboratory chemical management. The second, **"Hazardous Waste Management,"** is more general and seeks to describe the nature of the issue, the sources of complexities and uncertainties, and the various strategies being developed. The third, **"Chemical Risk: A Primer,"** focuses primarily on the scientific issues involved in determining the health risks arising from exposure to chemicals. Single copies of the publications are free. Contact the Office of Federal Regulatory Programs, ACS Department of Government Relations and Science Policy, 1155 16th St., N.W., Washington, D.C. 20036 (202-872-8725).

At this year's national meeting of the **American Association for Clinical Chemistry,** July 23–25, a new exposition will be featured called **SPOT** (Satellite and Physician Office Testing). The exhibit will be devoted exclusively to this market and will include chemistry, microbiology, and hematology systems and equipment for the physician's lab, test kits, quality control services, and computers. An educational program directed at physicians and practice managers will also be available, covering such topics as quality control, finance, training, and regulations. Contact the AACC, 1725 K St., N.W., Washington, D.C. 20006.

# Integrated solutions from IBM Instruments.

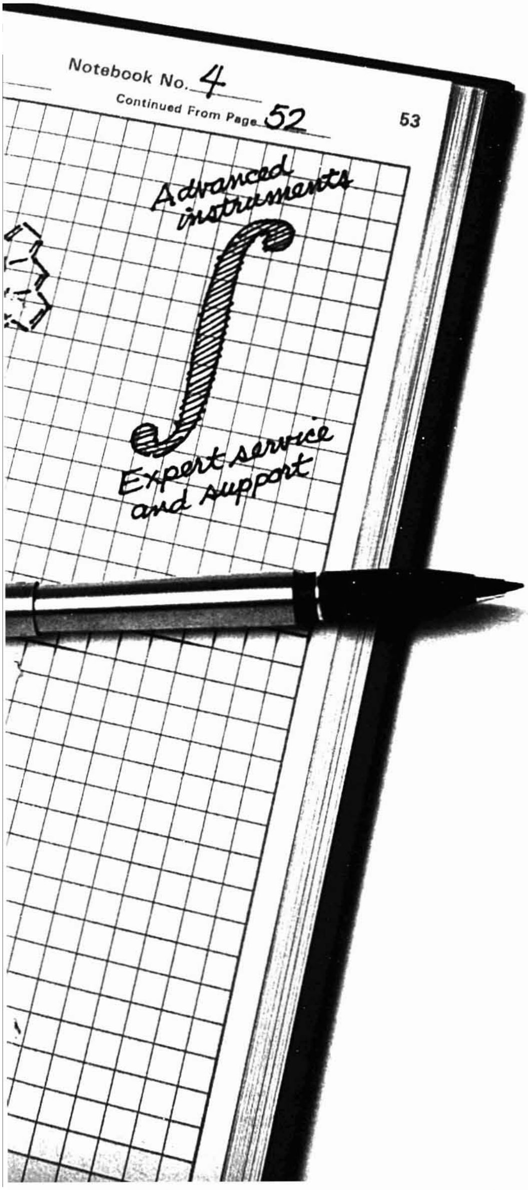

Our formula for solving analytical laboratory problems is a simple one.

We carefully study your current and future application requirements. Then, we work with you to develop a solution that addresses your analytical laboratory needs—in the most efficient, cost-effective manner possible.

We call this an integrated solution. Because it brings together all the necessary components that allow you to characterize, purify or quantify more productively than ever before. A solution that integrates the latest advances in instrument technology with the high levels of service and support associated with IBM.

**Family of Products.** We offer you a full family of spectrometers (NMR, EPR and FTIR), spectrophotometers (UV/Vis) and chromatographs (LC and GC). Plus powerful, real-time computers designed specifically for the laboratory.

But our quality products are only part of the formula. We also have expert applications scientists, customer service engineers and marketing representatives.

**Expertise and research.** When you sit down with us to discuss your analytical problems, you will be talking with someone who speaks your language. Who knows your application. Its chemistry. Its technology. And its critical requirements. Who can back you up with support centers, laboratories, methods analysis, equipment recommendations, documentation, training and service. Who can support you with expertise that is second to none.

And who knows how to work with you to develop the best solution for your application problem… an integrated solution.

**Call or write us today.** If you would like to find out how our formula for integrated solutions can work in your laboratory, call us at 1-800-243-7054 (in Connecticut, 1-800-952-1073), or write IBM Instruments, Inc., Orchard Park, P.O. Box 332, Danbury, CT 06810.

IBM Instruments Inc.

CIRCLE 104 ON READER SERVICE CARD

ION ANALYSIS PROBLEMS?

Lachat will spend the time to understand your problems before we offer a solution.

No two laboratories or chemical manufacturing processes are alike. Sample matrices, concentration ranges and analytes may vary even between companies analyzing the same types of samples.

That's why, at Lachat, we begin with a total analysis of your problem. Our Applications Support Group will work with you to evaluate all data necessary to meet your exact requirements. When we are satisfied that we understand your problem, our system recommendations will follow. We want to be certain that the correct ion analysis system is suggested for your application.

And . . . because Lachat is a leading manufacturer of both flow injection and ion chromatographic analyzers for laboratory and on-line applications, you can be assured that our Applications Support Group will provide the proper solution to your ion analysis problems.

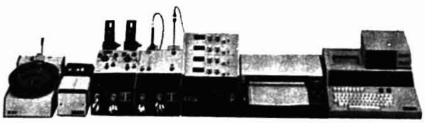

QuikChem® Automated Ion Analyzer

Call or write us today.
Our Applications Support
Group is at your service.

QuikChem®
Process
Monitor

FAST ACCURATE QuikChem QUALITY REPRODUCIBLE

LACHAT INSTRUMENTS
10500 N. Port Washington Road
Mequon, WI 53092
Phone (414) 241-3872
Telex: 26-9681
Innovators in ion analysis

CIRCLE 127 ON READER SERVICE CARD

The most complete listing of college chemistry faculties in the U.S. and Canada

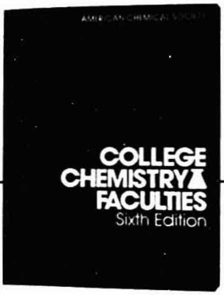

# College Chemistry Faculties

## Sixth Edition

Covering 2,400 two-year and four-year colleges and universities in the U.S. and Canada, COLLEGE CHEMISTRY FACULTIES lists the current affiliations and major teaching fields of over 18,000 faculty members.

A multi-purpose reference, COLLEGE CHEMISTRY FACULTIES is an important tool for researchers, recruiters, industrial chemistry labs, students and teachers as well as college and high school counselors and libraries. It provides:

1. State-by-state listings of institutions showing degrees offered, staff members and their major fields, department address and phone number.
2. Index of faculty members' names.
3. Index of institutions.

Soft cover, 8½" × 11". 204 pages...$34.00

**Call Toll Free**
**1-800-424-6747**
**(for credit card orders),**

**Or mail your order to:**
American Chemical Society
Distribution Office
1155 Sixteenth Street, N.W.
Washington, DC 20036

**APRIL 1985**

**VALID THROUGH AUGUST 1985**

| | | | | | | | | | | |
|---|---|---|---|---|---|---|---|---|---|---|
| ADVERTISED PRODUCTS: | | | | | 1 | 2 | 3 | 4 | 5 | 6 |
| 7 | 8 | 9 | 10 | 11 | 12 | 13 | 14 | 15 | 16 | 17 |
| 18 | 19 | 20 | 21 | 22 | 23 | 24 | 25 | 26 | 27 | 28 |
| 29 | 30 | 31 | 32 | 33 | 34 | 35 | 36 | 37 | 38 | 39 |
| 40 | 41 | 42 | 43 | 44 | 45 | 46 | 47 | 48 | 49 | 50 |
| 51 | 52 | 53 | 54 | 55 | 56 | 57 | 58 | 59 | 60 | 61 |
| 62 | 63 | 64 | 65 | 66 | 67 | 68 | 69 | 70 | 71 | 72 |
| 73 | 74 | 75 | 76 | 77 | 78 | 79 | 80 | 81 | 82 | 83 |
| 84 | 85 | 86 | 87 | 88 | 89 | 90 | 91 | 92 | 93 | 94 |
| 95 | 96 | 97 | 98 | 99 | 100 | 101 | 102 | 103 | 104 | 105 |
| 106 | 107 | 108 | 109 | 110 | 111 | 112 | 113 | 114 | 115 | 116 |
| 117 | 118 | 119 | 120 | 121 | 122 | 123 | 124 | 125 | 126 | 127 |
| 128 | 129 | 130 | 131 | 132 | 133 | 134 | 135 | 136 | 137 | 138 |
| 139 | 140 | 141 | 142 | 143 | 144 | 145 | 146 | 147 | 148 | 149 |
| 150 | 151 | 152 | 153 | 154 | 155 | 156 | 157 | 158 | 159 | 160 |
| 161 | 162 | 163 | 164 | 165 | 166 | 167 | 168 | 169 | 170 | 171 |
| 172 | 173 | 174 | 175 | 176 | 177 | 178 | 179 | 180 | 181 | 182 |
| 183 | 184 | 185 | 186 | 187 | 188 | 189 | 190 | 191 | 192 | 193 |
| 194 | 195 | 196 | 197 | 198 | 199 | 200 | 201 | 202 | 203 | 204 |
| 205 | 206 | 207 | 208 | 209 | 210 | 211 | 212 | 213 | 214 | 215 |
| 216 | 217 | 218 | 219 | 220 | 221 | 222 | 223 | 224 | 225 | 226 |
| 227 | 228 | 229 | 230 | 231 | 232 | 233 | 234 | 235 | 236 | 237 |
| 238 | 239 | 240 | 241 | 242 | 243 | 244 | 245 | 246 | 247 | 248 |
| 249 | 250 | 251 | 252 | 253 | 254 | 255 | 256 | 257 | 258 | 259 |
| 260 | 261 | 262 | 263 | 264 | 265 | 266 | 267 | 268 | 269 | 270 |
| 271 | 272 | 273 | 274 | 275 | 276 | 277 | 278 | 279 | 280 | 281 |
| 282 | 283 | 284 | 285 | 286 | 287 | 288 | 289 | 290 | 291 | 292 |
| 293 | 294 | 295 | 296 | 297 | 298 | 299 | 300 | 301 | 302 | 303 |
| 304 | 305 | 306 | 307 | 308 | 309 | 310 | 311 | 312 | 313 | 314 |

| | | | | | | | | | | |
|---|---|---|---|---|---|---|---|---|---|---|
| NEW PRODUCTS: | | | | 401 | 402 | 403 | 404 | 405 | 406 | 407 |
| 408 | 409 | 410 | 411 | 412 | 413 | 414 | 415 | 416 | 417 | 418 |
| 419 | 420 | 421 | 422 | 423 | 424 | 425 | 426 | 427 | 428 | 429 |
| 430 | 431 | 432 | 433 | 434 | 435 | 436 | 437 | 438 | 439 | 440 |
| 441 | 442 | 443 | 444 | 445 | 446 | 447 | 448 | 449 | 450 | 451 |
| 452 | 453 | 454 | 455 | 456 | 457 | 458 | 459 | 460 | 461 | 462 |
| 463 | 464 | 465 | 466 | 467 | 468 | 469 | 470 | 471 | 472 | 473 |
| 474 | 475 | 476 | 477 | 478 | 479 | 480 | 481 | 482 | 483 | 484 |
| 485 | 486 | 487 | 488 | 489 | 490 | 491 | 492 | 493 | 494 | 495 |

**TO VALIDATE THIS CARD, PLEASE CHECK ONE ENTRY FOR EACH CATEGORY BELOW:**

**Intensity of product need:**
☐ 1. Have salesman call
☐ 2. Need within 6 mos.
☐ 3. Future project

**Primary field of work:**
☐ A. Energy
☐ B. Environmental
☐ C. Medical/Clinical
☐ D. Drug/Toiletries
☐ E. Forensic/Narcotic
☐ F. Biotechnology
☐ G. Metals
☐ H. Pulp/Paper/Wood
☐ I. Soaps/Cleaners
☐ J. Paint/Coating/Ink
☐ K. Electrical/Electronic
☐ L. Instrument Dev./Des
☐ M. Plastic/Polymer/Rub
☐ N. Agricultural/Food
☐ O. Inorganic Chemicals
☐ P. Organic Chemicals

**Primary area of employment:**
INDUSTRIAL
☐ A. Research/Development
☐ B. Quality/Process Control
MEDICAL/HOSPITAL
☐ C. Research/Development
☐ D. Clinical/Diagnostic
GOVERNMENT
☐ E. Research/Development
☐ F. Regulate/Investigate
COLLEGE/UNIVERSITY
☐ G. Research/Development
☐ H. Teaching
INDEPENDENT/CONSULTING
☐ I. Research/Development
☐ J. Analysis/Testing

**CIRCLE 314 FOR SUBSCRIPTION FORM TO ANALYTICAL CHEMISTRY**

NAME: ____________________
TITLE: ____________________
FIRM: ____________________
STREET: ____________________
CITY: ____________________
STATE: ____________ ZIP: ________
PHONE: (___ ___) ___ ___ ___

**NEED MORE INFORMATION?**
**CIRCLE a key number. . .**
**SEND IN the postage paid reply card. . .**
**AND GET free data on any product advertised in this issue. . .**

NO POSTAGE NECESSARY IF MAILED IN THE UNITED STATES

**BUSINESS REPLY CARD**
FIRST CLASS Permit #27346 Philadelphia, Pa.

POSTAGE WILL BE PAID BY ADDRESSEE

analytical chemistry
**P.O. BOX #7826**
**PHILADELPHIA, PA 19101**

NO POSTAGE
NECESSARY
IF MAILED
IN THE
UNITED STATES

**BUSINESS REPLY CARD**

FIRST CLASS Permit #27346 Philadelphia, Pa

POSTAGE WILL BE PAID BY ADDRESSEE

**analytical**
chemistry

P.O. BOX #7826
PHILADELPHIA, PA 19101

## NEED MORE INFORMATION?
## CIRCLE a key number. . .
## SEND IN the postage paid reply card. . .
## AND GET free data on any product advertised in this issue. . .

**APRIL 1985**

VALID THROUGH
AUGUST 1985

| | | | | | | | | | | |
|---|---|---|---|---|---|---|---|---|---|---|
| ADVERTISED PRODUCTS: | | | | | 1 | 2 | 3 | 4 | 5 | 6 |
| 7 | 8 | 9 | 10 | 11 | 12 | 13 | 14 | 15 | 16 | 17 |
| 18 | 19 | 20 | 21 | 22 | 23 | 24 | 25 | 26 | 27 | 28 |
| 29 | 30 | 31 | 32 | 33 | 34 | 35 | 36 | 37 | 38 | 39 |
| 40 | 41 | 42 | 43 | 44 | 45 | 46 | 47 | 48 | 49 | 50 |
| 51 | 52 | 53 | 54 | 55 | 56 | 57 | 58 | 59 | 60 | 61 |
| 62 | 63 | 64 | 65 | 66 | 67 | 68 | 69 | 70 | 71 | 72 |
| 73 | 74 | 75 | 76 | 77 | 78 | 79 | 80 | 81 | 82 | 83 |
| 84 | 85 | 86 | 87 | 88 | 89 | 90 | 91 | 92 | 93 | 94 |
| 95 | 96 | 97 | 98 | 99 | 100 | 101 | 102 | 103 | 104 | 105 |
| 106 | 107 | 108 | 109 | 110 | 111 | 112 | 113 | 114 | 115 | 116 |
| 117 | 118 | 119 | 120 | 121 | 122 | 123 | 124 | 125 | 126 | 127 |
| 128 | 129 | 130 | 131 | 132 | 133 | 134 | 135 | 136 | 137 | 138 |
| 139 | 140 | 141 | 142 | 143 | 144 | 145 | 146 | 147 | 148 | 149 |
| 150 | 151 | 152 | 153 | 154 | 155 | 156 | 157 | 158 | 159 | 160 |
| 161 | 162 | 163 | 164 | 165 | 166 | 167 | 168 | 169 | 170 | 171 |
| 172 | 173 | 174 | 175 | 176 | 177 | 178 | 179 | 180 | 181 | 182 |
| 183 | 184 | 185 | 186 | 187 | 188 | 189 | 190 | 191 | 192 | 193 |
| 94 | 195 | 196 | 197 | 198 | 199 | 200 | 201 | 202 | 203 | 204 |
| 05 | 206 | 207 | 208 | 209 | 210 | 211 | 212 | 213 | 214 | 215 |
| 16 | 217 | 218 | 219 | 220 | 221 | 222 | 223 | 224 | 225 | 226 |
| 27 | 228 | 229 | 230 | 231 | 232 | 233 | 234 | 235 | 236 | 237 |
| 38 | 239 | 240 | 241 | 242 | 243 | 244 | 245 | 246 | 247 | 248 |
| 49 | 250 | 251 | 252 | 253 | 254 | 255 | 256 | 257 | 258 | 259 |
| 60 | 261 | 262 | 263 | 264 | 265 | 266 | 267 | 268 | 269 | 270 |
| 71 | 272 | 273 | 274 | 275 | 276 | 277 | 278 | 279 | 280 | 281 |
| 82 | 283 | 284 | 285 | 286 | 287 | 288 | 289 | 290 | 291 | 292 |
| 93 | 294 | 295 | 296 | 297 | 298 | 299 | 300 | 301 | 302 | 303 |
| 04 | 305 | 306 | 307 | 308 | 309 | 310 | 311 | 312 | 313 | 314 |

| | | | | | | | | | | |
|---|---|---|---|---|---|---|---|---|---|---|
| EW PRODUCTS: | | | | 401 | 402 | 403 | 404 | 405 | 406 | 407 |
| 08 | 409 | 410 | 411 | 412 | 413 | 414 | 415 | 416 | 417 | 418 |
| 19 | 420 | 421 | 422 | 423 | 424 | 425 | 426 | 427 | 428 | 429 |
| 30 | 431 | 432 | 433 | 434 | 435 | 436 | 437 | 438 | 439 | 440 |
| 41 | 442 | 443 | 444 | 445 | 446 | 447 | 448 | 449 | 450 | 451 |
| 52 | 453 | 454 | 455 | 456 | 457 | 458 | 459 | 460 | 461 | 462 |
| 63 | 464 | 465 | 466 | 467 | 468 | 469 | 470 | 471 | 472 | 473 |
| 74 | 475 | 476 | 477 | 478 | 479 | 480 | 481 | 482 | 483 | 484 |
| 85 | 486 | 487 | 488 | 489 | 490 | 491 | 492 | 493 | 494 | 495 |

TO VALIDATE THIS CARD, PLEASE CHECK
ONE ENTRY FOR EACH CATEGORY BELOW:

**Intensity of product need:**
- ☐ 1. Have salesman call
- ☐ 2. Need within 6 mos.
- ☐ 3. Future project

**Primary field of work:**
- ☐ A. Energy
- ☐ B. Environmental
- ☐ C. Medical/Clinical
- ☐ D. Drug/Toiletries
- ☐ E. Forensic/Narcotic
- ☐ F. Biotechnology
- ☐ G. Metals
- ☐ H. Pulp/Paper/Wood
- ☐ I. Soaps/Cleaners
- ☐ J. Paint/Coating/Ink
- ☐ K. Electrical/Electronic
- ☐ L. Instrument Dev./Des
- ☐ M. Plastic/Polymer/Rub
- ☐ N. Agricultural/Food
- ☐ O. Inorganic Chemicals
- ☐ P. Organic Chemicals

**Primary area of employment.**

INDUSTRIAL
- ☐ A. Research/Development
- ☐ B. Quality/Process Control

MEDICAL/HOSPITAL
- ☐ C. Research/Development
- ☐ D. Clinical/Diagnostic

GOVERNMENT
- ☐ E. Research/Development
- ☐ F. Regulate/Investigate

COLLEGE/UNIVERSITY
- ☐ G. Research/Development
- ☐ H. Teaching

INDEPENDENT/CONSULTING
- ☐ I. Research/Development
- ☐ J. Analysis/Testing

**CIRCLE 314 FOR SUBSCRIPTION FORM TO ANALYTICAL CHEMISTRY**

NAME: ____________________

TITLE: ____________________

FIRM: ____________________

STREET: ____________________

CITY: ____________________

STATE: ____________________ ZIP: __________

PHONE: (___ ___ ___) ____________________

# Key Chemicals & Polymers
## New 6th Edition

One-page reviews packed with data on the current economic status and short-tern outlook for 42 large-volume chemical industry products.

The 42 products are:

**Acrylic**
**Ammonia**
**Benzene**
**Butadiene**
**Carbon dioxide**
**Caustic soda**
**Chlorine**
**Cyclohexane**
**DMT/PTA**
**Epoxies**
**Ethanol**
**Ethylene**
**Ethylene oxide**
**Formaldehyde**
**High-density polyethylene**
**Lime**
**Low-density polyethylene**
**Methanol**
**Nitrogen**
**Nylon**
**Oxygen**
**Phenol**
**Penolics**
**Phosphoric acid**
**Phosphorus**
**Polyester**
**Polyesters**
**Polypropylene**
**Polystyrene**
**Polyvinyl chloride**
**Potash**
**Propylene**
**Soda ash**
**Styrene**
**Sulfur**
**Sulfuric acid**
**Titanium dioxide**
**Toluene diisocyanate (TDI)**
**Urea**
**Vinyl acetate**
**Vinyl chloride**
***p*-Xylene**

**Chemical & Engineering News**
Distribution Dept.
1155 — 16th St., N.W.
Washington, D.C. 20036

Please send ______ copies of Key Chemicals & Polymers (6th Edition) at $5.00 per copy ($4.00 per copy for orders of more than 10). On orders of $20 or less please send payment with order. California residents add 6% sales tax.

☐ Payment enclosed ☐ Bill me

Charge my ☐ MasterCard
☐ VISA ☐ American Express

Card # ____________________

Interbank # ____________________
(MasterCard only)

Exp. date ____________________

Signature ____________________

Name ____________________

Address ____________________

City ____________________

State ______________ ZIP __________

**Call Toll Free 800-424-6747**

# Elemental analyses that mean business.

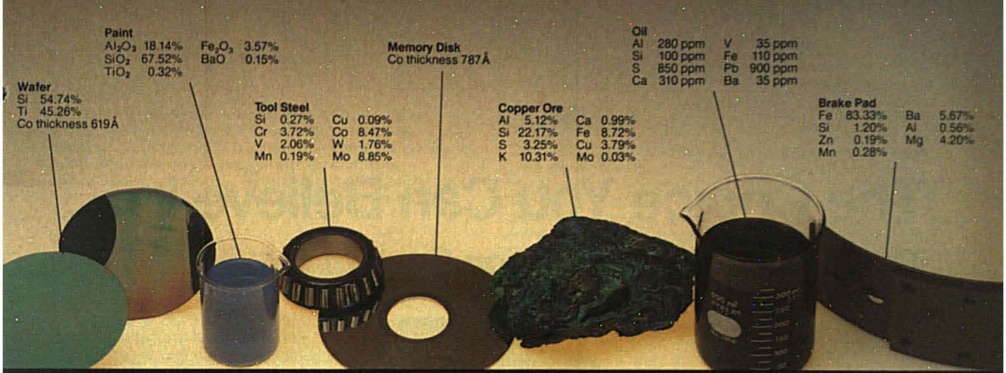
Paint
$Al_2O_3$ 18.14% $Fe_2O_3$ 3.57%
$SiO_2$ 67.52% BaO 0.15%
$TiO_2$ 0.32%
Wafer
Si 54.74%
Ti 45.26%
Co thickness 619Å
Tool Steel
Si 0.27% Cu 0.09%
Cr 3.72% Co 8.47%
V 2.06% W 1.76%
Mn 0.19% Mo 8.85%
Memory Disk
Co thickness 787Å
Copper Ore
Al 5.12% Ca 0.99%
Si 22.17% Fe 8.72%
S 3.25% Cu 3.79%
K 10.31% Mo 0.03%
Oil
Al 280 ppm V 35 ppm
Si 100 ppm Fe 110 ppm
S 850 ppm Pb 900 ppm
Ca 310 ppm Ba 35 ppm
Brake Pad
Fe 83.33% Ba 5.67%
Si 1.20% Al 0.56%
Zn 0.19% Mg 4.20%
Mn 0.28%

## The field-proven TEFA™ Monitor energy dispersive x-ray fluorescence analyzer.

The TEFA Monitor has what it takes to get down to the business of sample analysis for elemental composition, film thickness and material uniformity.

Versatile, fast and accurate, TEFA Monitor nondestructively and automatically analyzes inorganic samples—large and small. Solids, liquids or powders with quantitative and qualitative results you can trust. And the kind of reliability all types of industries have depended upon for years.

Only the Monitor with computer control provides simple push-button analysis...even for "unknowns."

Unique regression analysis (ATAC) and fundamental parameter (FPT) software automatically recalibrate and determine elemental composition. With no standards, one standard or a suite of standards—within minutes.

A wide dynamic range permits analysis from a few parts per million to 100%. All data is stored for immediate recall or comparative analysis.

And only the Monitor with its unique "X-Y" scanning feature can compare concentrations at one point on the sample surface with those at other points.

To support TEFA Monitor for your operation, EG&G ORTEC has fully functional applications laboratories staffed by experienced analytical chemists. Answers to any question about x-ray fluorescence analysis are just a phone call away.

We'd like to show you how the TEFA Monitor can benefit your application. Mail the coupon below and we'll send an application study for your sample type. Or call (615) 482-4411. Chances are you'll want to put x-ray fluorescence to work in your business.

☐ Yes! I'd like to know more about XRF and the TEFA Monitor.

☐ Yes! Please send me an Application Report for my ________ sample(s).

Name ____________________

Title/Position ____________________

Firm Name ____________________

City ____________________ State ________ Zip ________

Phone ____________________

Mail to: TEFA Monitor, EG&G ORTEC, 100 Midland Road, Oak Ridge, TN 37830

**EG&G ORTEC**

We put x-ray fluorescence to work.

CIRCLE 51 ON READER SERVICE CARD

SIEMENS

# The Choice You Can Believe In

## The D 500 X-ray Diffraction System

X-ray diffraction has become one of the most important and necessary tools for solving analytical and research problems in laboratories throughout the world, and the Siemens D 500 diffractometer provides the universal capabilities for satisfying the widest range of applications.

The D 500 is the one system that combines a wide selection of accessories with a comprehensive but user-oriented software package that enables you to perform routine powder diffraction analysis in production, control or sophisticated research by the addition of options, such as stress, texture, high-temperature, and Theta-Theta diffractometry — or dramatically speed up the analysis with the addition of a position sensitive detector.

Already operating in numerous laboratories worldwide, the D 500 is evidence of Siemens commitment to satisfying all your present and future needs in x-ray diffraction. Siemens is the choice that you can believe in for x-ray diffraction systems. For more information write or call: Siemens AG, Analytical Systems E 689, D 7500 Karlsruhe 21, P.O. Box 21 1262, Federal Republic of Germany, Tel: (0721) 595-2425, Telex: 7826851.
Siemens-Allis, Inc., Analytical Systems, One Computer Drive, P.O. Box 5477, Cherry Hill, NJ 08034, (609) 424-9210.

**Siemens. . . The company you can believe in.**

CIRCLE 186 ON READER SERVICE CARD

# FOUR FRACTION COLLECTORS AREN'T TOO MANY IF YOU'RE TRYING TO PLEASE 98,579 SCIENTISTS.

All four let you enter fraction size by time, drop, volume — even directly in ml if you have an ISCO WIZ peristaltic pump. ISCO fraction collectors are coldroom proof and hold any common test tube or mini scintillation vial. All but Cygnet also hold 28 mm vials, have LED readouts, and can collect from multiple columns.

## Workhorses

The Retriever III is our fraction collector for big jobs. It can hold 25 mm (70 ml!) tubes, and carries up to 380 smaller tubes.

Retriever II is the ISCO medium-capacity linear fraction collector. It holds up to 174 tubes but needs only a square foot of your bench space—perfect for crowded labs. We've made about 20,000 instruments using the patented Retriever linear mechanism and many are still going strong after 15 years!

## Budget

Cygnet is by far the least expensive fraction collector you can buy. Yet it still has all the basic features including drop counting. Stainless steel reels hold 100 tubes in a big range of sizes.

## Smart

FOXY™ matches fractions to your chromatogram—not to the clock. It rejects void volumes, locates and saves desired peaks, and controls valves and pumps to make gradients or automate your system. For HPLC, collect successive injections without resetting, and overlay repeated injections of the same sample to collect identical peaks in the same tubes. The sloped keyboard, 12-digit display, and logical programming make it all easy to do.

You can't beat an ISCO fraction collector for reliability, capability, or price. And you can't match the ISCO 3-year warranty. Phone toll-free [800]228-4250 for our complete catalog. Or write ISCO, P.O. Box 5347, Lincoln, NE 68505.

CIRCLE 103 ON READER SERVICE CARD

ISCO

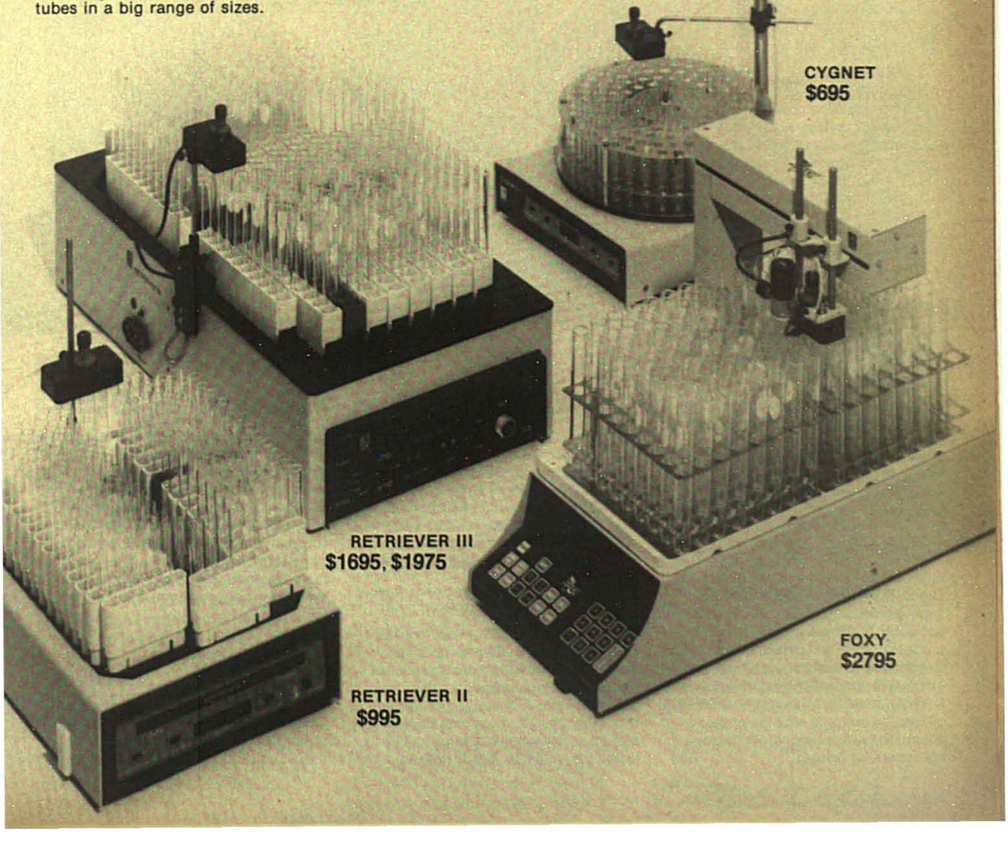

# New Products

### Surface analyzer

Model 4175 Rutherford backscattering surface analyzer provides routine nondestructive surface and depth analyses of any element from Li to U within 0.001% to 1% atomic detection limits. It furnishes quantitative results without calibration standards, and data acquisition is complete in less than 15 min per sample. General Ionex Corp. **405**

### GC

Model 3000's microprocessor controls temperature and detector electronic functions and is compatible with most data-handling systems. Options include subambient oven temperature control, up to four detectors (thermal conductivity, flame ionization, helium ionization, universal plasma ionization, thermionic electron capture, flame photometric, and chemiluminescent nitrogen), and capillary capability with on-column or split-splitless operation. Antek **406**

### Hydrogen safety system

HSS-4 consists of one central unit, placed anywhere in the lab, and from one to four satellite units that are placed near a GC. Satellites continuously measure $H_2$ concentration in the GCs and compare it to an alarm level. If this level is reached, an audible alarm is given on the central unit and power to that GC is shut off; operation of the other GCs continues uninterrupted. Chrompack **407**

### X-ray fluorescence

Extra II total-reflection X-ray fluorescence TXRF system consists of an X-ray generator, Si(Li) detector, and a computer-based analyzer system for process control and data analysis. It can detect elements in the picogram range, and applications include mineral analysis; trace metal detection in water, oil, and grease; and analysis of blood serum, tissue specimens, and biological materials. Scintag **408**

**TiterCalc** acquires, displays, processes, and stores data from ELISA readers, improving accuracy and reducing the time and effort necessary to transcribe and handle ELISA reader data. Operations that currently require about 1½ h to perform manually are completed in less than 2 min. HP Genenchem **403**

### UV–VIS spectrophotometer

UV 160 has a scanning speed of 2400 nm/min over the entire 200–1100-nm wavelength range. Other features include full-wavelength-range baseline correction within 1 min, full spectral manipulation, no baseline drift, wide range of quantitative functions, and modular convenience. Shimadzu **409**

### Multiport stream switch

MUST, designed to allow easy column switching in HPLC, permits heart cut, stripper, and backflush configurations. Two six-way high-pressure valves are activated independently, either manually or by a timer, and optional six-way solvent selector valve and manual injector are available. Spark Holland **411**

### Data-handling system

Labtec is a dedicated hardware and software system for food and feed laboratories. It consists of a central unit to which one or more satellite units can be linked and interfaced to balances and analytical instruments. Software routines for sample logging; reporting of results; and Kjeldahl, fat, fiber, and moisture analyses are provided. The system is user programmable. Tecator, Inc. **412**

---

**For more information on listed items, circle the appropriate numbers on one of our Readers' Service Cards**

---

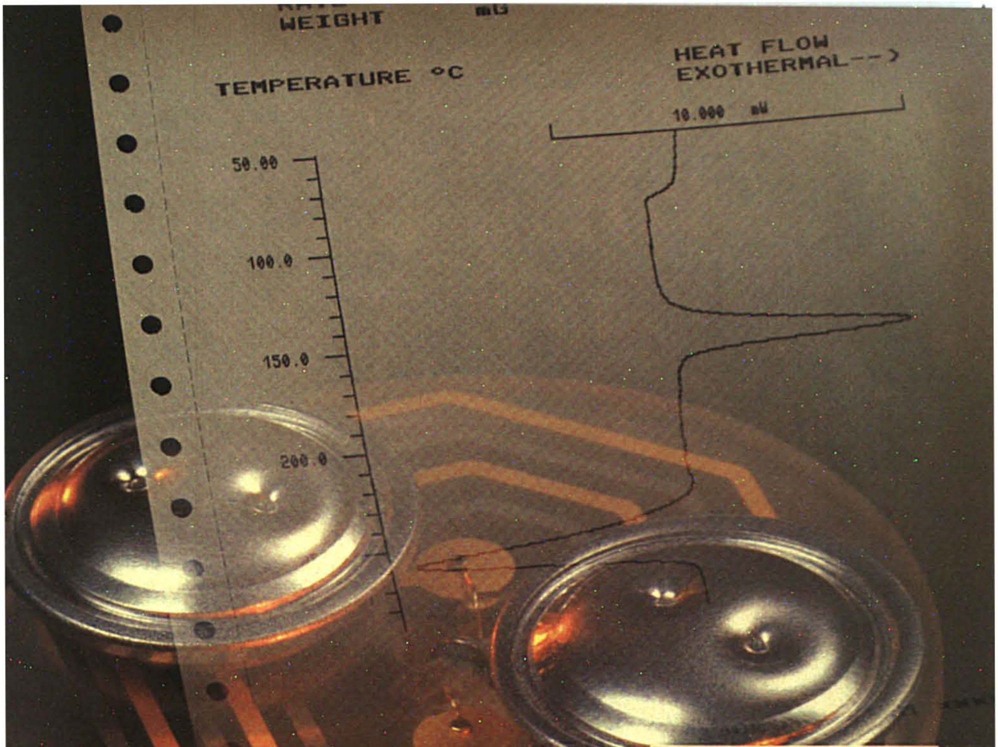

Mettler TA3200 System for DSC. Only $24,500...complete.

## Mettler Thermal Analysis.
## Gets you from problem to solution...every time.

***A measuring and evaluation system all in one.***
At last, your thermal analysis problems can be solved completely—down to the digital result—with one compact, inexpensive system. The Mettler TA3000 with powerful, new features.

Forget cumbersome manual and external computer data manipulation.

Instead, simply help yourself to indisputable, clear numeric interpretation of the measuring curve.

***New. The TC10A Processor.***
The heart of Mettler's TA3000, the TC10A, is the evaluation and control center for unique DSC, TMA and TG measuring modules.

Its comprehensive and advanced utilization of integral software enables automatic calibration, storage of methods and data, plotting and processing of information for each.

***Unique measuring modules.***
The DSC30 is the only DSC cell designed for full range work: -170°C to +600°C. It provides unsurpassed baseline stability and temperature control. The fully electronic TMA40, with static and dynamic load capability, features 4.5 nm resolution. It even measures absolute sample thickness. Utilizing Mettler's M3 microbalance, the TG50 assures easy, stable and accurate measurements.

***New. Personal computer interface.***
Should you need greater storage capacity, either for additional methods or later data retrieval, the TA3000 supplies a bidirectional RS232C port.

***New. Rugged metal sensor.***
There's even an extraordinarily rugged metal sensor for measuring accuracy in the harshest test conditions.

The TA3000 is everything you need for thermal analysis. See it by calling (609) 448-3000. Mettler Instrument Corporation, Box 71, Hightstown, NJ 08520. You'll be glad you did.

Mettler.

Breakthrough
in
BIOPOLYMER
SEPARATIONS

By using Shandon Wide-Pore packing materials, it is now possible to separate biopolymers in minutes using existing HPLC equipment.

- Pre-packed columns for separations of peptides, proteins and polynucleotides.
- Available in $C_4$ or $C_8$ fully endcapped bonded phases.
- Excellent recoveries.

Call or write for our **free** Wide-Pore literature.

**SEE US AT FASEB BOOTHS 1343-1345**

**SHANDON**

**Shandon Southern Instruments, Inc.**
515 Broad Street, Drawer 43
Sewickley, PA 15143
Phone 800/245-6212 (In PA 412/741-8400)

CIRCLE 190 ON READER SERVICE CARD

## New Products

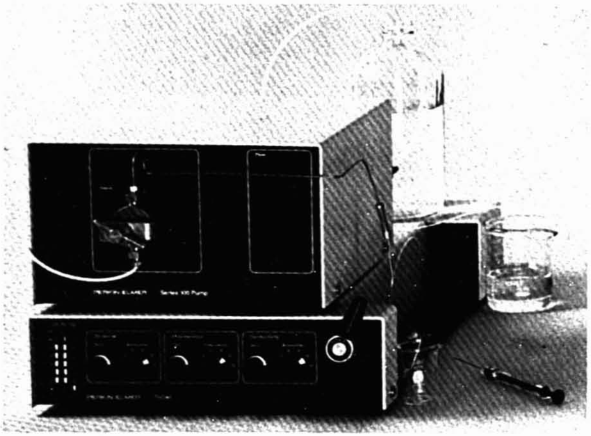

**3D HPLC system** is an isocratic HPLC system with simultaneous UV, conductivity, and fluorescence detection provided by a trifunctional detector. Applications include ion chromatography, content uniformity tests on tablet analgesics, monitoring of derivatized amino acids and phenols, and detection of therapeutic drugs and water-soluble vitamins. Perkin-Elmer **402**

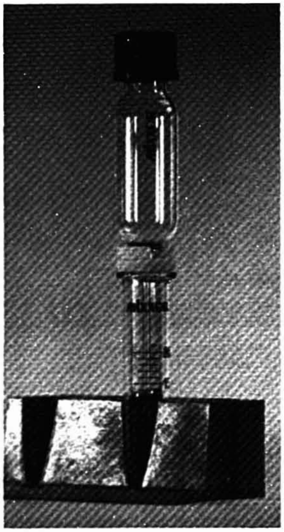

**Mixxor separatory cylinder** for liquid–liquid extractions is available in 2-, 5-, 10-, and 50-mL sizes. It consists of a lower mixing chamber and a piston–reservoir with an axial channel. Six piston strokes equal 40 separatory funnel shakes. After phase separation the upper phase can be poured into a container, and the lower phase is held in the Mixxor by capillary effect. Lidex Technologies, Inc. **401**

### GC

Model 9630 offers an optional multipurpose second column oven that makes possible simultaneous multiple analyses that cannot be accomplished with two or more separate GCs. It can be fitted with injectors, detectors, and heating blocks controlled by the host GC. Subambient oven temperature control and data system are available. IBM Instruments **410**

### GC detector

Flame photometric detector for the Sigma 2000 GC is sensitive to subnanogram quantities of sulfur and phosphorus compounds. It is also highly selective for these compounds. It is 10,000 times less sensitive to hydrocarbons than to sulfur compounds. Applications include analysis of sulfur- or phosphorus-containing pesticide residues and monitoring of ambient air and furnace stacks. Perkin-Elmer **413**

### Ozone monitor

Model 727-3, which is based on the UV absorption technique of ozone determination, measures ozone specifically; common gases occurring in ambient air will not interfere. Electronic circuitry automatically monitors and controls UV source drift and corrects instrument span over each sample–reference measurement cycle. Digital readout of 0.01 to 9.99 ppm is provided. Mast Development Co. **414**

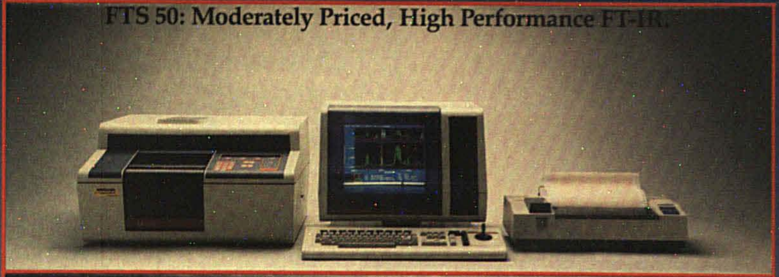

FTS 50: Moderately Priced, High Performance FT-IR.

FTS 60: High Performance With Research Quality GC/IR.

FTS 80: Our Most Powerful And Versatile FT-IR Spectrometer.

# DIGILAB FT-IR: RESEARCH GRADE PERFORMANCE IN THREE NEW CONFIGURATIONS

When you buy one of the three new FTS spectrometers shown above, you are buying a spectrometer that is discriminating enough to resolve even minor spectral components, sensitive enough to detect trace concentrations and fast enough for GC/IR and kinetics.

Research grade performance, applications experience, customer support, value…when you buy a Digilab FTS spectrometer, you are getting one of the industry's finest instruments.

For literature, send the coupon today to Bio-Rad, Digilab Division, 237 Putnam Avenue, Cambridge, MA 02139. Or call TOLL FREE (800) 225-1248.

Name Title:

Affiliation:

Street & No.:

City & State: Zip: Telephone: ( )

Applications:

Please send me a brochure on the (check one): FTS 50: ______ FTS 60: ______ FTS 80: ______

BIO-RAD Digilab Division

CIRCLE 20 ON READER SERVICE CARD

### GC

Model 412 GC, designed for the analysis of naphtha-type samples, can separate paraffins, naphthenes, and aromatics. It analyzes components by carbon number below the 200 °C boiling point and also analyzes components up to 275 °C in the backflush mode. Handling of $CO_2$ is eliminated by a Tenax trap. Packard Instrument Co. **415**

## Chemicals

### $^3$He

$^3$He is available in isotopic purities ranging from 99.9% up to 99.9995% or better. Applications include low-temperature physics, laser gas mixtures, and use in neutron detection equipment. Cambridge Isotope Laboratories **417**

### SRM

SRM 1586, Isotopically Labeled and Unlabeled Priority Pollutants in Methanol, can be used to test methods requiring the combined use of GC/MS and isotopically labeled internal standards. It is composed of two solutions: one containing 10 priority pollutants at $\mu g/g$ levels in methanol and the other containing the same compounds labeled with deuterium or carbon-13 at approximately the same concentrations in methanol. NBS **418**

### RM

RM 8409, Simulated Rainwater, is designed to aid in the analysis of acidic rainwater by providing a stable, homogeneous material as a control standard. It consists of two 50-mL solutions prepared by dissolving high-purity salts and acids in high-purity distilled/deionized water. Nominal pH of Level I is 4.3; that of Level II is 3.6. Acidity, specific conductance, and nominal concentrations of several major anions and cations are provided. NBS **416**

## Software

### Data acquisition and analysis

RS/1, BBN's data analysis system, includes data management and analysis, curve fitting, statistics, graphics, modeling, and reporting. Labtech Notebook is Laboratory Technology's package for data acquisition, monitoring, and real-time control. The systems have been integrated and run on the IBM PC XT and AT. BBN Software Products Corp. and Laboratory Technologies Corp. **420**

### IR spectrometry

Spectrafile is menu driven, runs on the Apple II+/IIe microcomputer, and will interface with any IR spectrophotometer that has an RS-23 or IEEE interface. It provides instrument control and allows data acquisition, storage, recall, and post-run analysis of spectra. Heyden Datasystems **421**

### Spectrophotometers

Data Capture Software interfaces the DU-50 series spectrophotometer with the IBM PC. Special features include real-time color graphics for wavelength, kinetics, and gel scans; spectral manipulation, including addition and subtraction; and instrument parameter setup by remote control from the computer. Beckman Instruments, Inc. **422**

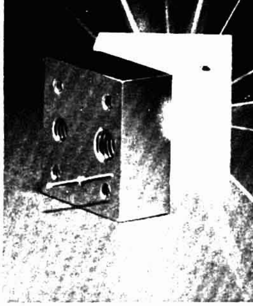

In LCEC, the DIFFERENCE is BAS!

**Versatility** Fraction Collection • Low Dead-Volume Cells for Microbore Chromatography • Chemically-Modified Electrodes • Single or Dual Electrode LCEC

**Sensitivity** It's not just how big the signal, but the signal-to-noise that counts! Amperometry is the only way to go, sooner or later all our imitators realize that.

**Selectivity** BAS offers different electrode materials tailored to individual reactions. BAS offers single or dual electrodes (in 2 configurations!). Why limit yourself to just one type of LCEC application when there are hundreds of possibilities? BAS has the technology, NOW!

**Support** BAS offers the largest, and best respected, LCEC research group in the world. We're the ones who have published over a hundred original papers in refereed scientific journals. BAS offers on-site and factory training courses. Our full line of COMPLETE LCEC analyzers are designed specifically for the needs of electroanalytical chemistry. Our applications notes are so good, everyone else copies them!

Are you considering the advantages of LCEC? Why not go with the leaders? In LCEC, the difference is BAS!

BAS
2701 Kent Ave
West Lafayette
Indiana 47906

Telex: 276141
(317) 463-4527

CIRCLE 16 ON READER SERVICE CARD

## All that you can ask for in a spectrophotometer.

Scientific and technical problems, today, demand quick, accurate analytical computation for their solution. Gilford meets the needs of laboratory research with the finest in analytical systems.

The Response™ spectrophotometer, by Gilford, combines photometric, optical and microprocessor technology to assure you of highly accurate, consistently reliable measurements.

**Standard features include:**

- Wavelength and time scanning, kinetics, multi-wavelength analysis and curve fitting routines.
- Graphic and tabular data display via high resolution CRT.
- Microprocessor controlled absorbance and wavelength calibration routines.
- Program storage and data storage to 10,000 points. RS-232C computer interface.
- Video copier for a publication quality hard copy.

## Response™ from Gilford.

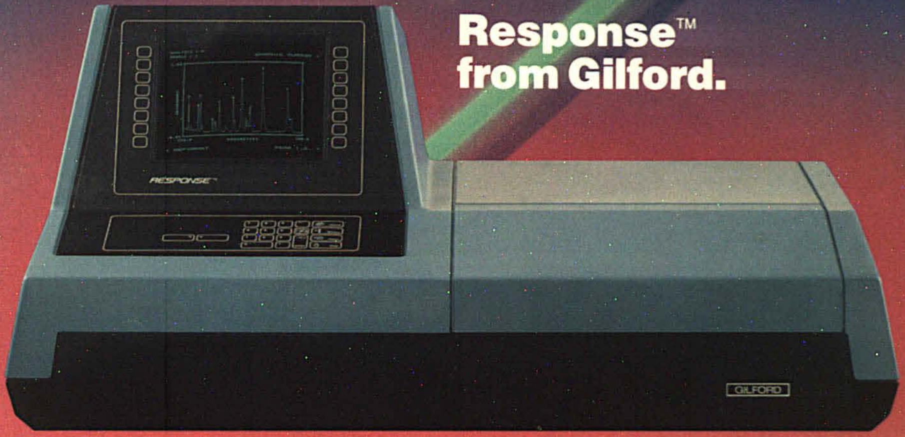

Circle 35 on Reader Service Card

### A combination of sophistication and efficiency.

Response™ was designed with the interaction in mind with easy-to-operate controls, dedicated function keyboard, function changing dynamic keys and a convenient, transverse sample compartment that accepts accessories including six-position cell holders, 20cm gel and film scanners and a rapid sampler.

NO POSTAGE
NECESSARY
IF MAILED
IN THE
UNITED STATES

**BUSINESS REPLY CARD**
FIRST CLASS PERMIT NO. 36 OBERLIN, OHIO

POSTAGE WILL BE PAID BY ADDRESSEE

**GILFORD**
**A CORNING Laboratory Sciences Company**
132 Artino Street
Oberlin, Ohio 44074-9984
U.S.A.

# Other fine analytical instruments in the Gilford line include...

**Fluoro IV™**
The Fluoro IV combines measuring power, flexibility, and simplified operation in a single instrument that meets customer requirements for both maximum sensitivity and reproduceability. It features dual monochromators for excitation, emission or synchroscanning, a 4-position thermostatted cell holder and an RS-232C interface. An optional printer/plotter allows both tabular and graphical data presentation.

**Series 260 UV/VIS Research Spectrophotometer**

The Gilford Model 260 Spectrophotometer is a UV/VIS instrument for the most rigorous analytical measurements. High resolution is achieved through narrow bandwidth operation in the wavelength range of 190 - 900nm. Absorbance or concentration data is presented on an LED display. This information can also be routed to an optional printer or recorder. A convenient optical bench rod system allows quick changeover from the standard 4-position cuvette holder to either a rapid sampler or gel scanner. Electronic temperature control at selectable fixed temperatures is available for the cuvette positioner or rapid sampler. These capabilities are also available in the Model 252 Modernization System.

**Stasar®**
The Gilford Stasar reference spectrophotometer provides absorbance or concentration data throughout the wavelength range of 335 to 700nm. The aspiration flow cell has a temperature range of 25 to 37°C and can be controlled to within ± 0.1°C for sensitive temperature dependent measurements. An optional printer or recorder can provide permanent data presentation.

Circle 36 on Reader Service Card

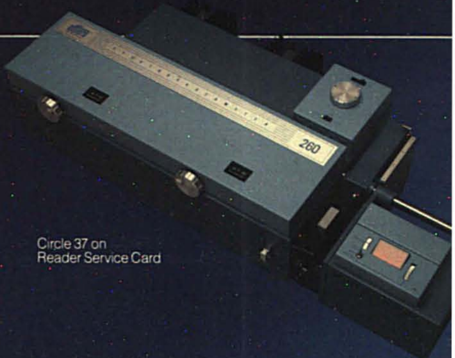

Circle 37 on
Reader Service Card

Circle 38 on
Reader Service Card

*I am interested in additional information about the following Gilford instruments:*

- ☐ Response™ Spectrophotometer
- ☐ Series 252 UV/VIS Modernization System
- ☐ Series 260 UV/VIS Spectrophotometer
- ☐ Fluoro IV™ Scanning Spectrophotometer
- ☐ Stasar Spectrophotometer

NAME ____________________

TITLE ____________________

COMPANY ____________________

ADDRESS ____________________

CITY ____________ STATE ________ ZIP ________

( )
AREA CODE, TELEPHONE ____________________

**GILFORD**
132 Artino Street
Oberlin, Ohio 44074-9984
800-221-7527

**For more information about Gilford analytical instruments, fill out this card and drop it in the mail today!**

Gilford
a CORNING
Laboratory Sciences Company

PrepSep
Extraction Columns

# Pour it on

## and Clean It Up with PrepSep™ Solid Phase Extraction Columns

**PrepSep column's unique conical shape** lets you pour your sample directly into the large 10mL sample reservoir. Permits easy sample addition and large sample volume. Made of polypropylene, with 300mg of selected packing sandwiched between two 20μm pore size polyethylene frits.

**Fast, easy extraction and elution** of pesticides, dyes, parabens, phthalate esters, and many other organic compounds. Speed up sample cleanup for HPLC, GC, TLC, and UV analysis, without jeopardizing separations. They replace many preparative techniques, even tedious liquid-liquid extractions.

**Six versatile packings:** Five are bonded-phase silica: $C_1$, $C_8$, $C_{18}$, cyano, and amino. The sixth is pure uncoated silica gel. All are 40μm particle size. Packing type is conveniently marked on upper rim of each column.

**Three convenient ways to achieve fast flow:** 1. Connect PrepSep column to a syringe via tubing and use the syringe's plunger to draw eluent through the packing. 2. Insert PrepSep column into a vacuum box to pull the eluent through the packing, into a test tube. 3. Place PrepSep column into a centrifuge tube. Use centrifuging speed and time to control rate and amount of sample flow through the packing.

**Each PrepSep column is individually sealed** for protection against contamination and moisture. They're inexpensive enough to be truly disposable, eliminating cross-contamination and messy cleanups.

**For more information,** including extraction procedures and analytical results using PrepSep columns, use Reader Service Number. Or write Fisher Scientific, 711 Forbes Ave., Pittsburgh, PA 15219.

ALLIED Fisher Scientific

CIRCLE 58 ON READER SERVICE CARD

# Manufacturers' Literature

**HPLC software.** Brochure describes the Data Master HPLC system software with combined gradient control and data analysis functions. Analysis functions include real-time and post-run quantification of peaks, automatic analysis and storage of multiple runs, and multilevel calibration; control functions include solvent and flow programming and automatic sample integration with sample injection. 11 pp. Gilson Medical Electronics 425

***Teknivent News.*** Volume I features articles on low-cost work stations for chromatography and mass spectrometry based on the IBM PC, a new data system to automate Hewlett-Packard mass spectrometers, and upgraded equipment for Finnegan 6000 series data systems. 4 pp. Teknivent 426

**"Topics in SIMS."** Topics covered in a series of short technical notes include validation of SIMS data, dopant concentrations near the $SiO_2$ interface, effects of primary ion energy and angle of incidence on yield, and profile distortions in SIMS depth profiling. Atomika, Inc. 427

**"Lock-In Applications Anthology."** Use of lock-in amplifiers in a variety of low-level signal measurements is illustrated. The booklet contains 20 application notes and is divided into six sections covering solid-state, spectroscopic, electrochemical, mechanical, instrumental, and engineering applications. 76 pp. EG&G Princeton Applied Research 428

**UV-VIS spectrophotometer.** Data sheet details the Lambda 1A instrument, which is designed specifically for quantitative applications and offers three operating modes, nine memory locations, and integration of absorbance value. Instrument specifications are listed along with available accessories. Perkin-Elmer 429

**Nonmetallic safety containers.** Literature describes use, capacity, and dimensions of Type I and Type II cans, oval cans, plunger cans, dispenser cans, disposal cans, and corrosives cans. 4 pp. Justrite Manufacturing Co. 430

**Elemental analyzer.** Brochure describes the Erba Model 1106 analyzer, which can perform 50 CHN, O, and S determinations in 6 h. A schematic diagram of the system is shown together with detailed explanations of operating principles, the instantaneous combustion–reduction system, detector, autosampler, chromatographic columns, and data processor. 7 pp. Erba Instruments, Inc. 431

**Food and beverage analysis.** Technical guide includes 21 methods for the use of pH and ion-selective electrodes in food and beverage analyses. Also included are information on measurement techniques, how to measure on a per-sample basis, temperature problems affecting pH, and a bibliography. 50 pp. Orion Research 432

**Optical multichannel spectrum analyzer.** Booklet discusses the features of the TN-6500 analyzer's diode array parallel detector system and their relation to stopped-flow, chemical kinetics, plasma etch, HPLC, UV-VIS, absorbance, Raman, and fluorescence applications. 20 pp. Tracor Northern 433

**Quick couplings.** Guide covers fittings, available in thermoplastic and metal, that can handle vacuum and pressure lines up to 120 psi (250 psi for metal) at −40 to 180 °F. It also points out when metal or plastic fittings are appropriate, and describes straight-through and automatic shutoff couplings, special manifolds, and multiple mountings that can handle up to 10 flexible lines in a single connector. 28 pp. Colder Products Co. 434

**Preparative LC.** Literature features an industrial system for process purification using both HPLC and LC at flow rates up to 100 L/h. The completely automated pump, detector operation, and microprocessor-based fraction collection package can be self-contained on a mobile LC bench. ISCO 435

**For more information on listed items, circle the appropriate numbers on one of our Readers' Service Cards**

***The Wescan Ion Analyzer.*** No. 8 features articles on pharmaceutical analysis, acid and plating bath analysis, pulp and paper analysis, and tips on column and eluant selection. 8 pp. Wescan Instruments, Inc. 436

## Catalogs

**Laboratory supplies.** Catalog 133 details instruments, apparatus, furniture, vacuum pumps, chemicals, and supplies. 1744 pp. Sargent-Welch 438

**Plasticware.** Catalog includes a guide to the structure and properties of resins, a chart of the chemical resistance of plastic resins, and a guide to the use and care of plasticware. 96 pp. Cole-Parmer 439

**Specialty gases and equipment.** Descriptions, illustrations, and specifications for pure, mixed, and electronics gases are featured. Also detailed are equipment and instrumentation used in GC, basic and industrial research, calibration procedures, and gas handling. 192 pp. Airco 440

**1985 price list.** Catalog is divided into sections covering products for chromatography, HPLC and IC, electrophoresis and molecular biology, and assays. 256 pp. Bio-Rad 441

**FT-IR/IR accessories.** Brochure includes IR solid-, liquid-, and gas-sampling accessories, IR reflectance devices, microsampling devices, accessory kits, and a guide to material selection. 17 pp. Janos Technology 442

**Separation supplies.** Catalog offers a complete line of hardware and supplies for HPLC, GC, TLC, column chromatography, electrophoresis, and tissue culture. American Laboratory Supply Co., Inc. 443

**Chemicals.** 1985 catalog features 1400 new products, including chemicals, lab equipment, liquid–liquid extractors, models, carbon-13 labeled compounds, and NMR supplies. 40 pp. Aldrich Chemical Co. 444

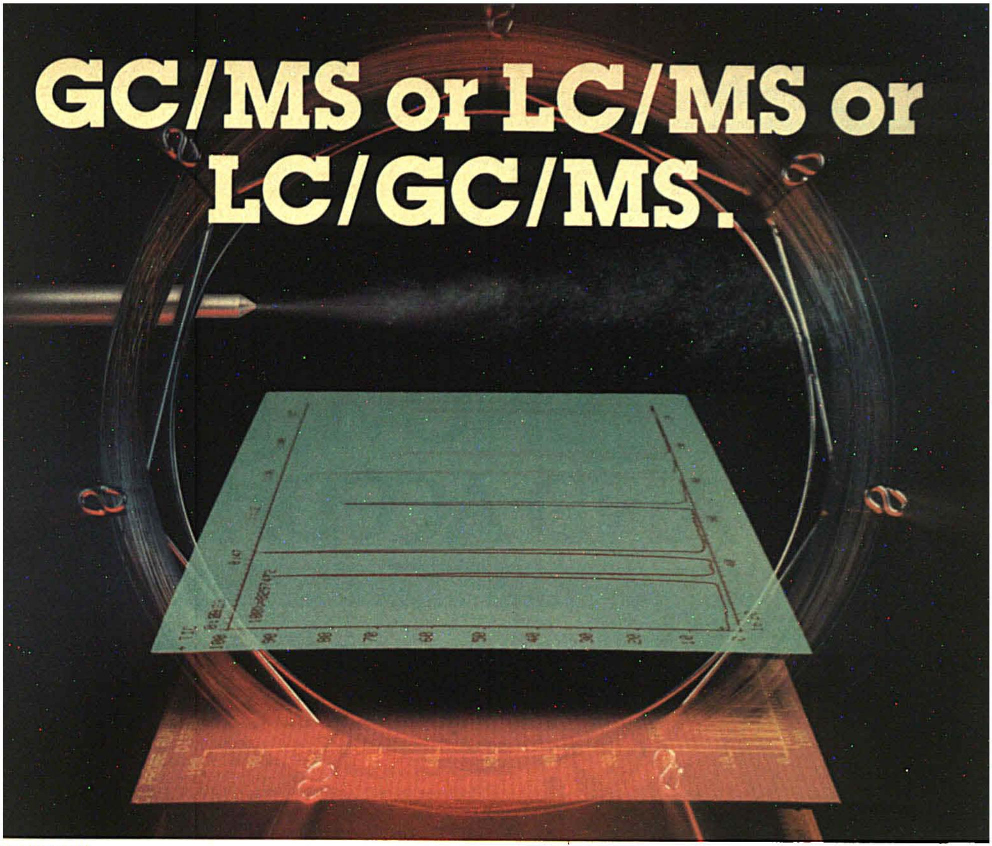

© Spectros Int'l 1985

# Your Choice.

The world's first *truly dedicated LC/MS system* is here. It integrates the best of Kratos MS with the best of Kratos LC via a unique thermospray interface. The Kratos MS 25 RFA also comes in a dedicated GC/MS or an integrated LC/GC/MS version. *All with MS facilities* not normally found in other routine systems. And all come with an automation package second to none in power and speed. The DS 90 color data system controls all instrument parameters, gives you convenient menu operation and easy to read, full color reports. *If the concept of integration in LC/MS or GC/MS or both, has appeal,* you must look into the MS 25 RFA. Ask for our new color brochure or a demo. Your choice. Kratos Analytical, 170 Williams Drive, Ramsey, NJ 07446.

*New dedicated LC/MS 25 RFA*

*New dedicated GC/MS 25 RFA*

**MS 25—the alternative with magnetism.**

KRATOS
ANALYTICAL
a division of SPECTROS

CIRCLE 120 ON READER SERVICE CARD

# SNOW PEAS AND ACEPHATE

## CONFIRMATION OF ILLEGAL PESTICIDE RESIDUES

There can be no doubt that chemical technology has greatly advanced the world's standard of living while simultaneously introducing a potential threat to the health of society. The legal, intelligent application of insecticides and fungicides to curb infestations and thereby increase crop yields accounts for a multibillion-dollar industry. Intensive legislative activity over the past two decades has dramatically increased the role of analytical chemistry in protecting the public health. Nowadays, therefore, the emphasis routinely placed on trace analysis of the food supply has mandated a new strategic analytical approach. The primary method of analysis is usually acetone extraction and methylene chloride partitioning followed by gas chromatography (GC) on various stationary phases (nonpolar, semipolar, and polar) with various detectors (P, S, N, Cl, etc.). During such regulatory analysis of the nation's food supply to ensure compliance with registered uses, violations are encountered that demand confirmation of a particular residue by mass spectrometry (MS).

We describe a recent domestic situation in which snow peas from a large number of individual growers in the same area in California were found to contain acephate. These findings revealed an unregistered use of acephate, i.e., no legal residue level had been established for snow peas. Under such circumstances, a scientifically supportable analytical determination of this residue is necessary if regulatory action is to be considered. Primary detection of the residue was made via GC with a flame photometric detector for phosphorus (FPD–P) followed by confirmation via GC/MS using ammonia chemical ionization (CI) and single ion monitoring (SIM).

Acephate (*O,S*-dimethyl acetylphosphoramidothioate) (I) (Figure 1) is a popular systemic insecticide widely used in the U.S. (more than three million pounds per year) in controlling a broad spectrum of arthropod pests of plants. Foliar studies on acephate in the cotton plant have revealed the ma-

This article not subject to U.S. Copyright
Published 1985 American Chemical Society

**Thomas Cairns**
**Emil G. Siegmund**
**Gregory M. Doose**
**Andrew C. Oken**
Department of Health and Human Services
Food and Drug Administration
Office of Regulatory Affairs
1521 West Pico Blvd.
Los Angeles, Calif. 90015

jor metabolite (9%) to be methamidophos (*O,S*-dimethyl phosphoramidothioate) (II) with two other metabolites (III and IV) at much lesser concentrations (<5%). Although acephate and methamidophos are of toxicological significance (i.e., cholinesterase-inhibiting compounds), the other metabolites pose no such threat.

Tolerances have been established for acephate on various raw agricultural commodities at concentration levels ranging from 0.1 to 10 ppm. At present, however, tolerance levels of acephate have been limited to such commodities as lettuce, celery, peppers, soybeans, beans, meat (including poultry), raisins, milk, and eggs. Although the potential theoretical dietary exposure is well below the acceptable daily intake of 0.2 mg/kg body weight/day set by the Environmental Protection Agency, the increased detection of acephate and methamidophos residues by this laboratory on both domestic and imported produce warranted continued surveillance for acephate and its metabolites.

## Gas chromatography

During routine surveillance monitoring of a large number of domestic and imported crops for pesticide residues, a sample of snow peas was initially determined to contain acephate (Figure 2).

In addition to acephate, its major metabolite, methamidophos was also detected, together with dimethoate and its oxygen analog (retention time of 3 min). The other response appear ing just before the elution of methamidophos was due to elemental sulfur; the peak at 1.5 min is an unknown

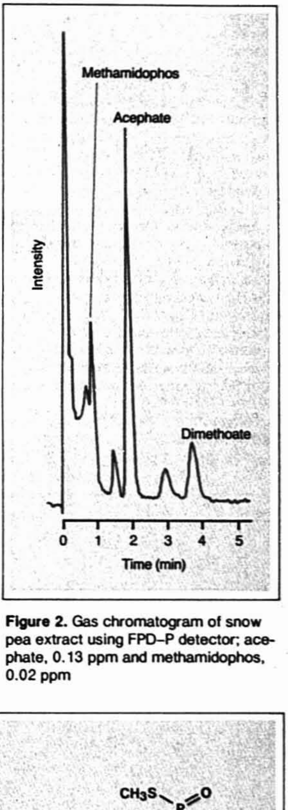

**Figure 2.** Gas chromatogram of snow pea extract using FPD–P detector; acephate, 0.13 ppm and methamidophos, 0.02 ppm

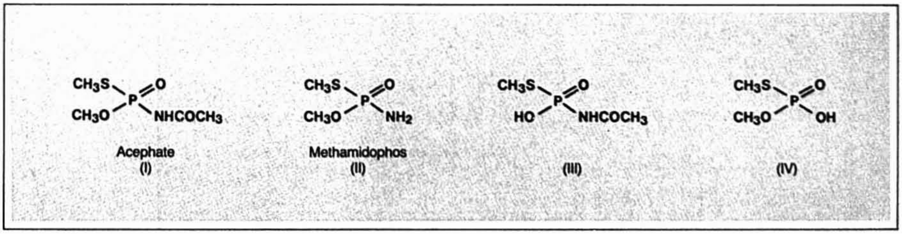

**Figure 1.** Structures of acephate and its metabolites

analytical response. This incidence of acephate on snow peas indicated an unregistered use, and further investigation into pesticide application in the general growing area was conducted.

Initially 119 samples were collected, each representing a different grower within the same general locale as the original sample found to contain acephate. The wide range of residue levels detected in the snow pea extracts indicated variations in the time of application. Clearly, the highest levels (four samples containing levels from 0.21 to 0.75 ppm) represented spraying with acephate just prior to harvest whereas extracts within the range 0.06–0.20 ppm (seven samples) could have resulted from spraying at least three days prior to harvest. Twenty samples (0.01 to 0.05 ppm) had obviously been sprayed with acephate at least one week before harvest. In 88 samples, no acephate was detectable below the instrumental level of detection (0.001 ppm).

Acephate has been shown by other workers to undergo rapid foliar absorption as well as translocation from roots to fruit. Further evidence of this was the concurrent incidence of methamidophos (Figure 2). The mean ratio of acephate to methamidophos for 25 samples with detectable levels of methamidophos was approximately 3.0 with the range of ratios from a low of 1 to a high of 9.5.

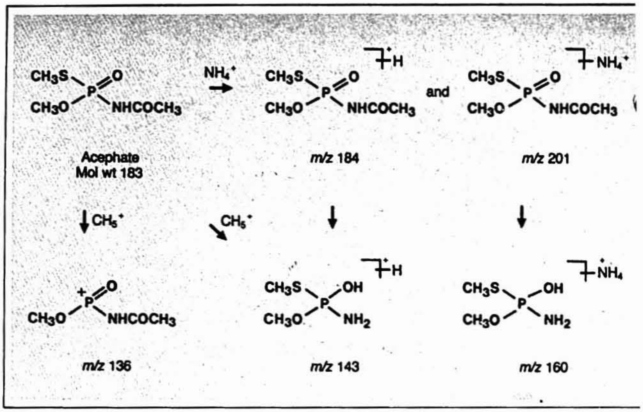

**Scheme 1.** Proposed fragmentation pathway of acephate under CI conditions

It has already been shown that the expected concentration level of methamidophos is about 9% of the absorbed dose of acephate within 24 h. The experimentally observed values of 9.5 to 1 are consistent with the timing of the application of acephate as outlined above. Ratio values in excess of 50% were indicative of fairly recent spraying, whereas lower values indicated spraying one to two weeks prior to harvest.

## Mass spectrometry

In developing an analytical protocol to confirm the presence of acephate, methamidophos, and its other metabolites in snow pea extracts, CI was selected to enhance the relative abundance of the $[M + H]^+$ ions for such low molecular weight compounds. In the case of acephate (Figure 3), ammonia was chosen as reagent gas for the actual analysis because of the availability of three prominent ions (*m/z* 143, 184, and 201) for single ion monitoring. It also enabled us to achieve the necessary sensitivity (as low as 10 ng injected). The ions at *m/z* 184 and 201 represent the ions $[M + H]^+$ and $[M + NH_4]^+$, respectively. However, the ions appearing at *m/z* 143 and 160 deserve special comment.

Empirically each represents a twin proton transfer with loss of the $COCH_3$ group after protonation or adduct formation with $[NH_4]^+$ (Scheme 1). This proton transfer is common under electron impact conditions for

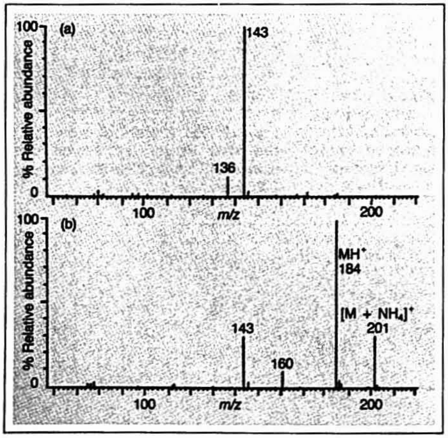

**Figure 3.** CI mass spectra of acephate with (a) methane as reagent gas, (b) ammonia as reagent gas

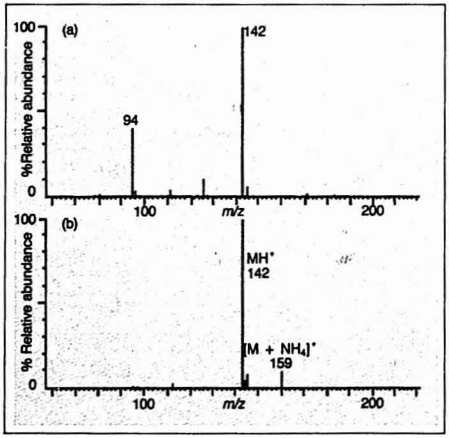

**Figure 4.** CI mass spectra of methamidophos with (a) methane as reagent gas, (b) ammonia as reagent gas

# Q. WHY IS OUR WORKSTATION DATA ACQUISITION SYSTEM THE COMPLETE SOLUTION?

*Keithley DAS' Series 500 workstation data acquisition system is the complete solution to your control and measurement needs, present and future. Even a basic configuration provides enough power and capacity for most lab and test bench applications. As your needs become greater, you can set it up to perform more complex or varied operations later on. The key is: you configure it for your needs, whenever you need to.*

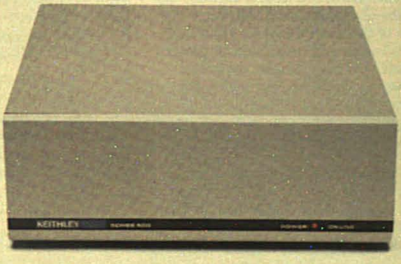

## A. A CHOICE OF PCs.

First of all, the Series 500 supports the PCs most commonly used in lab and R&D work: the IBM PC, PC-XT and Portable PC; the Apple II+ and IIe; and the Compaq Portable. We even support the 8087 coprocessor.

## A. A CHOICE OF SOFTWARE.

Our Soft500 package was written to give beginners the accessibility and ease of use they need to get results, yet it also offers more experienced users the depth and extra facilities necessary for more complex applications. Facilities like high-speed sampling, data storage, graphics, statistical analyses and memory-mapped I/O for high-speed data transfer. Our unique interrupt-driven architecture allows data acquisition in the background and simultaneous real-time analysis, control and display in the foreground. What's more, with our new Plus500 interface, you can also connect IEEE-488 instruments to your PC and put the same software environment in charge of both interfaces. For special needs, there's our Chem500 analytical chemistry software package for chromatography, spectroscopy, thermal analysis and colorimetry. And the Series 500 is also supported by the Macmillan ASYST™ and Lab Notebook™ software packages.

SOFT500
PLUS500
SOFT500
SERIES 500
IBM

## A. A CHOICE OF FUNCTIONS.

With the Series 500, you can choose from a larger library of plug-in function cards than any other company offers.

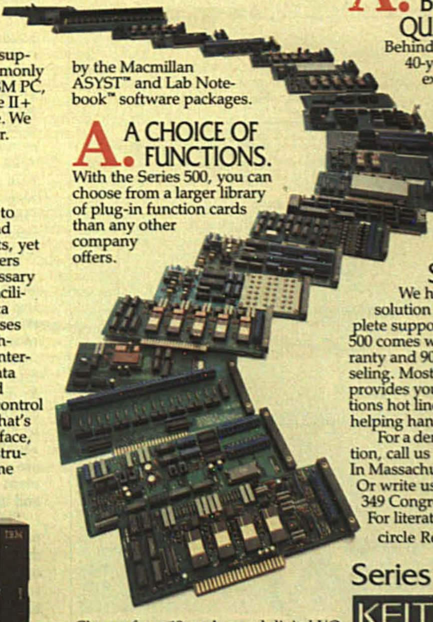

Choose from 18 analog and digital I/O modules; isolated and non-isolated analog input; direct connection of transducers: thermocouples, strain gauges and RTDs; pulse counting; 4-20 mA current loop input and output; direct switching and sensing of AC and DC power lines; and programmable excitation for transducers. All with full software support.

## A. ALL THIS, BACKED BY KEITHLEY QUALITY.

Behind the Series 500 is Keithley's 40-year reputation for engineering excellence and low-level measurement expertise. We designed it to provide the least noise, the highest accuracy and the greatest thermal stability of any PC-based data acquisition system.

## A. BACKED BY KEITHLEY SUPPORT, TOO.

We haven't provided a complete solution unless we provide complete support. And we do. Your Series 500 comes with a one-year full warranty and 90 days' free software counseling. Most important, Keithley DAS provides you with a toll-free applications hot line, for the times you need a helping hand.

For a demonstration or more information, call us toll-free at 1-800-552-1115. In Massachusetts call 617-423-7780. Or write us at Keithley DAS, 349 Congress Street, Boston, MA 02210. For literature on the Series 500. circle Reader Service Number 118.

**Series 500**

**KEITHLEY das**

© 1984 by Keithley DAS, Boston, Massachusetts

simple organophosphorus compounds. However, such behavior under CI conditions merits discussion. The site of initial protonation or adduct formation by $[NH_4]^+$ to permit such proton transfers must be viewed as occurring at the phosphorus site. Although the loss of the methyl ketonic grouping could occur with concomitant proton transfer to the nitrogen, the actual source of the second proton transfer to the oxygen of the P=O bond is not as clear. The most probable source under CI conditions would be the reagent gas.

Observance of the ion at *m/z* 160 presents the most interesting example of rearrangement while the electrophilic species $[NH_4]^+$ is still attached to the molecule. Such reactions are rare and demonstrate the feasibility of an $S_E2$ mechanism with tandem rearrangement. To date, no such examples of this extension of the $S_E2$ reaction with concurrent double-proton transfer have been reported. The remaining ion in the spectrum of acephate under methane CI conditions was at *m/z* 136 (Figure 3) corresponding to the loss of $SCH_3$.

In the case of methamidophos, the ammonia CI spectrum (Figure 4) exhibited only ions corresponding to $[M + H]^+$ and $[M + NH_4]^+$ at *m/z* 142 and 159, respectively. However, under methane CI conditions an additional ion at *m/z* 94 represented the loss of $SCH_3$ already observed under EI conditions. This ion was the homologue of *m/z* 136 observed for acephate.

### Residue confirmation

To match the sensitivity of the FPD–P detector used for primary detection of acephate and methamidophos, the snow pea extracts were examined by single ion monitoring using ammonia CI conditions. In the case of acephate the ions chosen for analysis were *m/z* 143, 184, and 201 and for methamidophos, *m/z* 142 and 159. Figure 5 illustrates the ion profiles obtained for a typical snow pea extract containing acephate at the 0.5-ppm level. Although the retention time and relative ratios are consistent with the presence of acephate, the broadening of the profile for *m/z* 143 could be explained by the presence of metabolite (III) as $[M + H]^+$. No evidence for the presence of metabolite (IV) could be found. In a similar manner, the presence of methamidophos was confirmed by observing ion profiles for *m/z* 142 and 159 at the correct retention time.

### Enforcement

How and when are such analytical results used to control interstate marketing of both domestic and imported food commodities that contain illegal residues of pesticides?

The Federal Food, Drug and Cosmetic Act authorizes the Food and Drug Administration (FDA) to initiate seizure of such shipments considered adulterated, to seek an injunction against further shipments, and to invoke criminal penalties against the firm and sometimes the individuals responsible for the adulteration. Historically about 3% of the surveillance samples examined contained illegal residues.

Enforcement is exercised through three main avenues. In cases where the sampled commodity stays in the state of origin, the results are communicated to state officials for intrastate regulatory action. In some cases, the interstate shipment is either voluntarily destroyed by industry upon notification of FDA findings or embargoed by state officials and then destroyed. Finally, by the time analytical results are completed and reviewed, the shipment may have moved even farther, and it cannot be traced.

This last situation is most often experienced with fresh agricultural produce such as snow peas. In spite of the inability to trace the fruit or vegetable to its final destination, the information acquired about specific growers and shippers is invaluable in monitoring future shipments from the same produce fields.

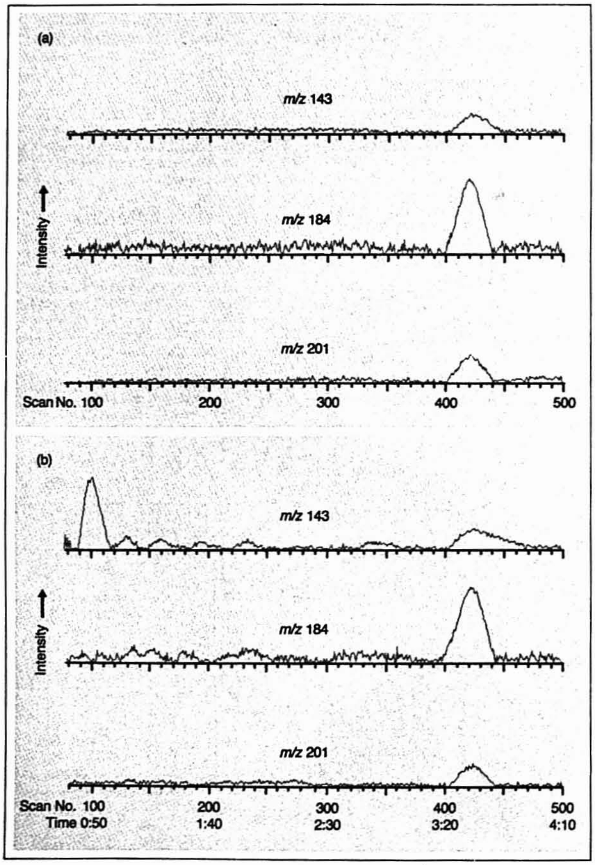

**Figure 5.** SIM chromatograms for (a) acephate reference standard, (b) snow pea extract containing 0.5-ppm acephate

# ANTEK 3000

## GAS CHROMATOGRAPH

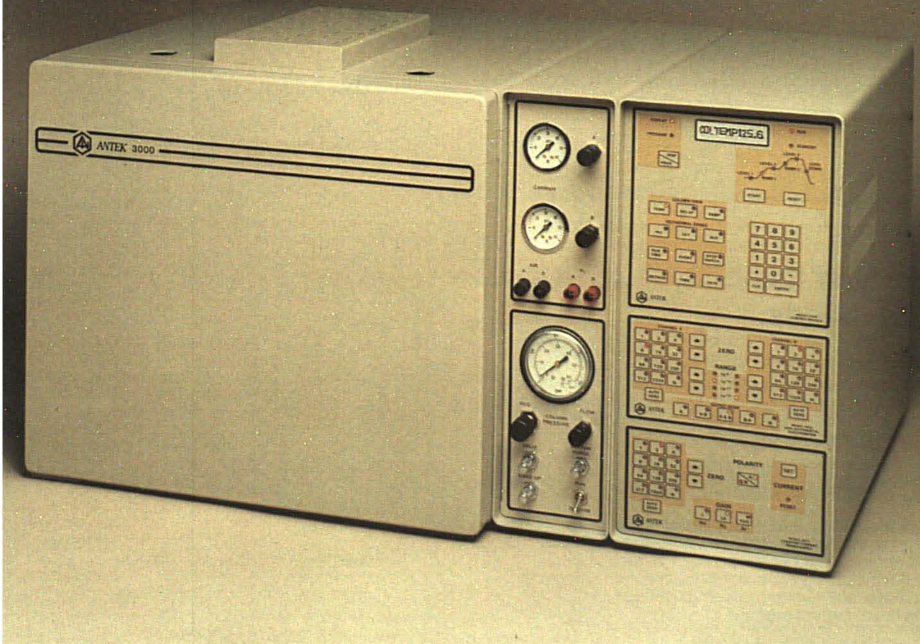
ANTEK 3000
COL.TEMP125.6
ZERO
RANGE
POLARITY
ZERO
CURRENT
GAIN

ANTEK®

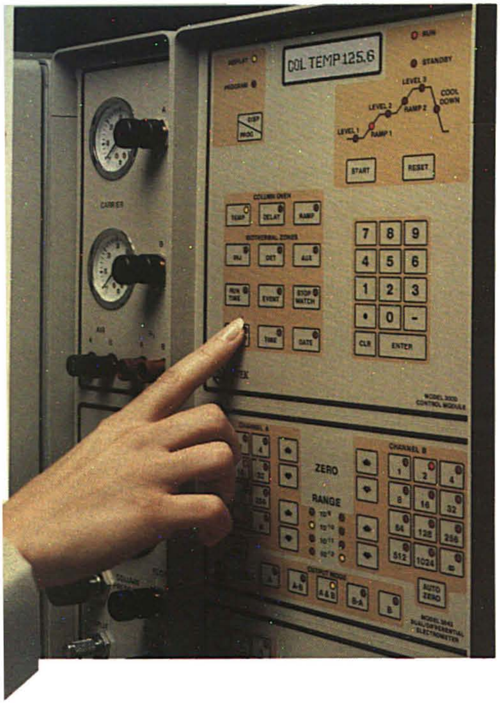
COL TEMP 125.6
RUN
STANDBY
DISPLAY
PROGRAM
LEVEL 1
RAMP 1
LEVEL 2
RAMP 2
LEVEL 3
COOL DOWN
START
RESET
COLUMN OVEN
TEMP
DELAY
RAMP
ISOTHERMAL ZONES
INJ
DET
AUX
RUN TIME
EVENT
STOP WATCH
TIME
DATE
CLR
ENTER
CARRIER
CHANNEL A
CHANNEL B
ZERO
RANGE
OUTPUT MODE
AUTO ZERO

# The ANTEK 3000 Gas Chromatograph puts you in control.

At last, the complete control of a gas chromatograph has been placed where it always belonged — in the hands of the chromatographer. ANTEK introduces state-of-the-art simplicity in an instrument so versatile, it can be programmed to your precise specifications at the touch of a finger.

**Simple touch pad** actuates the built-in microprocessor control functions and analytical parameters.

**Lighted display** buttons tell you at a glance precisely what conditions are being utilized and the status of the analysis.

**Analytical conditions** and control functions can be changed at any time by the simple touch of a button.

**Your methods** can be developed, stored, recalled and used with unprecedented ease.

## Modular flexibility — to fit your needs.

ANTEK 3000 GC offers the chromatographer maximum flexibility. Modular design lets you build the exact system you need for virtually any analysis. Just choose the desired combination of detector control modules, power supply modules and flow systems.

### Change the system by simply changing modules.

1. **Model 3000 Electronic Control Module** is the heart of the ANTEK system. It enables the chromatographer to input all temperature parameters — isothermal and programmed, timed events, analytical methods, and numeric values for voltage and current into the microprocessor.

2. **Detector Control and Power Supply Modules** plug into appropriate control panel positions. Select from four power modules and eight detectors to create the right detection system for your analytical needs.

3. **Flow Modules** offers even more versatility. ANTEK 3000 provides flow systems for thermal conductivity and/or ionization detectors, packed column, capillary or wide bore capability. With ANTEK 3000, the flexibility is built-in.

*Modular touch pad front panel and diverse flow panel provide maximum flexibility.*

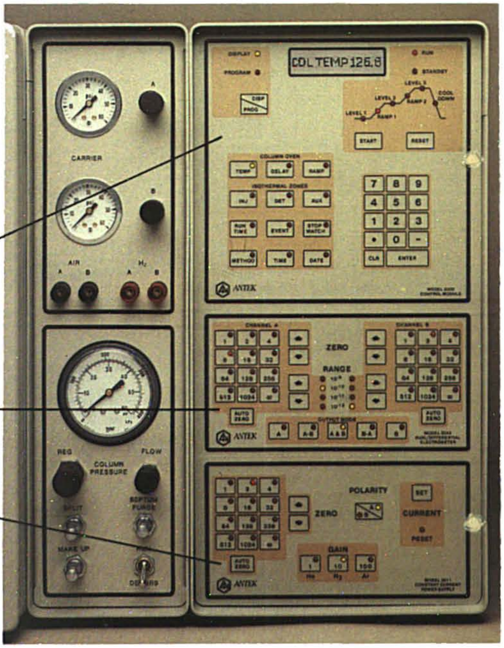
COL TEMP 125.8
RUN
STANDBY
DISPLAY
PROGRAM
START
RESET
COLUMN OVEN
TEMP
DELAY
RAMP
ISOTHERMAL ZONES
INJ
DET
AUX
RUN TIME
EVENT
STOP WATCH
METHOD
TIME
DATE
CLR
ENTER
CARRIER
AIR
H2
ANTEK
ZERO
RANGE
AUTO ZERO
REG
FLOW
COLUMN PRESSURE
SPLIT
SEPTUM PURGE
MAKE UP
POLARITY
SET
CURRENT
RESET
GAIN
He
N2
Ar

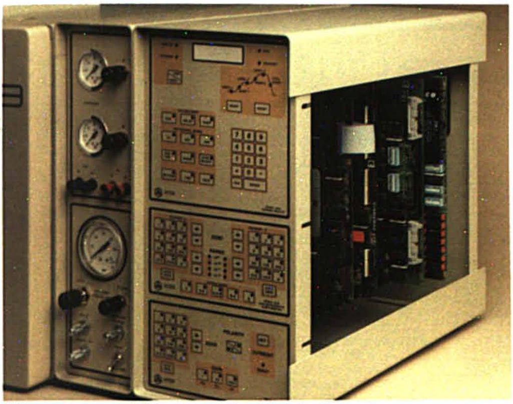

*Microprocessor and detector control printed circuit boards are easily accessed for speedy troubleshooting and service.*

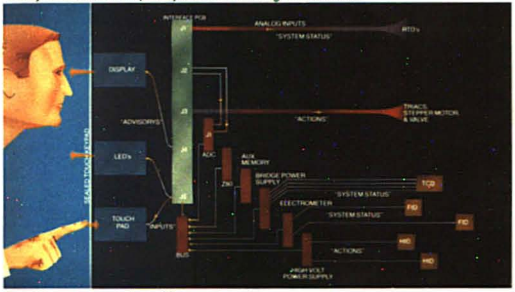

*Graphic representation of interaction of the chromatographer, interface, microprocessor and GC.*

# Now you can have direct control of GC functions.

Manipulating GC functions has never been so easy. Chromatographic parameters may be changed with as little as one key stroke.

A sealed, easy-touch front panel keypad controls communication with the microprocessor. LED's and intelligent alphanumeric displays guide the chromatographer during programming. The displays also give the status of the system.

For example. To set the column oven temperature to 60°C, simply touch.

DISP / PROG  TEMP ○  6  0  ENTER

To change attenuation on Electrometer Channel B to 64, simply touch: ● 64 (in Channel B section)

Setting or changing all parameters is just as easy as demonstrated above. During construction of the temperature programs, the alphanumeric display conveniently guides the chromatographer.

## Take a look inside the ANTEK 3000 microprocessor.

To the left, the diagram describes how the microprocessor works. The chromatographer has direct control of all GC operations through the sealed touch keypad.

As entries are keyed, the microprocessor controls all GC functions. Front panel LEDs reveal system status. The alphanumeric display provides meaningful messages to aid in both programming and trouble shooting.

Microprocessor electronics are housed in replaceable circuit boards for ease of service.

## The Oven.

**Large column oven** gives you maximum flexibility in the selection and placement of inlets, columns, valves and detectors. Oven size specifications are 35.0 cm wide X 24.9 cm high X 22 cm deep (13.8 in. x 9.8 in. x 8.8 in.) with a volume of 19522 cm$^3$ (1190 in.$^3$).

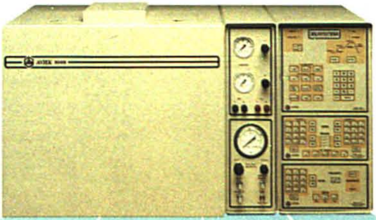

**Total microprocessor control** provides accurate, reproducible chromatography and activation of sampling and column switching valves. Temperature control software gives precise heating rates and very rapid cooldown (250 °C to 50 °C in just 3.5 minutes).

**Component flexibility** makes it easy to pick a system to fit your application. Accommodate from 1 to 4 injectors and detectors with 1 to 4 packed columns or up to 4 capillary columns.

## Components

**Capillary Injectors**

1. Cool-on-column
2. Split/Splitless

**Packed Column Injectors**

3. Flash vaporization
4. On-column

**Detectors** Installation of up to 4 of the 8 available detectors provides the versatility needed to meet today's demanding analytical tasks. All 8 detectors are compatable with packed or capillary columns.

1. TCD
2. FID
3. HID
4. UPID*
5. FPD
6. TID/CFID
7. ECD
8. CND*

Combined with autosamplers, sample valves, column switching valves, data systems and other accessories, the ANTEK 3000 has the versatility to put you in total control.

*New detector, see specifications.

## Options

*Model 736-2V Autosampler*

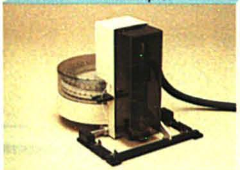

*Sampling and Column Switching Valves with Automation*

*Eight detectors available*

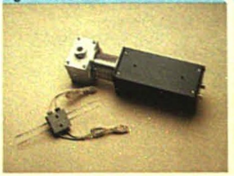

*Model 4270 Chromatography Integrator*

CIRCLE 8 ON READER SERVICE CARD

# ANTEK 3000

## Specifications

**Column Oven**
Size: Height 24.9 cm (9.8 in.)
Width 35.0 cm (13.8 in.)
Depth 22.4 cm (8.8 in.)
Volume: 19522 cm$^3$ (1190 in$^3$)
Capacity: up to four 30 ft. metal ⅛" OD columns or;
up to four 10 ft. glass ¼" OD columns or;
up to four 100 m capillary columns.
Temperature Range: 5 °C above ambient to 425 °C. −99 °C to 425 °C with cryogenic option.
Cooldown Rate: 250 °C to 50 °C in 3.5 minutes.

**Column Oven Temperature Control**
Miltilinear Temperature Program: 6 steps
Delay Times: 0 to 650 min. in 0. 1 min. increments
Ramp Rates: 0 to 20 °C/min. in 0.1 °C/min. increments

**Isothermal Zones**
Temperature Range: Ambient to 425 °C
Six independent isothermal zones are available: two injector, two detector and two auxillary.

**Methods**
Storage of 6 methods for exact reproduction of analytical parameters.

**Timed Events**
Eight programmable events for valve switching or actuation of other accessories.

**Injectors**
Flash vaporization, cool and heated on-column, ⅛" and ¼", for packed column.
Cool-on-column and split/splitless for capillary columns.

**Detectors**
Thermal Conductivity (TCD)
Sensitivity: 11 $\mu$v/ppm (5 x 10$^3$ mV-ml/mg) butane at 300 ma, 120 °C, He carrier.
Minimum Detectable Limit: 3 x 10$^{-10}$ g/ml butane.
Linearity: >10$^5$, butane.
Power Supply: constant current, 0 to 300 ma in 1 ma increments, filament protect.
Capillary Option: cell volume 30 $\mu$l.
Flame Ionization (FID)
Sensitivity: >0.015 coulombs/g C
Minimum Detectable Limit: 4 x 10$^{-12}$ g/sec.
Linearity: >10$^7$, butane
Noise: 2 x 10$^{-14}$ amperes
Electrometer: Single or Dual/Differential
Helium Ionization (HID)
Generally Licensed: No specific license required.
Minimum Detectable Limit: <20 ppb $N_2$
<10 ppb $CO_2$
<10 ppb $CH_4$
Linearity: >10$^4$
Ionization Source: 190 mc $^3$H
Power Supply: 0 to 1200 VDC in 1 volt increments
Electrometer: Single or Dual/Differential
Universal Plasma Ionization (UPID)
Generally Licensed: No specific license required.
Minimum Detectable Limit: <100 ppb for permanant gases and light hydrocarbons
Linearity: >10$^3$
Ionization Source: 190 mc $^3$H
Power Supply: 0 to 1200 VDC in 1 volt increments
Electrometer: Single or Dual/Differential
Flame Photometric (FPD)
Minimum Detectable Limit: Sulfur <10$^{-10}$ g/sec.
Phosphorus <10$^{-12}$ g/sec.
Range: Sulfur >10$^3$
Phosphorus >10$^5$
Thermionic Ionization (TID)
Minimum Detectable Limit: 1 x 10$^{-13}$ gN/sec. (azobenzene)
5 x 10$^{-14}$ gP/sec. (malathion)
Linearity: 2 x 10$^5$ for N
Electron Capture (ECD)
Minimum Detectable Limit: 0.1 picogram Aldrin
Dynamic Range: >10$^5$ for Aldrin
Cell Volume: 180 ul
Operating Temperature: up to 320 °C
Carrier Gas: Nitrogen or Argon/Methane
Chemiluminescent Nitrogen (CND)
Type: Pyro-chemiluminescent, totally specific for nitrogen
Minimum Detectable Limit: <1 nanogram N
Dynamic Range: >10$^5$

**Detector Controllers**
Electrometer
Used with: FID, HID, UPID, TID
Types: Single input with single output or Dual input with single, dual or dual/differential output.
Sensitivity: 5 x 10$^{-13}$ amperes/millivolt
Attenuator: Binary from 1 to 1024 and infinity.
Auto Zero: Standard
Drift: <10 $\mu$v/month at constant temperature.
Output: Recorder 0 — 1 mV
Computer 0 — 1 V
0 — 10 V
Constant Current Power Supply
Used With: TCD, FPD
Range: 0 to 300 ma in 1 ma increments
Amplifier Gain: selectable at 1X, 10X or 100X amplification
Attenuator: Binary from 1 to 1024 and infinity
Auto Zero: Standard
High Voltage Power Supply
Used With: HID, UPID, FPD
Range: 0 to 1200 volts DC in 1 volt increments
Polarity: + and −
Stability: better than 0.002%

**Flow System**
Carrier:
1) manual flow control
2) optional flow controller with pressure guage
3) optional digital flow controller
Air/$H_2$:
On/off valves with adjustable metering valves
Filters:
1) optional particulate filters
2) optional $H_20$/Hydrocarbon filters
Power Requirements
115 VAC 60 Hz 2200 watts
230 VAC 50/60 Hz 2200 watts

**Physical**
Height: 43.2 cm (17.0 in.)
Width: 78.2 cm (30.8 in.)
Depth: 53.3 cm (21.0 in.)
Weight: 61 kg (135 lbs.)

ANTEK® INSTRUMENTS, INC.

**ANTEK INSTRUMENTS, INC.**
6005 North Freeway
Houston, Texas 77076-3998
713/691-2265
TWX: 910 881-1792

**ANTEK INSTRUMENTS, GmbH**
Wacholderstrasse 7
D-4000 Dusseldorf 31 (BRD)
Telefon (0203) 74325/6
Telex: 8588297
Answerback: ANDU D

©Copyright Antek Instruments, Inc. 1985

Printed in USA
A-3000-85

# 3 important reasons to invest in a PACKARD GC NETWORK

- **Operational Simplicity and Security**
  Centralized network control on the compact Network Manager, in any convenient location. Place it on your office desk to program and monitor all network instruments, with instantaneous access to the status report of any network GC. And, since satellite GCs have no programming facilities of their own, they are completely secure against accidental or unauthorized changes to stored and active GC methods.

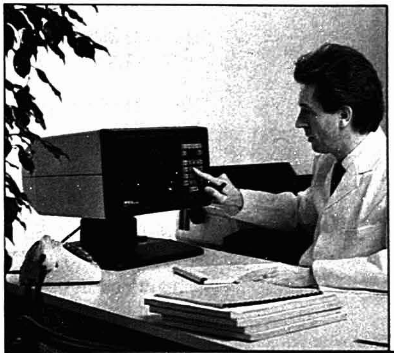

- **One-Shot Samplers**
  Are new automatic injection devices that offer extremely accurate and reproducible sample introduction. An ideal network accessory for routine process control environments as well as research labs, the One-Shot Samplers eliminate human error and save money on costly syringes.

- **Cost Savings**
  One Network Manager with two satellite GCs costs about the same as two conventional GCs, forming the ideal low-cost entry into the Network. Expand it as and when desired; the bigger it gets - the larger your accumulated savings.

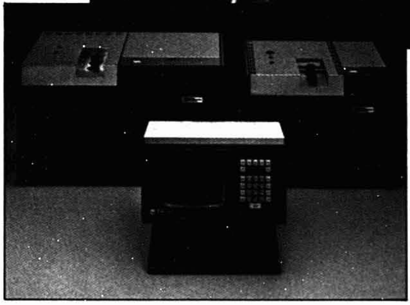

## Ask for our brochures!

---

**UNITED TECHNOLOGIES PACKARD**

**PACKARD INSTRUMENT B.V.**
P O Box 519/2600 AM Delft/The Netherlands

**PACKARD INSTRUMENT INTERNATIONAL S.A.**
Renggerstrasse 3/CH-8038 Zurich/Switzerland

**PACKARD INSTRUMENT COMPANY, INC.**
2200 Warrenville Road/Downers Grove, IL 60515/U.S.A.

CIRCLE 170 ON READER SERVICE CARD

# A closer look at the MTS800 Multi-Titration System

ENDPOINT PH

Radiometer presents the new MTS800 Multi-Titration System.

The MTS800 gives you unprecedented simplicity of operation on top of our world-famous Radiometer reliability.

The MTS800's microprocessor memory permanently stores up to 31 methods, and allows you to retrieve them at the push of a button and use your choice of titration modes: End-point, inflection points, or Karl Fischer. Titrant volume resolution of 0.1 $\mu$l helps you detect even the weakest equivalence points.

MTS800 will prove to be a faithful partner in the lab. Whether you work with large batch analyses or single titrations, you will find that the unique features of the MTS800 speed up work without compromising accuracy.

For all the facts ask for our free brochure. Call toll free, 1–800–321-9484. In Ohio, please call 1–216–871-8900.

RADIOMETER
COPENHAGEN
Analytical Instruments Division

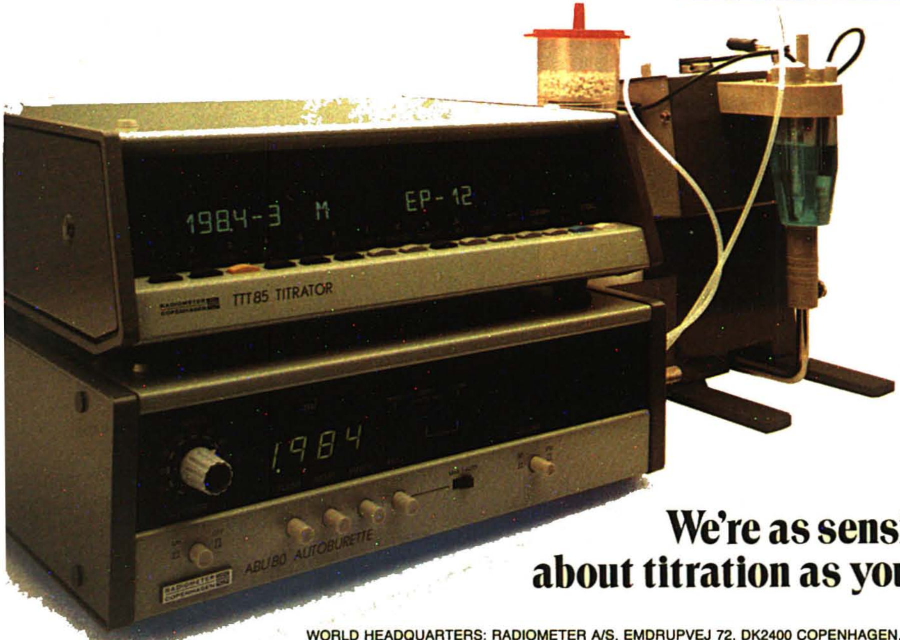

## We're as sensitive about titration as you are

WORLD HEADQUARTERS: RADIOMETER A/S, EMDRUPVEJ 72, DK2400 COPENHAGEN, DENMARK
IN THE U.S.: RADIOMETER AMERICA, INC., 811 SHARON DRIVE, WESTLAKE, OH 44145

CIRCLE 179 ON READER SERVICE CARD

# Books

## Useful Text for the Beginning Electroanalyst

**Laboratory Techniques in Electroanalytical Chemistry.** Peter Kissinger, William Heineman, Eds. xv + 751 pp. Marcel Dekker, 270 Madison Ave., New York, N.Y. 10016. 1984. $34.75

*Reviewed by Fred Anson, California Institute of Technology, Division of Chemistry and Chemical Engineering, Room 127-720, Pasadena, Calif. 91125*

Editors Kissinger and Heineman and the illustrious group of authors they have assembled have made a major contribution to electroanalytical chemistry with the appearance of this volume. The two editors also serve as authors or coauthors for 8 of the 24 chapters, which are admirably consistent in the style and level of the presentations. Some of the editors' intentions for their collection, as stated in the preface, do a good job of conveying the flavor of the book:

"... this book was conceived in 1970 ... to provide a means of enabling a neophyte ... to get started in the lab. During the decade over which this effort has spanned the emphasis ... expanded to include a pedagogical component."

"The emphasis of this book is entirely on *analytical* and mechanistic (homogeneous), kinetic (homogeneous), and synthetic (laboratory scale) applications."

"The organization of the book flows from principles through methodology to applications."

This book differs from most of its predecessors in studiously and unapologetically eschewing mathematical derivations as much as possible. In their place one is offered clear, carefully considered qualitative descriptions of the physical situations that are the cause and the result of the passage of current through electrochemical cells. The treatment is both appealing and stimulating. The more rigorous mathematical treatments available in the well-known books by Delahay and Bard and Faulkner may well receive added appreciation and understanding from readers who have been guided in their direction after being introduced to the topics in the informative and seductive forms employed in this book.

I concur with the editors' opinion "that Chapters 2 through 5 are suitable for use in graduate-level introductory courses in electroanalytical chemistry." (Indeed, several other chapters, e.g., 6, 16, and 12, could also serve this purpose admirably.) Chapters 2–5, written by the editors (and their associates in one case), treat the fundamental concepts underlying essentially all dynamic electroanalytical techniques with pedagogic insights and an arresting style uncommon to most previous monographs on electroanalytical chemistry. For example, a derivation of Fick's second law of diffusion is followed by these sentences: "The solution of diffusion equations has fascinated academic electroanalytical chemists for years and they naturally have a tendency to expound upon them at the slightest provocation. Fortunately the chemist using electrode reactions can accomplish a great deal without more than a cursory appreciation of the mathematics." The succeeding chapters in the collection amply support this contention. The topics treated cover virtually everything a beginning researcher needs to know to undertake laboratory work in electroanalysis: analog instrumentation; the virtues and limitations of electrodes made of mercury, carbon, or films; electrochemical cells and solvents; and useful techniques involving vacuum lines, controlled atmospheres, electron spin resonance, photochemistry, conductance, and digital simulation. Illustrative examples are used in discussions of organic electrode reaction mechanisms, transition metal electrochemistry, analysis of pharmaceuticals, applications of electrochemical detectors to chromatography, electrochemical preconcentration, and constant-current coulometry.

I have already found this book highly useful in assisting students and colleagues in trying out an unfamiliar electrochemical technique because the descriptions provided are both clear and encouraging. The book deserves the popularity with which it will undoubtedly be received. My advice to fellow electrochemists is to buy two copies—one to keep for handy reference and a second to lend to the army of friends and colleagues who are apt to descend upon us in search of the answers that they've heard the book can provide.

**Small Bore Liquid Chromatography Columns: Their Properties and Uses.** Raymond P.W. Scott, Ed. xiii + 271 pp. John Wiley & Sons, 605 Third Ave., New York, N.Y. 10016. 1984. $48.50

*Reviewed by Richard Hartwick, Department of Chemistry, Rutgers University, New Brunswick, N.J. 08903*

"Small Bore Liquid Chromatography Columns" is a timely addition to the Chemical Analysis Series, edited by one of the founders of the field of

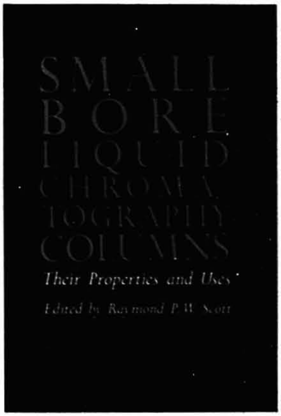
SMALL BORE LIQUID CHROMATOGRAPHY COLUMNS
Their Properties and Uses
Edited by Raymond P.W. Scott

UNION GIKEN

First choice for

STOPPED FLOW

reaction analysis

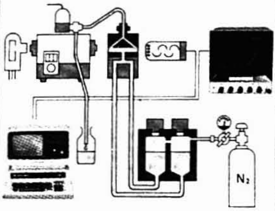

Union Giken apparatus achieves a dead time as short as ½ millisecond for measurement of fast reactions. Gas pressure is directly applied to the surface of the reactants in each reservoir, mixing and flow being controlled from the end of the system by a high-response stop valve. The RA-401 STOPPED FLOW SPECTROMETER is the ideal match for fast reactions.

The RA-451 DATA PROCESSOR generates a simulated reaction curve from the measured results and automatically calculates the rate constant.

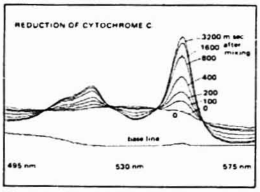

The RA-415 RAPID SCAN ATTACHMENT monitors the change in absorption spectrum during the reaction.

Other attachments are available for T-jump, P-jump, fluorescence and flash photolysis.

*Contact the sole export agent for more details:—*

**ATAGO BUSSAN CO., LTD.**
7-23, 5-chome Shimbashi, Minato-ku,
Tokyo 105, Japan
Telex: 28421 Cable: TAGOA TOKYO
Phone: (03) 432-8741

CIRCLE 2 ON READER SERVICE CARD

"microbore" HPLC. As stated by Scott in the preface, the term *microbore* has probably been rendered obsolete by advancing technology. He suggests instead that "small bore" columns be used as the generic appellation of columns in the range of 1–2-mm i.d. There is still no general consensus on the nomenclature of HPLC using columns smaller than the current standard of 3–5-mm i.d. Scott's suggestion is probably a good one, except that the term microbore in connection with 1-mm-i.d. columns is already so well established in the literature that a change at this late date is probably ill-advised. Besides, small bore is still a comparative, rather than an absolute, term and may in several years represent "conventional" or even "semipreparative" LC, depending on how far the trend toward miniaturization continues.

The book sets out with a deliberate bias in that it deals almost exclusively with 1–2-mm-i.d. column technology, as implied by the title. The extensive literature on packed fused-silica columns of several hundred micrometers i.d. is not addressed. This is not necessarily a weakness, because the book gains a certain strength from limiting its focus to one specific column type. However, this is mentioned for the sake of the reader who might expect a comprehensive treatise on all aspects of microbore column technology.

The book consists of 11 chapters, with the first six focusing on the theory and instrumentation of small-bore columns, whereas Chapters 7–11 review particular applications of these columns. In general, the information contained in the chapters is useful to the practicing chromatographer. The first four chapters, dealing with band dispersion and instrumentation, review basic chromatographic equations, expressed in terms of small-bore LC. The theoretical treatment suffers from being spread over several chapters by three different authors; however, the equations are unified in their nomenclature. A more comprehensive treatment by a single author of all the instrumental theory covered could have strengthened this aspect of the work. In fairness, however, such cohesiveness is virtually impossible to sustain in any multiauthored volume. Some sections, such as that on serpentine tubing, assemble in one place a variety of useful equations normally scattered about the literature.

The chapters on applications do a good job of covering 1-mm-i.d. column technology. Some of the more exciting work in narrow-bore instrumentation, such as laser-based detectors, is not adequately covered, since much of this is being done with packed fused-silica columns. Also, the field of LC/MS, which seems destined to become one of the primary driving forces for the trend toward micro-LC, is only superficially mentioned. A full chapter devoted to this topic could have added depth to the volume.

A strength of the book is the comprehensive manner in which all major aspects of chromatography with 1-mm-i.d. columns are covered. A chromatographer needing to do work with this type of instrumentation could successfully begin work in this area using only this book as a guide. Thus, the book should be useful for those chromatographers who are contemplating starting up a 1-mm-i.d. instrument in their own labs.

In summary, this volume should be a useful addition to the library of the chemist needing a handy reference to the literature and use of 1–2-mm-i.d. columns. As with any rapidly advancing field, some material is undoubtedly dated, but this does not detract from the utility of the book as a basic work. Overall, the editor and the contributors effectively present the advantages and limitations of small-bore columns and the role they play in the development of HPLC separations.

**Regulatory Compliance Monitoring by Atomic Absorption Spectroscopy.** Sidney Katz, Stephen Jenniss. vii + 278 pp. Verlag Chemie International, 303 N.W. 12th Ave., Deerfield Beach, Fla. 33441. 1983. $37.50

*Reviewed by Theodore Martin, U.S. Environmental Protection Agency, Environmental Monitoring and Support Laboratory, Cincinnati, Ohio 45268*

This book is a descriptive collection of various atomic absorption methodologies used for the analysis of environmental samples. The majority of the methods included are analytical procedures used for compliance monitoring. The text, which consists of eight chapters, is introduced by a general discussion on some practical aspects of atomic absorption analyses and concludes with a suitable discussion on the needs and requirements of a laboratory quality assurance program. Two chapters are specifically devoted to sampling, sample preservation, and preparation procedures, whereas the remaining four chapters address the analytical requirements of the monitoring methods for air, water, solid-type samples, and tissue analyses.

*(continued on p. 587A)*

# Now, improve microanalysis 6 ways. EDAX 9100-LX.

EDAX® answers your microanalytical needs with proven Application **Software** in EDS, EELS, diffraction, WEDAX, stage control and particle detection; and with Software that provides precise beam control in SEM and STEM. **EDscan™ X-ray and Electron Imaging** for spatially related chemical analyses in full color. And **Standardless Quantitative Analysis** with automatic peak identification. World renowned **ECON® Series Detectors** for light element analysis down to boron. User-definable **Dynamic Function Keys** for one-keystroke ease of operation. And the **Dynastatic Display** for smooth automatic vertical scaling change and easy-to-read spectral display.

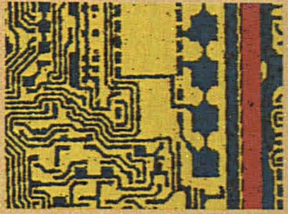

Color-coded digitized BSE image.

Composite x-ray image showing areas of B K = yellow, FeL = red, and SiK = blue.

System 9100-LX. The proven answer to your microanalytical needs.

**Ask about it.** Contact EDAX at (312) 634-0600.

ECON is a registered trademark and EDscan is a trademark of EDAX International, Inc.

EDAX INTERNATIONAL, INC., P.O. Box 135, Prairie View, IL 60069

EDAX®

FIRST NAME IN MICROANALYSIS

CIRCLE 50 ON READER SERVICE CARD

# Treat yourself to routine chromatographic analysis!

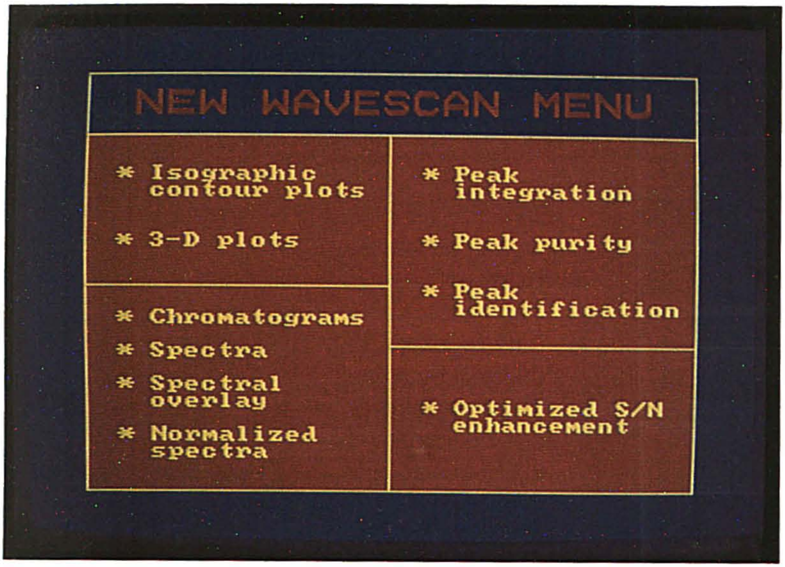

## Automated diode array detection gets your work done faster and more reliably

Save time, trouble and guesswork. Your existing HPLC system can now be completely automated for maximum QC productivity. Peak purity control and positive component identification is all yours at the touch of a button!

Using LKB's Rapid Spectral Detector and Wavescan software, your IBM XT/AT is powered to store multiple runs, however short or long. And fast access storage gives you the analytical control no other system offers. Manipulate raw data for more information, greater detail and increased certainty—you'll run every sample just once!

Wavescan equips you with multiple display formats, powerful deconvolution and sophisticated derivative techniques. Lets you explore the whole chromatographic landscape without missing a single peak!

Drive a cursor through colour coded isograms, and you'll instantly access optimal chromatograms. Now go ahead for peak integration. Track again and you'll generate optimal spectra. This is the kind of routine analysis you've always wanted, always needed. It will even find you peaks you might have missed in the noise!

From storage to hard colour copy, Wavescan automates diode array detection to give your HPLC a big boost in output. Now give your analysis work the breakthrough it deserves. Go on, treat yourself. Get in touch with LKB. You'll be glad you did!

LKB
BROMMA

LKB-Produkter AB, Box 305, S-161 26 Bromma, Sweden. Tel. +46 (8) 98 00 40, telex 10492

**Antwerp** (03) 218 93 35 · **Athens-Middle East** +30 (1) 894 73 96 · **Copenhagen** (01) 29 50 44 · **London** (01) 657 88 22
**Lucerne** (041) 55 44 57 · **Madras** (044) 45 28 74 · **Moscow** (095) 256-9002 · **Munich** (089) 85 830 · **Paris** (06) 92 86 507
**Rome** (06) 39 90 33 · **Stockholm** (08) 98 00 40 · **Tokyo** (03) 293-5141 · **Turku** (021) 678 111
**Vienna** +43 (222) 92 16 07 · **Washington** (301) 963 3200 · **Zoetermeer** (079) 31 92 01
Over 60 qualified representatives throughout the world.

CIRCLE 130 ON READER SERVICE CARD

**Environmental Sampling for Hazardous Wastes**

**Glenn E. Schweitzer and John A. Santolucito,** *Editors*
*U.S. Environmental Protection Agency*

**Underlines the concern and need for improved methods of environmental sampling. Surveys the problems of collecting representative samples, ensuring the chemical integrity of samples from collection to analyses, and characterizing and monitoring contamination sites. Examines the important aspects of designing and implementing sampling programs, emphasizing surface and subsurface sampling for hazardous wastes. Looks into the experiences of federal and state agencies, and academic and institutional organizations. Cites several successful field programs for sampling dioxin, lead, and cyanide.**

**CONTENTS**

Hazardous Waste: Questions and Issues from the Field • Uses of Environmental Testing in Human Health Risk Assessment • Assessing Cyanide Contamination from an Aluminum Smelter • 2,3,7,8-Tetrachlorodibenzo-*p*-dioxin Sampling Methods • Field Measurement of Polychlorinated Biphenyls in Soil and Sediment Using a Portable Gas Chromatograph • Using Geostatistics in Assessing Lead Contamination near Smelters • Lead Levels in Blood of Children Around Smelter Sites in Dallas • An Approach to Interdisciplinary Design of Multifactor Experiments • Statistical Methods in Environmental Sampling • Soil Sampling Quality Assurance and the Importance of an Exploratory Study • Quality Assurance for Measurement Program • New Ways of Assessing Spatial Distributions of Pollutants • Detecting Elevated Contamination by Comparison with Background

*Based on a workshop sponsored by the ACS Committee on Environmental Improvement, the U.S. Environmental Protection Agency, and the University of Nevada—Las Vegas*

ACS Symposium Series No. 267
144 pages (1984) Clothbound
LC 84-20480 ISBN 0-8412-0884-0
US & Canada **$34.95** Export **$41.95**

**Order from:**
**American Chemical Society**
**Distribution Office Dept. 18**
**1155 Sixteenth St., N.W.**
**Washington, DC 20036**
**or CALL TOLL FREE 800-424-6747**
**and use your VISA, MasterCard, or American Express credit card.**

The methods included are not limited to those published by the U.S. Environmental Protection Agency (EPA) and the National Institute for Occupational Safety and Health; methods from foreign governments, in particular the Canadian Department of the Environment, with references to work by professional scientific societies and other researchers, also have been included. The authors do not present a critical review of the methods, but list similar methods for each analyte for a comparative review by the reader. An important feature of the book is the interspersing of appropriate comments and references to related research work throughout the text.

The book is intended to be an aid to analysts in presenting the required details of official methodology with a brief statement on the purposes of regulatory compliance monitoring. The book is easy to read and for the most part accomplishes its goal. As with all texts a few typographical errors do appear as in the table on regulatory limits (p. 4), where the drinking water maximum contaminant level concentrations for cadmium and selenium are incorrect, and chromium is listed as a hexavalent measurement. Also, important sentences from the introduction to the EPA chelation extraction procedure (p. 65) as well as reagent preparation steps have been omitted, which significantly affects the reader's ability to understand the procedure.

Overall the book is useful and should be considered a resource. However, the reader should not substitute its use for original referenced material from which the methods have been extracted. The reader must also be aware that periodic updating of approved methodology and regulatory changes may date some information in the text. The *Federal Register* should be consulted for appropriate changes as they develop.

## Books Received

**The Analysis of Plastics.** T.R. Crompton. ix + 445 pp. Pergamon Press, Maxwell House, Fairview Park, Elmsford, N.Y. 10023. 1984. $49.50

**Official Methods of Analysis of the Association of Official Analytical Chemists.** 14th ed. Sidney Williams, Ed. 1141 pp. Association of Official Analytical Chemists, 1111 North 19th St., Suite 210, Arlington, Va. 22209. 1984. $133.95 (U.S. members); $148.50 (U.S. nonmembers)

TECHNICAL NOTES 6

**How to select LC filters to maximize resolution.**

A column inlet filter is usually necessary to capture contaminating particles, yet this filter may easily impair resolution if not wisely selected.

Rheodyne's Tech Note 6 reports experiments measuring how much filters of various sizes and flow geometry affect the resolution achieved by columns of several sizes.

The newer microbore columns and short 4.6-mm columns prove to be most sensitive to filter performance. If their resolution is to be preserved, an inlet filter with very little sample dispersion must be used.

The Tech Note helps the reader select the optimum filter for his application: one with little enough sample dispersion to preserve resolution, yet large enough capacity to prevent a rapid rise in backpressure.

**Send for Tech Note #6**

For a copy free of charge contact Rheodyne, Inc., P.O. Box 996, Cotati, California 94928, U.S.A. Phone (707) 664-9050.

RHEODYNE
THE LC CONNECTION COMPANY
CIRCLE 177 ON READER SERVICE CARD

# Perkin-Elmer continues its Lambda Array tradition . . . with the IBM PC

Lambda Array 3840 now interfaces with the IBM Personal Computer to provide the most versatile UV spectrophotometer and data handling system available: a state of the art diode array fast scan spectrophotometer using Perkin-Elmer's turnkey software, and a personal computer with the most extensive library of compatible software ever developed.

**Low cost fast scan**

Lambda Array 3840 brings you unmatched optical performance with the total capability of a diode array photometer. Now you can choose the controlling computer: either the Perkin-Elmer Series 7000 Professional Computer or the IBM PC. Both display spectra within two seconds . . . and one computer is best suited for your application.

**Optical performance you expect**

Lambda Array 3840 with the IBM PC provides the same high performance specifications: resolution up to 0.25 nm and stray light less than 0.05%T. This is because the optical module has not been changed or compromised. You choose the computer to fit your needs and budget.

**A new turnkey software package**

To bring you a low cost, diode array spectrophotometer, totally new spectroscopy software for the IBM PC was developed. The new software allows many of the features found on the Perkin-Elmer Series 7000 Professional Computers. We have taken the features you most often use: data acquisition and archiving; spectral difference and derivatives; spectral enhancement and calculations; and we have included them in our new software package, PECSS.

**We'll help you choose**

With the Lambda Array 3840 and the controlling computer of your choice, you're the winner. Call us toll free at (800) 323-7155, (in Illinois, call (312) 887-0770) and we will help you make the decision. Or contact one of the offices below.

Perkin-Elmer Corp., Analytical Instruments
Main Avenue. (MS-12), Norwalk, CT 06856
U.S.A. Tel (203) 762-1000. Telex 965-954

Bodenseewerk Perkin-Elmer & Co., GmbH,
Postfach 1120, 7770 Ueberlingen, Federal
Republic of Germany. Telex: (07551) 811

Perkin-Elmer Ltd., Post Office Lane,
Beaconsfield, Bucks, HP9 1QA, England.
Tel: Beaconsfield (049 46) 6161

**PERKIN-ELMER**

The science and computer company.
Where solutions come first.

CIRCLE 169 ON READER SERVICE CARD

# KONTRON INSTRUMENTS

## your partner in science and health

CENTRIFUGES

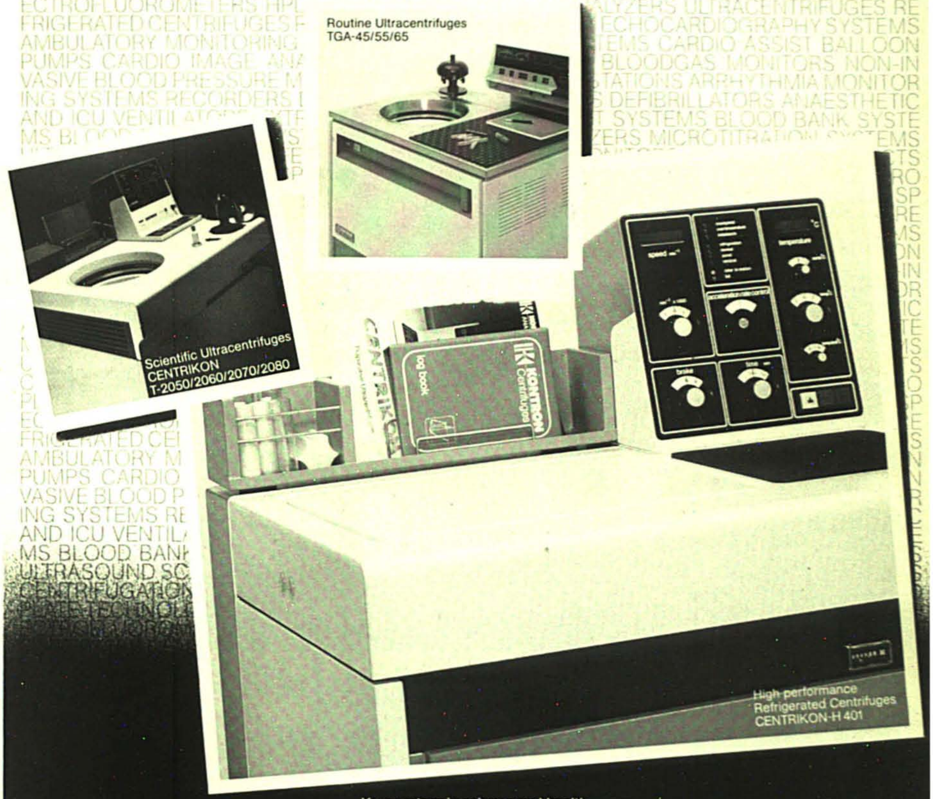

Routine Ultracentrifuges
TGA-45/55/65

Scientific Ultracentrifuges
CENTRIKON
T-2050/2060/2070/2080

High performance
Refrigerated Centrifuges
CENTRIKON-H 401

*Your partner in science and health*

**KONTRON**
INSTRUMENTS

*For further information please contact your local KONTRON Company*

| | | | |
|---|---|---|---|
| Austria (Vienna) | (0222) 670631 | Japan (Tokyo) | (03) 2634801 |
| France (Montigny le Br.) | (3) 0438152 | Scandinavia (Stockholm) | (08) 7567330 |
| Germany (Munich) | (08165) 771 | Spain (Madrid) | (01) 7291155 |
| Great Britain (St. Albans) | (0727) 66222 | Switzerland (Zurich) | (01) 4354111 |
| Italy (Milan) | (02) 50721 | USA (Everett/Mass.) | (617) 3896400 |

International Marketing Services, KONTRON AG, Bernerstrasse Süd 169, 8048 Zurich/Switzerland
Telephone (01) 435 41 11, Telex 822 191

CIRCLE 119 ON READER SERVICE CARD

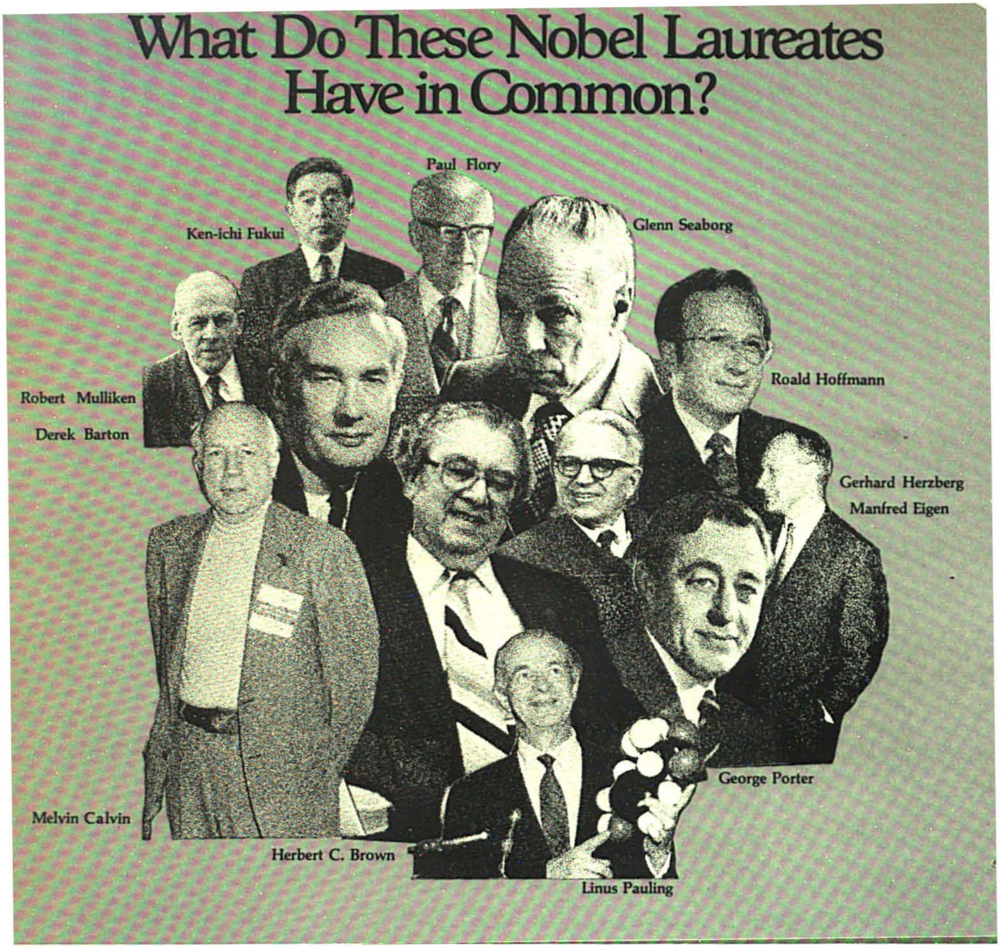
What Do These Nobel Laureates Have in Common?
Paul Flory
Ken-ichi Fukui
Glenn Seaborg
Roald Hoffmann
Robert Mulliken
Derek Barton
Gerhard Herzberg
Manfred Eigen
George Porter
Melvin Calvin
Herbert C. Brown
Linus Pauling

## They have all published articles in the journals of the American Chemical Society.

- Analytical Chemistry
- Chemical & Engineering News
- CHEMTECH
- Environmental Science & Technology
- Accounts of Chemical Research
- Biochemistry
- Chemical Reviews
- Industrial & Engineering Chemistry—Process Design and Development
- Industrial & Engineering Chemistry—Product R&D
- Industrial & Engineering Chemistry—Fundamentals
- Inorganic Chemistry
- Journal of Agricultural & Food Chemistry
- Journal of the American Chemical Society
- Journal of Chemical & Engineering Data
- Journal of Chemical Information and Computer Sciences
- Macromolecules
- Journal of Medicinal Chemistry
- The Journal of Organic Chemistry
- The Journal of Physical Chemistry
- ACS Single Article Announcement
- Journal of Physical and Chemical Reference Data
- Organometallics
- Langmuir

**American Chemical Society—chemical publishers since 1879.**

Send orders or inquiries to:

1155 Sixteenth Street, N.W.
Washington, D.C. 20036 U.S.A.

Cable Address: JIECHEM
Telex: 440159 ACSPUI or
892582 ACSPUBS
U.S.A. Call toll free: 800-424-6747

PHILIPS ANALYTICAL GAS CHROMATOGRAPHY

# The achievement

Superlatives have no relevance to the PU 4900 for they suggest comparisons which cannot be made.

Instead, its introduction invites an understanding by everyone involved with GC that the technique has finally achieved its true fulfilment.

The unique and essential principle behind this is termed "Total System-Power" by Philips Analytical and can be defined as the integration of chromatography and data handling in a single, uncompromised, analytical program.

Capillary, multi-dimensional or conventional, the implications for gas chromatography are sufficiently great to justify immediate examination. We, and the future, await your inquiry.

**Pye Unicam Ltd**
**York Street Cambridge**
**Great Britain CB1 2PX**
**Tel (0223) 358866 Telex 817331**

## *PU 4900 – the Total Analytical Chromatograph*

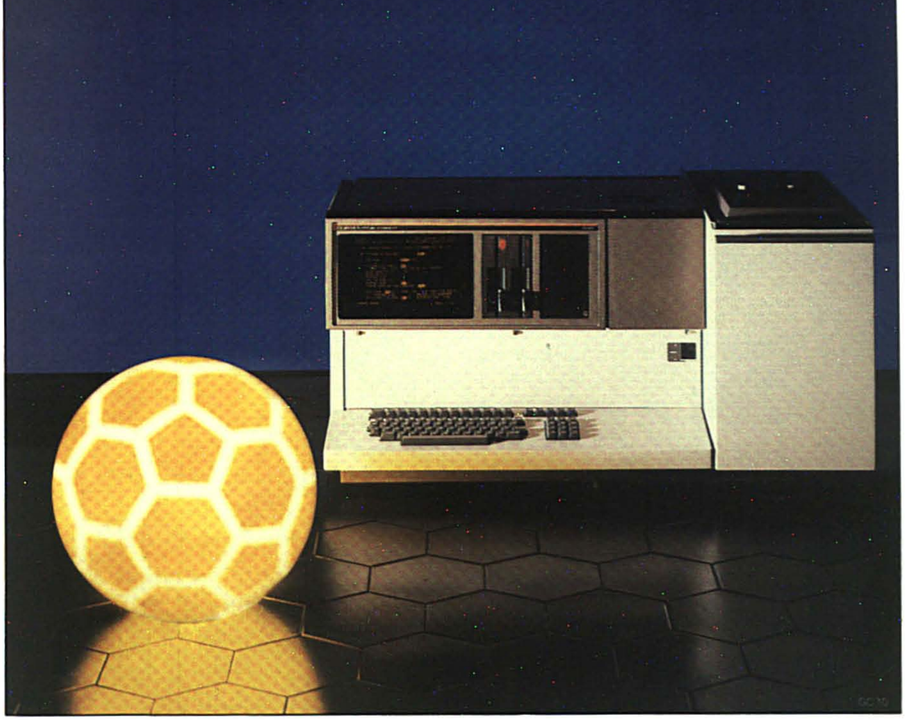

PHILIPS

**Scientific &**
**Analytical Equipment**

**PHILIPS**

CIRCLE 86 ON READER SERVICE CARD

# The Perfect "10"

**Your time is too valuable to waste on anything less than the top journal in your field. For 56 years, the highest standards for excellence have kept Analytical Chemistry ahead of the rest.**

And a personal subscription will help keep *you* ahead of the rest in at least ten ways:

1. Issue by issue, you build a personal desktop library of advanced research.

2. You get more pages of scholarly excellence in **Analytical Chemistry** than anywhere else in the field.

3. **Analytical Chemistry** publishes only the best in original research—each paper published has been subjected to rigid peer-review by recognized authorities.

4. Every paper is briefed in a single listing, saving you search time.

5. **Analytical Chemistry** is where the experts publish and where the experts go for information.

6. **Analytical Chemistry**'s vast informational resources will help you anticipate any developing technologies or methodologies that are likely to influence your functions.

7. Its broad scope provides complete and timely information on the varied facets of analytical chemistry. You'll be kept up-to-date on instrumentation, regulations, new product breakthroughs, literature and more.

8. Practical, hands on information is yours . . . our new column, *A/C Interface*, translates the intricate world of computers and relates it to you and your work.

9. **Analytical Chemistry**'s convenient subscriber service opens the door to the latest in product and literature resources. Simply use the reader service card for quick access to more information.

10. And, you'll receive two special BONUS issues each year: the annual LabGuide . . . your personal consultant to equipment and suppliers and the REVIEWS issue . . . 400 pages surveying the most recent literature, focusing on Fundamentals and Applications (in alternate years).

**So, why settle for anything less? Go right to the top with ANALYTICAL CHEMISTRY!**

For information, write
**ANALYTICAL CHEMISTRY,**
Circulation Office, The American Chemical Society, 1155 16th Street, N.W., Washington, D.C. 20036, or in the U.S. call
**TOLL FREE 800-424-6747.**

analytical chemistry

analytical
chemistry

LIQUID CHROMATOGRAPHY

# New peaks for LC

You're looking at the shape of the future in liquid chromatography.

Analysis by the dramatically effective new techniques of Microbore and FAST, plus the ability to enhance results using conventional columns.

It's all possible with a single system, if you invest in one of the new isocratic or gradient low dispersion LCs from Pye Unicam.

Their very low extra-column peak dispersion stems from a new range of pumps capable of exceptionally smooth and precise flow rates variable from 10 μl to 10 ml/min.

Flexibility and accuracy is maintained by the new PU 4025 variable wavelength UV detector offering 100 ms response time and available with a choice of four flowcells to suit every purpose.

Whether you are interested in better economy, sensitivity, sample throughput or simply better LC the new low dispersion range from Pye Unicam will help you achieve new peaks. Send today for full information.

0.05 4 10 5
235

**Pye Unicam Ltd**
**York Street Cambridge**
**Great Britain CB1 2PX**
**Tel (0223) 358866 Telex 817331**

LC06

**Analytical Equipment**

CIRCLE 87 ON READER SERVICE CARD

**PHILIPS**

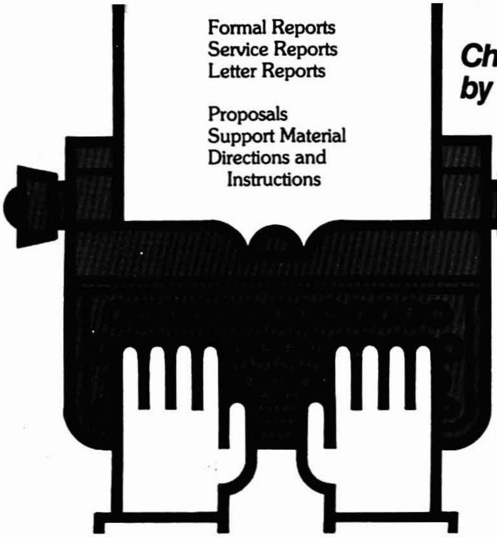

***Chemists are often judged by the papers they write***

**AMERICAN CHEMICAL SOCIETY'S AUDIO COURSE**

# PRACTICAL TECHNICAL WRITING

**SHOWS HOW TO WRITE TECHNICAL PAPERS WITH EASE, CLARITY AND CONFIDENCE**

The successful chemist writes a good many technical papers in a lifetime . . . some in-house, some for publication, some for clients or potential clients. In any case, careers are often helped—or hindered—by the caliber of those papers.

Fortunately, writing good, sound technical papers is a skill that can be mastered. The ACS Audio Course, PRACTICAL TECHNICAL WRITING, is designed to help scientists and engineers express themselves clearly, convincingly, and professionally.

Combining the ease of listening with the challenge of doing, the course consists of eight audiotape cassettes, with a total playing time of 5.3 hours, and an integrated manual which includes examples and exercises covered in the lecture, as well as additional information and instructions.

**NO RISK: 10-DAY FREE TRIAL**

Order your course in Practical Technical Writing now. Look over the manual . . . listen to some of the cassettes . . . see how comprehensively the manual and cassettes complement each other. Read the examples of sound technical writing. Notice the clear Do's and Don'ts spelled out in the easy-to-read sections. Then start the course. Try some of the exercises. If you are not satisfied, return it to us within ten days and all billing will be cancelled, or your money will be returned.

Practical Technical Writing
Practical Technical Writing

**THE INSTRUCTOR:** Professor Jay R. Gould, for many years Director of the Technical Writers' Institute and Master's Program in Technical Writing at Rensselaer Polytechnic Institute, is the author of "Opportunities in Technical Writing" and a revision of "Technical Reporting." While Professor of English and Communication at RPI, Professor Gould conducted in-house writing seminars for many companies and government agencies.

**INDIVIDUAL OR GROUP USE**

Individuals intent on improving their communications skills will find this course a worthwhile investment in their futures.

Groups, including companies, government agencies, universities, and professional clubs and associations will find that it lends itself to multi-person use, since individual manuals can be ordered for each participant.

**THE COST:**

The complete unit, including eight cassettes and a manual in a handsome, sturdy case . . . $265.00.
Additional manuals: $17.50 each.

Be prepared to write your next paper easily, quickly, confidently. Order your course under our no-risk, 10-day trial offer. Call TOLL FREE 1-800-424-6747 (Credit card orders only) or mail coupon.

**ACS Audio Courses**
**1155 Sixteenth Street, N.W., Washington, D.C. 20036**

Please send me ________ Practical Technical Writing Courses @ $265.00
Please send ______ additional manuals at a total cost of __________
☐ Please send me information on other available Audio Courses.
☐ Payment enclosed
Charge my ☐ VISA ☐ MasterCard ☐ ACCESS ☐ Barclay Card
Acct. No. ____________________
Exp. Date ________ Interbank Code ________ (MasterCard Only)
Name ____________________
Place of Employment ____________________
Address ☐ Home ☐ Business ____________________
City ____________ State ________ Zip ________

LATEST NEWS FROM PHILIPS ANALYTICAL

## Latest AA software

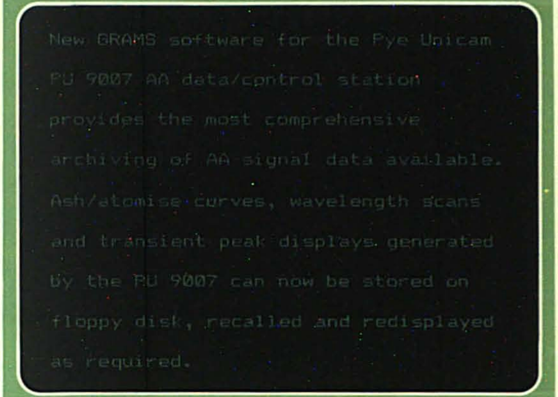

New GRAMS software for the Pye Unicam PU 9007 AA data/control station provides the most comprehensive archiving of AA signal data available. Ash/atomise curves, wavelength scans and transient peak displays generated by the PU 9007 can now be stored on floppy disk, recalled and redisplayed as required.

**Reader inquiry no. 70** AA27

## New LC detector

Interchangeable flowcells optimised for Microbore, FAST or conventional liquid chromatography are an important feature of the new PU 4025 variable wavelength UV detector from Philips Analytical.

It also offers push-button response time selection down to 100 ms, a master blazed holographic grating and silica coated optics.

**Reader inquiry no. 71** LC34

## Portable pH

A complete pH measuring package for applications away from the laboratory bench has been introduced by Philips Analytical.

It includes the new PW 9419 hand-held, battery operated pH meter, a tough, epoxy-bodied combination electrode, buffer sachets, bottles and battery, all contained in a compact carrying case.

**Reader inquiry no. 72** EC29

## UV/VIS flash

Here are facts you need to know about DERIVATIVE CONCENTRATION – unique to all Pye Unicam PU 8800 Video UV/VIS spectrophotometers.

- No more calibration curves – results directly in concentration
- Pre-treatment of difficult samples becomes unnecessary
- Offers significant improvement in sensitivity
- Removes sample background or matrix effects

**Reader inquiry no. 73** UV23

## For more information . . .

Use the reader inquiry service to obtain further details of the products which interest you.

| | Inquiry no. |
|---|---|
| **GRAMS AA software** | **70** |
| **PU 4025 LC detector** | **71** |
| **PW 9419 pH package** | **72** |
| **PU 8800 UV/VIS spectrophotometers** | **73** |
| **Other UV/VIS spectrophotometers** | **74** |
| **AA spectrophotometry** | **75** |
| **IR spectrophotometry** | **76** |
| **Gas chromatography** | **77** |
| **Liquid chromatography** | **78** |
| **pH, conductivity, ISE** | **79** |

**Pye Unicam Ltd**
**York Street Cambridge**
**Great Britain CB1 2PX**
**Tel (0223) 358866 Telex 817331** 11

**Scientific & Analytical Equipment**

**PHILIPS**

# CHEMICAL RESEARCH FACULTIES:

# *AN INTERNATIONAL DIRECTORY*

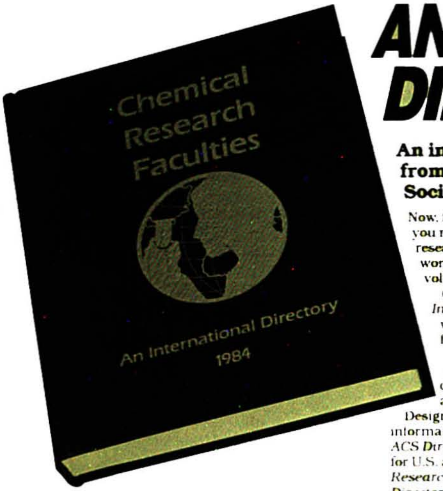

**$129.95** in the U.S. and Canada
**$155.95** in all other countries

## An invaluable new resource from the American Chemical Society.

Now, for the first time, *all* the information you need about chemical research and researchers at universities around the world has been gathered into one volume.

*Chemical Research Faculties: An International Directory* contains a wealth of facts on more than 8,900 faculty members and 737 departments in 62 countries. And it's a book no academic institution or chemically oriented business can afford to be without.

Designed to provide the same type of information on an international scale that the *ACS Directory of Graduate Research* gives for U.S. and Canadian schools, *Chemical Research Faculties: An International Directory* includes listings for chemistry, chemical engineering, biochemistry, and pharmaceutical/medicinal chemistry.

It offers informative statistical tables on graduate programs worldwide. Organizes data on 63 chemical societies in 51 nations. And is cross-referenced three ways—by faculty, institution, and research subject—for easy use.

## Indispensable for industry and academia alike.

If you're involved in chemical research, *Chemical Research Faculties: An International Directory* can keep you abreast of the latest developments in your area of specialization.

If you advise graduate students, it can help you steer them toward the programs they're seeking.

And if you're in a business even remotely related to chemical research, just one of the thousands of leads this book contains could pay for the purchase price many times over.

Why not fill out the order form right now? Or call 800/424-6747 and charge your VISA, MasterCard, or American Express.

And let *Chemical Research Faculties: An International Directory* open up a whole new world of professional possibilities.

**Departmental Information**
includes address and phone number, name of department head, advanced degrees offered, and principal areas of research

**Faculty Information**
includes name, year of birth, title, degrees (with years and institutions), areas of specialization, current research, and recent publications

**Chemical Society Information**
lists address, principal officer, publications, purpose, organizational structure, and number of members

**Guide to Chemical Research Institutions**
lists all countries, universities, and departments in order of appearance, providing an overview of each section

**Four Organizational Sections**
break down listings into chemistry, chemical engineering, biochemistry, and pharmaceutical/medicinal chemistry

**Faculty Index**
helps you keep up with colleagues' moves and learn more about others in your area of specialization

**Statistical Tables**
provide for each country the number of master's and doctoral degrees conferred in 1981 and 1982—as well as the number of full-time faculty, post-doctoral appointments, and students enrolled in advanced degree programs.

**Institutional Index**
provides a merged alphabetical listing that lets you find institutions known by name but not location

**Index of Research Subjects**
helps you locate universities, departments, and individuals doing research related to your own

800-424-6747

## ORDER FORM

☐ **YES! Please rush me my copy of the new international directory!**

| | *QTY* | *U.S./ CANADA* | *EXPORT* | *TOTAL* |
|---|---|---|---|---|
| **Chemical Research Faculties: An International Directory** | ______ | **$129.95** | **$155.95** | ______ |
| | | | California residents add 6% tax | ______ |
| | | | AMOUNT ENCLOSED | ______ |

☐ I have enclosed a check for $__________ payable to the American Chemical Society
☐ Purchase Order #______________ enclosed
Charge my ☐ VISA ☐ MasterCard ☐ American Express
☐ Barclaycard ☐ Access

Name of cardholder ______________________
Account # ______________________
Expires ______________ Interbank # ______________
(MasterCard and Access)
Signature ______________________

**Note:** Please allow four to six weeks for delivery. Foreign payment must be made in U.S. currency by international money order, UNESCO coupons, or U.S. bank draft. Order through your local bookseller or directly from the American Chemical Society. Orders from individuals must be prepaid.

**PLEASE SHIP BOOKS TO:**

Name ______________________
Address ______________________
______________________
______________________

33

**MAIL THIS ORDER FORM TO: American Chemical Society**
Distribution Office, Department 33
1155 16th Street, N.W.
Washington, D.C. 20036

☐ **Please send me more information about the *ACS Directory of Graduate Research 1983*, which gives similar data for U.S. schools.**

# You'll read it 1st

## LANGMUIR—*New in 1985!*

*Arthur Adamson, Editor; University of Southern California*

Bimonthly journal covering all areas of fundamental surface and colloid science…wet surface chemistry, 'uhv' surface chemistry, disperse systems, electrochemistry.

| | U.S. | Canada | Europe | All Other Countries |
|---|---|---|---|---|
| **Member** | $ 49 | $ 58 | $ 58 | $ 58 |
| **Nonmember** | $299 | $308 | $308 | $308 |

## ANALYTICAL CHEMISTRY

*George H. Morrison, Editor; Cornell University*

This monthly journal is the world's foremost publication in the vital field of measurement science.

| | U.S. | Canada | Europe | All Other Countries |
|---|---|---|---|---|
| **Member** | $ 20 | $ 40 | $ 57 | $ 80 |
| **Nonmember** | $ 30 | $ 50 | $ 99 | $122 |

## ACCOUNTS OF CHEMICAL RESEARCH

*Joseph F. Bunnett, Editor; University of California, Santa Cruz*

Monthly publication offering short, critical reviews written by scientists active in the research described.

| | U.S. | Canada | Europe | All Other Countries |
|---|---|---|---|---|
| **Member** | $ 22 | $ 26 | $ 28 | $ 31 |
| **Nonmember** | $ 96 | $102 | $102 | $105 |

## CHEMTECH

*Benjamin J. Luberoff, Editor; ACS*

Stimulating, personal monthly helping chemists and engineers arrive at innovative solutions to real problems.

| | U.S. | Canada | Europe | All Other Countries |
|---|---|---|---|---|
| **Member** | $ 27 | $ 33 | $ 37 | $ 44 |
| **Nonmember** | | | | |
| Personal | $ 38 | $ 44 | $ 48 | $ 55 |
| Institutional | $199 | $205 | $209 | $216 |

## ENVIRONMENTAL SCIENCE & TECHNOLOGY

*Russell F. Christman, Editor; Univ. of North Carolina, Chapel Hill*

Monthly for scientists engaged in study and maintenance of environment through the application of chemical principles.

| | U.S. | Canada | Europe | All Other Countries |
|---|---|---|---|---|
| **Member** | $ 26 | $ 34 | $ 40 | $ 49 |
| **Nonmember** | | | | |
| Personal | $ 35 | $ 43 | $ 49 | $ 58 |
| Institutional | $149 | $157 | $163 | $172 |

## JOURNAL OF THE AMERICAN CHEMICAL SOCIETY

*Allen J. Bard, Editor; University of Texas*

Most quoted biweekly journal of the widest possible interest to research workers and students in all areas of chemistry.

| | U.S. | Canada | Europe | All Other Countries |
|---|---|---|---|---|
| **Member** | $ 61 | $ 96 | $129 | $161 |
| **Nonmember** | $299 | $334 | $367 | $399 |

# in American Chemical Society Publications.

**From chemical news today to peer-reviewed research in print for the first time… ACS publishes worldwide developments in chemistry for you.**

**CALL TOLL FREE**
**800-424-6747**

***Air Service Delivery included in all rates listed for Europe and All Other Countries.**

**AMERICAN CHEMICAL SOCIETY, 1155 16th St., N.W., Washington, D.C. 20036** **1985**
**CALL TOLL FREE 800-424-6747**

**Please enter a one-year subscription for the following publications:**

PRICE PRICE

1. ____________________ 2. ____________________

3. ____________________ 4. ____________________

Name ____________________ Position ____________________

Company ____________________ Address ☐ Home ☐ Business ____________________

City ____________________ State ____________ Zip ____________

☐ Payment enclosed ____________ (Payable to American Chemical Society) ☐ Bill me ☐ Bill company

Charge my ☐ MasterCard ☐ VISA Account No. ____________________ Interbank No. ____________ (MasterCard only)

Expire Date ____________ Signature ____________________

Nature of Your Employer's Business: ☐ Manufacturing ☐ Government ☐ University

☐ Other (Please indicate) ____________________

☐ I am ☐ I am not an ACS member.

☐ Please send me information on how to become an ACS member.

**Member rates are for personal use only.**

Journal subscriptions start January 1985 and expire December 1985. Member subscriptions to Analytical Chemistry, Environmental Science & Technology, and CHEMTECH will start the month the order is placed and expire one year later unless subscriber requests a January start date.

Foreign payment must be made in U.S. currency by international money order, UNESCO coupons, U.S. bank draft, or through your subscription agency. For rates in Japan, contact Maruzen Co., Ltd.

**3147R**

## BIOCHEMISTRY

*Hans Neurath, Editor; University of Washington*

Offers results of original research in all recognized or developing areas of biochemistry. Biweekly.

| | U.S. | Canada | Europe | All Other Countries |
|---|---|---|---|---|
| **Member** | $ 59 | $ 92 | $117 | $149 |
| **Nonmember** | $303 | $336 | $361 | $393 |

## CHEMICAL & ENGINEERING NEWS

*Michael Heylin, Editor; ACS*

Chemical newsweekly and the official publication of the ACS that all members receive as part of their dues.

| | U.S. | Canada | Europe | All Other Countries |
|---|---|---|---|---|
| **Nonmember** | $ 37 | $ 61 | $ 88 | $116 |

(Via surface mail outside U.S. and Canada. $61)

## CHEMICAL REVIEWS

*Josef Michl, Editor; University of Utah*

Reviews of research of chemistry that eliminate the need to scan scores of articles concerning particular fields. Bimonthly.

| | U.S. | Canada | Europe | All Other Countries |
|---|---|---|---|---|
| **Member** | $ 19 | $ 24 | $ 28 | $ 33 |
| **Nonmember** | $ 76 | $ 81 | $ 85 | $ 90 |

## I&EC FUNDAMENTALS

*Robert L. Pigford, Editor; University of Delaware*

Publishes, quarterly, original scientific papers dealing with the very frontiers of chemical engineering understanding.

| | U.S. | Canada | Europe | All Other Countries |
|---|---|---|---|---|
| **Member** | $ 15 | $ 19 | $ 27 | $ 28 |
| **Nonmember** | $ 67 | $ 71 | $ 79 | $ 80 |

## I&EC PROCESS DESIGN AND DEVELOPMENT

*Hugh M. Hulburt, Editor; Northwestern University*

Quarterly contains original papers and occasionally critical reviews, that present theoretical and experimental results relating to the development of processes and process equipment.

| | U.S. | Canada | Europe | All Other Countries |
|---|---|---|---|---|
| **Member** | $ 15 | $ 19 | $ 30 | $ 32 |
| **Nonmember** | $ 76 | $ 80 | $ 91 | $ 93 |

## I&EC PRODUCT R&D

*Jerome A. Seiner, Editor; PPG Industries*

Publishes original research on broadly varied product related topics in an interdisciplinary manner. Quarterly.

| | U.S. | Canada | Europe | All Other Countries |
|---|---|---|---|---|
| **Member** | $ 15 | $ 19 | $ 30 | $ 32 |
| **Nonmember** | $ 76 | $ 80 | $ 91 | $ 93 |

## INORGANIC CHEMISTRY

*M. Frederick Hawthorne, Editor; University of California, Los Angeles*

Biweekly journal publishes fundamental studies, experimental and theoretical, in all phases of inorganic chemistry.

| | U.S. | Canada | Europe | All Other Countries |
|---|---|---|---|---|
| **Member** | $ 70 | $101 | $105 | $146 |
| **Nonmember** | $373 | $404 | $408 | $449 |

## JOURNAL OF AGRICULTURAL AND FOOD CHEMISTRY

*Irvin E. Liener, Editor; University of Minnesota*

Bimonthly reporting of original research into the chemical aspects of agriculture and food.

| | U.S. | Canada | Europe | All Other Countries |
|---|---|---|---|---|
| **Member** | $ 22 | $ 29 | $ 36 | $ 45 |
| **Nonmember** | $116 | $123 | $130 | $139 |

## JOURNAL OF CHEMICAL AND ENGINEERING DATA

*Bruno J. Zwolinski, Editor; Texas A & M University*

This quarterly journal is primarily concerned with the presentation of data of lasting value.

| | U.S. | Canada | Europe | All Other Countries |
|---|---|---|---|---|
| **Member** | $ 27 | $ 31 | $ 32 | $ 35 |
| **Nonmember** | $148 | $152 | $153 | $156 |

## JOURNAL OF CHEMICAL INFORMATION AND COMPUTER SCIENCES

*T. L. Isenhour, Editor; Utah State University*

Quarterly reporting on new R&D, concepts, systems, and programs in all areas of information and computers relevant to chemistry and chemical technology.

| | U.S. | Canada | Europe | All Other Countries |
|---|---|---|---|---|
| **Member** | $ 17 | $ 21 | $ 21 | $ 24 |
| **Nonmember** | $ 90 | $ 94 | $ 94 | $ 97 |

## JOURNAL OF MEDICINAL CHEMISTRY

*Phillip S. Portoghese, Editor; University of Minnesota*

Monthly journal concerned with the relationship of chemistry to biological activity, including rapid communication of major advances in drug design and development.

| | U.S. | Canada | Europe | All Other Countries |
|---|---|---|---|---|
| **Member** | $ 33 | $ 43 | $ 52 | $ 64 |
| **Nonmember** | $172 | $182 | $191 | $203 |

## THE JOURNAL OF ORGANIC CHEMISTRY

*Frederick D. Greene, Editor; Massachusetts Institute of Technology*

Biweekly offering critical accounts of original work and interpretative reviews of existing data that present new viewpoints.

| | U.S. | Canada | Europe | All Other Countries |
|---|---|---|---|---|
| **Member** | $ 45 | $ 71 | $ 95 | $110 |
| **Nonmember** | $233 | $259 | $283 | $298 |

## THE JOURNAL OF PHYSICAL CHEMISTRY

*Mostafa A. El-Sayed, Editor; University of California, Los Angeles*

Biweekly journal of experimental and theoretical research on fundamental aspects of physical chemistry and chemical physics.

| | U.S. | Canada | Europe | All Other Countries |
|---|---|---|---|---|
| **Member** | $ 56 | $ 86 | $108 | $145 |
| **Nonmember** | $333 | $363 | $385 | $422 |

## JOURNAL OF PHYSICAL AND CHEMICAL REFERENCE DATA

*David R. Lide, Jr., Editor; National Bureau of Standards*

Quarterly published with Amer. Inst. of Physics and N.B.S. presenting critically evaluated data on physical and chemical properties.

| | U.S. | Canada | Europe | All Other Countries |
|---|---|---|---|---|
| **Member (ACS, AIP, affiliated societies, personal)** | $ 50 | $ 60 | $ 75 | $ 85 |
| **Nonmember** | $200 | $210 | $225 | $235 |

## MACROMOLECULES

*Field H. Winslow, Editor; Bell Telephone Laboratories*

Monthly original material on all fundamental aspects of polymer chemistry.

| | U.S. | Canada | Europe | All Other Countries |
|---|---|---|---|---|
| **Member** | $ 44 | $ 57 | $ 68 | $ 82 |
| **Nonmember** | $254 | $267 | $278 | $292 |

## ORGANOMETALLICS

*Dietmar Seyferth, Editor*
*Massachusetts Institute of Technology*

Monthly journal with an interdisciplinary approach to organometallic chemistry: synthesis; structure and bonding; reactivity and mechanism; applications in organic, inorganic, polymer, and solid state chemistry, and materials science.

| | U.S. | Canada | Europe | All Other Countries |
|---|---|---|---|---|
| **Member** | $ 40 | $ 54 | $ 60 | $ 73 |
| **Nonmember** | $229 | $243 | $249 | $262 |

## ACS SINGLE ARTICLE ANNOUNCEMENT

Semi-monthly current awareness service reproduces contents pages of all ACS primary journals, so you may order articles of your choice using a form provided.

| | U.S. | Canada | Europe | All Other Countries |
|---|---|---|---|---|
| **Member** | $ 50 | $ 60 | $ 70 | $ 70 |
| **Nonmember** | $100 | $110 | $120 | $120 |

***Air Service Delivery included in all rates listed for Europe and All Other Countries.**

NO POSTAGE
NECESSARY
IF MAILED
IN THE
UNITED STATES

# BUSINESS REPLY CARD

FIRST CLASS PERMIT NO. 10094 WASHINGTON, D.C.

POSTAGE WILL BE PAID BY ADDRESSEE

**AMERICAN CHEMICAL SOCIETY**
**Attn: Periodicals Marketing Dept.**
**1155 Sixteenth Street, N.W.**
**Washington, D.C. 20036**

# Automated NMR? Varian generates MAGICAL™ results!

Total automation hardware and MAGICAL, Varian's new MAGnetics Instrument Control and Analysis Language, enhance both experiment flexibility and instrument ease of use on XL Series Systems to give you the best results — the first time, every time.

See us at the
FASEB in Anaheim, CA
April 21-26

## Here's how:

- New ASM-100 Automatic Sample Manager gives you the flexibility to load up to 100 samples individually or in batches.
- ASM-100 software lets you prioritize every sample and run them in any order.
- Fully automated spectrometer control, including AutoLock™ -Spin, -Shim,™ -Gain, -Phase,™ and -Eject.
- Unique quantitative analysis and customized report generation turn NMR data into useful answers.
- Automatic data acquisition, based on a pre-set signal-to-noise ratio, eliminates unnecessary acquisition time.
- Completely automates 2D experiment setup, making 2D NMR more routine.

**Call or write now.** Find out how you can get MAGICAL results with Varian XL Series NMR Spectrometers.

**Varian Instrument Group**, 220 Humboldt Court, Sunnyvale, CA 94089
• **In Canada:** 332 Guelph Street, Georgetown, Ontario L7G 4B5
• **In Europe:** Steinhauserstrasse, CH-6300 Zug, Switzerland

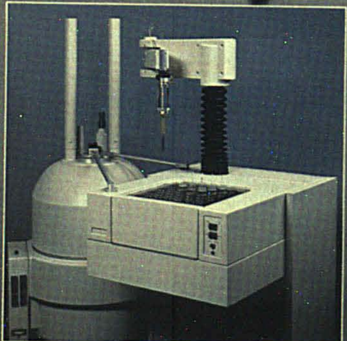

**For immediate assistance,**
**call 800-231-5572.**
**In Canada**, call 416-457-4130.
**In Europe**, call Zug, Switzerland, at (042) 23 25 75;
Darmstadt, Germany, at (06151) 7030.

varian

ANOTHER
variantelligent
INSTRUMENT

CIRCLE 219 ON READER SERVICE CARD

SPECTRONIC 20
BAUSCH & LOMB

# Breeding you can depend on. Stamina to spare.

## The SPEC 20™ tradition.

The SPEC 20™ has been the favorite spectrophotometer of more labs throughout the world than any other. And the "20" sired an entire breed of spectrophotometers like itself —instruments unsurpassed for dependability, performance, and value.

**Today there's a complete stable of SPECTRONIC® spectrophotometers,** from the basic value of the 21 line, through the microprocessor power of the 1001 split-beam and the sophistication of the 2000 double-beam, to the versatile new twins: the 501/601 single beams. And isn't it reassuring to know there'll always be a SPEC 20.

Which SPECTRONIC model should you harness for your lab? Contact your nearest Bausch & Lomb distributor or call Peg Moran (716) 338-8363. Then just use your own horse sense.

ANALYTICAL PRODUCTS
**BAUSCH & LOMB**

CIRCLE 22 ON READER SERVICE CARD

SPECTRONIC 21 series

NEW!

SPECTRONIC 501/601

SPECTRONIC 1001

SPECTRONIC 2000

2E023

# High Performance Gas Chromatography

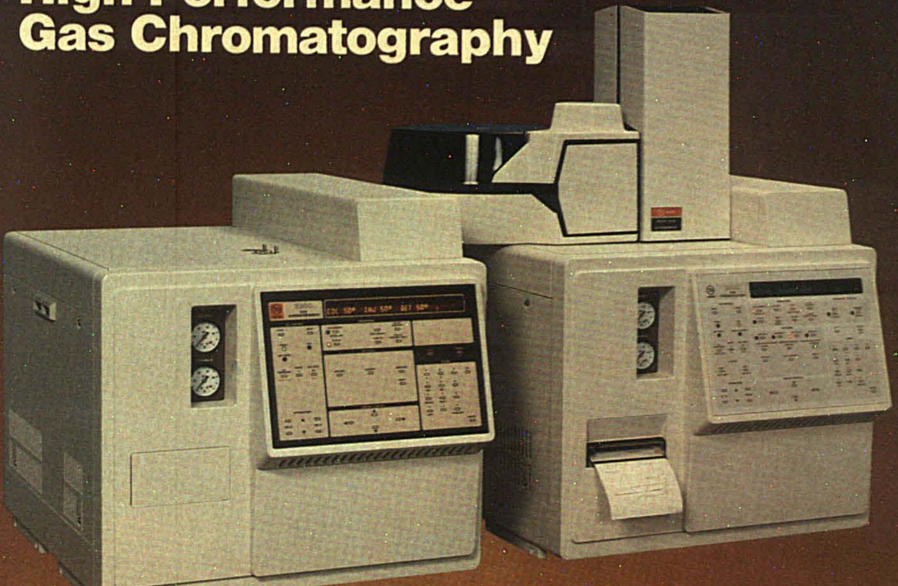

*Varian's high-reliability 3000 Series Gas Chromatographs perform more work at lower cost than any other GC in their class*

## New Model 3300

- Capillary and packed configurations with a complete choice of high performance injectors.
- Full line of high performance detectors—choose from TCD, FID, ECD, TSD, FPD and HECD.
- Provides full microprocessor control of injector/detector and auxiliary temperature zones, column oven temperature, detector ranges, and auto zero.
- Operates quickly and easily via touchpad keys and self-guiding display prompts.
- Offers maximum uptime with reliable design, unique self-checking diagnostics and user serviceability—saves service costs, too!
- Saves bench space with its 20″ width.
- Economical—from $6550.

## New Model 3400 . . . All 3300 benefits and these extra features:

- 4-method memory
- Optional printer/plotter built into the space-saving 20″ width.
- Powerful automation options:
  - Built-in method sequencing
  - Built-in control of powered relays and an autosampler.
- Serial I/O to Varian chromatography data systems, VAX LIMS, or external data systems.

**Call toll free 800-231-5772 (In Canada, call 416-457-4130) for immediate assistance.**

**Varian Instrument Group,** 220 Humboldt Court, Sunnyvale, CA 94089
· **In Canada:** 332 Guelph Street, Georgetown, Ontario L7G 4B5
· **In Europe:** Steinhauserstrasse, CH-6300 Zug, Switzerland

MORE
**varian***telligent*
INSTRUMENTS

See us at the FASEB in Anaheim, CA April 21-26

varian

CIRCLE 220 ON READER SERVICE CARD

# Is Your Compound Pure?

## The answer is automatic and instantaneous… only with Varian's exclusive PURITY PARAMETER™

*Varian introduces POLYCHROM™… a breakthrough in diode array HPLC detector technology.*

### The PURITY PARAMETER

- eliminates the need for subjective spectral overlays and 3-D presentations.
- provides peak confirmation even at trace levels.
- is far more than a ratio…an instantaneous, numerical and graphical presentation of spectral data for peak purity evaluation.
- eliminates laborious post run computer interrogation of data files.

**For immediate assistance, call**
**800-231-5772.**
**In Canada,** call 416-457-4130.

**Unique diode array technology** provides instantaneous spectral acquisition, simultaneous multiwavelength detection, and superior detection sensitivity.

**Complete stand-alone operation** for use with any liquid chromatograph.

**Fully automated diode array detector** with 16-bit internal computer enhances laboratory productivity.

**Less expensive than other diode array detectors** …the most cost effective LC detector on the market today!

**Varian Instrument Group,** 220 Humboldt Court,
Sunnyvale, CA 94089 • **In Canada:** 332 Guelph Street,
Georgetown, Ontario L7G 4B5 • **In Europe:** Steinhauserstrasse,
CH-6300 Zug, Switzerland

varian

MORE
**varian**telligent
INSTRUMENTS

See us at the
FASEB in Anaheim, CA
April 21-26

CIRCLE 221 ON READER SERVICE CARD

Instrumentation

**Stanford L. Smith**
Departments of Chemistry and Radiology
University of Kentucky
Lexington, Ky. 40506-0055

# Nuclear Magnetic Resonance Imaging

Proton nuclear magnetic resonance (NMR) imaging has provided a major breakthrough in diagnostic medical imaging and biomedical research. More than 200 instruments are now in use worldwide. Yet chemical analytical applications of the imaging techniques are virtually nonexistent. This article will discuss the basic principles and techniques of imaging, describe the instrumentation available, and consider some possible chemical applications.

The basic concept of imaging is simple (Figure 1). The Larmour equation

$$\omega = \gamma B$$

says the resonance frequency ($\omega$) is proportional to the field strength ($B$). In conventional NMR spectroscopy the magnetic field is extremely homogeneous, and the only variation in $B$ arises from the chemical environment of the nucleus leading to the usual kinds of NMR spectra. Imagers apply a relatively strong linear gradient, $\Delta G$, to the sample in a controlled manner, so $\omega$ depends on the location of the nuclei relative to the gradient. Conversion of frequency to distance is trivial for modern computerized equipment. The signal at any given frequency is still dependent on the concentrations of the nuclei and their relaxation times, $T_1$ and $T_2$. The actual process of obtaining an image is most conveniently considered in two sections: spatial encoding and factors determining information within the encoded volume.

## Spatial encoding

The simplest image is that of a single slice. Two steps are required: First, only nuclei in the slice of interest are excited; then the information from that slice is encoded in two dimensions. Slice thickness is determined by two factors, the slope of the gradient and the width of the rf pulse. Figure 2 illustrates the general principle. Since $\gamma$ for $^1H$ is 4250 Hz/gauss, a gradient of 0.1 gauss/cm produces a variation of 425 Hz over a distance of 1 cm. The pulse width, $PW$, of the exciting rf produces modulation of the carrier, giving a band of frequencies with bandwidth $1/PW$. For $PW = 2$ ms the bandwidth is 500 Hz. Only nuclei in a slice about 1.1 cm thick centered on the resonance point, $B_o + \Delta G$, will be

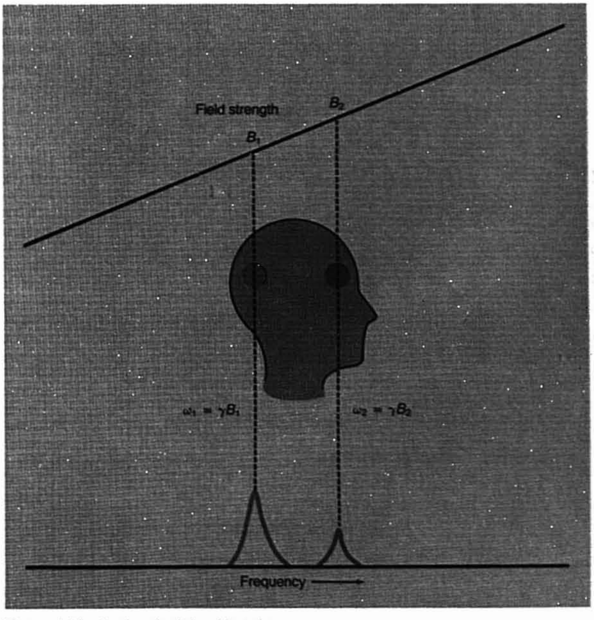

**Figure 1.** The basic principle of imaging
When the magnetic field strength varies systematically across an object, the resonance frequency of a group of nuclei is directly related to their position

0003-2700/85/0357-595A$01.50/0
© 1985 American Chemical Society

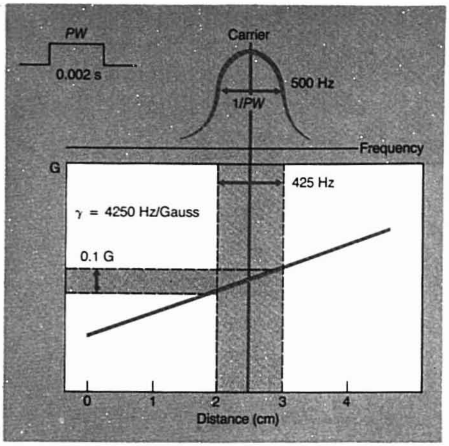
PW
0.002 s
Carrier
500 Hz
1/PW
Frequency
G
425 Hz
$\gamma$ = 4250 Hz/Gauss
0.1 G
0
1
2
3
4
Distance (cm)

**Figure 2.** Slice selection

Combination of a field gradient to produce a distribution of resonance frequencies and excitation of only a narrow band of frequencies by the rf pulse excites only the spins in a narrow region—in this case a slice ~1 cm thick

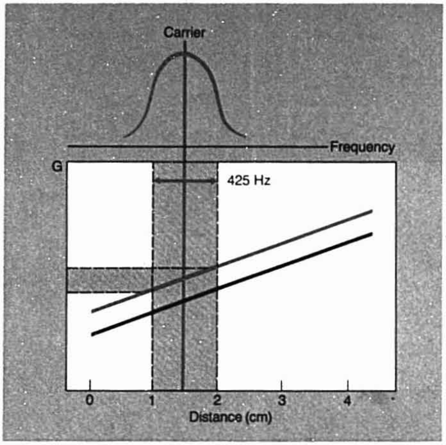
Carrier
Frequency
G
425 Hz
0
1
2
3
4
Distance (cm)

**Figure 3.** The location of a slice can be changed by applying a dc offset to the field gradient; this could also be accomplished by moving the rf carrier

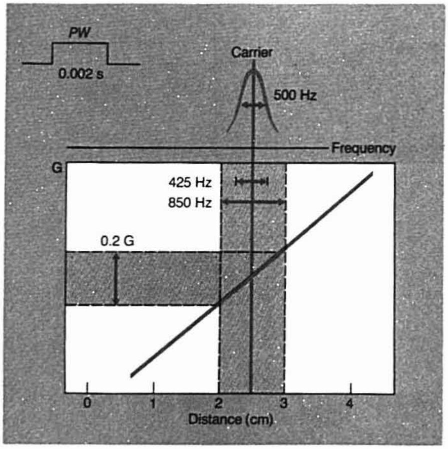
PW
0.002 s
Carrier
500 Hz
Frequency
G
425 Hz
850 Hz
0.2 G
0
1
2
3
4
Distance (cm)

**Figure 4.** Slice thickness is determined by the combination of the gradient slope and the rf pulse width and can be changed by varying either one (in this case changing the slope is illustrated)

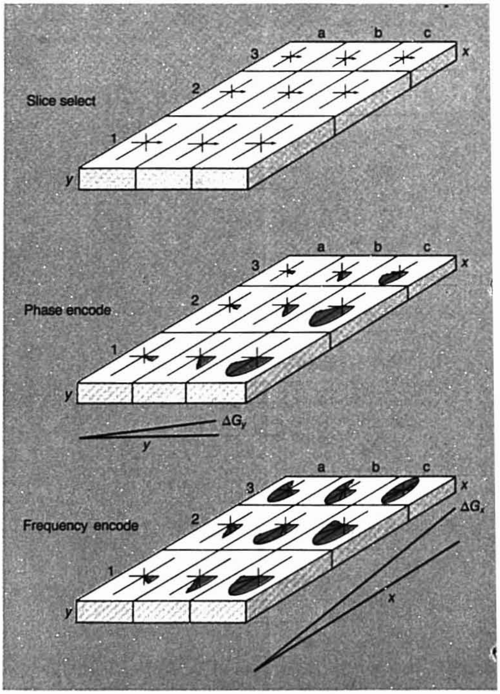
a
b
c
x
3
2
1
Slice select
y
a
b
c
x
3
2
1
Phase encode
y
$\Delta G_y$
y
a
b
c
x
$\Delta G_x$
3
2
1
Frequency encode
y
x

**Figure 5.** Spatial encoding within a slice is accomplished by applying a phase-encoding gradient and then a frequency or "read" gradient to the set of polarized spins in the slice

flipped by this soft rf pulse. If the gradient is turned off and the receiver turned on at this point, a single signal is observed from the nuclei in the region excited. As shown in Figures 3 and 4 the location of a slice can be changed by applying a dc offset to the gradient, and the thickness of the slice can be varied by changing either the gradient slope or the rf pulse width. Orientation of the slice relative to the sample (or the magnet) coordinates depends on whether the slice selection gradient is applied with the $x$, $y$, or $z$ gradient coil.

Spatial encoding within the slice is accomplished in a manner identical to that used for high-resolution 2D spectroscopy. A simplified picture of this is given in Figure 5. Following slice selection all the spins in the slice have been flipped. The slice selection gradient is turned off, and a second orthogonal gradient ($G_y$) is turned on for a fixed time period ($t_y$). Nuclei precess at different frequencies, depending on their position relative to this second gradient. In the example all spins in column a have precessed through a given phase angle. Spins in column b are in a stronger field and have precessed through a larger phase angle, etc. The end result is to phase encode distance information along the $y$ direction. After the phase-encoding gradient is turned off a third gradient ($G_x$) orthogonal to the previous two is turned on, as is the receiver for an appropriate time, $t_x$. A free induction decay (FID) is acquired in which spins in row 1 move at one frequency, spins in row 2 move at a greater frequency, etc., which provides the final spatial encoding along the $x$ axis. The process is repeated as often as desired for incrementally increasing values of the phase-encoding gradient. A typical experiment might obtain an FID of 256 or 512 data points for each of 128 different phase-encoding gradients. The result is a two-dimensional data set.

In a conventional high-resolution 2D experiment the raw data are a function of two time periods, an evolution time ($t_e$) and a detection time ($t_d$). Double Fourier transformation (FT) yields the conventional 2D spectrum with two frequency axes

$$S(t_e, t_d) \xrightarrow{\mathrm{FT}^2} S(\omega_e, \omega_d)$$

In 2D FT imaging the spins move at different frequencies during evolution and detection because of the strong gradient applied rather than from intrinsic chemical shift or coupling differences (which at the present time in current equipment are much smaller than the effects of the gradients). In this case it is convenient to keep $t_e$ fixed and increase the slope of the phase-encoding gradient rather than

Our MICRO/IR System runs transmittance or reflectance spectra on samples as small as 10 microns.

Integrated into the powerful Qualimatic FT-IR spectrometer, our MICRO/IR System features a microscope with a horizontal stage up to 6" × 6", a turret of objectives (4x, 32x) for easy sample location and uncompromised performance, Cassagrainian optics, and an integral, permanently aligned 0.25 mm MCT detector.

Send today for our MICRO/IR System Brochure to BIO-RAD, Digilab Division, 237 Putnam Avenue, Cambridge, MA 02139. Or call (800) 225-1248.

BIO-RAD Digilab Division

DIGILAB MICRO FT-IR

...because you never know when you'll need high performance.

CIRCLE 21 ON READER SERVICE CARD

Attention: Chemical Scientists

Do you want to . . .

- Keep up to date?
- Increase professional contacts?
- Receive substantial discounts on publications?
- Present your latest research?
- Receive assistance in financial planning?
- Attend chemical expositions?
- Find a new position?
- Continue your chemical education?

If you can say "yes" to even one of these the **ACS** should be *your* Society!

Write or call today for information about these and many other benefits.

**Membership Development Office**
**American Chemical Society**
**1155 16th St., N.W.**
**Washington, D.C. 20036**
**202-872-4437**

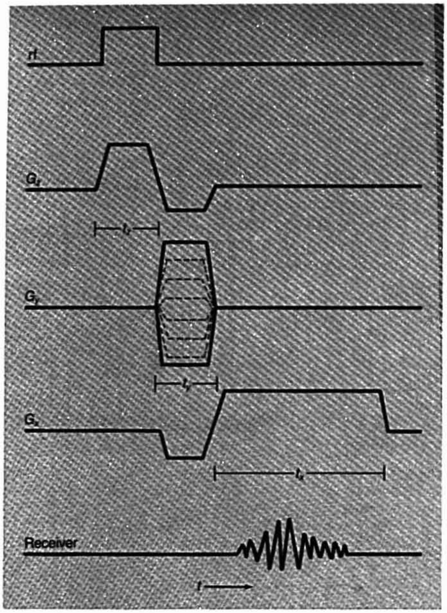

**Figure 6.** The imaging sequence for single-slice 2D FT imaging

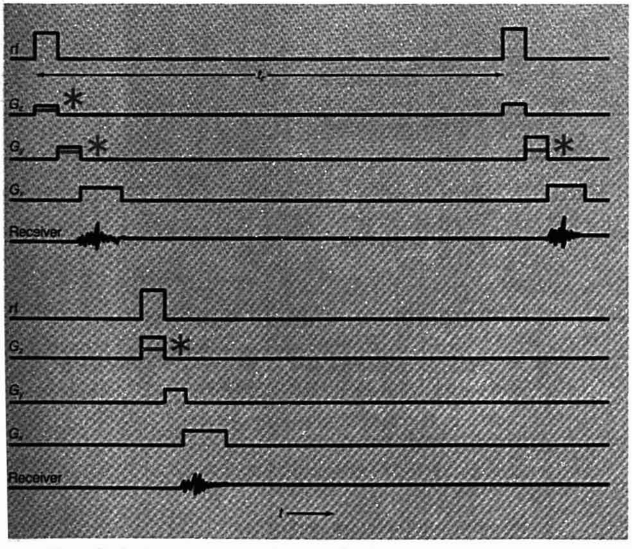

**Figure 7.** The imaging sequence for multislice imaging

In the upper sequence (identical to Figure 6) the data for one slice are encoded. The second set of pulses and gradients for this slice differs in the magnitude of the phase-encoding gradient (red asterisks). The second slice sequence is the same as the first, except that a different slice location is selected (blue asterisks)

increasing $t_e$ by increments as is done in 2D FT spectroscopy. Thus, a signal that is a function of two gradients is doubly Fourier transformed to a signal that is a function of two frequencies that are related to spatial distances

$$S(G_x, G_y) \xrightarrow{\text{FT}^2} [S(\omega_x, \omega_y)] \rightarrow S(D_x, D_y)$$

Unlike a 2D spectrum, which contains information at only a few locations, an image usually contains intensity information at all possible points. This is most conveniently displayed as a picture in which the white (or the red end of a color scale) indicates high intensities and black (or blue) indicates low intensities, rather than as a stack plot or contour plot used in 2D spectroscopy. It is, of course, possible to obtain plots or digital readouts of the intensity values for any desired row, column, or selected set of volume elements (voxels) represented in the picture.

Resolution in an image is, in principle, determined by the minimum volume that contains a sufficient number of nuclei to give a detectable signal. In current practice it is determined by the slice thickness, the number of phase encoding steps, and the number of data points acquired in each FID. Current commercial instruments produce images with 128 × 128, 256 × 256, or 512 × 512 horizontal elements on slices a few millimeters to 1.5 cm thick. Results from experimental high-field studies on small samples suggest that horizontal resolution of $\sim$100 $\mu$m on slices less than 1 mm thick is attainable.

Figure 6 is a typical imaging sequence for a single slice measurement by 2D FT showing the relative timing involved in turning on and off the rf, various gradients, and the receiver. The whole process for acquisition of a single FID requires a few hundred milliseconds at most. As for any pulse NMR experiment it is necessary to wait for a period of time (related to $T_1$) to permit recovery of equilibrium magnetization before repeating the sequence. This repeat or recycle time, $t_r$, is typically 0.5–2.0 s for biological, samples having $T_1$'s of 0.1 to 2–3 s. As a result it takes 2–10 min to acquire the raw data for a single slice image. Processing and display using array processors require a few minutes or less. An obvious extension, common on all imagers, is to use the time during which the spins in the first slice are recovering to obtain data from a different slice location that was left undisturbed by the first sequence. As shown in Figure 7, the timing and sequence are identical in all respects except that the second slice selection gradient is given a dc offset to select

# Ten years of research stand behind these LC injectors.

# And Rheodyne's not done yet.

You can expect Rheodyne always to be designing and testing new LC sample injectors. Doing just that, we've acquired a lot of valuable knowledge that we can pass on to you. Both in the form of better-designed sample injectors–and in the form of expert advice on the most effective way to use them.

Our aim has always been to make injectors more versatile and easier to use, while maximizing the precision and resolution of your liquid chromatograph. Rheodyne's Model 7125, pictured in the foreground below, is an excellent example of this philosophy. It injects sample either from a loop that's completely filled (to maximize precision) or from a loop that's partially filled using a syringe (to save time). The 7125 offers unexcelled versatility, ease of use, and reliability.

Expert advice on how to use sample injectors is available to you in Rheodyne's Technical Note No. 5. It tells how to achieve high precision while avoiding sample wastage and cross contamination. Ask your Rheodyne dealer for free copies of all our Technical Notes and our catalog.

Or contact Rheodyne, Inc., P.O. Box 996, Cotati, California 94928, U.S.A. Phone (707) 664-9050.

7000
LOAD
INJECT
7125
LOAD
INJECT

**RHEODYNE**

THE LC CONNECTION COMPANY

CIRCLE 178 ON READER SERVICE CARD

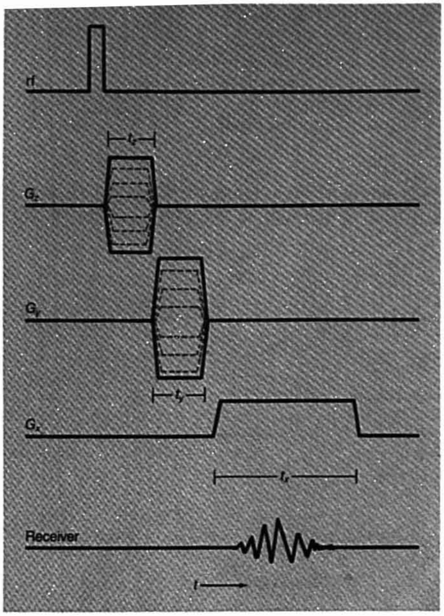

**Figure 8.** The imaging sequence for 3D FT imaging
A hard rf pulse produces excitation of all the spins in the sample, and two different phase-encoding gradients are applied before the read gradient

spins at a different location. This approach is known as multislice imaging and permits 2–32 slices to be obtained in the time previously required for a single slice. (Obviously the number of slices potentially obtainable is limited by $t_r$.) At present multislice imaging is the most efficient method used.

True 3D FT imaging is accomplished by a conceptually simple extension of the 2D method (Figure 8). A hard (i.e., narrow width) rf pulse is applied to polarize all spins in the sample. A gradient is applied to produce phase encoding along one axis ($z$). It is turned off, and an orthogonal gradient ($y$) is turned on to produce a second phase encoding along that axis. Finally, a read gradient orthogonal to the previous two ($x$) is turned on along with the receiver, and a FID is acquired. The process is repeated with the same value of the $z$ gradient, but an incrementally different value of the $y$ gradient. After a suitable number of $y$ gradient steps have been performed a new incrementally different value of the $z$ gradient is applied and, again, a set of $y$ increments is run. The final result is a 3D data set that can be Fourier transformed three times and converted to distance information

$$S(G_z, G_y, G_x) \xrightarrow{\mathrm{FT}^3} [S(\omega_z, \omega_y, \omega_x)] \rightarrow S(D_z, D_y, D_x)$$

Acquisition and processing of 3D images requires an hour or so and can be done on most commercial instruments. It is not commonly used for several reasons. In most cases almost the same information can be acquired more rapidly by the multislice technique. The requirement that the sample (patient or animal) not move for an hour is difficult to achieve, and more information is acquired than can practically be displayed and examined with present equipment.

Consideration of the relationship between 2D FT spectroscopy, 2D FT imaging, and 3D FT imaging leads to an understanding of how chemical shift imaging can be accomplished. The only requirement is that the magnet used for imaging have an extremely homogeneous field (0.1 ppm or better) when the gradients are not being applied. The only change in the sequence is to insert a variable evolution time, $t_e$, in the sequence whose function is identical to that of $t_e$ in conventional 2D spectroscopy. For example, during a time period following slice selection by a soft rf pulse and a gradient, individual spins will precess at different frequencies depending on their chemical shifts (and coupling), producing phase encoding. After that time period, spatial phase encoding and read gradients produce spatial encoding exactly as before. The process is repeated for an incrementally different $t_e$ exactly as is done in 2D spectroscopy. Triple Fourier transformation produces a data set in which one of the dimensions is chemical shift information and the other two are spatial information

$$S(t_e, G_y, G_x) \xrightarrow{\mathrm{FT}^3} S(\omega, D_y, D_x)$$

Conceptually, extension to four- or five-dimensional acquisition is obvious although the practical feasibility of such experiments remains to be demonstrated.

It should be noted in closing this section that the techniques described here are those currently used on commercially available equipment. There are several other ways to produce spatially encoded NMR information, but at this time they are not being commercially implemented.

## Image Intensity

Four factors control the intensity of the signal from a given voxel: the intrinsic sensitivity of the nucleus, concentration, $T_1$ (spin lattice), and $T_2$ (spin–spin) relaxation times.

Present commercial imagers detect only hydrogen, but satisfactory images have been obtained using other nuclei such as $^{19}$F, $^{31}$P, and $^{23}$Na. Signal averaging, the usual solution to low-sensitivity concentration problems, is relatively ineffective. During imaging the S/N ratio increases with $\sqrt[6]{n}$ ($n$ = the number of scans) rather than $\sqrt{n}$ as in one-dimensional averaging. Imaging with nuclei other than $^1$H obviously has considerable potential, and the next generation of equipment is being designed to be multinuclear. However, for the immediate future, sensitivity approaching conventional spectroscopy cannot be expected. Carbon-13 and $^{15}$N imaging are not likely to be very practical.

With a reasonable concentration of a suitable nucleus the critical factors determining whether an image can be obtained at all, and if it is obtainable, controlling the intensity, are the spin lattice ($T_1$) and spin–spin ($T_2$) relaxation times. Practical imaging presently requires that $T_2$ be at least a few milliseconds. $T_1$ and $T_2$ should not exceed a few seconds. (Recall that $T_2 \leq T_1$.) These values are typically found in liquids or liquidlike solids, but not in crystalline or rigid solids. For example, aqueous solutions, viscous liquids

INORGANIC ELEMENTAL ANALYSIS

Simultaneous, Non-Destructive, Wide Dynamic Range

EDXRF

- **Sample Form**
  Solid, Powder or Liquid
- **Dynamic Range**
  PPM to 100%
- **Ease of Use**
  Fully Automated, Single Pushbutton Analysis of up to Ten Samples
- **Analysis Time**
  All Elements Simultaneously, in Minutes

Tracor Xray

TEL. 415/967-0350

CIRCLE 201 ON READER SERVICE CARD

AIRCO
Pure Gases
Mixed Gases
Electronic Gases
Equipment
Instrumentation
Special Gases and Equipment

We're giving away our entire product line.

It's all in our free Special Gases & Equipment Catalog. It lists and describes pure, mixed and electronic gases from Argon to Zenon. Plus all the regulators, flowmeters, instrumentation, fittings, cylinders and other gas handling equipment you'll ever need. To get your free copy of everything we sell, just fill out the information below and mail.

Name ______
Title ______
Company ______
Address ______
City ______ State ______
Zip ______ Phone ______

AIRCO

Airco Special Gases, 575 Mountain Avenue
Murray Hill, New Jersey 07974

CIRCLE 7 ON READER SERVICE CARD

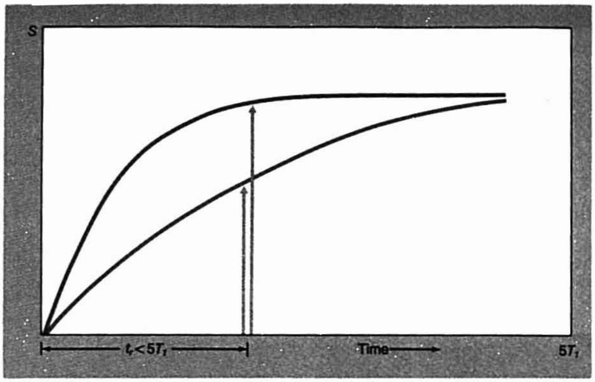

**Figure 9.** Spin lattice, $T_1$, relaxation curves for two different species

When the repeat or recycle time, $t_r$, for the sequence is less than 5 × $T_1$, the relative intensity of the signal observed depends on the relaxation rate

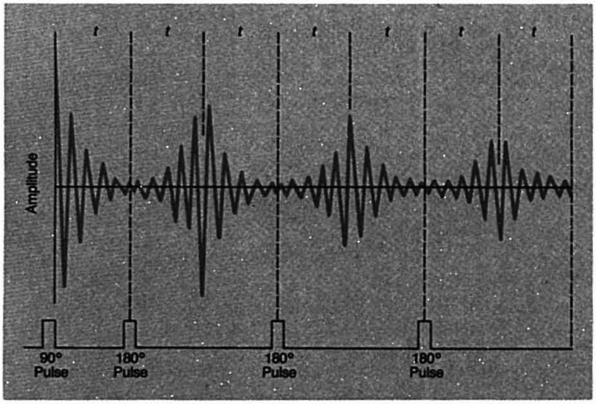

**Figure 10.** The signal available following a 90° pulse decays rapidly as a function of both natural $T_2$ processes and experimental conditions such as field inhomogeneity, as illustrated at the beginning of this figure

Application of a 180° pulse at some time *t* following the initial 90° pulse reverses these experimental effects and produces an echo (at a time 2*t* after the 90° pulse) that is diminished only by the natural $T_2$ processes. A series of 180° pulses known as a Carr–Purcell sequence can be used to obtain a series of echoes that can be sampled at any time in the natural decay curve, such as at the point illustrated in Figure 11

such as glycols, and soft solids such as lard or grease give excellent images. Materials such as polymethyl methacrylate and wood do not, but "liquid" regions or inclusions in such materials do. Materials with suitable $T_1$ and $T_2$ values also have reasonably narrow spectral lines obviating the problems implicit in the very wide powder patterns characteristic of rigid solids.

Within the above limits, intensity data are determined in an image exactly the same way they are in a conventional spectrum—by the rf pulse sequence and its timing. In conventional pulse FT spectroscopy a time $\geq 5T_1$ is required between the rf pulses to permit complete recovery of magnetization (Figure 9). If a sample contains species with different $T_1$'s and the recycle time, $t_r$, is less than five times the longest $T_1$ value, the intensities of all the lines in a spectrum are distorted; those with short $T_1$'s are enhanced and those with longer $T_1$'s are diminished. The $t_r$ recycle time in the imaging sequences (Figures 6, 7, and 8) produces exactly the same effect in

**VG MASSLAB**
**Automated Mass Spectrometry**

**VG 12-250**
A NEW CONCEPT IN LC-MS/GC-MS

- SIMPLE KEYBOARD CONTROL
- 2000 AMU MASS RANGE
- THERMOSPRAY LC INTERFACE
- FAST ATOM BOMBARDMENT
- FAST ALTERNATE +EI/+CI/–CI

With the development of the VG12-250 LC-MS/GC-MS quadrupole, VG MassLab has opened up new areas of analysis and brought automated mass spectrometry to the analytical scientist who demands optimum results.

Combining the VG12-250 mass spectrometer with one of the most powerful data systems available, has produced a flexible, high performance, research grade instrument with simple keyboard control – whilst VG's unique Thermospray inlet provides the ultimate in detection limits and ease of operation with LC.

To find out more about the capabilities of the VG12-250 contact:

**VG MASSLAB**
Automated mass spectrometry

**VG INSTRUMENTS INC.**, 300 Broad Street, Stamford, CT 06901.
Tel: (203) 322-4546 Telex: 230965999
**VG MASSLAB**, Tudor Road, Altrincham, Cheshire WA145RZ, England.
Tel: 061-941 3552 Telex: 669964

CIRCLE 224 ON READER SERVICE CARD

an image as it does in a conventional spectrum. In an image a bright or high-intensity voxel corresponds to a site with a relatively short $T_1$ value that has recovered considerable magnetization during $t_r$ as compared to a dark (low intensity) voxel that has not. (This assumes, of course, that the concentration in the two voxels is substantially the same.) The unique feature of the image is that the chemical species in the different voxels may be the same, e.g., water, but still report different $T_1$ effects at different sites for a variety of reasons, such as degree of hydration, concentration and nature of dissolved species, and temperature. If $T_1$ remains constant but concentration varies, the image will provide a concentration map. Obviously, both effects can occur simultaneously.

Images acquired in this way are labeled SR images because of the equivalence of the imaging sequence to the $(90° - \tau)_n$-acquire saturation recovery $T_1$ measurement sequence of conventional spectroscopy. Greater dynamic range and image contrast are obtained by applying a 180° inverting pulse followed by a time interval before beginning the imaging sequence. This is identical to the $(180° - \tau - 90°)$ inversion–recovery $T_1$ measuring sequence of conventional spectroscopy, and such images are labeled IR images. Images obtained by either technique are collectively called $T_1$ weighted images.

Spin-spin ($T_2$) relaxation causes loss of detectable magnetization, resulting in a decrease or decay of the signal (FID) with time (Figure 10). Both natural factors, depending on the nature of the sample, and instrumental factors, most notably field inhomogeneity, contribute to this decay. Elimination of the instrumental effects and measurement of the true or natural $T_2$ is accomplished by the formation of *spin echoes.* In either conventional spectroscopy or imaging, initial detectable magnetization is produced by a 90° pulse. If after some time $t$ a 180° pulse is applied, the instrumental effects on the signal decay are reversed and magnetization is refocused, reaching a maximum at a time $t$ after the 180°pulse. A series of such pulses, known as a Carr–Purcell sequence, will produce a set of echoes, each of which is diminished slightly in amplitude from the previous echo only by natural $T_2$ processes as shown in Figure 11.

Although not shown earlier, all imaging sequences normally include at least one 180° rf pulse and actually detect an echo rather than the initially produced FID. The primary reason is to correct for various instrumental effects that decrease signal intensity during the time period between the initial 90° pulse and the time the receiver is turned on, but selection of the echo time ($2t$ in Figure 10) provides another means of controlling image and intensity. Images produced in this manner are called $T_2$ weighted images or sometimes SE (spin echo) images.

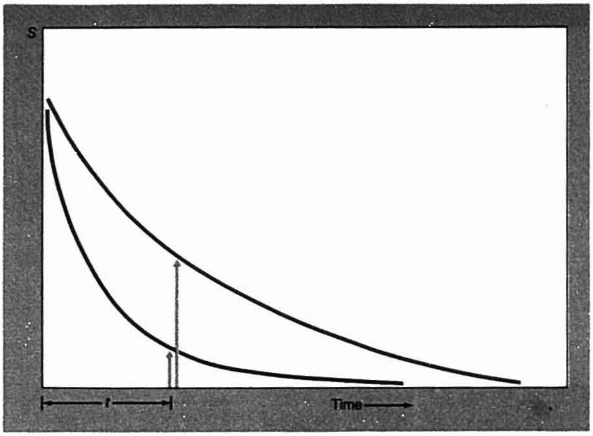

**Figure 11.** Spin-spin ($T_2$) relaxation curves for two different species
When acquisition of the FID is delayed, the magnitude of the acquired signal depends on the spin-spin relaxation time constant

Some instruments are able to apply a Carr–Purcell sequence and collect data from several echoes following a single spatial encoding sequence. For example, four images corresponding to echo times, $t_e$, of 30, 60, 90, and 120 ms might be acquired for a single slice in the same time otherwise required for a single image. Combinations of techniques lead to multislice–multiecho imaging whereby a total of perhaps 64 images (16 slices with four echoes for each slice) can be obtained in the time originally required for a single slice.

As was the case with $T_1$ effects, different materials or the same substance in different environments can have different $T_2$ values. As shown in Figure 11 a voxel in which the $T_2$'s are long will still give appreciable signal (and hence appear relatively bright) at longer echo times whereas a voxel in which the $T_2$'s are short will have a very weak signal (and hence appear darker).

In summary, the operator can select single-slice, multislice, or 3D spatial encoding. In the former cases the plane of the slice can correspond to whatever gradient is used for slice selection. Within any spatial encoding scheme the operator can select $t_r$ and $t_e$ (and also the options of inversion–recovery and Carr–Purcell sequences). A sufficiently long $t_r$ and a short $t_e$ will produce images in which contrast or intensity depends primarily on concentration. A long $t_r$ and longer $t_e$ produce $T_2$ weighted images. A shorter $t_r$ and short $t_e$ produce primarily $T_1$ weighted images. In practice most images contain all three effects. Acquisition of several images with different $t_r$'s or $t_e$'s permits calculation of the actual $T_1$ and $T_2$ value corresponding to each voxel. An image can then be presented in which the intensity in each voxel corresponds to the numerical value of $T_1$ or $T_2$. Such images are called $T_1$ (or $T_2$) images or maps. (In actual practice more complicated combinations of pulse sequences and timings permit calculation of $T_1$ (or $T_2$) maps from only two or three image data sets. The results are less accurate, but much more rapidly obtained.) The same kind of approach can be used to obtain concentration maps from several image data sets containing concentration, $T_1$, and $T_2$ effects.

## Instrumentation

Imaging equipment is divided into three groups. Whole-body medical imagers have large magnets with a 1-m free bore in which a human (or other object of similar size) can be placed. Electromagnets with field strengths of 0.15 or 0.3 Tesla (1 T = 10,000 gauss) detecting protons at 6 MHz or 12 MHz and superconducting solenoids with 0.5 T (21 MHz) or 1.0 T (42.5 MHz) are common. A few experimental instruments operate at 1.5 T or 2.1 T, but only the lower field instruments are presently approved for

# There's more in a new Model 8300 Gas Chromatograph than meets the eye!

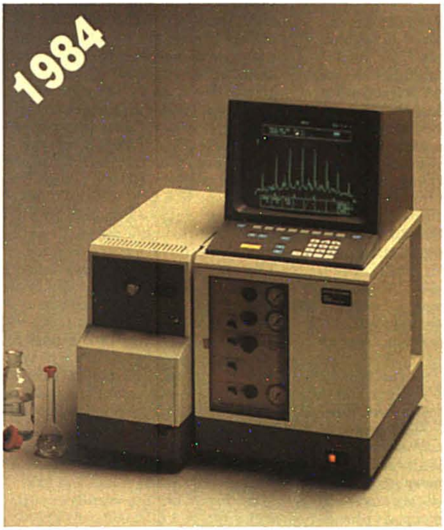

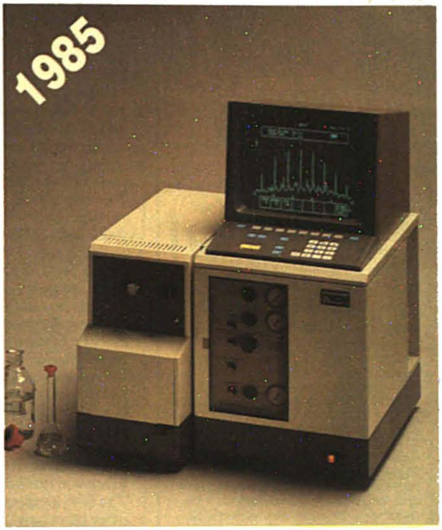

**Our 1985 Model 8300 appears no different from last year's model – but take a closer look! It now offers even greater versatility and performance.**

New features include:

☐ The PTV (Programmable Temperature Vaporiser) for capillary chromatography – an outstanding new split/splitless injector allowing cold injection from syringe or autosampler, with major improvements in analytical precision and greater security with thermally labile substances.

☐ A data handling option providing re-integration of raw data in addition to real time graphics and data handling.

☐ Electronic pressure readout of capillary column head pressure up to 100 psi – ideal for the whole range of columns from micro-bore to wide bore.

☐ Four ramp temperature programming with column oven ranges covering -80°C to +500°C with liquid nitrogen or carbon dioxide accessories.

Combined with the other unique features of the Model 8300 – ease of operation, automated bleed compensation, real time graphics/data handling and the AS-8300 autosampler – these new features maintain the Model 8300 as the world's most advanced, yet friendly gas chromatograph.

Why not see for yourself?

For further information please contact:
Perkin-Elmer Corp., Analytical Instruments.
Main Ave. (MS-12), Norwalk, CT 06856
U.S.A. Tel: (203) 762-1000.
Perkin-Elmer Ltd., Post Office Lane,
Beaconsfield, Bucks HP9 1QA, England.
Tel: Beaconsfield (049 46) 6161.
Bodenseewerk Perkin-Elmer & Co., GmbH,
Postfach 1120, 7770 Ueberlingen, Federal
Republic of Germany. Tel: (07551) 811.

**PERKIN-ELMER**

The science and computer company.
Where solutions come first.

CIRCLE 167 ON READER SERVICE CARD

**Mapping Strategies in Chemical Oceanography**

Mapping Strategies in Chemical Oceanography
209
NEW!

**Alberto Zirino**, *Editor*
*Naval Ocean Systems Center*

**For the first time—a practical overview of the novel and recent approaches in ocean mapping technology. Focuses on environmental applications as well as on methods used for chemical and biological mapping of the marine environment. Discusses the interdisciplinary character of method development, sampling, data collection, and analysis. Presents the experiences of well-known authorities in developing and applying new instrumentation. Vital reading for anyone involved in making marine assessments.**

**CONTENTS**

New Problems for Chemical Oceanographers • Flow-Injection Analysis for Seawater Micronutrients • Determining Trace Gases in Air and Seawater • Measurement Strategy for Sea-Salt Aerosols • Dependence of Sea-Salt Aerosol Concentration on Environmental Parameters • Sediment Sampling System for Trace Metal Surficial Sediment Studies • Shipboard Copper Analyses by Atomic Absorption Spectroscopy • On-Line Shipboard Determination of Trace Metals in Seawater • Multiple-Unit Large-Volume In Situ Filtration System • Oxygen Consumption in the Ocean • Bioluminescence • Distributions of Epipelagic Bioluminescence • Fluorescence Spectral Signatures for Studies of Marine Phytoplankton • Underway Analysis of Suspended Biological Particles • Biological Profiling in Upper Oceanic Layers with Batfish Vehicle • Undulating Oceanographic Recorder Mark 2 • Sampling Upper 100m of Warm Core Ring • Airborne Mapping of Laser-Induced Fluorescence • Application of Satellites to Chemical Oceanography • pH–Temperature Relationships in Gulf of California • Air–Sea Exchange of $CO_2$ and O Induced by Phytoplankton

*Based on a symposium sponsored by*
*the Division of Analytical Chemistry*
*of the American Chemical Society*

Advances in Chemistry Series No. 209
465 pages (1985) Clothbound
LC 84-20265 ISBN 0-8412-0862-X
US & Canada **$89.95** Export **$107.95**

**Order from:**
**American Chemical Society**
**Distribution Office Dept. 24**
**1155 Sixteenth St., N.W.**
**Washington, DC 20036**
**or CALL TOLL FREE 800-424-6747**
**and use your VISA, MasterCard**
**or American Express credit card.**

human investigations. Several low-field (0.15 T and 0.3 T) instruments are available that use permanent magnets. Most of the magnets have a homogeneity of several parts per million over the region of interest. Recently units with homogeneity on the order of 0.1 ppm have become available. Sensitivity increases with increasing field strength. Unfortunately, so do most $T_1$'s and $T_2$'s.

The large open bore of these magnets leads to a number of installation siting problems. For example, for a 1.0-T solenoid, a fringe field of 5 gauss or more extends out 37 ft from either end of the magnet along the field axis and 25 ft radially. Many kinds of equipment and materials located within this volume affect and are affected by the field. The large open bore also means that the rf coils are exposed, and both broadcast the rf pulse and receive all sorts of extraneous rf signals. These considerations, particularly for the higher field equipment, frequently lead to their installation in a separate specially designed building. Alternatively, substantial site preparation costs are incurred for installation in existing facilities.

The remainder of these units, rf electronics, computer systems, and the like, are quite similar to conventional NMR spectrometers. The rf power requirements are substantially greater—typically several kilowatts compared to a few watts for most spectrometers. The field gradient coils are larger, require more current, and must provide computer-controlled switching. Computer systems must handle large arrays of data so array processors and large disk systems (>160 Mbyte) are mandatory. Operator consoles usually have two screens, one for entering and displaying information and one dedicated to displaying images. Images are most conveniently stored and transported as pictures so photographic reproduction and processing equipment are required. The total cost for a whole-body imaging installation currently runs between $1 and $2.5 million.

The second class of imagers is known as "animal units" or, by comparison with whole-body units, "small bore" imagers. They are really hybrid units. The magnets are superconducting solenoids with a bore of 30–40 cm operating at fields of 2.1 to 4.7 T (proton frequencies of 90–200 MHz). The stronger fields and smaller bore still result in substantial fringe fields (±26 ft axially for a 4.7-T unit) and installation problems similar to those of the whole-body units. The consoles and electronics for these units are essentially identical to those of modern spectrometers with the addition of gradient supplies and controls, increased rf power, and frequently a second display device. Operationally these units are multinuclear spectrometers that also do multinuclear imaging. Such units are also known as topical spectrometers because they permit in vivo spectroscopy using surface coils. In many respects these are perhaps the most versatile instruments available today because they combine the capability to do most modern spectroscopy experiments and multinuclear imaging with a magnet having a bore capable of accepting good-size samples. The stronger field strength, greater homogeneity, and smaller bore result in substantially greater resolution and sensitivity than are possible with whole-body units. The cost for these kinds of instruments (installed) is in the range of $800,000 to $1 million.

The last group of imagers is conventional high-resolution NMR spectrometers that can also perform imaging. These are sometimes referred to as NMR microscopes. Because spectrometer magnets have very small bores (5–9 cm), only very small objects can be imaged. Sensitivity can be quite high, and resolution of 100 $\mu$m or better is possible. Installation considerations are the same as for any spectrometer. Multinuclear operations and the full range of spectroscopic experiments can be applied. At the present time only one manufacturer produces such an instrument, but others have been announced. It presently appears that it will cost $100,000 to $150,000 to add imaging capability to a new spectrometer system that already includes an array processor and sufficient mass storage.

## Chemical applications of imaging

As noted earlier, chemical, as opposed to biochemical or physiological, applications of imaging are essentially nonexistent. Therefore, this is a discussion of possible or potential applications. Basically, any sample for which it is necessary or desirable to obtain qualitative or quantitative information nondestructively as a function of spatial location is a candidate for analysis by imaging. The first applications using existing equipment will probably address moisture content and distribution. Diffusion of water (or other solvents) into plastics and fiber products has already been demonstrated. Water and fat distribution in meats, fruits, and vegetables can be observed. (The very first images were of peppers, lemons, etc.) Examination of products in sealed packages can be advantageous.

Research concerning growth of animal or plant products can be followed without sacrificing the sample. For example, we have observed hole size and

*At last, for solids and liquids:*

# NMR power spanning seven orders of magnitude.

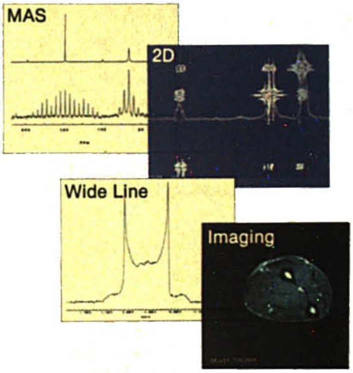

## The new MSL Series spectrometer covers the complete range of linewidths from 0.2 Hz up to 1 MHz.

Bruker has now married the performance of a routine high resolution NMR spectrometer with the power and versatility of a solids instrument without compromising either ease-of-use or analytical capabilities.

With MSL systems you can now perform virtually all known magnetic resonance experiments:

☐ High Resolution in Liquids
☐ 2D NMR in Liquids and Solids
☐ MAS (Magic Angle Spinning) with Variable Temperature
☐ Wide Line FT
☐ Multipulse Line Narrowing (MREV-8, BR-24, etc.)
☐ ADRF/ARRF Experiments
☐ Multiple Quantum NMR
☐ NMR Diffusion Measurements
☐ NMR Imaging
☐ In-vivo Spectroscopy
☐ NQR (Nuclear Quadrupole Resonance)
☐ Ferromagnetic Resonance

The new design of the MSL Series console reflects a quantum jump in high resolution/broadline spectroscopy instrumentation. It offers: full automation and complete keyboard control; sample changer; color raster; compu-shim and autolock feature; a new fast and versatile pulse programmer; provisions for interfacing user devices, such as gradient control, etc.

Your range of samples, liquid or solid, and your experimental freedom is only limited by your imagination. You'll find it difficult to compare the MSL to anything else available today.

Now, if you want to combine performance, convenience and ease of use with analytical versatility and the power of wideline NMR, ask for details on the new MSL Series.

*Bruker Instruments, Inc.*
*Manning Park, Billerica, MA 01821.*
*In Europe: Bruker GmbH,*
*Silberstreifen, D-7512*
*Rheinstetten 4, W. Germany.*

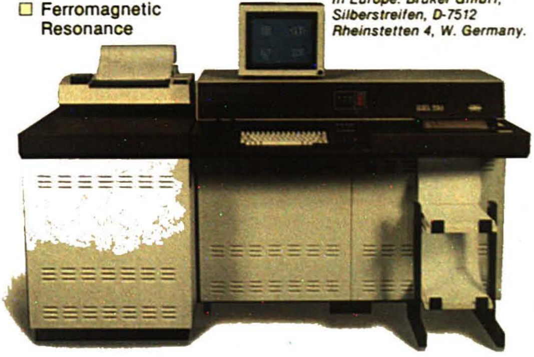

**BRUKER** *NMR systems designed to solve problems.*

CIRCLE 18 ON READER SERVICE CARD

distribution in Swiss cheese and curd size and distribution in cottage cheese. Voids, liquids, and regions of liquid-like disorder in soft polymers (above the glass transition temperature), foams, solid fuel elements, gels, etc., should be amenable to study. Composition and distribution of gels, greases, lubricants, and the like in or around solid objects should also be addressable. The reverse experiment should not be discounted. The size and distribution of solid objects (which themselves do not give a signal) in a soft matrix (which does give a signal) can be observed as the presence of "black holes."

Because $T_1$ and $T_2$ are sensitive to the presence of paramagnetic species (such as $O_2$, free radicals, and many metal species), the presence, distribution, and concentration of such materials is "reported" by observed $T_1$ (or $T_2$) variations of signals from $^1H$ or $^{19}F$ intrinsically present in the sample of interest or added as reporter molecules. $^{19}F$ tags offer the potential to follow dynamic chemical and biochemical processes in a manner analogous to that presently done by positron emission tomography (PET) scanning. The size and distribution of particles and also the distribution and flow of fluids as a function of operating conditions in separation columns, reactor beds, and the like could be examined. Multinuclear studies with NMR microscopes will permit analysis of seeds, tablets, pellets, etc. Problems associated with the mixing, storage, application, and curing of coatings such as paints, varnishes, and adhesives are another area of potential interest. All of these areas and many more can be addressed with existing commercially available equipment.

The future is even more speculative. Multinuclear applications will undoubtedly be forthcoming with improvements in field strength and sensitivity. Extension of imaging techniques to hard solids will occur. Three- and four-dimensional extensions to chemical shift imaging and examination of dynamic processes will occur. And, combination of NMR imaging with other techniques will open entirely new approaches to a wide variety of problems.

## Additional reading

Hinshaw, W. S.; Lent, A. H. "An Introduction to NMR Imaging: From the Block Equation to the Imaging Equation," *Proc. IEEE* **1983**, *71*, 338.

Ljunggern, S. "A Simple Graphical Representation of Fourier-Based Imaging Methods," *J. Magn. Res.* **1983**, *54*, 338.

Mansfield, P.; Morris, P. G. "NMR Imaging in Biomedicine"; Suppl. 2, Advances in Magnetic Resonance; Waugh, J. S., Ed.; Academic Press: New York, N.Y., 1982.

Partain, C. L.; James, A. E., Jr.; Rollo, F. D.; Price, R. R. "Nuclear Magnetic Resonance (NMR) Imaging"; W. B. Saunders: Philadelphia, Pa., 1983.

Witcofski, R. L.; Karstaedt, N.; Partain, C. L., Eds. "NMR Imaging: Proceedings of an International Symposium on Nuclear Magnetic Resonance Imaging"; Bowman Gray School of Medicine of Wake Forest University, Winston-Salem, N.C., 1982.

*Stanford L. Smith is professor of chemistry and radiology at the University of Kentucky. He received his PhD from Iowa State University and his AB degree from Albion College. His research interests cover all aspects of NMR with particular emphasis on applications of 2D spectroscopic techniques and imaging methods.*

Answers out of the blue

NEWPORT 4000

How much Hydrogen in fuel? Oil in seeds? Fat in foodstuffs? The Newport 4000 provides the answers – simply, safely and fast.

Rapid, accurate analysis is vital to quality control and cost-effective production throughout industry.

Now, Newport 4000 makes it so much easier. Ask us about it. Providing answers is our business.

OXFORD

**Oxford Analytical Instruments Limited**
20 Nuffield Way, Abingdon
Oxon OX14 1TX, England
Telephone (0235) 32123 Telex 83621

2 Elm Square, Andover, MA 01810 /
617-470-3700 / 1-800-447-4717

A member of the Oxford Instruments Group plc

CIRCLE 157 ON READER SERVICE CARD

PYREX
100 ML
PYREX
100 ML
100
PYREX

# SHAKE A TOUGHNECK

You see vision in the unique design of every Pyrex® Volumetric Flask.

- Beefier, thicker neck on sizes that need it.
- Wide mouth, optimized for easy pipeting and a good meniscus.

Widest choice of closures.

- Barrelheads that avoid contamination.
- Standard tapers in glass or plastic.
- Snap caps or phenolic screw-on caps.
- Bareheaded without caps, if you prefer.

And more…

- Choice of certified, class A or B accuracy.
- Shrink wrap cases on sizes 25 ml and up for easier, safer handling and storage.

We originated low-expansion borosilicate labware with the Pyrex® beaker in 1915. We've been innovating, modifying and updating our labware ever since. It's a vision that's evolved for 70 years. And it takes us to outer space, for example, in shuttle windows and heat shielding.

CIRCLE 31 ON READER SERVICE CARD

70 YEARS OF VISION
1915-1985 CORNING

AC-04-85-VV

**FREE SHUTTLE BEAKER**

For additional information and free commemorative shuttle beaker, mail this coupon on your letterhead with name and address to Corning Glass Works, Science Products, P.O. Box 1150, Elmira, New York 14902-9944. Offer ends November 29, 1985.

The Most Trusted Tools Of Science

CORNING

# The data/control station that thinks like a chromatographer, now thinks like a lab manager, too. The Waters™ 840.

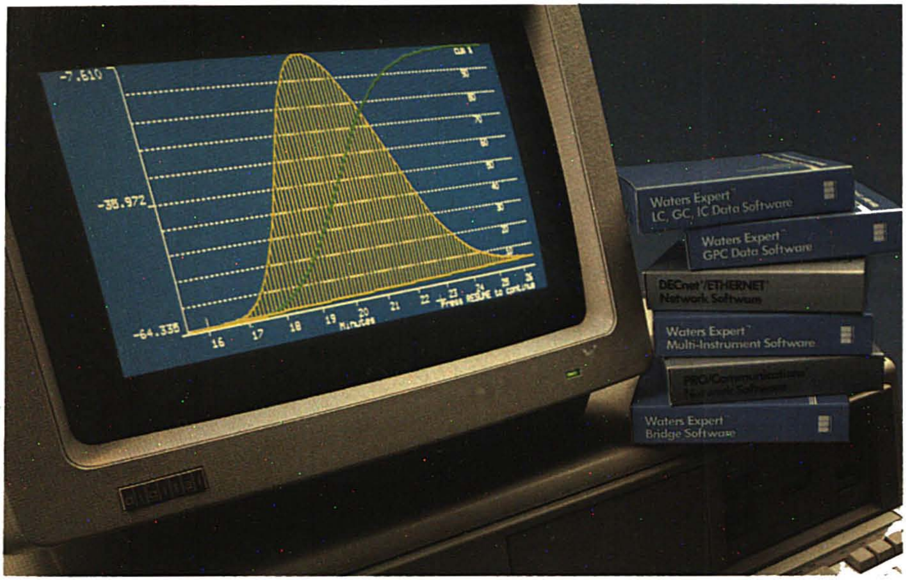
-7.610
-35.972
-64.335
16
17
18
19
20
21
22
23
24
25
26
Minutes
Press RESUME to continue
Waters Expert™ LC, GC, IC Data Software
Waters Expert™ GPC Data Software
DECnet™/ETHERNET® Network Software
Waters Expert™ Multi-Instrument Software
PRO/Communications Network Software
Waters Expert™ Bridge Software

**Now get expanded capability for HPLC, GPC, IC and GC data reduction.** The Waters 840 has set a new standard for ease and sophistication in HPLC data management and system control – as the only data/control station that works the way a chromatographer thinks. Now you get even more capability with new Waters Expert™ chromatography software for GPC, GC, ion chromatography, post-run statistical analysis, and more.

Plus, new multi-instrument software allows data acquisition from up to 4 different systems and 16 detectors simultaneously.

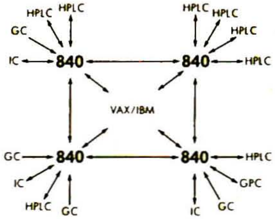
HPLC
HPLC
GC
IC
840
HPLC
HPLC
HPLC
840
HPLC
VAX/IBM
GC
840
IC
HPLC
GC
840
HPLC
GPC
IC
GC

The Waters 840 gives you virtually unlimited communications capabilities, including ETHERNET® compatibility for high speed data transfer. No matter what your current data management requirements are, the Waters 840 can meet them – and expand as your needs grow.

No other data/control station gives you so much multi-tasking capability. Acquire and store months of raw data, and reprocess it in seconds. At the same time you can also watch your separations as they run, or use the screen to set up new methods, or perform other computer tasks such as word processing.

See the new power of the Waters 840. Call now: (617) 478-2000, or write Millipore, Waters Chromatography Division, 34 Maple St., Milford, MA 01757.

MILLIPORE
Waters Chromatography Division

ETHERNET is a registered trademark of Xerox Corporation. VAX, DECnet and PRO/Communications are registered trademarks of Digital Equipment Corporation.
Waters and Waters Expert are trademarks of Millipore Corporation. © 1984 Millipore Corporation

CIRCLE 231 ON READER SERVICE CARD

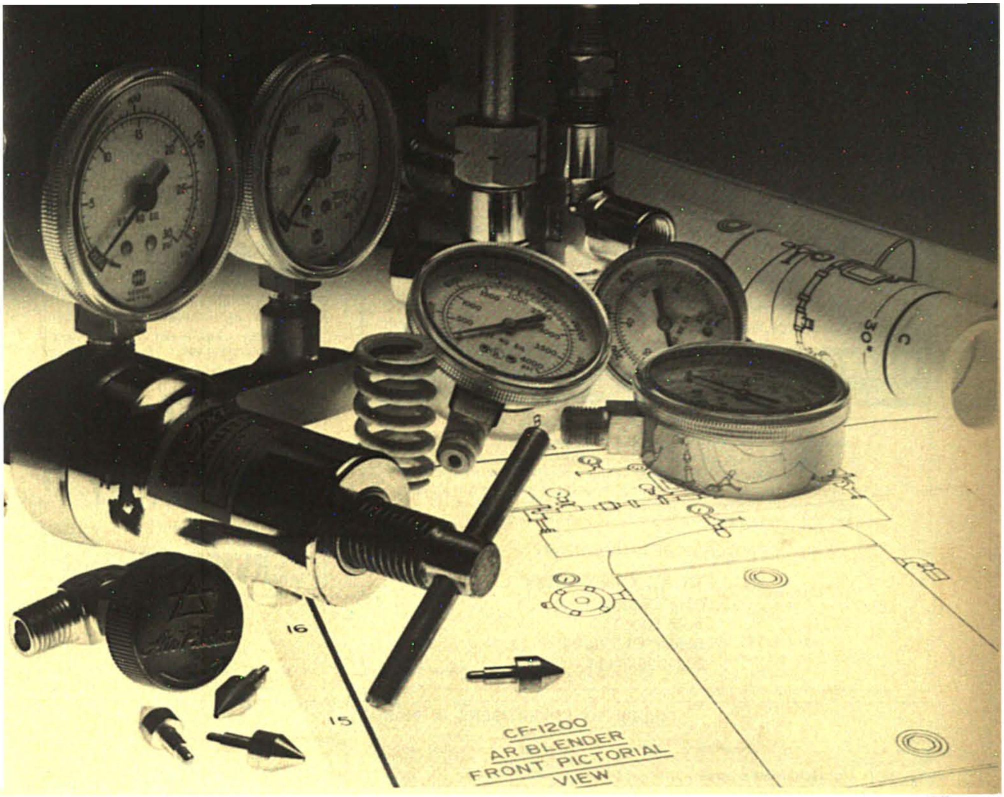

# Why it pays to buy gas equipment made by Air Products.

Few gas suppliers actually make the equipment they sell.

At Air Products, we design and manufacture almost all of the gas regulating equipment we sell. So we offer some distinct advantages.

Right off, we can keep a tight rein on quality. You get equipment you can depend on. But if service is ever needed, it's conveniently and quickly available through one of our repair stations strategically located across the country.

As a gas supplier, we know what equipment is best for any given job. And when economics point to the advantages of manifolding or custom blending, we can design and build the system that's right for you. But before we make any recommendations, of course, we first consider your total system and safety requirements.

A full line of specialty gases. A full line of compatible gas-handling equipment. All from one dependable supplier—with over 80 stocking locations—to make your job a lot easier.

For a copy of our Specialty Gas and Equipment Catalog, simply use the coupon. Or call (215) 481-8257. Canadian address: Air Products, 209 Steeles Avenue East, Brampton, Ontario L6T 1A7.

Air Products and Chemicals, Inc.
Specialty Gas Department
Box 538, Allentown, PA 18105

Please send me your complete catalog and price list.

Name__________ Title__________

Company__________

Address__________

City__________

State__________ Zip__________

Telephone__________

**AIR PRODUCTS**

© 1982 Air Products and Chemicals, Inc.

CIRCLE 4 ON READER SERVICE CARD

# LABORATORY SERVICE CENTER

Alizarin Complexone • p-Aminohippuric Acid • 3-Aminophthalhydrazide
Bicine • 2-Bromoethylamine HBr • Cellubiose • Chloranil • 2,2'-Dipyridyl
Disodium Malonate • Glucose-1-Phosphate • Glutaric Acid & Anhydride
Levulose • o-Methoxybenzoic Acid • Methyl Acetate • Mucobromic Acid
Nadic Anhydride • Ninhydrin • 4-(4-Nitrobenzyl)pyridine • Orcein
m-Phenylenediamine DiHCl • Phenylthiourea • Pyruvic Acid & Sodium Salt
Quinic Acid • DL-Tartaric Acid • Toluene-3,4-Dithiol & Zinc Salt
2,4,6-Tribromoaniline • Tripalmitin • 2,3,5-Triphenyltetrazolium Chloride

*Write for our Products List of over 3000 chemicals*

Tel: 516-273-0900 • TOLL FREE: 800-645-5566 TWX: 510-227-6230

**EASTERN CHEMICAL**
A Division of UNITED-GUARDIAN, INC.

P. O. Box 2500
DEPT. AC
SMITHTOWN, N. Y. 11787

LIQUID CHROMATOGRAPHY SPECIALISTS

POLYMER PROBLEMS?

WE OFFER:
- Complete Polymer Deformulation
- Good vs Bad Comparison
- Gel Permeation Chromatography MWD Mn Mw Mz
- Additive Package Analysis

All work done is treated as strictly confidential. For more information please write or call us at

617-376-8883

JORDI
ASSOCIATES INC
397 Village Street
Millis, Massachusetts 02054

**Laboratory Service Center** (Equipment, Materials, Services, Instruments for Leasing), Maximum space — 4 inches per advertisement. Column width, 2-3/16"; two-column width, 4-9/16". Artwork accepted. No combination of directory rates with ROP advertising. Rates based on number of inches used within 12 months from first date of first insertion. Per inch: **1" — $125; 12" — $123; 24" — $120; 36" — $115; 48" — $112.**

*CALL OR WRITE JANE GATENBY*

**ANALYTICAL CHEMISTRY**
**25 Sylvan Road South**
**P.O. Box 231**
**Westport, Ct. 06881**
**203-226-7131**

USE
LABORATORY
SERVICE CENTER

## INDEX TO ADVERTISERS IN THIS ISSUE

| CIRCLE INQUIRY NO. | ADVERTISERS | PAGE NO. |
|---|---|---|
| 7 | ***Airco Industrial Gases**<br>Hammond Farrell Inc. | 602A |
| 4 | ***Air Products and Chemicals**<br>Lewis, Gilman & Kynett Inc. | 611A |
| 3 | **Allied Analytical Systems**<br>Aries Advertising, Inc. | 550A |
| 5–6 | ***American Burdick & Jackson**<br>Nordstrom/Cox Marketing | 500A, 504A |
| 1 | **The Anspec Company**<br>JJ&K Advertising | 518A |
| 8 | **Antek Instruments** | 577A–580A |
| 2 | ***Atago Bussan Company Ltd.**<br>Echo Japan Corp. | 584A |
| 22 | **Bausch & Lomb, Inc.**<br>Blair Advertising, Inc. | 592A |
| 16 | **Bioanalytical Systems**<br>Kissinger Advertising | 566A |
| 20–21 | **Bio-Rad Digilab Division** | 565A, 597A |
| 17 | **Bomem, Inc.** | 505A |
| 18 | ***Bruker Instruments**<br>Techmarketing, Inc. | 607A |
| 19 | **Burrell Corporation**<br>David J. Westhead Co. | 514A |
| 32 | ***Cajon Company**<br>Falls Advertising | 548A |
| 30–31 | **Corning Glass Works/Science Products**<br>Winterkorn Lillis, Inc. | 531A, 609A |
| xx | **CRC Press** | 495A |
| 42 | **Dialog Information Services**<br>McCann-Erikson, Inc. | 516A |
| 41 | ***Dionex Corporation**<br>LaPointe, Schott & Smith, Inc. | 537A–540A |
| 50 | **Edax International**<br>STG Marketing | 585A |
| 51 | **EG&G/Ortec**<br>Charles Tombras Advertising | 559A |
| 48–49 | **EG&G/PARC**<br>The Message Center | 502A, 542A |
| 65–66 | **Finnigan MAT** | 527A |
| 58 | ***Fisher Scientific Company**<br>Tech-Ad Associates | 569A |
| 57 | **FTS Systems**<br>DJ Moore Advertising, Inc. | 528A |
| 56 | ***Gelman Sciences, Inc.** | 492A–493A |
| 67 | **General Motors**<br>N.W. Ayer, Inc. | 507A–509A |
| 35–38 | ***Gilford Instruments**<br>Oberlin Industrial Advertising | 567A–568A |
| 63–64 | ***Gilson Medical Electronics**<br>LaPointe, Schott & Smith, Inc. | 513A |
| 68 | **Gow-Mac Instruments**<br>Kenyon Hoag Associates | 499A |
| 95 | ***Hamilton Company** | 535A |
| 96–99 | ***Hewlett-Packard Company**<br>Pinné, Garvin, Herbers & Hock | 489A, 515A |
| 104 | ***IBM Instruments, Inc.**<br>Marquardt & Roche | 555A |
| 103 | ***ISCO**<br>Farneaux Associates | 561A |
| 118 | **Keithley das**<br>McKinney, Inc. | 575A |
| 119 | ****Kontron**<br>Promotion Kontron AG | 588B |
| 120 | ***Kratos**<br>Techmarketing, Inc. | 571A |

# INDEX TO ADVERTISERS IN THIS ISSUE

| CIRCLE INQUIRY NO. | ADVERTISERS | PAGE NO. |
|---|---|---|
| 121 | ***Kratos**<br>Studio 21 Advertising | 530A |
| 127 | **Lachat Instruments**<br>Lighthouse Communications | 556A |
| 131 | **LDC/Milton Roy**<br>HRS Communications | 529A |
| 128 | ***Leco Corporation** | 503A |
| 125-126 | **Leeman Laboratories**<br>Bell & Wilson, Inc. | 506A |
| 133 | **Lidex Technologies, Inc.**<br>Scicom Advertising | 546A |
| 132 | **Liquid Carbonic Corporation** | 534A |
| 130 | **LKB-Produkter AB**<br>Marketing Service | 586A |
| 137 | **Malvern Instruments** | 520A |
| 138 | ***Matheson Gas Products**<br>Schaefer Advertising | 501A |
| 139 | ***Mattson Instruments**<br>Lucarelli Ltd. | OBC |
| 142 | **Merck & Company**<br>Dugan/Farley Communications | 536A |
| 140-141 | ***Mettler Instruments**<br>McKinney, Inc. | 521A, 563A |
| 152 | ***Nelson Analytical**<br>Moran, Lanig & Duncan | 517A |
| 153 | ***Nicolet Corporation**<br>Technical Communications | 545A |
| 156 | ***Omnitherm Corporation** | 522A |
| 157 | **Oxford Analytical**<br>Vap Group Ltd. | 608A |
| 170 | **Packard Instrument** | 581A |
| 166-167 | ***Perkin-Elmer Corporation**<br>AC&R Advertising | 525A, 605A |
| 169 | **Perkin-Elmer/Oakbrook Instrument Division** | 588A |
| 168 | **Precision Systems**<br>Productive Marketing Service | 530A |
| 70-79, 86-87 | ****Pye Unicam Ltd.**<br>Connors Publicity Ltd. | 588D, 588F, 588H |
| 179 | ***Radiometer America**<br>Forte Communications | 582A |
| 177-178 | ***Rheodyne, Inc.**<br>Bonfield Associates | 587A, 599A |
| 194-200 | **Sargent-Welch Scientific Company**<br>Polytech Advertising | 547A |
| 187 | **Seastar Instruments** | 504A |
| 185 | ***Separations Group**<br>Pan & Associates | 552A |
| 190 | **Shandon Southern Instruments**<br>Downing Industrial Advertising | 564A |
| 192-193 | ***Shimadzu Scientific Instruments**<br>General Advertising | 549A, 551A |
| 186 | **Siemens AG**<br>Barbeau-Hutchings Advertising | 560A |
| 188 | ***Spectra-Physics** | 541A |
| 189 | **Spectrofuge Corporation** | 500A |
| 202 | **Tecator, Inc.** | 553A |
| 201 | ***Tracor X-Ray** | 601A |
| 211 | **UIC, Inc.**<br>Hoffman Associates | IFC |
| 213 | ***U.S. Analytical Instruments**<br>Silverstein Associates | 510A |
| 218 | ***Valco Instruments**<br>Technical Advertising Assoc. | 497A |
| 222 | ***Varian**<br>La Centra Advertising Inc. | 614A |
| 219-221 | ***Varian**<br>Moran, Lanig, Duncan | 591A, 593A, 594A |
| 223 | **VG Instruments**<br>Barbeau-Hutchings Advertising | 519A |
| 224 | **VG Masslabs**<br>ICA Publicity Ltd. | 603A |
| 231-232 | **Waters Associates**<br>Mintz & Hoke, Inc. | 523A, 610A |
| 230 | ***Whatman, Inc.**<br>Communique | 533A |
| 242 | **Yellow Springs Instruments**<br>B.Y.O. Horn Advertising | 498A |

** See ad in ACS Laboratory Guide*

*** Company so marked had advertisement in Foreign Regional edition only.*

*Advertising Management for the American Chemical Society Publications*

**CENTCOM, LTD**

*President*
**Thomas N. J. Koerwer**

*Executive Vice President* *Senior Vice President*
**James A. Byrne** **Benjamin W. Jones**

**Alfred L. Gregory**, *Vice President*
**Clay S. Holden**, *Vice President*
**Robert L. Voepel**, *Vice President*
**Joseph P. Stenza**, *Production Director*

25 Sylvan Rd. South
P.O. Box 231
Westport, Connecticut 06881
(Area Code 203) 226-7131
Telex No. 643310

ADVERTISING SALES MANAGER
**James A. Byrne, VP**

ASSISTANT SALES MANAGER
**Bruce E. Poorman**

ADVERTISING PRODUCTION MANAGER
**Jane F. Galenby**

SALES REPRESENTATIVES

**Philadelphia . . . Storey L. Johnson, Patricia O'Donnell, CENTCOM, LTD., GSB Building, Suite 425, 1 Belmont Avenue, Bala Cynwyd, Pa. 19004. Telephone: 215-667-9666**

**New York . . . Dean A. Baldwin, Storey L. Johnson, CENTCOM, LTD., 60 East 42nd St., New York, N.Y. 10165. Telephone: 212-972-9660**

**Westport, CT . . . Edward M. Black, CENTCOM, LTD., 25 Sylvan Rd. South, P.O. Box 231, Westport, Ct. 06881. Telephone: 203-226-7131, Telex 643310**

**Cleveland . . . Bruce E. Poorman, CENTCOM, LTD., 325 Front St., Suite 2, Berea, Ohio 44017. Telephone: 216-234-1333**

**Chicago . . . Michael J. Pak, CENTCOM, LTD., 540 Frontage Rd., Northfield, Ill. 60093. Telephone: 312-441-6383**

**Houston . . . Michael J. Pak, CENTCOM, LTD. Telephone: 312-441-6383**

**San Francisco, CA . . . Paul M. Butts, CENTCOM, LTD., Suite 1070, 2672 Bayshore Frontage Road, Mountainview, CA 94043. Telephone: 415-969-4604**

**Los Angeles . . . Clay S. Holden, CENTCOM, LTD., Newton Pacific Center, 3142 Pacific Coast Highway, Suite 200, Torrance, CA 90505. Telephone: 213-325-1903**

**Boston, MA . . . Edward M. Black, CENTCOM, LTD. Telephone: 203-226-7131**

**Atlanta, GA . . . Edward M. Black, CENTCOM, LTD. Telephone: 203-226-7131**

**Denver . . . Paul M. Butts, CENTCOM, LTD. Telephone: 415-969-4604**

**United Kingdom**
- **Reading, England . . . Malcolm Thiele, Technomedia Ltd., Wood Cottage, Shurlock Row, Reading RG10 0QE. Berkshire, England. Telephone: 073-434-3302**
- **Lancashire, England . . . Technomedia Ltd., c/o Meconomics Ltd., Meconomics House, 31 Old Street, Ashton Under Lyne, Lancashire, England. Telephone: 061-308-3025**

**Continental Europe . . . Andre Jamar, International Communications, Inc., Rue Mallar 1, 4800 Verviers, Belgium. Telephone: (087) 22-53-85, Telex #49263**

**Tokyo, Japan . . . Shuji Tanaka, International Media Representatives Ltd., 2-29 Toranomon, 1-Chome Minato-ku Tokyo 105 Japan. Telephone: 502-0656, Telex #22633**

**Need improved chromatography instrument control and data handling?**

**Varian's new VISTA 600 Series is the most advanced system available today for LC and GC.**

varian
DS 604

**For immediate assistance, call 800-231-5772.**
**In Canada,** call 416-457-4130

**Here's why:**

- Automated, simultaneous control of up to four LC or GC instruments
- Software based on the powerful, proven VISTA 402 System Software
- Automatic bidirectional communication to LIMS or other external computers
- High-resolution, real-time graphics for easy-to-read, accurate results
- Inboard BASIC programming performs more complex experiments easily
- Completely automated system with modular hardware and software for easy upgrading

**Call or write today.** Varian VISTA 600 Series Chromatography Data Systems will improve the data handling and instrument control in your lab.

**Varian Instrument Group,** 220 Humboldt Court, Sunnyvale, CA 94089
• **In Canada:** 332 Guelph Street, Georgetown, Ontario L7G 4B5
• **In Europe:** Steinhauserstrasse, CH-6300 Zug, Switzerland

varian

MORE
**varian***telligent*
INSTRUMENTS

VARIAN NO. SEP-4072/553

CIRCLE 222 ON READER SERVICE CARD

For over
six decades
analytical chemistry
ANALYTICAL CHEMISTRY
PRODUCT TAMPERING: TRACING THE SOURCE
...the
leader in
the field.

☐ **YES,** send me my own personal copy of **Analytical Chemistry.**

| Published monthly<br>One Year | U.S. | Mexico &<br>Canada | Europe | All Other<br>Countries |
|---|---|---|---|---|
| **ACS Members*** | ☐ $20 | ☐ $40 | ☐ $57 | ☐ $ 80 |
| **Nonmembers*** | ☐ $30 | ☐ $50 | ☐ $99 | ☐ $122 |

☐ Payment Enclosed (Payable to American Chemical Society)
☐ Bill Me ☐ Bill Company Charge my: ☐ VISA ☐ MasterCard

Card No. ______

Exp. Date ______ Interbank # ______ (Mastercard Only)

Signature ______

Name ______

Title ______ Employer ______

Address ______

City, State, Zip ______

Employer's Business: ☐ Manufacturing, type ______

☐ Academic ☐ Government ☐ Other ______

***Subscriptions at these rates are for personal use only.**
**All foreign subscriptions** are now fulfilled by air delivery. Foreign payment must be made in U.S. currency by international money order, UNESCO coupons, U.S. bank draft, or order through your subscription agency. For nonmember subscription rates in Japan, contact Maruzen Co., Ltd.
Please allow 45 days for your first copy to be mailed.
Redeem until December 31, 1985.

1985

**MAIL THIS POSTAGE-PAID CARD TODAY!**

☐ **YES,** send me my own personal copy of **Analytical Chemistry.**

| Published monthly<br>One Year | U.S. | Mexico &<br>Canada | Europe | All Other<br>Countries |
|---|---|---|---|---|
| **ACS Members*** | ☐ $20 | ☐ $40 | ☐ $57 | ☐ $ 80 |
| **Nonmembers*** | ☐ $30 | ☐ $50 | ☐ $99 | ☐ $122 |

☐ Payment Enclosed (Payable to American Chemical Society)
☐ Bill Me ☐ Bill Company Charge my: ☐ VISA ☐ MasterCard

Card No. ______

Exp. Date ______ Interbank # ______ (Mastercard Only)

Signature ______

Name ______

Title ______ Employer ______

Address ______

City, State, Zip ______

Employer's Business: ☐ Manufacturing, type ______

☐ Academic ☐ Government ☐ Other ______

***Subscriptions at these rates are for personal use only.**
**All foreign subscriptions** are now fulfilled by air delivery. Foreign payment must be made in U.S. currency by international money order, UNESCO coupons, U.S. bank draft, or order through your subscription agency. For nonmember subscription rates in Japan, contact Maruzen Co., Ltd.
Please allow 45 days for your first copy to be mailed.
Redeem until December 31, 1985.

1985

**MAIL THIS POSTAGE-PAID CARD TODAY!**

**CALL TOLL FREE**
(800) 424-6747 (U.S. only)

NO POSTAGE
NECESSARY
IF MAILED
IN THE
UNITED STATES

**BUSINESS REPLY CARD**
FIRST CLASS PERMIT NO 10094 WASHINGTON D C

POSTAGE WILL BE PAID BY ADDRESSEE

**American Chemical Society**
Periodicals Marketing Dept.
1155 Sixteenth Street, N.W.
Washington, D.C. 20036

---

**CALL TOLL FREE**
(800) 424-6747 (U.S. only)

NO POSTAGE
NECESSARY
IF MAILED
IN THE
UNITED STATES

**BUSINESS REPLY CARD**
FIRST CLASS PERMIT NO 10094 WASHINGTON D C

POSTAGE WILL BE PAID BY ADDRESSEE

**American Chemical Society**
Periodicals Marketing Dept.
1155 Sixteenth Street, N.W.
Washington, D.C. 20036

analytical
chemistry

*EDITOR:* **GEORGE H. MORRISON**

EDITORIAL HEADQUARTERS
1155 Sixteenth St., N.W.
Washington, D.C. 20036
Phone: 202-872-4570 Teletype: 710-8220 151

*Executive Editor:* Josephine M. Petruzzi
*Associate Editors:* Stuart A. Borman, Marcia S. Vogel
*Assistant Editors:* Rani A. George, Louise Voress, Mary D. Warner
*Production Manager:* Leroy L. Corcoran
*Art Director:* Alan Kahan
*Designer:* Sharon Harris Wolfgang
*Production Editor:* Gail M. Mortenson
*Circulation:* Cynthia G. Smith
*Editorial Assistant, LabGuide:* Joanne Mullican

**Journals Dept., Columbus, Ohio**
*Associate Head:* Marianne Brogan
*Associate Editor:* Rodney L. Temos

**Advisory Board:** Shier S. Berman, Brian S. Bidlingmeyer, Henry N. Blount, Gary D. Christian, Dennis H. Evans, Jack W. Frazer, Gary M. Hieftje, William R. Heineman, Harry S. Hertz, Roland F. Hirsch, Atsushi Mizuike, Melvin W. Redmond, Jr., Herbert L. Retcofsky, Martin A. Rudat, Wilhelm Simon, Charles L. Wilkins. *Ex Officio:* Donald D. Bly

**Instrumentation Advisory Panel:** Richard S. Danchik, Thomas C. Farrar, Larry R. Faulkner, John F. Holland, F. James Holler, Peter N. Keliher, Curt Reimann, D. Warren Vidrine, Andrew T. Zander

*Contributing Editor, A/C Interface:* Raymond E. Dessy

**The Analytical Approach Advisory Panel:** Edward C. Dunlop, Robert A. Hofstader, Wilbur D. Shults

*Published by the*
**AMERICAN CHEMICAL SOCIETY**
1155 16th Street, N.W.
Washington, D.C. 20036

**Books and Journals Division**
*Director:* D. H. Michael Bowen
*Journals:* Charles R. Bertsch
*Production:* Elmer Pusey, Jr.
*Research and Development:* Lorrin R. Garson

Manuscript requirements are published in the January 1985 issue, page 395. Manuscripts for publication (4 copies) should be submitted to ANALYTICAL CHEMISTRY at the ACS Washington address.

The American Chemical Society and its editors assume no responsibility for the statements and opinions advanced by contributors. Views expressed in the editorials are those of the editors and do not necessarily represent the official position of the American Chemical Society.

# ACS Editors Conference

Some authors and readers of the scientific literature may be of the opinion that editors set the policies of their journals somewhat arbitrarily—oblivious to the methods used by other journals. This is certainly not the case for editors of American Chemical Society journals, who hold periodic meetings to compare notes. The 1985 Conference of Editors of ACS Publications was held recently in California, and editors of the 20 journals had an opportunity to review once again the operation of their respective publications. These conferences provide an ideal forum for discussing common problems confronting the editors and generating ideas for new and improved methods of carrying out their responsibilities.

One of the important continuing topics on the agenda was that of dealing with authors. Not surprisingly, problems encountered are not unique to any one journal. Issues of policy, ethics, and technical considerations were discussed. Another topic discussed is the perpetual concern of all ACS editors—that of identifying good reviewers to maintain the health of the peer review system.

For some time the editors of the ACS journals have been striving to publish "Ethical Guidelines to Publication of Chemical Research," and the final touches to this important document were completed at the meeting. The guidelines covered include those for the ethical obligations of editors, authors, and reviewers. The publication of these guidelines, which is expected shortly, should be of great use to the scientific community.

Other items covered at the conference included a review of the objectives and status of selected journals—giving the editors an opportunity to evaluate their programs with the help of their peers. Finally, operational matters such as circulation, copyright, manuscripts in electronic form, and ACS journals online were discussed.

Periodic meetings such as these are of inestimable value to the editors, who often have the feeling that they are all alone in the world. I am happy to report that ANALYTICAL CHEMISTRY is highly respected by our colleagues and continues to be one of the most successful in the ACS family.

G. H. Morrison

Anal. Chem. 1985, 57, 786–789

# Neutral Reactions in Gas Chromatography/Chemical Ionization Mass Spectrometry

**Patrick Rudewicz and Burnaby Munson***

*Department of Chemistry, University of Delaware, Newark, Delaware 19716*

**The use of $NH_3$ as a carrier gas and as a reagent gas produces neutral reactions between $NH_3$ and carbonyl compounds to give basic products which are detected by $NH_3$ chemical ionization (CI) in the mass spectrometer. Reactions are observed with aldehydes and ketones but not alcohols, ethers, or esters. Postcolumn addition of $NH_3$ or $CH_3NH_2$ also gives neutral products which can be detected by $NH_3$ CI. On-column reactions are observed with carbonyl compounds by the injection of an amine immediately after the introduction of the sample. On-column reactions are also observed by adding acetone or acetic anhydride to a mixture of amines.**

The ammonia chemical ionization ($NH_3$ CI) mass spectra of certain aldehydes and ketones contain ions corresponding to protonated Schiff bases or imines which are also isobaric with the molecular ions. The mechanism of formation of the imines has not been clearly established. An early report indicated that aldehydes but not ketones formed protonated imines in a two-step process involving a neutral gas phase reaction between ammonia and the aldehyde to form the imine and subsequent protonation of the imine by $NH_4^+$ (*1*). In a later study, however, the ammonia CI spectrum of cyclohexanone was reported to contain the protonated imine formed not by a two-step mechanism involving a neutral reaction but by a single-step ion/molecule reaction (*2*). Finally, it has been suggested that protonated imines in the $NH_3$ CI mass spectra of 3-keto bile acid derivatives are formed by the two-step process of neutral reaction with $NH_3$ followed by protonation by $NH_4^+$ (*3*). Protonated imines were not observed with 7-keto or 12-keto bile acid derivatives.

We have observed neutral reactions between ammonia and various ketones and aldehydes on packed GC columns, using ammonia as the GC carrier gas. The products of these on-column reactions elute from the gas chromatograph into the source of the mass spectrometer and are protonated under ammonia CI conditions. Alcohols, ethers, and esters do not react with ammonia in neutral on-column reactions to give detectable products under ammonia CI conditions.

These on-column reactions with $NH_3$ as the carrier gas are very similar to experiments in reaction chromatography which have been reported previously (*4, 5*). In reaction chromatography, compounds having a particular functional group may be completely removed from the chromatogram (subtractive chromatography) (*6*) or converted to volatile derivatives (peak shifting) (*7*) by precolumn, on-column, or postcolumn reactions. Pyrolytic and catalytic reactions have also been employed (*8, 9*). On-column hydrogen/deuterium exchange reactions have been carried out using Carbowax columns pretreated with deuterium oxide (*10*). Somewhat more recently, reaction chromatography has been combined with mass spectrometry for the conversion of selected classes of compounds to derivatives whose electron ionization mass spectra are more informative (*11*).

## EXPERIMENTAL SECTION

These experiments were done with a Du Pont 21-492B mass spectrometer (Hewlett-Packard 21MX computer, Du Pont data system) and a Varian 2740 gas chromatograph. The source pressure was measured with a MKS Baratron capacitance manometer (MKS Instruments, Burlington, MA) connected to the source through the probe inlet. The reagent gas pressure was 0.5 torr and the source temperature was kept between 160 °C and 180 °C. The ammonia, used for both the reagent gas and the GC carrier gas, was obtained from Matheson (anhydrous 99.99% min). The electron energy was 75 eV and the emission current was 250 $\mu$A. The repeller voltage was set to zero and the accelerating voltage was approximately 1750 V.

The majority of the experiments were done with a 6 ft × $^1/_4$ in. glass column, packed with 3% SP-2100 on 80/100 mesh Supelcoport. The performance of the column before and after aproximately 80 h of use with ammonia as the carrier gas was checked with a standard polarity mixture. No significant degradation in column performance was noted. The resolution for the separation of 2,4-dimethylaniline and naphthalene in a programmed temperature experiment was 1.2 before and 1.2 after 80 h of use with ammonia as the carrier gas. Chromatographic efficiency appeared to be about the same, but full characterization studies were not performed.

For the postcolumn derivatization experiments, He was used as the GC carrier gas and the reactive gas was introduced via a Swagelok tee placed directly behind the GC column.

## RESULTS AND DISCUSSION

The ammonia CI mass spectrum of acetophenone is shown in Figure 1. This spectrum was obtained from a GC/CIMS experiment with He as the carrier gas in the gas chromatograph and ammonia as the CI reagent gas in the mass spectrometer source: $P(\mathrm{He}) = 0.07$ torr; $P(\mathrm{NH_3}) = 0.46$ torr; $t = 175$ °C. In this spectrum there are essentially no ions at $m/z$ 120, neither $C_8H_8O^+$ from acetophenone nor $C_8H_{10}N^+$ as the protonated imine; $I(120) < 0.1\%$ of the total sample ionization. The spectrum is a very simple one: predominantly the $(M + NH_4)^+$ adduct with a small amount of solvated adduct, $(M + N_2H_7)^+$, and small traces of $(M + H)^+$ ions. This spectrum agrees with earlier work (*1*). The reaction time for neutral acetophenone with ammonia within the source of the mass spectrometer is not known; however, experiments under similar conditions with another instrument (CEC-110) suggest that the residence times of neutral molecules within the source of the mass spectrometer in these experiments are only a few tenths of a second (*12*). Comparisons of peak widths obtained with a flame ionization detector (FID) and with the mass spectrometer give no indications of significant peak broadening due to retention within the source of the mass spectrometer.

With ammonia as a GC carrier gas, acetophenone forms an imine in a condensation reaction in the gas chromatograph

$$C_6H_5COCH_3 + NH_3 \rightarrow C_6H_5C(NH)CH_3 + H_2O \quad (1)$$

The imine elutes from the column and is protonated in the ion source to give $m/z$ 120 as the major ion in the spectrum

$$NH_4(NH_3)_x^+ + C_6H_5C(NH)CH_3 \rightarrow C_6H_5C(NH_2)CH_3^+ + (x + 1)NH_3 \quad (2)$$

Precise mass measurements show that the ion at $m/z$ 120 in these experiments is $C_8H_{10}N^+$, not the molecular ion for acetophenone, $C_8H_8O^+$. Not all of the acetophenone is converted to the imine and the unreacted acetophenone elutes and forms an adduct ion, $(M + NH_4)^+$, at $m/z$ 138. Selected

0003-2700/85/0357-0786$01.50/0 © 1985 American Chemical Society

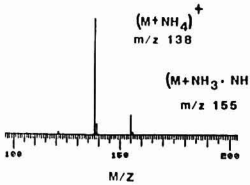

**Figure 1.** Ammonia GC CI mass spectrum of acetophenone using He as a carrier gas and ammonia as a reagent gas: source pressure, 0.07 torr He, 0.046 torr $NH_3$; source temperature, 175 °C.

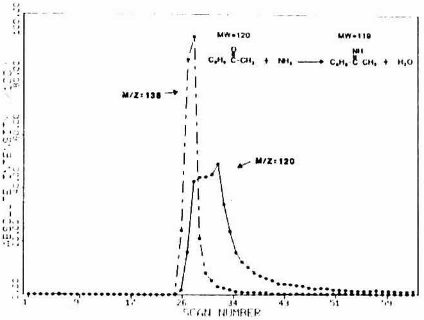

**Figure 2.** Single ion traces for the protonated imine of acetophenone, *m/z* 120, and the adduct ion for the unreacted acetophenone, *m/z* 138, using ammonia as the GC carrier gas and the CI reagent gas.

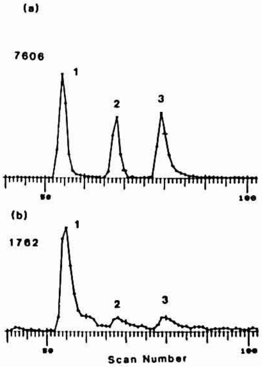

**Figure 3.** (a) Single ion traces for the $(M + NH_4)^+$ adduct ions of (1) cyclohexanone, (2) acetophenone, and (3) 2-octanone. He is the GC carrier gas with postcolumn introduction of ammonia for reaction and as the CI reagent gas. (b) Single ion traces for the $(M + H)^+$ ions of imine derivatives with $NH_3$ of (1) cyclohexanone, (2) acetophenone, and (3) 2-octanone. He is the GC carrier gas with postcolumn introduction of ammonia for reaction and as the CI reagent gas.

ion monitoring shows that the imine and the unreacted acetophenone have different chromatographic peak profiles, Figure 2. The ratio of the areas of the two peaks is an indication of the extensive conversion of acetophenone to the imine. However, the ratio of the peak areas is not the same as the mole ratio since the CI sensitivity for acetophenone with ammonia is much less than the sensitivities for amines and by inference the sensitivity of the imine.

Imine formation is observed with several aliphatic and aromatic ketones and aldehydes and appears to be a general process under the relatively mild conditions of 100–150 °C and on-column times of a few minutes. For many of the compounds the imines elute as well-defined peaks which partially overlap the peak for the unreacted ketones and have widths at half-height that are significantly wider than the half-widths of the peaks for the unreacted ketones and which have retention times that are slightly longer than the retention times of the corresponding unreacted ketones. A decrease in the flow of ammonia through the gas chromatograph increases the retention and reaction time of the carbonyl compounds and increases the extent of conversion to the imines. Slow flow rates and long reaction times induce extensive tailing in the peak profile for the imine without a similar effect on the peak profile for the unreacted ketone. Peak profiles for the imine depend on the chemical nature of the carbonyl compound as well as the physical parameters of the separation.

Comparisons were made for several ketones between experiments with ammonia as the GC carrier gas and the CI reagent gas and with He as the GC carrier gas and ammonia as the CI reagent gas. For all these compounds trace amounts or none of the protonated imines was observed unless ammonia was the GC carrier gas and the CI reagent gas. With 5-nonanone, for example, with ammonia as the GC carrier gas and the CI reagent gas, the ratio of $(M + NH_4 - H_2O)^+/(M + NH_4)^+$ is about 15, whereas in the conventional CI experiment, with He as the carrier gas and ammonia as the reagent gas, virtually no $(M + NH_4 - H_2O)^+$ ions are detected. Consequently, under our conditions, the overwhelming amount of $(M + NH_4 - H_2O)^+$ ions are protonated imines formed by a two-step process with the neutral reaction occurring prior to entry of the sample into the source of the mass spectrometer.

The sometimes surprisingly well-shaped chromatographic peaks for the imines suggested formation in a narrow region or short time. Consequently, experiments were performed at different temperatures of the GC injection port and the same temperature for the GC oven and column. No significant and systematic changes were noted in the ratios of concentrations of unreacted carbonyl compounds to imines, as indicated by the ratios of the ion currents, $(M + NH_4)^+/(M + NH_4 - H_2O)^+$. Consequently, only a very small extent of reaction can be occurring in the injection port.

Postcolumn reaction with ammonia (through the flame ionization detector oven at approximately 300 °C and the transfer line at approximately 125 °C for less than 7 s) gave small extents of conversion of carbonyl compounds to imines (Figure 3). Retention times for the imines and unreacted ketones are the same, although the half-widths of the peaks for the imines are somewhat larger than the half-widths of the peaks for the unreacted ketones. The peak broadening and tailing, shown in Figure 3, probably result from adsorption of the imines on the unsilanized glass transfer line betwen the gas chromatograph and the mass spectrometer and are not dependent on the reaction. The ratio of the ion currents for the protonated imine to that for the ammonium ion adduct of the ketone is roughly proportional to the extent of conversion. For a few ketones, this ratio was about 50 times larger (range of 15–70) for the on-column experiments than for the postcolumn experiments. Consequently, we consider that the reactions with ammonia as the GC carrier gas are occurring almost entirely within the chromatographic column.

Figure 3 also shows differences in the extents of reaction of ammonia with three ketones. Previous experiments indicate that the sensitivities with ammonia for strongly basic secondary amines are essentially constant; therefore, we assume that the sensitivities of these imines are roughly the same and that the areas under the peaks for the protonated imine ions are directly proportional to the extents of reaction with the same proportionality constant. Since there are equimolar amounts of cyclohexanone, 2-octanone, and acetophenone in the mixture and, in the postcolumn experiment, the reaction times are the same for all three compounds, we say that the neutral reaction of ammonia with cyclohexanone is much faster (approximately a factor of 10) than the reaction of neutral ammonia with 2-octanone or with acetophenone. The data from the on-column experiments do not provide so direct a comparison, but they also indicate a greater reactivity of ammonia with cyclohexanone than with 2-octanone or acetophenone. One cannot determine the extent of conversion for aldehydes because the ammonia CI sensitivity for the unreacted aldehyde is too low to provide reliable data. However, postcolumn experiments, like those of Figure 3, indicate a slightly higher reactivity for ammonia with hexanal than with cyclohexanone.

The postcolumn experiments clearly indicate that some of the reaction can be occurring in the gas phase in the chromatographic column. However, we have not determined if the dominant process occurs in the gas phase or in the liquid coating of the support. One preliminary experiment indicated an increase in the extent of conversion of acetophenone to the imine for on-column reactions using a Carbowax rather than a silicone column.

The order of reactivity of these compounds with ammonia in the gas chromatograph roughly correlates with the reported reactivity of carbonyl compounds with ammonia in solution: i.e., aldehydes are more reactive than ketones with sterically hindered ketones being particularly unreactive (*13*). Aromatic ketones are even less reactive than aliphatic ketones. In solution, the condensation of acetophenone and ammonia requires an aluminum chloride catalyst and a 4-h reaction time at 180 °C (*14*).

The diones, 2,4-pentanedione and 2,3-pentanedione, primarily condense with ammonia at one carbonyl site, since essentially none (<0.2%) of the protonated diimine is noted for 2,4-pentanedione and no more than 3% of the protonated diimine is noted for 2,3-pentanedione. Apparently the reaction time is not long enough for significant condensation at both sites. Although 2,5-hexanedione gives some ionization indicative of monocondensation, at *m/z* 114, the majority of the ionization for the compound occurs at *m/z* 96. The precise mass for this ion is 96.081, $C_6H_{10}N^+$. The occurrence of this ion can be explained by a cyclization of 2,5-hexanedione with ammonia to give 2,5-dimethylpyrrole, which is subsequently protonated in the source of the mass spectrometer

$$CH_3COC_2H_4COCH_3 + NH_3 \rightarrow C_6H_9N + 2H_2O \quad (3)$$

$$C_6H_9N + NH_4(NH_3)_x^+ \rightarrow C_6H_{10}N^+ + (x + 1)NH_3 \quad (4)$$

In the condensed phase, 2,5-dimethylpyrrole is formed by the condensation of 2,5-hexanedione with ammonia (*15*).

Two problems exist with the use of a polar carrier gas like ammonia. There is a small amount of ammonia in the chromatographic column which is eluted with He as the carrier gas for an extended period of time. Consequently, the CI spectra which one obtains for several hours after the use of ammonia contain ions resulting from the reactions of $NH_4^+$ if one uses methane or isobutane as the reagent gas. Another problem was that after extended ammonia use, peaks corresponding to alcohols were broader and their retention times were shifted. More experiments are planned to determine the effects that a continued ammonia flow has on the performance of various packed GC columns.

One method of avoiding the adsorption and desorption problems which also maintains the chromatogrphic integrity of the sample is the postcolumn introduction of the reactive gas which we have discussed previously. The extents of conversion are relatively small in our experiments, but provide sufficient amounts of the derivatives that they could be diagnostically useful. Methylamine was also tried as a postcolumn CI reagent gas, and reactions were also observed between methylamine and carbonyl compounds which were analogous to those observed with ammonia, including a cyclization reaction which produces *N*-methyl-2,5-dimethylpyrrole. The reactions of methylamine with hexanal and cyclohexanone were much faster than the reaction with acetophenone. Since $(M + H)^+$ ions were observed for all of these Schiff bases, their proton affinities must be greater than the proton affinity of methylamine, 214.1 kcal/mol (*16*). Sensitivities of the carbonyl compounds with methylamine are quite low. The present experiments in GC/CIMS with postcolumn introduction of reactive gases which also serve as the CI reagent gases are similar to those reported previously on the postcolumn exchange of labile hydrogens using $CH_3OH$ and $CH_3OD$ as the reactive reagent gas (*17*).

There is another method of inducing on-column reactions which does not contaminate the column, which allows the use of any CI reagent gas in the source of the mass spectrometer, and which gives reasonable chromatography for the samples and their derivatives. With He as the carrier gas, Schiff bases can be formed from carbonyl compounds by the injection of a large amount of a low molecular weight amine after the injection of the carbonyl compounds. For example, injection of 5 μL of *n*-propylamine immediately after the injection of 0.02 μL of benzaldehyde results in an on-column conversion of roughly 30% of the aldehyde to the corresponding substituted imine, as shown by the FID chromatographic trace in Figure 4a. The imine is protonated in the mass spectrometer as before

$$C_6H_5CHO + C_3H_7NH_2 \rightarrow C_6H_5CH{=}NC_3H_7 + H_2O \quad (5)$$

$$C_6H_5CH{=}NC_3H_7 + NH_4(NH_3)_x^+ \rightarrow C_6H_5CHNHC_3H_7^+ + (x + 1)NH_3 \quad (6)$$

The reaction time between the amine and the aldehyde, estimated from the width of the chromatographic peak for propylamine, is approximately 30 s. Figure 4b shows mass spectrometric detection of these compounds with ammonia as the CI reagent gas. Selected ion traces are indicated for benzaldehyde as the $(M + NH_4)^+$ ion and the imine as the $(M + H)^+$ ion. The very large difference in relative sensitivities of the two detectors is indicated by comparison of the two traces: ammonia CI is obviously very insensitive for aldehydes. Under similar conditions acetophenone gives less than 0.1% conversion.

Other examples of reaction chromatography were tried in chemically similar systems. Injection of a large amount (5 μL) of acetone onto the column immediately after the injection of a mixture of *n*-hexylamine, diallylamine, and tripropylamine gave a small, but readily detectable, amount of the imine from *n*-hexylamine detected on both the FID trace and as the $(M + H)^+$ ion under ammonia CI conditions. The other two compounds gave no indications of reaction products. Acetone, however, is not the most reactive compound which can be tried with amines.

More dramatic results were achieved by using acetic anhydride as the on-column reagent with amines. Figure 5a shows the FID trace for an equimolar mixture of pyridine, aniline, *m*-methylaniline, *N*-ethylaniline, *N,N*-diethylaniline, and dibenzylamine. Each of these compounds was detected as $(M + H)^+$ ions and/or $(M + NH_4)^+$ ions with ammonia as the reagent gas. Figure 5b shows the FID trace for the same mixture when a large amount (5 μL) of acetic anhydride was injected onto the column immediately after the injection of the amine mixture. Essentially quantitative removal of the

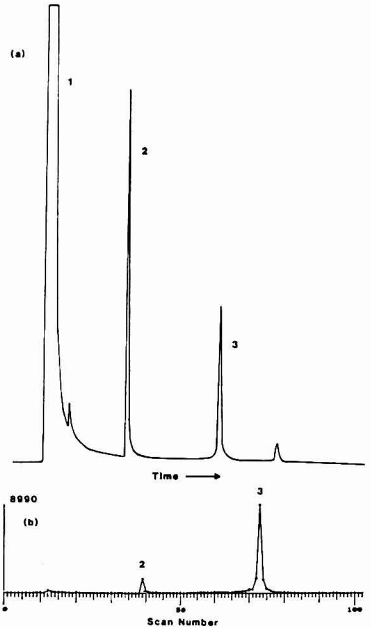

**Figure 4.** (a) FID trace for 0.04 μL of benzaldehyde followed by a 5-μL injection of *n*-propylamine: (1) *n*-propylamine, (2) benzaldehyde, (3) imine; mol wt 147. (b) Single ion traces for (2) the $(M + NH_4)^+$ for benzaldehyde and (3) the $(M + H)^+$ for the imine, *m/z* 148.

primary and secondary amines is noted on the FID trace and also in the ammonia GC CIMS single ion traces (reaction time, approximately 2.5 min). Four major new peaks appear in the chromatogram shown in Figure 5b, which also appear in the ammonia CI spectra with similar profiles. The heterocyclic amine, pyridine, and the tertiary amine, *N,N*-diethylaniline, do not react with acetic anhydride: their retention times from the FID traces and their mass spectra are the same in the two experiments. The four acetamide derivatives give very simple spectra, corresponding to protonated ions and ammonium adduct ions. More extensive characterization of the compounds could be achieved by using a more reactive CI reagent gas like methane. On-column derivatization of steroids and alkaloids with acetic or propionic anhydride was reported previously with chromatographic retention times used for identification (*18*).

We have made no effects to investigate the kinetics of the on-column reactions. However, such analyses may be possible for systems like these since the kinetics of simple elimination reactions have been studied on chromatographic columns using gas/solid chromatography (*19*).

In conclusion, ammonia, when used as a GC carrier gas as well as a CI reagent gas, reacts with ketones and aldehydes to form imines which are more basic than ammonia and are easily detected by their $(M + H)^+$ ions. Since ammonia CI sensitivity is greater for nitrogen-containing compounds than for oxygenated compounds, derivatization with ammonia may be a method of increasing the ammonia CI sensitivities of ketones and to a greater extent aldehydes. With He as a GC carrier gas, derivatization of carbonyl compounds may be accomplished by the postcolumn addition of ammonia or methylamine or by the injection of a low molecular weight amine after sample injection. On-column reaction chromatography can also be combined with ammonia CI to characterize mixtures of amines.

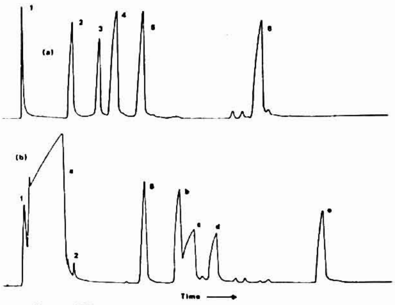

**Figure 5.** (a) FID trace for amine mixture of (1) pyridine, (2) aniline, (3) *m*-toluidine, (4) *N*-ethylaniline, (5) *N,N*-diethylaniline, and (6) dibenzylamine. He is the GC carrier gas. (b) FID trace of amine mixture after on-column derivatization with acetic anhydride: (1) pyridine, (a) acetic anhydride, (5) *N,N*-diethylaniline, (b) *N*-ethyl-*N*-phenylacetamide, (c) *N*-phenylacetamide, (d) aceto-*m*-toluidide, and (e) *N,N*-dibenzylacetamide.

**Registry No.** $NH_3$, 7664-41-7; methylamine, 74-89-5; acetone, 67-64-1; acetic anhydride, 108-24-7; acetophenone, 98-86-2; cyclohexanone, 108-94-1; 2-octanone, 111-13-7; aniline, 62-53-3; *m*-toluidine, 108-44-1; *N*-ethylaniline, 103-69-5; dibenzylamine, 103-49-1; benzaldehyde, 100-52-7; propylamine, 107-10-8.

## LITERATURE CITED

(1) Hunt, D. F. In "Advances in Mass Spectrometry"; West, A. R., Ed.; Applied Science Publishers: London, 1974; Vol. 6.
(2) Tabet, J. C.; Fraisse, D. *Org. Mass Spectrom.* **1981**, *16*, 45–47.
(3) DeMark, B. R.; Klein, P. D. *J. Lipid Res.* **1981**, *22*, 166–177.
(4) Perry, S. G. *Chromatogr. Rev.* **1967**, *9*, 1–22.
(5) Harris, W. E. *J. Chromatogr. Sci.* **1975**, *13*, 514–515.
(6) Sugii, A.; Harada, K. *J. Chromatogr.* **1981**, *206*, 485–491.
(7) James, A. T.; Martin, A. J. P. *Biochem. J.* **1956**, *63*, 144.
(8) Kosa, W. C.; MacGee, J.; Ramachandran, S.; Webber, A. J. *J. Chromatogr. Sci.* **1979**, *17*, 177–187.
(9) Beroza, M. *Anal. Chem.* **1962**, *34*, 1801–1811.
(10) Senn, M.; Richter, W. J.; Burlingame, A. L. *J. Am. Chem. Soc.* **1965**, *87*, 680–681.
(11) Mikaya, A. I.; Smetanin, V. I.; Zaikin, V. G.; Antonova, A. V.; Prostakov, N. S. *Org. Mass Spectrom.* **1983**, *18*, 99–104.
(12) Goren, A. Ph.D. Thesis, University of Delaware, Newark, DE, 1975.
(13) Reeves, R. L. In "The Chemistry of the Carbonyl Group"; Patai, S., Ed.; Interscience: New York, 1966; Chapter 12.
(14) Strain, H. H. *J. Am. Chem. Soc.* **1930**, *52*, 820–823.
(15) Norman, R. O. C. "Principles of Organic Synthesis", 2nd ed.; Chapman and Hall: London, 1978; Chapter 10.
(16) Lias, S. G.; Liebman, J. F.; Levin, R. D. *J. Phys. Chem. Ref. Data*, in press.
(17) Blum, W.; Schlumpf, E.; Liehr, J. G.; Richter, W. J. *Tetrahedron Lett.* **1976**, *7*, 565–568.
(18) Anders, M. W.; Mannering, G. J. *Anal. Chem.* **1962**, *34*, 730–733.
(19) Matsen, J. M.; Harding, J. W.; Magee, E. M. *J. Phys. Chem.* **1965**, *69*, 522–527.

RECEIVED for review September 17, 1984. Accepted January 4, 1985. The authors wish to express their appreciation to the National Science Foundation (CHE-8312954) for the financial support of this work.

*Anal. Chem.* **1985,** *57,* 790–792

# Gas Chromatography/Mass Spectrometry Determination of Water-Soluble Primary Amines as Their Pentafluorobenzaldehyde Imines

**Michael J. Avery* and Gregor A. Junk**

*U.S. Department of Energy, Ames Laboratory, Ames, Iowa 50011*

**Primary aliphatic amines present at trace levels in water samples were converted to imine derivatives using pentafluorobenzaldehyde. The derivatives were extracted into hexane and measured by combined high-resolution gas chromatography/mass spectrometry using multiple ion monitoring. The detection limit of this method for determining amines was 10 ppb for 0.5-mL samples of tap, river, and oil shale process waters.**

The determination of primary aliphatic amines present in various liquids is an important problem. These compounds can be found in biological fluids, environmental samples, and industrial process streams, usually in aqueous solutions and often at trace levels. Amines are difficult to extract from water and are not easily chromatographed due to their polarity. Previous determinations of amines present in water have utilized three approaches: (1) direct gas chromatographic (GC) analysis of the aqueous samples; (2) concentration of the amines followed by separation and detection; (3) alteration of the amines by derivative formation.

Direct analysis of aqueous samples minimizes sample preparation, thereby improving precision and reducing sample contamination. Direct methods include GC with an amine-deactivated column (*1–3*) and ion chromatography (*4*). Both techniques are limited to parts-per-million level determinations.

Detection limits can be improved by concentrating the aqueous sample before measurement. Purging the compounds from water onto a Cu(II) absorber column (*5*), steam distillation (*6*), vacuum distillation (*7*), and sorption onto a XE-340 column (*8*) have been reported. These methods lower the detection limit to about 0.1 ppm but also concentrate impurities leading to possible false positives or high results.

Amines have been derivatized to fluoroacetates (*9*), boron chelates (*10*), and *m*-toluamides (*11*) to improve their chromatographic separations and their detection limits. The reagents used in these derivatizations have the disadvantage of reacting with water, which limits their applicability to organic solvent extracts of amines. Direct derivatization of amines in water with reagents such as *o*-phthaladehyde (*12*), dinitrofluorobenzene (*13, 14*), and 2-methoxy-2,4-diphenyl-3(2*H*)-furanone (*15*) have been reported. These direct methods lack one or more of the following desirable features: sensitivity, selectivity for primary amines, and chromatographic resolution. Pentafluorobenzaldehyde (PFB) has been reported as a selective reagent for primary amines (*16*), but the derivatizations were performed in ethanol rather than water samples.

A new procedure has been developed, in this laboratory, to determine trace levels of primary aliphatic amines in aqueous solutions. It involves the direct derivatization of the amines present in the water sample using PFB to form imines of the amines. The procedure requires minimal sample manipulation and is completed within 30 min and the imine derivatives can be readily extracted into hexane. High-resolution gas chromatography/mass spectrometry (HRGC/MS) analysis of the hexane extract is used to ensure that all imine isomers will be measured separately, with no interferences.

## EXPERIMENTAL SECTION

**Reagents.** Amines and amine hydrochlorides were obtained from Fluka Chemical Corp. (Hauppauge, NY), pentafluorobenzaldehyde from PCR (Gainesville, FL), organic-free water from J. T. Baker (Phillipsburg, NJ), pesticide grade hexane from MC/B (Norwood, OH), and HPLC grade acetonitrile from Burdick and Jackson (Muskegon, MI). Standard solutions of methyl-, ethyl- and *n*-propylamines were made up at the 1 mg/mL level by dissolving the amine hydrochloride in organic-free water and adding 0.1 N NaOH until the solution was basic. All other amines were dissolved in acetonitrile.

The PFB imine standard, used for comparing efficiencies of imine derivatization, was prepared by standard Shiff base reaction of *n*-butylamine with PFB.

**Samples.** Tap water was obtained from the City of Ames, IA, water system. River water was sampled from the North Skunk River at a point approximately 1 mile north of the Ames city limits and was centrifuged to remove particulate matter. Process water from a simulated in situ oil shale retort procedure was obtained from the Laramie Energy Technology Center.

**Derivatization Procedure.** A 0.5-mL aqueous sample was mixed in a 5-mL Reacti-vial (Pierce Chemical Co., Rockford, IL) with 1 mL of acetonitrile containing 40 $\mu$g of PFB, heated to 85 °C, and held at that temperature for 30 min. After cooling to ambient temperature, the imines were extracted by adding 0.5 mL of organic-free water and 1.0 mL of hexane to the reaction mixture and shaking vigorously for 15 s. No further treatment of the hexane solution was necessary to achieve a detection limit of 10 ppb.

If detection limits below 10 ppb were desired, a larger sample size and slightly modified procedure were required. For example, methylamine at a concentration of 1 ppb in water was derivatized by heating to 85 °C for 30 min a mixture of 5 mL of aqueous sample and 10 mL of acetonitrile containing 0.5 mg of PFB. Five milliliters of organic-free water was added to the cooled reaction mixture prior to extraction of the imine into 10 mL of hexane. The hexane layer was collected and reduced to 1 mL with a rotary evaporator.

**Instrumentation.** A Finnigan Model 4000 combination GC/MS with an INCOS 2300 data system was used for all imine analyses. The GC/MS was operated in the electron impact mode using full scan ($m/z$ 45–400) or multiple-ion-monitoring ($m/z$ 57 + 208 + 222) detection. The instrument was fitted with a 30 m × 0.25 mm i.d. DB5 (J&W, Rancho Cordova, CA) fused silica capillary column which was led directly into the mass spectrometer ion source; helium was the carrier gas at 24 cm/s linear velocity at 45 °C. For each run, 1.8 $\mu$L of hexane extract was injected splitless at 45 °C for 30 s. The column temperature was held at 45 °C for 4 min and then programmed to 200 °C at 4 °C/min. Quantitations were performed by using three-point standard additions.

**Mass Spectra.** The 70-eV electron impact mass spectra of the imine derivatives are as follows: methylamine, 208 (100), 209 (85), 181 (29), 117 (18), 93 (16), 161 (15), 104 (9), 99 (9); ethylamine, 208 (100), 181 (24), 194 (12), 223 (7), 161 (7), 117 (7), 104 (7), 93

0003-2700/85/0357-0790$01.50/0 © 1985 American Chemical Society

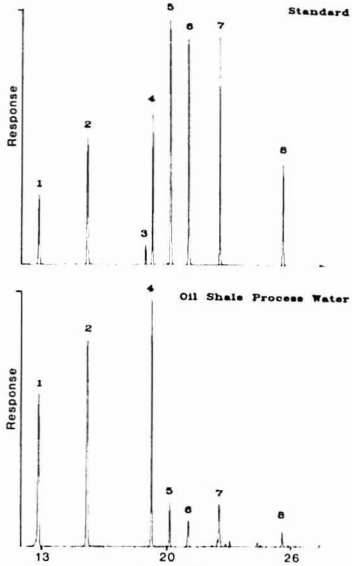

**Figure 1.** Mass chromatograms ($m/z$ 57 + 208 + 222) of derivatized amine samples. Numbered peaks refer to the pentafluorobenzaldehyde imines of (1) methylamine, (2) ethylamine, (3) *tert*-butylamine, (4) *n*-propylamine, (5) *sec*-butylamine, (6) isobutylamine, (7) *n*-butylamine, and (8) *n*-pentylamine.

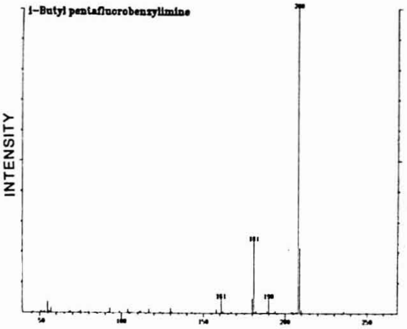

**Figure 2.** Mass spectrum of the pentafluorobenzaldehyde imine of isobutylamine.

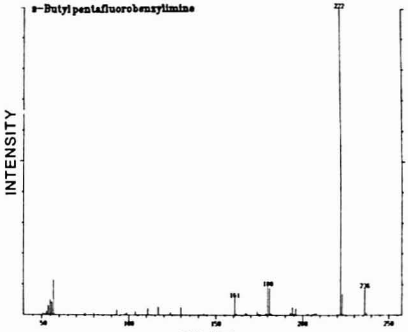

**Figure 3.** Mass spectrum of the pentafluorobenzaldehyde imine of *sec*-butylamine.

(6); *n*-propylamine, 208 (100), 181 (35), 209 (27), 161 (8), 190 (6), 117 (6), 180 (6), 236 (4); *n*-butylamine, 208 (100), 181 (61), 209 (41), 190 (37), 222 (12), 161 (11), 194 (11), 180 (10); isobutylamine, 208 (100), 181 (23), 209 (20), 161 (4), 190 (4), 180 (4), 55 (3), 130 (3); *sec*-butylamine, 222 (100), 57 (12), 180 (9), 181 (9), 236 (9), 161 (9), 223 (6), 194 (3); *tert*-butylamine, 57 (100), 236 (20), 180 (6), 56 (3), 161 (3), 58 (3), 111 (2), 196 (1); *n*-pentylamine, 208 (100), 181 (77), 250 (45), 190 (45), 209 (30), 194 (18), 222 (13), 55 (13).

## RESULTS AND DISCUSSION

**Derivatization.** One of the reasons for derivatizing alkylamines is to improve their chromatographic behavior. A mass chromatogram of standard imine derivatives, shown at the top of Figure 1, illustrates the peak shapes obtained by injecting a sample containing about 1 ng of each component. This excellent chromatographic behavior was observed for amounts as low as 10 pg. Electron impact mass spectra of imine derivatives of alkylamines are dominated by α-cleavage as illustrated below for pentafluorobenzaldehyde *n*-butylimine.

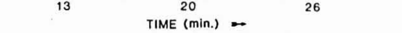

$$C_6F_5CH{=}\overset{+\bullet}{N}{-}CH_2{-}C_3H_7 \longrightarrow C_6F_5CH{=}\overset{+}{N}{=}CH_2 + \cdot C_3H_7$$

If the α-position of the amine is unsubstituted, the base peak will be $m/z$ 208, illustrated by the mass spectrum of pentafluorobenzaldehyde isobutylimine in Figure 2. The addition of a methyl group at the α-position increases the base peak to $m/z$ 222 as shown in Figure 3. The *tert*-butyl isomer, with both α-positions occupied by methyl groups, produces $m/z$ 236 with a relative abundance of 20%. The base peak for the *tert*-butyl isomer, $m/z$ 57, is produced by inductive cleavage. The aforementioned ions are characteristic of the imine derivatives, so mass chromatograms can be used to obtain structural information about the alkyl groups of the parent primary amines. Primary aromatic amines, such as aniline, will not interfere because these ions are not produced from its imine. Detection limits for the derivatives are in the low picogram range when using SIM of the base peaks. Although electron-capture detection would give comparable sensitivity and reasonable selectivity, unreacted PFB would have to be removed in a separate cleanup step (*16*) and structural information would be lacking. Nitrogen-specific detection would provide some selectivity but the sensitivity would be much less than electron capture and SIM.

When the derivatization was attempted without diluting the water sample 2:1 with acetonitrile, very poor conversion to the imine was realized. Full-scan GC/MS analysis of the reaction mixture revealed that a side product, tentatively identified as a PFB dimer, was produced in amounts much greater than the desired imine.

Although the formation of the imine derivatives is selective for primary amines, not all primary amines will react with the reagent with the same efficiency. The relative reactivities for the reaction of PFB with the four isomers of butylamine are *n*-butyl (1.00), isobutyl (0.91), *sec*-butyl (0.37), and *tert*-butyl (0.09). The amount of derivative decreases as steric hinderance of the amine group increases. In general, detection limits for hindered amines will be much higher than those for the *n*-alkyl isomers.

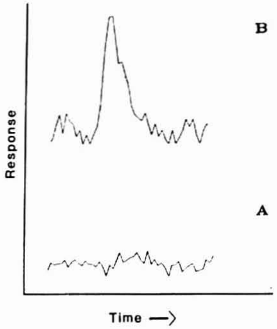

**Figure 4.** Mass chromatograms (*m/z* 208) of derivatized samples of 5 mL each of (A) river water and (B) river water spiked with 1 ppb methylamine.

**Methodology Tests.** The derivatization of *n*-butylamine to pentafluorobenzaldehyde *n*-butylimine at the 100 ppb level was found to have an overall efficiency of 30%. This value includes the efficiency of derivative formation and extraction into hexane.

The detection limit for the method described here is 10 ppb with no sample transfers or manipulations being necessary for sample volumes of 0.5 mL. The sensitivity can be improved by evaporation of the hexane from the 1 mL hexane extract, but care must be taken to avoid losses of the imines. The detection limit can also be lowered by increasing the sample size. Figure 4 illustrates the signal obtained by application of the method to a 5-mL sample of a surface water spiked with 1 ppb methylamine. Disadvantages to the use of sample sizes greater than 0.5 mL are increased sample manipulation, leading to poorer precision and more chances for sample contamination, and an increase in extract volume, necessitating a volume reduction step.

The accuracy and reproducibility of the PFB derivatization scheme were determined by spiking the target compounds into tap water and river water at levels ranging from 50 ppb to 10 ppm. Quantitative values obtained for seven compounds were within ±10% of the true values. Mean relative standard deviations for triplicate determinations ranged from ±9% at 10 ppm to ±25% at 50 ppb.

Obtaining quantitative values for the PFB derivatives by the usual method of external standards requires that pure samples of each derivative be synthesized. This problem was circumvented by using the method of standard additions since all that is required is to add easily obtainable amines or amine salts to the sample. In addition, this method corrects for the nonquantitative nature of imine formation.

**Applications.** The developed methodology was applied to samples of Ames tap water, water from the Skunk River, and a sample of oil shale retort water. No target amines were detected in the tap water or river water. A process retort water, produced as an emulsion with shale oil during in situ retorting, proved to be rich in the target amines as well as many other organic compounds (*6, 7*). A mass chromatogram of the derivatized retort water is shown at the bottom of Figure 1. The selectivity of the method is illustrated by the clean base line. The peaks not identified are probably due to isomers of pentylamine for which standards were not available. Quantitative values for six amines present in the sample were determined and are compared to published values in Table I.

**Table I. Determination of Amines Present in a Shale Oil Retort Water**

| | concn, ppm | | |
|---|---|---|---|
| amine | PFB derivatization | GC direct[a] | steam distillation[a] |
| methyl | 14.3 | 13 | 10 |
| ethyl | 10.2 | 11 | 9 |
| *n*-propyl | 5.7 | 4 | 4 |
| *n*-butyl | 1.6 | 2 | 2 |
| *sec*-butyl | 1.4 | ND[b] | ND |
| iso-butyl | 0.8 | ND | ND |
| *n*-pentyl | 2.2 | ND | ND |

[a] Taken from ref 6. [b] Not determined.

## CONCLUSION

The sensitivity and selectivity described in this report suggest that this procedure for determining primary amines is generally applicable to environmental waters, wastewaters, and process streams and is particularly well-suited to biofluids and homogenized tissues where only small sample sizes are available. Studies of these applications are currently in progress.

## ACKNOWLEDGMENT

The technical assistance of John Richard and the administrative assistance of Ray W. Fisher and V. A. Fassel are acknowledged.

## LITERATURE CITED

(1) Onuska, F. I. *Water Res.* **1973**, *7*, 835.
(2) Umbreit, G. R.; Nygrean, R. E.; Testa, A. J. *J. Chromatogr.* **1969**, *43*, 25.
(3) Moser, A. R.; Andre, C. E.; Viets, F. G., Jr. *Environ. Sci. Technol.* **1973**, *7*, 642.
(4) Bouyoucos, S. A. *Anal. Chem.* **1977**, *49*, 401.
(5) Chriswell, C. D.; Fritz, J. S. *J. Chromatogr.* **1977**, *136*, 371.
(6) Richard, J. J.; Junk, G. A. *Anal. Chem.* **1984**, *56*, 1625.
(7) Leenheer, J. A.; Noyes, T. I.; Stuber, H. A. *Environ. Sci. Technol.* **1982**, *16*, 714.
(8) Smith, J. S.; Hanrahan, J. M. *J. Chromatogr.* **1980**, *193*, 271.
(9) Donike, M. *J. Chromatogr.* **1973**, *78*, 273.
(10) Hohaus, E. *Bunseki Kagaku* **1984**, *33*, E55.
(11) Wellons, S. L.; Carey, M. A. *Chromatographia* **1978**, *10*, 808.
(12) Petty, R. L.; Michel, W. C.; Snow, J. P.; Johnson, K. S. *Anal. Chim. Acta* **1982**, *142*, 299.
(13) Day, E. W., Jr.; Golab, T.; Koons, J. R. *Anal. Chem.* **1966**, *38*, 1053.
(14) Koga, P.; Akiyama, T.; Shinohara, R. *Bunseki Kagaku* **1981**, *30*, 745.
(15) Nakamura, H.; Takagi, K.; Tamura, Z.; Yoda, R.; Yamamoto, Y. *Anal. Chem.* **1984**, *56*, 919.
(16) Hoshika, Y. *Anal. Chem.* **1977**, *49*, 541.

RECEIVED for review October 1, 1984. Accepted December 26, 1984. This work was performed in the laboratories of the U.S. Department of Energy and supported under Contract No. W-7405-Eng-82. The work was supported by the Office of Health and Environmental Research, Office of Energy Research and the Assistant Secretary for Fossil Energy, Division of Coal Utilization, through the Laramie Energy Technology Center.

# Rapid and Precise Method for the Measurement of Vapor/Liquid Equilibria by Headspace Gas Chromatography

**Abul Hussam and Peter W. Carr***

*Department of Chemistry, Smith and Kolthoff Hall, University of Minnesota, Minneapolis, Minnesota 55455*

**This work describes a device designed to allow the rapid measurement of vapor/liquid equilibria, including vapor pressure and solute activity coefficients, in an automated fashion based on a conventional gas chromatograph. Various correction factors needed to convert the analytical signal (peak area) to the desired thermodynamic quantities have been developed. In general, activity coefficients at low concentration (mole fraction less than 0.01) are in good agreement with literature values (ca. 2%). Similarly, vapor pressures can be measured with good accuracy. The precision of measurement is often better than 0.5%. The major limitation in the accuracy of the method appears to be the lack of high quality experimental gas phase virial coefficients.**

Virtually since its inception, gas chromatography has been recognized as a powerful method for the study of vapor/liquid equilibria, in particular, for the measurement of infinite dilution activity coefficients of nonelectrolytes (*1, 2*). There are many possible chromatographic approaches to the determination of such phase transfer equilibria, including the dynamic, static (*3*), and saturation or stripping methods (*4*). The most common and thermodynamically well-defined methods include the dynamic approach, in which the retention volume of a solute molecule is measured and the static or headspace (*5–7*) analysis technique, in which the chromatograph is used in a conventional fashion, i.e., as a selective and sensitive gas analyzer. Each of these approaches has distinct advantages and disadvantages.

In principle, the dynamic method is the faster because it does not entail the preparation of solutions of the solute in the solvent of interest. Once a column with an *accurately* (*8*) known amount of well-defined stationary phase (the solvent) is available, one merely measures the column dead volume and retention volume of the solutes of interest. Thus, it is possible to inject mixtures of solutes and generate data quite rapidly. In practice the method is limited to solvents of low volatility. Column preparation (including support deactivation) and determination of the mass of stationary phase liquid is tedious; indeed, this step is the limitation of the accuracy and precision of the method (*8, 9*). Corrections for the compressibility of the mobile phase and the pressure differential across the column must be made quite accurately and the effect of adsorption at the high surface area gas/solid or gas/liquid interface must be assessed and a correction made when significant. Clearly, when a mixture of solutes is injected, it must be well separated under isothermal conditions (note that temperature programmed elution is not permissible since the relevant thermodynamic parameters, i.e., vapor pressures, stationary phase density, and activity coefficient, are all temperature dependent). Finally, to obtain infinite dilution activity coefficients, the solutes must be injected at quite low concentration to avoid nonlinear isotherms. It should be noted that activity coefficients at finite concentrations can be obtained by dynamic GC by the use of frontal analysis (*10*). A major advantage of the approach is that where it is applicable, very precise results can be obtained (0.2%) (*9*). Additional advantages include the fact that the detector need not be calibrated. Elution time and eluent flow rates are the critically important measurements. Because the flow rate and temperature must be known quite accurately, most workers who use the dynamic method have modified the flow controllers and ovens of commercial equipment or designed their own system. A nontrivial advantage of the method is the possibility of obtaining the solute–carrier gas virial coefficient by varying the pressure drop across the column via a change in the flow rate (*11*). The retention time of a peak can be used to measure the thermodynamic retention only when the peak is symmetric or nearly so. When asymmetric peaks are encountered, the first moment must be computed, thus requiring on-line acquisition of the signal and postrun data analysis. Consequently, conventional integrators cannot be used.

The static or headspace technique was adopted in this work for several reasons. First, our primary interest, and, indeed, of most chemists, is in rather volatile solvents, e.g., mixtures of water and methanol, microemulsions, etc. The dynamic method can be used with volatile solvents, but the mobile phase must be presaturated with the liquid, and the pressure drop across the column must be small. Second, the headspace method is more readily amenable to the measurement of vapor pressure, as well as activity coefficients over a finite concentration range. Thus, the entire phase diagram can be assessed. A headspace device with the following operational features was developed: (1) rapid analysis of samples; (2) accurate temperature control of samples (better than ±0.01 °C); (3) ability to work at low sample concentration (mole fraction <0.01); (4) minimal perturbation of the equilibrium by the sampling process; (5) ability to vary composition of the solvent automatically.

The device which was designed is shown schematically in Figure 1. In order to allow high sensitivity and analysis of complex mixtures of gases, a commercial temperature programmed capillary (macrobore) gas chromatograph was used as the analyzer. Preliminary work indicated that microbore capillaries and their attendant splitter systems (*12*) were not acceptable in terms of the ultimately desired accuracy and precision (ca. 1%). For our purposes a macrobore capillary provided an excellent compromise in terms of the desired resolution and analytical sample capacity between a conventionally packed column and a microbore capillary.

Most commercial headspace analyzers transfer the sample by over pressuring the sample and timing the flow of gas from the sample chamber to the column. A vacuum transfer system was used in this work to achieve the precision inherent in the sample loop valve and to minimize the perturbation of the vapor/liquid equilibrium by use of a very small sample (~200 μL). Commercial headspace analyzers also employ some type of septum which may be attacked by the solvent or imbibe sample. This potential problem was avoided wherever possible, thus, with one exception, a system with only glass or metal components was designed.

Headspace analysis has a number of significant advantages over the use of conventional classical measurement approaches (*13*). First, the solvent need not be degassed nor must more volatile impurities be removed since these can be easily sep-

0003-2700/85/0357-0793$01.50/0 © 1985 American Chemical Society

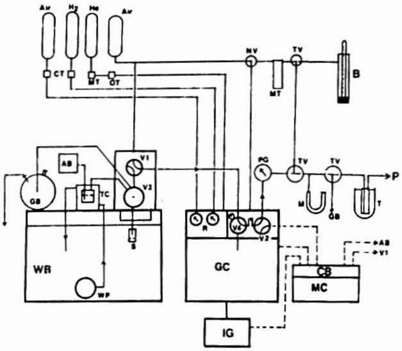

Figure 1. A schematic diagram of the experimental setup.

arated from the sample in the capillary column. Obviously, the solvent must be sufficiently pure that it, and not impurities in it, establish the activity coefficient of the solute. This issue is distinct from the pressure measurement problem involved when there is a small amount of a volatile liquid in a much less volatile solvent. Second, one can work at extremely low concentrations and can simultaneously study several solutes provided that they can be separated. In general, nonchromatographic methods for the measurement of activity coefficients require a series of studies to be carried out over a considerable range in composition and the data extrapolated, sometimes over a wide interval, to obtain infinite dilution activity coefficients. In contrast, the sensitivity and detection capabilities of a chromatographic system are such that one can easily work at solute concentrations where Henry's law is accurately obeyed and, consequently, no extrapolation to infinite dilution is needed. The separations are generally trivial since a temperature program can be used, and the column can be chosen to achieve the desired resolution. The method requires much less material than recirculation stills (*14*) and equilibrium can be established quite rapidly provided the liquids are not excessively viscous since small cells (less than 20 mL) can be used. A comprehensive review of a number of nonchromatographic methods for the study of vapor/liquid equilibria can be found in ref 15 and 16. Where applicable, such techniques can have extremely high accuracy and precision. The headspace method and apparatus described here cannot achieve the same degree of certitude as the classical methods. In contrast they are far less cumbersome and can produce reasonably reliable data in far less time.

The chief drawbacks of headspace methods in comparison to dynamic chromatographic methods are the need to calibrate the detector response, the requirement of detector linearity over the range of concentrations to be studied, and the need for information on gas-phase compressibilities to correct the analytical data (peak area) to pressure.

This work describes an apparatus and the theoretical correction factors which allow the convenient measurement of a number of important vapor/liquid properties.

## EXPERIMENTAL SECTION

**Chemicals.** *n*-Alkanes (*n*-pentane through *n*-decane) were obtained from Aldrich Chemical Co. Prior to use they were passed through silver nitrate impregnated activated silica to remove unsaturated hydrocarbons and stored over phosphorus pentoxide. *n*-Octadecane (purity 99%) was obtained from Alfa Chemical Co. and used without purification. Benzene, toluene, nitromethane, methyl ethyl ketone, acetonitrile, and dioxane were either HPLC grade or spectrophotometric quality (Fisher Chemical Co.) and were kept over molecular sieve (5 Å). Ethanol and octanol were Gold Label grade reagents from Aldrich Chemical Co.

**Table I. Critical Dimensions of the Gas Transfer Lines**

| transfer line | inside diameter, in. | volume, μL |
|---|---|---|
| S–V3 | 0.01 | 16 |
| V3–V1 | 0.01 | 2.5 |
| V1–V4 | 0.01 | 33 |
| V4–V2 | 0.04 | 202 |
| V3–GB | 0.01 | 25 |
| V3–TC | 0.01 | 16 |
| sample loop | 0.02 | 20 |

**Apparatus.** A schematic diagram of the experimental setup is shown in Figure 1. The headspace analyzer was designed around an HP-5790A (Hewlett-Packard Instrument Co.) capillary gas chromatograph (GC), equipped with a gas sampling valve (V4) and a four-port valve (V2). The gas sampling valve (V4) was connected to another four-port valve (V1) (Model AH-6-CV-9H7A, Valco Instruments, Inc., Houston, TX) and to a 16-port sample selection valve (V3) (Model CSD16T, Valco Instruments, Inc., Houston, TX). The valves are housed in two heated boxes at a temperature of 150 °C (±2 °C). The sample cells are glass vessels (volume ca. 12 mL) connected via glass–metal seals to $^1/_4$ in. to $^1/_{16}$ in. zero dead volume Swagelok stainless steel fittings and placed in a water bath (WB), the temperature of which is controlled by a PTC-40 temperature controller (Tronane Inc., Provo, UT). The temperature of the water bath is constant with a tolerance of ±0.001 °C. Temperature measurements were performed with a calibrated thermometer (ASTM-56C, Fisher Scientific Co.). Two of the ports from the 16-port selection valve are reserved for a thermostated cell (TC) (volume ca. 60 mL) and a gas bulb (GB). The thermostated cell is used for studies in which an accurately known amount of a liquid can be added by means of a precalibrated autoburet (AB) (Model ABU-11, Radiometer, Copenhagen, Denmark). Water is circulated around the thermostated cell by a water pump (WP), immersed in the water bath. To hold standards, a large gas bulb of accurately known volume is fitted with a "mininert" Teflon valve for sample introduction and a Teflon needle valve for evacuating the bulb. All gas transfer lines are heated to 150 °C. Heating is provided by an insulated nichrome wire heater. The gas transfer lines are $^1/_{16}$ in. o.d. precleaned nickel tubing (grade 200, Alltech Associates). Dimensions of the transfer lines are listed in Table I. The transfer line from the sample cell is inserted some distance into the cell so that vapor can be sampled from near the liquid surface. The transfer lines from V1 to V2 are evacuated by a vacuum pump (P), which is connected to a cold trap (T), a manometer (M) (Model G-1700, Gilmont Instruments Inc, NY), and a pressure gauge (PG). A vacuum on the order of 0.5 torr of Hg can be generated in 2 min. Atmospheric pressure is monitored by a barometer (B) (Model G-4400, Gilmont Instruments, Inc., New York). A high-pressure air tank is used to supply the necessary pressure for the actuation of valves V1, V4, and V2. This tank can also be used to pressurize the sample if necessary, by using the manostat (MT) (Model C-2200, Gilmont Instruments, Inc., New York) and two needle valves (NV) (Type CP1, Parker Fluidics).

Helium, which serves as the carrier gas, passes through a moisture trap (MT) and an oxygen trap (OT). Hydrogen and air for the flame ionization detector (FID) pass through a charcoal trap (Model HC-2445, Supelco, Inc.). Precision pressure regulators (Perkin-Elmer Corp, Norwalk, CT) maintain a stable flow rate for the FID gases. These pressure regulators are thermally insulated because room temperature fluctuations can cause a change in the flow rate of the FID gases and thus alter the response of the detector.

The GC is interfaced to an integrator (IG) (HP-3390A). Automation of the system is provided by a microcomputer (MC) (Model TS-1000, Timex Corp.) interfaced to a controller board (CB) (Model BB-1, Byte Back Co.). Valves V1, V2, the GC, the integrator, and the autoburet are actuated at precise time settings by the computer. All reasonable precautions have been taken to ensure stable and reproducible responses. This is essential because high analytical accuracy and precision are needed to detect the small differences in the thermodynamic measurements of interest.

**Sample Preparation.** For the measurement of the vapor pressure of a pure liquid, approximately 2 mL of the liquid is transferred to the sample cell (ca. volume 12 mL). Hydrocarbons in *n*-octadecane were prepared by weighing each component in a glass vial fitted with a "mininert" valve. Weighing accuracy was better than 0.01%. To avoid loss of volatile hydrocarbons (e.g., pentane) the samples were kept in a refrigerator. Rapid condensation (solidification) of *n*-octadecane at room temperature (ca. 25 °C) prevents the use of a gastight syringe for transferring such samples. During transfer, the closed samples in octadecane were melted in a water bath and about 2 mL of the stock is immediately transferred to a headspace vial by using a Pasteur pipet. We chose to study the system *n*-alkane/ocatadecane because we believe that the literature values for the infinite dilution activity coefficient in this system are extremely reliable. Further, the values are close to unity and, therefore, constitute a difficult test of the methodology described here. Clearly, the inconveniently high melting point of this solvent places considerable demands on the care which must be exercised to obtain reliable results with the more volatile solutes. Other binary mixtures were also prepared by weighing the components in a glass vial fitted with a "mininert" valve.

For the study of the vapor/liquid equilibria of the dioxane–acetonitrile system, one of the components was delivered to a known weight of the other component by a precalibrated autoburet under computer control. The mixture was continuously stirred for 20 min for rapid equilibration before the headspace was sampled for GC analysis.

**Procedure.** *Sampling Procedure.* To sample the headspace, the transfer lines V1 to V2 are evacuated for 2 min and then valve V2 is closed and V1 is opened for 30 s to allow the sample vapor to fill the 20-μL sample loop of valve V4. Valve V1 is then closed and the gas sample is immediately injected into a wide bore high capacity fused silica capillary column (HP Series 530 μ methyl silicone) without any sample splitting. A narrow bore column can be used with sample splitting provided that there is no preferential splitting of the components. This is particularly important during a multicomponent analysis. Typical GC operating conditions are as follows: He flow, 21.4 mL/min; air flow, 292 mL/min; $H_2$ flow, 88 mL/min; auxiliary He, 17 mL/min; temperature program, 35 °C for 2 min then increase at 30 °C/min.

*Standard Preparation.* Details of the standard preparation and calibration procedure have been described elsewhere (*17*). Briefly, gas standards (multicomponent or single component) are prepared in a large (~12 L) gas bulb (GB), of precisely known volume, by injecting a known weight of standard sample and allowing it to evaporate completely. The weight of the liquid must be low enough to avoid saturation of the gas phase and concomitant condensation. In a second method, the headspace vapor above a pure liquid of known vapor pressure is used for calibration. Both techniques are applied whenever necessary. Experimentally, the second method is faster and simpler than the first.

## THEORY

When the gas phase can be assumed to be a perfect gas, the equations needed to calibrate the vapor/liquid equilibrium parameters are very straightforward. The approach given below is a good deal more complex to account for gas phase nonideality even though in most cases the corrections are small (<10%).

At equilibrium, the fugacities of any solute must be equal in the liquid and vapor phases

$$f_i^{l} = f_i^{v} \tag{1}$$

At a given temperature the fugacities in the liquid and vapor phase are functions of only the composition, concentration, and pressure as follows:

$$f_i^{l} = \gamma_i x_i f_i^{\circ} \tag{2}$$

$$f_i^{v} = \phi_i y_i P \tag{3}$$

where $\gamma_i$ is the activity coefficient of species $i$, $x_i$ is its mole fraction, and $f_i^{\circ}$ is the fugacity of pure liquid $i$. Similarly, in the vapor phase, $\phi_i$ is the fugacity coefficient, $y_i$ is its mole fraction, and $P$ is the total pressure. For pure $i$

$$f_i^{\circ} = P_i^{\circ}\phi_i^{\circ} \exp[\nu_i^{l}(P - P_i^{\circ})/RT] \tag{4}$$

where $\phi_i^{\circ}$ is the fugacity coefficient of pure $i$ which corrects for the deviation of the saturated vapor pressure, $P_i^{\circ}$, from ideal gas behavior, the exponential term accounts for the effect of applied pressure, and $\nu_i^{l}$ is the molar volume of pure liquid $i$. Combining eq 1–4, we obtain eq 5 (*18*)

$$\ln \gamma_i = \ln (y_i P/x_i P_i) + \ln (\phi_i/\phi_i^{\circ}) - [\nu_i^{l}(P - P_i^{\circ})/RT] \tag{5}$$

Gas-phase fugacity coefficients $\phi_i$ can be approximated at low pressure by the virial equation of state truncated after the second virial coefficient

$$\ln \phi_i = (2/\nu) \sum_{j=i}^{m} y_j B_{ij} - \ln Z_{\text{mix}} \tag{6}$$

where $\nu$ is the molar volume of the mixture and $Z_{\text{mix}}$ is the compressibility of the mixture. $Z_{\text{mix}}$ can be related to the virial coefficients by the equation

$$Z_{\text{mix}} = 1 + PB_{\text{mix}}/RT \tag{7}$$

where

$$B_{\text{mix}} = \sum_{i}^{n}\sum_{j}^{n} y_i y_j B_{ij} \tag{8}$$

and $B_{\text{mix}}$ is the mixture virial coefficient. Equation 5 along with eq 6–8 are the basis for the thermodynamic correction for the nonideality of gases.

**Case I: Use of Gas Standard.** To apply eq 5 to the headspace method, the following consideration has to be made. Assuming the detector is linear over the measured concentration range, the peak area will be related to the molar concentration $C_i$ of sample gas by the equation

$$A_i = kV_{\text{loop}}C_i \tag{9}$$

and for the gas standard (GS)

$$A_{\text{GS}} = kV_{\text{loop}}C_{\text{GS}} \tag{10}$$

where $k$ is a constant response factor and $V_{\text{loop}}$ is the volume of the sample loop. The partial pressure of $i$ in the headspace can be related to the vapor-phase concentration by the equation

$$p_i = C_i RTZ_{\text{mix}} \tag{11}$$

Combining eq 9–11, we get

$$p_i = (A_i/A_{\text{GS}})C_{\text{GS}}RTZ_{\text{mix}} \tag{12}$$

where $Z_{\text{mix}}$ is due to solute $i$, solvent, and the air present in the headspace. Since $C_{\text{GS}}$ (known from the weight of standard and volume of the bulb) is the analytical concentration of the solute in the standard gas bulb, no assumption regarding nonideality of gases in the standard is required. By definition $p_i = y_i P$, then eq 5 can be combined with eq 12

$$\ln \gamma_i^{\text{GS}} = \ln (A_i C_{\text{GS}}/A_{\text{GS}}x_i) + \ln (RTZ_{\text{mix}}/P_i^{\circ}) + \ln (\phi_i/\phi_i^{\circ}) - [\nu_i^{l}(P - P_i^{\circ})/RT] \tag{13}$$

Equation 13 relates the activity coefficient of solute $i$ to the peak areas $A_i$ and $A_{\text{GS}}$ when a gas standard of known composition is used.

**Case II: Use of Pure Liquid Standard in Presence of Air.** The situation is much more complicated when the pure liquid vapor is used as the standard. For a pure liquid (LS) in the presence of air, the peak area will be

$$A_{\text{LS}} = kV_{\text{loop}}C_{\text{LS}} \tag{14}$$

Combining eq 9 and 14 we obtain

$$C_i = C_{LS}A_i/A_{LS} \qquad (15)$$

We know

$$P_i^* = C_{LS}RTZ_{mix}^* \qquad (16)$$

where $P_i^*$ is the vapor pressure of the liquid in the presence of air and $Z_{mix}^*$ is the compressibility under the same conditions. The compressibilities $Z_{mix}$ and $Z_{mix}^*$ refer to the sample condition and not that in the sampling loop. Combining eq 11, 15, and 16, we obtain

$$P_i = P_i^*(A_i/A_{LS})(Z_{mix}/Z_{mix}^*) \qquad (17)$$

To obtain $P_i^*$, we must consider the vapor/liquid equilibrium of the liquid standard in the presence of air. If we assume that the solubility of air in the pure liquid is negligible, then for pure liquid

$$f_i^l = f_i^\circ = P_i^\circ\phi_i^\circ \exp[\nu_i^l(P - P_i^\circ)/RT] \qquad (18)$$

For the vapor phase

$$f_i = \phi_i^* P_i^* \qquad (19)$$

where $P_i^* = y_iP$ and $\phi_i^*$ is the fugacity coefficient of pure vapor in the presence of air. Combining eq 18 and 19 we obtain

$$P^* = P_i^\circ(\phi_i^\circ/\phi_i^*) \exp[\nu_i^l(P - P_i^\circ)/RT] \qquad (20)$$

Equation 20 corrects the true (saturated liquid vapor) pressure ($P_2^\circ$) to that which should be observed in the presence of air at total pressure $P$. Combining eq 5, 17, and 20, the activity coefficient based on a liquid standard can be calculated as

$$\gamma_i^{LS} = (A_i/A_{LS}x_i)(\phi_i/\phi_i^*)(Z_{mix}/Z_{mix}^*) \qquad (21)$$

In many cases it should be possible to assume that when the partial pressure of the solute and solvent pairs are very low, the terms $\phi_i/\phi_i^*$ and $Z_{mix}/Z_{mix}^*$ will be very close to unity. Thus when virial coefficients are unknown, the use of the pure liquid solute as the analytical standard can be quite advantageous. In eq 13, the first two terms are the uncorrected activity coefficient of the solute; the terms after that are usually very small and close to unity, particularly when the solute is at infinite dilution.

It is important to understand we have assumed the detector response is linear and there is no intercept in the calibration curve. By use of two distinct standards the assumption can be checked.

## RESULTS AND DISCUSSION

**Preliminary Experiments.** Before describing the quantitative results of the study a number of operational features of the system must be made clear. First, the pneumatic characteristics of the transfer system were assessed. As shown in Figure 2, transfer of the sample to the sampling valve is almost instantaneous and does not change by more than 0.5% when V1 is open from 5 to 300 s. This indicates that the gas sample moves very rapidly into the transfer line. It is possible to calculate the linear velocity of a gas, when there is a pressure difference (1 atm in this work) between valve V1 and V2 by using the Poiseuille equation. Such calculations show that flow at a rate of ca. 500 μL s$^{-1}$ through a 0.01-in. i.d., 135 cm long tube will require 0.1 s to reach the other end of the tube. We have chosen a 30–60 s V1 open period for convenience. Once the gas sample is in the transfer line, i.e., when V1 and V2 are closed, there should be no movement of the gas by diffusion or by pressure variation. This was confirmed, i.e., the peak area did not change by more than 0.5% as a function of residence time (see Table II). Figure 1 and Table II show that a representative sample of the gas phase is in the sample loop.

It is also critically important that the ballast volume, i.e., the volume between V4 and V2 (202 μL) be sufficiently large compared to the sum of the volume of the transfer line and the gas sampling valve to ensure that a representative sample of the gas in the cell is delivered to the capillary column, i.e., the ballast must be large enough to completely sweep the preceding sample (or air) from the transfer line to waste. As seen in Table I, the ballast volume is approximately 4 times larger than the transfer line; a ballast volume the same or less than that of the transfer line showed almost no transfer (<1%) of the gas sample.

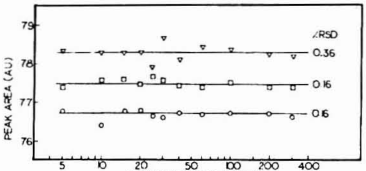

**Figure 2.** Peak area of pentane (○), hexane (▽), and octane (□) as a function of V1 opening time; solution, ca. $10^{-3}$ M each in *n*-octadecane at 30 °C.

**Table II. Effect of Sample Residence Time on Peak Areas**

| residence time,[a] s | peak area × $10^{-3}$, arb. units |
|---|---|
| 0 | 3114 |
| 7 | 3105 |
| 15 | 3107 |
| 30 | 3124 |
| 60 | 3142 |
| 300 | 3144 |
| | 3123 av |
| | 0.5% RSD |

[a] Sample is the vapor above air-saturated *n*-hexane at 25 °C. Transfer line temperature is 150 °C.

**Table III. Effect of Volume of the Sample Vessel on the Peak Areas of *n*-Hexane in Vapor/Liquid Equilibrium[a]**

| volume, mL | | volume ratio vapor/liquid | peak area × $10^{-3}$, arb. units |
|---|---|---|---|
| liquid sample | total cell | | |
| 1.00 | 12.00 | 11.00 | 1934 |
| 6.00 | 12.00 | 1.00 | 1947 |
| 1.00 | 81.00 | 80.00 | 1922 |
| 30.00 | 81.00 | 1.7 | 1960 |
| | | | 1940 av |
| | | | 0.73% RSD |

[a] Split vent flow, 385 mL/min; column, 12 m 0.1 μm methyl silicone. In another experiment, the vapor pressure of toluene was measured in a 12 mL, 30 mL (stainless steel), and a 81 mL sample vessel. The values of $p^\circ$ obtained was in excellent agreement with the literature value with a relative accuracy better than 1%.

If a representative sample of gas is being taken, the peak area should be quite independent of the ratio of vapor to liquid volume in the cell and of the total cell volume. Results for such experiments are shown in Table III.

Table IV shows the results when air is readmitted to the system after a sample is taken and when it is not. Clearly the difference is insignificant. Provided that equilibrium is established rapidly (see footnote of Table IV, 3 min is the minimum time between runs) the volume of the ballast system should be unimportant. This was checked by using a large gastight syringe to rapidly remove a large volume of the headspace and immediately sampling the vapor. The results are shown in Table V. Clearly, the vapor/liquid equilibrium is perturbed momentarily only when the volume of the vapor

**Table IV. Effect of Repressurization with Air on the Sample Peak Area of Octane**[a]

| | peak area × $10^{-3}$, arbitrary units | |
|---|---|---|
| | no air readmitted | air readmitted |
| | 468.2 | 464.5 |
| | 465.2 | 464.2 |
| | 463.1 | 463.9 |
| | 467.3 | 463.9 |
| | 463.5 | 464.6 |
| av | 465.5 | 464.2 |
| % RSD | 0.43 | 0.07 |

[a] Time between runs varied from 3 to 22 min.

**Table V. Perturbation of Vapor/Liquid Equilibrium of *n*-Octane**[a]

| mL of air injected | peak area × $10^{3}$, arb. units | mL of headspace withdrawn | peak area × $10^{-3}$, arb. units |
|---|---|---|---|
| 0.0 | 464.5 | 0.0 | 465.4 |
| 2.0 | 466.7 | 2.0 | 464.3 |
| 4.0 | 466.9 | 4.0 | 463.6 |
| 6.0 | 466.4 | 8.0 | 455.7 |
| 10.0 | 464.9 | 10.0 | 455.4 |
| 0.0 | 464.9 | 0.0 | 465.2 |

[a] Sample volume and headspace volume are 2 and 10 mL, respectively, with 3 to 5 min interval between runs.

**Table VI. Port to Port Reproducibility of Multiport Selection Valve**

| port no. | peak area × $10^{-3}$, of hexane | port no. | peak area × $10^{-3}$, of hexane |
|---|---|---|---|
| 1 | 3831 | 13 | 3841 |
| 2 | 3836 | 15 | 3836 |
| 4 | 3879 | 16 | 3868 |
| 5 | 3803 | | |
| 6 | 3833 | av | 3840 |
| 7 | 3836 | % RSD | 0.54 |

sampled is nearly equal to the headspace volume. In the present apparatus only 20 μL of the 250-μL gas sample is injected onto the column. Since the total volume of gas sampled is insignificant compared to the headspace volume (10–80 mL), the perturbation of the vapor/liquid equilibrium does not occur. The rate of equilibration can also be checked by deliberately injecting a large volume of air into the cell and running an assay of the headspace. Table V shows that volumes of up to 10 mL of air can be injected with no effect. The equilibrium is reestablished within 3 min.

Since a 16-port sample selection valve is used, it is important to certify the port to port reproducibility of the system. Table VI shows the results with hexane as the sample. It is clear from the result that port to port reproducibility is well within experimental error.

As a final preliminary check of the system, the temperature of the transfer line from the top of the sample cell to the bottom of the valve box oven was varied while the rest of the transfer lines were maintained at 150 °C. It is important to maintain the tubing at a temperature high enough so that condensation and adsorption of the sample do not occur. Figure 3 shows that octane vapor does condense when the transfer tube line is at 33 °C. This is evidenced by raising the transfer tubing to 77 °C; the peak area increased dramatically and then decreased almost monotonically in successive runs. It takes a very large number of runs to remove all of the condensate at 77 °C. Therefore, the sample was disconnected and a vacuum applied to the tubing until no octane peak was observed. After this cleaning procedure, the headspace was sampled 30 times (3 to 5 min between runs) with a relative standard deviation of 0.3% with no systematic trends in the data (Figure 3c). The vapor pressure of octane measured under these conditions is in excellent agreement with the literature value (% error = −0.2%). To avoid adsorption and condensation problems, we have used precleaned nickel tubing and a transfer line temperature of 110–150 °C. At this elevated temperature, the tubing must be carefully thermally insulated to avoid temperature fluctuations in the water bath. It should be noted, however, that one of the functions of the ballast volume is to draw enough sample from the cell so that the walls of the tubing are freed of condensed and adsorbed material. If necessary, one could use uncoated fused silica transfer lines for use with highly adsorptive test systems. Their fragility mitigates against routine use.

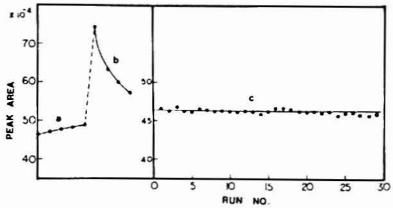

Figure 3. Effect of temperature variation of the transfer line between sample and oven on the peak areas of pure octane vapor: temp, (a) 33 °C, (b) 77 °C, and (c) flushed at 77 °C. Each point (●) indicates a single run.

**Measurement of Vapor Pressure of Pure Liquids.** After performing the preliminary experiments described above, we measured the vapor pressure of 11 polar and nonpolar liquids (see Table VII). For these measurements the chromatographic system was calibrated with a pure gas standard of the respective substance. In Table VII the lowest ratios of the sample area ($A_i$) to that of the gas standard ($A_{GS}$) are listed. At least three different concentrations of gas standards were used for calibration. For example the highest $A_i/A_{GS}$ for pentane and hexane were 292 and 254, respectively. A six-point calibration curve of hexane gas standard (from $5.44 \times 10^{-6}$ M to $2.61 \times 10^{-3}$ M) was prepared. This calibration yielded a straight line through the origin (intercept = $(0.035 \pm 0.025) \times 10^{-5}$ M) and a correlation coefficient of 0.9999 ($F = 51703$). Again, using pure liquid hydrocarbons (*n*-pentane to *n*-decane), we have shown (*17*) that a plot of the response factor per mole of carbon as a function of log (molar concentration) of the saturated vapor as determined by its vapor pressure has a slope of 0.026 ± 0.028 at the 90% confidence level and an overall coefficient of variation of 0.4%. These results show that the detector response is linear over a wide range of concentration. Since the amount of sample injected is limited by its vapor pressure and the volume of the sample loop (20 μL), the upper limit of the dynamic range is never reached in headspace analysis. Therefore, the detector (FID) is never "overloaded" in this work.

It is clear from Table VII that the precision of the measurement (% RSD) is considerably better than is the accuracy. Because the gas phase is nonideal and the measurements are made with air in the sample cell, eq 20 was used to correct the observed vapor pressure. The primary data needed for correction of the observed vapor pressure are the second virial coefficient, $B_{11}$, for the pure compound and the cross-virial coefficient, $B_{12}$, where 2 is the co-gas, which is primarily nitrogen in this case. For nonpolar hydrocarbons $B_{11}$ and $B_{12}$ can be calculated from the correlation of Pitzer and Curl (*19*),

Table VII. Measured Vapor Pressure of Pure Liquids at 298.16 K

| compounds | $A_i/A_{GS}$[a] | $p^\circ$ (exptl), atm | % RSD[b] | $p^\circ$ (corr),[c] atm | $p^\circ$ (Antoine),[e] atm | % error exptl–Ant. | % error corr–Ant. |
|---|---|---|---|---|---|---|---|
| pentane | 38.60 | 0.6890 | 0.1 | 0.6798 | 0.6743 | +2.2 | +0.8 |
| hexane | 3.80 | 0.2043 | 0.3 | 0.1992 | 0.1990 | +2.6 | +0.1 |
| heptane | 11.37 | 0.0603 | 0.2 | 0.0588 | 0.0601 | +0.3 | -2.1 |
| octane | 6.92 | 0.0183 | 0.1 | 0.0179 | 0.0183 | 0.0 | -2.1 |
| benzene | 12.56 | 0.1255 | 0.4 | 0.1231 | 0.1252 | +0.24 | -1.7 |
| toluene | 2.28 | 0.0374 | 0.6 | 0.0366 | 0.0374 | 0.0 | -2.1 |
| nitromethane | 2.04 | 0.0470 | 0.3 | 0.0464 | 0.0469 | +0.21 | -1.0 |
| acetonitrile | 3.99 | 0.1176 | 0.4 | 0.1145 | 0.1136 | +3.5 | +0.8 |
| methyl ethyl ketone | 6.87 | 0.1219 | 0.3 | *d* | 0.1187 | +2.7 | *d* |
| dioxane | 4.02 | 0.0459 | 0.3 | 0.0451 | 0.0463 | +0.8 | -2.6 |
| ethanol | 2.96 | 0.0812 | 0.2 | *d* | 0.0788 | +3.0 | *d* |

[a] Peak area ratio of sample to gas standard for the highest gas standard concentrations. [b] Percent relative standard deviation of at least ten measurements. [c] Corrected experimental vapor pressure using eq 20. [d] Accurate $B_{12}$ values were not available. [e] Antoine values obtained by using Antoine constants *A*, *B*, and *C* (*22*).

Table VIII. Measurement of Infinite Dilution Activity Coefficient of Some n-Hydrocarbons in n-Octadecane at 303.16 K

| compounds (*i*) | $A_i/A_{LS}$[a] | $x_i$ | $\gamma_i^{\infty}$[b] | % RSD[f] | $\gamma_i^{\infty}$[c] | $\gamma_i^{\infty}$[d] (lit.) | % error |
|---|---|---|---|---|---|---|---|
| | | | A. Mixtures of all Solutes + *n*-Octadecane | | | | |
| pentane | 0.0157 | 0.0195 | 0.805 | 0.12 | 0.817 | 0.854 | -4.2 |
| hexane | 0.0140 | 0.0167 | 0.838 | 0.36 | 0.845 | 0.869 | -2.8 |
| heptane | 0.0123 | 0.0139 | 0.887 | 0.22 | 0.888 | 0.889 | -0.1 |
| octane | 0.01067 | 0.0114 | 0.936 | 0.11 | 0.936 | 0.917[e] | +1.9 |
| | | | B. Binary Mixtures of One Solute + *n*-Octadecane | | | | |
| pentane | 0.0151 | 0.0191 | 0.794 | 0.13 | 0.805 | 0.854 | -5.7 |
| hexane | 0.0125 | 0.0151 | 0.831 | 0.18 | 0.844 | 0.869 | -2.9 |
| heptane | 0.0157 | 0.0179 | 0.878 | 0.42 | 0.880 | 0.889 | -1.0 |
| octane | 0.01607 | 0.0177 | 0.908 | 0.31 | 0.906 | 0.917[e] | -1.2 |

[a] Peak area ratio of solute *i* to the liquid standard. [b] Uncorrected values based on $\gamma_i^{\infty} = A_i/(A_{LS}x_i)$. [c] Thermodynamically corrected values (eq 21). [d] See ref 23. [e] Extrapolated value obtained from a plot of ln $\gamma_i^{\infty}$ vs. carbon number. [f] Percent relative standard deviation of replicate runs. A minimum of 13 replicate analyses is included.

and the necessary values for critical constants are obtained from the literature (*20*). Although it is more difficult to estimate the second virial coefficient of polar gases, empirical correlations have been established (*21*). The agreement between experimental values and values using the Antoine equation (*22*) is excellent and the overall absolute error is 1.2% in comparison to that between corrected and Antoine values (1.7%). Therefore the correction factors are small for nonassociating compounds (i.e., hydrocarbon) and somewhat larger for strongly associated compounds. However, for many practical purposes, the thermodynamic correction factor can be neglected. Although we have taken the Antoine equation vapor pressure ($P^\circ$) as the correct absolute value, occasionally the literature values for $P^\circ$ can deviate as much as 5% from the Antoine value. Therefore it is important to measure the vapor pressure of pure components for any vapor/liquid equilibrium studies.

Inspection of Table VII does not indicate any correlation between the accuracy of the measured vapor pressure and the ratio of sample area to standard area. This substantiates our belief that detector nonlinearity is not the dominant source of the residual analytical error.

The present technique for the measurement of vapor pressure is only limited by the lower limit of the FID's dynamic range, in other words, the vapor pressure of a liquid that can be measured (with a 20-μL sample loop) for which the signal is at least three times the standard deviation of the background which amounts to ca. $3 \times 10^{-7}$ atm for decane. For less volatile liquids one can use a large sample loop, but care must be taken not to perturb the vapor/liquid equilibrium by withdrawing excessive amounts of sample. For low volatile liquids, conventional vapor pressure measurements are difficult due to the removal of all gases and isomers of similar volatility. Headspace techniques are not subject to such problems. They are very flexible and limited only by the ability to accurately standardize the system.

**Direct Measurement of Infinite Dilution Activity Coefficients.** Since we were able to measure the vapor pressure of pure liquids; the measurement of infinite dilution activity coefficient ($\gamma^{\infty}$) of solutes was also assessed. The results are compiled in Table VIII. In Table VIIIA the $\gamma^{\infty}$ of several alkanes (*n*-pentane to *n*-octane) in *n*-octadecane are given when all solutes were present as a mixture in the solvent at the indicated mole fraction. In Table VIIIB, the $\gamma^{\infty}$ of some solutes are given for binary mixtures of that solute and *n*-octadecane. All $\gamma^{\infty}$ values are obtained with a relative precision better than 1%. Thermodynamically corrected $\gamma^{\infty}$ are obtained by applying eq 21 based on pure liquid standards of the solute. Because the detector linearity has been checked for *n*-hydrocarbons (*17*) over a wide range of concentration and the vapor pressures of *n*-hydrocarbons have been measured with excellent accuracy using the same technique, the pure liquid solute can therefore be used as the standard. Pure liquid standards are much easier to prepare and use. They also allow us to monitor the vapor pressure and therefore the overall instrument performance. The only problem with pure liquid standards is the thermodynamic correction terms become complicated, particularly when both solute and solvent are volatile.

It is clear from Table VIII that the corrected $\gamma^{\infty}$ values are in good agreement with literature values (*23*). It should be mentioned that the literature values of $\gamma^{\infty}$ compared well to values calculated using the Flory–Huggins equation where the interaction parameter was taken to be a linear function of the

**Table IX. Infinitely Dilute Activity Coefficients of Some Other Binary Mixtures**

| solute | solvent | temp, K | $\gamma_i^{\infty a}$ | $\gamma_i^{\infty}$ (lit.) | % error | ref |
|---|---|---|---|---|---|---|
| benzene | toluene | 298.16 | 0.984[c] | 0.99 | −0.6 | 26 |
| benzene | methanol | 303.16 | 7.17 | 7.18[b] | | 26 |
| benzene | water | 303.16 | 2402[d] | 2422 | 0.8 | 27 |
| toluene | methanol | 303.16 | 9.97 | 10.8 | | 26 |
| toluene | octanol | 298.16 | 2.11 | 2.19 | −3.6 | 24 |
| acetonitrile | dioxane | 298.16 | 1.520[c,d] | 1.542 | −1.3 | 25 |
| dioxane | acetonitrile | 298.16 | 1.310[c,d] | 1.330 | −1.5 | 25 |
| nitromethane | octanol | 298.16 | 8.58 | 8.52 | +0.7 | 24 |

[a] Based on pure liquid standard using $\gamma_i^{\infty} = A_i/(A_{\mathrm{LS}}\chi_i)$. [b] Temperature was 308.1 K. [c] Thermodynamic and analytical corrections based on eq 21 were applied. [d] Values obtained from extrapolation of $\gamma_i^{\infty}$ as $\chi_i \rightarrow 0$.

volume fraction of the solute. Using the same equations the ratio for pentane $\gamma^{\infty}_{\mathrm{VIII(A)}}/\gamma^{\infty}_{\mathrm{VIII(B)}}$ was found to be within 1% of the calculated values. Because the error in $\gamma^{\infty}$ is the largest for pentane, we attribute this to the loss of pentane (the most volatile solute) during sample transfer. The same is true for other solutes, but in decreasing order.

One can see from Table VIII that our solute concentrations are ten times lower than those used to establish the literature values. Solute mole fractions below $10^{-3}$ can be easily measured by headspace capillary GC, but difficulties in the accurate preparation of the sample, due to the high volatility of the solutes, limits the technique. However, literature values show $\gamma/\gamma^{\infty}$ to be greater than 1.01 when the mole fraction of solute exceeds 0.04 and 0.05 for pentane and hexane or heptane, respectively. Therefore, our $\gamma$ values are essentially in the infinite dilution region. The results show that $\gamma^{\infty}$ of all solutes can be measured simultaneously, possibly in a single run, provided that the mole fractions of the solutes are kept in the infinite dilution range.

Measurements of the infinite dilution activity coefficients for other systems are given in Table IX. The results show that a wide range of $\gamma^{\infty}$ values for a variety of solute–solvent systems can be studied. The agreement between measured and literature values is excellent. Thermodynamic and analytical corrections for some of the systems could not be done because $B_{11}$ and $B_{12}$ values for those systems were not available. It should, however, be remembered that both thermodynamic and analytical correction terms become important when $\gamma^{\infty}$ is close to unity.

We have also measured $\gamma^{\infty}$ for a series of *n*-alkylbenzenes (benzene to *n*-butylbenzene) in a series of methanol–water mixtures (*28*). For this system the mole fraction of *n*-alkylbenzenes ranges from $10^{-3}$ in pure methanol to $10^{-5}$ in methanol–water mixtures rich in water (ca. 0.9 mole fraction). With these systems no correction factors were applied, since they are insignificant compared to ln $\gamma^{\infty}$ (which is the quantity related to the excess free energy of solution). Even at very low mole fractions of the alkylbenzenes (ca. $10^{-6}$–$10^{-7}$) in water-rich mixed solvents, the gas-phase concentration of the solute is high enough to measure peak areas with a relative precision better than 1%. This is due to the strong hydrophobic effect forcing the solute out of the solution. However, as mentioned earlier, preparation of such a dilute solution is very difficult and loss of solute by adsorption on the container surface is a strong possibility. In general, it is possible to measure $\gamma^{\infty}$ quite accurately and simultaneously for a number of solutes in a single solvent (volatile or nonvolatile) as long as solute–solute interactions are negligible in comparison to the solute–solvent interactions, essentially in the Henry's law region. Work is under way (*29*) in this laboratory to measure $\gamma^{\infty}$ of six Rohrschneider solutes (*3*) in a large number of solvents and compare the results with theoretically obtained values (*30*).

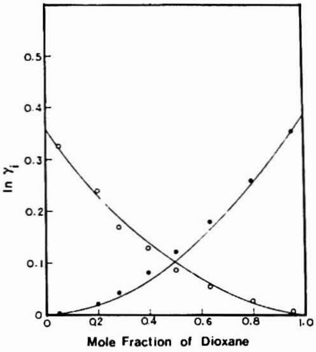

**Figure 4.** Activity coefficients vs. mole fraction of dioxane (○) in dioxane–acetonitrile (●) mixture at 298.16 K.

**Table X. Second Virial Coefficients (cm³ mol⁻¹) of Dioxane–Acetonitrile–Nitrogen Systems at 298.16 K**

| | dioxane (1) | acetonitrile (2) | nitrogen (3) |
|---|---|---|---|
| dioxane (1) | −1717 | −2734 | −159 |
| acetonitrile (2) | −2734 | −3713 | −140 |
| nitrogen (3) | −159 | −140 | −4.34 |

**Vapor/Liquid Equilibria of *p*-Dioxane–Acetonitrile Mixtures.** Headspace GC has been applied to solute–solvent systems that show both positive and negative deviations from Raoult's law, from which activity coefficients at various concentrations and related functions, such as partial and total molar free energy of mixing and excess functions were obtained (*31, 32*). We studied the *p*-dioxane–acetonitrile system and the effect of thermodynamic and analytical correction factors on the observed $\gamma$. This system is nearly an ideal mixture.

The measured $\gamma$ of *p*-dioxane (component 1) and acetonitrile (component 2) as a function of the solvent composition are shown in Figure 4. The results are in excellent agreement with literature values (*25*) except in the middle composition range (mole fractions in the range 0.3–0.6) where the errors are about 5%. Since the experimental $\gamma$ values are based on the analytical gas standard, poor agreement between experimental and literature values in the middle composition range are attributed to the error in calculating $Z_{\mathrm{mix}}$ of eq 13. From eq 7 it can be seen that $Z_{\mathrm{mix}}$ is related to $B_{ij}$ and the mole fraction of the components in the gas phase. For dioxane–acetonitrile and nitrogen (component 3) in the gas phase, $B_{\mathrm{mix}}$ can be written as

$$B_{\mathrm{mix}} = y_1^2B_{11} + y_2^2B_{22} + y_3^2B_{33} + 2y_1y_2B_{12} + 2y_1y_3B_{13} + 2y_2y_3B_{23} \quad (22)$$

The second virial coefficients $B_{ii}$ and $B_{ij}$ are listed in Table X. In the intermediate composition range, all terms in eq

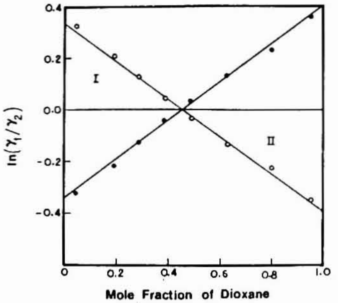

**Figure 5.** Test of thermodynamic consistency of dioxane (O)–acetonitrile (●) system by using the Gibbs–Duhem equation (eq 23).

21 are significant. To calculate $Z_{mix}$, $B_{ii}$ and $B_{ij}$ have to be known accurately while the gas-phase composition is accurately measured by the use of headspace GC. Since no experimental values of $B_{ii}$ and $B_{ij}$ are available, we used the general empirical correlation of O'Connell and Prausnitz (*21*). The values thus estimated can deviate considerably from experimental values and are very sensitive to the choice of components *i* and *j*. On the other hand, at infinite dilution of one of the components, some of the terms in eq 22 will drop out (as the corresponding gas phase mole fractions approach zero) and directly minimize the error in calculating $Z_{mix}$. Since $\phi_i$ is also related to $B_{ij}$ and $Z_{mix}$, similar conclusions can also be drawn for the third term in eq 13, although in the term $\phi_i/\phi_i^\circ$ some of the errors cancel. Comparing the second and third terms in eq 13, the second term is larger than the third term. Note, however, the correction terms become somewhat significant when $\gamma$ of the solute approaches unity. This is one of the reasons why acetonitrile–dioxane is a good test system; another is that the $\gamma$ values are not very variable (<40%) over the entire composition range.

The data in Figure 4 have been tested for thermodynamic consistency by using the integrated Gibbs–Duhem equation

$$\int_0^1 \ln (\gamma_1/\gamma_2)\, \mathrm{d}\chi_1 = 0 \qquad (23)$$

A plot of such a test is shown in Figure 5. It shows that the experimental data over the entire composition range is 14% inconsistent compared to 2% for the literature value. However, the $\gamma^\infty$ values are in excellent agreement with the literature values (see Table IX) and none of the $\gamma$ values at other compositions are more than 5% in error. It is well-known (*33*, *34*) that if accurate $\gamma^\infty$ are available, the two parameters in expressions for the excess Gibbs energy, i.e., the van Laar (*35*), Wilson (*36*), and UNIQUAC (*37*) equations can be obtained and thus the entire *y*–*x*, *P*–*x*, and $\gamma$–*x* curves for the system can be predicted with good accuracy.

To evaluate the relative merits of the two types of standards, we used both procedures. Based on the two standards, the $\gamma$ of acetonitrile and dioxane are compared in Table XI. The two standards are in good agreement (2%) considering the different nature of the correction terms involved. Finally, we conclude that in the middle composition range, accurate $\gamma$ values for systems in which both solute and solvent are volatile can be obtained if accurate experimental $B_{ii}$ and $B_{ij}$ values are obtained.

In view of the excellent precision (relative precision better than 1%) for the experiments described above, the accuracy is poor. Although in many cases the accuracy obtained is acceptable, we feel that it can be improved by carefully considering the various analytical and thermodynamic factors involved. Work is under way to achieve that goal.

**Table XI. Comparison of Activity Coefficient of Acetonitrile in Dioxane Based on Liquid and Gas Standard at 298.16 K**

| $\chi_{CH_3CN}$ | $\gamma$(GS)[a] | $\gamma$(LS)[b] | \|%Δ\|[c] | $\gamma$ (lit.) |
|---|---|---|---|---|
| 0.7186 | 1.051 | 1.074 | 2.1 | 1.031 |
| 0.6037 | 1.092 | 1.116 | 2.1 | 1.067 |
| 0.5021 | 1.136 | 1.161 | 2.1 | 1.105 |
| 0.3646 | 1.194 | 1.220 | 2.1 | 1.173 |
| 0.1994 | 1.284 | 1.313 | 2.2 | 1.289 |
| 0.0403 | 1.397 | 1.428 | 2.2 | 1.419 |

[a] Based on eq 13. [b] Based on eq 21. [c] $|\Delta\%| = |(\gamma_{GS} - \gamma_{LS})/\gamma_{LS} \times 100|$.

## CONCLUSION

This work shows that headspace gas chromatographic methods can be used for the precise (<1%) and accurate (typically 3%) measurement of vapor/liquid equilibria in a wide variety of systems (pure component vapor pressure, infinite dilution activity coefficients) encompassing nonpolar and polar species. The methodology does not require rigorous degassing of samples nor must all volatile impurities be removed. The chief drawback of the approach is the need for complex thermodynamic and analytical correction factors which must be obtained from other experimental measurements or empirical correlations. In many instances such corrections are often small (e.g., in highly nonideal mixtures). Operationally the methodology is quite rapid and flexible. It does not have the extremely high accuracy (<1%) provided by classical techniques but it can provide data of sufficient accuracy for predictive purposes needed by analytical chemists, chemical engineers, and others for the design of separation systems and establishing experimental data bases for correlating molecular properties (*30*).

## ACKNOWLEDGMENT

The authors wish to express their appreciation to Donald F. Hagen of the 3M Co. for his invaluable technical advice and guidance in the design of the system.

## LITERATURE CITED

(1) Conder, J. R.; Young, C. L. "Physicochemical Measurements by Gas Chromatography"; Wiley: New York, 1979.
(2) Laub, R. J.; Pecsok, R. L. "Physicochemical Applications of Gas Chromatography"; Wiley: New York, 1978.
(3) Abraham, M. H. *J. Chem. Soc. A* **1971**, 1061–1071.
(4) Lerol, J. C.; Mason, J.-C.; Renon, H.; Fabrics, J.-F.; Jarrier, H. *Ind. Eng. Chem., Process Des. Dev.* **1977**, *16*, 139–144.
(5) Hachenberg, H.; Schmidt, A. P. "Gas Chromatographic Headspace Analysis"; Heyden: London and Philadelphia, 1977.
(6) Kolb, B., Ed. "Applied Headspace Gas Chromatography"; Heyden: London and Philadelphia, 1980.
(7) Ioffe, B. V.; Vitenberg, A. G. "Headspace Analysis and Related Methods in Gas Chromatography"; Wiley: New York, 1984.
(8) Wicarova, O.; Novak, J.; Janak, J. *J. Chromatogr.* **1970**, *51*, 3.
(9) Oweimreen, G. A.; Lin, G. C.; Martire, D. E. *J. Phys. Chem.* **1979**, *83*, 2111–2119.
(10) Glueckauf, E. *J. Chem. Soc.* **1947**, 1302.
(11) Cruickshank, A. J. B.; Windsor, M. L.; Young, C. L. *Proc. R. Soc. London, Ser. A* **1966**, *295*, 271.
(12) Jennings, W. "Gas Chromatography with Glass Capillary Columns", 2nd ed.; Academic Press: New York, 1980; pp 63–77.
(13) Hala, H.; Pick, J.; Fried, V.; Vilim, V. "Vapor-Liquid Equilibrium", 2nd English ed.; Pergamon: Oxford, 1967.
(14) Brown, I. *Aust. J. Sci. Res., Ser. A* **1952**, *5*, 530.
(15) McGlashan, M. L. "Chemical Thermodynamics"; Academic Press: London, 1979; pp 244.
(16) Marsh, K. N. "Experimental Thermodynamics of Gas Liquid Equilibria"; Vol. 2 of Chemical Thermodynamics, McGlashan, M. L., Ed.; Chemical Society: London.
(17) Hussam, A.; Carr, P. W., submitted for publication.
(18) Prausnitz, J. M. "Molecular Thermodynamics of Fluid Phase Equilibria"; Prentice-Hall: Englewood Cliffs, NJ, 1969.
(19) Pitzer, K. S.; Curl, R. F., Jr. *J. Am. Chem. Soc.* **1957**, 79, 2369.
(20) Kudchadker, A. P.; Alani, G. R.; Zwolinski, B. J. *Chem. Rev.* **1968**, *68*, 659–735.
(21) O'Connel, J. P. O.; Prausnitz, J. M. *Ind. Eng. Chem. Process Des. Dev.* **1967**, 6, 245–250.

(22) Dreishbach, R. R. "Physical Properties of Chemical Compounds"; American Chemical Society: Washington, DC, **1959**; Vol. II.
(23) Vogel, G. L.; Hamzavi-Abdel, M. A.; Martire, D. E. *J. Chem. Thermodyn.* **1983**, *15*, 739–745.
(24) Rohrschneider, L. *Anal. Chem.* **1973**, *45*, 1241–1247.
(25) Davolio, F.; Pedrosa, G. C.; Katz, M. *J. Chem. Eng. Data* **1981**, *26*, 26–27.
(26) Thomas, E. R.; Eckart, C. A., *Ind. Eng. Chem. Process Des. Dev.* **1984**, *23*, 194–209.
(27) Tucker, E. E.; Lane, E. H.; Christian, S. D. *J. Soln. Chem.* **1981**, *10*, 1–20.
(28) Hussam, A.; Carr, P. W., submitted for publication.
(29) Fritz, D. W.; Carr, P. W., unpublished results.
(30) Fredenslund, A.; Jones, R. L.; Prausnitz, J. M. *AIChE J.* **1975**, *21*, 1086.
(31) Kolb, B. *J. Chromatogr.* **1975**, *112*, 287–295.
(32) Shaw, D. A.; Anderson, T. F. *Ind. Eng. Chem. Fundam.* **1983**, *22*, 79–83.
(33) Eckert, C. A.; Newman, B. A.; Nicolaides, G. L.; Long, T. C. *AIChE J.* **1981**, *27*, 33–40.
(34) Loblen, G. M.; Prausnitz, J. M. *Ind. Eng. Chem. Fundam.* **1982**, *21*, 109–113.
(35) Van Laar, J. J. *Z. Phys. Chem.* **1910**, *72*, 723.
(36) Wilson, G. M. *J. Am. Chem. Soc.* **1964**, *86*, 127.
(37) Abrams, D. S.; Prausnitz, J. M. *AIChE J.* **1975**, *21*, 116.

RECEIVED for review October 29, 1984. Accepted December 17, 1984. This work was supported in part by grants from the University of Minnesota Graduate School and the National Science Foundation.

# Determination of Chlorinated Benzenes in Bottom Sediment Samples by WCOT Column Gas Chromatography

**F. I. Onuska* and K. A. Terry**

*National Water Research Institute, Canada Centre for Inland Waters, Burlington, Ontario, Canada L7R 4A6*

**An integrated analytical procedure for determining chlorinated benzene contaminants that enables quantitation of individual isomers as low as 0.4 μg/kg in sediment samples has been developed. Preparation of the sample can be performed by using one of three techniques, namely, Soxhlet extraction and ultrasonic extraction or steam distillation. Chlorinated benzenes are then characterized and quantified by open tubular column gas chromatography with electron capture detection. Recoveries of individual chlorinated benzene isomers at three different levels from two different types of sediment, one low and one high in organic matter, were evaluated. Although all three methods are quantitative, the steam distillation method was found to be the most efficient for the determination, insofar as time and simplicity are concerned. Data presented indicate that detection limits of this method are 0.4 to 10 μg/kg of individual chlorobenzene isomers. Chlorobenzene recovery from bottom sediment samples at concentration levels between 1 and 100 μg/kg is 86 ± 14%.**

The occurrence of chlorinated benzenes in environmental systems has created concern about environmental chemicals, regarding the fate and transport of these contaminants in air (*1*), natural waters (*2*), and sediments (3). Chlorinated benzenes have been used as raw materials and intermediates in the manufacture of pesticides and chlorinated phenols and as process solvents. They are produced in amounts in excess of 500 metric tons annually in the United States (*1*). Information on their toxicity (*4*) and metabolic studies of individual isomers after ingestion or exposure are also well documented (*4–6*).

Chau and Babjak have reported an ultrasonic extraction technique which in our hands did not provide consistent recoveries for chlorinated benzenes (*7*). Oliver reports a Soxhlet extraction procedure which is quite time-consuming (*8*). This paper describes improved analytical methodology for quantitative determination of all the chlorinated benzene isomers in sediment samples. The main objective was to evaluate the efficiency of the exhaustive steam distillation method (*9*) vs. Soxhlet and ultrasonic extraction followed by centrifugation. Both blank and environmentally contaminated sediments were investigated to study recoveries.

**Table I. Standard Mixtures Used for Quantitation**

| isomer | mixture 1, pg/μL | mixture 2, pg/μL |
|---|---|---|
| 1,3-dichlorobenzene | 100 | 25 |
| 1,4-dichlorobenzene | 100 | 25 |
| 1,2-dichlorobenzene | 100 | 25 |
| 1,3,5-trichlorobenzene | 10 | 5 |
| 1,2,4-trichlorobenzene | 10 | 5 |
| 1,2,3-trichlorobenzene | 10 | 5 |
| 1,2,3,5-tetrachlorobenzene | 10 | 5 |
| 1,2,4,5-tetrachlorobenzene | 10 | 5 |
| 1,2,3,4-tetrachlorobenzene | 10 | 5 |
| pentachlorobenzene | 10 | 5 |
| hexachlorobenzene | 10 | 10 |
| hexachlorethane | | 1 |
| hexachlorobutadiene | | 5 |

The efficiency of the extraction techniques for recoveries was determined by using open tubular column (WCOT) gas chromatography and electron capture detection (ECD). All chlorinated benzenes can be detected in bottom sediment samples at low microgram-to-kilogram levels. Before applying this methodology to bottom sediment samples, the methods were validated for accuracy, precision, and minimum detection limits for individual chlorinated benzene isomers.

## EXPERIMENTAL SECTION

**Reagents.** Pesticide quality *n*-hexane, benzene, acetone, diethyl ether, and 2,2,4-trimethylpentane was used.

Two high purity chlorinated benzene standard solutions were prepared from pure individual isomers obtained from RFR Corp., Hope, RI. The specific isomers and their concentration in these solutions are given in Table I.

It should be noted that the concentrations of dichlorobenzenes are 5 to 10 times higher than the remaining higher chlorinated isomers.

Copper was activated by washing Cu powder in 6 N HCl for 15 min and storing under *n*-hexane.

Mercury was triple distilled.

**Sediment Samples.** Wet sediment (approximately 5000 g) taken from Lake Superior (Isle Royale, Blake Pt.) was spread

0003-2700/85/0357-0801$01.50/0 © 1985 American Chemical Society

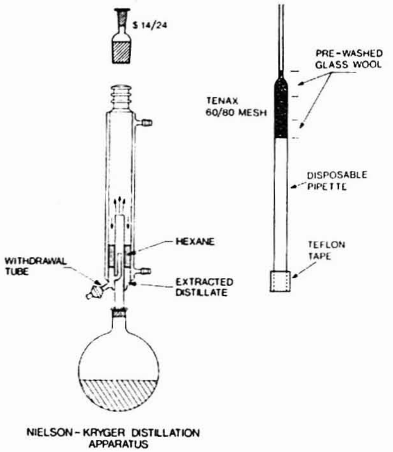

**Figure 1.** Nielson–Kryger steam distillation apparatus with an adsorption adaptor.

evenly in a large shallow glass dish and allowed to air-dry at room temperature in a contaminant-free area. The sample was stirred and mixed occassionally during drying to break it into small pieces. This process was continued until the sample appeared visually dry and free flowing. The dried sample was then manually ground to a fine powder with a mortar and pestle. This homogenized sample was used as a blank because it contained no chlorobenzenes as was determined by the analysis.

Two environmentally contaminated sediments were used: Hamilton Harbour (74.6% water) and an EC-2 sediment sample. The EC-2 sample was a mixture of the Hamilton Bay sediment and a Lake Ontario sediment was used as a standard reference (*2*).

**Spiking Procedure.** Ten grams of blank sediment was added to the extraction vessel; 10 mL of organic-free water was added to wet the sample. The appropriate spike was then added and the sample swirled to mix it as evenly as possible. The vessel was then sealed and allowed to equilibrate for 10 h.

Similarly, 10 g of wet sediment from Hamilton Harbour was weighed into the extraction vessel and 10 mL of organic-free water was added. The spike was then introduced over the sample in a manner described elsewhere (*10*). Equilibration time was 10 h.

**Apparatus.** *Soxhlet Extractor.* The apparatus includes a 500-mL round-bottom flask, heating mantle with variable voltage control, Soxhlet extractor (100-mL capacity), and a Liebig water-cooled condenser.

*Sonifier/Cell Disruptor.* The apparatus, from Ultrasonics Inc., Model W-350, includes the following: power supply, 120 V, 5 A, 60 Hz, output power 350 W to the converter, frequency of 20 kHz, continuous and intermittent duty cycle; converter with 95% efficiency in converting electrical energy to mechanical vibrations (20 cm long × 62.5 mm diameter); Sonabox enclosure for decreasing cavitation sound; horn, standard distruptor horn of titanium alloy (17.5 cm long × 19 mm diameter) and high gain disruptor horn (6.25 cm × 19 mm diameter); cooling bath, ground ice in a 1-L beaker; centrifuge, 2000 rpm at 10 °C by Internation Refrigerated, Model PR-6, or equivalent.

*Steam Distillation Apparatus.* A Nielson-Kryger distillation apparatus available from ACE Glass Co., Vineland, NJ, was used with a Tenax trap made from a disposable pipet with silanized glass wool plug and approximately 1 g of 80/100 mesh Tenax followed by another short silanized glass wool plug as shown in Figure 1.

**Extraction of Sediments.** (*1*) *Soxhlet Extraction Method.* A 25-mm layer of solvent extracted Celite was placed in an extraction thimble. A 10 g equivalent of sediment was placed over the Celite. A 300 mL volume of *n*-hexane–acetone (1:1) plus 50 mL of 2,2,4-trimethylpentane (isooctane) and some boiling chips were added to the round-bottom flask. Extraction was carried out continuously for 18 h. This time was selected experimentally, because it provided 100% recovery for hexachlorobenzene. After cooling, the extract was transferred with 2 × 25 mL *n*-hexane rinsings to a 1000-mL separatory funnel. One hundred milliliters of organic-free water was added and the separatory funnel was shaken lightly. The aqueous layer was transferred to a 500-mL separatory funnel and extracted with 100 mL of benzene. If an emulsion was formed, 10 mL of saturated sodium sulfate solution was added. The organic layers were combined, and the aqueous layer was discarded. The organic layer was dried over 5 cm of anhydrous $Na_2SO_4$ in a suction filtration funnel.

The 1000-mL separatory funnel was rinsed two times with 25 mL of *n*-hexane and the extract was passed through the anhydrous $Na_2SO_4$. The sodium sulfate was rinsed with two 25-mL portions of *n*-hexane and the sample was then evaporated on the rotary evaporator to 5 mL for further Florisil column chromatography cleanup. The standard Florisil column cleanup procedure was used for Soxhlet extracted samples. Since the samples were analyzed solely for chlorinated benzenes, only the 200 mL of *n*-hexane eluate was collected and concentrated in a rotary evaporator. Isooctane (10 mL) was added as a keeper before the preconcentration step by rotary evaporation in each extraction method. In addition to the Florisil cleanup, it was necessary to treat the extract for removal of sulfur, if interferences occurred. This was done by shaking it with mercury until newly added mercury no longer dulled (*11*). For less contaminated samples activated copper should be used. The treated eluates were analyzed by WCOT column gas chromatography and electron capture detector (ECD).

(2) *Ultrasonic Extraction.* A 10-g dry weight equivalent of sediment was placed in a 200-mL centrifuge bottle. Approximately 160 mL of *n*-hexane–acetone (1:1) was added to the sample. The bottle was then placed into an ice bath on an adjustable stand. The purpose of the ice was to minimize losses by volatilization. In areas where the sediment was badly contaminated with sulfur, the use of mercury was necessary and was added to the final organic extract. The sample was then sonified for 3 min at 50% duty cycle and output 5, with the mouth of the bottle butted up against the base of the horn. After this time, the horn was rinsed with 2 mL of hexane–acetone into the extract. The bottle was then capped and centrifuged at 2000 rpm at 10 °C for 3 min. The solution was then decanted into a 1000-mL separatory funnel where 100 mL of organic-free water was added to the combined extracts and shaken for 1 min with venting at 20-s intervals. The aqueous portion was drained into a secondary separatory funnel (500 mL capacity) and extracted with two 60-mL portions of benzene. The combined organic extracts were dried through a 5-cm column of anhydrous $Na_2SO_4$ in an Alihn filter into a 500-mL round-bottom flask. Vacuum was applied only after all of the solvent had apparently passed through. The sample was concentrated to 5 mL of isooctane by rotary evaporation at 35–40 °C under aspirator vacuum.

(3) *Steam Distillation.* An equivalent of 10 g of dry sediment was weighed and quantitatively transferred into a 1000-mL round-bottom flask with 250 mL of organic-free water. Approximately 10 mL of water was added into the condenser followed by 10 mL of *n*-hexane. One gram of Tenax was placed into a Pasteur pipet secured by glass wool which was then joined to the flask on the top of the condenser as shown in Figure 1. An asbestos jacket connected to a Variac transformer was placed around the flask and the water was boiled for 3 h. The condenser was cooled by water at 1 L/min to condense the steam containing the volatile organics. After 3 h, the hexane was drained out from the withdrawal tube by opening the stopcock. The *n*-hexane was dried through sodium sulfate. The Tenax column was washed with 10 mL of *n*-hexane and was combined with the dried *n*-hexane from the condenser. This volume was made up to 10 mL with isooctane. No cleanup or Florisil was required, but if sulfur contamination was evident, mercury was added to the extract.

**Gas Chromatographic Analyses.** All GC/ECD analyses were performed with a Varian Vista 6000 gas chromatograph equipped with the splitless injector as described earlier (*12*). We used open

**Table II. Retention Times, Relative Retention Times, and Response Factors for Chlorinated Benzenes on Carbowax 20M WCOT Column**[a]

| chlorobenzene isomer | retention time, min | rel retention time | concn, pg/μL | response factor, counts/pg |
|---|---|---|---|---|
| 1,3-di- | 5.90 | 0.227 | 25 | 280 |
| hexachloroethane | 6.21 | 0.239 | 1 | 690 |
| 1,4-di- | 6.52 | 0.251 | 25 | 155 |
| 1,2-di- | 7.42 | 0.286 | 25 | 135 |
| hexachloro-butadiene | 7.82 | 0.301 | 5 | 355 |
| 1,3,5-tri- | 8.06 | 0.310 | 5 | 1010 |
| 1,2,4-tri- | 11.17 | 0.430 | 5 | 1070 |
| 1,2,3-tri- | 13.29 | 0.512 | 5 | 1205 |
| 1,2,3,5-tetra- | 14.72 | 0.567 | 5 | 1690 |
| 1,2,4,5-tetra- | 15.02 | 0.578 | 5 | 1440 |
| 1,2,3,4-tetra- | 18.28 | 0.704 | 5 | 1650 |
| pentachlorobenzene | 20.82 | 0.802 | 5 | 1965 |
| hexaachlorobenzene | 25.97 | 1.000 | 10 | 1900 |

[a] Column and conditions described in the text earlier using Hewlett-Packard instrument.

**Table III. Replicate Analyses of Chlorinated Benzenes in EC-2 Sediment, Sample Extracts and Their Minimum Detection Limits**[a]

| chlorobenzene | amt found, pg/μL | MDL, μg/kg |
|---|---|---|
| 1,3-di- | 4.7 ± 0.1 | 1.5 |
| hexachlorobutadiene | 20.6 ± 0.3 | 0.7 |
| 1,3,5-tri- | 7.1 ± 0.1 | 1.0 |
| 1,2,4-tri- | 12.3 ± 0.1 | 0.8 |
| 1,2,3-tri- | 0.9 ± 0.1 | 0.8 |
| 1,2,3,5-tetra- | 1.7 ± 0.1 | 0.5 |
| 1,2,4,5-tetra- | 23.8 ± 0.2 | 0.5 |
| 1,2,3,4-tetra- | 13.7 ± 0.2 | 0.5 |
| penta- | 20.9 ± 0.2 | 0.4 |
| hexa- | 93.8 ± 0.3 | 0.4 |
| total | 199.5 ± 1.7 | |

[a] Data were calculated from four replicate samples using cool on-column injection.

tubular column chromatography and 50 m × 0.25 mm i.d. Carbowax 20M coated on fused silica capillary ($d_f$ = 0.2 μm) having 207 000 effective plates for hexachlorobenzene as $k'$ = 21.7. Hydrogen was used as a carrier gas with a linear velocity of 65 cm/s. An initial temperature of 75 °C was held for 2 min followed by temperature programming to 180 °C at 4 °C/min. The final temperature was held for 5 min. The injector temperature was 200 °C, the detector temperature was 350 °C, and the flow rate of 3.2 mL/min was employed to sweep the septum. The detector makeup gas was nitrogen at 30 mL/min. Splitless time was 35 s.

**Quantitation and Data Collection.** Data were reported on a Spectra Physics reporting integrator, Model SP-4100. The WCOT column chromatographic peaks were identified by using a method of relative retention time matching (RRT). This also allowed summing selected peak areas assignable to the homologues of chlorinated benzenes similar to the method reported for the quantitation of PCBs (*13*).

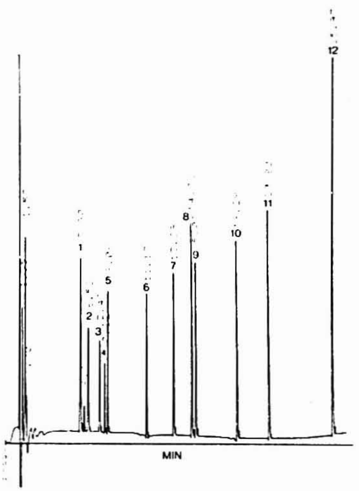

**Figure 2.** Separation of chlorinated benzenes on the Carbowax 20M WCOT column (50 m × 0.25 mm i.d.): column at 75 °C for 2 min programmed at 4 °C/min to 180 °C and held at final temperature for 5 min; attenuator at 64×.

## RESULTS AND DISCUSSION

A gas chromatogram of the chlorinated benzene standards is shown in Figure 2. All isomers are separated on the Carbowax 20M WCOT column. The retention times, the relative retention times and an appropriate response factor for the particular isomers are given in Table II.

The response factors were not found to vary widely when hydrogen was used as a carrier gas in contrast to data reported by Oliver et al. (2). Detector response is linear over 3 orders of magnitude. A chromatogram showing an EC-2 sample extract is given in Figure 3 and quantitative results are provided in Table III.

The minimum detection limit (MDL) for chlorinated benzenes at 3:1 $S/N$ and attenuation of 32× corresponds to approximately 15 pg for dichlorobenzenes and approximately between 0.4 and 1.0 pg for the remaining chlorinated benzenes. Calculated minimum detection values (MDL) are given in Table III.

**Table IV. Recoveries of Chlorinated Benzenes from Lake Superior Sediment Using Soxhlet Extraction**

| chlorinated benzene isomers | spiked concn, μg/g | recovery, % | RSD, % | spiked concn, μg/g | recovery, % | RSD, % | spiked concn, μg/g | recovery, % | RSD, % |
|---|---|---|---|---|---|---|---|---|---|
| 1,3-dichlorobenzene | 1000 | 55.4 | 0.3 | 100 | 48.1 | 1.2 | 10 | 34.5 | 4.3 |
| 1,4-dichlorobenzene | 1000 | 53.9 | 0.7 | 100 | 50.2 | 1.2 | 10 | 37.3 | 1.5 |
| 1,2-dichlorobenzene | 1000 | 54.1 | 0.6 | 100 | 54.0 | 0.7 | 10 | 49.8 | 1.6 |
| 1,3,5-trichlorobenzene | 100 | 67.9 | 15.8 | 10 | 68.0 | 10.8 | 1 | 54.0 | 9.3 |
| 1,2,4-trichlorobenzene | 100 | 69.7 | 13.6 | 10 | 67.0 | 5.3 | 1 | 66.0 | 12.9 |
| 1,2,3-trichlorobenzene | 100 | 72.0 | 14.2 | 10 | 73.0 | 6.9 | 1 | 43.0 | 15.6 |
| 1,2,3,5-tetrachlorobenzene | 100 | 69.9 | 9.8 | 10 | 73.0 | 11.5 | 1 | 48.0 | 11.0 |
| 1,2,4,5-tetrachlorobenzene | 100 | 69.4 | 12.2 | 10 | 71.0 | 12.2 | 1 | 47.0 | 12.3 |
| 1,2,3,4-tetrachlorobenzene | 100 | 71.7 | 10.1 | 10 | 77.0 | 6.0 | 1 | 46.0 | 8.7 |
| pentachlorobenzene | 100 | 73.3 | 9.0 | 10 | 79.0 | 3.4 | 1 | 46.0 | 7.8 |
| hexachlorobenzene | 100 | 78.2 | 8.9 | 10 | 81.0 | 2.9 | 1 | 58.0 | 1.7 |

**Table V. Recoveries of Chlorinated Benzenes from Lake Superior Sediment Using Ultrasonic Extraction Method**

| chlorinated benzene isomers | spiked concn, μg/g | recovery, % | RSD, % | spiked concn, μg/g | recovery, % | RSD, % | spiked concn, μg/g | recovery, % | RSD, % |
|---|---|---|---|---|---|---|---|---|---|
| 1,3-dichlorobenzene | 1000 | 46.6 | 0.1 | 100 | 50.5 | 0.8 | 10 | 18.0 | 3.3 |
| 1,4-dichlorobenzene | 1000 | 44.1 | 0.5 | 100 | 52.9 | 0.2 | 10 | 43.0 | 4.9 |
| 1,2-dichlorobenzene | 1000 | 45.2 | 0.5 | 100 | 52.2 | 0.6 | 10 | 39.2 | 4.0 |
| 1,3,5-trichlorobenzene | 100 | 61.7 | 0.5 | 10 | 71.0 | 9.8 | 1 | 32.0 | 17.5 |
| 1,2,4-trichlorobenzene | 100 | 62.7 | 3.2 | 10 | 75.0 | 6.9 | 1 | 39.0 | 13.6 |
| 1,2,3-trichlorobenzene | 100 | 63.8 | 3.2 | 10 | 72.0 | 8.4 | 1 | 52.0 | 9.2 |
| 1,2,3,5-tetrachlorobenzene | 100 | 70.2 | 0.8 | 10 | 78.0 | 9.1 | 1 | 35.0 | 18.9 |
| 1,2,4,5-tetrachlorobenzene | 100 | 71.3 | 0.1 | 10 | 79.0 | 6.2 | 1 | 37.0 | 13.8 |
| 1,2,3,4-tetrachlorobenzene | 100 | 71.5 | 1.3 | 10 | 79.0 | 6.2 | 1 | 35.0 | 19.1 |
| pentachlorobenzene | 100 | 76.7 | 0.1 | 10 | 80.0 | 5.3 | 1 | 41.0 | 31.7 |
| hexachlorobenzene | 100 | 88.6 | 3.6 | 10 | 82.0 | 3.4 | 1 | 44.0 | 11.6 |

**Table VI. Recoveries of Chlorinated Benzenes from Lake Superior Sediment Using Steam Distillation Method**

| chlorinated benzene isomers | spiked concn, μg/g | recovery, % | RSD, % | spiked concn, μg/g | recovery, % | RSD, % | spiked concn, μg/g | recovery, % | RSD, % |
|---|---|---|---|---|---|---|---|---|---|
| 1,3-dichlorobenzene | 1000 | 75.9 | 0.6 | 100 | 71.3 | 2.1 | 10 | 73.8 | 1.4 |
| 1,4-dichlorobenzene | 1000 | 80.9 | 0.6 | 100 | 73.2 | 2.0 | 10 | 71.8 | 2.3 |
| 1,2-dichlorobenzene | 1000 | 80.6 | 0.5 | 100 | 75.0 | 2.2 | 10 | 76.1 | 3.9 |
| 1,3,5-trichlorobenzene | 100 | 89.3 | 20.8 | 10 | 75.0 | 33.2 | 1 | 66.0 | 17.3 |
| 1,2,4-trichlorobenzene | 100 | 89.6 | 18.8 | 10 | 84.0 | 2.9 | 1 | 82.0 | 7.8 |
| 1,2,3-trichlorobenzene | 100 | 90.5 | 14.6 | 10 | 84.0 | 2.9 | 1 | 79.0 | 5.4 |
| 1,2,3,5-tetrachlorobenzene | 100 | 86.6 | 9.8 | 10 | 82.0 | 2.5 | 1 | 89.0 | 10.2 |
| 1,2,4,5-tetrachlorobenzene | 100 | 93.6 | 11.0 | 10 | 83.0 | 1.4 | 1 | 89.0 | 10.4 |
| 1,2,3,4-tetrachlorobenzene | 100 | 90.8 | 8.9 | 10 | 88.0 | 25.4 | 1 | 84.0 | 5.0 |
| pentachlorobenzene | 100 | 90.5 | 1.0 | 10 | 80.0 | 12.3 | 1 | 84.0 | 9.4 |
| hexachlorobenzene | 100 | 87.5 | 4.2 | 10 | 82.0 | 7.5 | 1 | 80.0 | 16.6 |

**Table VII. Analysis of Chlorinated Benzenes from Hamilton Harbour Sediment Samples by Soxhlet Extraction, Sonification, and Steam Distillation ($n = 3$)**

| isomers | concn found by steam distillation, ng/g dry wt | RSD, % | concn found by Soxhlet, ng/g dry wt | RSD, % | concn found by sonification, ng/g dry wt | RSD, % |
|---|---|---|---|---|---|---|
| 1,3-dichlorobenzene | 31.0 | 3.6 | | | | |
| 1,4-dichlorobenzene | 68.6 | 0.5 | 81.4 | 13.0 | 39.4 | 3.6 |
| 1,3,5-trichlorobenzene | 2.9 | 3.4 | 4.5 | 19.2 | 2.8 | 39.4 |
| 1,2,4-trichlorobenzene | 13.0 | 13.9 | 20.2 | 21.4 | 5.8 | 6.2 |
| 1,2,3-trichlorobenzene | | | | | | |
| 1,2,3,5-tetrachlorobenzene | 3.0 | 21.9 | 4.4 | 37.1 | 3.4 | 3.7 |
| 1,2,4,5-tetrachlorobenzene | | | | | | |
| 1,2,3,4-tetrachlorobenzene | | | | | | |
| pentachlorobenzene | 3.8 | 15.2 | 3.6 | 44.9 | | |
| hexachlorobenzene | 6.0 | 11.7 | 7.0 | 18.0 | 5.2 | 9.5 |

**Table VIII. Comparison of Spiked Hamilton Harbour Sediment Analysis Using Three Different Techniques**[a]

| | steam distillation | | | Soxhlet extraction | | | sonification | | |
|---|---|---|---|---|---|---|---|---|---|
| chlorinated benzene isomers | 1 | 2 | % | 1 | 2 | % | 1 | 2 | % |
| 1,3-dichlorobenzene | 131.0 | 127.0 | 97 | 100.0 | 72.7 | 73 | 100.1 | 42.9 | 43 |
| 1,4-dichlorobenzene | 168.6 | 149.5 | 89 | 181.4 | 112.0 | 62 | 139.4 | 60.1 | 43 |
| 1,2-dichlorobenzene | 100.0 | 88.9 | 89 | 100.0 | 66.4 | 66 | 100.0 | 45.8 | 46 |
| 1,3,5-trichlorobenzene | 12.9 | 10.6 | 82 | 14.5 | 10.5 | 72 | 12.8 | 6.3 | 49 |
| 1,2,4-trichlorobenzene | 23.0 | 19.1 | 83 | 30.2 | 23.0 | 76 | 15.8 | 7.3 | 46 |
| 1,2,3-trichlorobenzene | 10.0 | 8.9 | 89 | 10.0 | 8.0 | 80 | 10.0 | 6.3 | 63 |
| 1,2,3,5-tetrachlorobenzene | 13.0 | 11.2 | 86 | 14.4 | 10.7 | 74 | 13.4 | 7.5 | 56 |
| 1,2,4,5-tetrachlorobenzene | 10.0 | 8.8 | 88 | 10.0 | 7.6 | 76 | 10.0 | 6.1 | 61 |
| 1,2,3,4-tetrachlorobenzene | 10.0 | 8.3 | 83 | 10.0 | 8.8 | 88 | 10.0 | 6.8 | 68 |
| pentachlorobenzene | 13.8 | 11.6 | 34 | 13.6 | 12.5 | 92 | 10.0 | 7.4 | 74 |
| hexachlorobenzene | 16.0 | 14.4 | 90 | 17.0 | 14.0 | 82 | 15.2 | 9.1 | 60 |

[a] 1, spike + amount found in the sample (ng/g); 2, recovered amount (ng/g); %, percentage of the recovered amount. All samples were spiked with mixture no. 1 (see Table I).

When environmental sediment samples are analyzed for chlorinated benzenes, drying and grinding should be eliminated. A wet sediment sample (15 g) should be weighed for each analysis. Moisture content can be determined on a separate portion of the sample and incorporated into the calculation for reporting data on a dry weight basis.

Data to define recoveries and accuracy for the Soxhlet extraction, the sonification, and the steam distillation are shown in Tables IV–VI. Three replicate samples and a blank of the prepared dry sediment (10 g each, dry weight) were

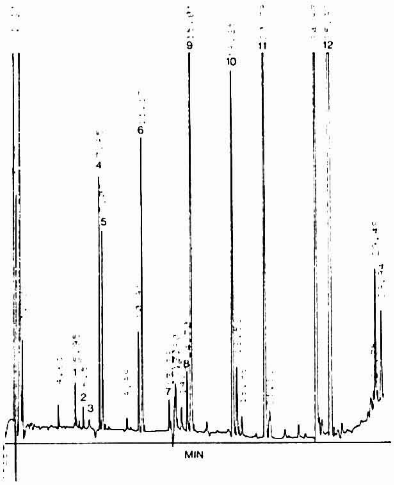

**Figure 3.** Hamilton Harbour sample (EC-2) chromatographed under the identical conditions as Figure 2: (1) 1,3-dichlorobenzene; (2) 1,4-dichlorobenzene; (3) 1,2-dichlorobenzene; (4) hexachlorobutadiene; (5) 1,3,5-trichlorobenzene; (6) 1,2,4-trichlorobenzene; (7) 1,2,3-trichlorobenzene; (8) 1,2,3,5-tetrachlorobenzene; (9) 1,2,4,5-tetrachlorobenzene; (10) 1,2,3,4-tetrachlorobenzene; (11) pentachlorobenzene; (12) hexachlorobenzene.

extracted, concentrated, and analyzed according to the previously described procedures. Recoveries of chlorobenzenes from spiked sediment samples averaged 55 ± 11% for the Soxhlet extraction, 48 ± 12% for the sonification–centrifugation, and 81 ± 12% for the steam distillation method.

To demonstrate the effectiveness of discussed preconcentration methods and the gas chromatography with open tubular column separation, we determined the concentrations of chlorinated benzenes in Hamilton Harbour bottom sediment samples and the same sample spiked with 10 μg/g of chlorinated benzenes. Results are given in Tables VII and VIII.

In addition, a study of the recovery of the Hamilton Harbour sediment spiked with 10 μg/g of chlorinated benzenes was carried out by using three methods: Soxhlet extraction, sonification, and steam distillation. Results of these tests show the superiority of the steam distillation procedure over the other extraction procedures as far as bottom sediments are concerned (Table VIII). Steam distillation produced good recoveries after just 3 h of extraction time. The results of this study show this technique to be the most efficient method for recovery of chlorinated benzenes from bottom sediment samples of different matrices and is the method of choice due to its simplicity and time efficiency. Even at low concentrations, recoveries of chlorinated benzenes were over 82%. In general, the recoveries obtained are significantly greater than any of the other procedures tested.

The Soxhlet extraction procedure provided consistent recoveries at medium and higher concentrations with recovered amounts in range of 66–92%. The lower efficiency is probably due to the matrix variability. As was observed, the many evaporation and preconcentration steps and solvent changes could also be responsible for lower recoveries.

The sonification procedure did not provide quantitative results. The volatile dichloro- and trichlorobenzene isomer quantitation was not reproducible.

In conclusion, the steam distillation procedure appears satisfactory for extracting chlorinated benzenes from bottom sediment samples. Extracts can be directly used for determination of chlorinated benzenes by means of WCOT column gas chromatography using an electron capture detector.

## LITERATURE CITED

(1) Langhorst, M. L.; Nestrick, T. J. *Anal. Chem.* **1979**, *51*, 2018–2025.
(2) Oliver, B. G.; Bothen, K. D. *Anal. Chem.* **1980**, *52*, 2066–2069.
(3) Onuska, F. I.; Thomson, R.; Terry, K. CCIW-Internal Report, 13-AMD-3-81, Burlington, Ontario, 1981.
(4) Rofman, K.; Mueller, W. F.; Coulston, F.; Korte, F. *Chemosphere* **1978**, *7*, 177–184.
(5) Kohli, J.; Jones, D.; Safe, S. *Can. J. Biochem.* **1976**, *54*, 203–208.
(6) Morita, M.; Oishi, S. *Bull. Environ. Contam. Toxicol.* **1975**, *14*, 313–318.
(7) Chau, A. S. Y.; Babjak, L. J. *J. Assoc. Off. Anal. Chem.* **1979**, *62*, 107–113.
(8) Oliver, B. G.; Bothen, K. D. *Int. J. Environ. Anal. Chem.* **1982**, *12*, 131–139.
(9) Veith, G. D.; Kiwus, L. M. *Bull. Environ. Contam. Toxicol.* **1977**, *14*, 631–636.
(10) Bellar, T. A.; Lichtenberg, J. J. *ASTM Spec. Tech. Publ.* **1975**, *No. 573*, 206–219.
(11) Goerlitz, D. F.; Law, L. M. *Bull. Environ. Contam. Toxicol.* **1971**, *6*, 9–10.
(12) Onuska, F. I.; Kominar, R. J.; Terry, K. *J. Chromatogr. Sci.* **1983**, *21*, 512–518.
(13) Onuska, F. I.; Kominar, R. J.; Terry, K. *J. Chromatogr.* **1983**, *279*, 111–118.

RECEIVED for review October 10, 1984. Accepted December 26, 1984.

# Industrial Wastewater Analysis by Liquid Chromatography with Precolumn Technology and Diode-Array Detection

**M. W. F. Nielen, U. A. Th. Brinkman, and R. W. Frei***

*Department of Analytical Chemistry, Free University, De Boelelaan 1083, 1081 HV Amsterdam, The Netherlands*

**Small precolumns packed with C18, PRP$_1$, and cation-exchange materials have been used for the on-line group separation and trace enrichment of industrial wastewater samples. The sample is divided into three main groups: a fraction containing nonpolar compounds, a second fraction containing medium polarity compounds and certain polar substituted aromatics, and a third fraction containing polar anilines and other polar bases. Each precolumn fraction is subsequently chromatographed on a C18 analytical column with a methanol gradient and detected by a diode-array UV-Vis detector. Multisignal plots and three-dimensional spectrochromatograms are used to get information about the identity of the pollutants present. The completely automated system is optimized for 29 selected chemicals of particular interest. Some of these compounds were found in the wastewater samples tested and were quantitated.**

Industrial wastewater represents a very complex matrix, containing organic pollutants over a wide range of polarity. There are several considerations for analyzing such samples: to check efficiency of production processes, to control the functioning of a wastewater treatment plant via fingerprinting techniques, and to maintain the stringent governmental rules for the discharge of industrial effluents into surface water and the environmental contamination with hazardous materials.

The complexity of the sample demands high resolution of the chromatographic system including the necessary sample pretreatment. Sample handling of wastewater was frequently done by liquid–liquid extraction (*1*, *2*) but such procedures made automation of the analysis more difficult. Recently, an on-line extraction and evaporation procedure was described for liquid chromatography (*3*), but this system seems to be rather complex. Nowadays, cleanup and trace enrichment via precolumn techniques is widely used in water (*4*) and biological (*5–7*) analysis. Although many sample pretreatments are still done with off-line disposable columns, the on-line techniques will be favored because of the automation aspect.

We analyzed industrial effluents by liquid chromatography with an on-line precolumn for trace enrichment (*8*) but the system described could only deal with (a small group of) specific compounds. By combining different types of precolumns, one should be able to handle wastewater samples containing pollutants of very different polarities. Little et al. (*9*) described a microprocessor controlled valve-switching unit for automated sample cleanup and trace enrichment in HPLC. Such equipment is very suitable for automated group separation and on-line trace enrichment on different types of precolumns.

In wastewater analysis, more sophisticated detection principles such as diode-array UV-Vis detectors may be helpful to search for particular pollutants in the samples and give a first indication about the identity of the substances present. If necessary, such detection techniques can be optimized to yield high signal-to-noise ratios for some compounds of special interest and/or can give information about peak inhomogeneity (*10*, *11*).

In the present paper both principles, precolumn technology for on-line group separation and trace enrichment and diode-array detection for peak and pattern recognition have been combined in an automated LC system for the analysis of 29 selected compounds in industrial wastewater.

## EXPERIMENTAL SECTION

**Apparatus.** A Kontron (Zürich, Switzerland) LC system consisting of two Model 410 pumps, equipped with a high-pressure dynamic mixer and a pulse dampener, a MCS 670 Tracer valve switching unit, and a Model 200 programmer was used (this setup is shown in Figure 1). A HP 1040A (Hewlett-Packard, Palo Alto, CA) diode-array UV-Vis detector was used with a HP 85 microcomputer, a HP 9121 dual disk drive, and a HP 7225 B plotter. Chromatograms were also analog recorded on a W + W 900 (Kontron) recorder.

**Reagents.** HPLC-grade methanol, perchloric acid, potassium acetate, acetic acid, and sodium oxalate were obtained from J. T. Baker (Deventer, The Netherlands). EDTA was obtained from Sigma Chemicals (St. Louis, MO). All reagents but methanol were of analytical grade. Demineralized water was purified in a Milli-Q (Millipore, Bedford, MA) filtration system to obtain LC-grade water for use in mobile phases and standard solutions. Eluents were degassed in an ultrasonic bath under vacuum.

Twenty-nine pollutants were selected to be analyzed in the wastewater samples (Table I). These solutes were of more than 90% purity and supplied by Fluka, Merck, and Aldrich.

**Stationary Phases and Columns.** Wastewater samples were preconcentrated on homemade 2 × 4.6 and 4 × 4.6 mm i.d. stainless steel precolumns (*12*), which are also commercially available from Chrompack (Middelburg, The Netherlands). The precolumns were hand-packed with a microspatula, with 10 $\mu$m silica-based RP18 (Merck, Darmstadt, G.F.R.), with the spherical 10 $\mu$m styrene–divinylbenzene copolymer PRP$_1$ (Hamilton, Reno, NV), or with the 13 $\mu$m resin-based Aminex A5 (Bio-Rad, Richmond, CA) sulfonic acid cation exchanger. The analytical column was a 25 cm × 4.6 mm i.d. stainless steel column prepacked with 8 $\mu$m CP-Spher C 18 (Chrompack).

**Procedures.** Stock solutions of the selected pollutants were prepared by weighing and dissolving them in methanol. These solutions were diluted with LC-grade water adjusted to pH 3.0 to obtain standard solutions at the parts-per-billion level. The wastewater samples were pretreated as follows: to 50 mL of (acidic) wastewater were added 5 mL of a saturated sodium oxalate solution, 0.75 mL of an EDTA solution (18 g/L), and 45 mL of a $10^{-3}$ M perchloric acid solution (see also Table II). The final solution was filtered over a 0.8-$\mu$m membrane filter to remove calcium oxalate (cf. ref 13) and adjusted to pH 3.0 with perchloric acid, if necessary.

Breakthrough curves of the selected pollutants from the precolumns were recorded according to the procedure as outlined in ref 14 with 250 ppb standard solutions (pH 3) at a flow rate of 5 mL min$^{-1}$.

The automated precolumn group separation and trace enrichment and the subsequent on-line gradient elution of the precolumns were performed by use of the experimental setup given in Figure 1. Five milliliters of sample was introduced via pump C to the three precolumns in series. The first, C18 precolumn trapped the nonpolar dye stuffs and other nonpolar solutes; the second, PRP$_1$ precolumn trapped the more polar aromatics like *p*-chloro- and *p*-nitrophenol and *p*-chloroaniline; the third, cation-exchange precolumn trapped the polar phenylenediamines and other anilines. After this sample introduction the precolumns were flushed in series with 10 mL of $10^{-3}$ M perchloric acid to

0003-2700/85/0357-0806$01.50/0 © 1985 American Chemical Society

**Table I. Breakthrough Volumes of 29 Selected Pollutants on Short Precolumns Packed with Various Sorbents**[a]

| no. | compound | breakthrough volume (mL) on RP 18, 10 μm 2 × 4.6 mm i.d. | PRP$_1$, 10 μm 4 × 4.6 mm i.d. | Aminex A5, 13 μm[b] 4 × 4.6 mm i.d. |
|---|---|---|---|---|
| 1 | *p*-aminophenol | 0 | 0 | > 100 |
| 2 | *p*-phenylenediamine | 0 | 0 | > 100 |
| 3 | *m*-phenylenediamine | 0 | 1 | > 100 |
| 4 | 4-methyl-*m*-phenylenediamine | 0 | 1 | > 100 |
| 5 | *o*-phenylenediamine | 0 | 1 | > 100 |
| 6 | aniline | 0 | 2 | > 100 |
| 7 | *p*-anisidine | 0 | 1 | > 100 |
| 8 | *p*-nitroaniline | 1 | 10 | > 100 |
| 9 | 3-amino-4-ethoxyacetanilide | 1 | 7 | > 100 |
| 10 | *o*-anisidine | 1 | 6 | > 100 |
| 11 | *o*-toluidine | 1 | 3 | > 100 |
| 12 | picramic acid | 2 | > 100 | –[c] |
| 13 | *p*-chloroaniline | 2 | 30 | – |
| 14 | *p*-nitrophenol | 1 | 25 | – |
| 15 | 3,5-dinitro-*o*-cresol | 10 | > 100 | – |
| 16 | *m*-cresol | 1 | 37 | – |
| 17 | nitrobenzene | 2 | > 100 | – |
| 18 | *p*-chlorophenol | 2 | 72 | – |
| 19 | *p*-chloronitrobenzene | 3 | > 100 | – |
| 20 | pentachlorophenol | > 100 | – | – |
| 21 | *o*-dianisidine | 10 | 78 | – |
| 22 | 2-aminoanthraquinone | >100 | – | – |
| 23 | 3,3′-dichlorobenzidine | 72 | – | – |
| 24 | 3-amino-9-ethylcarbazole | 50 | – | – |
| 25 | *p*-aminoazobenzene | >100 | – | – |
| 26 | 1-aminoanthraquinone | >100 | – | – |
| 27 | *p*-dichlorobenzene | 17 | – | – |
| 28 | 2-phenylaminonaphthalene | >100 | – | – |
| 29 | 1,2,5-trichlorobenzene | >100 | – | – |

[a] LC-water samples containing 250 ppb of test solute; pH adjusted to 3.0 with perchloric acid; sampling rate 5 mL min$^{-1}$. [b] Maximum values (cf. ref 13). [c] –, not determined.

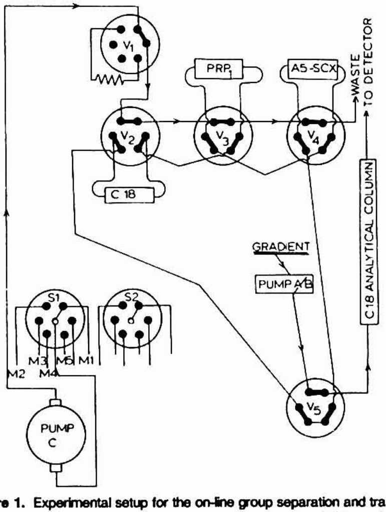

**Figure 1.** Experimental setup for the on-line group separation and trace enrichment of wastewater samples: V, high pressure switching valve; S, low pressure selector valve; M1, sample; M2, $10^{-3}$ M $HClO_4$; M3, 50% methanol; M4, 0.02 M $HClO_4$; M5, $10^{-3}$ M $HClO_4$. Precolumns: 2 × 4.6 mm i.d. (RP18), 4 × 4.6 mm i.d. (PRP$_1$), and 4 × 4.6 mm i.d. (Aminex A5). Analytical column: 25 cm × 4.6 mm i.d. CP-Spher C18.

complete the desired group separation. Only the cation-exchange precolumn could be flushed with 3 mL of 50% methanol as an extra clean-up step.

**Table II. General Procedure Using the Setup of Figure 1**[a]

1 precipitation and complexation of interferences by oxalate and EDTA, respectively
2 filtration and adjustment to pH 3.0 (if necessary)
3 group separation and trace enrichment on C18, PRP$_1$, and Aminex A5 precolumns (in series)
4 flushing the C18, PRP$_1$, and Aminex A5 precolumns (in series) with $10^{-3}$ M perchloric acid
5 further cleanup of the cation exchanger by flushing with 50% methanol
6 backflush desorption from cation exchange fraction to C18 analytical column
7 backflush desorption from PRP$_1$ fraction to C18 analytical column
8 desorption from C18 precolumn to C18 analytical column
9 regeneration of the precolumns in series with $10^{-3}$ M perchloric acid

[a] Steps 3–9 are fully automated. The time-based column switching program is given in Table III.

Next the ion-exchange precolumn was eluted on-line with the methanol–potassium acetate (pH 6) gradient to the C18 separation column. After the separation of this ion-exchange fraction, the PRP$_1$ and, finally, the C18 precolumn were eluted. The precolumns were regenerated on-line with dilute perchloric acid while analytical separations took place simultaneously. The entire procedure has been summarized in Table II.

Sample introduction, column switching, solvent selection, gradient elution, and start of detector and recorder were all controlled by the Model 200 Programmer. The diode-array detector was programmed to store four chromatograms (at 222, 390, 244, and 295 nm, respectively) and spectra (from 200 to 500 nm; at the peak apex and the base line after each peak) on flexible disk.

## RESULTS AND DISCUSSION

**Breakthrough Volumes.** Table I shows the retention behavior of the 29 selected pollutants on the various preco-

**Table III. Automated Procedure Using a Kontron Model 200 Programmer and a Kontron MCS 670 Tracer Switching Unit**[a]

| time, min | call file no. | event | time, min | call file no. | event |
|---|---|---|---|---|---|
| 0.00 | 88 | reset | 18.5 | 84 | regenerate A5 (30 ml) |
| 0.09 | flow 1.5 % B 10 | start pump A/B | 28.5 | 86 | switch to $10^{-3}$ M $HCLO_4$ |
| 0.1 | 81 | start pump C | 33.5 | 91 | stop pump C |
| 2.1 | 82 | sample through C18 | 40.0 | 82 | |
| 2.2 | 83 | sample C18 + $PRP_1$ | 40.1 | 83 | |
| 2.3 | 84 | sample C18 + $PRP_1$ + A5 | | | |
| 4.0 | 86 | switch to $10^{-3}$ M $HClO_4$ | 40.3 | 85 | |
| 9.6 | 92 | C18 bypass | 40.7 | 93 | desorption $PRP_1$ |
| 9.7 | 93 | C18 + $PRP_1$ bypass | 40.8 | % B 50 dur 6 | gradient |
| 10.5 | 86 | switch to 50% MeOH | 45.8 | 95 | precolumns bypass |
| 12.5 | 91 | stop pump C | 45.9 | 83 | |
| 12.6 | 82 | | 70.0 | 85 | |
| 12.7 | 83 | | 71.0 | 92 | desorption RP 18 |
| 12.8 | 85 | | 71.1 | % B 80 dur 10 | gradient |
| 13.1 | aux 8 dur 0.01 | start detector | 76.0 | 95 | precolumns bypass |
| 13.2 | 94 | desorption A5 | 76.1 | 82 | |
| 13.3 | chart 2 | start recorder | 76.2 | 81 | start pump C } regenerate |
| 13.4 | % B 30 | step gradient | 91.2 | 91 | stop pump C } precolumns |
| 16.2 | 95 | precolumns bypass | 105 | % B 10 dur 10 | reset gradient |
| 16.3 | 93 | | 149 | flow 0.0 chart 0.0 | stop pump A/B and recorder |
| 16.4 | 92 | | 150 | end | |
| 16.5 | 86 | switch to 0.02 M $HClO_4$ | | | |
| 16.6 | 81 | start pump C | | | |

[a] Precolumns: 2 × 4.6 mm i.d. (RP 18), 4 × 4.6 mm i.d. ($PRP_1$) and 4 × 4.6 mm i.d. (Aminex A5). Analytical column: 25 cm × 4.6 mm i.d. CP-Spher C18; eluent, 0.1 M potassium acetate (pH 6.0) + methanol gradient (10–80%). Flow rates: pump A/B (gradient) 1.5 mL $min^{-1}$; pump C, 2.0 mL $min^{-1}$.

lumns connected in series (see also Figure 1) at pH 3. The samples are introduced through the precolumns in the order C18–$PRP_1$–Aminex A5. The nonpolar compounds (no. 20–29) are trapped on the C18 precolumn but the retention for *p*-dichlorobenzene and *o*-dianisidine is rather low. The *o*-dianisidine plus the chloro- and nitro-substituted aromatic compounds (no. 12–19) are, on the other hand, well retained on the $PRP_1$ material and can be preconcentrated on the $PRP_1$ precolumn. Of these, only 3,5-dinitro-*o*-cresol will also be partly retained on the C18 precolumn and hence be present in the C18 fraction. The remaining 11 compounds (1–11) which are polar anilines, can be successfully preconcentrated at pH 3 on the cation-exchange precolumn from relatively large sample volumes (cf. ref 13). Of these, only nitroaniline will have been partly absorbed on the $PRP_1$ precolumn.

To summarize, when the sample is pumped through the series of precolumns in the order C18–$PRP_1$–Aminex A5, a certain percentage of the compounds from the $PRP_1$ and Aminex A5 fraction will remain on the previous precolumns (C18 and $PRP_1$, respectively). When the precolumns are flushed in series with 10 mL of $10^{-3}$ M perchloric acid after the sample introduction, the desired group separation can be achieved. After this step, only *p*-nitroaniline and 3,5-dinitro-*o*-cresol appeared in more than one precolumn fraction.

**Diode-Array Detection.** Figure 2 shows a multisignal chromatogram obtained with 5 mL of standard solution (pH 3.0) containing 200 ppb of each of the 29 pollutants of interest. With the gradient profile, as included in this figure, acceptable resolution was obtained. The first 28 min of the chromatograms correspond to the ion-exchange precolumn (the polar aniline fraction). The period between 28 and 58 min corresponds to the $PRP_1$ precolumn (other medium polar aromatics) and the final period, from 58 to 90 min, to the C18 precolumn (nonpolar compounds). Trace B, the chromatogram recorded at 222 nm, shows all peaks of interest and can be regarded as a nonselective "total-peak chromatogram". It is clearly shown here that only *p*-nitroaniline (no. 8) and 3,5-dinitro-*o*-cresol (no. 15) appear in more than one fraction. Trace C at 390 nm gives a very selective chromatogram, only nitro aromatics and *p*-aminoazobenzene will appear. Traces D and E (at 244 and 295 nm) give additional information. The polar anilines (no. 1–11) for instance will appear at these wavelengths; their secondary maximum around 290 nm may be an aid for group identification. At 244 nm, *p*-chloroaniline (no. 13) will be relatively intense as compared to 222 nm which is verified by trace D. The dichloro- and trichlorobenzene (no. 27 and 29) show only a reasonable absorbance at low wavelengths; they appear only at 222 nm and not at one of the other wavelengths investigated.

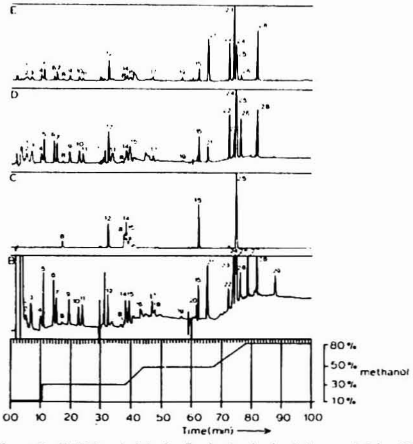

**Figure 2.** Multisignal plot of a 5-mL standard solution containing 200 ppb of the selected pollutants from Table I. Gradient elution with 0.1 M potassium acetate (pH 6.0) and methanol (10–80%) as indicated. Detection at 222 (B), 390 (C), 244 (D), and 295 nm (E). Attenuation was 0.2 aufs. Peak numbers correspond to the compounds listed in Table I.

These examples show that multisignal plots obtained with diode-array detectors can be used to give preliminary information about the identity of the compounds present and such

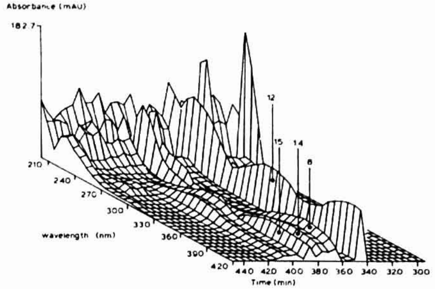

**Figure 3.** Spectrochromatogram of a part of the $PRP_1$ fraction from the analysis of Figure 2. Spectra were memorized automatically at the peak apex and at the base line after the peak. Conditions are given in Figure 2.

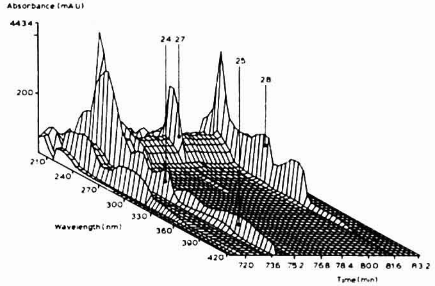

**Figure 4.** Spectrochromatogram of a part of the C18 fraction from the analysis of Figure 2. Conditions are given in Figure 3.

profiles may be helpful for peak recognition in unknown samples. Figures 3 and 4 represent spectrochromatograms of some parts of the same run. In the $PRP_1$ fraction (Figure 3) the nitro compounds (no. 8, 14, and 15) are recognized by their maxima at 400 nm. The picramic acid (no. 12) spectrum is clearly shown and a good example for the validity and usefulness of such plots for compounds with well-defined UV spectra. As a further example, compounds no. 24, 25, 27, and 28 can be identified with the aid of the 3D plot of Figure 4.

**Application to Real Samples.** Figure 5 is a multisignal plot obtained with a 5-mL industrial wastewater sample, collected after a biological step in the water treatment plant. The first part (the ion-exchange fraction) shows peaks at 222, 244, and 295 nm but not at 390 nm, indicating that there are no nitroanilines present but many other polar anilines. The spectrochromatogram of this region (Figure 6) shows the similarity in the UV spectra of these compounds, hence identification of these compounds is not possible via these spectra. On the other hand, comparison of retention times of polar anilines with the data obtained with well-defined standard samples will give more information. *m*-Phenylenediamine, aniline, and *o*-anisidine could be identified in this way. The second and third part of the chromatogram ($PRP_1$ and C18 fraction) contained only two peaks of the pollutants of interest. *p*-Nitrophenol and 3-amino-9-ethylcarbazole were identified through their UV spectra. Spectra of the other peaks did not resemble the 29 reference spectra of the standard mixture, nor did their retention times.

Figure 7 was obtained by analyzing industrial wastewater before the treatment. It should be noticed that the chromatograms in Figure 7 are plotted at a two times reduced

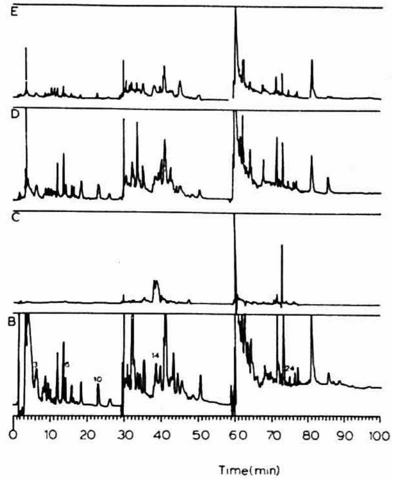

**Figure 5.** Multisignal plot of a 5-mL industrial wastewater sample, taken after a biological treatment plant. Conditions are given in Figure 2.

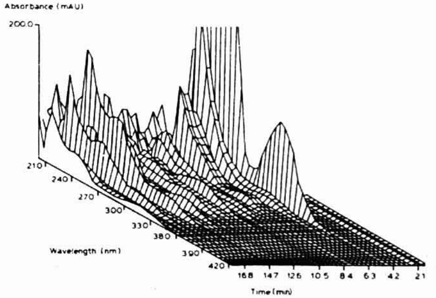

**Figure 6.** Spectrochromatogram of a part of the Aminex A5 fraction from the analysis of Figure 5. Spectra were memorized automatically at the peak apex and at the base line after the peak. Conditions are given in Figure 2.

sensitivity of the detector, indicating that the UV absorbance of the pollutants is much higher before than after the biological treatment step, as was to be expected. Again, the aniline fraction was identified based on retention times and general spectral information. No *p*-nitroaniline was present but *m*-phenylenediamine, *o*-phenylenediamine, *o*-anisidine, and, especially, 4-methyl-*m*-phenylenediamine and aniline were present in relatively high concentrations. Unfortunately, there were no known species in the $PRP_1$ fraction, but in the C18 fraction *o*-dianisidine and *p*-dichlorobenzene could be identified.

The compounds tentatively identified in the wastewater sample which was collected after biological treatment (see Figure 5) were quantitated by standard addition: 100 ppb of the standard mixture was added to the wastewater sample which was reanalyzed. The concentrations were calculated from the relative peak heights with respect to the dilution factor and are given in Table IV. The homogeneity of these spiked peaks was tested in the same experiment by memorizing also spectra on the slopes of the peaks and by plotting

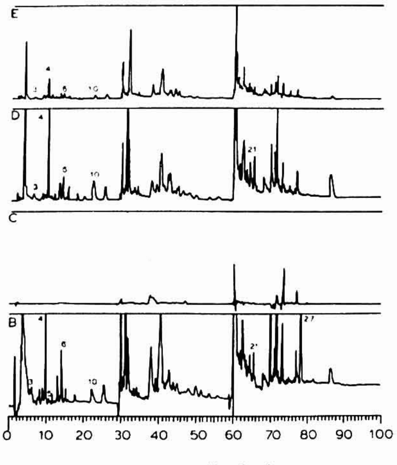

**Figure 7.** Multisignal plot of a 5-mL industrial wastewater sample taken before a biological treatment plant. Attenuation was 0.4 aufs. Other conditions are given in Figure 2.

**Table IV. Concentration of Identified Pollutants in Wastewater after Biological Treatment**

| compound | concn, ppb |
|---|---|
| *m*-phenylenediamine | 262 |
| aniline | 150 |
| *o*-anisidine | 286 |
| *p*-nitrophenol | 260 |
| 3-amino-9-ethylcarbazole | 58 |

these spectra afterward overlapping each other. No peak inhomogeneity was observed in this experiment. Other peak homogeneity tests—such as ratio chromatograms—were obstructed by the background absorption of the mobile phase below 240 nm (caused by the high acetate concentration) which can lead to wrong conclusions about the peak homogeneity.

## CONCLUSIONS

Precolumn technology offers the desired selectivity and sensitivity needed for industrial wastewater analysis with subsequent UV detection. Combination of different types of precolumns, optimized for pollutants of special interest, gives satisfactory group separations prior to the actual analysis. Unattended analysis is possible and easily done by using a time-based valve and solvent switching program.

The applicability of diode-array detectors to such complex matrices has been demonstrated. The choice of selective wavelengths and multisignal plotting may be an aid for a first identification. In addition three-dimensional spectrochromatograms will give UV spectra and the possibility of identification for those compounds having characteristic spectra. Of course systems like this can be made more powerful if more compounds present in wastewater are being considered. Spectra of unknowns can be compared automatically to reference data previously stored and peak inhomogeneity can be checked. Although UV spectra alone can never give absolute certainty about the identity of a compound, combination of selective sample handling with sophisticated detector software will reach the point where there is reasonable certainty about the compounds of interest. Further extension of this technique by including, i.e., functional group specific detectors such as electrochemical (cf. ref 13) and reaction detectors, should provide additional evidence without necessarily having to resort to MS methodology.

## ACKNOWLEDGMENT

The Hewlett-Packard analytical division (Waldbronn, G.F.R) is acknowledged for the loan of the 1040 diode-array detector and peripherals. Kontron is acknowledged for the loan of HPLC equipment and the programmer. Chrompack, Merck, and Hamilton are thanked for the gift of packing materials and columns.

## LITERATURE CITED

(1) Riggin, R. M.; Cole, T. F.; Billets, S. *Anal. Chem.* **1983**, *55*, 1862–1869.
(2) Folke, J. *HRC CC, J. High Resolut. Chromatogr. Chromatogr. Commun.* **1984**, *7*, 25.
(3) Oka, K.; Minagawa, K.; Hara, S. *Anal. Chem.* **1984**, *56*, 24–27.
(4) Fishman, M. J.; Erdmann, D. E.; Garbarino, J. R. *Anal. Chem.* **1983**, *55*, 102R–133R.
(5) Werkhoven-Goewie, C. E.; Brinkman, U. A. Th.; Frei, R. W.; de Ruiter, C.; de Vries, J. *J. Chromatogr. Biomed. Appl.* **1983**, *276*, 349–357.
(6) Bjerg, B.; Olsen, O.; Rasmussen, K. W.; Sorensen, H. *J. Liq. Chromatogr.* **1984**, *7*, 691–707.
(7) Cox, J. W.; Pullen, R. H. *J. Chromatogr. Biomed. Appl.* **1984**, *307*, 155–171.
(8) Zygmunt, B.; Visser, J.; Brinkman, U. A. Th.; Frei, R. W. *Int. J. Environ. Anal. Chem.* **1983**, *15*, 263–280.
(9) Little, C. J.; Tompkins, D. J.; Stahel, O.; Frei, R. W.; Werkhoven-Goewie, C. E. *J. Chromatogr.* **1983**, *264*, 183–196.
(10) Clark, B. J.; Fell, A. F.; Scott, H. P.; Westerlund, D. *J. Chromatogr.* **1984**, *286*, 261–273.
(11) Fell, A. F.; Scott, H. P.; Gill, R.; Moffat, A. C. *J. Chromatogr.* **1983**, *282*, 123–140.
(12) Goewie, C. E.; Nielen, M. W. F.; Frei, R. W.; Brinkman, U. A. Th. *J. Chromatogr.* **1984**, *301*, 325–334.
(13) Nielen, M. W. F.; Frei, R. W.; Brinkman, U. A. Th. *J. Chromatogr.* **1984**, *317*, 551–567.
(14) Werkhoven-Goewie, C. E.; Brinkman, U. A. Th.; Frei, R. W. *Anal. Chem.* **1981**, *53*, 2072.

RECEIVED for review September 10, 1984. Accepted December 21, 1984.

# Computer-Based Numerical Integration for the Calculation of Retention Times in Gradient High-Performance Liquid Chromatography

**Sterling A. Tomellini and Richard A. Hartwick***

*Department of Chemistry, Rutgers University, P.O. Box 939, Piscataway, New Jersey 08854*

**Hugh B. Woodruff**

*Merck Sharp & Dohme Research Laboratories, P.O. Box 2000, Rahway, New Jersey 07065*

**An approach to the calculation of solute retention under gradient elution conditions using numerical approximations on a DEC VAX 11/780 computer is presented. This approach eliminates the need for exact solutions of the inherently complex gradient integrals. The programs developed can be used for any solvent composition vs. solute capacity factor or solvent composition vs. time relationships and are, therefore, universal in nature. Gradient microbore HPLC in the reversed-phase mode was used to demonstrate the accuracy of the approach. The assumption of a quadratic dependency between ln *k′* and solvent composition allowed for the least-squares fitting of solute isocratic retention with a minimal number of experiments. By use of this approach and the corresponding FORTRAN program, prediction of solute retention under complex multiple-linear gradient shapes was achieved with an accuracy of better than 5%.**

The chromatographic experiment is somewhat unique in that more time and effort are normally invested in determining the required experimental conditions than in interpreting the resulting data. Research has thus been directed at finding efficient ways to "optimize" an HPLC separation. Drouen et al. (*1*) have characterized the two major optimization schemes in HPLC as being either of the sequential simplex or of the lattice type design. While automated optimization programs of either design can be useful in finding adequate separation conditions, it must be realized that a separation can be "optimized" according to many different criteria. Thus, an optimization scheme should be flexible to the specific demands of a particular separation problem and not be user independent, contrary to the philosophy being adopted by numerous instrument companies in automated methods development.

An alternative to the completely automated methods development approach is to permit the scientist to use the computer as an interactive tool, without the restriction of a single optimization algorithm. In order to permit this, versatile calculation procedures must be available. Jandera and Churacek (*2–11*), Schoenmakers et al. (*12–14*), Snyder (*15*), and others (*16–18*) have demonstrated that exact mathematical solutions can be derived for certain gradient conditions and that these solutions can predict the retention time of a compound with good accuracy. Such mathematical solutions can then form the basis for subsequent optimization procedures.

The problem with using exact mathematical solutions is that the form of the solution depends upon a number of factors, including the gradient shape and number of components in the mobile phase, the function describing the capacity factor ($k'$) and mobile phase composition for each solute and the instrumental delay volume. As the complexity of these factors increases, exact solutions become progressively more difficult to implement. In addition, programming effort becomes excessive when writing algorithms to handle any of a variety of potential conditions within a single computer program. Due to the inflexibility of the existing solutions and the mathematically intractable nature of other solutions for more complex cases, it was decided to develop an approach and corresponding computer programs which could more easily handle the various conditions often used by the scientist attempting to develop a separation.

The strength of the approach presented arises by the separation of the solute–solvent composition relationship from the mathematics of the gradient integral. Complex equations of this type are often most easily solved by using numerical integration techniques. Such approximate solutions require numerous calculations and therefore must run on relatively fast computers. The reward for using approximate solutions and larger computers is that a single program can handle complex solute–solvent relationships as well as complex isocratic and gradient elution conditions with reasonable calculation time. This paper will report on the results obtained with a program written to determine retention times for binary, ternary, quaternary, etc. gradient elution conditions with single or multiple linear gradient segments based on limited isocratic chromatographic data. Multiple linear gradient segments were chosen since these are widely used on commercial HPLC instruments.

## THEORY

**Isocratic Data.** The first step in deriving solutions for the prediction of retention times for solutes eluted under gradient conditions is to know the capacity factor, $k'$, for each solute as a function of solvent composition. For the reversed-phase mode of HPLC, using a binary solvent, a logarithmic function of the following form can usually be assumed (*18*)

$$\ln k' = AC_1 + BC_1^2 + D \quad (1)$$

where $A$, $B$, and $D$ are constants and $C_1$ is the concentration of organic modifier which is generally given in volume percent. For an aqueous solution containing two organic modifiers, the relationship of solvent composition to $k'$ can be expected to be in the form

$$\ln k' = AC_1 + BC_1^2 + DC_2 + EC_2^2 + FC_1C_2 + G \quad (2)$$

where $A$, $B$, $D$, $E$, $F$, and $G$ are constants. A cross term has been included which varies as a function of both $C_1$ and $C_2$. By use of similar mathematical fitting, any number of organic modifiers can be used. Also, if a different function is followed, as for example a reciprocal function as is often observed in ion exchange, similar equations of the same general type can be derived.

0003-2700/85/0357-0811$01.50/0 © 1985 American Chemical Society

Once the expected relationship between $k'$ and organic modifier is known, the values of the constant coefficients must be determined by using a linear least-squares fit. The minimum number of data points required varies with the number of terms in the equation being fit. A binary mobile phase (single organic modifier) fit to eq 1 requires at least three experimentally determined data points. Likewise, six and ten data points are required for ternary and quaternary mobile phases, respectively.

**Calculation of Retention Times.** Liquid chromatography is often treated as a volume problem but is in fact fundamentally a length problem since the column length, $L_{\mathrm{col}}$, is a limiting parameter. All separations must be completed by the time the compounds have traveled the length of the column. Thus

$$L_{\mathrm{col}} = \text{velocity of solute} \times \text{retention time} \tag{3}$$

In the isocratic case the velocity may be assumed to be constant and eq 3 becomes

$$L_{\mathrm{col}} = U_{\mathrm{band}} t_{\mathrm{R}} \tag{4}$$

where $t_{\mathrm{R}}$ is the retention time for a given solute and $U_{\mathrm{band}}$ is the linear velocity of that solute band. In gradient elution the velocity is not constant, and the integral solution for eq 3 must be used which is given as

$$L_{\mathrm{col}} = \int_0^{t_{\mathrm{R}}} U'_{\mathrm{band}}\,\mathrm{d}t \tag{5}$$

where $U'_{\mathrm{band}}$ is the instantaneous velocity of the solute band and the integration limits are from time = 0 to time = $t_{\mathrm{R}}$.

The velocity of a band can be found for the isocratic case by first rearranging the often used expression for $k'$

$$t_{\mathrm{R}} = t_{\mathrm{M}}(1 + k') \tag{6}$$

where $t_{\mathrm{M}}$ is the elution time of an unretained solute. $U_{\mathrm{band}}$ for elution under isocratic conditions can be calculated by dividing the column length by $t_{\mathrm{R}}$ (as given in eq 6) resulting in

$$U_{\mathrm{band}} = L_{\mathrm{col}}/(t_{\mathrm{M}}(1 + k')) \tag{7}$$

Under gradient conditions where $k'$ is changing throughout, the instantaneous band velocity is of interest. From eq 7, $U'_{\mathrm{band}}$ can be found in terms of the instantaneous $k'$, $k'_{\mathrm{inst}}$, such that

$$U'_{\mathrm{band}} = L_{\mathrm{col}}/(t_{\mathrm{M}}(1 + k'_{\mathrm{inst}})) \tag{8}$$

Thus the fundamental equation for gradient elution becomes

$$L_{\mathrm{col}} = \int_0^{t_{\mathrm{R}}} L_{\mathrm{col}}/((1 + k'_{\mathrm{inst}})t_{\mathrm{M}})\,\mathrm{d}t \tag{9}$$

Equation 9 reduces to eq 4 for isocratic cases where $k'_{\mathrm{inst}}$ is constant with respect to time.

With eq 9, it is in theory possible to solve exactly for the retention time of any band knowing the instantaneous $k'$ of a solute as a function of time. If, however, the instantaneous $k'$ vs. time relationship is mathematically complex or the gradient shape is very complex, then an exact solution for $t_{\mathrm{R}}$ can be difficult if not impossible to derive.

An alternative to using exact mathematical solutions to eq 9 is to use numerical integration. Approximate solutions have two major advantages. First, approximate solutions of eq 9 are always solvable, and second, the flexibility of approximate calculations reduces the amount of programming effort and program size necessary when multiple experimental conditions are to be allowed.

**Corrections for Gradient Delay.** Several corrections are necessary for the solution of eq 9 under actual experimental conditions. First the distance traveled by the solute under the initial isocratic conditions before being overtaken by the gradient front must be calculated. This delay has two sources. First, due to a physical instrumental delay time, $t_{\mathrm{D}}$, the solute band will move down the column at a velocity inversely proportional to $(1 + k')$ (eq 7) while the gradient front travels to the column head. Secondly, the solute band continues to advance at the same rate until overtaken by the gradient traveling at a rate equal to the mobile phase velocity, $u$, i.e., $L_{\mathrm{col}}/t_{\mathrm{m}}$. Knowing the instrumental time delay of the solute band allows for the calculation of a time correction, $t_{\mathrm{corr}}$. Simply stated the distance traveled by the solute band during the instrumental delay plus the time until overtaken by the gradient front in the column must be equal to the distance traveled by the gradient front at the time the two are coincidental, or

$$(L_{\mathrm{col}}/(t_{\mathrm{M}}(1 + k'))t_{\mathrm{corr}}) + ((L_{\mathrm{col}}/t_{\mathrm{M}})t_{\mathrm{D}}) = (L_{\mathrm{col}}/t_{\mathrm{M}})t_{\mathrm{corr}} \tag{10}$$

Solving eq 10 for $t_{\mathrm{corr}}$ gives

$$t_{\mathrm{corr}} = ((1 + k')/k')t_{\mathrm{D}} \tag{11}$$

The distance traveled by the solute band isocratically, $L_{\mathrm{iso}}$, can be found by multiplying $t_{\mathrm{corr}}$ as defined in eq 11 by $U_{\mathrm{band}}$ as given in eq 7, yielding

$$L_{\mathrm{iso}} = (L_{\mathrm{col}}k')/t_{\mathrm{M}} \tag{12}$$

Knowing the time spent by the solute band traveling isocratically and its position in the column when the gradient takes effect allows the calculation of the distance over which the gradient will affect the solute since

$$L_{\mathrm{iso}} + L_{\mathrm{grad}} = L_{\mathrm{col}} \tag{13}$$

Thus, $L_{\mathrm{grad}}$ can be substituted into eq 9 for $L_{\mathrm{col}}$ to become

$$L_{\mathrm{grad}} = \int_0^{t_{\mathrm{R'}}} [1/(k' + 1)]u\,\mathrm{d}t \tag{14}$$

where

$$t_{\mathrm{R}} = t_{\mathrm{corr}} + t_{\mathrm{R'}} \tag{15}$$

**Solution of the Gradient Integral by Approximation.** An exact solution of eq 14 is often not possible under complicated gradient profiles or when complex $k'$ vs. solvent concentration relationships exist. It is easier, therefore, to evaluate the integral in a stepwise manner by incrementing the time by some small step (0.01 min for this study), calculating the corresponding $k'$ for the resulting time and then calculating the length traveled during the time interval. The sum of the time steps will equal $t_{\mathrm{R'}}$ when the sum of the lengths traveled is equal to $L_{\mathrm{grad}}$. A continuous correction must be made, however, since the actual time spent traveling and the time corresponding to the gradient concentration which the solute band encounters are generally not the same. The reason for this difference is that the gradient concentration at the band is dependent not only upon the time after which the gradient has started but also upon the position of the band in the column. The simplest way to eliminate length from the problem is to calculate a "gradient" time, $t_{\mathrm{g}}$, as well as an actual time, $t_{\mathrm{a}}$. While the actual time interval is specified, the "gradient" time interval, $t_{\mathrm{g}}$, can be calculated by using the relationship

$$t_{\mathrm{g}} = t_{\mathrm{a}} - L_{\mathrm{a}}/u \tag{16}$$

where $L_{\mathrm{a}}$ is the length traveled by the solute band in the actual time interval and $u$ is the linear velocity of the gradient front. Thus, the sum of the $t_{\mathrm{g}}$ intervals is equal to the "gradient" time seen by the solute band, and it is this time that must be used to calculate the instantaneous capacity factors for the stepwise integration.

**Calculation of Bandwidths.** The desire to calculate chromatographic resolution in addition to solute retention time requires estimation of the elution width for each solute. Under isocratic conditions the calculation of bandwidth is straightforward assuming that the number of theoretical plates is constant for a given solute. The relationship between $t_W$ ($4\sigma$ in time units) and the last capacity factor of the band center as it emerges from the column, $k'_L$, is found to be

$$T_W = (4t_M(1 + k'_L))/(N^{1/2}) \qquad (17)$$

This is essentially identical with the derivations of Jandera et al. (*5*) and Snyder et al. (*15, 19*) except that no "band compression" factor has been included. In practice it was found that eq 17 describes the actual width of low molecular weight solutes to an acceptable accuracy.

## EXPERIMENTAL SECTION

**Apparatus and Reagents.** Five test solutes were used to determine the accuracy of the predictive capabilities of the developed program. They were uracil, phenol, acetophenone, nitrobenzene, and methyl benzoate. All compounds used were reagent grade or better. HPLC grade (J. T. Baker, Inc., Phillipsburg, NJ) methanol, acetonitrile, and tetrahydrofuran were used as organic modifiers. Mobile phases were prepared volumetrically with double-distilled, deionized water and were sparged with helium before use.

The chromatographic system consisted of a Brownlee MPLC MicroPump (Brownlee Labs., Santa Clara, CA) using a nominal 150-μL packed-bed mixing chamber to ensure the reproducibility of the gradient concentration, a Rheodyne variable sample loop injection valve (Rheodyne, Cotati, CA) Model 7413, set at 0.5 μL, and a Kratos (Kratos Analytical Instruments, Ramsey, NJ) Model SF 769 U.V. detector operating at 254 nm with a 0.5-μL flow cell. The analog output of the detector was recorded with a Kipp & Zonen, BD-40 series, strip chart recorder.

Laboratory-bonded octyl stationary phases were prepared with either Whatman Partisil-10 10-μm silica gel (batch no. 4116-100) (Whatman Inc., Clifton, NJ) or Shandon MOS-Hypersil 5-μm spherical support (batch no. 10/899) (Shandon Products, Ltd., Cheshire, England). Both phases were bonded by refluxing 3 g of silica gel with a 5-fold excess of chlorodimethyloctylsilane in toluene, using 5 mL of pyridine as an acid scavenger. Reaction was allowed to proceed at 65–70 °C for 24 h. Phases were then washed in methanol, dried, and exhaustively end capped with trimethylchlorosilane. Stationary phases were packed into 250 × 1 mm i.d. glass-lined columns by slurrying 300 mg of packing into 3 mL of isopropyl alcohol, at a pressure of 10 000 psi for approximately 15 min, using acetone as the packing solvent (*20*). The MOS-Hypersil bonded phase was used for the binary gradient studies while the Partisil-10 bonded phase was used for ternary and quaternary gradient experiments.

Computer programs were written in FORTRAN using a Digital Equipment Corp. (Maynard, MA) VAX 11/780.

**Procedure.** Since the MPLC MicroPump is a dual-syringe pump, only two solvent concentrations were used for ternary and quaternary gradients. Solvent proportioning was made by the pump in all cases to obtain the required isocratic data. The flow rate throughout the entire study was kept constant at 50 μL/min. In order to test the capabilities of the approach and corresponding program, chromatographic evaluations were performed for binary, ternary, quaternary, linear, and multiple linear gradients. The instrumental delay volume was varied by injecting the solutes at various times before and after the gradient was started.

## RESULTS AND DISCUSSION

**Isocratic Data.** As previously described, mobile phases containing one modifier require at least three isocratic data points to allow fitting the expected $k'$ vs. modifier concentration curve. Methanol was used as an organic modifier to test the capabilities of the program on binary gradients. The retention times of the five test solutes were determined under four isocratic conditions (35%, 45%, 55%, and 65% methanol). The retention data are given in Table I. Retention times were generally found to vary by less than 0.2 min between runs for a given isocratic solvent concentration. Given the excellent reproducibility of retention times observed, single data points at any given solvent composition were subsequently used for the fitting of $k'$ vs. solvent composition data. Multiple experiments could be performed for each composition if desired; however, in practice this was not found to be necessary.

Table I. Binary Isocratic Data

Retention Time[a]

| solute | 1 | 2 | 3 | 4 |
|---|---|---|---|---|
| uracil | 3.1 | 3.2 | 3.2 | 3.2 |
| phenol | 4.1 | 5.2 | 6.9 | 10.4 |
| acetophenone | 4.8 | 6.4 | 10.2 | 18.6 |
| nitrobenzene | 5.4 | 7.4 | 12.0 | 20.6 |
| methyl benzoate | 6.2 | 9.7 | 18.9 | 41.4 |

Mobile Phase Concentration

| point no. | % methanol |
|---|---|
| 1 | 65.0 |
| 2 | 55.0 |
| 3 | 45.0 |
| 4 | 35.0 |

[a] All times are in minutes. [b] All solvent compositions are in volume percent.

**Binary Gradients.** Retention data for a number of binary gradients were acquired and compared to predicted values. The instrumental delay volume was determined to be 190 μL. The actual and calculated retention times (along with the percent difference) for a 10-min gradient from 35% to 65% methanol are given in Table IIA. The same gradient was run with a 290-μL instrumental delay simulated by injecting the solutes 100 μL (2.0 min) before starting the gradient. The retention data for this gradient are also given in Table IIA. The program easily accommodated the varying instrumental delays, allowing the scientist to evaluate quickly the effects of such a delay.

Data were also acquired for binary multiple linear gradients. The actual and calculated retention data for one of these gradients are presented in Table IIB. In this instance, only the last two compounds, nitrobenzene and methyl benzoate, ever experienced the second segment of the gradients. The actual and calculated retention values are again in excellent agreement, demonstrating the accuracy of both the mathematical approach and program. Total error in both the generation of the gradient and computer calculations was better than 2.1% for the demonstrated cases.

**Ternary Gradient Systems.** While the fitting of the isocratic concentration vs. retention relationship is fairly straightforward for mobile phases containing one modifier, it becomes increasingly difficult as the number of modifiers increase. Ternary solvent systems contain two independent and one dependent variables and require at least six isocratic data points to fit to eq 2.

Theoretically a well-designed multivariate experiment should be used for determining the capacity factor response surface for ternary and higher order systems. Experimentally, however, such multivariate experiments can be extremely difficult to perform due to instrumental and time limitations. To demonstrate the approach of numerical integration for complicated relationships between capacity factor and solvent composition, as are typically encountered in ternary and quaternary chromatographic systems, it was decided to acquire data along a solvent "line" generated by allowing the binary HPLC pump to proportion two ternary (or higher) reservoir solvents to obtain the required number of isocratic data points.

Table II. Binary Gradient Data[a]

A: Single Segment Linear Binary Gradient Profile

Conditions
solvents: methanol/water
gradient: 35.0:65.0 $CH_3OH:H_2O$ to 65.0:35.0 $CH_3OH:H_2O$ over 10 min

| solute | obsd $t_R$ | calcd $t_R$ | % diff |
|---|---|---|---|
| 1. 190 μL Instrumental Delay | | | |
| uracil | 3.2 | | |
| phenol | 9.2 | 9.0 | 2.1 |
| acetophenone | 12.2 | 12.0 | 1.6 |
| nitrobenzene | 13.0 | 12.9 | 0.8 |
| methyl benzoate | 15.4 | 15.5 | 0.6 |
| 2. 290 μL Instrumental Delay | | | |
| uracil | 3.2 | | |
| phenol | 9.6 | 9.8 | 2.1 |
| acetophenone | 13.4 | 13.2 | 1.5 |
| nitrobenzene | 14.4 | 14.2 | 1.4 |
| methyl benzoate | 17.2 | 17.1 | 0.6 |

B: Multiple Linear Binary Gradient Profile

Conditions
solvents: metnaol/water
gradient: 35.0:65.0 $CH_3OH:H_2O$ to 50.0:50.0 $CH_3OH:H_2O$ over 5 min and then 50.0:50.0 $CH_3OH:H_2O$ to 65.0:35.0 $CH_3OH:H_2O$ over 10 min
delay volume: 190 μL

| solute | obsd $t_R$ | calcd $t_R$ | % diff |
|---|---|---|---|
| uracil | 3.2 | | |
| phenol | 9.0 | 9.0 | 0 |
| acetophenone | 12.0 | 12.0 | 0 |
| nitrobenzene | 13.0 | 13.1 | 0.8 |
| methyl benzoate | 16.2 | 16.4 | 1.2 |

[a] All retention times are in minutes. All solvent compositions are in volume percent.

**Table III. Ternary Isocratic Data**

Retention Time (min)

| compound | 1 | 2 | 3 | 4 | 5 | 6 |
|---|---|---|---|---|---|---|
| uracil | 3.2 | 3.0 | 3.0 | 3.0 | 2.8 | 2.8 |
| phenol | 11.8 | 9.2 | 7.7 | 6.4 | 5.8 | 5.4 |
| acetophenone | 21.0 | 15.0 | 11.9 | 9.4 | 8.2 | 7.5 |
| nitrobenzene | 29.4 | 21.6 | 16.8 | 12.8 | 11.0 | 9.7 |
| methyl benzoate | 41.0 | 26.6 | 19.3 | 14.0 | 11.8 | 10.4 |

Mobile Phase Concentration

| point no. | % acetonitrile | % methanol |
|---|---|---|
| 1 | 14.0 | 26.0 |
| 2 | 20.8 | 23.0 |
| 3 | 27.5 | 20.0 |
| 4 | 34.3 | 17.0 |
| 5 | 38.8 | 15.0 |
| 6 | 43.3 | 13.0 |

These isocratic data were then fit to expected $k'$ vs. solvent composition relationships. Such "line" experiments have inherent mathematical limitations and instabilities of which the user must be aware. A fit is being forced to a given relationship and this relationship may have no physical meaning; therefore, useful results if any can only be expected within the chosen boundry conditions. Furthermore, good fits may exist between other, possibly less complicated relationships and the experimental data. However, the use of a solvent "line" represented a practical means to simulate the complexity of a full surface map utilizing the available instrumentation.

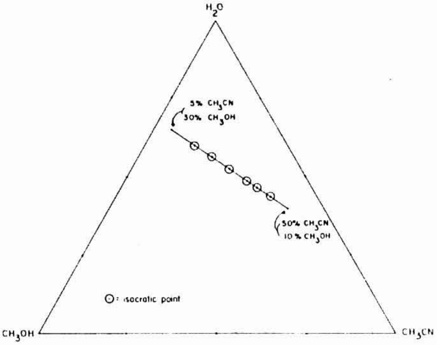

**Figure 1.** Ternary solvent diagram indicating mobile phase concentrations for isocratic data points.

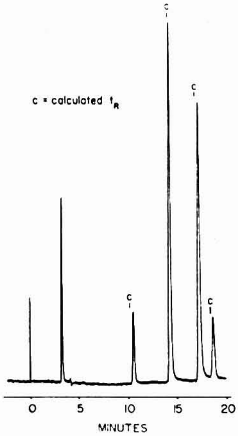

**Figure 2.** Microbore HPLC of test solutes showing actual and calculated (c) retention times for a 10-min linear ternary gradient (conditions listed in Table IVA) using a 190 μL instrumental gradient delay: column, 250 × 1 mm; laboratory bonded Partisil 10 $C_8$; flow rate, 50 μL $min^{-1}$; detector, Kratos 769, fitted with a 0.5 μL flow cell; wavelength, 254 nm; sensitivity, 0.1 aufs; pump, Brownlee MPLC micobore gradient pump; injector, Rheodyne 7413 with a 0.5-μL injection loop.

Ternary gradients were run with aqueous solutions containing methanol and acetonitrile as organic modifiers. A solution of 50:10:40 acetonitrile:methanol:water was used as the high strength solvent while the low strength solvent was a mixture of 5:30:65 acetonitrile:methanol:water. The pump itself was used to proportion these two solvents for the isocratic experiments. The ternary isocratic retention data are given in Table III. Figure 1 illustrates by use of a ternary diagram both the solvent compositions which are possible using the solvents chosen for the reservoirs and also the points at which isocratic data were acquired.

By use of the fitted ternary data, a 10-min gradient was run from 14.0% methanol. The gradient was run with a 190-μL instrumental delay, producing the chromatogram shown in Figure 2. The corresponding data are presented in Table IVA. The gradient used is graphically illustrated in Figure 3. Another 10-min, ternary gradient was run from 27.5% ace-

**Table IV. Single Segment Linear Ternary Gradient Profiles**

A.

Conditions
solvents: acetonitrile/methanol/water
gradient: 14.0:26.0:60.0 $CH_3CN:CH_3OH:H_2O$ to 41.0:14.0:45.0 $CH_3CN:CH_3OH:H_2O$ over 10 min
delay volume: 190 μL

| solute | obsd $t_R$ | calcd $t_R$ | % diff |
|---|---|---|---|
| uracil | 3.2 | | |
| phenol | 10.5 | 10.2 | 2.9 |
| acetophenone | 14.4 | 14.2 | 1.4 |
| nitrobenzene | 17.4 | 17.0 | 2.3 |
| methyl benzoate | 18.8 | 18.6 | 1.1 |

B.

Conditions
solvents: acetonitrile/methanol/water
gradient: 28.0:20.0:52.0 $CH_3CN:CH_3OH:H_2O$ to 43.0:13.0:44.0 $CH_3CN:CH_3OH:H_2O$ over 10 min
delay volume: 190 μL

| solute | obsd $t_R$ | calcd $t_R$ | % diff |
|---|---|---|---|
| uracil | 3.0 | | |
| phenol | 7.4 | 7.5 | 1.4 |
| acetophenone | 10.7 | 10.7 | 0 |
| nitrobenzene | 13.9 | 13.7 | 1.4 |
| methyl benzoate | 15.0 | 15.0 | 0 |

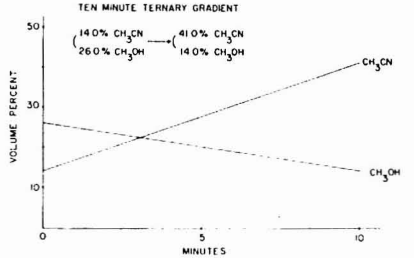

**Figure 3.** Ten-minute ternary gradient for the chromatogram shown in Figure 2, as entered into gradient generator.

**Table V. Quaternary Isocratic Data**

| | Retention Time (min) | | | | | |
|---|---|---|---|---|---|---|
| compound | 1 | 2 | 3 | 4 | 5 | 6 |
| uracil | 3.1 | 3.0 | 3.1 | 3.0 | 3.0 | 2.9 |
| phenol | 17.0 | 15.8 | 14.8 | 13.8 | 13.0 | 12.0 |
| acetophenone | 21.0 | 18.4 | 17.0 | 15.8 | 14.6 | 13.4 |
| nitrobenzene | 35.4 | 32.4 | 30.0 | 27.6 | 25.6 | 23.5 |
| methyl benzoate | 43.0 | 38.2 | 34.4 | 31.0 | 28.2 | 25.4 |

| | Retention Time (min) | | | | |
|---|---|---|---|---|---|
| compound | 7 | 8 | 9 | 10 | 11 |
| uracil | 3.2 | 3.2 | 2.8 | 3.0 | 3.0 |
| phenol | 11.7 | 11.2 | 10.0 | 9.4 | 8.8 |
| acetophenone | 13.0 | 12.3 | 11.1 | 10.2 | 9.6 |
| nitrobenzene | 22.3 | 20.7 | 19.0 | 16.6 | 15.6 |
| methyl benzoate | 23.8 | 21.7 | 19.8 | 16.9 | 16.0 |

Mobile Phase Composition

| point no. | % tetrahydrofuran | % acetonitrile | % methanol |
|---|---|---|---|
| 1 | 5.50 | 7.75 | 21.25 |
| 2 | 6.00 | 8.63 | 20.63 |
| 3 | 6.50 | 9.50 | 20.00 |
| 4 | 7.00 | 10.38 | 19.38 |
| 5 | 7.50 | 11.25 | 18.75 |
| 6 | 8.00 | 12.13 | 18.13 |
| 7 | 8.50 | 13.00 | 17.50 |
| 8 | 9.00 | 13.88 | 16.88 |
| 9 | 9.50 | 14.75 | 16.25 |
| 10 | 10.50 | 16.50 | 15.00 |
| 11 | 11.00 | 17.38 | 14.38 |

**Table VI. Linear Quaternary Gradient Data**

A. Single Segment Linear Profile

Conditions
solvents: THF/acetonitrile/methanol/water
gradient: 6.0:8.6:20.6:64.8 $THF:CH_3CN:CH_3OH:H_2O$ to 11.0:17.4:14.4:57.2 $THF:CH_3CN:CH_3OH:H_2O$ over 20 min
delay volume: 190 μL

| solute | obsd $t_R$ | calcd $t_R$ | % diff |
|---|---|---|---|
| uracil | 3.0 | | |
| phenol | 14.2 | 14.2 | 0 |
| acetophenone | 15.8 | 16.2 | 2.5 |
| nitrobenzene | 24.1 | 23.6 | 2.1 |
| methyl benzoate | 25.4 | 25.0 | 1.6 |

B. Multiple Linear Quaternary Profile

Conditions
solvents: THF/aceto/methanol/water
gradient: 6.0:8.6:20.6:64.8 $THF:CH_3CN:CH_3OH:H_2O$ to 10.0:15.6:15.6:58.8 $THF:CH_3CN:CH_3OH:H_2O$ over 10 min and then 10.0:15.6:15.6:58.8 $THF:CH_3CN:CH_3OH:H_2O$ to 11.0:17.4:14.4:57.2 $THF:CH_3CN:CH_3OH:H_2O$ over 10 min
delay volume: 190 μL

| solute | obsd $t_R$ | calcd $t_R$ | % diff |
|---|---|---|---|
| uracil | 3.0 | | |
| phenol | 13.8 | 13.6 | 1.4 |
| acetophenone | 15.2 | 15.2 | 0 |
| nitrobenzene | 22.4 | 21.7 | 3.1 |
| methyl benzoate | 23.5 | 22.9 | 2.6 |

tonitrile, 20.0% methanol to 43.3% acetonitrile, 13.0% methanol with a 190-μL instrumental delay. The results for this gradient are given in Table IVB. The results for the ternary gradients clearly show that even though ternary systems are mathematically and experimentally very complex, they can be handled with an accuracy exceeding 97%.

**Quaternary Gradients.** In order to test the applicability of the program and instrumentation under rigorous conditions, quaternary solvent systems were investigated for both linear and multiple linear gradient shapes. Quaternary gradients have not been exploited fully, possibly because of the tremendous complexity of such solvent systems. A solvent concentration line was again evaluated as opposed to the entire response surface. It should be noted that quaternary and higher order systems pose additional problem since their response surfaces require four or more dimensions to visualize. While a minimum of ten isocratic data points are necessary to fit the equation for aqueous solutions containing three organic modifiers, 11 data points were acquired. The high strength mobile phase reservoir contained an aqueous 12.5% tetrahydrofuran, 20.0% acetonitrile, and 12.5% methanol solution and the low strength mobile phase was an aqueous 2.5% tetrahydrofuran, 2.5% acetonitrile, and 25.0% methanol solution. The 11 isocratic data points used are given in Table V. Both linear and multiple-linear quaternary gradients were run. The results for a 20-min gradient from 6.0% THF, 8.6% acetonitrile, and 20.6% methanol to 11.0% THF, 17.4% acetonitrile, and 14.4% methanol with a 190-μL instrumental

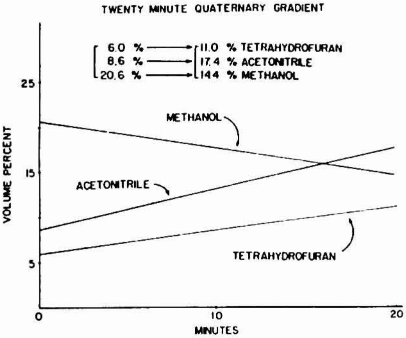

**Figure 4.** Twenty-minute quaternary gradient profile as entered into the gradient generator.

delay are given in Table VIA. A graphical illustration for this gradient is presented in Figure 4. Changing the instrumental delay had little effect on the accuracy of the calculations.

Finally, a multiple linear quaternary gradient was run consisting of a first segment from 6.0% THF and 8.6% acetonitrile and 20.6% methanol to 10.0% THF, 15.6% acetonitrile, and 15.6% methanol in 10.0 min followed by a 10.0-min segment to 11.0% THF, 17.4% acetonitrile, and 14.4% methanol. Like the previous quaternary gradients, the THF and acetonitrile concentrations rise from the initial to the final concentrations while the methanol concentration falls. The results for the multiple linear quaternary gradient are presented in Table VIB.

The overall accuracy of the quaternary gradient experiments was slightly worse than for the simple binary gradients, but in no case was the error between predicted and observed more than 6%. It was felt given the complexity of the system, that these errors were sufficiently small for prediction purposes.

## CONCLUSIONS

The algorithms derived using integration by parts on a larger computer avoid the problems of attempting to derive exact mathematical solutions to the gradient integral equations. Computation times are fast, even for complicated gradient shapes and long elution times. Calculations required at most only a few seconds. In addition, excellent flexibility is achieved by using this computational approach, since virtually any $k'$ vs. solvent composition relationship can be accommodated. The same type of flexibility is expected to be found for different gradient shapes, especially those of unusual profiles not readily described by any particular function. Multiple linear gradients were utilized for this work, since most new instruments construct gradients by linking linear segments. However, complicated gradients of any mathematical form can be handled as readily with little programming effort.

## ACKNOWLEDGMENT

We extend our appreciation to Peter Carr, University of Minnesota, for his guidance on aspects of this work.

## LITERATURE CITED

(1) Drouen, A. C. J.; Billiet, H. A. H.; de Galan, L. *Anal. Chem*. **1984**, *56*, 971.
(2) Jandera, P.; Churacek, J. *J. Chromatogr*. **1974**, *91*, 223.
(3) Jandera, P.; Churacek, J. *J. Chromatogr*. **1974**, *93*, 17.
(4) Jandera, P.; Churacek, J. *J. Chromatogr*. **1975**, *104*, 9.
(5) Jandera, P.; Churacek, J. *J. Chromatogr*. **1979**, *170*, 1.
(6) Jandera, P.; Churacek, J. *J. Chromatogr*. **1974**, *91*, 207.
(7) Jandera, P.; Churacek, J.; Svoboda, L. *J. Chromatogr*. **1980**, *192*, 37.
(8) Jandera, P.; Churacek, J. *J. Chromatogr*. **1980**, *192*, 19.
(9) Handera, P.; Churacek, J. *J. Chromatogr*. **1980**, *192*, 1.
(10) Jandera, P.; Churacek, J.; Colin, H. *J. Chromatogr*. **1981**, *214*, 35.
(11) Jandera, P.; Churacek, J. *J. Chromatogr*. **1975**, *104*, 23.
(12) Shoenmakers, P. J.; Billiet, H. A. H.; de Galan, L. *Chromatographia* **1982**, *15*, 205.
(13) Schoenmakers, P. J.; Billiet, H. A. H.; Tijssen, R.; de Galan, L. *J. Chromatogr*. **1978**, *149*, 519-537.
(14) Shoenmakers, P. J.; Billiet, H. A. H.; de Galan, L. *J. Chromatogr*. **1983**, *282*, 107.
(15) Snyder, L. R. In "High Performance Liquid Chromatography. Advances and Perspectives"; Horvath, Cs., Ed.; Academic Press: New York, 1980; Vol. 1, pp 207-316.
(16) Borowko, M.; Jaroniec, M.; Narkiewicz, J.; Patryklejew, A.; Rudzinski, W. *J. Chromatogr*. **1978**, *153*, 309.
(17) Borowko, M.; Jaroniec, M.; Narkiewicz, J.; Patryklejew, A. *J. Chromatogr*. **1978**, *153*, 321.
(18) Hartwick, R. A.; Grill, C. M.; Brown, P. R. *Anal. Chem*. **1979**, *51*, 34.
(19) Snyder, L. R.; Saunders, D. L. *J. Chromatogr. Sci*. **1969**, *7*, 195.
(20) Meyer, R. F.; Hartwick, R. A. *Anal. Chem*. **1984**, *56*, 2211.

RECEIVED for review October 9, 1984. Accepted December 10, 1984. S.A.T. acknowledges the financial support of Merck Sharp & Dohme Research Laboratories, Rahway, NJ. Acknowledgment is also given to the National Science Foundation, Grant No. 8100224, and to the donors of the Petroleum Research Fund, administered by the American Chemical Society.

# Polarity of Chemically Modified Silica Surfaces and Its Dependence on Mobile-Phase Composition by Fluorescence Spectrometry

**Jan Ståhlberg***

*Astra Pharmaceutical Production AB, Quality Control, S-151 85 Södertälje, Sweden*

**Mats Almgren**

*Institute of Physical Chemistry, P.O. Box 532, S-751 21 Uppsala, Sweden*

**Pyrene was adsorbed on RP-2 and RP-18 surfaces and its excitation and emission spectra showed that pyrene has the same photophysical properties as in solution. By an analysis of the fine structure of the emission spectrum it was possible to determine the polarity of the surfaces when they are surrounded by water–methanol and water–acetonitrile mixtures (0–30% (w/w) organic solvent). It was found that with increasing concentration of methanol in the solvent, there was a decrease in the polarity of RP-2 and RP-18 surfaces. The influence of acetonitrile on surface polarity was found to be more complex. A molecular model based on these results is discussed.**

It is generally acknowledged (*1–4*) that there is a lack of understanding of the mechanism of solute retention in reversed-phase liquid chromatography. One of the reasons for this is that the knowledge of the physical nature of the chemically modified surface and its dependence of mobile-phase composition is incomplete.

Many chromatographic studies correlating changes in solute retention with properties of the bonded phase have been performed. The literature is overwhelming and a short review is found in ref 3. A number of spectrometric techniques have been used to provide information which complements these chromatographic data. Besides infrared spectrometry (*5, 6*), UV–visible spectrometry (*7*), photoacoustic spectroscopy (*8, 9*), and NMR (*10–12*) spectrometry, fluorescence spectrometry is a technique which has been used, however, only to a limited extent (*4, 13, 14*). Much of the spectrometric work to date has been focused on the analysis of spectrometric data of the chemically bound species. In this work, however, we are using fluorescence spectrometry to examine pyrene molecules that are adsorbed on the surface. The purpose is to investigate the polarity of the chemically modified surface and its dependence on the composition of the surrounding solvent.

During the last years a number of papers have appeared dealing with the photophysical properties of organic molecules adsorbed on solid surfaces. Pyrene is a molecule that has been extensively used, and several studies of its photophysical properties when adsorbed on silica (*15–18*), aluminium oxide (*19*), $TiO_2$ (*20, 21*), and montmorillonite (*22*) have been performed. In some of these papers (*15–19, 21*) the effect of coadsorbed organic molecules on the photophysical properties of pyrene is reported. Before discussing these results it may be useful to recall the pertinent photophysical properties of pyrene in fluid solutions. The important processes are

$$P + h\nu_0 \rightarrow P^* \quad (1)$$

$$P^* \rightarrow P + h\nu_1 \quad (2)$$

$$P^* + P \rightleftarrows P_2^* \text{ (excimer formation)} \quad (3)$$

$$P_2^* \rightarrow P + P + h\nu_2 \quad (4)$$

The emission spectrum of the monomer in solution shows a significant fine structure (vibronic bands) and is situated in the region 370–400 nm. On the other hand, the emission spectrum of the excimer is a broad and structureless band situated at ~470 nm. On solid surfaces one additional process may be of importance, the excitation of a ground-state dimer with a subsequent emission in the same region as the excimer emission, i.e.

$$P_2 + h\nu_0 \rightarrow P_2^* \quad (5)$$

$$P_2^* \rightarrow P_2 + h\nu_3 \quad (6)$$

In addition to this, there is another important feature of the monomer emission that is extensively used in this work. It was first found by Kalyanasundaram and Thomas (*23*) that the intensities of the various vibronic bands show a strong dependence on the solvent environment. The emission spectrum consists of five major vibronic bands usually labeled I–V in progressive order, i.e., the 0–0 band is labeled I etc. In the presence of polar solvents, there is a significant enhancement in the intensity of the 0–0 vibronic band at the expense of other bands. The ratio of the emission intensities for bands III and I serves as a measure of solvent polarity. We found, for example, that the III/I ratio was 1.63 in hexane and 0.51 in $H_2O$. It must be pointed out that no theory is available for a quantitative explanation of this effect, but qualitatively, the III/I ratio is a measure of the extent of interaction between the solvent dipoles and the excited singlet state of pyrene (*23*).

Some relevant results concerning the behavior of pyrene adsorbed on solid surfaces, as obtained by others with fluorescence spectrometry can be summarized as follows:

The monomer emission for pyrene adsorbed on silica (*16, 17*) is similar in detail to what is observed in solution, indicating little perturbation by the oxide support. The monomer emission for pyrene adsorbed on aluminum oxide is slightly distorted (*19*) and on $TiO_2$ it is strongly distorted (*20*), indicating a strong binding to the $TiO_2$ surface.

Formation of ground-state dimer is found on both silica (*17*) and aluminum oxide (*19*), but not on $TiO_2$ (*20*).

Coadsorbed alcanols (*17*) and nonionic surfactants (*18*) solubilize pyrene on the silica surface and the former increases the intensity of excimer emission (*17*).

The III/I ratio for pyrene adsorbed on silica (*16*) and aluminum oxide (*19*) is characteristic of a polar environment and coadsorbtion of alcanols increases the III/I ratio. The III/I ratio for pyrene adsorbed on silica modified with trimethylsilyl chloride is characteristic of a nonpolar environment (*16*).

In this work it was shown that when pyrene was adsorbed on RP-2 and RP-18 particles suspended in water, the emission spectrum had the same characteristic as in fluid solutions. In addition, no ground-state dimerization of adsorbed pyrene was

0003-2700/85/0357-0817$01.50/0 © 1985 American Chemical Society

found in the concentration range studied. The polarity of RP-2 and RP-18 surfaces in contact with water was found to be comparable to the polarity of 1-octanol. However, when methanol was gradually substituted for water, in the range 0–30% (w/w) methanol, there was a gradual decrease in surface polarity for both RP-2 and RP-18 surfaces. However, when acetonitrile was substituted for water, in the range 0–30% (w/w) acetonitrile, the behavior of surface polarity was found to be more complex. An interpretation of the results on the molecular level is discussed.

The preceding discussion demonstrates that fluorescence spectrometry is a useful tool in the examination of chemically modified silica surfaces. Additional information concerning the physical nature of these surfaces can be obtained from quenching studies, the relative intensity of monomer–excimer emission, and fluorescence decay methods. Such studies are currently in progress.

## EXPERIMENTAL SECTION

**Materials.** LiChrosorb RP-2 and RP-18 (5 μm) (Merck, Darmstadt, G.F.R.) were used. According to the manufacturer they have the following characteristics: RP-2, surface area (BET) 350 $m^2/g$, surface coverage $5.5 \times 10^{-6}$ mol/$m^2$; RP-18, surface area (BET) 150 $m^2/g$, surface coverage $3.3 \times 10^{-6}$ mol/$m^2$. Pyrene (Kodak) was used as received, the purity was found, by LC analysis, to be 99.5%. All the solvents used were of spectroscopic, chromatographic, or analytical grade and were used without further purification; in addition they were controlled with respect to spectral impurities by UV–vis and fluorescence spectrometry. Sodium tetradecylsulfate and $CuSO_4 \cdot 5H_2O$ of analytical grade (Merck) were used as supplied.

**Fluorescence Studies.** All fluorescence spectra were obtained with a Perkin-Elmer Model MPF-3 scanning fluorescence spectrophotometer using an excitation and emission slit width of 2 nm (except when excitation spectra were collected with the emission monochromator set at 470 nm, then the emission slit width was 7 nm). A suspension of RP-18 was prepared by adding 2 or 8 mg of particles/g of $H_2O$ and in most cases 0.5 mg of sodium tetradecylsulfate/g of $H_2O$ to deionized water whereupon the mixture was intensively shaken until all particles were suspended. A suitable amount of pyrene dissolved in methanol (~$1 \times 10^{-3}$ M) was then added. The methanol concentration in the suspension never exceeded 0.6% (w/w). In the experiments with varying concentrations of methanol or acetonitrile, the suspension was prepared in ~0.05 M or ~0.10 M $CuSO_4$ solution instead of water. When methanol or acetonitrile is added to this suspension, flocculation may occur, particularly when added to an RP-18 suspension. Therefore, to minimize systematic errors in the measurements of fluorescence intensity, an elaborated procedure was used. Approximately 2.5 g of the suspension was added into a 10-mm quartz cell and approximately 125 mg of methanol or acetonitrile was subsequently added with a Hamilton syringe directly into the cell. All amounts were weighed on an analytical balance. After each addition and between each measurement the cell was put into an ultrasonic bath for 1 min. After this treatment the emission intensity was measured within 10–15 s at 373 or 383 nm. For each solvent composition, four measurements were performed in three different cells. So, by this procedure all the measurements, with different methanol–water or acetonitrile–water mixtures, were carried out with the same sample.

In addition, a suspension with exactly the same composition as in the cells was centrifuged and the emission intensity at 383 and 373 nm of the supernatant was measured. The excitation wavelength was 337 nm. All measurements were performed in the right angle mode and a correction for the light scattered by the particles was made by measuring a suspension of the same composition, with the exception that pyrene was not added.

## RESULTS AND DISCUSSION

**Fluorescence Measurements in Highly Scattering Media.** All fluorescence intensity measurements in this work are carried out with right angle illumination on suspensions that strongly scatter the incident light. To validate such a procedure, pyrene was dissolved in methanol and varying amounts of RP-2 particles (0–10 mg of particles/mL of methanol) were added, whereupon the emission intensity was measured at both 373 and 383 nm. To investigate the influence of absorbance, the measurements were carried out in two solutions containing different amounts of pyrene, the absorbances at 336 nm in these solutions were 0.11 and 0.45, respectively. After a proper correction for the amount of light scattered by the particles, it was found that the emission intensity, for both wavelengths, was independent of the particle concentration. The difference of absorbance of the solutions was found to have no influence on the result. It is worth pointing out that in the solution containing the lesser concentration of pyrene and the highest concentration of particles, the emission intensity from pyrene and the intensity of the scattered light were approximately equal.

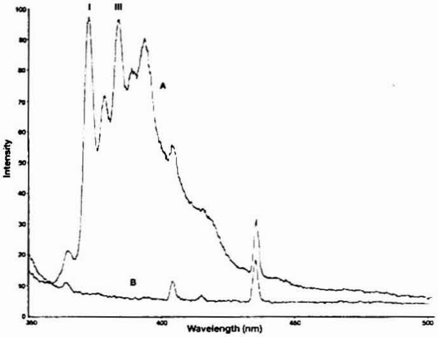

Figure 1. (A) Emission spectrum of pyrene adsorbed on RP-18. Composition of suspension: 2.01 mg of RP-18 particles/g of $H_2O$, 0.15 mg of sodium tetradecylsulfate/g of $H_2O$, $1.88 \times 10^{-6}$ mol of pyrene/g of RP-18. (B) Background spectrum, the peaks are unidentified.

An explanation of the insensitivity of the corrected emission intensity to particle concentration is the following: The particles scatter the emitted light randomly in all directions, but since the pyrene molecules emit randomly also in a nonscattering medium, the emission intensity will be the same, if the fraction of the incident light that is directly backscattered by the particles is negligible. In conclusion, the procedure that was used in this investigation, i.e., subtraction of the intensity of scattered light by the particles and of emission from the supernatant solvent, obtained through centrifugation, is valid. However, care must be taken when working with suspensions with such absorbances that the emission intensity is not linearly related to concentration.

**Emission and Excitation Spectra of Pyrene on RP-2 and RP-18 Surfaces.** Because of its interesting photophysical properties and its strong hydrophobicity, pyrene is a suitable probe molecule in the study of hydrophobic surfaces. It is seen in Figure 1 that the emission spectrum for pyrene adsorbed on RP-18 has the same vibronic fine structure as that in a solvent; for comparison, emission spectra for pyrene in various solvents can be found in ref 23. This indicates that there is no strong binding between the pyrene molecule and the RP-18 surface. The emission spectrum for pyrene adsorbed on RP-2 has the same characteristics. Furthermore, it is seen that, at this pyrene concentration, the formation of excimers is small.

It has been shown by others (*17, 19*) that ground-state dimers of pyrene may exist on solid surfaces. However, it is possible to differentiate the monomeric state from the dimeric state by an analysis of the excitation spectra with observation in the monomer (383 nm) and excimer regions (470 nm). In

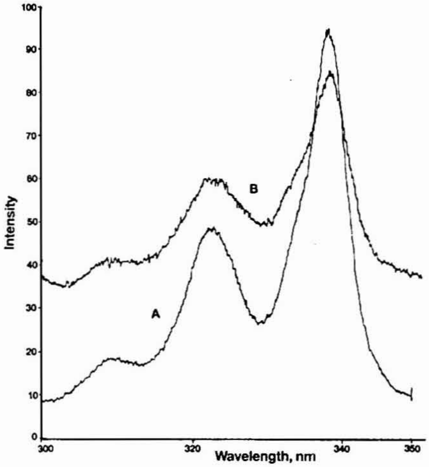

**Figure 2.** Excitation spectrum of pyrene adsorbed on RP-18 (A) with observation in the monomer region (383 nm) and (B) with observation in the excimer region (470 nm). For composition of suspension, see caption to Figure 1.

Figure 2 it is seen that the absorption peaks in the monomer and excimer excitation spectra, for pyrene adsorbed on RP-18, occur at the same wavelengths. The excitation spectra for pyrene adsorbed on RP-2, observed in the monomer and excimer regions, overlap in the same way as they do with RP-18. If ground-state dimers were present, the excitation spectrum with observation in the excimer region should have been red-shifted by 5–7 nm in relation to the excitation spectrum of the monomer.

In summary, it has been shown that pyrene adsorbed on RP-2 and RP-18 surfaces retains the same photophysical properties as it has in solution. It has also been shown that no ground-state dimers are formed under the conditions that are used in this work.

**Polarity of RP-2 and RP-18 Surfaces.** It has been shown that the relative intensity of peak III and peak I in the emission spectrum of pyrene, the III/I ratio, can be used as a measure of solvent polarity (*23*). Since the reported III/I ratios (*23*) are based on uncorrected spectra, we had to repeat the measurements with our equipment. The obtained III/I ratios are summarized in Table I, the reproducibility of the reported values is ±0.01. It is readily seen that the III/I ratio correlates well with the chemists practical experience of solvent polarity. The term "solvent polarity" has, however, no physical definition. It can be shown that the effective polarity of a molecule increases with increasing size of the ratio $D^2/\sigma^3kT$ where $D$ is the permanent dipole moment, $\sigma$ is the collision diameter, $k$ is the Boltzmann constant, and $T$ is the absolute temperature.

However, even this expression is unable to show the increase in effective polarity that occurs in a molecule with an unsymmetrical disposition of the polar group as in, e.g., alcohols (*24*). Still it is a parameter with physical significance and it is therefore interesting to correlate this parameter with the III/I ratio. The term $\sigma^3$ in the denominator is somewhat inconvenient to use and will here be substituted by the molar volume, $V$, of the solvent. To extend this correlation to mixtures of hexane and octanol, the term $D^2/V$ must be substituted by an expression that takes the dilution of the polar molecules into consideration. It is therefore reasonable to use the following expression for this mixture:

**Table I. Solvent Dependence of III/I Ratio for Pyrene Monomer Fluorescence**

| solvent | III/I ratio |
|---|---|
| water | 0.51 |
| acetonitrile | 0.52 |
| acetone | 0.55 |
| dichloromethane | 0.68 |
| methanol | 0.69 |
| trichloromethane | 0.72 |
| tetrahydrofuran | 0.72 |
| ethanol | 0.78 |
| 1-propanol | 0.84 |
| 2-propanol | 0.89 |
| 1-butanol | 0.92 |
| 1-hexanol | 0.98 |
| 1-octanol | 1.03 |
| 1-octanol (87.7 mol %) + *n*-hexane | 1.07 |
| 1-octanol (74.5 mol %) + *n*-hexane | 1.11 |
| 1-octanol (56.8 mol %) + *n*-hexane | 1.16 |
| 1-octanol (49.6 mol %) + *n*-hexane | 1.20 |
| 1-octanol (39.7 mol %) + *n*-hexane | 1.26 |
| 1-octanol (24.8 mol %) + *n*-hexane | 1.34 |
| 1-octanol (10.4 mol %) + *n*-hexane | 1.49 |
| *n*-hexane | 1.63 |

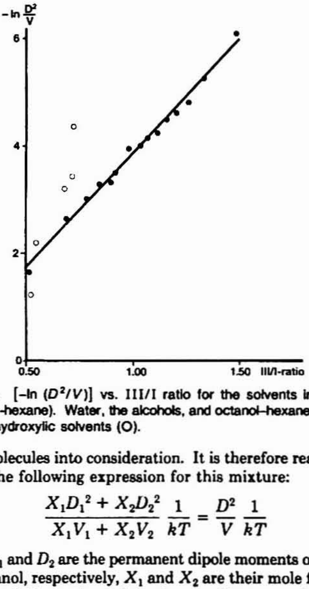

**Figure 3.** [$-\ln (D^2/V)$] vs. III/I ratio for the solvents in Table I (except *n*-hexane). Water, the alcohols, and octanol–hexane mixtures (●); nonhydroxylic solvents (○).

$$\frac{X_1D_1^{\,2} + X_2D_2^{\,2}}{X_1V_1 + X_2V_2}\,\frac{1}{kT} = \frac{D^2}{V}\,\frac{1}{kT} \tag{7}$$

where $D_1$ and $D_2$ are the permanent dipole moments of hexane and octanol, respectively, $X_1$ and $X_2$ are their mole fractions and $V_1$ and $V_2$ are the molar volumes of hexane and octanol, respectively. In Figure 3 a plot of [$-\ln (D^2/V)$] as a function of the III/I ratio is presented for the solvents and solvent mixtures in Table I (except for hexane). Since the temperature is constant (room temperature), it is omitted in the calculations together with Boltzmann's constant.

It is seen that a linear correlation is obtained between these parameters for water, for the different alcohols, and for the hexane–octanol mixtures. The nonhydroxylic solvents do not fit the straight line (except for acetone) and this may be explained by the high polarizability of THF, $CH_2Cl_2$, and $CHCl_3$ and the low polarizability of acetonitrile. It must be emphasized that the correlation between [$-\ln (D^2/V)$] and the III/I ratio is an empirical correlation and, as such, it is not based on any physical insight into the influence of solvent on the deexcitation process of the singlet excited pyrene molecule. Despite this, it can be concluded that it is possible to set up a polarity scale based on the III/I ratio.

Since the RP-2 and RP-18 surfaces are not wetted by water, the corresponding particles are not readily suspended in it. Therefore, to lower the interfacial surface tension, the tenside sodium tetradecylsulfate was added. The influence of the tenside on the III/I ratio was investigated by measuring it for different tenside concentrations. To suspensions containing 2.0 mg of RP-2 or RP-18/g of $H_2O$, the total amount tenside was varied between 0.023 and 0.63 mg/g of $H_2O$ for RP-2 and between 0.076 and 0.87 mg/g of $H_2O$ for RP-18. It has been shown by us (*25*) that when the total amount of added tenside corresponds to 1.03 mg/g of $H_2O$ in a suspension containing 2.0 mg of RP-18/g of $H_2O$, the concentration of sodium tetradecylsulfate in the surrounding water is equal to CMC ($2.2 \times 10^{-3}$ M (*26*)).

All these measurements were thus performed with tenside concentrations below CMC. It was found that these large differences in tenside concentration in neither case had no effect on the III/I ratio, and it can be concluded that the influence of the tenside on the polarity of the surface layer is negligible.

In summary, it has been demonstrated that all requirements for measurement of polarity of the RP-2 and RP-18 surfaces are fullfilled.

So, the III/I ratios for these surfaces were measured in a suspension containing 2.0 mg of particles/g of $H_2O$, 0.15 mg of tenside/g of $H_2O$ (RP-18) or 0.38 mg of tenside/g of $H_2O$ (RP-2), and $2.0 \times 10^{-6}$ mol of pyrene/g of particles. After centrifugation of these suspensions, the emission intensity of the supernatant was measured. It was found that the emission intensity was negligible of the supernatant from the RP-18 suspension but for RP-2 it contributed with ca. 30% of the total emission intensity from the suspension. After proper correction for this and for background scattering by the particles, the III/I ratios are found to be 1.06 ± 0.02 for RP-2 and 1.03 ± 0.02 for RP-18. Examination of the data in Table I shows that the polarity of the RP-18, in contact with water, is the same as for octanol while the RP-2 surface probably has a slightly lower polarity. This is explained by the higher surface coverage of hydrophobic groups on RP-2 compared with RP-18, which consequently gives fewer silanol groups and hydrogen bonded water molecules on the surface.

It is also interesting to investigate how the polarity of the surfaces varies with the composition of the surrounding solvent. Since methanol– and acetonitrile–water mixtures are the most used solvents in reversed-phase liquid chromatography, our work was focused on these mixtures. When these solvents are added to the previous suspension, the concentration of pyrene rapidly increases in the liquid phase and it becomes inconvenient to correct for such high emission intensities from the supernatant. It has, however, been shown by us (*25*) that the $Cu^{2+}$ ion only partially quenches the emission from pyrene molecules adsorbed on the RP-2 and RP-18 surfaces. Thus, by making the suspension in $CuSO_4$ solutions, the emission from pyrene molecules in the solution is almost entirely quenched but the emission from pyrene adsorbed on the surfaces is only partially quenched. In addition, the presence of $Cu^{2+}$ ion in the solution does not alter the measured III/I ratio. Hence such a procedure is valid for measurements of the dependence of surface polarity on the composition of the surrounding solvent. The results from the measurements with the RP-18 surface are shown in Figure 4 and with the RP-2 surface in Figure 5.

It is readily seen that there are large differences between the influence of acetonitrile and methanol on the polarity for both RP-18 and RP-2 surfaces. On the other hand, methanol has a similar effect on the polarity of RP-2 and RP-18 surfaces, but the effect of acetonitrile differs slightly between them. Due to flocculation in the measuring cell, the reproducibility of the III/I ratio in these measurements is lower than that in solvents. Each point in the figures is based on measurements in three different systems with the same composition and for every point four measurements with each system were performed. From the *t* distribution the 95% confidence limit for the indicated mean value can be estimated to ±0.05 for the RP-18-acetonitrile system and ±0.04 for the others.

The results of these measurements show that there is a large difference between acetonitrile and methanol in their interaction with the RP surfaces. The results for RP-18 in contact with methanol-water mixtures indicate that the methanol molecules that enter between the long alkyl chains are hydrogen bonded to the free silanol groups on the surface. By turning out the methyl group from the surface, the polarity of the surface decreases. Since no increase in polarity was detected when the concentration of methanol increases in the solvent, the concentration of freely moving methanol molecules

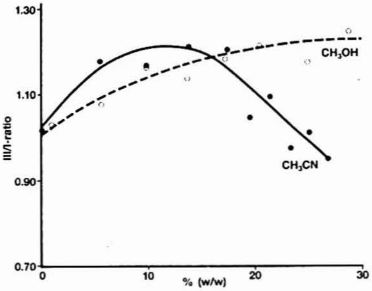

**Figure 4.** Dependence of III/I ratio for RP-18 on the composition of the surrounding solvent in weight percent of organic modifier: water–methanol mixture (O), water–acetonitrile mixture (●). Initial composition of suspensions: $H_2O$–$CH_3OH$ mixture, 8.50 mg of RP-18/g of $H_2O$, 0.48 mg of tenside/g of $H_2O$, $1.30 \times 10^{-6}$ mol of pyrene/g of RP-18, 0.055 M $CuSO_4$; $H_2O$–$CH_3CN$ mixture, 8.09 mg of RP-18/g of $H_2O$, 0.45 mg of tenside/g of $H_2O$, $1.15 \times 10^{-6}$ mol of pyrene/g of RP-18, 0.10 M $CuSO_4$.

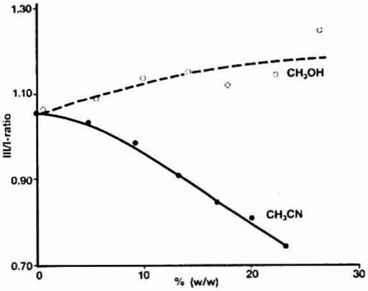

**Figure 5.** Dependence of III/I ratio for RP-2 on the composition of the surrounding solvent in weight percent of organic modifier: water–methanol mixture (O), water–acetonitrile mixture (●). Initial composition of suspensions: $H_2O$–$CH_3OH$ mixture, 8.91 mg of RP-2/g of $H_2O$, 0.51 mg of tenside/g of $H_2O$, $0.74 \times 10^{-6}$ mol of pyrene/g of RP-2, 0.054 M $CuSO_4$; $H_2O$–$CH_3CN$ mixture, 8.38 mg of RP-2/g of $H_2O$, 0.47 mg of tenside/g of $H_2O$, $0.78 \times 10^{-6}$ mol of pyrene/g of RP-2, 0.053 M $CuSO_4$.

between the alkyl chains is probably very low. Several studies have been performed concerning the selective adsorption of acetonitrile and methanol on RP surfaces (2, 27). It is interesting to compare this interpretation with the results from RP-18–methanol isotherm measurements made by Slaats et al. (27).

With the assumption that methanol is selectively adsorbed on the surface, they found that the amount of methanol adsorbed is 1.24 mmol/g RP-18 when the solvent contained 24.7% (w/w) methanol. Moreover it was found that with higher concentration of methanol in the solvent, there was only a small increase in the amount of adsorbed methanol molecules. Since the concentration of free silanol groups on the surface probably is in the range of 0.8–1.6 mmol/g RP-18, i.e., of the same magnitude as the concentration of adsorbed methanol molecules, the results of Slaats et al. support the above interpretation of our results. In summary, the majority of the adsorbed methanol molecules are probably hydrogen bonded to free silanol groups, and by turning out the methyl group from the surface, the polarity of the surface decreases.

In the case of acetonitrile–water mixture in contact with RP-18 the results show that the behavior is more complicated than for methanol–water mixtures. For low concentrations of acetonitrile in the solvent there is a decrease in surface polarity. This indicates that the adsorbed acetonitrile molecules are hydrogen bonded to the silanol groups, and by turning out the methyl group from the surface, the polarity of the surface decreases, i.e., an identical mechanism as for methanol–water mixtures. For higher concentrations, 14–28% (w/w) of acetonitrile in the solvent, the polarity of the surface layer increases which indicates that additional acetonitrile molecules enter between the alkyl chains and that these are more or less freely moving, which leads to an increase in polarity of the surface layer. It is also in this case interesting to compare the interpretation with the results from measurement of the absorption isotherm for acetonitrile–water solvent mixtures on RP-18 (27). It was found, with the assumption that acetonitrile is selectively adsorbed, that for a mixture containing 16.1% (w/w) acetonitrile, 1.72 mmol of acetonitrile is adsorbed per g of RP-18. This amount is slightly higher than the amount of available silanol groups on the surface and in Figure 4 it is seen that the polarity of the surface at this composition increases. When the concentration of acetonitrile in the solvent is 29.8% (w/w), it was found that 3.01 mmol of acetonitrile is adsorbed per gram of RP-18 and thus the amount of adsorbed acetonitrile greatly exceeds the number of silanol groups, in contrast to the behavior of methanol. It can be be concluded, therefore, that these results also agree well with the above interpretation of our results.

The influence of the methanol–water mixture on the polarity of the RP-2 surface is seen to be similar as on the RP-18 surface and an identical explanation is suggested; i.e., the adsorbed methanol molecules are hydrogen bonded to the silanol groups. Unfortunately Slaats et al. (27) did not determine the isotherm for methanol on RP-2 surface, so a direct comparison cannot be made. For the RP-2 surface in contact with acetonitrile–water mixtures, the results show an increase in polarity for all concentrations. However, the increase is very small for low concentrations of acetonitrile in the solvent which probably is due to a combination of hydrogen bonding of the acetonitrile molecules (decrease the polarity) and of an increasing concentration of more or less freely moving acetonitrile molecules on the surface (increase the polarity). When the majority of the silanol groups are shielded by acetonitrile molecules, additional acetonitrile molecules are more or less freely moving and the polarity rapidly increases. That the polarity of an RP-2 surface in contact with an acetonitrile–water mixture is higher than the corresponding RP-18 surface is in agreement with the findings of Slaats et al., who found that within this concentration range of solvent the amount of acetonitrile adsorbed on RP-2 is about 25–30% higher than on RP-18.

## ACKNOWLEDGMENT

Thanks are due to M. A.-L. Pettersson for assistance with the experiments and to D. Westerlund for valuable discussion of the manuscript.

**Registry No.** $CH_3OH$, 67-56-1; $CH_3CN$, 75-05-8; pyrene, 129-00-0.

## LITERATURE CITED

(1) Berendsen, G. E.; de Galan, L. *J. Chromatogr.* **1980**, *196*, 21.
(2) McCormick, R. M.; Karger, B. L. *J. Chromatogr.* **1980**, *199*, 259.
(3) Martire, D. E.; Boehm, R. E. *J. Phys. Chem.* **1983**, *87*, 1045.
(4) Lochmüller, C. H.; Colborn, A. S.; Hunnicutt, M. L.; Harris, J. M. *Anal. Chem.* **1983**, *55*, 1344.
(5) Sander, L. C.; Callis, J. B.; Field, L. R. *Anal. Chem.* **1983**, *55*, 1068.
(6) Leyden, D. E.; Kendall, D. S.; Burggraf, L. W.; Pern, F. J.; De Bellow, M. *Anal. Chem.* **1982**, *54*, 101.
(7) Mimms, L. T.; McKnight, M. A.; Murray, R. W. *Anal. Chim. Acta* **1977**, *89*, 355.
(8) Lochmüller, C. H.; Marshall, S. F.; Wilder, D. R. *Anal. Chem.* **1980**, *52*, 19.
(9) Lochmüller, C. H.; Hill, W. B., Jr. *Anal. Chim. Acta* **1984**, *157*, 65.
(10) Bayer, E.; Albert, K.; Reiners, J.; Nieder, M.; Müller, D. *J. Chromatogr.* **1983**, *264*, 197.
(11) Gilpin, R. K.; Gangoda, M. E. *Anal. Chem.* **1984**, *56*, 1470.
(12) Sindorf, D. W.; Maciel, G. E. *J. Am. Chem. Soc.* **1983**, *105*, 3767.
(13) Lochmüller, C. H.; Marshall, D. B.; Harris, J. M. *Anal. Chim. Acta* **1981**, *131*, 263.
(14) Lochmüller, C. H.; Marshall, D. B.; Wilder, D. R. *Anal. Chim. Acta* **1981**, *130*, 31.
(15) Bauer, R. K.; Borenstein, R.; de Mayo, P.; Okada, K.; Rafalska, M.; Ware, W. R.; Wu, K. C. *J. Am. Chem. Soc.* **1982**, *104*, 4635.
(16) Francis, C.; Lin, J.; Singer, L. A. *Chem. Phys. Lett.* **1983**, *94*, 162.
(17) Bauer, R. K.; de Mayo, P.; Okada, K.; Ware, W. R.; Wu, K. C. *J. Phys. Chem.* **1983**, *87*, 460.
(18) Levitz, P.; Van Damme, H.; Keravis, D. *J. Phys. Chem.* **1984**, *88*, 2228.
(19) Beck, G.; Thomas, J. K. *Chem. Phys. Lett.* **1983**, *94*, 553.
(20) Chandrasekaran, K.; Thomas, J. K. *J. Am. Chem. Soc.* **1983**, *105*, 6383.
(21) Chandrasekaran, K.; Thomas, J. K. *J. Colloid Interface Sci.* **1984**, *100*, 116.
(22) Della Guardia, R. A.; Thomas, J. K. *J. Phys. Chem.* **1984**, *88*, 964.
(23) Kalyanasundaram, K.; Thomas, J. K. *J. Am. Chem. Soc.* **1977**, *99*, 2039.
(24) Rowlinson, J. S.; Swinton, F. L. "Liquids and Liquid Mixtures", 3rd ed.; Butterworth & Co: London, 1982.
(25) Ståhlberg, J.; Almgren, M., in preparation.
(26) Rosen, M. J. "Surfactants and Interfacial Phenomena"; Wiley: New York, 1978.
(27) Slaats, E. H.; Markovski, W.; Fekete, J.; Poppe, H. *J. Chromatogr.* **1981**, *207*, 299.

RECEIVED for review October 15, 1984. Accepted December 10, 1984.

# Interface of a Microbore High-Performance Liquid Chromatograph with a Diffuse Reflectance Fourier Transform Infrared Spectrometer

**Christine M. Conroy**[1] **and Peter R. Griffiths***
*Department of Chemistry, University of California, Riverside, California 92521*

**Kiyokatsu Jinno**
*School of Materials Science, Toyohashi University of Technology, Toyohashi 440, Japan*

**Some of the problems commonly encountered in high-performance liquid chromatography (HPLC)/Fourier transform infrared spectrometry (FT-IR) can be alleviated through the use of microbore HPLC (μHPLC) columns. An interface based on a solvent elimination technique and utilizing the microsampling capability of diffuse reflectance (DR) FT-IR has been designed for use with μHPLC. Detection limits achieved with the interface are about an order of magnitude lower than those previously reported. Several different microbore columns were studied and the relative advantages and disadvantages of each, with respect to the interface, are discussed.**

Over the past decade, several authors have reported interfaces between a high-performance liquid chromatograph (HPLC) incorporating conventional 4.6 mm internal diameter (i.d.) columns and a Fourier transform infrared (FT-IR) spectrometer. Two fundamentally different types of HPLC/FT-IR interfaces have been developed. In the first the effluent from the column is passed directly through a flow cell (*1–4*), while the second approach involves the use of solvent elimination techniques (*5–7*). In both approaches, the high flow rate required for 4.6 mm i.d. columns (typically about 1 mL/min) has represented a major limitation. When flow cells are used, minor peaks elute at a concentration which is well below the detection limit for FT-IR absorption spectrometry. This is partly because of reduced transmittance in the spectral regions where the solvent absorbs and partly because only a very small fraction of each eluate is present in the flow cell at any instant during the measurement. In solvent elimination techniques, the generation of large volumes of solvent vapor presents an environmental hazard unless great care is taken.

The development of columns of smaller cross-sectional area has allowed the use of lower flow rates to achieve the same linear velocity and approximately the same chromatographic resolution as 4.6-mm columns with the same packing (*8–10*). Microbore columns have internal diameters between 0.25 and 2 mm, so that they operate with flow rates between 3 and 200 μL/min. The low flow rates required for microbore HPLC (μHPLC) have permitted on-line mass spectrometry with direct liquid introduction (*11–13*) and several other detection systems which only operate at high efficiency when the flow rate is significantly less than 1 mL/min (*14*). It has also been noted (*15*) that the use of expensive solvents becomes less prohibitive as the flow rate decreases. As a result of the lower flow rates, the increased concentration of minor components, and the possibility of using deuterated solvents, the use of microbore HPLC also alleviates several of the problems associated with HPLC/FT-IR interfaces using flow cells. The first μHPLC/FT-IR measurement using a flow cell was reported by Teramae and Tanaka (*16*), in which a two-component mixture was separated by size exclusion chromatography (SEC) using $CCl_4$ as the mobile phase. Subsequently Brown and Taylor (*15*) reported a normal-phase μHPLC/FT-IR measurement of phenols and amines separated on a 1 m × 1 mm i.d. PAC column using $CDCl_3$ as the mobile phase, while Amateis and Taylor (*17*) used an amino bonded phase microbore column for the separation of aromatic bases. Injected minimum detectable quantities for the stronger solute bands were approximately 1 μg.

Because of the high density (1.48 g/mL) and viscosity (0.58 cP) of chloroform relative to hexane (0.66 g/mL and 0.32 cP, respectively), chloroform is not commonly used as a mobile phase for normal-phase (NP) HPLC; indeed it can only be used at all when rather polar molecules are to be separated. It is much more common to use hexane, sometimes in conjunction with a polar modifier such as methanol, 2-propanol, or ethyl acetate, as the mobile phase for NP-HPLC. The absorptivities of the major absorption bands of hexane and each of the modifiers are significantly stronger than those of chloroform at all wavenumbers above 850 $cm^{-1}$. A flow cell with a shorter path length is therefore needed for hexane-based mobile phases. Typical path lengths are 100–200 μm for hexane and 500 μm for chloroform (*18*). As a result, the detection limits for NP-HPLC/FT-IR using hexane as the mobile phase are at least twice those found for chloroform. The very polar solvents used for reverse-phase (RP) HPLC absorb infrared radiation much more strongly than any of the solvents listed above. Thus few RP-HPLC/FT-IR measurements using flow cells have been reported. Recently, however, Jinno et al. (*19*) reported reversed-phase μHPLC/FT-IR data using a flow cell, with a mobile phase of 90% $CD_3CN$ and 10% $D_2O$. Although much of the fingerprint region of the spectrum was obscured, C—H and C=O stretching modes could be observed.

The first μHPLC/FT-IR results using solvent elimination techniques were also reported by Jinno and his co-workers (*20, 21*). Applications both of SEC, using tetrahydrofuran as the mobile phase, and normal-phase adsorption chromatography, using hexane/dichloromethane mixtures, were reported. In this work the column effluent was deposited on a KBr plate which was slowly translated across the exit of the column. Each eluate was deposited as a "buffer memory" on the plate. After the chromatogram was complete, the plate was simply transferred to the spectrometer and transmittance spectra were measured continuously across the region of the plate where the peaks had been deposited. Detection limits are usually between 100 ng and 1 μg, and no spectral region is obscured by the solvent.

The use of microbore columns does, of course, present several disadvantages for μHPLC/FT-IR measurements. The principal problem is the capacity of the columns which is often

---

[1] Present address: Alcoa Technical Center, Alcoa Center, PA 15069.

0003-2700/85/0357-0822$01.50/0 © 1985 American Chemical Society

equal to, or even less than, the detection limits of the spectrometer. Column capacity decreases in proportion to cross-sectional area, thus the capacity of a 1 mm i.d. column is 20 times less than that of a 4.6 mm i.d. column. These columns are also susceptible to severe extracolumn band broadening (*22, 23*) and care must be taken to minimize dead volume if chromatographic resolution is to be maintained.

We believe that in view of the excellent microsampling capability of diffuse reflectance (DR) infrared spectrometry, the detection limits of the buffer memory μHPLC/FT-IR technique could be reduced if the peaks could be efficiently deposited on a powdered alkali halide in an analogous fashion to the early HPLC/FT-IR interface reported by Kuehl and Griffiths for 4.6 mm i.d. columns (*5*). In this paper we report the measurement of μHPLC/FT-IR spectra using a device based on this principle. Detection limits of less than 10 ng can be achieved, which is over an order of magnitude less than the capacity of 1 mm i.d. microbore columns.

## EXPERIMENTAL SECTION

**Chromatography.** Three microbore columns of different dimensions were used. These were a 1 mm i.d. × 500 mm long stainless steel column packed with 10-μm silica (Alltech Associates, Waukegan, IL) and two poly(tetrafluoroethylene) (PTFE) columns (0.5 mm × 120 mm and 0.35 mm × 150 mm) also packed with 10-μm silica. These columns were fabricated at Toyohashi University of Technology. A Gilson Model 302 pump, Kratos Model SF 769 variable wavelength detector equipped with a 0.5-μL flow cell, and a Rheodyne 7413 injection valve equipped with a 1-μL loop were used with the Alltech column. All separations on the PTFE columns were effected with a Familic 100 microbore liquid chromatograph (JASCO International, Easton, MD).

**Spectrometry.** FT-IR spectra were measured with a Digilab Model 296 interferometer, a medium range ($\nu_{\min}$ = 600 cm$^{-1}$) mercury cadmium telluride detector (Infrared Associates, New Brunswick, NJ), and an optical system for DR spectrometry which has been described previously (*24*). Spectra were acquired at a nominal resolution of either 4 cm$^{-1}$ or 8 cm$^{-1}$, and 64 or 256 scans were signal averaged. Powdered KCl was used as the substrate for sample deposition and also as the reference material. For most measurements the optical system was not purged with dry air because of a major and long-term problem with air dryers in our laboratory, so that evidence of atmospheric water vapor is seen in several spectra.

**Solvents and Chemicals.** Solvents were all HPLC Grade and were obtained from Fisher Scientific. Stahl's test dye solution was purchased from Alltech Associates; this is a three-component mixture containing Butter Yellow, Indophenol Blue, and Sudan Red, each present at 0.1% in benzene. All other chemicals were Reagent Grade; their purity as estimated by HPLC was always better than 95%.

**μHPLC/FT-IR Interface.** An interface designed for the measurement of DR spectra of peaks eluting from microbore columns was constructed. This interface was based on the principle developed previously by Kuehl and Griffiths (*5, 6*) but with several modifications to facilitate operation with the low flow rates of μHPLC. The carousel comprised a light aluminum annulus, 120 mm in diameter, in which 180 cups were drilled. Each cup was 2.0 mm in diameter and 2.5 mm deep. In view of the low flow rates involved, the sample concentration step was eliminated. A 0.25 mm i.d. stainless steel capillary, which was bent to an angle of 65° to the vertical, was attached to the end of the column. A drop monitor was mounted at the exit of this tube; it consisted of a light-emitting diode on one side and a photodiode on the other. Only one drop was allowed to fall on each cup. After each drop had fallen, the carousel was rotated by exactly 2° using a stepping motor so that the next cup was in place to receive the subsequent drop. From the drop rate and the flow rate of the mobile phase, the size of each drop was calculated to be between 8 and 10 μL.

The best results both in terms of base line flatness and band intensity were found when the KCl was tamped gently into each cup rather than being loosely packed. The carousel was preheated under an infrared heat lamp so that when the solute was deposited the solvent evaporated rapidly. In this way the sample was contained in the top millimeter of KCl powder, thereby maximizing the sensitivity of the measurement (*24*). Occasionally the sample cups were heated both before and after deposition to ensure complete evaporation of the solvent prior to the infrared measurement. In practice this precaution was rarely found to be necessary, and the spectra shown in this paper were all measured by preheating the cup but without the postheating step.

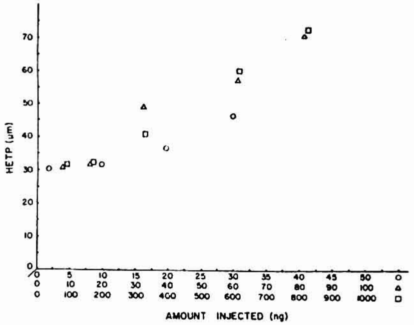

**Figure 1.** Plot of HETP vs. amount injected for (□) 500 mm × 1 mm column, (△) 120 mm × 0.5 mm column and (○) 150 mm × 0.35 mm column. The probe was nitrobenzene and it had *k′* values of 1.25, 1.32, and 1.26, respectively. The mobile phase was 2% methanol in hexane and the flow rates were close to the optimum linear velocity for each column, 45, 15, and 6 μL/min, respectively.

## RESULTS AND DISCUSSION

If an HPLC/FT-IR interface is to be used to identify the components of complex mixtures, the spectra of both major and minor components must be able to be measured. The capacities of the columns were determined by plotting the height equivalent to a theoretical plate (HETP) against the quantity of sample injected, as shown in Figure 1. For each column, solutions of nitrobenzene in hexane were eluted by using 2% methanol in hexane as the mobile phase. The *k′* values for the nitrobenzene peak separated on the 1 mm, 0.5 mm, and 0.35 mm i.d. columns were 1.25, 1.32, and 1.26, respectively. For all three columns, the limiting HETP for low injected quantities was 30 μm (i.e., about 3 particle diameters). The column capacities, defined as the quantity required to increase the HETP by 10%, were 230 ng, 23 ng, and 14 ng, respectively. Sample capacities would be expected to increase considerably at higher values of *k′* and with smaller particle size packings.

The 1 mm i.d. column was used for the initial μHPLC/FT-IR investigations since its capacity was so much larger than that of either of the PTFE columns. A chromatogram of Stahl's test dye solution, measured with an ultraviolet detector, is shown in Figure 2. Spectra of two of the components (Butter Yellow and Indophenol Blue) are shown in Figure 3. The difference in intensity of these two spectra illustrates the well-known fact that HPLC/FT-IR detection limits depend on both the nature of the analyte and its retention time. Not only are the absorptivities of the stronger bands in the spectrum of Butter Yellow somewhat greater than those for Indophenol Blue, but under these chromatographic conditions the full width at half height (fwhh) of the Indophenol Blue peak is about 1.5 times that of the Butter Yellow peak. The broader peaks can elute over several drops, so that although equivalent amounts of sample were injected, the quantities collected per cup may be quite different. Ideally gradient elution techniques should be applied to make the fwhh of all

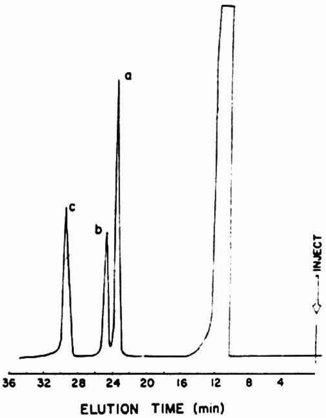

**Figure 2.** Chromatogram of Stahl's dye separated into its three components (a) Sudan Red, (b) Butter Yellow, and (c) Indophenol Blue using a 500 mm × 1 mm 10 μm silica gel column with mobile phase of 2% methanol in hexane at a flow rate of 40 μL/min.

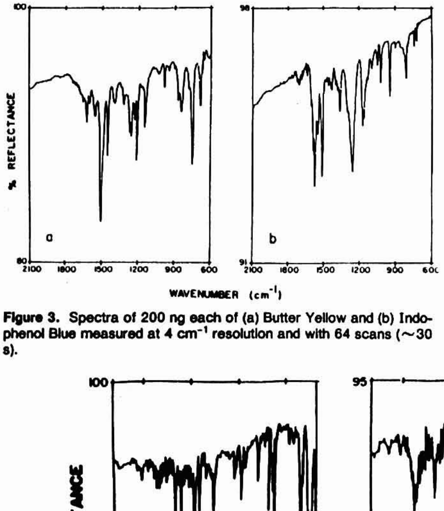

**Figure 3.** Spectra of 200 ng each of (a) Butter Yellow and (b) Indophenol Blue measured at 4 cm$^{-1}$ resolution and with 64 scans (~30 s).

peaks identical throughout the chromatogram, but in practice this goal is not readily achieved for μHPLC.

Another major problem with depositing amounts of μHPLC eluates less than 100 ng is the fact that impurities and atmospheric absorption bands can lead to severe interferences in the DR spectrum. To illustrate the effect of these problems, the spectra of decreasing amounts of tetraphenylporphyrin injected into the chromatograph are shown in Figure 4. Although the strongest bands below 1200 cm$^{-1}$ are still observable at greater than three times the noise level, lines in the vibration–rotation spectrum of atmospheric water vapor are beginning to obscure much of the spectral region between 1900 and 1300 cm$^{-1}$ when less than 75 ng of tetraphenylporphyrin is in injected. (It should be remembered that these measurements were made on a poorly purged instrument.) Since one of the major advantages of FT-IR spectrometry over other detection systems is its capability to identify unknowns, it is important that no spectral region should be obscured, whether by atmospheric interferences or by solvent bands.

The most crucial step in the interface is undoubtedly the deposition of the analyte. The problems that can occur may be demonstrated by comparing μHPLC/FT-IR spectra obtained by using the 0.5 mm i.d. PTFE column and the 1 mm i.d. stainless steel column. At the very low flow rates required with the 0.5 mm column (typically 10 μL/min), it was found to be very difficult to deposit the solute efficiently. Apparently the eluent creeps up the outside of the stainless steel capillary mounted at the end of the column. We believe that some of the solvent evaporates, leaving a fraction of solute deposited on the outer surface of the capillary. It is also possible that solutes having an appreciable vapor pressure can evaporate along with the solvent.

To illustrate the difference in performance associated with low flow rates, a mixture of nitrobenzene and 4-chloronitrobenzene was separated by using the 1 mm and 0.5 mm columns. The same mobile phase and linear velocity was employed for each separation. The spectra of 4-chloronitrobenzene obtained during these runs are shown in Figure 5. Spectra are not shown above 2000 cm$^{-1}$ for these molecules in view of the low absorptivities of the aromatic C–H stretching bands near 3050 cm$^{-1}$ and the lack of any other fundamentals in the region between 2000 and 4000 cm$^{-1}$. (Even poorer spectra were obtained when the 0.35 mm i.d. PTFE column was used.) The results seem to indicate that the higher flow rates which can be tolerated by the 1-mm

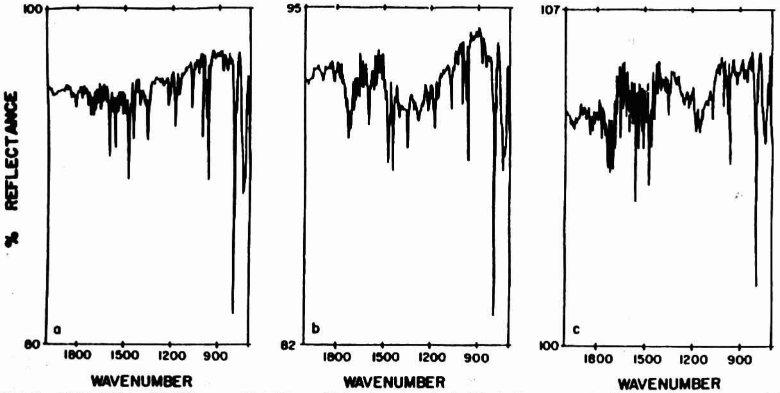

**Figure 4.** Spectra of (a) 500 ng, (b) 125 ng, and (c) 75 ng of tetraphenylporphyrin (injected), measured with 4 cm$^{-1}$ resolution and 256 scans after elution from a 120 mm × 0.5 mm 10 μm silica gel PTFE column using a 90:10 chloroform:acetone mobile phase.

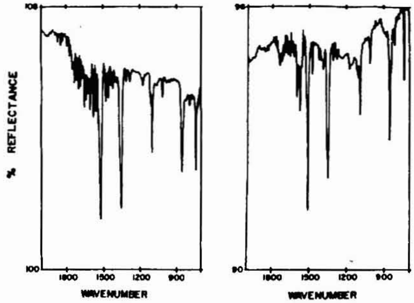

**Figure 5.** Spectra measured with 8 $cm^{-1}$ resolution and 128 scans of (left) 10 ng and (right) 15 ng of 4-chloronitrobenzene separated on a 1.0 mm i.d. and a 0.5 mm i.d. column, respectively. The mobile phase was 2% methanol in hexane and the flow rates were 35 $\mu$L/min and 10 $\mu$L/min, respectively.

column improve the deposition characteristics, since a smaller fraction of the solvent evaporates while each drop is being formed. The signal-to-noise ratio of the spectrum of 10 ng of 4-chloronitrobenzene is sufficiently good that we hoped to be able to obtain a recognizable spectrum from 1 ng of this material. We were not able to achieve this goal, presumably because of evaporation by the solute. Indeed evaporation of the solute appears to be the fundamental limitation of $\mu$HPLC/FT-IR for small molecules.

A conservative estimate for the dynamic range of the $\mu$HPLC/FT-IR interface for the 1 mm column, i.e., the ratio of the column capacity at low $k'$ to the detection limit, is about 20:1. This is almost an order of magnitude better than that of any $\mu$HPLC/FT-IR interface which has been reported previously and is obviously the result of the significantly decreased detection limits.

At this time we believe that we are in a position to judge whether the use of microbore columns has extended the usefulness of HPLC/FT-IR interfaces using solvent elimination techniques. For this purpose we may compare the data obtained with the 1 mm i.d. microbore column reported in this paper with the results obtained earlier with conventional (4.6 mm i.d.) columns (*5*). Detection limits are about ten times lower for the 1 mm column, while the capacity of the 4.6 mm column is $(4.6)^2$, i.e. 20, times greater. Thus the dynamic range of the "conventional" HPLC/FT-IR interface is slightly greater than that of the $\mu$HPLC/FT-IR system. The chromatographic resolution of the two columns is about the same, being determined by the particle diameter of the packing. Thus in spite of the excellent detection limits reported in this paper, the main practical advantage of the $\mu$HPLC/FT-IR interface over previous HPLC/DR-FT-IR systems is related to the reduced solvent consumption.

It is interesting to speculate on the application of the technique described in this paper for microbore reverse-phase HPLC. Certainly the use of KCl as a substrate is inappropriate for direct RP-HPLC/FT-IR measurements; substrates which are insoluble in water, in particular diamond powder (*25, 26*), would seem to be more suitable. Rapid elimination of the solvent with a nebulizer (*27*) or thermospray (*26*) followed by deposition of the solute on diamond powder has been demonstrated using 4.6 mm i.d. RP-HPLC columns. An analogous technique should be applicable for RP-$\mu$HPLC/FT-IR after relatively minor modifications. Similarly the technique developed by Kalasinsky et al. (*28*) in which water in the column effluent is reacted with 2,2′-dimethoxypropane before elimination of the remaining organic solvents should also be able to be scaled down for RP-$\mu$HPLC/FT-IR.

In summary, the use of the 1 mm i.d. columns with their intermediate flow rates (20–50 $\mu$L/min) and intermediate capacities (200–300 ng) appears to be the best compromise in the construction of a simple yet sensitive HPLC/FT-IR interface. This interface allows the detection of both major and minor components eluting from this column and there is little problem evaporating and disposing of the mobile phase at these relatively low flow rates.

## ACKNOWLEDGMENT

We wish to thank JASCO International for the loan of the Familic 100 chromatograph.

**Registry No.** DMMP, 756-79-6; TMP, 512-56-1; DIMP, 1445-75-6.

## LITERATURE CITED

(1) Vidrine, D. W. *J. Chromatogr. Sci.* **1979**, *17*, 477.
(2) Shafer, K. H.; Lucas, S. V.; Jakobsen, R. J. *J. Chromatogr. Sci.* **1979**, *17*, 464.
(3) Brown, R. S.; Hausler, D. W.; Taylor, L. T.; Carter, R. C. *Anal. Chem.* **1981**, *53*, 197.
(4) Johnson, C. C.; Taylor, L. T. *Anal. Chem.* **1983**, *55*, 436.
(5) Kuehl, D. T.; Griffiths, P. R. *J. Chromatogr. Sci.* **1979**, *17*, 471.
(6) Kuehl, D. T.; Griffiths, P. R. *Anal. Chem.* **1980**, *52*, 1394.
(7) Conroy, C. M.; Griffiths, P. R.; Duff, P. J.; Azarraga, L. V. *Anal. Chem.* **1984**, *56*, 2636.
(8) Scott, R. P. W.; Kucera, P. J. *J. Chromatogr.* **1979**, 169, 51.
(9) Ishii, D.; Asai, K.; Hibi, K.; Jonokuchi, T.; Nagaya, M. *J. Chromatogr.* **1977**, *144*, 157.
(10) Novotny, M. *Anal. Chem.* **1979**, *51*, 1807.
(11) Krien, P.; Devant, G.; Hardy, M. *J. Chromatogr.* **1981**, *251*, 129.
(12) Henion, J. D.; Maylin, G. A. *Biomed. Mass Spectrom.* **1980**, *7*, 115.
(13) Shafer, K. M.; Levsen, K. *J. Chromatogr.* **1981**, *206*, 245.
(14) McGuffin, V. L.; Novotny, M. *Anal. Chem.* **1981**, *53*, 946.
(15) Brown, R. S.; Taylor, L. T. *Anal. Chem.* **1983**, *55*, 1492.
(16) Teramae, N.; Tanaka, S. *Spectrosc. Lett.* **1980**, *13*, 117.
(17) Amateis, P. T.; Taylor, L. T. *Anal. Chem.* **1984**, *56*, 966.
(18) Vidrine, D. W. In "Fourier Transform Infrared Spectroscopy: Applications to Chemical Systems"; Ferraro, J. R.; Basile, L. J., Eds.; Academic Press: New York, 1979; Chapter 4.
(19) Jinno, K.; Fujimoto, C.; Uematsu, G. *Am. Lab.* (*Fairfield, Conn.*) **1983**, *16* (2), 39.
(20) Jinno, K.; Fujimoto, C. *HRC CC, J. High Res. Chromatogr. Chromatogr. Commun.* **1981**, *4*, 532.
(21) Jinno, K.; Fujimoto, C.; Ishii, D. *J. Chromatogr.* **1982**, *239*, 625.
(22) Jinno, K.; Fujimoto, C. *HRC CC, J. High Res. Chromatogr. Chromatogr. Commun.* **1980**, *3*, 313.
(23) Tsuda, T.; Novotny, M. *Anal. Chem.* **1978**, *50*, 632.
(24) Fuller, M. P.; Griffiths, P. R. *Appl. Spectrosc.* **1980**, *34*, 533.
(25) Brackett, J. M.; Azarraga, L. V.; Castles, M. A.; Rogers, L. B. *Anal. Chem.* **1984**, *56*, 2007.
(26) Griffiths, P. R.; Conroy, C. M. *Adv. Chromatogr.*, in press.
(27) Azarraga, L. V. Paper presented at the Eastern Analytical Symposium, New York, 1983.
(28) Kalasinsky, K. S.; Smooter Smith, J. A.; Kalasinsky, V. F. Paper No. 659, Pittsburgh Conference on Analytical Chemistry and Applied Spectroscopy, Atlantic City, NJ, 1984.

RECEIVED for review August 3, 1984. Accepted December 26, 1984. Although the information in this document has been funded in part by the United States Environmental Protection Agency under assistance agreement CR-810430 to the University of California, Riverside, it does not necessarily reflect the views of the agency and no official endorsement should be inferred.

*Anal. Chem.* **1985,** *57,* 826–829

# Pulse Residence in Short Chromatographic Columns

**Dwight W. Underhill**

*Department of Industrial and Environmental Health Sciences, Graduate School of Public Health, University of Pittsburgh, Pittsburgh, Pennsylvania 15261*

**By a simple geometric construction the mean residence time in linear chromatography is shown to be independent of the degree with which equilibrium is attained. The general relationship is that if a constant input of $m$ mol/s leads to a steady-state accumulation of $M$ moles in the column, the mean residence time for a pulse input is $M/m$ s. This leads to simple calculations of the effects of input and effluent boundary conditions on the mean residence time. Although an irreversible chemical reaction reduces the residence time, a procedure is available to determine the residence time in the absence of chemical reaction. The residence times following inputs into the mobile and stationary phases, respectively, differ by a constant.**

The calculation of pulse residence times in short chromatographic columns would appear to be complex, for in a short column severe inequilibrium may be expected between the moving and stationary phases. Furthermore boundary conditions at the inlet and outlet would, in view of the shortness of the column, have a relatively greater effect. Yet for the case of linear chromatography, many of these difficulties are a mirage. It has been known for some time that the mean residence time in a linear system—a system in which the equilibrium and diffusion coefficients are independent of concentration—should be absolutely independent of any rate constants for mass transfer (*1*, *2*). Yet research reports have appeared in which it appeared that the mean residence time was affected by mass transfer effects (*3–5*). Here we will examine some specific examples of holdup in linear chromatographic systems, showing precisely how mass transfer affected the mean residence time. Finally a general procedure will be developed which permits the mean residence time to be determined without having to solve fully the partial differential equations governing mass transfer within chromatographic columns.

## INEQUILIBRIUM BETWEEN MOVING AND STATIONARY PHASES

Young (*6*) gave an exact solution to the simplest possible model for interphase inequilibrium in a chromatographic column. His partial differential equation assumes that the mass transfer to and from the stationary phase is proportional to the concentrations in each phase, viz.

$$\frac{\partial F}{\partial x} = -\alpha\left(F - \frac{Q}{k'}\right) \tag{1}$$

where $F$ is the molar flux, defined as the moles per second flowing past the point "$x$" at a time "$t$" (mol/s), $Q$ is the uptake of sorbate in stationary phase (mol/cm), $\alpha$ is the constant for mass transfer from mobile to stationary phase ($cm^{-1}$), and $k'$ is the constant giving equilibrium uptake in the stationary phase per unit flux of sorbate in the mobile phase. $k'$ has units of s/cm. By a mass balance the uptake of sorbate in the stationary phase must be

$$Q = -\int_0^t \frac{\partial F}{\partial x}\,\mathrm{d}t \tag{2}$$

Assuming the boundary condition of a pulse input of $m$ moles into the mobile phase at $t = 0$, $x = 0$, the solution for the above equations is

$$F = me^{-N}\delta(0) + \frac{mN}{(tt')^{1/2}}e^{-N(1+(t/t'))}I_1\left(2N\left(\frac{t}{t'}\right)^{1/2}\right) \tag{3}$$

where $t' = k'L$, $N = \alpha L$, $L$ is the length of column (cm), $I_1$ is the modified Bessel function of order 1, and $\delta(0)$ is the unit delta function at time $t = 0$. The purpose of giving the above equation is to illustrate the effects of interphase mass transfer under conditions of very poor mass transfer efficiency. In eq 3, the number of theoretical plates, $N$, describes the kinetics of mass transfer within the column. The greater the number of theoretical plates, the more efficient the mass transfer. This can be seen in Figure 1, which shows breakthrough curves calculated for various values of $N$. In eq 3, the factor $e^{-N}\delta(0)$ represents the fraction of the initial input that leaves the column before passing at least once into the stationary phase. Normally this equation would be applied to columns for which $N > 100$, and in these cases the fraction of the input that passes through the column without being adsorbed at least once is negligible. But suppose that $N$ is equal to 0.5. In this case 61% of the input passes through the column unadsorbed. Yet, remarkably, the mean residence time, $t_h$, calculated from the integral

$$t_h = \int_0^\infty tF\,\mathrm{d}t \Big/ \int_0^\infty F\,\mathrm{d}t \tag{4}$$

remains unchanged and, regardless of the value for $N$, is precisely equal to $t'$. The importance of this calculation is that it shows that interphase mass transfer resistance cannot, ipso facto, alter the mean residence time. On first appearance it would seem that this conclusion is belied by eq 4 of Galán et al. (*4*), which predicts the mean residence time from an equation containing rate constants. But the two rate constants given are the forward and reverse rate constants which determine an equilibrium coefficient. And in fact the mean residence time depends on their ratio (or equilibrium coefficient) and not to the degree to which equilibrium was attained. This is just what Galan et al. want to demonstrate.

## INTERPHASE DIFFUSION

Dispersion of an injected pulse occurs also from diffusion in the mobile phase as the sorbate is transported across the column. The high diffusion coefficients of sorbates in gases make this effect especially important in gas chromatography at low carrier gas velocities.

To determine the effect that dispersion in the mobile phase has on the mean residence time, we begin with the partial differential equation describing the combined effects of diffusion and convection on concentration

$$D\frac{\partial^2 C}{\partial x^2} - V\frac{\partial C}{\partial x} = (k + 1)\frac{\partial C}{\partial t} \tag{5}$$

where $C$ is the concentration of sorbate ($mol/cm^3$), $D$ is the diffusion coefficient for the sorbate in the carrier gas ($cm^2/s$), $V$ is the interparticle carrier gas velocity (cm/s), equal to $\upsilon/\epsilon A$, $\upsilon$ is the flow of carrier gas ($cm^3/s$), $A$ is the cross-sectional area

0003-2700/85/0357-0826$01.50/0 © 1985 American Chemical Society

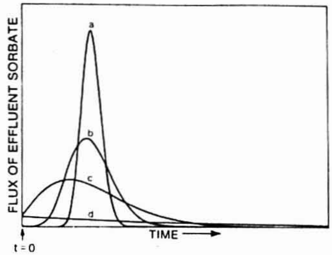

**Figure 1.** Breakthrough curves from columns having different mass transfer efficiencies. Curves a, b, c, and d show, respectively, breakthrough curves calculated from eq 3, with $N$, the number of theoretical plates, equal to 100, 20, 5, and 0.5, respectively. In the text it is shown that in spite of the effect that the value of $N$ has on the shape of the breakthrough curve, the mean retention time is independent of the value of $N$.

of column (cm$^2$), $\epsilon$ is the fractional interparticle void volume, and $k$ is the equilibrium partition coefficient between moving and stationary phases (dimensionless). The solution to this equation, for a pulse input of $m$ moles at time $t = 0$ into a seminfinite column ($0 < x < \infty$), with no mass transfer out of the column (i.e., $VC - D(\partial C/\partial x) = 0$ at $x = 0$) is

$$C = \frac{m}{\epsilon A(1+k)x}\left\{\left(\frac{2Nt'}{\pi t}\right)^{1/2} e^{-(N/2)[(t'/t)^{1/2}-(t/t')^{1/2}]^2} - Ne^{2N}\operatorname{erfc}\left[\left(\frac{N}{2}\right)^{1/2}\left(\left(\frac{t}{t'}\right)^{1/2}+\left(\frac{t'}{t}\right)^{1/2}\right)\right]\right\} \quad (6)$$

where $N = Vx/2D$ and $t' = (1+k)x/V$. The flux of sorbate in the column, now determined by the combined effects of convection and diffusion, is in general

$$F = \epsilon A\left(CV - D\frac{\partial C}{\partial x}\right) \quad (7)$$

and in particular, from eq 6, the flux becomes

$$F = \frac{m}{t}\left(\frac{Nt'}{2\pi t}\right)^{1/2} e^{-(N/2)[(t/t')^{1/2}-(t'/t)^{1/2}]^2} \quad (8)$$

From eq 4 and 8 the mean residence time in this system is now

$$t_{\mathrm{h}} = t' \quad (9)$$

Again the result is that the mean residence time is unaffected by the rate constant describing mass transfer, in this case the constant describing interparticle diffusion.

Others (*7, 8*) have used as the breakthrough curve under these conditions the results calculated from a unit pulse *concentration* input, i.e., $C_{x=0} = \delta(0)$. It turns out that with this input function the resultant equation for the concentration is identical in form with eq 8, used above to describe the flux following a pulse mole input. Further examination of this result shows that instead of a finite mole input, the boundary conditions now demand that there be an input of an infinite number of moles, with all but an infinitely small fraction being resorbed at the point of input. This is not a realistic model of the results following a finite input into a column with essentially no resorption at the point of input.

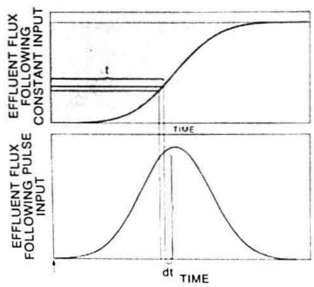
EFFLUENT FLUX FOLLOWING CONSTANT INPUT
t
TIME
EFFLUENT FLUX FOLLOWING PULSE INPUT
dt
TIME

**Figure 2.** Geometric relationship between breakthrough curves obtained from constant and pulse inputs. See text for procedure used to determine mean residence time from the geometrical relationship between these curves.

## STEADY-STATE MODEL

There is a simple geometric construction that shows it is reasonable to expect residence time to be independent of all factors describing rates of mass transfer in the column. Figure 2 shows two breakthrough curves describing mass transfer within two identical columns, the difference being that the lower curve resulted from a unit pulse input at time $t = 0$ whereas the upper curve was from a constant input of one unit per second, also starting at $t = 0$. Because (1) these columns behave as a linear system and (2) the constant input is mathematically the integral of the pulse input, then the output from the constant input must be precisely the integral of the output from the pulse input. From the integral/differential relationship between the two curves, the width of the differential strip, d$F$, in the upper curve is equal to the area of the differential strip, $F\,\mathrm{d}t$, in the lower curve. As the length of the upper differential strip is equal to $t$, the area of this differential strip must therefore be equal to $tF\,\mathrm{d}t$, which was used earlier in eq 4 to define the mean residence time. Therefore, the stippled area in the upper curve, which corresponds exactly to the value of the integral in eq 4, must equal the mean residence time. By a mass balance this must also be equal to the sorbate retained in the column at steady state. The general relationship between accumulated mass and residence time is that if following a constant input of $m$ moles per second of sorbate, $M$ moles accumulate in the column at steady state, then the mean residence time in the column for a pulse input is $M/m$ seconds. This allows us to use steady-state retention in a column, which must be independent of all rate constants, to determine *exactly* the mean residence time of an injected pulse. All that is necessary is that mass transfer within the column be described by linear partial differential equations. This proof is still valid if the carrier gas velocity and adsorption coefficients vary as a function of position within the column.

Huang and Madey (*3*) give through a series of complex, approximate calculations, results that state that the mean residence time of a pulse in a linear system may be affected by incomplete mass transfer. The general proof given above shows that such a conclusion must be in error.

## EDGE EFFECTS

Suppose the chromatographic column were not closed at $x = 0$, but instead were to extend infinitely in both the $+x$ and $-x$ directions. We feel from experience that even if the volume of the column in the upstream direction were infinite, the residence time would remain finite, although somewhat larger than if upstream diffusion were not permitted. Figure 3 shows the differences resulting from permitting upstream diffusion. The simplest way to calculate the effect that this has on the overall residence time is to use the steady-state model developed in the previous section. At steady state the

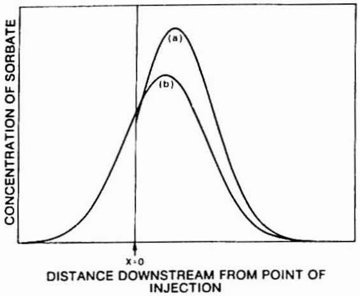

**Figure 3.** Effect of boundary conditions on spatial distribution of sorbate. Both curves show the combined effect of convection and diffusion on a pulse of sorbate injected earlier at $X = 0$. For curve A an impervious barrier was at $X = 0$, whereas for curve B no such barrier existed.

partial differential equation in $x$ and $t$ that described mass transfer now reduces to the ordinary differential equation

$$D\frac{d^2C}{dx^2} - V\frac{dC}{dx} = 0 \tag{10}$$

The general solution to this equation is

$$C = a + b\exp\left(\frac{Vx}{D}\right) \tag{11}$$

For positive values of $x$ (i.e. after the point of injection), $b$ must be equal to 0 to keep the solution finite and the obvious solution for this half of the column is

$$C = m/v \tag{12}$$

But for negative values of $x$, $C$ must decrease to 0 with increasingly negative values of $x$. Here then

$$C = \left(\frac{m}{v}\right)\exp\left(\frac{Vx}{D}\right) \tag{13}$$

Integration gives the moles of sorbate upstream of the point of injection as

$$M = \frac{m(1 + k)D}{V^2} \tag{14}$$

In the previous section a direct relationship was established between the moles retained at steady state and the residence time for a pulse input. From this relationship the increased residence time for a pulse input is

$$t_h = \frac{(1 + k)D}{V^2} \tag{15}$$

As a sample calculation, if we take $D = 0.1$ cm$^2$/s, $V = 10$ cm/s, and $k = 1000$, then diffusion upstream will increase the observed residence time for a pulse input by 1.0 s, which is small but perhaps detectable in some systems.

Because Kucera (5) assumed an infinite column, we would expect that edge effects would contribute to his calculated mean residence time, and in fact this is what his equations show.

Theoretically the opposite effect—a decrease in residence time—could occur if at the effluent end of the column a detector were placed which acted as a perfect sink for the sorbate. For such a case it turns out that the decrease in residence time is exactly the same magnitude as the increase in residence time given by eq 15.

## IRREVERSIBLE CHEMICAL REACTION

The above relationships do not hold if there is an irreversible chemical reaction taking place with the sorbate as it passes through the column. Such a chemical reaction reduces the measured residence time by selectively removing those molecules that otherwise would be retained the longest in the column, thereby biasing the result toward those molecules having shorter residence times. This effect can be illustrated by an example. For a column filled with a homogeneous spherical packing which not only adsorbs but also reacts irreversibly in a first-order reaction with the sorbent, the residence time of an injected pulse is reduced by a percent equal to (*9*)

$$R = 100\left\{1 - \frac{1 + \frac{3k}{2}\left(\frac{\coth\phi}{\phi} - \operatorname{csch}^2\phi\right)}{(1 + k)\left[1 + \frac{12\beta D}{V^2}\left(\frac{\coth\phi}{\phi} - \frac{1}{\phi^2}\right)\right]^{1/2}}\right\} \tag{16}$$

where $R$ is the percent reduction in residence time (dimensionless), $D_p$ is the intraparticle diffusion coefficient (cm$^2$/s), $d$ is the particle diameter (cm), $\beta$ is the first-order reaction constant (s$^{-1}$), $\phi = (\beta d^2/4D_p)^{1/2}$, and $D$, $V$, and $k$ are defined as before. A similar result was derived by Galan et al. (*4*). Note that the percent reduction in residence time does not depend on column length, although it does depend on other factors including the reaction rate and the carrier gas velocity.

The simplest procedure for determining the "true" residence time in the presence of an irreversible first-order chemical reaction is to multiply the effluent at each time, $t$, by a correction factor, $e^{\lambda t}$, such that the "corrected" effluent has the same mass as the input. Specifically, after finding the value of $\lambda$, such that the measured flux, following an input of $m$ moles, when integrated with $e^{\lambda t}$, gives

$$m = \int_0^\infty e^{\lambda t}F(t)\,dt \tag{17}$$

the mean residence time in the absence of chemical reaction is then estimated as

$$t_h = \int_0^\infty e^{\lambda t}tF(t)\,dt/m \tag{18}$$

This correction procedure has the effect of removing the bias against the slower moving molecules.

## STATE OF INJECTED SORBATE

It can make a difference if the sorbate is injected into the stationary rather than the mobile phase. As an example, Perry et al. (*10*) using the same differential equation for mass transfer as Young, but assuming instead that the injected material is added to the stationary phase, calculate the flux to be

$$F = \frac{mN}{t'}e^{-N[1+(t/t')]}I_0\left[2N\left(\frac{t}{t'}\right)^{1/2}\right] \tag{19}$$

One noteworthy difference between this equation and eq 3 is that now there is no initial rapid movement in the mobile phase (no $\delta(0)$ term). Instead there is an exponentially decreasing factor at $x = 0$ representing the transfer of the injected sorbate into the mobile phase. The mean retention time, as calculated from eq 4 and 19, is

$$t_h = t' + t'/N \tag{20}$$

The second term results from the finite time required for the injected sorbate to pass into the mobile phase.

For large values of $N$, Perry et al. suggest using the approximation

$$F \approx \frac{m(N/\pi)^{1/2}e^{-N[1-(t/t')^{1/2}]^2}}{2t^{1/4}(t')^{3/4}} \tag{21}$$

which under the same conditions should be an equally good approximation to Young's equation. But in a short column where this approximation is not valid, differences brought about by the state of the injected sorbate might be noted.

## LITERATURE CITED

(1) Gibilaro, L. G. *Nature (London)* **1977**, *270*, 47–48.
(2) Buffham, B. A. *Proc. R. Soc. London, Ser. A* **1973**, *333*, 89–98.
(3) Huang, Jan-Chan; Madey, Richard *Anal. Chem.* **1982**, *54*, 326–328.
(4) Galan, M. A.; Suzuki, M.; Smith, J. M. *Ind. Eng. Chem. Fundam.* **1975**, *14*, 273–275.
(5) Kucera, Eugene *Chromatography* **1965**, *19*, 237–248.
(6) Young, J. K. "Gas Chromatography 1957"; Academic Press: New York, 1958; Chapter 2.
(7) Wicar, Stanislav; Novak, Josef; Ruseva-Rakshieva, Nedjalka *Anal. Chem.* **1971**, *43*, 1945–1950.
(8) Madey, Richard; Fiore, Ronald A.; Pflumm, Eugene; Stephenson, Thomas *Trans. Am. Nucl. Soc.* **1962**, *5*, 465–466.
(9) Underhill, Dwight W. U.S. AEC Report CONF-700816, 1970, pp 600–606.
(10) Perry, Robert H. "Chemical Engineers' Handbook", 4th ed.; McGraw-Hill: New York, 1963; Chapter 2.

RECEIVED September 20, 1984. Accepted December 26, 1984. This study was supported by NIOSH Grant 1 R01 OHO1644-01.

# Potassium Hydroxide Eluent for Nonsuppressed Anion Chromatography of Cyanide, Sulfide, Arsenite, and Other Weak Acids

**Tetsuo Okada* and Tooru Kuwamoto**

*Department of Chemistry, Faculty of Science, Kyoto University, Sakyo-ku, Kyoto 606, Japan*

**Potassium hydroxide solution was found to be an effective eluent for nonsuppressed anion chromatography. Polyvalent ions, $SCN^-$, and $ClO_4^-$, which are strongly retained by an anion-exchange resin, could not be quantitatively measured, because potassium hydroxide was too weak an eluent. However, this method was applicable to the determination of 15 inorganic monovalent anions ($F^-$, $Cl^-$, $ClO_3^-$, $Br^-$, $BrO_3^-$, $I^-$, $IO_3^-$, $NO_3^-$, $NO_2^-$, $CN^-$, $HS^-$, $CNO^-$, $BF_4^-$, silicate, arsenite). The main advantage is that weak acids of $pK_a > 7$ (cyanide, sulfide, arsenite, silicate, and phenol compounds) which cannot be detected by conventional ion chromatography using a conductivity detector can be determined by this method. The detection limits for cyanide, sulfide, and arsenite were 0.1 ppm, 0.1 ppm, and 0.2 ppm (as As), respectively.**

Since ion chromatography (IC) was introduced by Small et al. (*1*) in 1975, it has been applied to the analysis of anions and cations in various fields (*2–6*). To improve problems with column efficiency and conductivity detection, other systems for the anion analyses, such as ion-exchange chromatography or reversed-phase chromatography with UV (*7, 8*), electrochemical (*9–12*), and atomic absorption spectrometric (*13–16*) detectors, have been developed recently. However, IC using a conductivity detector is still a powerful method for anion analysis which has often proved difficult and tedious using conventional analytical methods. IC has been applied to the determination of organic (*17*) and oxo acids (*18, 19*) in addition to some common inorganic anions ($F^-$, $Cl^-$, $Br^-$, $NO_2^-$, $NO_3^-$, etc.). With suppressed IC, weak acids of $pK_a > 7$ could not be detected because the conductance of the effluent was measured in a neutral or acidic solution (*20*). Nonsuppressed IC using a basic eluent permitted detection of weak acids but the determination of cyanide, sulfide, and arsenite has been shown to be inadequate.

The authors previously reported the nonsuppressed IC of anions using a potassium hydroxide eluent (*3, 17, 21, 22*). This method has two advantages. First, it is sensitive because of the large ion equivalent conductance of hydroxide ion, and second, weak acids such as phenol (*17*) and silicic acid (*21, 22*) can be determined since the separation and detection are carried out in a basic solution. Although this eluent is a weak eluent relative to a carbonate eluent or organic acid eluents, it can quantitatively elute monovalent anions. For example, silicic acid which is essentially a tetravalent ion could be determined, because it dissolved as the monovalent ion ($H_3SiO_4^-$) in potassium hydroxide eluent (*22*).

In this paper, the applicability of this method to the analysis of some weak acids (cyanide, sulfide, and arsenite) is discussed.

## EXPERIMENTAL SECTION

**Apparatus.** A Toyo Soda Model nonsuppressed ion chromatograph HLC-601 equipped with an anion exchange column (50 mm × 4.6 mm i.d.) packed with TSKgel IC-Anion-PW (particle size 10 ± 1 μm; capacity 0.03 ± 0.005 mequiv/g) was used. HLC-601 consisted of a computer-controlled pump, conductivity detector, a sample injector (100 μL), and an oven. Two separation columns were connected, if necessary. The flow rate was maintained at 1 mL/min under a pressure of 15–25 kg/cm$^2$. The separator columns and a conductivity detector were set in an oven regulated at 30 °C.

**Reagents.** The eluent was prepared daily by dissolving analytical grade potassium hydroxide in distilled deionized water and deaerating it. Stock solutions (1000 ppm) of cyanide and sulfide were prepared weekly by dissolving the analytical grade potassium cyanide and sodium sulfide in water, respectively. Their working standard solutions were prepared daily by diluting the stock solutions with water. A silicate standard solution was prepared according to the previous reports (*21, 22*). Stock solutions (1000 ppm) of the other inorganic anions were prepared by dissolving their potassium or sodium salts, dried under vacuum at 110 °C overnight if necessary, in water. Standard solutions of heavy metal ions were prepared by dissolving the analytical grade reagents of their nitrate or sulfate salts in water. Working standard so-

0003-2700/85/0357-0829$01.50/0 © 1985 American Chemical Society

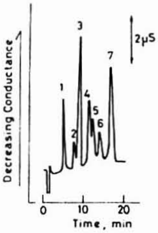

**Figure 1.** Typical ion chromatogram of seven inorganic anions: 1, fluoride (1 ppm); 2, bromate (3 ppm); 3, chloride (5 ppm); 4, nitrite (3 ppm); 5, cyanate (3 ppm); 6, bromide (3 ppm); 7, nitrate (10 ppm). The eluent was 1 mM KOH.

lutions were prepared by diluting the stock solutions with water and were stored in plastic bottles.

## RESULTS AND DISCUSSION

Figure 1 shows a typical ion chromatogram of seven anions obtained with 1 mM potassium hydroxide as eluent. The first large negative peak is the "dip peak" which is caused by sample water, sample cations ion-excluded by the anion exchange resin, and an eluent anion ($OH^-$) replaced by sample anions (*23*). This peak often interfers with anions which elute rapidly. For example, it restricts the linear range of the calibration curves of fluoride and chloride (*17*) and interfers with the analysis of silicic acid when the concentration of electrolyte was ten times lager than that of an eluent (*22*). All elution peaks were detected as negative peaks because of the large ion equivalent conductance of hydroxide ion (198 $\Omega^{-1}$ $cm^2$ $mol^{-1}$ at 25 °C). The analysis of some weak acids (cyanide, sulfide, arsenite, etc.) by this method is discussed below.

**Cyanide and Sulfide.** Because of concern for the toxicity of sulfide and cyanide, many analytical methods for their determination have been investigated. Methods studied include the solid membrane ion selective electrodes using AgI or $Ag_2S$ (*24, 25*), polarography (*26, 27*) or amperometry (*28*) with Ag or Hg electrodes, and direct (*29*) or indirect spectrophotometry (*30*). Those methods using silver or mercury, however, have the serious common disadvantages that some ions (e.g., halide ions), which form complexes or insoluble salts with silver and mercury, interfere with the determination and that sulfide and cyanide frequently interfere with the analysis of each other. Therefore, a method is required that separates cyanide and sulfide from each other and from interfering ions.

Since sulfide ($pK_1$ = 6.02, $pK_2$ = 14.0) and cyanide ($pK_a$ = 9.32) are dissolved as monovalent anions at pH 10–11, they can be quantitatively eluted and detected by nonsuppressed IC using the potassium hydroxide eluent. They eluted between chloride and nitrite and were completely separated from the other anions ($Br^-$, $NO_3^-$, $I^-$, $F^-$, etc.). Since it is possible that chloride and nitrite will be present in a sample solution, it is important that these four anions ($Cl^-$, $HS^-$, $CN^-$, $NO_2^-$) are separated for accurate determination. Two separation columns were connected in order to enhance efficiency. A marked increase in pressure was avoided because the columns were short (50 mm long) and the packed resin was small and spherical. The actual increase of pressure was below 10 $kg/cm^2$. Figure 2 shows the variation of resolution between pairs of anions eluting adjacently ($Cl^-$–$HS^-$, $HS^-$–$CN^-$, $CN^-$–$NO_2^-$), with the eluent concentration. The resolution of $Cl^-$–$HS^-$ and $HS^-$–$CN^-$ hardly varied with changing the eluent concentration, but that of $CN^-$–$NO_2^-$ was affected (the resolution was 1.03 with 0.5 mM KOH and 0.46 with 3 mM KOH). Figure 3 shows the separations of $Cl^-$–$HS^-$, $HS^-$–$CN^-$, and $CN^-$–$NO_2^-$ at various eluent concentrations. An increase in the eluent concentration increased the peak heights of these anions but degraded the separations. These facts are also shown in Figure 2. Therefore, as a result of the consideration of the separation and the time required for the analysis, 1.5

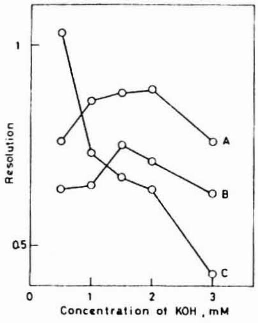

**Figure 2.** Variation of resolution between anion pairs eluting adjacently, with the concentration of the eluent: A, $Cl^-$–$HS^-$; B, $HS^-$–$CN^-$; C, $CN^-$–$NO_2^-$. Two separation columns were connected and used.

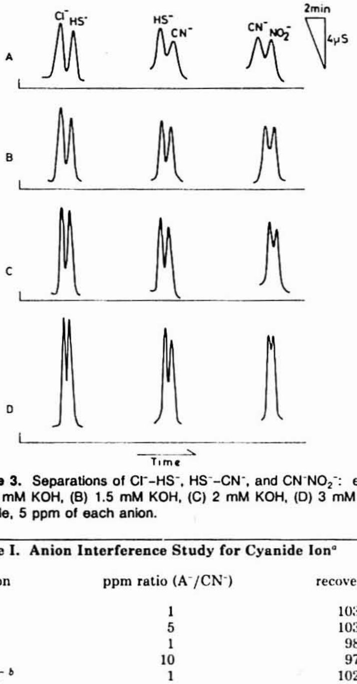

**Figure 3.** Separations of $Cl^-$–$HS^-$, $HS^-$–$CN^-$, and $CN^-NO_2^-$: eluent, (A) 1 mM KOH, (B) 1.5 mM KOH, (C) 2 mM KOH, (D) 3 mM KOH; sample, 5 ppm of each anion.

**Table I. Anion Interference Study for Cyanide Ion**[a]

| anion | ppm ratio ($A^-/CN^-$) | recovery, % |
|---|---|---|
| $Cl^-$ | 1 | 103.8 |
| | 5 | 103.3 |
| $Br^-$ | 1 | 98.1 |
| | 10 | 97.3 |
| $NO_2^-$ [b] | 1 | 102.5 |
| | 5 | 109.0 |
| $NO_3^-$ | 1 | 100.3 |
| | 10 | 98.8 |
| $S^-$ | 1 | 106.0 |
| | 2 | 115.6 |

[a] Sample contained 5 ppm of cyanide ion. [b] Eluent was 0.5 mM KOH, 1.5 mM KOH for other cases.

**Table II. Anion Interference Study for Sulfide Ions**[a]

| anion | ppm ratio ($A^-/CN^-$) | recovery, % |
|---|---|---|
| $Cl^-$ | 1 | 100.4 |
| | 5 | 120.9 |
| $Br^-$ | 1 | 105.8 |
| | 5 | 99.4 |
| $NO_2^-$ | 1 | 102.5 |
| | 5 | 98.6 |
| $NO_3^-$ | 1 | 102.1 |
| | 5 | 99.4 |
| $CN^-$ | 1 | 97.8 |
| | 2 | 93.5 |

[a] Sample contained 5 ppm of sulfide ion. Eluent was 1.5 mM of KOH.

**Table III. Cation Interference Study for Cyanide Ion**[a]

| metal ion | log[b] | molar ratio ($M^{2+}/CN$) | concn, ppm | recovery, % |
|---|---|---|---|---|
| Hg(II) | 40.9 | 0.1 | 3.85 | *c* |
| Co(II) | 19.1 | 0.1 | 1.13 | 62.7 |
| Ni(II) | 30.2 | 0.1 | 1.13 | 35.5 |
| Cu(II) | 28 | 0.1 | 1.22 | 60.0 |
| Pb(II) | 10.3 | 0.1 | 3.98 | 95.5 |
| | | 0.5 | 19.9 | 80.6 |
| Zn(II) | 16.8 | 0.1 | 1.26 | 101.7 |
| | | 1 | 12.6 | 97.3 |
| Cd(II) | 17.1 | 0.1 | 2.16 | 102.3 |

[a] Sample contained 5 ppm of cyanide. [b] Formation constant of cyanide complex (literature value). [c] Small and distorted peak.

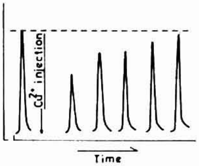

**Figure 4.** Depression of cyanide peak by $Cu^{2+}$ retained by the resin. 5 ppm of cyanide was injected.

**Table IV. Anion Interference Study for Arsenite Ion**[a]

| anion | ppm ratio ($A^-/H_2AsO_3^-$) | recovery, % |
|---|---|---|
| silicate | 1 | 97.7 |
| | 5 | 70.1[b] |
| $F^-$ | 1 | 103.7 |
| | 5 | 103.4 |
| $Cl^-$ | 1 | 100.7 |
| | 10 | 85.2[b] |
| arsenate | 1 | 98.8 |
| | 10 | 102.5 |

[a] Sample contained 5 ppm (as As) of arsenite. [b] The peak was broadened.

mM of KOH eluent was used for the following investigation.

Tables I and II show the interference of anions to the analysis of cyanide and sulfide, respectively. All sample solutions contained 5 ppm of cyanide or sulfide. The interference caused by chemical reactions in the sample solution or the separator column, as occurred in the case of fluoride interference with silicic acid (*22*), was not observed in either case. Bromide and nitrate which were completely separated from cyanide and sulfide did not interfere even if their concentrations were 25–50 ppm. However, 25 ppm of chloride which did not interfere with the determination of cyanide, caused an increase of 20% in sulfide recovery. Ten parts per million of cyanide caused a decrease of 6.5% in sulfide recovery, and 10 ppm of sulfide also caused an increase of 15.6% in cyanide recovery.

Table III shows cation interference with cyanide. Hg(II), Cu(II), Co(II), and Ni(II) seriously interfered but Pb(II), Zn(II), and Cd(II) did not. Hg(II) markedly depressed the cyanide peak and even $1.92 \times 10^{-5}$ M of Hg(II) (molar ratio of Hg to cyanide is 0.1) abolished it. The degree of the interference of metal ions (Hg > Ni > Cu > Co > Cd > Zn > Pb) was related to the magnitude of the formation constants of the cyanide complexes (Hg > Ni > Cu > Co > Pb = Zn = Cd). The concentration of free cyanide in a sample solution containing metal ions may decrease during IC analysis, because cyanide complexes of metal ions are easily formed in a basic solution. However, Pb(II), Zn(II), and Cd(II), the cyanide complexes of which are comparatively stable, did not depress the peak height of cyanide. Considering these facts, free cyanide must be measured by this method though its concentration may be slightly decreased by the formation of cyanide complexes during IC.

As sulfide and heavy metal ions form insoluble salts, sulfide measured by this method must be sulfide free. When only heavy metal ions were injected into this system, they were adsorbed as hydroxides by the anion-exchange resin. These hydroxides were retained in the column and affected the elution of cyanide and sulfide. Figure 4 shows the peak depression of cyanide by Cu(II) remaining in a column. The recovery of cyanide was 57% at the first injection after injecting 5 ppm of Cu(II) and six injections of cyanide were necessary in order to reach the original peak height.

Calibration curves for cyanide and sulfide were linear over the ranges 0.5–5 ppm, respectively. The percent deviations were 1.6% and 1.7% at 5 ppm cyanide and sulfide levels, respectively. Each detection limit was 100 ppb (the detection limit was defined as the concentration corresponding to twice the value of the noise of the base line).

For chromatographic methods for cyanide and sulfide, Rocklin et al. (*11*) determined parts-per-billion levels of these anions with an amperometric detection system, but these anions were determined with detection limits only in the parts-per-million to sub-part-per-million range by the other systems such as potentiometric (*31*) and coulometric detection (*12*). Cyanide has also determined by the conductivity detection after conversion to other detectable anions by the following reactions (*32, 33*).

$$I_2 + HCN = H^+ + \mathit{I^-} + ICN$$

$$NaCN + 2H_2O = NH_3 + \mathit{HCOO^-} + Na^+$$

The italic anions were detected by conventional IC. In both cases, parts-per-million levels of cyanide were detectable. The present method has the following itemized advantages for the determination of cyanide and sulfide compared with these conventional methods.

(1) The procedure is simple and safe, because pretreatment is unnecessary and cyanide and sulfide are always in a basic solution.

(2) Other anions can be simultaneously determined.

(3) The sensitivity is satisfactory compared with the other chromatographic methods.

**Arsenite.** Arsenate ($pK_1 = 2.2$, $pK_2 = 6.9$, $pK_3 = 11.5$), which is a comparatively strong acid, can be detected by the conventional IC (*34*), but arsenite ($pK_1 = 9.2$, $pK_2 = 12.1$, $pK_3 = 13.4$) has only been detected by an atomic absorption spectrometric system (*15, 16*).

Arsenite eluted between fluoride and chloride using this system. Table IV shows the interference of anions in the determination of arsenite. Silicate and chloride caused the broadening of the arsenite peak and lessened the peak height, when they were present in high concentration in a sample

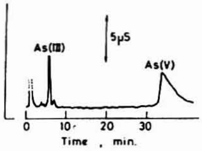

**Figure 5.** Separation of arsenic species. 5 ppm (as As) for each anion.

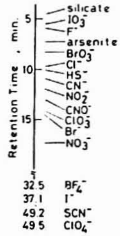

**Figure 6.** Fifteen anions determined by the present method. The eluent was 1 mM KOH.

solution. Arsenite could be determined separately from arsenate which eluted with a longer retention time. Figure 5 shows the separation of arsenite and arsenate. Organoarsenic compounds were not investigated, but the separation of arsenite from organoarsenic species should be possible since separation using the Dionex system and atomic absorption spectrometric detection were reported by Ricci et al. (*15*). The peak of arsenate was broadened and overlapped with the "absent peak" of carbonate contained in the eluent as an impurity (*17, 23*). Therefore, arsenate could not be determined accurately by this system.

The calibration curve for arsenite was linear over the range 0.5–10 ppm (as As). The percent deviation was 1.8% at the 5 ppm As level. The detection limit was 200 ppb, corresponding to that of flame atomic absorption spectrometry (*35*).

**Silicate.** As mentioned in previous papers (*21, 22*), fluoride, magnesium, and calcium ions interfere with the determination of silicic acid. However, the interference of fluoride ion was reduced by adding boric acid to the sample solution and interference from magnesium and calcium ions was eliminated by pretreatment with a $H^+$ form cation-exchange column. The detection limit was 22 ppb (as Si). This method was practical for the analysis of silic acid and applicable to its determination in natural water.

**Phenol Compounds.** Phenol and its derivatives (cresols, dimethylphenol, and ethylphenol) were detectable by this system as already reported (*17*). Nitrophenols and picrate were not eluted because of their strong adsorption on the anion-exchange resin. A detailed investigation of phenol compounds was not carried out because UV detection is more practical for these compound than conductivity detection. However, a $10^{-6}$ M level of phenol compounds was detectable by the present method. There was a possibility that phenol compounds would interfere with the determination of inorganic anions which should be detected by IC. However, the interference was not serious for the determination of most monovalent anions because the retention time of phenol, which eluted most rapidly among the phenol compounds studied, was longer than that of nitrate.

**Table V. Anions Detected by Conventional IC Using Conductivity Detector**[a]

| anions | ref |
|---|---|
| $F^-$, $Cl^-$, $Br^-$, $I^-$, $ClO_3^-$, $BrO_3^-$, $IO_3^-$, $ClO_4^-$, $NO_2^-$, $NO_3^-$, $SCN^-$, $CNO^-$, $N_3^-$, $SO_4^{2-}$, $SO_3^{2-}$, $S_2O_3^{2-}$, $PO_4^{3-}$, $PO_3^{3-}$, $BF_4^-$, $CrO_4^{2-}$, $WO_4^{2-}$, $MoO_4^{2-}$, Se(IV), Se(VI), As(V) | 1, 18, 19, 36–43 |

[a] Phenate, carbonate, and borate solutions were used for suppressed IC (*1, 18, 19*). Phthalate, tartrate, and citrate solutions were used for nonsuppressed IC (*36–43*).

**Table VI. Detection Limits and Linear Ranges of Calibration Curves of Four Weak Acids**

| anion | detection limit, (ppb) | linear range of calibration curve, ppm |
|---|---|---|
| silicate | 22 (as Si) | 0.1–2.5 |
| cyanide | 100 | 0.5–5 |
| sulfide | 100 | 0.5–10 |
| arsenite | 200 (as As) | 0.5–10 |

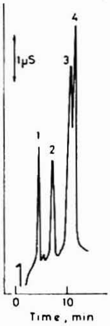

**Figure 7.** Ion chromatogram of four weak acids: 1, silicic acid (1 ppm); 2, arsenite (5 ppm); 3, sulfide (5 ppm); 4, cyanide (5 ppm).

**Comparison with Conventional IC.** Figure 6 shows the retention times of monovalent anions eluted with 1 mM KOH. The quantitative peaks for $SCN^-$ and $ClO_4^-$ were not obtained because their elution was delayed by hydrophobic interactions with the resin matrix (a polyacrylic acid resin was used for this study). Similarly, polyvalent anions were not quantitatively eluted by this eluent. It is necessary to use a more concentrated eluent to obtain quantitative elution of these anions retained by the resin. However, the use of such an eluent is impractical, since the noise of the base line increases because of the increase in the background conductance. Table V shows inorganic anions detected by the conventional suppressed and nonsuppressed IC. Some polyvalent anions, which were determined with difficulty by the present method, could be measured by the conventional methods. However, 15 inorganic anions eluting ahead of iodide could be determined by the present method as shown in Figure 6. Above all, this method has an advantage that four weak acids (cyanide, sulfide, silicate, and arsenite) can be simultaneously determined, together with other inorganic anions without the need for selective detection systems. Figure 7 shows an ion chromatogram of these four weak acids. The applicability of this method will be increased by the complete separation of cyanide and sulfide. Although arsenate is not quantitatively measured as mentioned above, arsenite and arsenate can be separately determined by the combined use of this method and other methods (e.g., atomic absorption spectrometry) since arsenite can be determined without interference from arsenate. Table VI shows the detection limits of this method for these four weak acids. These values will be improved upon by the elimination of pulses from the pump, temperature deviation in the oven, and the dissolution of carbon dioxide into the eluent.

In conclusion, 15 inorganic anions, which included cyanide, sulfide, arsinite, and silicic acid, could be determined with detection limits in sub-part-per-million by the present method. This method is practical to the analysis of anions which were determined with difficulty by conventional methods and will be applied to the anion analysis in wider fields.

**Registry No.** $ClO_3^-$, 14866-68-3; $BrO_3^-$, 15541-45-4; $IO_3^-$, 15454-31-6; $NO_3^-$, 14797-55-8; $NO_2^-$, 14797-65-0; $CN^-$, 57-12-5; $HS^-$, 15035-72-0; $CNO^-$, 661-20-1; $BF_4^-$, 14874-70-5; $H_3SiO_4^-$, 18102-72-2; $H_2AsO_3^-$, 14102-45-5; $S^-$, 18496-25-8; $F^-$, 16984-48-8; $Cl^-$, 16887-00-6; $Br^-$, 24959-67-9; $I^-$, 20461-54-5; KOH, 1310-58-3.

## LITERATURE CITED

(1) Small, H.; Stevens, T. S.; Bauman, W. C. *Anal. Chem.* **1975**, *47*, 1801–1809.
(2) Legrand, M.; Angelis, M.; Delmas, R. J. *Anal. Chim Acta* **1984**, *156*, 181–192.
(3) Okada, T.; Kuwamoto, T. *Bunseki Kagaku* **1983**, *32*, 595–599.
(4) Stevens, T. S.; Turkelson, V. T.; Albe, W. R. *Anal. Chem.* **1977**, *49*, 1176–1178.
(5) Sunden, T.; Lindgren, M.; Cedergren, A.; Siemer, D. D. *Anal. Chem.* **1983**, *55*, 2–4.
(6) Sevenich, G. J.; Fritz, J. S. *Anal. Chem.* **1983**, *55*, 12–16.
(7) Rokushika, S.; Qui, Z. Y.; Sun, Z. L.; Hatano, H. *J. Chromatogr.* **1983**, *280*, 69–76.
(8) Reeve, R. N. *J. Chromatogr.* **1979**, *177*, 393–397.
(9) Wang, C. Y.; Bunday, S. D.; Tartar, J. G. *Anal. Chem.* **1983**, *55*, 1617–1619.
(10) Pyen, G. S.; Erdmann, D. E. *Anal. Chim. Acta* **1983**, *149*, 355–358.
(11) Rocklin, R. D.; Johnson, E. L. *Anal. Chem.* **1983**, *55*, 4–7.
(12) Girard, J. E. *Anal. Chem.* **1979**, *51*, 836–839.
(13) Parks, E. J.; Brinckman, F. E.; Blair, W. R. *J. Chromatogr.* **1979**, *185*, 563–572.
(14) Messman, J. D.; Rains, T. C. *Anal. Chem.* **1981**, *53*, 1632–1636.
(15) Ricci, G. R.; Shepards, L. S.; Colovos, G.; Hester, N. E. *Anal. Chem.* 1981, *53*, 610–613.
(16) Grabinski, A. A. *Anal. Chem.* **1981**, *53*, 966–968.
(17) Okada, T.; Kuwamoto, T. *Anal. Chem.* **1983**, *55*, 1001–1004.
(18) Zolotov, Yu. A.; Shpigun, O. A.; Bubchikova, L. A. *Fresenius Z. Anal. Chem.* **1983**, *316*, 8–12.
(19) Ficklin, W. H. *Anal. Lett.* **1982**, *15*, 865–871.
(20) Pohl, C. A.; Johnson, E. L. *J. Chromatogr. Sci.* **1980**, *18*, 442–452.
(21) Okada, T.; Kuwamoto, T. *Anal. Lett.* **1984**, *17*, 1743–1751.
(22) Okada, T.; Kuwamoto, T.; *Anal. Chem.*, in press.
(23) Okada, T.; Kuwamoto, T. *Anal. Chem.* **1984**, *56*, 2073–2078.
(24) Pungor, E.; Toth, K. *Analyst (London)* **1970**, *95*, 625–648.
(25) Cusbert, P. J. *Anal. Chim. Acta* **1976**, *87*, 429–435.
(26) Turner, J. A.; Abel, R. H.; Osteryoung, R. A. *Anal. Chem.* **1975**, *47*, 1343–1347.
(27) Davison, W.; Gabbutt, C. D. *J. Electroanal. Chem.* **1979**, *99*, 311–320.
(28) McCloskey, J. A. *Anal. Chem.* **1961**, *33*, 1842–1843.
(29) Chambers, W. E.; Coulter, P. D.; Greinke, R. A. "Treatise on Analytical Chemistry"; Kolthoff, I. M., Elving, P. J., Eds.; Wiley: New York, 1978; Part II, Vol. 10, pp 175–177.
(30) Blanco, M.; Maspoch, S. *Talanta* **1983**, *31*, 85–87.
(31) Wang, W.; Chen, Y.; Wu, M. *Analyst (London)* **1984**, *109*, 281-286.
(32) DuVal, D. L.; Fritz, J. S.; Gjerde, D. T. *Anal. Chem.* **1982**, *54*, 830–832.
(33) Dolzine, T. W.; Esposito, G. G.; Rinehart, D. S. *Anal. Chem.* **1982**, *54*, 470–473.
(34) Hansen, L. D.; Richter, B. E.; Rollins, D. K.; Lamb, J. D.; Eatough, D. J. *Anal. Chem.* **1979**, *51*, 633–637.
(35) Skoneiczny, R. F.; Han, R. B. "Treatise on Analytical Chemistry"; Kolthoff, I. M., Elving, P. J., Eds.; Wiley: New York, 1978, Part II, Vol. 10, pp 247–249.
(36) Hill, C. J.; Lash, R. P. *Anal. Chem.* **1980**, *52*, 24–27.
(37) Hoover, T. B.; Yager, G. D. *Anal. Chem.* **1984**, *56*, 221–225.
(38) Mackie, H.; Speciale, S. J.; Throop, L. J.; Yang, T. *J. Chromatogr.* **1982**, *242*, 177–180.
(39) Matsushita, S.; Tada, Y.; Baba, N.; Hosako, K. *J. Chromatogr.* **1983**, *259*, 459–464.
(40) Gjerde, D. T.; Fritz, J. S.; Schmuckler, G. *J. Chromatogr.* **1979**, *186*, 509–519.
(41) Gjerde, D. T.; Schmuckler, G.; Fritz, J. S. *J. Chromatogr.* **1980**, *187*, 35–45.
(42) Gjerde, D. T.; Fritz, J. S. *Anal. Chem.* **1981**, *53*, 2324–2327.
(43) Fritz, J. S.; DuVal, D. L.; Barron, R. E. *Anal. Chem.* **1984**, *56*, 1177–1182.

RECEIVED for review October 26, 1984. Accepted December 17, 1984. This work has been supported by Grant-in-Aid for Scientific Research (NO. 58470029) from the Ministry of Education, Science and Culture, Japan.

# Electrokinetic Chromatography with Micellar Solution and Open-Tubular Capillary

**Shigeru Terabe,* Koji Otsuka, and Teiichi Ando**

*Department of Industrial Chemistry, Faculty of Engineering, Kyoto University, Sakyo-ku, Kyoto 606, Japan*

**Fundamental characteristics of a new type of chromatography with micellar solutions of ionic surfactants were examined. Electrokinetic phenomena in open-tubular capillaries move two phases, aqueous and micellar, with different velocities and micellar solubilization operates as the distribution process of solutes. Sodium dodecyl sulfate (SDS) solutions and a 0.05 mm i.d. × 650 mm fused silica tube were employed and high dc voltages up to 25 kV were applied. Linear relationships were observed between current and migration velocities of water, micelle, and any solute, but not between applied voltages and the velocities. This discrepancy can be reasonably interpreted in terms of the temperature rise of the solution in the tube resulting from Joule heating. Optimum resolutions can be obtained when the capacity factor is about 2, because retention times are limited between those of an insolubilized solute or water and a totally solubilized solute or micelle. Observed dependence of capacity factors on current can also be explained by the temperature rise. Thermodynamic parameters in micellar solubilization were presented.**

In conventional liquid chromatography, the stationary phase is immobilized in a column, while the mobile phase is percolated through the stationary bed. When a sample is added to the top of the column, components of the sample distribute themselves between mobile and stationary phases in the ratio of the capacity factor while mobile phase flows down continuously through the column. It is, however, not essential in chromatography that one phase is rigidly fixed in the column; the relative movement of two phases between which a solute is distributed is satisfactory for the chromatographic separation. Thus, instead of the forced flow of the mobile phase through the stationary phase, any means of continuous displacement between two phases can be utilized to constitute a chromatographic system. The two phases need not always be heterogeneous if any distribution process of a solute can be held between them; they may be solvent and a pseudophase like micelle, or even a molecule. In this paper we report a new type of chromatographic technique based on electrokinetic migrations and the micellar solubilization phenomenon which extends the scope of liquid chromatography to that of a homogeneous solution alone.

In a previous paper (*1*) we briefly described the results of preliminary experiments and adopted the term "electrokinetic separation" for this technique according to the suggestion of a reviewer. However, we now prefer using the term "electrokinetic chromatography" because this obviously belongs to a branch of chromatography, which is probably close to liquid–liquid partition chromatography. Nakagawa (*2*) first proposed to apply the micellar solubilization phenomenon to chromatography in combination with electrophoresis of an ionic micelle and called this technique "solubilization chromatography" after the partition mechanism. When electrophoresis is exclusively operating in the relative migration between the aqueous and micellar phases, the aqueous phase is considered to be stationary and the micellar phase mobile. Although micelles are understood as dynamic structures with a liquid core (*3*), it may be possible in the following discussion in this paper to depict micelles as a liquid phase distinct from the surrounding aqueous solution.

Among various techniques available in electrophoresis we have employed free zone electrophoresis in open-tubular capillaries (*4, 5*) because of its high efficiency in separation and ease of instrumentation for continuous on-line detection. In free zone electrophoresis with an open-tubular glass capillary, it has been reported (*5*) that the strong electroosmotic flow of the electrolyte solution occurs in the tube to an extent that even small, triply charged anions are carried toward the negative electrode. This electroosmotic flow provides another advantage of shortening the analysis time.

In this paper, we will first present some features of the electrokinetic migration from the practical point of view, i.e., how electrokinetic velocities can be related to experimental variables. Then some fundamental characteristics of this technique as a chromatographic method will be described in comparison with conventional chromatography because the limited range of retention times requires different expressions of chromatographic parameters. Last, distribution coefficients and thermodynamic parameters in micellar solubilization will be discussed.

## EXPERIMENTAL SECTION

**Apparatus, Reagents, and Procedure.** The same apparatus as described previously (*1*) was placed in a thermostated oven. Although the oven was not equipped with a circulating fan, a fan incorporated in a JASCO UVIDEC-100-II spectrophotometric detector to dissipate the heat from a UV lamp served as a substitute. The solution was allowed to stand in the oven more than 1 night before use to equilibrate at the temperature. Sodium tetradecyl sulfate (STS) supplied by Nikko Chemicals (Tokyo, Japan) and sodium dodecylsulfonate purchased from Tokyo Kasei Kogyo (Tokyo, Japan) were used as received. Compounds employed as solutes were of analytical-reagent grade and used without further purification. Concentrations of test samples were arbitrarily adjusted to give suitable peak heights, and estimated to be in the range from 0.1 to 1.0 mg $mL^{-1}$ except for methanol and Sudan III. About 1% of methanol was added to each sample solution. Injection volume was about 2 nL throughout the experiment. Other reagents and the experimental procedure were described in the previous paper (*1*).

## RESULTS AND DISCUSSION

**Electrokinetic Migration.** The electrokinetic chromatogram shown in Figure 1 was obtained with a 0.05 M sodium dodecyl sulfate (SDS) solution and a 0.05 mm i.d. × 500 mm tube at 35 °C. All the solutes injected at the positive end of the tube were detected with a UV photometer positioned at the negative side. Methanol is regarded as an insolubilized solute, i.e., as existing only in the aqueous phase, and Sudan III is assumed to be completely solubilized, i.e., to exist only in the micellar phase. The assumed behavior of methanol was justified by gel filtration chromatography with SDS solutions (*6*): The distribution coefficient of methanol between SDS micelle and water was found to be 0.3 at 40 °C (*7*). The validity of the use of a water-insoluble dye as a tracer of the micelle has been discussed by Stigter and Mysels (*8*).

0003-2700/85/0357-0834$01.50/0 © 1985 American Chemical Society

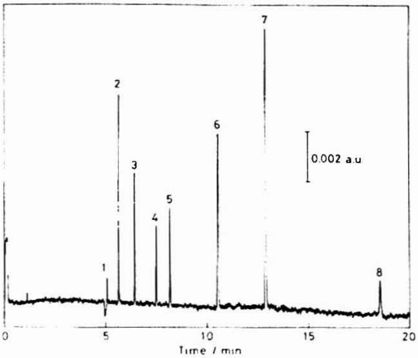

**Figure 1.** Electrokinetic chromatogram of some test samples: (1) methanol, (2) resorcinol, (3) phenol, (4) *p*-nitroaniline, (5) nitrobenzene, (6) toluene, (7) 2-naphthol, (8) Sudan III; micellar solution, 0.05 M SDS in 0.1 M borate–0.05 M phosphate buffer, pH 7.0; separation tube, 0.05 mm i.d. × 650 mm; length of the tube used for separation, 500 mm; total applied voltage, ca. 15 kV; current, 26 μA; detection wavelength, 210 nm; temperature of oven, 35 °C.

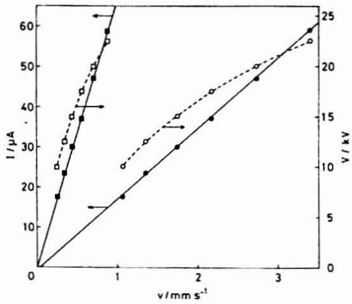

**Figure 2.** Dependence of migration velocities *v* of methanol (○, ●) and Sudan III (□, ■) on applied voltage (dashed line) and current (solid line). Conditions are the same as those given in Figure 1 except for applied voltage and current.

Methanol is usually not detected by the absorption of UV light but absorbs here due to the slight change of the refractive index. The cylindrical cell employed in this work is susceptible to the influence of refraction when it is irradiated at right angles to the axis of the tube. Since other solutes are considered to be un-ionized under the conditions used, the retention times of these solutes fall between those of methanol and Sudan III as mentioned previously (*1*). The retention parameters in this method will be discussed later.

Dependences of the migration velocities of these solutes on the electrical field strength and the current were examined under various applied voltages, and the results for methanol and Sudan III are given in Figure 2. Similar dependences as shown in Figure 2 were always recognized at different SDS concentrations. The migration of the aqueous phase which is indicated by the methanol band is interpreted to be brought about by electroosmosis and, therefore, the velocity of the methanol band should be essentially equal to the electroosmotic velocity $v_{eo}$. The Sudan III band is considered to represent the migration of the micelle as mentioned above. The velocity of the micelle should be equal to the difference between electroosmotic velocity of the aqueous phase and the electrophoretic one of the micelle, because the negatively charged SDS micelle is subject to both effects in opposite directions. The electroosmotic velocity is observed to be much larger than the electrophoretic one for the SDS micelle under the conditions employed.

Linear relationships were noticed between velocities of any solutes and the electrical current but not between velocities and applied voltages as shown in Figure 2 for methanol and Sudan III. A similar deviation from linearity has been reported by Jorgenson and Lukacs (*5*) and they suggested that Joule heating is responsible for this deviation.

The theoretical work of Rice and Whitehead (*9*) on electroosmotic flow in narrow cylindrical capillaries indicates that when the reciprocal of the Debye–Huckel parameter, $1/\kappa$, is much smaller than the radius of a capillary $r$, $v_{eo}$ is described by the classical formula (*10*)

$$v_{eo} = -\frac{\epsilon\zeta}{\eta}E \tag{1}$$

where $\epsilon$ is the permittivity of the liquid, $\zeta$ is the zeta potential, $\eta$ is the viscosity of the liquid, and $E$ is the electrical field strength. The negative sign means that when $\zeta$ is negative, the liquid flow is toward the negative electrode (*10*). In the case of the buffer solution employed in this study, 0.1 M borate–0.05 M phosphate, pH 7.0, the value of $1/\kappa$ is estimated from electrolyte concentrations to be 0.8 nm, much smaller than the radius of the tube, 50 μm. Since the surface conductivity may be neglected in this case, Ohm's law

$$E = \frac{l}{\pi r^2 \sigma} I \tag{2}$$

where $l$ is the length of the tube, $\sigma$ is the specific conductivity of the liquid, and $I$ is the current due to transport of charge by the fluid, can be used to rewrite eq 1 into the expression

$$v_{eo} = -\frac{l}{\pi r^2}\frac{\epsilon\zeta}{\sigma\eta} I \tag{3}$$

The specific conductivity $\sigma$ is given by Kohlrausch's law of independent migration of ions

$$\sigma = \sum_j c_j z_j \lambda_j \tag{4}$$

where $c_j$, $z_j$, and $\lambda_j$ are the number of moles per unit volume, charge number, and equivalent conductivity of the $j$th ion, respectively. Here, $\lambda_j$ can be related to the viscosity by the combination of the Stokes–Einstein relation and the Nernst–Einstein equation (*11*) as

$$\lambda_j = \frac{z_j e F}{6\pi a_j \eta} \tag{5}$$

where $e$ is the elementary charge, $F$ is the Faraday constant, and $a_j$ is the radius of the solute ion $j$. Combination of eq 3 with eq 4 and 5 gives

$$v_{eo} = -\frac{6\epsilon\zeta l}{r^2 e F}\sum_j \frac{a_j}{c_j z_j^2} I \tag{6}$$

One should note that $\eta$ is not included in eq 6.

The dependence of $v_{eo}$ on current and the applied voltage $V$ shown in Figure 2 may be explained in terms of the decrease of $\eta$ with increase of $V$ or $I$. That is, if $c_j$, $z_j$, and $a_j$ are assumed to be constant, $v_{eo}$ increases linearly with increase of $I$ as predicted from eq 6, but the deviation from linearity may be predicted between $v_{eo}$ and $V$ as a result of the change of $\eta$ with $V$ in eq 1. The experimental results strongly support this view and, in addition, indicate that the product of permittivity and the zeta potential remains virtually constant regardless of $E$

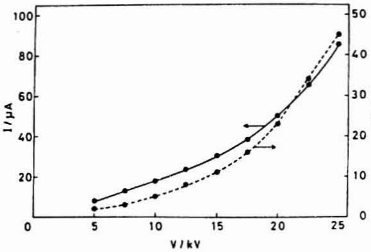

**Figure 3.** Dependence of current (solid line) and rise in surface temperature, $\Delta T$, of the tube (dashed line) on applied voltage; length of the tube was 610 mm. Other conditions are given in Figure 2.

and $I$. The rise in temperature of the liquid in the tube by Joule heating must be the reason for the decrease of $\eta$ as the applied voltage increases. In order to confirm this interpretation, the surface temperature of the tube was measured with a thermocouple under the same conditions as employed for obtaining Figure 2. The rise in temperature observed reached 45 °C higher than the ambient temperature at 25 kV/610 mm as shown in Figure 3, although the exact temperature was uncertain because of the relatively large contact point (0.2 mm o.d., of 0.1 mm o.d. alumel–chromel wire) compared with the diameter of the tube, 0.2 mm o.d. The temperature rise was proportional to the power dissipated per unit length of the tube and amounted to about 2.8 °C mW$^{-1}$ cm for 0.05 M SDS solution. Rather high temperature at the surface reveals that heat dissipation is not efficient because of a low film coefficient of heat transfer from the surface of the tube into the air.

The variation of current with the applied voltage is also illustrated in Figure 3. By considering the rise in temperature mentioned above, the nonlinear relationship between $V$ and $I$ can also be understood from a viewpoint of the alteration in conductivity as a result of the viscosity change as predicted from eq 5. It follows, therefore, that low viscosity at a high voltage causes positive deviation in the plot of $I$ vs. $V$ as shown in Figure 3.

By taking into account the sign of the migrating direction, we can describe the velocity of the micelle $v_{mc}$, as

$$v_{mc} = v_{eo} + v_{ep} \qquad (7)$$

where $v_{ep}$ is the electrophoretic velocity of the micelle. The velocity $v_{ep}$ is given by

$$v_{ep} = \frac{2\epsilon\zeta}{3\eta} f(\kappa a)\ E \qquad (8)$$

where function $f(\kappa a)$ depends on the particle shape and, for sphere of $\kappa a = \infty$, is 1.50 and $a$ is the radius of the particle (*10*). It should be noted that the zeta potential in eq 8 is for the micelle, while that in eq 1 is for fused silica. Substitution of eq 1 and eq 8 into eq 7 gives

$$v_{mc} = -\frac{\epsilon}{\eta}\left\{\zeta_1 - \frac{2}{3}\zeta_2 f(\kappa a)\right\}E \qquad (9)$$

where subscripts 1 and 2 denote fused silica and micelle, respectively. The observed movement of the methanol band from the positive end to the negative means that $\zeta_1$ is negative. The fact that the Sudan III band moved in the same direction as the methanol but with lower velocity implies that $\zeta_2$ is lower than $\zeta_1$ in absolute value, because $\zeta_2$ should also be negative for the negatively charged SDS micelle. The linear relationship of $v_{mc}$ vs. $I$ and the nonlinear one of $v_{mc}$ vs. $E$ as shown in Figure 2 agree with the probable change of viscosity as discussed above. Although the micellar size of an ionic surfactant is reported to decrease with an increase of temperature (*12*), the observed linearity between $v_{mc}$ and $I$ or $v_{ep}$ and $I$ indicates that $f(\kappa a)$ may be regarded as unaltered in the temperature range of 35–80 °C.

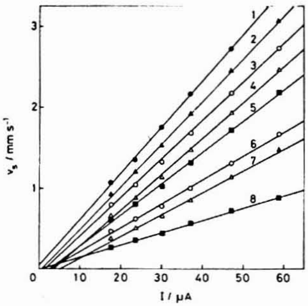

**Figure 4.** Velocities of solutes as a function of current. Solutes are indicated by the same numbers as given in Figure 1. Conditions are the same as those given in Figure 2.

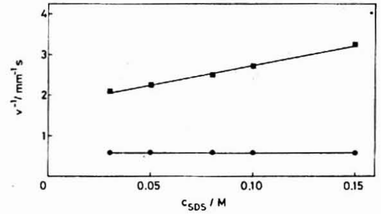

**Figure 5.** Reciprocal velocities of Sudan III (■) $v_{mc}^{-1}$ and methanol (●) $v_{eo}^{-1}$ as a function of SDS concentration; applied voltage was 15 kV. Other conditions are given in Figure 1.

Velocities of the solutes $v_s$ are shown in Figure 4 as a function of the current. All the solutes have linear dependence but extrapolated values of $v_s$ at $I = 0$ do not coincide with zero. These deviations seem to exceed the experimental error and may be ascribed to the small variation of the zeta potential for the micelle with temperature when the micelle contains solutes. The number of solutes solubilized into the micelle is roughly estimated to be less than 5 to 10 molecules per micelle under the condition shown in Figure 1 except for Sudan III where less than one molecule is solubilized.

At a constant voltage applied, $v_{eo}$ remained virtually constant irrespective of the SDS concentration $c_{SDS}$, while the reciprocal of $v_{mc}$ increased with an increase of $c_{SDS}$ as shown in Figure 5. In this case, current was observed to increase linearly with $c_{SDS}$ from 22 μA at 0.03 M to 45 μA at 0.15 M as predicted from eq 2 and 4. Independence of $v_{eo}$ from $c_{SDS}$ suggests that the viscosity $\eta$ remains approximately unchanged as expected from eq 1: The effect of the temperature rise by increasing current on $\eta$ is accidentally compensated by that of increasing $c_{SDS}$. Thus, the viscosity of the aqueous SDS solution has been reported to increase linearly with the concentration (*13*). The constant $v_{eo}$ regardless of $c_{SDS}$ also suggests that SDS has no effect on the zeta potential of the glass/solution interface. The observed increase of $v_{mc}^{-1}$ with $c_{SDS}$, i.e., the increase of the electrophoretic velocity, is in contrast to the result of Stigter et al. (*8*) that the electrophoretic mobility of the SDS micelle decreases linearly with the increase of $c_{SDS}$. This discrepancy may be interpreted in terms of differences in temperature rise by Joule heating, i.e.,

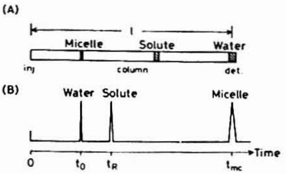

**Figure 6.** Schematic illustration of zones separated in the tube (A) and chromatogram (B) of the hypothetical mixture of water, solute, and micelle. Plate number, capacity factor of solute, and $v_0/v_{mc} = t_{mc}/t_0$ are arbitrarily assigned as 14 000, 1, and 4, respectively.

2.8 °C mW$^{-1}$ cm in this work and 0.2 °C mW$^{-1}$ cm in the case of Stigter et al. (*8, 14*). Thus, in this work $\eta$ happened to be held nearly constant as described above but in the case of Stigter et al. (*8, 14*) the increase of $\eta$ with $c_{SDS}$ caused decrease of $v_{ep}$ as anticipated from eq 8.

**Retention Parameters.** The retention behavior characteristic of electrokinetic chromatography has been discussed briefly in the previous paper (*1*). Figure 6A schematically illustrates migrating zones of water, a solute, and the micelle at the time $t_0$, elution time of water, after a hypothetical mixture of the three is injected at the left end of the tube. Here, it is assumed that the zeta potential for fused silica has the same sign as that for the micelle, and the absolute value of the former is higher than the latter. The velocity $v_{eo}$, which is equal to $l/t_0$, is presumed to be four times as large as the $v_{mc}$ in Figure 6A. Figure 6B displays the schematic chromatogram of the three zones observed with an imaginary detector situated at length $l$ from the injection point. The number of theoretical plates $N$ is arbitrarily assigned as 14000. Experimentally, the retention time of water $t_0$ is measured with methanol and that of the micelle $t_{mc}$ with Sudan III as described above. The most significant difference in this method from conventional chromatography lies in the fact that the range of retention times of electrically neutral solutes are limited between $t_0$ and $t_{mc}$. The chromatogram given in Figure 1 shows an example of the total range of retention.

The capacity factor $\tilde{k}'$ defined by the ratio, $n_{mc}/n_{aq}$, where $n_{mc}$ and $n_{aq}$ are the total moles of the solutes in the micelle and in the aqueous phase, respectively, can be calculated (*1*) from retention times by

$$\tilde{k}' = \frac{t_R - t_0}{t_0(1 - t_R/t_{mc})} \tag{10}$$

where $t_R$ is the retention time of the solute. Equation 10 can be written in another form as

$$t_R = \frac{1 + \tilde{k}'}{1 + (t_0/t_{mc})\tilde{k}'}t_0 \tag{11}$$

In this paper, the capacity factor is given the symbol $\tilde{k}'$ instead of widely accepted $k'$ in order to emphasize the difference in the relationship of the capacity factor to $t_R$ from the well-known equation

$$t_R = (1 + k')t_0 \tag{12}$$

The value of $t_{mc}/t_0$ can be regarded as a parameter to indicate the width of the total range of elution for electrically neutral solutes. When $t_{mc}$ becomes infinite, eq 11 is equivalent to eq 12. It should be stressed that the capacity factor of infinity in this method implies that the solute stays in the micellar phase at all times.

It is interesting to compare the retention behavior observed in this method whose total range of retention is limited between $t_0$ and $t_{mc}$ with that obtained under the gradient elution in conventional liquid chromatography. The relationship between the retention time and the capacity factor in this method can be calculated from eq 11, and an example is shown on a solid line in Figure 7, where the following conditions are assumed: $t_0 = 200$ s, $t_{mc} = 800$ s, and tube length $l = 500$ mm. Similar relationship between the retention time for a concave gradient elution and the capacity factor $k_w'$ in water under reversed-phase chromatography is calculated for two cases according to the procedure described in the Appendix. The result for a concave gradient from water to methanol ($S = 3.0$ (*15*)) is shown on the dashed line, and that for the case from water to tetrahydrofuran ($S = 4.4$ (*15*)) is on the dotted line. In both cases, column length and $t_0$, the retention time of an unretained solute, are taken as the same value as the above example, and $t_G$ as 600 s, that is, pure methanol or tetrahydrofuran reaches the exit of the column at 800 s. The gradient shapes are chosen to give a curve close to that for the above example: $m = 2.1$ in eq A1 for water–methanol and $m = 3.0$ for water–tetrahydrofuran. Although the curve for electrokinetic chromatography is not in good agreement with those for the concave gradient, it can be said that the relationship between the capacity factor and the retention time in electrokinetic chromatography is roughly approximated to that in reversed-phase chromatography with the concave gradient elution technique from water to methanol except for solutes having larger capacity factors than 150 in water.

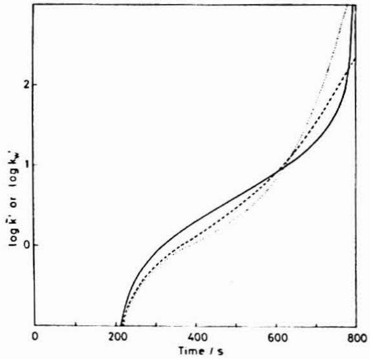

**Figure 7.** Logarithmic capacity factor as a function of retention time for electrokinetic chromatography (solid line) and for concave gradient elution in liquid chromatography from water to methanol (dashed line) and from water to tetrahydrofuran (dotted line).

**Resolution Equation, Effective Plates, and Peak Capacity.** The following resolution equation can be derived by considering eq 10 in the same manner (*16*) as in usual elution chromatography:

$$R_s = \frac{N^{1/2}}{4}\left(\frac{\alpha - 1}{\alpha}\right)\left(\frac{\tilde{k}_2'}{1 + \tilde{k}_2'}\right)\left(\frac{1 - t_0/t_{mc}}{1 + (t_0/t_{mc})\tilde{k}_1'}\right) \tag{13}$$

Here, $R_s$ is the resolution, $N$ is the plate number, and $\alpha$ is the separation factor which is equal to $\tilde{k}_2'/\tilde{k}_1'$. Owing to the last term, the selectivity term in this chromatography is not independent of the capacity factor term in contrast to conventional chromatography (*16*).

$$R_s = \frac{N^{1/2}}{4}\left(\frac{\alpha - 1}{\alpha}\right)\left(\frac{k'}{1 + k'}\right) \tag{14}$$

The last term in eq 13 reveals again the characteristic of this method. The infinite value of $t_{mc}$ reduces the last term of eq 13 to unity, and then eq 13 becomes equal to eq 14. To evaluate the effect of $\tilde{k}'$ on resolution, the approximation, $\tilde{k}_1'$

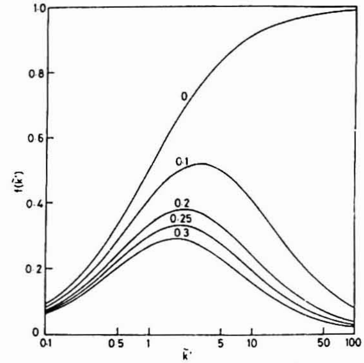

**Figure 8.** Dependence of $f(\tilde{k}')$ on capacity factor $\tilde{k}'$. The values of $t_0/t_{mc}$ are given on each line.

$= \tilde{k}_2' = \tilde{k}'$, is made for closely eluting peaks. The function $f(\tilde{k}')$, the product of the last two terms in eq 13, is written as

$$f(\tilde{k}') = \left(\frac{\tilde{k}'}{1 + \tilde{k}'}\right)\left(\frac{1 - t_0/t_{mc}}{1 + (t_0/t_{mc})\tilde{k}'}\right) \qquad (15)$$

The dependence of the function $f(\tilde{k}')$ on $\tilde{k}'$ is shown in Figure 8 for some different values of $t_0/t_{mc}$. The value of zero for $t_0/t_{mc}$ corresponds to conventional chromatography, where the larger capacity factor leads to the better resolution as generally known. Large $\tilde{k}'$ values, however, are unfavorable to obtain good resolutions in this method because the last term in eq 13 approaches zero. The optimum value of $\tilde{k}'$ depends on the ratio $t_0/t_{mc}$ as shown in Figure 8. The ratio $t_0/t_{mc}$ remains constant for an SDS concentration irrespective of $V$ or $I$ as found from Figure 2 but decreases from 0.28 for 0.03 M SDS to 0.18 for 0.15 M SDS as found from Figure 5. For example, since $t_0/t_{mc}$ is about 0.22 for 0.1 M SDS solution, the optimum range of $\tilde{k}'$ lies between 0.84 and 5.4 which gives $f(\tilde{k}')$ values between 0.30 and 0.36. The maximum value 0.36 is found at $\tilde{k}' = 2.13$. Although Figure 8 is calculated based on the assumption $\tilde{k}_1' = \tilde{k}_2'$, if we set 1.1 for $\tilde{k}_2'/\tilde{k}_1'$ in the above example, the range of $\tilde{k}'$ which gives the value higher than 0.30 for the product of the last two terms in eq 13 becomes 0.74 to 5.6 and the maximum value of the product increases to 0.37 at $\tilde{k}_1' = 2.0$. That is, the better resolution will be attained for actual cases than predicted from eq 15 only from the viewpoint of the last two terms in eq 13 in addition to the selectivity term.

The smaller maximum value of $f(\tilde{k}')$ than that of the term $k'/(1 + k')$ in eq 14, which may be close to unity, implies a disadvantage of this method in view of maximum resolution. However, the smaller value of this can be well compensated by the large plate numbers, e.g., 250 000 obtained for a 500 mm tube as will be discussed in a separate paper. The smallest value of $\alpha$ to obtain $R_s = 1$ calculated by eq 13 is 1.023 at $\tilde{k}' = 2.13$ for $N = 250\,000$ and $t_0/t_{mc} = 0.22$.

Since the capacity factor $\tilde{k}'$ is proportional to the volume ratio of a micelle to an aqueous phase, the $\tilde{k}'$ value can be easily adjusted by changing the concentration of a micelle to yield an appropriate value for optimum resolution. The dependence of $\tilde{k}'$ on the concentration of a surfactant and temperature will be discussed later in this paper. Any of the three parameters, $\tilde{k}'$, $\alpha$, and $t_0/t_{mc}$, may be altered by the structure of a surfactant molecule. Examples of variations of these parameters are given in Table I for three surfactant solutions at 0.05 M along with current, $v_{eo}$, $v_{mc}$, and $v_{ep}$. It is obvious from Table I that changes in ratio $t_0/t_{mc}$ among three solutions are mainly attributable to the changes in electrophoretic velocities which depend on both surface charges and micellar sizes as predicted from eq 8. The alteration of elution order is not observed for listed solutes but values of $\tilde{k}'$ are significantly different among three solutions. Since critical micelle concentrations (CMC) of these surfactants are different, the effect of the structural change of a surfactant molecule on the capacity factor should be examined at the same micellar concentration or with the distribution coefficient as discussed below.

**Table I. Comparison of Current, Velocities, and Capacity Factors among Three Anionic Surfactant Solutions at Constant Applied Voltage**[a]

| | surfactant | | |
|---|---|---|---|
| | $R_{12}SO_4Na$[b] | $R_{14}SO_4Na$[c] | $R_{12}SO_3Na$[d] |
| $I/\mu A$ | 44.6 | 41.4 | 41.0 |
| $v_{eo}/mm\ s^{-1}$ | 2.67 | 2.62 | 2.50 |
| $v_{mc}/mm\ s^{-1}$ | 0.685 | 0.769 | 0.674 |
| $v_{ep}/mm\ s^{-1}$ | 1.985 | 1.851 | 1.826 |
| $t_0/t_{mc}$ | 0.257 | 0.294 | 0.270 |
| $\tilde{k}'$(resorcinol) | 0.158 | 0.207 | 0.155 |
| $\tilde{k}'$(phenol) | 0.378 | 0.509 | 0.326 |
| $\tilde{k}'$(*p*-nitroaniline) | 0.657 | 0.860 | 0.454 |
| $\tilde{k}'$(nitrobenzene) | 0.986 | 1.37 | 0.693 |
| $\tilde{k}'$(toluene) | 2.27 | 3.56 | 1.80 |
| $\tilde{k}'$(2-naphthol) | 3.79 | 5.74 | 3.35 |

[a] Electrical field strength, 308 V cm$^{-1}$; concentration of surfactant, 0.05 M; oven temperature, 35 °C. [b] Sodium dodecyl sulfate (SDS). [c] Sodium tetradecyl sulfate (STS). [d] Sodium dodecylsulfonate.

In regard to the resolution equation, the number of effective plates $N_{eff}$ is given for this method as

$$N_{eff} = N\left(\frac{\tilde{k}'}{1 + \tilde{k}'}\right)^2\left(1 - \frac{t_0}{t_{mc}}\right)^2 \qquad (16)$$

To see the performance of this method, the maximum effective plates per second is calculated by setting $N = 250\,000$, $l = 500$ mm, $v_{eo} = 2$ mm s$^{-1}$, and $t_0/t_{mc} = 0.22$ to give 148 s$^{-1}$ at $\tilde{k}' = 5.9$. This suggests that the efficiency of this method is comparable to that of gas chromatography with open-tubular glass capillaries.

Peak capacity is defined as the maximum number of peaks that can be resolved within a specified range of retention time. For cases in which peaks are to be separated with $4\sigma$ resolution, where $\sigma$ is the standard deviation of the peak, under a constant plate number $N$, peak capacity $n$ is given according to Giddings (*17*) as

$$n = 1 + \frac{N^{1/2}}{4} \ln \frac{t_{mc}}{t_0} \qquad (17)$$

If we take the parameters again as $N = 250\,000$ and $t_0/t_{mc} = 0.22$, $n$ becomes 190.

**Capacity Factor $\tilde{k}'$ and Distribution Coefficient $K$.** The dependence of the capacity factor $\tilde{k}'$ on electroosmotic velocity $v_{eo}$ was observed to be remarkable as shown in Figure 9. The velocity $v_{eo}$ can be related to current as shown in Figure 2 and, therefore, a similar relationship obviously applies between $\tilde{k}'$ and $I$. The capacity factor $\tilde{k}'$ linearly decreased with an increase of $v_{eo}$, but slopes of these plots were different from one another. The similar plots were obtained with other concentrations of SDS and with other surfactant solutions. In order to eliminate the effect of $v_{eo}$ or $I$ on $\tilde{k}'$, each line of the plot was extrapolated to the intercept at $v_{eo} = 0$, and the value of $\tilde{k}'$ at $v_{eo} = 0$ was designated $\tilde{k}_0'$. The capacity factor $\tilde{k}_0'$ may be taken as $\tilde{k}'$ at the ambient temperature in the oven thermostated at a constant temperature, because the tem-

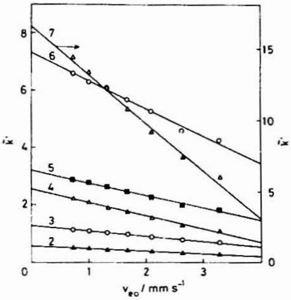

**Figure 9.** Dependence of capacity factor $\tilde{k}'$ on velocity $v_{eo}$. The number on each plot corresponds to the solute shown in Figure 1; concentration of SDS was 0.10 M. Other conditions are the same as those in Figure 1 except for applied voltages.

perature of liquid in the tube should be higher than the ambient unless $v_{eo}$ is equal to zero as described above.

The capacity factor $\tilde{k}'$ can be related to the distribution coefficient $K$ of a solute between micellar and aqueous phases through

$$\tilde{k}' = K\frac{V_{mc}}{V_{aq}} \tag{18}$$

where $V_{mc}$ and $V_{aq}$ are volumes of micellar and aqueous phases. Here, $V_{mc}$ can be determined from a micellar concentration $c_{mc}$, which is equal to the concentration of a surfactant $c_{sf}$ minus CMC, and partial specific volume $\bar{v}$ of micelle, and $V_{aq}$ can be regarded as the difference between the total internal volume of the tube and $V_{mc}$. Thus, the distribution coefficient can be easily calculated from the capacity factor in contrast to conventional chromatography.

Equation 18 means that $\tilde{k}'$ is proportional to the phase ratio $V_{mc}/V_{aq}$ which is described as

$$\frac{V_{mc}}{V_{aq}} = \frac{\bar{v}(c_{sf} - \mathrm{CMC})}{1 - \bar{v}(c_{sf} - \mathrm{CMC})} \tag{19}$$

When micellar concentrations are low, the denominator at the right side of eq 19 may be approximated to be equal to unity, i.e.

$$\tilde{k}' \simeq K\bar{v}(c_{sf} - \mathrm{CMC}) \tag{20}$$

The plots of $\tilde{k}_0'$ vs. concentration of SDS, $c_{SDS}$, are given in Figure 10. The linear relationship observed in these plots implies that the distribution coefficients remain constant at least at the SDS concentrations below 0.15 M. Similar linear plots were recognized for STS and sodium dodecylsulfonate solutions.

Distribution coefficients at 35 °C calculated from slopes of these plots are listed in Table II for three surfactants. It is interesting to note that distribution coefficients are almost the same between SDS and STS for less solubilized solutes from resorcinol to nitrobenzene in Table II but significantly different for toluene and 2-naphthol. On the other hand, the situation is reversed between SDS and sodium dodecylsulfonate. These data indicate that distribution coefficients of solutes partially soluble in water are more sensitive to the change of the polar moiety of a surfactant molecule than to that of the nonpolar moiety and that distribution coefficients of solutes almost insoluble in water are sensitive to the length of the alkyl chain. These facts suggest that solutes partially miscible with water are solubilized by adsorption on the micellar surface with orienting polar groups toward the aqueous phase and nonpolar groups inside the micelle, and that less water-soluble solutes are uptaken into the interior of the micelle in agreement with the postulated modes of incorporation (*19*). The differences in capacity factors of solutes from resorcinol to nitrobenzene listed in Table I between SDS and STS are exclusively ascribed to the difference in micellar volume, that is, differences in CMC and the partial specific volume, because distribution coefficients are almost the same between the two solutions.

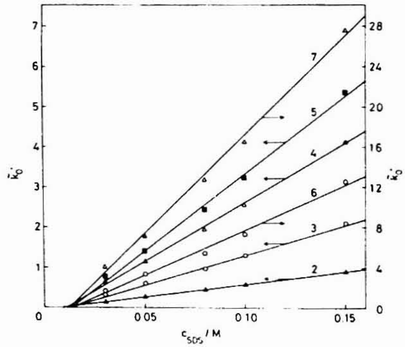

**Figure 10.** Dependence of capacity factor $\tilde{k}_0'$ on the concentrations of SDS. Solutes are indicated by the same numbers as those in Figure 1.

**Table II. Distribution Coefficients at 35 °C Calculated from Slopes of Plots $\tilde{k}_0'$ vs. $c_{SDS}$ in Figure 10**

| solute | distribution coefficient[a] | | |
|---|---|---|---|
| | $R_{12}SO_4Na$[b] | $R_{14}SO_4Na$[b] | $R_{12}SO_3Na$[b] |
| resorcinol | 21.6 | 20.8 | 27.7 |
| phenol | 52.1 | 52.3 | 56.1 |
| *p*-nitroaniline | 103 | 100 | 84.3 |
| nitrobenzene | 135 | 138 | 111 |
| toluene | 318 | 345 | 288 |
| 2-naphthol | 656 | 789 | 698 |

[a] Partial specific volumes ($\bar{v}$) at 35 °C used to calculate distribution coefficients are taken from Shinoda et al. (*18*): for SDS, $\bar{v}$ = 0.8721 mL g$^{-1}$; for STS, $\bar{v}$ = 0.9019 mL g$^{-1}$; for sodium dodecylsulfonate, $\bar{v}$ = 0.8809 mL g$^{-1}$. [b] See Table I for abbreviations.

Intercepts of plots in Figure 10 extrapolated to $\tilde{k}_0' = 0$ are virtually concentrated at around 10 mM (averaged value 10.4 mM) and this concentration can be interpreted to be CMC under these conditions. This value of CMC seems too high in comparison with the reported value of 8.6 mM in water at 35 °C (*20*), since CMC is generally reduced with additions of electrolytes (*21*). The values of CMC for STS and sodium dodecylsulfonate at 35 °C found from similar plots as in Figure 10 are 2.2 mM and 12.1 mM. Reported values for STS in water at 35 °C is 2.12 mM (*20*) and for sodium dodecylsulfonate in water at 25 °C 8.1 mM (*22*). Thus, this method seems not to be reliable to obtain CMC.

Temperature dependence of the distribution coefficient can be described as

$$\ln K = -\frac{\Delta H^\circ}{RT} + \frac{\Delta S^\circ}{R} \tag{21}$$

where $\Delta H^\circ$ is the enthalpy change associated with micellar solubilization, $\Delta S^\circ$ is the corresponding entropy change, and $R$ is the gas constant. Logarithms of distribution coefficients determined from $\tilde{k}_0'$ through eq 18 at different temperatures

**Table III. Enthalpy, Entropy, and Gibbs Free Energy Changes in Micellar Solubilization with SDS Solution**[a]

| solute | $\Delta H°$/kJ mol$^{-1}$ | $\Delta S°$/J mol$^{-1}$ K$^{-1}$ | corr coeff | $\Delta G°$(35 °C)/kJ mol$^{-1}$ |
|---|---|---|---|---|
| resorcinol | −17 | −30 | 0.990 | −7.8 |
| phenol | −13 | −7.8 | 0.991 | −11 |
| *p*-nitroaniline | −19 | −22 | 0.982 | −12 |
| nitrobenzene | −10 | 8.5 | 0.953 | −13 |
| toluene | −17 | −5.7 | 0.792 | −15 |
| 2-naphthol | −20 | −9.8 | 0.995 | −17 |

[a] 0.1 M, pH 7.0. Calculated from distribution coefficients measured at four different temperatures: 31, 35, 40, and 45 °C.

**Table IV. Estimated Temperature of the Solution from Capacity Factor with Enthalpy and Entropy Changes Listed in Table III**[a]

| solute | $\bar{k}'$ | $T_{\mathrm{calcd}}$/°C |
|---|---|---|
| resorcinol | 0.29 | 59 |
| phenol | 0.72 | 68 |
| *p*-nitroaniline | 1.18 | 65 |
| nitrobenzene | 1.86 | 77 |
| toluene | 4.40 | 59 |
| 2-naphthol | 6.78 | 68 |

[a] Solution, 0.1 M SDS, pH 7.0; electrical field strength, 308 V cm$^{-1}$; current, 61.4 $\mu$A; oven temperature, 35 °C. Values of CMC and partial specific volume of micelle are taken as those at 35 °C to estimate the phase ratio.

were plotted against the reciprocal temperature according to eq 21 to give straight lines. The values of $\Delta H°$ and $\Delta S°$ calculated from the above van't Hoff plots are listed in Table III for six solutes along with correlation coefficients of the plots and Gibbs free energies $\Delta G°$ for micellar solubilization at 35 °C. Since the range of the temperature change is only 14 °C, accuracies of these thermodynamic data may be low. There were no available thermodynamic data in the literature concerning micellar solubilization of these solutes with SDS. These data will be helpful in understanding this phenomenon and the present method may provide a useful technique to determine these thermodynamic quantities as well as a high resolution separation method.

Since the capacity factor should be constant irrespective of the velocity $v_{\mathrm{eo}}$, we may assume that the decrease of $\bar{k}'$ with an increase of $v_{\mathrm{eo}}$ or current is ascribed to the rise in temperature resulting from Joule heating. On the basis of this assumption, it is possible to estimate the temperature which gives the $\bar{k}'$ value observed at any $v_{\mathrm{eo}}$ or current by using eq 18 and 21 from values of $\Delta H°$ and $\Delta S°$ listed in Table III. Thus, calculated temperatures of the solution corresponding to the observed $\bar{k}'$ values at the oven temperature of 35 °C under the applied field of 308 V cm$^{-1}$ are listed in Table IV. Although the calculated temperatures are scattered between 59 and 77 °C, these discrepancies may be accounted for by taking into account the fact that $\Delta H°$ and $\Delta S°$ are determined over a narrow range of temperatures. The average value of 66 °C is close to the observed surface temperature of 65 °C. The temperature gradient in the liquid and the wall of the tube is estimated to be negligibly small from coefficients of heat transfer in the solution and the wall of fused silica tubing. The agreement between the calculated and actual temperatures strongly suggests that the observed dependence of $\bar{k}'$ on the $v_{\mathrm{eo}}$ or current is attributable to the temperature rise by Joule heating.

In conclusion, the heat dissipation in open-tubular capillaries is not efficient and, therefore, the effect of the temperature rise of the solution by Joule heating should be taken into account in the interpretation of experimental results. Thus, since the capacity factor or distribution coefficient is dependent on both current and applied voltage, it is desirable to keep the energy dissipated per unit time constant throughout a series of runs in order to eliminate the temperature effects. The technique described here is the first example of chromatography with a homogeneous solution alone as the phases or entities between which the solute is distributed. This concept of chromatography with a homogeneous solution and electrokinetic migrations can be readily extended to the incorporation of the solute through some specific interactions, e.g., complexation or clathration, by a molecule differentially migrating from the surrounding solvent. The greatest advantage of this technique as a new separation method lies in its high efficiency because of the low axial dispersion in open-tubular capillaries with the electroosmotic flow and the electrophoretic migration of micelles and the rapid establishment of the distribution equilibrium in micellar solubilization. Band broadening in this method will be discussed in a separate paper.

## ACKNOWLEDGMENT

We thank Y. Ito and Z. Ogumi for their helpful suggestions and discussions about the temperature effects in electrokinetic migrations.

## APPENDIX

The relationship between the retention time and the capacity factor in water under the concave gradient elution in reversed-phase liquid chromatography was calculated with a personal computer as follows: The concave gradient shape can be written as

$$\phi_{\mathrm{b}} = (t/t_{\mathrm{G}})^m \qquad \text{(A1)}$$

where $\phi_{\mathrm{b}}$ is the volume fraction of organic solvent B in the mobile phase entering the column at time $t$ and $t_{\mathrm{G}}$ is the time from the beginning to the end of gradient at the inlet of column. The dependence of logarithm of the capacity factor $k'$ on $\phi_{\mathrm{b}}$ is assumed as (*15*)

$$\log k' = \log k_{\mathrm{w}}' - S\phi_{\mathrm{b}} \qquad \text{(A2)}$$

where $k_{\mathrm{w}}'$ is the capacity factor obtained in water. The parameter $S$ is the value of the negative slope of plots of $\log k'$ vs. $\phi_{\mathrm{b}}$.

In order to make numerical calculation possible, the gradient shape was approximated by the stepwise elution with 1000 steps of equal change of $\phi_{\mathrm{b}}$, i.e., $\phi_{\mathrm{b}}(i+1) - \phi_{\mathrm{b}}(i) = 1/1000$ for $i = 1$ to 1000. After setting an arbitrary value for $m$ in eq A1, time $t_i$ when the $i$th solvent enters the inlet of the column is determined for $\phi_{\mathrm{b}}(i) = i/1000$ with eq A1. The moving length of the mobile phase during the $i$th step, $x_{\mathrm{m}}(i)$, is given as

$$x_{\mathrm{m}}(i) = u(t_{i+1} - t_i) \qquad \text{(A3)}$$

where $u$ is the linear velocity of the mobile phase. The capacity factor $k_i'$ of a given solute in the $i$th solvent is calculated from eq A2. Since the velocity $u_{\mathrm{s}}(i)$ of the solute in the $i$th solvent is given by

$$u_{\mathrm{s}}(i) = u/(1 + k_i') \qquad \text{(A4)}$$

the differential velocity $\nu_{\mathrm{m}}(i)$ of the mobile phase relative to $u_{\mathrm{s}}(i)$ can be expressed as

$$\nu_{\mathrm{m}}(i) = u - u_{\mathrm{s}}(i) = k_i'u/(1 + k_i') \qquad \text{(A5)}$$

The period $\tau_{\mathrm{s}}(i)$ that the solute spends in the $i$th solvent is described as

$$\tau_{\mathrm{s}}(i) = x_{\mathrm{m}}(i)/\nu_{\mathrm{m}}(i) \qquad \text{(A6)}$$

Then, the distance $x_{\mathrm{s}}(i)$ that the solute travels in the $i$th solvent can be calculated from eq A6 in combination with eq A4 and A5 as

$$x_s(i) = u_s(i)\tau_s(i) = x_m(i)/k_i' \qquad (A7)$$

When the condition

$$\sum_{1}^{i} x_s(i) = l \qquad (A8)$$

where $l$ is the column length, is established, the solute should be eluted from the exit of the column. The retention time $t_R$ can be written as

$$t_R = \sum_{1}^{i} \tau_s(i) \qquad (A9)$$

When $t$ in eq A1 is equal to $t_G$, pure solvent B will begin to enter the column, and the column will be entirely filled with solvent B after $l/u$ from $t_G$. The concave gradient is considered to be completed at this time. A solute whose retention time is equal to $(t_G + l/u)$ is eluted at last while the gradient elution is running, and $k_w'$ of the last eluting solute is regarded as the maximum value. Thus, the relationship between $t_R$ and $k_w'$ is calculated for $k_w'$ from 0.1 to the maximum.

**Registry No.** SDS, 151-21-3; STS, 1191-50-0; resorcinol, 108-46-3; phenol, 108-95-2; *p*-nitroaniline, 100-01-6; nitrobenzene, 98-95-3; toluene, 108-88-3; 2-naphthol, 135-19-3; sodium dodecanesulfonate, 2386-53-0.

## LITERATURE CITED

(1) Terabe, S.; Otsuka, K.; Ichikawa, K.; Tsuchiya, A.; Ando, T. *Anal. Chem.* **1984**, *56*, 111–113.

(2) Nakagawa, T. *Newsl., Div. Colloid Surf. Chem., Chem. Soc. Jpn.* **1981**, *6* (3), 1.

(3) Attwood, D.; Florence, A. T. "Surfactant Systems: Their Chemistry, Pharmacy and Biology"; Chapman and Hall: London, 1983; Chapter 3.

(4) Mikkers, F. E. P.; Everaerts, F. M.; Verheggen, Th. P. E. M. *J. Chromatogr.* **1979**, *169*, 11–20.

(5) Jorgenson, J. W.; Lukacs, K. D. *Anal. Chem.* **1981**, *53*, 1298–1302.

(6) Herries, D. G.; Bishop, W.; Richards, F. M. *J. Phys. Chem.* **1964**, *68*, 1842–1852.

(7) Terabe, S.; Tanaka, H.; Otsuka, K.; Ando, T., unpublished work, Kyoto University, 1984.

(8) Stigter, D.; Mysels, K. D. *J. Phys. Chem.* **1955**, *59*, 45–51.

(9) Rice, C. L.; Whitehead, R. *J. Phys. Chem.* **1965**, *69*, 4017–4024.

(10) Hunter, R. J. "Zeta Potential in Colloid Science"; Academic Press: London, 1981; Chapter 3.

(11) Bockris, J. O'M.; Reddy, A. K. N. "Modern Electrochemistry"; Plenum: New York, 1970; Vol. 1, Chapter 4.

(12) Kuriyama, K.; Inoue, H.; Nakagawa, T. *Kolloid Z. Z. Polym.* **1962**, *183*, 68–71.

(13) Hess, K.; Philippoff, W.; Kiessig, H. *Kolloid Z.* **1939**, *88*, 40–51.

(14) Hoyer, H. W.; Mysels, K. J.; Stigter, D. *J. Phys. Chem.* **1954**, *58*, 385–388.

(15) Snyder, L. R.; Dolan, J. W.; Grant, J. R. *J. Chromatogr.* **1979**, *165*, 3–30.

(16) Karger, B. L.; Snyder, L. R.; Horvath, C. "An Introduction to Separation Science"; Wiley: New York, 1973; Chapter 5.

(17) Giddings, J. C. *Anal. Chem.* **1967**, *39*, 1027–1028.

(18) Shinoda, K.; Soda, T. *J. Phys. Chem.* **1963**, *67*, 2072–2074.

(19) Shinoda, K.; Nakagawa, T.; Tamamushi, B.; Isemura, T. "Colloidal Surfactants: Some Physicochemical Properties"; Academic Press: New York, 1963; p 140.

(20) Flockhart, B. D. *J. Colloid Sci.* **1961**, *16*, 484–492.

(21) Corrin, M. L.; Harkins, W. D. *J. Am. Chem. Soc.* **1947**, *69*, 683–688.

(22) Williams, R. J.; Phillips, J. N.; Mysels, K. J. *Trans. Faraday Soc.* **1955**, *51*, 728–737.

RECEIVED for review October 10, 1984. Accepted January 2, 1985. This work has been supported in part by the Grant-in-Aid for Scientific Research (No. 59550512) from the Ministry of Education, Science and Culture, Japan.

---

# Rotating Arc Direct Current Plasma as an Emission Excitation Source

**L. Y. Hara**[1] **and M. L. Parsons***[2]

*Department of Chemistry, Arizona State University, Tempe, Arizona 85287*

**A rotating arc direct current plasma system has been developed and evaluated as a spectroscopic excitation source for atomic emission spectrometry. It operates by forcing a dc arc to rotate reproducibly on the surface of a graphite anode disk by introducing argon gas tangentially to the anode. Sample aerosol is introduced into the plasma concentrically through an orifice in the graphite disk. Spectroscopic measurements are made directly in the current carrying region of the plasma. The design of this device was thoroughly examined and each parameter affecting its analytical performance was evaluated. The performance figures of merit for this device showed linearity over 5 orders of magnitude. The detection limits were comparable to a commercially available direct current plasma for several elements. While further work is required to completely characterize this device, this study shows that it has potential for becoming an alternate excitation source.**

Plasma emission spectrometry has become one of the most common methods to perform trace elemental analysis. The inductively coupled plasma (ICP) and direct current plasma (DCP) are used extensively in a variety of applications.

Both excitation sources provide a high-energy environment that ensures atomization and excitation. Detection limits and precision are nearly comparable. An area of common research interest with the ICP and DCP is sample introduction. Many studies have been performed to determine the means and mechanism of sample introduction and droplet size (*1*).

One problem with the commercially available DCP (SpectraJet III, SpectraMetrics, Inc., Division of Beckman Instruments, Andover, MA) is the comparatively inefficient manner of sample introduction into the plasma. Only a few percent of the sample is actually consumed by the plasma (*2*). If the analyte were forced directly into the plasma, a higher atom density should result, providing greater intensity for a given concentration and lowering detection limits.

A DCP which addressed the problem of sample introduction was first described by Rippetoe and Vickers (*3*) in 1972. They observed that in dc arc methods, arc wander is inevitable. Rather than trying to eliminate this, they took advantage of

---

[1] Current address: Air Products and Chemicals, Inc., P.O. Box 538, Allentown, PA 18105.

[2] Current address: The Los Alamos National Laboratory, CHM-1, MS-G740, Los Alamos, NM 87545.

0003-2700/85/0357-0841$01.50/0 © 1985 American Chemical Society

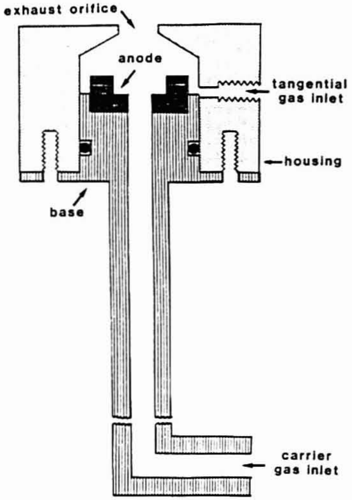

**Figure 1.** Diagram of RA-DCP: Macor (dotted segment); graphite (segment marked anode); brass (ruled segment); Viton (solid).

the "problem" of arc wander by permitting the discharge to rotate reproducibily around a circular disk anode up to a rate of 600 Hz.

An advantage to this rotating arc DCP (RA-DCP) system was that the life of the electrode could be extended and interaction between the sample aerosol (which was introduced concentrically through the anode) and arc discharge was enhanced. This occurred because the arc rotation rate was sufficiently rapid compared to the time required for an aerosol particle to cross the interelectrode space. The analyte species was constrained to trvel in a channel heated by the surrounding high temperature arc column. It should be noted however, that desolvation and a nebulizer that operated with low sweep gas flow rates were required to maintain this rapid rotation.

An RA-DCP designed by Owen (*4*) was examined in this study. It is a miniature version of that originally designed by Margoshes and Scribner (*5*, *6*). Though similar in design to that of Rippetoe and Vickers (*3*), there are two major differences: First, spectroscopic measurements were made directly in the current carrying portion of the plasma where the highest energy exists. Second, the cathode is placed on a vertical, rather than horizontal, axis. In this manner, the upward gas flow will carry any ablated cathode material away from the spectroscopic region. The evaluation of this RA-DCP is the subject of this investigation.

## EXPERIMENTAL SECTION

**Apparatus.** The housing of the RA-DCP was constructed of Macor (trademark of Corning Glass Works, NY), a machinable glass ceramic. The diameters of the exhaust and tangential gas inlet orifices, position of tangential gas inlet, and geometry of the housing were evaluated by varying the dimensions until a stable plasma could be sustained for 3 h without undue wear or destruction.

The anode was constructed by modifying a graphite disklike cylinder (National Spectroscopic, part number L4072, Cleveland, OH) to a step-design, as shown in Figure 1. An anode design described by Keirs (*7*) and an unmodified disk were constructed and tested. Contamination from the machining process was removed by soaking the graphite in 7 M nitric acid, rinsing with deionized water, and drying in an oven at 110 °C for 8 h.

**Table I. Apparatus Used**

| | |
|---|---|
| power supply | SpectraMetrics Model 53020 (SpectraMetrics, Inc., Andover, MA) |
| gas | argon, welding grade (Airco Industrial Gases, Murray Hill, NY) |
| flowmeters | Brooks Instruments Model 1335-8506A with R-2-15-B tube (Brooks Instruments Division, Emerson Electric Co., Hatfield, PA) |
| sample introduction | concentric glass nebulizer (constructed according to Scott (8)) |
| peristaltic pump | Cole-Parmer Model 7545-10 (Cole-Parmer Co., Chicago, IL) |
| optics | 8 cm focal length, 2.5 cm diameter quartz focusing lens |
| monochromator | Health Model EU 700-70 scanning monochromator with 1180 grooves mm$^{-1}$ grating blazed at 2500 Å (Schoeffel McPherson, Acton, MA) |
| detector | Health Model EU-701-30 photomultiplier module; RCA 1P28A PMT (RCA Solid State Division, Somerville, NJ) |
| electrometer | constructed in-house |
| chart recorder | Varian Model 135-1 (Varian Instruments, Palo Alto, CA) |
| desolvator | constructed similar to that described by Veillon and Margoshes (*9*) |

**Table II. RA-DCP Operating Conditions**

| | |
|---|---|
| applied current | 7.5 Å |
| electrode gap | 7 mm |
| gas flow rates: | |
| tangential | 3.3 L min$^{-1}$ |
| carrier | 1.8 L min$^{-1}$ |
| solution flow rate | 3.5 mL min$^{-1}$ |
| height of observation | 1.5 mm above the RA-DCP housing |
| monochromator settings: | |
| slit width | 35 $\mu$m |
| slit height | 1 mm |
| measurement time constant | 1 s |

The cathode consisted of either a pure tungsten (Specialty Steels, Pittsburgh, PA), 2% zirconiated tungsten, or 2% thoriated tungsten rod (Union Carbide, New York, NY) shaped to a 30° tip with an electric grinder. Each rod was tested in 3.1 and 6.3 mm diameters.

The completed RA-DCP and housing with optimized dimensions was then mounted on a brass base (Figure 1). To eliminate continuum from the cathode, a mechanical occluder was placed between the RA-DCP and focusing lens. The RA-DCP was placed in a dc arc stand and measurements were made with the apparatus summarized on Table I. Figure 2 shows a schematic diagram of the RA-DCP system.

**Reagents.** Analytical reagent grade chemicals (Mallinkrodt Chemical Works, St. Louis, MO) were dissolved to prepare 100 $\mu$g mL$^{-1}$ stock solutions by the method described by Smith and Parsons (*10*). Lower concentrations were prepared by serial dilution with distilled, deionized water.

**Simplex Optimization.** A simplex optimization similar to that described by Deming and Morgan (*11*) was performed to obtain parameter values for the best signal-to-noise ratio ($S/N$).

A 50 $\mu$g mL$^{-1}$ solution of Cu at the 3247.540-Å emission line was used to measure the $S/N$ ratio while performing the optimization. This was repeated with Mg, at the 2795.53-Å line.

Table II summarizes the optimized operating conditions of the RA-DCP.

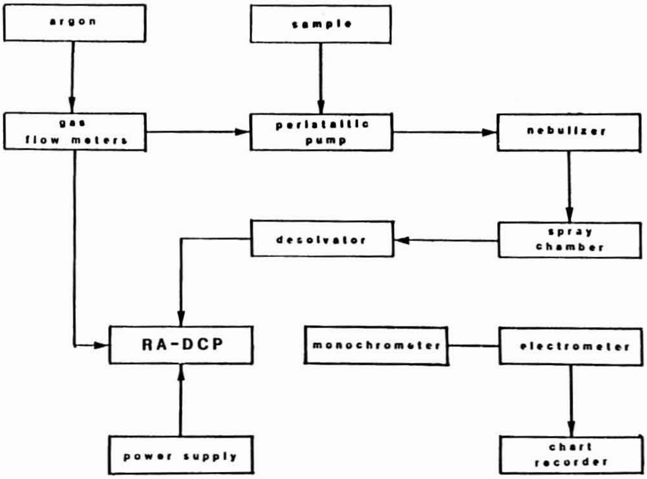

**Figure 2.** Schematic of RA-DCP experimental system.

**Procedure.** Fifteen minutes prior to ignition, the heating chamber of the desolvator was heated to 125 °C. The condenser and arc stand jaws were cooled by a recirculating chilled water bath maintained at 0 °C. The flow of argon gas was set to the operating conditions; and when ready, the anode and cathode were electrically contacted through the housing orifice with a graphite rod mounted on a Teflon holder. The rod was quickly removed and the plasma was allowed to equilibrate for 15 min. Distilled, deionized water was then introduced to the nebulizer to establish a base line.

Since the excitation source was not fully characterized, the best analytical line for each element using the RA-DCP was determined by scanning the five most intense lines as listed on the NBS tables (*12*) within 5 Å, while aspirating a 50 $\mu$g mL$^{-1}$ standard solution. The line that resulted in the best $S/N$ was chosen for subsequent analytical work.

**Arc Rotation Rate.** The arc rotation rate was measured by focusing an enlarged image of the plasma onto a UDT-500UV photodiode (United Detector Technology, Culver City, CA). To ensure that the rotating arc passed the detector only once per revolution, a 1.0 mm × 1.5 mm slit was used to isolate a section of the inverted cone image 1.5 mm above the housing. Thus, each time a segment of the arc traversed 360° and passed this "window", the photodiode received a pulse of radiation. The frequency of the impulses was monitored with an Tektronix Model T912 storage oscilloscope (Tektronix, Inc., Beaverton, OR).

**Performance Figures of Merit.** An analytical calibration was constructed by aspirating concentrations of 0.01, 0.05, 0.1, 0.5, 1.0, 5.0, 10.0, 50.0, 100, 500, and 1000 $\mu$g mL$^{-1}$ standard solutions and recording each intensity. Linear least-square regressions were performed for statistical analyses.

Detection limits were determined by aspirating a 0.5 $\mu$g mL$^{-1}$ standard solution (with the exception of boron, chromium, indium, iron, lead, and potassium for which a concentration of 10 $\mu$g mL$^{-1}$ was used) and recording the signal and noise (background of the blank measurement) at the wavelength previously selected. The detection limits were calculated according to IUPAC recommendations of a concentration equivalent to a signal three times the standard deviation of the blank.

**Analyses of Environmental Samples.** Groundwater was prepared by using the method described by Holloway and Kacoyannakis (*13*). River water and sediment were obtained from the Verde River located in Maricopa County, Arizona. An extract of the sediment was obtained by the method described by Sinex, Cantillo, and Heltz (*14*).

Comparison analyses of these samples were performed with a Jarrel-Ash Model 965 Atom Comp ICP (Jarrel Division, Fisher Scientific Co., Waltham, MA).

## RESULTS AND DISCUSSION

**Electrodes.** Keirs previously reported that using a zirconiated tungsten (Zr/W) rod as a cathode enhanced plasma stability. This was attributed to the arc "...completely engulfing the tip of the electrode..." which prevented cathode wander (*7*). Enhancement was not observed for our RA-DCP. The Zr/W electrodes of both dimensions performed poorly. Ignition was much more difficult since the arc traveled the length of the electrode making the distance between the cathode spot and the anode so great that the arc could not be sustained.

A pure tungsten electrode was also tested, but an arc could not be struck. The only electrode that initiated a stable plasma consisted of Th/W. These observations may be explained by considering the work function of the constituent elements of the electrodes. The work function increases in the order of Th, Zr, and W. While the thorium and zirconium make up only 2% of the electrode, this is sufficient to lower the work function of the alloy. Thus, as was observed, ignition would likely be easiest for the Th/W electrode. This conclusion is in agreement with the experiments of Scribner and Margoshes (*6*).

It was also noted that a 3.0 mm diameter Th/W electrode did completely engulf the tip as Keirs reported; however, the rod was consumed rapidly. The 6.0 mm diameter Th/W electrode provided the best stability by forming a bead of W at its tip. Without the formation of this bead, the arc would occasionally wander, causing spectroscopic flares.

Of the three anode designs tested, the stepped design functioned best. The anode with no alterations resulted in consumption by the arc rotating on the edge of the inner diameter wall. The truncated cone design resulted in an arc that traversed down the cone until a stable RA-DCP no longer existed and spectroscopic measurements could not be made; an excessive amount of noise was present. The stepped-design anode permitted the arc to rotate about a well-defined flat surface.

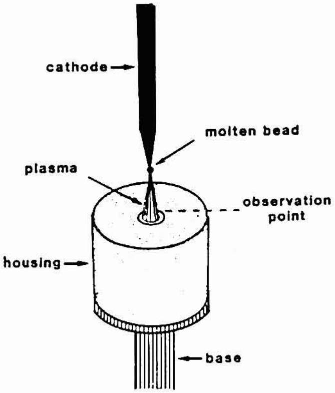

Figure 3. Schematic of RA-DCP in operation.

**Observations.** The RA-DCP, after being allowed to stabilize, features two unique characteristics. These are illustrated in Figure 3. First, the discharge arcs between the cathode and rotates about the anode disk in a conical manner. Second, a molten bead of thoriated tungsten (Th/W) is located at the upper vertex of the cone.

To maintain the bead at one point, gas flow rates must be carefully regulated. A change in flow dislodges the bead and reestablishment is necessary. Bead movement changes the resistance and power of the plasma. Consequently, stability, excitation capabilities, and analytical performance are degraded.

It is important to maintain the cathode along the same vertical axis as the anode. Failure to do so results in an asymmetric plasma. This causes the molten bead to form at locations other than the tip of the cathode, and electrode consumption is uneven.

Spectroscopic measurements are made in the inner region of the cone where advantages of the high temperature excitation capabilities can be utilized. This observation region differs from other DCPs in which measurements are made outside the plasma where the continuum is not as intense. The area of observation is limited to 1 mm$^2$. The excitation source thus behaves as a point source where emission is concentrated.

**Background Spectrum.** An emission continuum is observed between 2500 Å and 7000 Å; however, it appears to be substantially less than with other DCP designs.

Hydroxyl rotational band spectrum between 3064 Å degrading to 3245 Å was observed as well as much of the expected Ar atomic line spectrum, since Ar was the inert gas used to sustain the plasma. Its spectrum was observed predominantly at wavelengths greater than 4300 Å. Interference from this was not a severe problem, as the most useful region of the spectrum for most elements lies between 2000 and 4000 Å.

A carbon atom emission line at 2478.573 Å was also observed which can be attributed to the consumption of the graphite anode.

Some of the previous DCPs showed spectral interference from the cathode material (*3*). Since tungsten emits over 1000 lines, this potentially presented a problem. No W emission was observed with the RA-DCP because spectroscopic measurements were made 4 mm below the cathode. Any ablated cathode material was removed from the spectroscopic zone by the upward gas flow. Thorium, present in 2% composition in the cathode, did not emit any radiation in the observation zone.

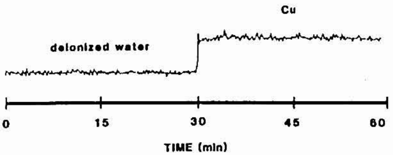

Figure 4. Stability of RA-DCP using the Cu I 3247.540 Å transition.

Table III. Detection Limits

| element | wavelength, Å | RA-DCP, μg mL$^{-1}$ | DCP (*16*), μg mL$^{-1}$ |
|---|---|---|---|
| Al I | 3961.520 | 1.0 | 0.002 |
| As I | 2780.22 | 0.1 | 0.045 |
| B I | 2497.733 | 0.28 | 0.005 |
| Cd I | 2288.002 | 0.03 | 0.008 |
| Ca II | 3933.676 | 0.001 | 0.0002 |
| Cr I | 3593.49 | 0.44 | 0.002 |
| Cu I | 3247.54 | 0.006 | 0.002 |
| In I | 4101.76 | 10.0 | 0.038 |
| Fe I | 3734.864 | 0.6 | 0.003 |
| Pb I | 3683.462 | 6.0 | 0.023 |
| Li I | 6707.76 | 0.02 | 0.002 |
| Mg II | 2795.53 | 0.0001 | 0.0002 |
| Mn I | 4033.07 | 0.003 | 0.002 |
| K I | 7664.907 | 0.36 | 0.015 |
| Ag I | 3280.683 | 0.003 | 0.003 |
| Na I | 5S95.924 | 0.003 | 0.002 |
| Zn I | 2138.56 | 0.033 | 0.002 |

**Stability of the RA-DCP.** Figure 4 shows the signal from the background emission of the Cu I line at 3247.540 Å while operating under optimum conditions and taken over a 1-h period. The figure also shows a signal that resulted from nebulizing a 10 μg mL$^{-1}$ Cu solution. The relative precision of the signal taken every 5 min over a 1-h period was 3.2%, which showed good short-term stability.

**Arc Rotation Rates.** Previous studies on an RA-DCP by Rippetoe and Vickers suggested that arc rotation improved source stability and sample interaction with the plasma by maximizing the arc rotation rate (*3*). In this manner, the analyte is frequently affected by the discharge while passing through the excitation zone. Some of the factors that determine arc rotation rate include gas composition, flow rates, and use of a desolvator.

Argon gas was used in this study because of its inert properties, low cost, and density. A density of 1.7837 g cm$^{-3}$ was well suited to provide an atmosphere to perturb the discharge and cause it to rotate repeatedly. Use of helium, with a density of 0.17847 g cm$^{-3}$, was attempted, but rotation could not be sustained even at maximum flow rates of 4.0 L min$^{-1}$.

The arc rotation rate varied linearly with the tangential gas flow, confirming Rippetoe and Vickers observations (*3*). In this study, the total gas flow of 5.06 L min$^{-1}$, arc rotation rate of 250 Hz, and interelectrode gap of 7 cm permitted the analyte to experience its effect for a period of $2.2 \times 10^{-4}$ s or 0.55 times while passing through the discharge.

The arc rotation rate was observed to be a function of the applied current. This linear relation observed was contrary to what Rippetoe and Vickers had found (*3*). While it would seem that arc rotation rate would depend only on gas flow dynamics, this difference may be attributed to higher temperatures arising from greater currents and electron density. The increase in temperature causes a less dense media, higher gas velocities, and, consequently, increased rotation rates.

**Detection Limits.** Table III lists the detection limits obtained from this study as well as limits from a commercially

**Table IV. Linear Least Squares Regression of Analytical Calibration Curves**

| element | slope | linear corr coeff |
|---|---|---|
| Ag | 0.9255 | 0.9459 |
| Al | 1.3275 | 0.9962 |
| As | 0.9748 | 0.9937 |
| B | 0.9238 | 0.9994 |
| Ca | 1.0244 | 0.9988 |
| Cd | 1.0439 | 0.9976 |
| Cr | 0.8380 | 0.9983 |
| Cu | 2.3739 | 0.9962 |
| Fe | 0.9367 | 0.9949 |
| In | 0.8599 | 0.9990 |
| K | 1.0562 | 0.9928 |
| Li | 1.0311 | 0.9983 |
| Mg | 0.9113 | 0.9895 |
| Na | 1.3333 | 0.9699 |
| Zn | 1.1181 | 0.9963 |

available DCP. In this study, to accommodate the fact that there are differences due to instruments, techniques, and researcher (*15*), two detection limits will be considered to be comparable if their values agree within a factor of 5.

A comparison of the detection limits of the RA-DCP to the commercially available DCP reveal that comparable results are found for Ag, As, Cu, Mg, Mn, and Na.

For Ca, Li, K, and Zn detection limits for the RA-DCP were an order of magnitude higher than those for the DCP, while Al, B, Fe, In, and Pb showed poorer results. Optimization was not performed for each element.

Spectral interferents can account for a poor detection limit with Pb. In this case, the most sensitive line at 4057.807 Å could not be used because of an interferent at 4060.599 Å from argon. Use of the less sensitive line at 3683.462 Å was required. A higher resolution monochromator could circumvent the problem by giving the dispersion necessary to separate the two lines.

**Analytical Curves.** Analytical curves were obtained for several elements. These curves showed good linearity, which was confirmed by the correlation coefficient calculated from a linear least-squares regression for log $C = f(\log I)$, as shown in Table IV. Deviations from linearity at concentrations greater than 100 $\mu$g mL$^{-1}$ because of self-absorption (which frequently occurs in other atomic emission techniques) were not observed.

The slope of the calibration curves varied from 0.8380 to 2.3739, indicating differing sensitivities. Theoretically, the slope of this curve should be 1.0000. The deviation from ideality may be attributed to lack of thermodynamic equilibrium.

**Analyses of Environmental Samples.** River water, sediment extract, and groundwater were analyzed with the RA-DCP. The results are shown in Table V along with a comparison of those obtained by an ICP. The data show comparable results.

## CONCLUSION

The performance of a RA-DCP has been evaluated with respect to its utility as an excitation source in AES.

**Table V. Analyses of Environmental Samples**

| sample | element | concentration, $\mu$g mL$^{-1}$ RA-DCP | ICP |
|---|---|---|---|
| river water | Na | 40 | 41 |
| | Mg | 20 | 24 |
| | Ca | 26 | 33 |
| groundwater | Na | 406 | 408 |
| | Mg | 0.1 | 0.09 |
| | Ca | 1.1 | 1.3 |
| sediment extract | Na | 75 | 79 |
| | Mg | 275 | 271 |
| | Ca | 400 | 395 |
| | Cu | 1.2 | 1.7 |

The background spectrum was studied and found to consist primarily of a relatively weak continuum, hydroxyl rotational band spectra, and argon emission.

Examination of the performance figures of merit showed linearity over 5 orders of magnitude. The detection limits were determined to be comparable to a commercially available instrument for several elements. Further optimization is required for better detection limits. Stability measurements showed a relative standard deviation of 3% over a 1-h period. The results show that the RA-DCP has a strong potential as a good spectroscopic excitation source.

**Registry No.** Al, 7429-90-5; As, 7440-38-2; B, 7440-42-8; Cd, 7440-43-9; Ca, 7440-70-2; Cr, 7440-47-3; Cu, 7440-50-8; In, 7440-74-6; Fe, 7439-89-6; Pb, 7439-92-1; Li, 7439-93-2; Mg, 7439-95-4; Mn, 7439-96-5; K, 7440-09-7; Ag, 7440-22-4; Na, 7440-23-5; Zn, 7440-66-6; $H_2O$, 7732-18-5.

## LITERATURE CITED

(1) Boyko, W. J.; Kelliher, P. N.; Patterson, J. M. *Anal. Chem.* **1982**, *54*, 191R.

(2) Gilbert, T. R.; Hildebrand, K. J. *Am. Lab.* (*Fairfield, Conn.*) **1982**, *14*, 72.

(3) Rippetoe, W. E.; Vickers, T. J. *Anal. Chem.* **1975**, *47*, 2082.

(4) Owen, L. E., personal communication, Tomorrow Enterprises, March, 1978.

(5) Margoshes, M.; Scribner, B. F. *Spectrochim. Acta* **1959**, *15*, 138.

(6) Scribner, B. F.; Margoshes, M. "Actes dv IX Colloquim Spectroscopium Internationale" Lyon 1961, G.A.M.S. Paris, 1963.

(7) Keirs, C. D. Ph.D. Dissertation, Florida State University, Tallahassee, FL, 1977.

(8) Scott, R. H. *ICP Inf. News*. **1978**, *3*, 425.

(9) Veillon, C.; Margoshes, M. *Spectrochim. Acta, Part B* **1959**, *23B*, 553.

(10) Smith, B. W.; Parsons, M. L. *J. Chem. Educ.* **1973**, *50*, 679.

(11) Deming, S. N.; Morgan, S. L. *Anal. Chem.* **1973**, *45*, 278A.

(12) Meggers, W. F.; Corliss, C. H.; Scribner, B. F. "Tables of Spectral-line Intensities, Part I-Arranged by Elements"; U.S. Government Printing Office: Washington DC, 1975; NBS Monograph 145.

(13) Holloway, J. R.; Kacoyannakis, J. F. "Preparation of Synthetic Grande Ronde Basalt (Umtanum) Ground Water"; Rockwell Int. Subcontract SA-865, Richland, WA, 1980.

(14) Sinex, S. A.; Cantillo, A. Y.; Helz, G. R. *Anal. Chem.* **1980**, *52*, 2342.

(15) Parsons, M. L. Seventh Annual Meeting of FACSS, Abstract 172, Sept 1980.

(16) "Plasma Emission Spectrometers for Atomic Analysis"; SpectraMetrics, Inc.: Andover, MA, 1980.

RECEIVED for review March 9, 1983. Resubmitted January 7, 1985. Accepted January 7, 1985.

*Anal. Chem.* 1985, *57*, 846–851

# Moderate-Power Helium Plasma as an Element-Selective Detector for Gas Chromatography of Dioxins and Other Halogenated Compounds

**David L. Haas[1] and Joseph A. Caruso***

*Department of Chemistry, University of Cincinnati, Cincinnati, Ohio 45221*

**A moderate-power helium microwave discharge is characterized as an element-selective detector for the gas chromatography of halogenated compounds. Plasma power and gas flow are optimized utilizing a mixture of chlorinated dioxins and pesticides. Not surprisingly, the lowest flows possible with the tangential flow torch produced the best sensitivity. Unlike earlier solution nebulization work, the higher plasma powers utilized led to poorer *S/N*. Multielement chromatograms are determined at several wavelengths corresponding to the elemental emission available from specific compounds. Detection limits and linear ranges are presented. In addition to the quantitative importance of this technique, elemental ratios (leading to empirical formulas) are determined with high accuracy by using an off-line background correction scheme. On-line background correction schemes were also useful although inferior to the off-line method. When no background correction is employed, the accuracy of the elemental ratio is considerably degraded.**

During the last 20 years, the microwave-induced plasma (MIP) has become popular as an element-selective detector for gas chromatography (*1, 2*). Selectivity in the detection of chromatographic eluents is gained since the He-MIP responds primarily to the elemental constituents of a compound, rather than to the entire compound. The element-selective capability of the microwave discharge allows more flexibility in the determination of gas chromatographic eluents, vs. electron capture and flame ionization detectors which respond nonselectivity to all compounds or to a given class of compounds.

Multielement determinations are facilitated by the utilization of a polychromator for the spectrometric determination of many compounds. The grating of the polychromator disperses radiation from the plasma along a focal curve, which contains exit slits and photomultiplier detectors for emitted radiation of the elements of interest. Ideally, all elements in the periodic table could be determined simultaneously provided data acquisition could be performed at a rapid rate, and a sufficient number of detectors could be positioned within the instrument. Commercial Ar-ICP/polychromator systems claim the capability of determining many elements simultaneously. Also, the time required for multielement determination of a sample is greatly decreased vs. single channel or slew-scanning monochromator systems. Gas chromatographic (GC) separations have been reported utilizing both an Ar-ICP (*3*) and He-MIP (*4–8*) in conjunction with polychromatic detection. In addition, the simultaneous multielement capability of the He-MIP/polychromator has allowed determination of elemental ratios of compounds eluting from a gas chromatograph (*4–7*).

**Table I. Components, Models, and Manufacturers for a Moderate-Power MIP/GC System**

| component | model or type | manufacturer |
|---|---|---|
| gas chromatograph | 570 | F&M Scientific |
| 3-way valve | 2033 | Carle Instruments |
| transfer block power supply | 120 V, 85 W | Chromalox |
| polychromator | 66-000 1.5 m, 1180 G/mm | Jarrell-Ash |
| stepper motor | M061-F608 | Slo-Syn (McGraw Edison) |
| photomultiplier | 1P28<br>R426 | RCA<br>Hamamatsu |
| amplifier | i to e | laboratory built |
| computer | Intel-8080 64K micro | laboratory built |
| resonant cavity | $TM_{010}$ internally tuned | laboratory built |
| generator | 420-1, 600 W | Micro-Now |
| tangential flow torch | 8/6 o.d./i.d. quartz | laboratory built |
| helium | 99.0% | Wright Brothers |

The elution of C-containing compounds presents a potential source of error in multielement determination, due to background shifts at the elemental line of interest caused by emission from molecular species such as CN, $C_2^+$, and CO. Relatively poor selectivities for C vs. such elements as Cl and Br have been attributed to this continuum shift (*9*). As a C-containing compound enters the plasma detector, the background continuum increases producing intensity at all spectral lines. Since this intensity is not due to the element of interest, "false peaks" in the chromatograms and nonlinear response are common problems with determinations at elemental lines other than carbon. To avert this problem, either on-line (*10*) or off-line (*8*) background correction schemes may be employed. On-line background correction involves monitoring the background intensity shift caused by C at all spectroscopic lines when the element of interest is not present. This background response due to C is then subtracted from the signal intensity when the element of interest is present, to yield the net signal intensity (in area or peak height) for the element. Off-line background correction can be performed utilizing an oscillating refractor plate which shifts the spectra on and off the emission lines of interest. Data collection, both on-line and off-line, thereby allows calculation of net signal intensity.

Many workers have employed the low-power He-MIP for the determination of halogenated compounds. With the availability of moderate-power microwave generators for analytical work (*11, 12*), a moderate-power He-MIP is potentially an attractive alternative as an excitation source for GC detection. The object of this work is to characterize a moderate-power He discharge as an element-selective detector for the gas chromatography of a variety of halogenated compounds, including the environmentally important dioxin group.

---

[1] Present address: Union Carbide Corp., P.O. Box 8361, South Charleston, WV 25303.

0003-2700/85/0357-0846$01.50/0 © 1985 American Chemical Society

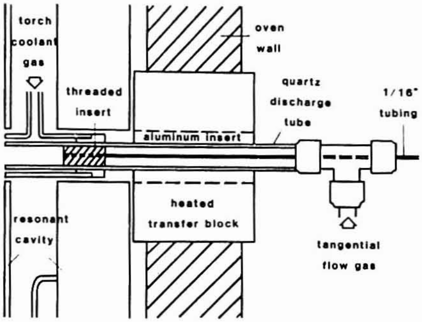

Figure 1. Modified tangential flow torch/GC interface. A heated transfer block prevents condensation of analyte in route to the plasma.

## EXPERIMENTAL SECTION

**Instrumentation.** The system schematic diagram is similar to that reported earlier (*8*). Experimental components and model numbers are listed in Table I. The internally tuned resonant cavity (*11*) was mounted on a gas chromatographic oven (F & M Scientific, Hewlett-Packard). To provide a means of venting a solvent peak, a three-way valve (Carle Instruments, Model 2033) was placed after the chromatographic column ($^1/_4$ in. × 3 ft quartz packed with 2% OV-101 on a silica support). The solvent peak must be vented with a low-power He-MIP to avoid extinguishing the plasma. At moderate power levels, the plasma was stable with the introduction of relatively large amounts (ca. 5 $\mu$L) of organic solvent. As might be expected, however, C background increased dramatically and thus solvent venting was employed throughout the investigation. During solvent venting, the plasma was maintained with a tangential flow gas as discussed below. Provisions were made to heat the tangential gas by passing it through 30 ft of $^1/_8$ in. stainless tubing before entry to the plasma. To minimize peak broadening, all existing union and "T" connectors were replaced with low dead volume fittings (Swagelok fittings, Cincinnati Valve and Fitting, Cincinnati, OH).

**Torch Design and Chromatographic Interface.** To avoid decomposition of the containment tube, it is critical that the moderate-power plasma remain centered. To satisfy this requirement, a torch was designed similar to the modified tangential torch discussed recently (*12, 13*). The torch design and chromatographic interface are given in Figure 1. A $^1/_{16}$ in. × 0.010 in. stainless steel tube from the chromatographic column passed through one end of a $^5/_{16}$ in. "T" connector and into a threaded, stainless steel insert placed within the discharge tube. This threaded insert is also threaded onto the low volume $^1/_{16}$ in. tubing from the column, both securing the insert in position and allowing its easy replacement. The stainless steel insert was quadrathreaded (four threads, 90° apart), with a thread depth of 0.020 in. and a pitch of 3-1/4 turns/in. The threaded insert fits snugly into a quartz discharge tube (8 mm o.d., 6 mm i.d.) which is secured in the other end of the "T" connector. To dissipate additional heat, the discharge tube was cooled by flowing $N_2$ gas through an outer cooling tube. To prevent condensation of the analyte as it is transported from the column to the plasma, the quartz discharge tube was passed through an aluminum insert ($^1/_2$ in. o.d., 8 mm i.d. × 3 in.) which was secured in a $^1/_2$ in. hole of an aluminum heating block. Power for the heating blocks (Chromlox, 120 V, 85 W) and thermocouples were provided with the controls of the gas chromatograph.

**Emission Lines.** Four emission lines (channels) were available for spectral observation. Namely C I at 247.9 nm; Br II at 470.5 nm; Cl II at 479.5 nm; and H I at 656.3 nm. The H I line was monitored with a red-sensitive photomultiplier (Hamamatsu R-446). The others were as described previously (*8*).

**Data Acquisition.** The plasma image was focused through a quartz lens (4 cm, 15 cm focal length, Ealing Optical) onto the entrance slit of the polychromator. Emission from the plasma passed through an oscillating quartz refractor plate and onto a concave grating where the radiation was dispersed along the Rowland circle of the polychromator. A stepper motor controller (*8*) oscillates the refractor plate to allow dynamic off-line background correction. The current of each photomultiplier is converted to voltage and sent to the PMT data preprocessor which "latches" the data before it is sent to the ADC board of the 8080 microcomputer for digitization.

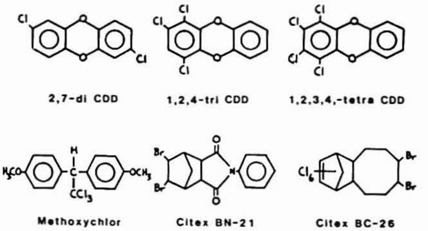

Figure 2. Chlorinated dioxins and pesticides.

**Sample Preparation and Procedures.** 2,7-Dichlorodioxin (2,7-di CDD), 1,2,4-trichlorodioxin (1,2,4-tri CDD), 1,2,3,4-tetrachlorodioxin (1,2,3,4-tetra CDD, also given as TCDD in some of the figures), Citex BC-26, Citex BN-21, Methoxychlor, and hexachlorocyclohexane (BHC) solutions all were prepared by weighing on a microbalance the amount of compound needed to prepare a 10 000 ppm stock solution, followed by dilution with benzene or isooctane in a 10.0-mL volumetric flask. These compounds were provided by the U.S. FDA. The dioxins also were obtained from Chem Service, Inc. BHC was obtained from the U.S. EPA. Diethyl phthalate (DEP) and dibutyl phthalate (DBP) are liquids and were obtained through the U.S. EPA. They were prepared by removal of the volume needed to produce a 10 000 ppm stock solution, followed by dilution with benzene in a 10.0-mL volumetric flask. Serial dilutions were then performed to obtain desired solution concentrations. Five microliters of the appropriate mixture was injected onto the chromatographic column.

## SOFTWARE

Data manipulation was performed utilizing appropriate software as discussed in an earlier work (*8*) but modified to provide additional features to store the chromatographic data on disk, recall of a chromatographic data set from the disk, calculation of detection limits and elemental ratios, and output of all calculations on the printer.

## RESULTS AND DISCUSSION

**(1) Plasma Power.** A study was performed to determine the effect of applied power to the helium discharge on the Cl signal intensity and signal-to-noise ratio of C and Cl in several halogenated compounds. A test mixture containing 2,7-di CDD, 1,2,4-tri CDD, 1,2,3,4-tetra CDD, Methoxychlor, Citex BN-21, and Citex BC-26 was selected due to the environmental significance of these compounds. Their structures are presented in Figure 2. All compounds except BN-21 contain chlorine. Citex BC-26 contains both chlorine and bromine. The mixture, consisting of 1000 ng (6.94 $\mu$L of 144 ppm) of each compound was injected. Off-line background correction was used throughout the experiment. The resulting separation is shown in Figure 3. Chromatographic operating conditions for this separation are listed in Table II

The effect of power on the signal intensity and signal-to-noise ratio for C and Cl emission illustrates a similar trend, as is illustrated in Figure 4 for C with a decrease followed by a slower increase in intensity and signal-to-noise ratio for both C and Cl, as power to the discharge is increased from 145 to 425 W (as measured at the generator). The noise on both channels (elements) steadily increases with power, and thus the optimal power level is the lowest (ca. 145 W) that could be obtained with this generator/cavity configuration. Un-

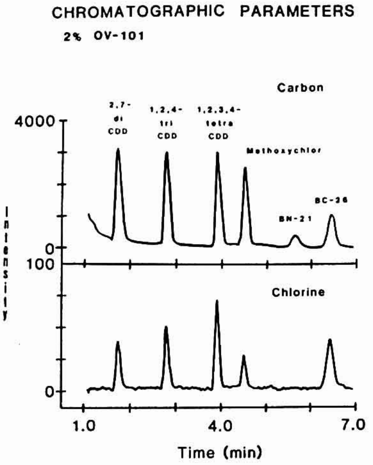

**Figure 3.** Gas chromatographic separation of chlorinated dioxins and pesticides, 190 W He plasma.

Table II. Moderate-Power He-MIP/GC Operating Conditions Utilized in Optimizing Plasma Conditions and Calculations of C/Cl Ratios

| | plasma optimization | | calculation of C/Cl ratios | |
|---|---|---|---|---|
| | Plasma Conditions | | | |
| forward power | 190 W | | 190 W | |
| reflected power | 0 W | | 0 W | |
| He flow (tangential) | 750 mL/min | | 750 mL/min | |
| He flow (column) | 25 mL/min | | 25 mL/min | |
| | GC Conditions | | | |
| column size | 1/4 in. × 3 ft | | 1/4 in. × 3 ft | |
| column packing | 2% OV-101 | | 2% OV-101 | |
| column flow | 25 mL/min | | 25 mL/min | |
| temp (injection port) | 300 °C | | 300 °C | |
| temp (transfer block) | 300 °C | | 300 °C | |
| temp gradient | time, min | temp, °C | time, min | temp, °C |
| | 0 | 190 | 0 | 100 |
| | 2 | 190 | 2.3 | 240 |
| | 3 | 240 | 7 | 240 |
| | 7 | 240 | | |
| injection volume | 6.9 μL | | 5.0 μL | |

fortunately, the plasma would not center at 145 W, preferring to cling to the wall of the discharge tube. To avoid etching the containment vessel, 190 W was chosen for the remainder of the studies as the plasma was easily centered at this power level.

**(2) Plasma Gas Flow.** The identical separation discussed above was utilized to determine the flow rate which yielded the greatest increase in C and/or Cl signal intensity and signal-to-noise ratio in a 190-W He discharge. Again, relative intensities for C and Cl responses were averaged over all compounds and are depicted in Figure 5. Both C and Cl responded similarly and showed increased intensity and *S/N* (results not shown) with decreased flow. This phenomenon is common with plasma sources and indicated a response dependent upon analyte residence time in the discharge. A tangential flow of 750 mL of He/min was needed to center the discharge and thus to avoid degradation of the containment vessel. The remainder of the studies were run at this flow.

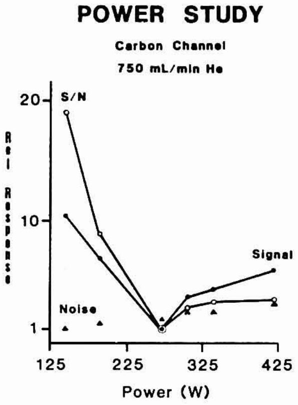

**Figure 4.** Power study on the C channel. Increased C signal-to-noise ratio in the He plasma discharge was obtained at lowest powers. The chlorine channel shows similar trends.

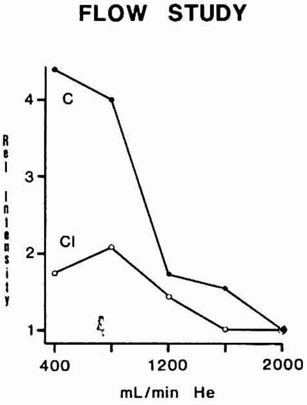

**Figure 5.** Tangential flow study with C and Cl. Low flows provided increased intensity and *S/N* on the C and Cl channels, 190 W He plasma.

**(3) Chromatography.** To investigate on-line vs. off-line background correction, and background interference due to C on the Cl channel, a test mixture was produced which contained three chlorinated compounds (Lindane (BHC), 1,2,3,4-tetra CDD, and Methoxychlor) and two non-chlorinated compounds (DEP and DBP). Chromatographic conditions are listed in Table II. The chromatographic separation, monitoring the C, Cl, and H channels, is presented in Figure 6.

**(4) Detection Limits and Precision.** Detection limits and percent relative standard deviations for C and Cl were calculated from averages of five replicates of the mixture described below. A 5.0-μL injection, containing 500 ng of DEP, 500 ng of BHC, 500 ng of DBP, 360 ng of 1,2,3,4-tetra CDD, and 440 ng of Methoxychlor, was used for all detection limit and precision studies. The detection limits and precision for

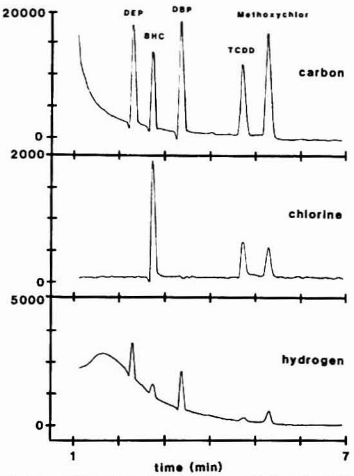

**Figure 6.** Separation of chlorinated and nonchlorinated priority pollutants. Responses on the C, Cl, and H channels are indicated. Relative intensities are given on the vertical axis.

**Table III. Comparison of Detection Limits and Precision of the Moderate vs. Low Power He-MIP/GC**

| element (channels) | mod power (single)[a] | mod power (multiple)[b] | low power (8) (multiple)[b] |
|---|---|---|---|
| | Detection Limits (pg/s) | | |
| C | 76 | 100 | 24 |
| Cl | 120 | 250 | 76 |
| H | ND[c] | 50 | ND |
| | Precision (% RSD) | | |
| C | 3.0 | 2.7 | 2.6 |
| Cl | 6.7 | 4.6 | 3.8 |

[a] Single element monitoring. [b] Multielement monitoring. [c] ND, not determined.

carbon, chlorine, and hydrogen determined in the moderate power helium discharge are listed in Table III. Data are compared for multielement acquisition using off-line correction vs. single channel determination utilizing on-line background correction. Detection limits were roughly 25 to 100% higher with off-line vs. on-line correction. This appears reasonable as the oscillating refractor plate allows less time for actual data acquisition on a given channel. The direct comparison of off-line vs. on-line correction (in the multielement mode) could not readily be accomplished with the present instrumentation. For comparison purposes, detection limits and precision values determined in a low power helium discharge on the same polychromator are also presented (*8*).

Detection limits for C and Cl determined in the moderate power He-MIP are approximately 4 times higher than C and Cl determined in a low-power He-MIP on the same polychromator system (*8*). These increased levels of detection might be attributed to several factors: (*a*) *Helium Flow.* Large He flows are required to maintain a centered plasma arrangement within the discharge tube. Larger flows decrease analyte residence time in the discharge and thus produce decreased signal intensity. The total He flow is 775 mL/min (750 mL/min tangential flow + 25 mL/min column flow) in the moderate power system vs. 80 mL/min He flow (20 mL/min auxiliary flow + 60 mL/min column flow) for the low power system (8). (*b*) *Elevated Background Excitation and Emission.* It is possible that complete molecular fragmentation also occurs at the lower power levels (*10, 14, 15*). If this is the case, then the higher power available from the moderate power discharge may be further exciting the molecular background of the sample and thereby degrading the *S/N* (resulting in higher detection limits). (*c*) *Optical Coupling.* The optical coupling to the polychromator was performed with different lenses in the two studies (this work and ref 8). The internally tuned cavity resonator possesses two stubs which protrude from the face plate of the cavity, limiting the focal length of the lens selected to focus the plasma image at the entrance slit. A 4.0 cm diameter, 15 cm focal length quartz lens was used vs. a 5.0 cm diameter, 10 cm focal length quartz lens in the low power system (*8*). The smaller lens limits the solid angle of light collected, allowing less light to the polychromator.

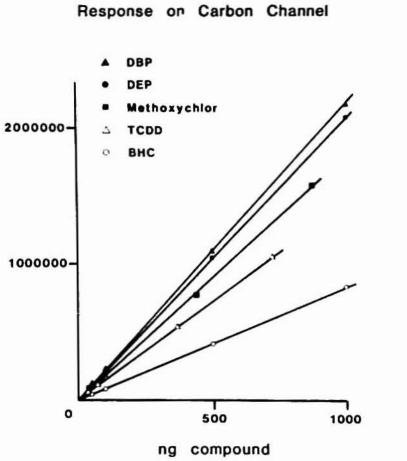

**Figure 7.** Carbon response per nanograms of compound. Relative intensity given on vertical axis. The chlorine response is similar.

Although it was initially anticipated that the detection limits would be lowered with the use of higher plasma powers, the data suggest that the lower power plasmas may be even better suited for gas analysis and will allow high-quality analytical results.

**(5) Linear Dynamic Ranges.** Single channel determinations for C and Cl were performed utilizing duplicates of 5-$\mu$L injections of the test mixture described above. The refractor plate at the entrance slit was placed in a fixed position, and thus no background correction was performed. The C (247.9 nm) channel response of DBP, BHC, DBP, 1,2,3,4-tetra CDD, and Methoxychlor in a 190-W He-MIP (750 mL/min flow) per ng of compound and ng of C is presented in Figures 7 and 8. The Cl (479.5 nm) channel response to BHC, 1,2,3,4-tetra CDD, and Methoxychlor per nanogram of compound and nanogram of Cl is similar to that given for C so the figures are not reproduced here. Both channels demonstrate linearity from 10 to 1000 ng of compound injected. Also a plot of intensity per nanogram of compound collapses to yield a constant slope when plotted as intensity per nanogram of element. This universal response, regardless of compound structure, indicates that reproducible fragmenta-

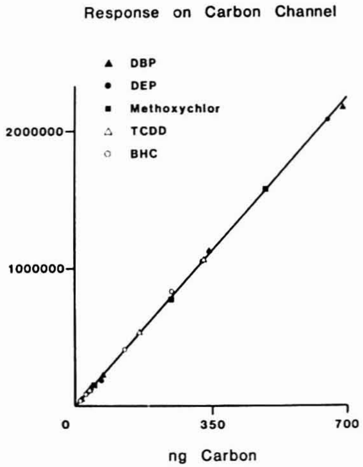

**Figure 8.** Carbon response per nanograms of carbon. Relative intensity given on vertical axis. The chlorine response is similar.

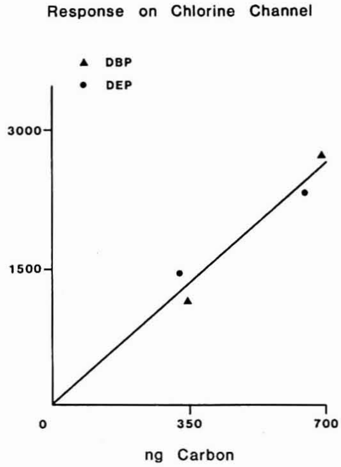

**Figure 10.** Carbon response on chlorine channel. Relative intensity is given on vertical axis.

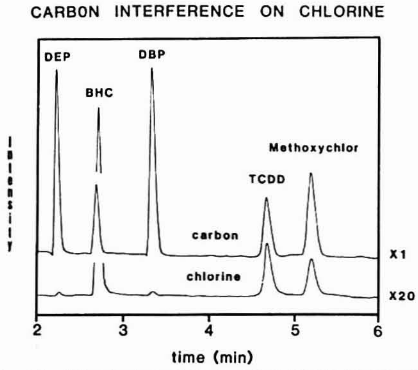

**Figure 9.** Carbon background interference on the chlorine channel. The chlorine channel was amplified 20-fold. Notice two "false peaks" appearing on the Cl channel are caused by non-Cl containing compounds.

**Table IV. Elemental C/Cl Ratios and Percent Error in Determination**[a]

| compound | actual C/Cl ratio | single element no bkg corr | single element on-line bkg corr | multielement off-line bkg corr |
|---|---|---|---|---|
| BHC | 1.00 | 0.95 (−5.0) | 0.96 (−4.0) | 1.00 (0) |
| 1,2,3,4-tetra CDD | 3.00 | 2.92 (−2.7) | 3.00 (0) | 3.02 (+.67) |
| Methoxychlor | 5.33 | 4.89 (−8.3) | 5.12 (−3.9) | 5.36 (+.56) |

[a] Percent error in determination of actual C/Cl ratio is given in parentheses.

tion of analyte occurs in the discharge. A plot of intensity vs. nanogram of element with constant slope, regardless of compound size or structure, is critical if elemental ratios are to be calculated.

**(6) Background Correction Schemes.** A system utilizing multielement data acquisition (with off-line correction) was compared with single element data acquisition (with and without on-line correction) for the determination of C/Cl ratios. The first system utilized the multielement capabilities of the polychromator in conjunction with an oscillating refractor plate which facilitated stepping "on and off" (ca. 0.2 nm) the spectrometric line of interest. Data acquisition was synchronized so that off-line data (background) could be dynamically subtracted from on-line data (background + signal), resulting in a background corrected chromatogram.

The second system involved monitoring C and Cl channels individually with the identical polychromator used in the former study (*8*). As C-containing compounds eluted from the chromatograph into the plasma, the background intensity increased due to molecular species such as CN, CO, $C_2^+$, etc. The rise and fall in background emission, as the C-containing compound eluted, produced a "false peak" on the Cl channel. This effect is illustrated in Figure 9. Both DEP and DBP (neither contain Cl) appear on the Cl channel. In addition, it is reasonable to assume a slightly inflated Cl intensity for compounds containing both C and Cl due to the above cited background shift. Background correction was performed by monitoring the intensity on the Cl channel due to compounds containing no Cl (DEP and DBP). In theory, intensity on the Cl channel per nanogram of C can then be subtracted from the Cl intensity to give a net Cl intensity corrected for the background interference. A plot of intensity on the Cl channel per nanogram of C (C-containing compounds with no chlorine) is given in Figure 10.

**(7) Elemental Ratios.** Elemental C/Cl ratios were calculated with five replicates of the mixture described above. Calculations using multiple channel acquisition were performed with the software described above. Elemental ratio calculations performed by monitoring the C and Cl channels individually must first be corrected for the background interference due to C on the Cl channel. Background correction is performed by subtracting the amount of emission on the Cl channel which corresponds to the amount (ng) of C in the chromatographic peak. Elemental C/Cl ratios as determined by multiple channel acquisition with off-line correction, and single channel acquisition with and without on-line correction are listed in Table IV. The percent error on determination as compared with the actual C/Cl ratio is also presented.

Single channel determinations of the C/Cl ratio of BHC, 1,2,3,4-tetra CDD, and Methoxychlor are all lower than the actual values for these compounds. As expected, the background interference due to C on the Cl channel does lead to significant error on the determination of the C/Cl ratio of a compound. This interference inflates the value of the Cl intensity, resulting in low C/Cl ratios. Subtraction of the Cl channel interference decreases the error in the determination of these ratios.

Multiple channel analysis with off-line correction leads to the determination of C/Cl ratios which are very close (<1% error) to the actual elemental ratios of the compounds studied. Here, C and Cl intensities are measured from a chromatographic eluent at the same time, rather than from separate chromatograms as in the above correction technique. The more interesting comparison of multichannel determination with off-line vs. on-line background correction of elemental ratios is now being pursued.

## ACKNOWLEDGMENT

The authors are grateful to Dr. Firestone and F. L. Fricke of the U.S. FDA for providing several of the compounds. We also acknowledge S. M. Pyle of the U.S. EPA for the BHC and the dialkyl phthalates. This work was supported by the National Institute of Environmental Health Sciences through Research Grant No. ES-03221.

**Registry No.** 2,7-Di CDD, 33857-26-0; 1,2,4-tri CDD, 39227-58-2; 1,2,3,4-tetra CDD, 30746-58-8; DEP, 52-68-6; DBP, 84-74-2; BHC, 58-89-9; Methoxychlor, 72-43-5; Citex BN-21, 40703-79-5; Citex BC-26, 51936-55-1; He, 7440-59-7.

## LITERATURE CITED

(1) Carnahan, J. W.; Mulligan, K. J.; Caruso, J. A. *Anal. Chim. Acta* **1981**, *130*, 227.
(2) Risby, T. H.; Talmi, Y. *CRC Crit. Rev. Anal. Chem.* **1983**, *14*, 231.
(3) Windsor, D. L.; Denton, M. B. *J. Chromatogr. Sci.* **1979**, *17*, 492.
(4) Brenner, K. S. *J. Chromatogr.* **1978**, *1967*, 365.
(5) Bonnekessel, J.; Klier, M. *Anal. Chim. Acta* **1978**, *103*, 29.
(6) McLean, W. R.; Stanton, D. L.; Penketh, G. E. *Analyst (London)* **1973**, *98*, 432.
(7) Dingjan, H. A.; De Jong, H. J. *Spectrochim. Acta, Part B* **1981**, *36B*, 325.
(8) Eckhoff, M. A.; Ridgway, T. H.; Caruso, J. A. *Anal. Chem.* **1983**, *55*, 1004.
(9) Estes, S. A.; Uden, P. C.; Barnes, R. M. *Anal. Chem.* **1981**, *53*, 1829.
(10) Hagen, D. F.; Belisle, J.; Marhevka, J. S. *Spectrochim. Acta, Part B* **1983**, *38B*, 377.
(11) Haas, D. L.; Carnahan, J. W.; Caruso, J. A. *Appl. Spectrosc.* **1983**, *37*, 82.
(12) Haas, D. L.; Caruso, J. A. *Anal. Chem.* **1984**, *56*, 2014.
(13) Bollo-Kamara, A.; Codding, E. G. *Spectrochim. Acta, Part B* **1981**, *36B*, 973.
(14) Qing-Yu, O.; Guo-Chuen, W.; Ke-Wei, Z.; Wei-Lu, Y. *Spectrochim. Acta, Part B* **1983**, *38B*, 419.
(15) Ke-Wei, Z.; Qing-Yu, O.; Guo-Chuen, W.; Wei-Lu, Y. "1984 Winter Conference on Plasma Spectrochemistry"; San Diego, Jan 1984; Paper 60.

Received for review August 27, 1984. Accepted January 2, 1985.

# Improved Detection Limits in Inductively Coupled Plasma Multichannel Spectrometry of Uranyl Nitrate Solutions by Compensation of Nonrandom Background Fluctuations

**Avraham Lorber,* Michael Eldan, and Zvi Goldbart**

*Nuclear Research Centre—Negev, P.O. Box 9001, Beer-Sheva 84190, Israel*

**Detection limits in nonrandom (flicker) noise dominated signals are directly proportional to the noise level in the signals. However, the nonrandom noise may be removed by a mathematical technique that requires dedicating several channels to monitoring background fluctuations. The applicability of the correction method to atomic emission spectra generated by an inductively coupled plasma (ICP) is tested for the determination of the detection limits of 20 analytes dissolved in uranyl nitrate solutions. A direct-reading spectrometer commonly used for routine multielement atomic emission analysis was employed. Up to 20-fold improvement in detection limit was achieved. Statistical measures were used to determine which analytical channel can be compensated for and also to determine whether a satisfactory correction could be achieved during the analytical run.**

The evaluation of the background contribution to the gross analyte signal is a critical step in any analytical quantification. The intense emission from atomic emission sources is also responsible for their greatest drawback—spectral interferences that complicate the analyte signal determination. Continuum and structured radiation from the source, spectral lines from the matrix, and scattered light, all contribute to this spectral interference problem. Blank subtraction will not give the sought-for correction in atomic emission spectrometry, because the blank and sample are not measured simultaneously. Source fluctuations, drift, and sample to sample variations all contribute to the uncertainty in the background corrected (or "net") analyte signal determination. Deterioration of more than 1 order of magnitude in detection limits in "real samples" is frequently encountered even without spectral overlap. A commonly used method for background subtraction is extrapolation of the value of the background at the analytical wavelength from the background in its vicinity. This approach is preferred over blank subtraction as it allows simultaneous, or quasi-simultaneous, determination during the analytical run, thus reducing the uncertainty in the net signal. Modern multielement analytical apparatus are equipped with both the hardware (refractor plate, fast scan drive, or array detectors) and the software to perform this determination. However, this method has two shortcomings: (a) the analysis duration

0003-2700/85/0357-0851$01.50/0 © 1985 American Chemical Society

is lengthened at least by a factor of 3 (except for array detectors), and (b) determination of the background is complicated when the matrix constituents contribute to the spectrum in the vicinity of the analytical wavelength (or even impossible when there is an overlap (*1*)).

A method that will combine the advantages of both blank subtraction and simultaneous background determination will result in better analytical performance. Weekly and Norris (*2*) monitored one readout channel in a direct reading spectrometer, in order to correct background fluctuations at the analytical wavelengths. Their method was based on the same assumption as the internal reference method, i.e., that a change in background intensity at the monitored wavelength is accompanied by a directly proportional change in background at all analytical channels. Thompson and Bankston (*3*) used several background monitor positions to calculate a regression equation for the background intensity. Attempts to apply this concept to microwave plasmas (*4*) were not successful in terms of precision. Replacing the above with a correlation of the analytical channel to the monitored one will greatly diminish the disadvantage of the simple model. Schmidt and Slavin (*5*) and Myers and Tracy (*6*) applied correlated monitoring to spectra from inductively coupled plasma (ICP). Myers and Tracy claimed that a high degree of correlation occurs between any two points in the plasma background over the wavelength interval from 200 to 760 nm. However, when matrix concomitants also contribute to the background at the analytical channel, one monitoring channel will not suffice. Thus, the benefits that may be gained by applying this method to "real samples" are not clear.

Lorber and Goldbart (*7*) suggested a modification of the internal reference method by a generalized one (GIRM). The GIRM is based on simultaneous measurements of several channels that respond differently to variations of parameters of the analytical system. Temporal characteristics of the monitored channels help to determine the fluctuations in the background at the analytical channels. The method is applicable when the factors affecting fluctuations in the monitored channels are the same as those affecting the analytical channel's background. The method was applied to correct fluctuations in signals that were free from interferences (*8*). The aim of the present work is to test the applicability of GIRM to background fluctuation correction. GIRM performs better in term of nonrandom noise removal than the internal reference projection method (IRPM) (*9*). However, we make use of IRPM as it allows real time compensation and there is no need to add an internal reference element. In order to demonstrate the usefulness of the method, we applied it to the uranium matrix, whose spectral interferences are the most severe in atomic emission spectrometry.

## EXPERIMENTAL SECTION

**Apparatus.** A direct reading spectrometer, Jobin-Yvon Model JY48, with 44 standard analytical channels and 4 external channels, was used in this study. The spectrometer incorporates a holographic grating ruled with 2550 grooves/mm, giving spectral coverage from 160 to 410 nm, and is equipped with fixed slits with widths of 37 μm, resulting in a resolution of 0.014 nm. Twenty six channels of the spectrometer were used. Two external channels were used: a monochromator, Jobin-Yvon Model H20 located at 595 nm, and an interference filter, Spectro-Film Inc, peak wavelength 766 nm with bandwidth of 10 nm. The photomultipliers used were standard type Hamamatsu R300. All other experimental facilities and operating conditions are given elsewhere (*8*).

**Reagents.** Stock solutions were prepared by dissolving pure metals or reagents (Specpure grade, Johnson-Matthey) in dilute acids (Suprapur grade, Merck) and deionized distilled water. Uranyl solutions, 0.5% (wt uranium), were prepared by dissolving uranyl nitrate in a mixture of 5% (vol) nitric acid. Analyte solutions were stored as 1000 μg/g stock solutions. Limits of detection (LOD) were determined from fresh multielement solutions containing concentrations 1000 × LOD (in water).

**Procedure.** Each measurement consisted of three successive 10-s integrations.

*Calibration of the Response of the Background to Variations in Plasma Parameters.* A 0.5% solution (wt uranium) is used. No internal standard is added to this solution, and the emission signals from uranium and the plasma on monitored channels are used. The calibration is accomplished by deliberately altering all parameters of the instrumental system. The first measurement is taken at the set point of the system, and the data obtained are used for "blank subtraction" from the subsequent measurements. The number of measurements should be greater than the number of monitored channels. The data from the calibration are processed by the singular value decompositon (SVD) (*10*), as described elsewhere (*9*). The results of the calibration step are projection matrices that include numerical values which are used for compensation.

*Compensation.* At the first measurement a blank solution is aspirated and the collected data are used for blank subtraction from the subsequent standard and samples. The compensation for background fluctuations at the *i*th channel is accomplished according to

$$\text{corrected background value} = (I_i^R - 1) - \sum_{i=1}^{p} z_{i,j}\hat{x}_j/(1 - z_{i,p+1}) \tag{1}$$

All the symbols in the equation are as defined in ref 9. However, this equation differs from eq 6 in ref 9 in that compensation is carried out by subtraction rather than by division.

*Calibration for the Response of "Net" Analyte Signals to Concentration.* After the compensated background is subtracted, the calibration is performed by regression to a zero intercept curve.

**Computation.** Subroutines were written in FORTRAN IV, and added to the original software that operates the JY48 spectrometer. Several modifications in the original program that allow for real time compensation were also incorporated. The SVD is computed by SVDRS subroutine of Lawson and Hanson (*10*). A Digital PDP 11/23 minicomputer was used.

## RESULTS AND DISCUSSION

**Selection of Monitored Channels.** There are several criteria that should be considered when deciding which channel to select; (a) The monitored channel fluctuations should not be affected by unexpected variations, such as emission from an analyte that may be present in the solution. (b) The fluctuations should be governed by nonrandom (flicker) noise. This is ensured by selecting channels with sufficiently high signals. (c) The factors that cause fluctuations of the selected monitored channel must also affect fluctuations in the analytical channels. The last criterion is a requirement of the computation method. As the similarity between the factors affecting the monitored set and the analytes increases, the quality of the compensation will also increase. In multielement analysis the background of the various analytical channels may be affected by several factors. In order to ensure that the set of monitored channels will be able to compensate for the various analytical channels, the factors affecting them should be as large as possible. The fulfillment of the first two criteria is quite obvious. However, the fulfillment of the last criterion is achieved by examining the calibration data by factor analysis techniques, as will be described.

In order to avoid the need to add internal reference material, we selected channels so that the above mentioned three criteria will be met by the data from the uranium and argon emission signals. Table I presents the eight channels chosen to monitor background fluctuations.

**Calibration.** For the purpose of calibration nine sets of measurements are sufficient, of which the first serves as the blank and the others for the determination of the fluctuations. However, the amount of data will not allow statistical inference regarding the adequacy of the monitored channel set to the

**Table I. Monitored Channels and Their Projection Matrix**[a]

| wavelength, nm | 361.384 | 326.990 | 316.340 | 318.341 | 385.958 | 404.442 | 766 | 595 |
|---|---|---|---|---|---|---|---|---|
| 361.384 (Sc II) | 0.343 | −0.062 | −0.039 | 0.398 | 0.126 | 0.197 | −0.073 | 0.040 |
| 326.990 (Sc I) | −0.062 | 0.492 | 0.341 | −0.185 | 0.272 | 0.118 | 0.079 | −0.036 |
| 316.340 (Nb II) | 0.039 | 0.341 | 0.770 | 0.133 | −0.166 | −0.103 | −0.054 | 0.025 |
| 318.341 (V II) | 0.398 | −0.185 | 0.133 | 0.612 | −0.081 | 0.100 | 0.089 | −0.049 |
| 385.958 (U II) | 0.126 | 0.272 | −0.166 | −0.081 | 0.539 | 0.353 | −0.014 | −0.007 |
| 404.442 (Ar I) | 0.197 | 0.118 | −0.103 | 0.100 | 0.353 | 0.274 | −0.019 | 0.025 |
| 766 | −0.073 | 0.079 | −0.054 | 0.089 | −0.014 | −0.019 | 0.976 | 0.012 |
| 595 | 0.040 | −0.036 | 0.025 | −0.049 | −0.007 | 0.025 | 0.012 | 0.993 |

[a] The signals of the monitored channels are due to uranium and argon emission.

**Table II. Correction Coefficient Values for the Listed Background Positions and Corresponding Elements in the Channel's Position**

| element and spectral position (nm) | monitored wavelengths, nm | | | | | | | | |
|---|---|---|---|---|---|---|---|---|---|
| | 361.384 | 326.990 | 316.340 | 318.341 | 385.958 | 404.442 | 766 | 595 | |
| Cr II, 205.552 | −0.075 | 0.119 | 0.224 | −0.031 | −0.053 | −0.081 | 0.052 | 0.014 | 0.909 |
| B I, 208.959 | 0.017 | −0.050 | −0.012 | 0.108 | −0.038 | −0.026 | 0.190 | −0.067 | 0.939 |
| Ni II, 221.647 | 0.064 | −0.106 | −0.049 | 0.156 | −0.046 | −0.013 | 0.163 | −0.049 | 0.920 |
| Cd I, 228.807 | 0.053 | −0.076 | 0.039 | 0.213 | −0.086 | −0.049 | 0.271 | −0.096 | 0.820 |
| Ba II, 230.424 | 0.142 | −0.159 | −0.014 | 0.287 | −0.079 | −0.008 | 0.173 | −0.061 | 0.786 |
| Co II, 236.379 | 0.028 | 0.159 | 0.417 | 0.125 | −0.130 | −0.073 | 0.086 | −0.009 | 0.431 |
| Al I, 237.336 | 0.120 | −0.182 | −0.026 | 0.288 | −0.071 | −0.013 | 0.096 | −0.034 | 0.221 |
| Fe II, 249.064 | −0.039 | 0.168 | 0.365 | −0.012 | −0.055 | −0.075 | −0.124 | 0.059 | 0.743 |
| Si I, 251.611 | 0.054 | −0.107 | −0.076 | 0.116 | −0.028 | 0.018 | 0.088 | −0.020 | 0.955 |
| Mn II, 257.610 | 0.239 | −0.170 | 0.035 | 0.386 | −0.070 | 0.043 | 0.056 | −0.024 | 0.558 |
| Mg II, 280.270 | −0.022 | −0.018 | 0.005 | 0.025 | 0.042 | −0.029 | −0.001 | 0.002 | 0.996 |
| V II, 310.230 | 0.013 | 0.277 | 0.263 | −0.007 | 0.113 | 0.063 | 0.110 | −0.053 | 0.231 |
| Mo I, 313.259 | 0.240 | −0.028 | 0.133 | 0.344 | 0.015 | 0.091 | 0.043 | −0.044 | 0.292 |
| Cu I, 324.754 | 0.211 | −0.026 | 0.158 | 0.330 | −0.034 | 0.057 | 0.092 | −0.044 | 0.263 |
| As I, 328.068 | 0.258 | −0.091 | −0.113 | 0.281 | 0.137 | 0.181 | 0.014 | 0.007 | 0.322 |
| Ti II, 334.941 | 0.254 | −0.112 | −0.040 | 0.349 | 0.046 | 0.122 | 0.102 | −0.045 | 0.357 |
| Zr II, 343.823 | 0.038 | 0.220 | 0.388 | 0.067 | −0.021 | −0.008 | −0.003 | 0.012 | 0.289 |
| Ca II, 393.366 | 0.150 | −0.186 | −0.191 | 0.252 | 0.055 | 0.076 | 0.080 | −0.029 | 0.777 |
| Th II, 401.913 | 0.230 | −0.044 | −0.174 | 0.206 | 0.256 | 0.223 | −0.026 | −0.000 | 0.418 |
| Sr II, 407.771 | 0.211 | −0.013 | −0.140 | 0.158 | 0.233 | 0.216 | −0.054 | 0.055 | 0.268 |

determination of fluctuations in the background signals. Twenty one measurements were taken, one served for blank subtractions, eight monitored free drift, and the rest monitored deliberate changes in plasma parameters. Four parameters were varied: sample uptake rate (varying feed rate), incident power, and plasma and aerosol carrier gas flow rates. Three measurements were taken for each parameter, varying its value up to 5%. Decomposition of the data matrix of order 20 × 8 (20 measurements and 8 monitoring channels) by the singular value decomposition (*10*) gave the following singular values; 0.5321, 0.2232, 0.0931, 0.0629, 0.0155, 0.0043, 0.0031, and 0.0023. Application of abstract factor analysis resulted in conflicting values for the number of significant factors. When Malinowski's RELI and IND functions (*11*) were used, five factors were obtained, while other methods resulted in four factors. Five factors were chosen because the last three singular values have very close values, which indicate that they result from errors in the data matrix. Finding five factors does not necessarily mean that the background signals are affected by five different plasma parameters but merely that they are described by five linear factors. In the case of a nonlinear response to a variable variation, more than one factor will be detected by abstract factor analysis.

The projection matrix obtained for the eight monitored channels is presented in Table I. Details of how to construct the projection matrix, together with a numerical example were presented in ref 9. Projection matrices act as a filter upon multiplication by a vector. When the vector is affected by the same factors that affect the projection matrix, the resultant vector will be the same. In actual measurements the vector contains random errors, and its multiplication by the projection matrix will result in noise rejection. The value of each off-diagonal element, when compared to the value of the element on the diagonal in the same row or column (they are identical), reflects the correlation between these channels. High correlation is indicated by approximately the same values. Low correlation is indicated by relatively low value for the off-diagonal elements compared to the elements in the diagonal. In extreme cases, when a channel is not correlated to any of the other channels, the diagonal value approaches unity. Thus, it is obvious that both the channels located at 766 and 595 nm are not correlated to the others, because their diagonal values are close to unity. The channels of Nb II, V II, and U II exhibit unique response to the parameters of the systems while behavior of the remaining three is well explained by fluctuations of the others. Even though monitoring of the five above mentioned channels is sufficient, we monitored the other three as well, in order to have sufficient degrees of freedom to decide whether the observed fluctuations during an analytical run are within the calibrated range.

Table II presents correction coefficients which are used in eq 1 to compensate for nonrandom fluctuations in the analytical channels. The row corresponding for each channel is taken from a projection matrix that is constructed from the calibration data for the eight monitored channels, together with the corrected analytical channel. The comparison of the off-diagonal elements to the diagonal element is valid also for the rows in this table. The diagonal elements in Table II are contained in the ninth matrix column. This comparison may give a quick indication of the validity of the calculation of the analyte's background fluctuations by the monitored channels. However, a more accurate analysis is obtained by applying

**Table III. Variance Ratio for the Errors in the Computed Background Values and Their Corresponding Intensities**

| element | intensity, counts | variance ratio |
|---|---|---|
| Cr | 1 100 | 28.0 |
| B | 4 400 | 23.0 |
| Ni | 10 700 | 18.5 |
| Cd | 6 700 | 11.0 |
| Ba | 11 500 | 6.00 |
| Co | 238 000 | 1.10 |
| Al | 16 700 | 12.4 |
| Fe | 66 000 | 5.10 |
| Si | 37 500 | 29.0 |
| Mn | 190 000 | 3.60 |
| Mg | 277 000 | 57.0 |
| V | 270 000 | 0.50 |
| Mo | 187 000 | 1.40 |
| Cu | 261 000 | 0.90 |
| Ag | 397 000 | 0.70 |
| Ti | 250 000 | 0.20 |
| Zr | 298 000 | 0.22 |
| Ca | 27 000 | 6.30 |
| Th | 288 000 | 3.50 |
| Sr | 342 000 | 1.60 |

tools developed for the validation of hypothesis on data matrix.

In order to examine the validity of a set of monitored channels to the calculation of background fluctuations in an analytical channel, the difference between the calculated fluctuations and the measured ones in this channel should be calculated. When the random error in the channel is not known in advance, as in our case, statistical inference to the adequacy is obtained by the Fisher variance-ratio test (*12*). Table III presents the variance ratios for the analytical channels. The variance ratios were calculated from the calibration data of each channel by eq 29 of ref 12. The variance ratio in our case is distributed as $F(11,21)$ degrees of freedom. A 95% significance level for the hypothesis that an analytical channel can be corrected by the monitored channels is obtained for a value of 2.1 for the variance ratio. In order to explain high variance-ratio values, background intensity values (arbitrary units) are also presented in Table III. Most channels located at the low UV region exhibit low background values, because background emissions resulting from both the source and the uranium are low in this region. Thus, the main cause for noise is random noise, which cannot be compensated for by internal reference methods. The high variance-ratio values for the channels of Fe, Si, Mg, and Ca may be explained by fluctuations due to a signal from the corresponding elements that are present in the surrounding atmosphere and in the torch.

**Quality of Compensation.** The IRPM, besides compensating for background fluctuations, enables one to check at each measuring interval whether the experienced fluctuations are within the calibrated range. The check is done by summing the differences between the measured fluctuations of the monitored channels and the results of multiplying them by their projection matrix. The sum is distributed as $\chi^2$ with degrees of freedom equal to the number of monitored channels minus the number of factors from which the projection matrix is constructed. A value of 0.1% RSD was taken for the random noise in the channels. For the chosen set of eight monitored channels whose projection matrix was constructed from five factors, the degrees of freedom are three. Statistical inference on the hypothesis that the experienced fluctuations are describable by the calibrated factors with a 97.5% significance level is obtained for $\chi^2 < 9.35$. The importance of this statistical measure in multielement analysis, where one cannot follow every channel's fluctuation, is quite critical. Error amplification, instead of compensation, may be obtained when the system parameters differ from their value at calibration.

The analysis of the quality of compensation was carried out by deliberately changing the four plasma parameters in a range of 10%. Tables IV–VII present the relative variation of the various signals from the fixed parameters, as well as the $\chi^2$ values. The results in the tables confirm the importance of using the $\chi^2$ test. Inspection of Table IV, for example, shows that regarding the absolute change in signals variation, of +5% and −5%, results in approximately the same values. Nevertheless, the $\chi^2$ values succeed in determining that varying the incident power by −5% results in signal variations which are outside the calibrated factors. The compensated signal values show that this finding is indeed true. This effect is more distinguished in Table V, where variation of +5% in the nebulizing pressure caused relatively high signal variations

**Table IV. Deviation of Background Signals (%) Caused by Varying Incident Power to Plasma and the Remaining Noise after Compensation by the IRPM**

| | % change in incident power to plasma | | | | | | | |
|---|---|---|---|---|---|---|---|---|
| | −10 | | −5 | | +5 | | +10 | |
| element | obsd | corrected | obsd | corrected | obsd | corrected | obsd | corrected |
| Cr | −24 | 4.0 | −15 | 3.4 | 12 | 0.76 | 32 | 2.3 |
| B | −28 | 2.7 | −18 | 1.8 | 12 | −1.4 | 35 | −2.6 |
| Ni | −29 | 2.1 | −18 | 0.67 | 11 | −2.1 | 34 | −2.3 |
| Cd | −24 | 1.8 | −15 | 1.5 | 11 | 0.15 | 30 | 0.41 |
| Ba | −25 | 1.5 | −16 | 1.1 | 11 | −0.07 | 31 | 0.64 |
| Co | −16 | 0.25 | −10 | 0.45 | 7.0 | 0.32 | 18 | 0.58 |
| Al | −24 | 3.2 | −16 | 1.9 | 13 | 1.7 | 34 | 3.6 |
| Fe | −18 | 1.6 | −11 | 1.2 | 8.5 | 1.0 | 22 | 1.7 |
| Si | −28 | 0.64 | −19 | −0.51 | 12 | −0.50 | 43 | 9.0 |
| Mn | −20 | −0.93 | −12 | 0.83 | 9.1 | 0.52 | 24 | 1.0 |
| Mg | −10 | 3.4 | −5.3 | 2.9 | 8.6 | 1.6 | 17 | 0.78 |
| V | −9.2 | −0.52 | −5.8 | −0.23 | 3.6 | −0.12 | 9.4 | −0.28 |
| Mo | −15 | 0.73 | −9.5 | −0.56 | 6.7 | 0.23 | 17 | 0.03 |
| Cu | −15 | −0.28 | −9.6 | −0.08 | 6.1 | −0.04 | 16 | −0.20 |
| Ag | −12 | −0.74 | −7.6 | −0.57 | 4.9 | 0.12 | 13 | 0.48 |
| Ti | −14 | 0.04 | −8.8 | 0.10 | 6.1 | 0.19 | 16 | 0.16 |
| Zr | −12 | 0.32 | −7.6 | 0.40 | 5.5 | 0.47 | 14 | 0.50 |
| Ca | −11 | 2.3 | −6.4 | 2.2 | 8.2 | 2.2 | 18 | 2.3 |
| Th | −8.0 | 1.5 | −4.8 | 1.2 | 4.6 | 0.37 | 10 | −0.14 |
| Sr | −8.1 | −0.58 | −5.1 | −0.40 | 3.5 | 0.15 | 8.8 | 0.42 |
| $\chi^2$ | 18 | | 16 | | 8.4 | | 18 | |

Table V. Deviation of Background Signals (%) Caused by Varying Nebulizing Pressure and the Remaining Noise after Compensation by the IRPM

| | % change in nebulizing pressure | | | | | | | |
|---|---|---|---|---|---|---|---|---|
| | -10 | | -5 | | +5 | | +10 | |
| element | obsd | corrected | cbsd | corrected | obsd | corrected | obsd | corrected |
| Cr | 15 | 1.6 | 8.0 | -1.9 | -14 | 3.0 | -23 | 6.8 |
| B | 12 | -0.10 | 5.4 | -12 | -13 | -0.86 | -21 | -2.5 |
| Ni | 10 | -0.80 | 4.9 | -6.9 | -13 | -0.69 | -22 | -2.8 |
| Cd | 12 | 1.4 | 6.2 | -4.4 | -12 | 0.13 | -21 | -0.29 |
| Ba | 12 | 1.8 | 5.8 | -1.6 | -12 | 0.74 | -21 | 0.44 |
| Co | 7.7 | 1.2 | 4.2 | 0.3 | -8.7 | 0.24 | -15 | 0.47 |
| Al | 16 | 4.1 | 8.3 | 1.1 | -14 | 0.97 | -23 | 1.8 |
| Fe | 12 | 2.6 | 6.7 | 3.3 | -11 | 1.8 | -20 | 3.7 |
| Si | 8.3 | 1.0 | 3.6 | -5.2 | -11 | -3.1 | -17 | -5.9 |
| Mn | 9.0 | 2.4 | 5.1 | 1.8 | 9.2 | 0.51 | -16 | 0.66 |
| Mg | 0.70 | 3.4 | 1.1 | 2.9 | 0.06 | 0.02 | -1.5 | -2.0 |
| V | -0.65 | -0.40 | -0.10 | -0.68 | -1.8 | -0.10 | -4.0 | -0.56 |
| Mo | 3.8 | 0.41 | 2.0 | 0.26 | -5.9 | 0.28 | -11 | 0.38 |
| Cu | 3.6 | -0.16 | 1.8 | -0.31 | -6.3 | -0.14 | -11 | -0.41 |
| Ag | -1.0 | 0.11 | -0.58 | 0.21 | -16 | -0.29 | -3.3 | -0.66 |
| Ti | 1.8 | 0.27 | 0.90 | -0.16 | -4.1 | -0.05 | -7.5 | -0.42 |
| Zr | 3.4 | 0.19 | 1.9 | 0.20 | -5.2 | 0.31 | -9.7 | 0.21 |
| Ca | 0.8 | 1.7 | 0.83 | 0.79 | -0.54 | 0.73 | -2.2 | -0.36 |
| Th | -3.5 | 0.7 | -1.6 | 0.93 | -1.8 | 0.43 | 2.2 | 0.45 |
| Sr | -3.7 | -0.03 | -1.8 | 0.47 | 1.4 | 0.00 | 1.9 | -0.02 |
| $\chi^2$ | 22 | | 60 | | 7.9 | | 26 | |

Table VI. Deviation of Background Signals (%) Caused by Varying Cooling Gas Flow Rate and the Remaining Noise after Compensation by the IRPM

| | % change in cooling gas flow rate | | | | | | | |
|---|---|---|---|---|---|---|---|---|
| | -20 | | -10 | | +10 | | +20 | |
| element | obsd | corrected | obsd | corrected | obsd | corrected | obsd | corrected |
| Cr | 31 | 5.0 | 13 | -0.62 | -13 | -2.3 | -23 | -5.5 |
| B | 25 | 4.6 | 12 | -0.65 | -15 | -0.25 | -26 | -10 |
| Ni | 6.5 | 4.6 | 4.2 | 1.2 | -6.1 | 0.38 | -11 | -4.0 |
| Cd | 11 | 1.9 | 6.5 | -0.3 | -9.7 | 0.47 | -18 | -3.9 |
| Ba | -0.1 | 1.9 | 1.5 | 1.0 | -5.6 | 0.33 | -14 | -3.2 |
| Co | 4.6 | 0.49 | 3.6 | 0.34 | -5.7 | -0.33 | -12 | -1.3 |
| Al | -3.4 | 3.2 | -0.2 | 1.3 | -3.4 | 1.6 | -9.6 | 0.01 |
| Fe | 4.8 | -0.03 | 3.7 | 0.24 | -5.8 | 0.56 | -12 | 2.3 |
| Si | -12 | 2.2 | -4.7 | 0.68 | 5.7 | 3.2 | -9.0 | 1.3 |
| Mn | -5.6 | 1.3 | -0.8 | 0.82 | -2.7 | 0.67 | -8.7 | -0.14 |
| Mg | -14 | 3.2 | 24.8 | 0.68 | 4.4 | 3.2 | 3.4 | 5.3 |
| V | 1.1 | -0.01 | 2.0 | 0.14 | -3.6 | -0.44 | -8.1 | -1.3 |
| Mo | -3.9 | 0.52 | -0.14 | 0.30 | -3.0 | 0.48 | -8.1 | 0.6 |
| Cu | -2.6 | 0.12 | 0.45 | 0.31 | -3.55 | -0.16 | -8.6 | -0.81 |
| Ag | -8.9 | 0.28 | -2.9 | -0.10 | 0.27 | -0.08 | -3.3 | -0.91 |
| Ti | -5.7 | 0.30 | -1.0 | 0.42 | -1.8 | -0.02 | -6.4 | -0.87 |
| Zr | 1.1 | 0.12 | 1.9 | 0.16 | -3.4 | 0.17 | -7.9 | 0.22 |
| Ca | -13 | 1.8 | -4.7 | 0.85 | 2.7 | 1.0 | 1.4 | 0.93 |
| Th | -9.8 | 1.2 | -3.4 | 0.39 | 2.1 | 0.9 | 0.06 | 2.0 |
| Sr | -9.5 | -0.4 | -3.3 | -0.02 | 2.0 | -0.02 | -0.09 | -0.48 |
| $\chi^2$ | 8.6 | | 6.3 | | 6.0 | | 16 | |

compared to -5%. Contrary to intuitive prediction, the $\chi^2$ test determines that the +5% variation may be handled. This insensitivity to the magnitude of signal variations is also seen by comparison of Table IV to Tables V and VI. In Table IV, although variation of +5% in incident power caused large signal variations, the compensation was successful. Much smaller signal variations caused by altering the nebulizing gas pressure to -10% and the cooling gas flow rate to +20%, cannot be compensated.

When a single element analysis is performed, one may find a spectral wavelength whose background fluctuation data may describe well the fluctuation at the analytical wavelength. However, in multielement analysis several monitored channels are a necessity. This can be seen from the tables. Variation of incident power and uranium concentration (Tables IV and VII) cause all signals to vary in the same direction. Altering both gas flow rates (Tables V and VI) does not result in the same phenomenon. Thus, it is obvious that multielement analysis is possible only through compensation by several monitored channels.

For all variations presented in the tables no error propagation due to the computation method is observed, even for channels for which the Fisher test showed that minor or no compensation is possible. Comparison of the actual quality of compensation to that predicted from the Fisher variance-ratio values shows that this ratio succeeded to predict the degree of compensation.

The compensation performance was also examined for free drift. Table VIII presents results of two set of measurements each of which was carried out for 2 h. The fluctuations ex-

**Table VII. Deviation of Background Signals (%) Caused by Varying Uranium Concentration and the Remaining Noise after Compensation by the IRPM**

| | % change in uranium concentration | | | | | | | |
|---|---|---|---|---|---|---|---|---|
| | -17 | | -7 | | +2.6 | | +7.5 | |
| element | obsd | corrected | obsd | corrected | obsd | corrected | obsd | corrected |
| Cr | -14 | 15 | -7.3 | 5.7 | 1.7 | -1.2 | 5.9 | -3.3 |
| B | -16 | 7.2 | -7.1 | 3.3 | 1.1 | -1.3 | 5.8 | -2.1 |
| Ni | -15 | 3.7 | -7.0 | 1.3 | 1.0 | -1.0 | 5.2 | -1.7 |
| Cd | -16 | 4.2 | -7.1 | 1.8 | 1.4 | -0.8 | 5.5 | -2.3 |
| Ba | -16 | 3.7 | -6.7 | 1.7 | 1.70 | -0.50 | 5.6 | -1.6 |
| Co | -17 | 0.52 | -7.1 | 0.31 | 1.5 | -0.41 | 5.9 | -0.81 |
| Al | -15 | -0.48 | -6.6 | -0.10 | 1.2 | -0.43 | 4.8 | -0.46 |
| Fe | -17 | 3.3 | -7.4 | 1.4 | 1.9 | -0.36 | 5.8 | -2.0 |
| Si | -15 | -5.4 | -7.3 | -2.8 | 0.60 | -0.61 | 4.1 | 0.81 |
| Mn | -17 | 1.4 | -7.4 | 0.44 | 2.3 | 0.13 | 5.7 | -1.3 |
| Mg | -17 | 4.5 | -6.3 | 2.2 | 2.8 | -0.64 | 6.5 | -1.7 |
| V | -17 | -0.14 | -7.1 | -0.12 | 2.1 | -0.07 | 6.7 | -0.07 |
| Mo | -17 | 2.0 | -7.1 | 0.81 | 2.1 | -0.27 | 6.6 | -0.73 |
| Cu | -17 | -0.28 | -7.2 | -0.20 | 2.0 | -0.05 | 6.5 | 0.09 |
| Ag | -17 | -0.19 | -7.2 | -0.21 | 2.2 | -0.11 | 6.8 | 0.17 |
| Ti | -17 | 0.48 | -7.1 | 0.13 | 2.1 | -0.19 | 6.5 | -0.24 |
| Zr | -17 | -0.32 | -7.1 | -0.08 | 2.0 | 0.03 | 6.5 | 0.00 |
| Ca | -17 | -2.8 | -7.9 | -1.8 | 1.7 | -0.50 | 6.7 | 0.97 |
| Th | -17 | 2.8 | -6.8 | 1.3 | 2.7 | -0.14 | 7.1 | -0.89 |
| Sr | -17 | -1.4 | -7.2 | -0.72 | 2.4 | 0.10 | 7.0 | -0.64 |
| $\chi^2$ | 62 | | 18 | | 2.3 | | 13 | |

**Table VIII. Free Fluctuations of Background Signals Which Occurred during a 2-h Run and the Compensated Results**

| | low fluctuations | | high fluctuations | |
|---|---|---|---|---|
| element | obsd | corrected | obsd | corrected |
| Cr | 1.80 | 0.70 | 7.3 | 1.00 |
| B | 1.80 | 1.00 | 8.7 | 1.10 |
| Ni | 1.70 | 0.80 | 8.0 | 0.60 |
| Cd | 1.50 | 0.70 | 7.4 | 0.60 |
| Ba | 1.30 | 0.50 | 7.8 | 0.50 |
| Co | 0.90 | 0.20 | 4.8 | 0.15 |
| Al | 1.40 | 0.50 | 7.2 | 0.60 |
| Fe | 1.20 | 0.40 | 5.4 | 0.40 |
| Si | 2.20 | 2.20 | 7.1 | 0.80 |
| Mn | 1.00 | 0.30 | 5.9 | 0.20 |
| Mg | 0.70 | 0.50 | 3.7 | 0.70 |
| V | 0.40 | 0.05 | 2.6 | 0.13 |
| Mo | 0.70 | 0.12 | 4.4 | 0.14 |
| Cu | 0.60 | 0.13 | 4.4 | 0.12 |
| Ag | 0.40 | 0.14 | 3.4 | 0.19 |
| Ti | 0.50 | 0.08 | 4.0 | 0.09 |
| Zr | 0.60 | 0.08 | 3.6 | 0.07 |
| Ca | 0.70 | 0.50 | 3.8 | 0.40 |
| Th | 0.50 | 0.11 | 2.5 | 0.30 |
| Sr | 0.50 | 0.08 | 2.3 | 0.11 |

perienced at one run were minor while at the second run they were severe. From the results in the table it may be seen that although the magnitude of the fluctuations differs largely from set to set, the residual noise values are very similar.

**Detection Limits.** The detection limit of an analytical signal is directly proportional to its noise level. In ICP emission spectrometry a value of 1% RSD for spectral lines above 230 nm is usually accepted (*13*). As may be seen from Table VIII, noise levels of a signal vary from run to run. Nevertheless, for comparison of detection limits obtained by the IRPM to those obtained without correction, we used the 1% RSD convention. The RSD values of signals whose RSD was larger than 1% (in the first column of Table VIII) were taken for detection limit computation. A number three times the RSD values was used to calculate detection limits. The detection limits obtained are presented in Table IX. The improvement in detection limits varies from 0 to 20-fold.

**Table IX. Detection Limits (μg/g U, 0.5% wt Uranium in Solution) Obtained without and with IRPM Treatment**

| element | without treatment | with IRPM treatment |
|---|---|---|
| Cr | 12 | 4.5 |
| B | 13 | 7.0 |
| Ni | 24 | 11.0 |
| Cd | 5 | 2.3 |
| Ba | 8 | 2.9 |
| Co | 7 | 1.3 |
| Al | 62 | 22.0 |
| Fe | 8 | 2.6 |
| Si | 100 | 100.0 |
| Mn | 5 | 1.5 |
| Mg | 10 | 5.0 |
| V | 230 | 12.0 |
| Mo | 170 | 22.0 |
| Cu | 50 | 6.8 |
| Ag | 50 | 7.2 |
| Ti | 12 | 1.0 |
| Zr | 11 | 1.0 |
| Ca | 0.3 | 0.2 |
| Th | 220 | 25.0 |
| Sr | 2 | 0.1 |

There is no need to recalibrate the instrument when plasma parameters are kept constant from run to run.

**Registry No.** U, 7440-61-1; Cr, 7440-47-3; B, 7440-42-8; Ni, 7440-02-0; Cd, 7440-43-9; Ba, 7440-39-3; Co, 7440-48-4; Al, 7429-90-5; Fe, 7439-89-6; Si, 7440-21-3; Mn, 7439-96-5; Mg, 7439-95-4; V, 7440-62-2; Mo, 7439-98-7; Cu, 7440-50-8; Ag, 7440-22-4; Ti, 7440-32-6; Zr, 7440-67-7; Ca, 7440-70-2; Th, 7440-29-1; Sr, 7440-24-6; uranyl nitrate, 10102-06-4.

## LITERATURE CITED

(1) Koirtyohann, S. R.; Glass, E. D.; Yates, D. A.; Hinderberger, J. E.; Lichte, F. E. *Anal. Chem.* **1977**, *49*, 1121–1126.

(2) Weekley, B. E.; Norris, J. A. *Appl. Spectrosc.* **1964**, *18*, 21–25.

(3) Thompson, G.; Bankston, D. C. *Spectrochim. Acta, Part B* **1969**, *24B*, 335–350.

(4) Skogerboe, R. K.; Lamothe, P. J.; Bastiaans, G. J.; Freeland, S. J.; Coleman, G. N. *Appl. Spectrosc.* **1976**, *30*, 495–500.

(5) Schmidt, G. J.; Slavin, W. *Anal. Chem.* **1982**, *54*, 2491–2495.

(6) Myers, S. A.; Tracy, D. H. *Spectrochim. Acta, Part B* **1983**, *38B*, 1227–1253.

(7) Lorber, A.; Goldbart, Z. *Anal. Chem.* **1984**, *56*, 37–43.

(8) Lorber, A.; Goldbart, Z.; Eldan, M. *Anal. Chem.* **1984**, *56*, 43–48.
(9) Lorber, A. *Anal. Chem.* **1984**, *56*, 1404–1409.
(10) Lawson, C. L.; Hanson, R. J. "Solving Least Squares Problems"; Prentice-Hall: Englewood, NJ, 1974.
(11) Malinowski, E. R.; Howery, D. G. "Factor Analysis in Chemistry"; Wiley: New York, 1980.
(12) Lorber, A. *Anal. Chem.* **1984**, *56*, 1004–1010.
(13) Boumans, P. W. J. M.; McKenna, R. J.; Bosveld, M. *Spectrochim. Acta, Part B* **1981**, *36B*, 1031–1058.

RECEIVED for review August 20, 1984. Accepted November 26, 1984.

# Determination of Gallium in Sediment, Coal, Coal Fly Ash, and Botanical Samples by Graphite Furnace Atomic Absorption Spectrometry Using Nickel Matrix Modification

**Shan Xiao-quan, Yuan Zhi-neng, and Ni Zhe-ming***

*Institute of Environmental Chemistry, Academia Sinica, P.O. Box 934, Beijing, People's Republic of China*

**A method has been developed for the determination of gallium in environmental samples at the level of 0.069–58 $\mu$g/g by graphite furnace atomic absorption spectrometry using nickel matrix modification. The sensitivity for determining gallium was improved by a factor of 6 in the presence of nickel as compared to that of pure gallium standard. The related mechanism of enhancement effect is discussed. The suppression effect of perchloric acid on the determination of gallium was probably due to the formation of GaCl originating from the condensed phase reaction at low $HClO_4$ concentration and the vapor phase reaction would also be recognized to occur at higher $HClO_4$ concentration.**

Gallium is not found as a major constituent of minerals and is widely distributed in nature. The concentration of gallium in silicate rocks is normally in the range of 10 to 100 $\mu$g/g (*1*). The methods present in use for the determination of gallium in rocks, ores, metals, and other inorganic materials have included flame atomic absorption spectrometry after solvent extraction (*2*) or anion exchange separation (*3*) and graphite furnace atomic absorption spectrometry using conventional graphite tube atomization (*4*), Zr-coating technique (*5*), metal atomizer (*6*), or atomization from platform (*7*). In general, graphite furnace atomic absorption spectrometry is sensitive enough to be applicable to a variety of samples. However, severe interferences are frequently encounterred. Pelosi and Attolini (*4*) stated that gallium absorption signal was masked by 1000- and 5000-fold amounts of zinc and indium and selective volatilization with thermal programming was unsuccessful, and a solvent extraction procedure was employed to determine gallium impurities in semiconducting materials. Nakamura et al. (*8*) reported that nitric acid, hydrochloric acid and phosphoric acid as well as a variety of common salts seriously influenced the results. When EDTA was used, the interference of hydrochloric acid and nitric acid was suppressed completely and the interference of phosphoric acid was suppressed partly. Koirtyohann et al. (*9*) investigated the interference effect of perchloric acid on the determination of the group 3 elements and 0.5 M $HClO_4$ caused over 95% reduction in peak absorbance for gallium. This suppression effect persisted even though the furnace tube was heated far above the boiling point of perchloric acid during the ashing step. The authors assumed that the acid or one of its decomposition products reacted with graphite to form thermostable products. Decomposition or release of this residual product resulted in a gas-phase reaction which inhibited atomization of gallium. This suppression effect was removed by addition of a certain carbonate or ammonium sulfate. Nevertheless, no molecular form of analyte escape was established. In order to reduce such interferences or to match the sample matrices, solvent extraction (*6*) or standard addition techniques (*1*, *4*, *8*) were frequently used in sample analyses.

The purpose of the present study is to develop a method for determining gallium in sediments, coal, coal fly ash, and botanical samples by graphite furnace atomic absorption spectrometry using nickel matrix modification. In the presence of nickel the tolerable charring temperature for gallium was raised to 1200 °C, and the sensitivity was improved by a factor of 6 compared to that of aqueous gallium standard. In addition, the interferrences from sample matrices were greatly reduced. And the machanism of enhancement effect of nickel on the determination of gallium and the interference from perchloric acid was discussed.

## EXPERIMENTAL SECTION

**Apparatus.** A Perkin-Elmer Model 4000 atomic absorption spectrometer, equipped with a Model HGA-400 graphite furnace and Model 056 chart recorder, was employed for the measurement of gallium absorbances at a resonance line of 287.4 nm under the conditions of "gas stop" and "maximum power". The spectral bandwidth was set at 0.7 nm. A hollow cathode lamp of gallium was operated at 15 mA. Deuterium arc background correction facility was used throughout. A 20-$\mu$L Eppendorf microliter pipet fitted with disposable polypropylene tips was employed to introduce sample solution into the graphite tube atomizer.

**Reagents.** Gallium stock solution, 1000 $\mu$g/mL, was prepared by dissolving 0.100 g of gallium (99.999%, Shanghai Chemical Co., China) in 10 mL of 7 M nitric acid. The solution was boiled to expel nitrogen oxide and diluted to 100 mL with deionized water. Working standards were prepared by appropriate dilution with 0.1 M nitric acid.

Nickel solution, 5 mg/mL, and ammonium sulfate solution, 25 mg/mL, were prepared by dissolving suitable amounts of nickel nitrate and ammonium sulfate (analytical reagent grade) in demineralized water.

All other chemicals used in this study were of analytical reagent grade.

**Procedures.** (*1*) *Decomposition of Peach Leaves and Tomato Leaves.* The method used to decompose 300 mg of sample by pressure decomposition was basically the same as that given in ref 10 except that 2 mL of 67% nitric acid, 1 mL of 72% perchloric acid, and 1 mL of 35% hydrofluoric acid were used and the final

0003-2700/85/0357-0857$01.50/0 © 1985 American Chemical Society

**Table I. Experimental Conditions for Measurement of Molecular Absorption**

| | GaO | GaCl | $NiCl_2$ |
|---|---|---|---|
| analyte | 1 μg of Ga + 50 μg of Ni | 0.5 μg of Ga + 50 μg of Ni + 10 μL of 0.2 M $HClO_4$ | 20 μg of Ni + 20 μL of 0.1 M $HClO_4$ |
| wavelength, nm | 244.5[a] | 248.1[a] | 346.8[b] |
| drying temp, °C | 110 | 110 | 110 |
| ramp/holding time, s | 1/30 | 1/30 | 1/30 |
| charring temp, °C | 300 | 1100 | 250 |
| ramp/holding time, s | 1/30 | 4/30 | 1/30 |
| vaporization temp, °C | varying | varying | varying |
| ramp/holding time, s | 0/10 | 0/10 | 0/10 |
| cleaning temp, °C | 2650 | 2650 | 2650 |
| ramp/holding time, s | 1/6 | 1/6 | 1/6 |

[a] From ref 11. [b] From ref 12.

volume of sample solution was defined as 5.0 mL for the determination of gallium by graphite furnace atomic absorption spectrometry.

(2) *Decomposition of Drainage Sediments, Coal, and Coal Fly Ash.* The method was similar to procedure 1 but the operation of standing overnight was omitted before the pressure attack procedure. In addition, the final content obtained by the pressure decomposition method was transferred to a 50-mL volumetric flask and diluted to the mark with 0.1 M nitric acid.

(3) *Determination of Gallium.* According to gallium content in drainage sediment, coal, and coal fly ash, the digested sample solution prepared by procedure 2 was appropriately diluted, 20 μL of the sample solution was introduced into the pyrolytically coated graphite furnace along with the same volume of a mixture of 1 mg/mL of nickel and 5 mg/mL of ammonium sulfate, the sample was dried at 110 °C for 30 s, charred at 1100 °C for 30 s, atomized at 2400 °C for 5 s using "maximum power" mode, and gallium absorbances were measured under the condition of "argon gas flow interrupted". Finally the tube was cleaned at 2650 °C for 5 s.

(4) *Measurement of Molecular Absorption of GaCl, GaO, and $NiCl_2$.* When the Perkin-Elmer Model 4000 atomic absorption spectrometer was used for the measurement of molecular absorbance, the spectral bandwidth was set at 0.07 nm and a deuterium arc lamp or tungsten halide lamp was used as a continuous light source. The wavelengths for measuring GaCl, GaO, and $NiCl_2$ were 248.1, 244.5, and 346.8 nm (*11, 12*), respectively. The experimental procedures and the operation conditions are summarized in Table I. First, the analyte solutions were introduced into the graphite furnace followed by drying and charring and then molecular absorption was measured at the vaporization stage using "maximum power" and "gas stop" modes in order to make the absorption. Finally a cleaning stage was employed.

(5) *Measurement of Appearance Temperature of Gallium in the Absence or Presence of Matrix Modifiers.* The procedure used for this purpose was the same as that described by Campbell and Ottaway (*13*).

## RESULTS AND DISCUSSION

**Selection of Matrix Modifiers.** In order to search suitable matrix modifiers, a variety of metal ions were tested. The absorbance obtained by injecting 20 μL of 0.025 μg/mL of gallium aqueous standard was set as unity, and the relative absorbances of gallium in various matrix modifiers were calculated, and all of these results are summarized in Table II. As can be seen from the data, the sensitivity for determining gallium is slightly higher in the presence of chromium and magnesium than in the presence of nickel. However, more severe interferences are encountered using chromium and magnesium since only lower charring temperatures were tolerated. Considering the sufficiently high sensitivity for determining gallium and the highest allowable charring temperature of 1200 °C, only nickel was used in the remainder of this study.

**Table II. Comparison of Various Matrix Modifiers for Gallium (20 μL of 0.025 μg/mL of Ga and Various Matrix Modifiers)**

| matrix modifier | as added | concn, mg/mL | tolerable charring temp, °C | rel absorbance |
|---|---|---|---|---|
| none | | | 900 | 1.0 |
| $Zn^{2+}$ | $Zn(NO_3)_2$ | 1.0 | 900 | 4.1 |
| $V^{5+}$ | $NH_4VO_3$ | 1.0 | 900 | 5.6 |
| $Cr^{6+}$ | $K_2Cr_2O_7$ | 1.0 | 900 | 6.8 |
| $Ba^{2+}$ | $Ba(NO_3)_2$ | 1.0 | 1000 | 4.9 |
| $Sr^{2+}$ | $Sr(NO_3)_2$ | 1.0 | 1000 | 4.9 |
| $Co^{2+}$ | $Co(NO_3)_2$ | 1.0 | 1000 | 5.7 |
| $Mo^{6+}$ | $(NH_4)_4Mo_7O_{24}·6H_2O$ | 1.0 | 1000 | 5.3 |
| $Al^{3+}$ | $Al(NO_3)_3$ | 1.0 | 1000 | 5.8 |
| $Mg^{2+}$ | $Mg(NO_3)_2$ | 1.0 | 1000 | 6.5 |
| $Pd^{2+}$ | $PdCl_2$ | 0.1 | 1100 | 4.7 |
| $Ca^{2+}$ | $Ca(NO_3)_2$ | 1.0 | 1100 | 4.9 |
| $Ni^{2+}$ | $Ni(NO_3)_2$ | 1.0 | 1200 | 6.1 |

[b] Lys-C peptide cleaved with trypsin.

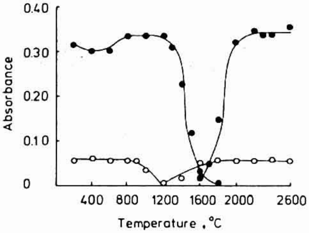

**Figure 1.** Effect of ashing and atomization temperature on the atomic absorption for gallium in the absence or presence of nickel: (○) 0.8 ng of Ga; (●) 0.8 ng of Ga + 20 μg of Ni.

The effect of charring and atomization temperature on gallium absorbances was examined, and the results are schematically shown in Figure 1. The left-side branches refer to the effect of charring temperatures on gallium absorbances obtained under the optimum atomization temperature in the absence or presence of nickel. The right-side branches refer to the effect of atomization temperatures on gallium absorbances with or without addition of nickel under the optimum charring temperature in each case. In the presence of nickel the tolerable charring temperature for gallium could be raised up to 1200 °C and the sensitivity improved by a factor of 6. The appearance temperatures of gallium in the absence and presence of nickel were 1100 and 1530 °C, respectively.

The mechanism of the enhancement effect of nickel matrix modification on the determination of gallium is ascribed to the formation of more thermostable solid solution and/or alloys (*14*), thus resulting in reduction of analyte loss in preatomization stage. In order to verify this assumption the molecular absorption of GaO was measured following procedure 4 and the results are shown in Figure 2. When no nickel was added, the molecular absorption of GaO increased with increasing vaporization temperature from 800 to 1300 °C,

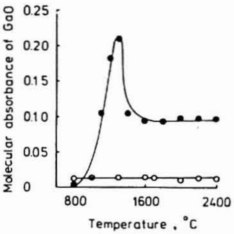

**Figure 2.** Effect of vaporization temperature on the molecular absorption of GaO in the absence or presence of nickel: (●) 1 μg of Ga; (○) 1 μg of Ga + 50 μg of Ni.

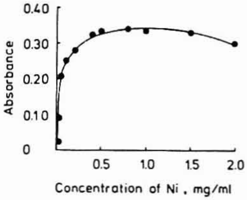

**Figure 3.** Dependence of the absorbance for 0.8 ng of gallium on the concentration of the nickel solution added (20 μL).

reached a maximum at 1300 °C, and then decreased with further increase in temperature; there was a plateau over the temperature range of 1600–2400 °C. However, a very small absorption of GaO and very little change in the absorption of GaO was observed when vaporization temperature was varied over the above range if nickel was used as a matrix modifier.

The stablilizing effect of nickel depended upon the amounts added, and this is shown in Figure 3. When the charring temperature of 1100 °C was used and 20 μL of various concentrations of nickel solution was added to the graphite atomizer, the absorbance for 0.8 ng of gallium increased with increasing nickel concentration from 0.02 to 0.5 mg/mL, then a nearly constant absorbance was obtained over the range 0.5–1.5 mg/mL, and a slight reduction was observed with further increase in nickel concentration. Therefore 20 μL of 1 mg/mL of nickel was used in the remainder of this study.

**Study of Interferences.** In order to examine the applicability of the recommended method for the real sample analyses, a series of experiments were undertaken to test the interference effects of a variety of foreign ions. Twenty milliliters of 0.020 μg/mL of gallium solution containing 1 mg/mL of nickel and 5 mg/mL of ammonium sulfate and the same volume of various foreign ions was introduced to the pyrolytically coated graphite furnace and procedure 3 was followed. The interference effect of each foreign ion was estimated by reference to the absorbance obtained by the same amount of gallium standard. It was found that there were no interferences from 0.05 mg/mL of $Li^+$ and $F^-$, 0.10 mg/mL of $Fe^{3+}$, $Sb^{5+}$, and $Te^{6+}$, 0.25 mg/mL of $K^+$, $Na^+$, $Mg^{2+}$, $Cr^{6+}$, $BO_3^{3-}$, and $SiO_3^{2-}$, 1.0 mg/mL of $Sr^{2+}$, $Mn^{2+}$, $Co^{2+}$, $Ca^{2+}$, $Ba^{2+}$, $Zn^{2+}$, $Cu^{2+}$, $Pb^{2+}$, $Cd^{2+}$, $Bi^{3+}$, $As^{3+}$, $Tl^{3+}$, $Se^{4+}$, and $V^{5+}$.

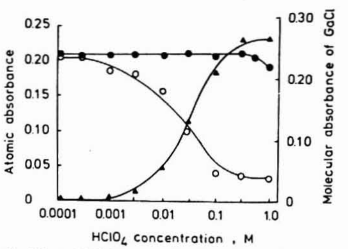

**Figure 4.** Effect of $HClO_4$ on atomic absorption of Ga and molecular absorption of GaCl: atomic absorption, (○) 0.5 ng of Ga + 20 μg of Ni + 20 μL of $HClO_4$, (●) 0.5 ng of Ga + 20 μg of Ni + 100 μg of $(NH_4)_2SO_4$ + 20 μL of $HClO_4$; molecular absorption, (▲) 0.5 μg of Ga + 50 μg of Ni + 20 μL of $HClO_4$.

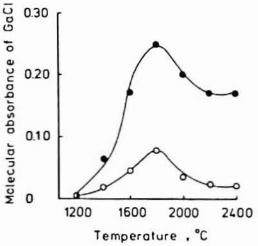

**Figure 5.** Relationship between vaporization temperature and the molecular absorption of GaCl in the absence or presence of ammonium sulfate: (●) 0.5 μg of Ga + 50 μg of Ni + 10 μL of 0.25 M $HClO_4$; (○) 0.5 μg of Ga + 50 μg of Ni + 100 μg of $(NH_4)_2SO_4$ + 10 μL of 0.25 M $HClO_4$.

Since perchloric acid was frequently used in sample preparation and its suppression effect on the determination of gallium by graphite furnace atomic absorption spectrometry was not fully elucidated, a series of experiments were conducted to study the mechanism of perchloric acid interference and to explain the reason of effectiveness of excess ammonium sulfate in overcoming this interference. As can be seen from Figure 4 gallium atomic absorbances decreased with increasing perchloric acid concentration even when nickel was employed as a matrix modifier. However, no interference at 0.3 M $HClO_4$ and only a reduction of 7% in peak absorbance were observed when excess ammonium sulfate was added. To elucidate the mechanism of the suppression effect of perchloric acid on gallium, the molecular absorption of GaCl was measured at 248.1 nm as a function of perchloric acid concentration or the vaporization temperature using a deuterium arc lamp. The results are shown in Figures 4 and 5, respectively. As the concentration of perchloric acid increased, the absorption of GaCl increased while atomic absorption of gallium decreased. This fact indicated that the suppression effect of perchloric acid was primarily due to the formation of GaCl by the following reactions:

$$Ga(ClO_4)_3 \rightarrow Ga^* + 3Cl^- + 6O_2 \qquad (1)$$

$$HClO_4 \rightarrow Cl^* + OH + {}^3/_2O_2 \qquad (2)$$

$$Ga^* + Cl^* \rightarrow GaCl \qquad (3)$$

Similar reactions have been used to elucidate the mechanism of perchloric acid interference with the determination of indium by flame atomic absorption spectrometry (*15*).

Koirtyohann et al. (*9*) reported that the interference effect of perchloric acid persisted at very high temperatures. This finding was confirmed in this study. Molecular absorbance of GaCl increased with increasing vaporization temperature from 1200 to 1800 °C and reached a maximum at 1800 °C which was higher than the appearance temperature of 1530 °C for gallium in the presence of nickel. Contrastly, the molecular absorbance of GaCl was remarkably reduced when

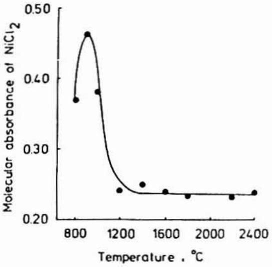

**Figure 6.** Effect of vaporization temperature on the molecular absorption of $NiCl_2$: (●) 20 μg of Ni + 20 μL of 0.1 M $HClO_4$.

excess ammonium sulfate was added although the trends remain the same. The reason for the effectiveness of ammonium sulfate in removing the interference of perchloric acid was probably due to the following reaction which was recognized to be a useful means of destroying perchlorate (*16*)

$$3ClO_4^- + 8NH_4^+ \rightarrow 3Cl^- + 4N_2 + 12H_2O + 8H^+ \qquad (4)$$

Therefore, no suppression effect was observed over the concentration of perchloric acid ranging from 0.0001 to 0.3 M, but some reduction in gallium absorbance existed when the concentration of perchloric acid exceeded this limit.

In addition to the analyte loss as GaCl, the less important factor resulting in suppression effect in the presence of both perchloric acid and nickel was the loss of nickel as $NiCl_2$ at charring stage (Figure 6). Because the stabilizing effect of nickel depends on the amount of nickel present in the graphite tube (Figure 3), the nickel remaining after charring at 1200 °C was insufficient to stabilize gallium. If more nickel was added, the suppression effect would become less severe (not given in Figure 4).

Koirtyohann et al. (*9*) concluded that the interference of perchloric acid was due to the gas-phase reaction when a relatively high concentration of perchloric acid was used. It is difficult to establish whether GaCl being lost during atomization would have originated from condensed phase or vapor phase interaction. In order to make this investigation, a homemade platform with two troughs was used, the breadth and depth of each trough were the same as those of the standard platform while the length was only half that of the standard platform. Gallium aqueous standard solution containing nickel was added in one of the troughs and perchloric acid of various concentrations was added in the other to avoid the physical contact of the two solutions, or a mixture of the two solutions was added in the single trough of a standard platform. The solutions were dried under infrared lamp, the platform was inserted into the graphite tube, and the normal furnace cycle was run. The absorbances obtained by using the above two types of platforms for gallium in the presence or absence of perchloric acid were compared and the results are shown in Figure 7. There is no interference over the concentration of perchloric acid ranging from 0.001 to 0.3 M if the two-trough platform was used, although the suppression effect was obvious when higher concentrations of perchloric acid were added. However, the suppression effect was most marked on the standard platform. It seems that the interference of perchloric acid on gallium determination was mainly due to the condensed phase reaction, though the gas phase reaction may also occur at higher concentrations of perchloric acid.

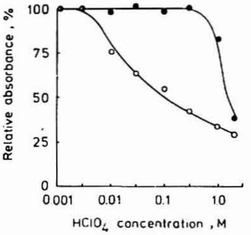

**Figure 7.** Comparison of $HClO_4$ interference from two-troughs platform (●) with that from the conventional platform (O): 0.5 ng of Ga + 20 μg of Ni + 10 μL of $HClO_4$.

**Table III. Recovery Study**

| sample | amt weighed, mg | Ga in sample μg | amt Ga added, μg | total Ga found, μg | recovery, % |
|---|---|---|---|---|---|
| 81–101, river sediment (China) | 100 | 1.95 | 1.0 | 3.0 | 105 |
| | | | 2.0 | 3.9 | 98 |
| | | | 3.0 | 4.8 | 95 |
| 82-201, coal fly ash (China) | 100 | 2.81 | 1.0 | 3.75 | 94 |
| | | | 2.0 | 4.69 | 94 |
| | | | 3.0 | 5.69 | 96 |
| 82-301, peach leaves (China) | 200 | 0.078 | 0.050 | 0.128 | 100 |
| | | | 0.100 | 0.175 | 97 |
| | | | 0.150 | 0.235 | 105 |

**Table IV. Determination of Gallium in Samples**

| | | gallium content, μg/g | | |
|---|---|---|---|---|
| sample | amt weighed, mg | this work | information value | lit. value |
| NBS SRM 1633a coal fly ash | 100 (0.2 mg/mL) | 58.7<br>56.3 | 58 | |
| 82-201, coal fly ash (China) | 100 (0.4 mg/mL) | 28.1<br>28.3 | | |
| NBS SRM 1632a coal | 100 (1.0 mg/mL) | 8.0<br>8.3 | 8.49 | |
| GSD-8, drainage sediment (China) | 100 (1.0 mg/mL) | 11.0<br>11.0 | 10.7 | |
| 81-101, river sediment (China) | 100 (0.5 mg/mL) | 19.5<br>18.5 | | 22.0 (7) |
| NBS SRM 1573 tomato leaves | 300 (60 mg/mL) | 0.083 | | 0.069 (17) |
| 82-301, peach leaves (China) | 200 (20 mg/mL) | 0.375<br>0.390 | | |

**Recovery Study.** Varied known amounts of pure gallium standards were added to drainage sediments, coal fly ash, and peach leaves, and then the entire procedure was carried out. The recovery was estimated by reference to the calibration curve constructed from gallium standards and an average recovery of 94 to 105% was achieved (Table III).

**Determination of Gallium in Real Samples.** Since no serious interferences were encountered and quantitative recoveries were obtained, the recommended method has been applied to the determinations of gallium in a variety of samples omitting the standard addition method or any separation procedures which were frequently used in the literature. The results of sample analyses are summarized in Table IV, and

*Anal. Chem.* **1985,** *57,* 861–864

a good agreement was obtained with the information values reported by NBS or other workers (*7*, *17*). The relative standard deviation was 3.7% for 11 replicate determinations of a drainage sediment in which gallium content was found to be 10.8 $\mu$g/g.

**Registry No.** Ni, 7440-02-0; Ga, 7440-55-3.

## LITERATURE CITED

(1) Langmyhr, F. J.; Rasmussen, S. *Anal. Chim. Acta* **1974**, *72*, 79–84.
(2) Lypka, G. N.; Chow, A. *Anal. Chim. Acta* **1972**, *60*, 65–70.
(3) Korkisch, J.; Steffan, I.; Nonaka, J. *Anal. Chim. Acta* **1979**, *109*, 181–185.
(4) Pelosi, C.; Attolini, G. *Anal. Chim. Acta* **1976**, *84*, 179–183.
(5) Kuga, K. *Bunseki Kagaku* **1981**, *30*, 529–534.
(6) Ohta, K.; Suzuki, M. *Anal. Chim. Acta* **1976**, *85*, 83–88.
(7) Han, Heng-bin; Ni, Zhe-ming *Funxi Huaxe* **1983**, *11*, 571–575.
(8) Nakamura, K.; Fujimori, M.; Tsuchiya, H.; Orii, H. *Anal. Chim. Acta* **1982**, *138*, 129–136.
(9) Koirtyohann, S. R.; Glass, E. D.; Lichte, F. E. *Appl. Spectrosc.* **1981**, *35*, 22–26.
(10) Shan, Xiao-quan; Ni, Zhe-ming; Zhang, Li *At. Spectrosc.* **1984**, *5*, 1–4.
(11) Dittrich, K.; Schneider, S. *Spectrochim. Acta, Part B* **1979**, *34B*, 257–268.
(12) Yasuda, S.; Kakiyama, H. *Anal. Chim. Acta* **1976**, *84*, 291–298.
(13) Campbell, W. C.; Ottaway, J. M. *Talanta* **1974**, *21*, 837–844.
(14) Wade, K.; Banister, A. J. In "Comprehensive Inorganic Chemistry"; Bailar, J. C. Jr., Emeléus, H. J., Nyholm, R., Trotman-Dickenson, A. F., Eds.; Pergamon Press: New York, 1973; Vol. 1, p 1074.
(15) Haraguchi, H.; Fuwa, K. *Bull. Chem. Soc. Jpn.* **1975**, *48*, 3056–3059.
(16) Burns, D. T.; Townshend, A.; Carter, A. H. "Inorganic Reaction Chemistry"; Ellis Horwood Limited: England, 1981; Vol. 2, Part A, Chapter 14, p 138.
(17) Gladney, E. *Anal. Chim. Acta* **1980**, *118*, 385–396.

RECEIVED for review October 1, 1984. Accepted December 18, 1984.

---

# Determination of Formaldehyde with the Thermal Lens Effect

**Jan A. Alfheim and Cooper H. Langford***

*Department of Chemistry, Concordia University, 1455 de Maisonneuve, West, Montreal, Quebec H3G 1M8, Canada*

**The laser thermal lens analysis of formaldehyde is reported. Two systems were tested, the first using a single laser in combination with a single diode detector and the second using two lasers in conjunction with a photodiode array detector. The formaldehyde solutions were prepared for colorimetry using the NIOSH method based on chromotropic acid. Improved sensitivity over standard absorption techniques is observed with enhancement factors up to 20.0 based on detection of absorptivity as low as 9 × $10^{-5}$ $cm^{-1}$ which corresponds to a concentration of 1.5 × $10^{-8}$ M. With collection efficiency of 95% for sampling solutions, this supports facile detection of formaldehyde in the parts-per-billion region in air.**

Current interest in the quantitative analysis of formaldehyde stems from its potential as a human health hazard (*1*). Formaldehyde polymers are used in the fabrication of wood products and home insulation and are known to emit low concentrations of formaldehyde into the surrounding environment (*2*, *3*). A recent trend in pollution analysis is toward decrease of the sample volume by means of an increase of analytical sensitivity. Thermal lens analysis is attractive in this context because it "improves" classic and well-tested methods.

Several methods to analyse formaldehyde have been developed (*4–6*) using both chromatographic and optical techniques. A close examination of the pararosaniline method (*7*) has shown it to be pH dependent (*8*) and seriously effected by $SO_2$ (*9*), thus limiting its potential.

In this study the NIOSH method for formaldehyde analysis has been modified to improve its sensitivity from 0.1–2 ppm to the parts-per-billion level where it can compete with GC and HPLC methods (*4–6*). The modifications to technique include diluting the chromotropic acid solutions 10-fold and then analyzing the samples with a laser thermal lens (LTL) spectrometer rather than a standard absorption spectrophotometer.

A thermal lens works on the principle that the passage of a laser beam through a material with a finite optical absorption generates thermal energy which heats the sample. The temperature gradient causes a refractive index gradient. For a Gaussian laser intensity distribution, a well-defined tranverse gradient in the refractive index will be established. In most materials $dn/dt$ is negative and thus this gradient has the same optical effect on the laser beam as a diverging lens.

It should be noted that a thermal lens is a function of true absorption in the same fashion as other calorimetric techniques and not absorption plus scattering as in transmittance techniques. The intensity of the thermal lens effect is proportional to the absorbed light energy.

LTL is a very sensitive method (*10*, *11*) which has already been used to measure pollutants in the micrograms per liter and lesser regions in both liquid and gaseous samples (*12*, *13*).

In keeping with the goal of minimizing apparatus complexity, both simple single and more complex dual laser systems were used in our experiments to evaluate their detection capabilities for quantitative formaldehyde determination. The admittedly primitive single laser experiments were performed to demonstrate that using the most basic of components to design a system one can still obtain relatively high sensitivity. The dual laser experiments were designed to demonstrate the true potential of LTL as a means of trace pollutant analysis, specifically formaldehyde. We encourage laboratories with one laser available to consider using the thermal lens effect.

## EXPERIMENTAL SECTION

**Instrument.** Figure 1A shows a block diagram for the simplified experimental setup. The optical train and lasers were fixed to a workbench which was isolated from building vibrations with a three-ply "sandwich" consisting of a sheet of cork, a piece of sheet metal, and a layer of sponge rubber. The Coherent CR-6 argon ion laser (A) was used to drive the Coherent CR-590 dye laser (B) which was run at 150 mW at $\lambda$ = 600 nm. The power was measured in front of the cell holder to account for power loss due to reflections of preceding optical components. The beam was elevated to the height of the optical train by means of a dual mirror system (C). The lens (D) which brought the light to a focus has a focal length of 23 cm. A manual shutter (E) was used to block the pump beam. The cell holder (F) was placed one confocal

0003-2700/85/0357-0861$01.50/0 © 1985 American Chemical Society

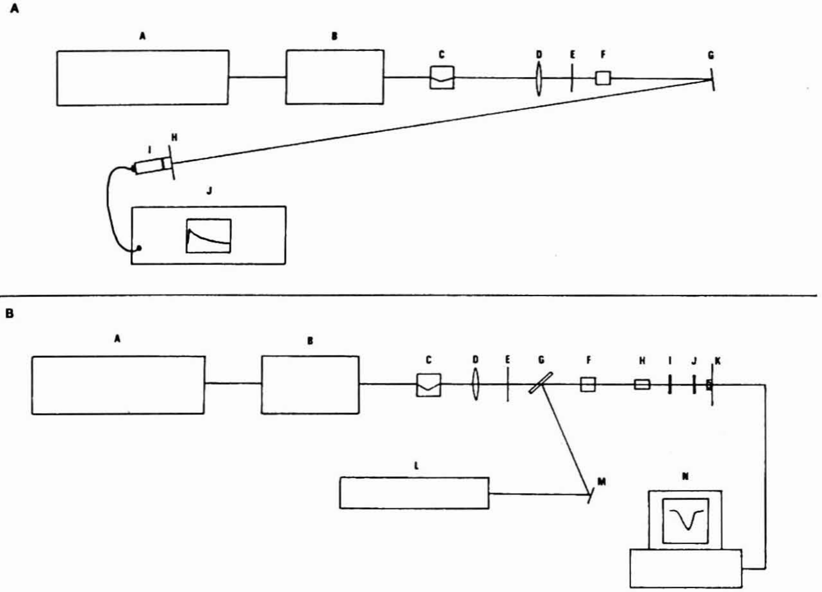

**Figure 1.** Block diagram of the laser thermal Lensing systems. Part A shows the pinhole/single laser system. The pinhole (H) was placed 403 cm from the lens (D). Part B shows the modifications to the system including the addition of a second laser (L), an optical flat (G), Nichol prism (H), and photodiode array (K).

distance (5 cm) beyond the focal point (*10, 11*). The cell used was a Canlab blue label 1-cm square cell. A flat mirror in an adjustable mount (G) was used to direct the beam toward the pinhole detector. The pinhole was 0.1 mm. The photodiode detector (I) behind the pinhole (H) was linked to a Tektronix oscilloscope (J) which had a Type 2A63 differential amplifier, and a 2B67 time base with single sweep capabilities. The lens formation was recorded at various sweep rates to record the initial ($I_0$) and final steady-state ($I_\infty$) intensities following opening the laser beam shutter. The data were then read off the screen and recorded.

Figure 1B is a block diagram of the dual laser thermal lens system. It is comprised of the six first components of the simplified system plus eight new additions. A Siemens 10 mW HeNe laser (L) was used as a probe beam which was directed to and aligned with the pump beam by means of a mirror (M) and an optical flat (G). A polarizing Nicol prism (H) was used to reduce the polarized pump beam intensity to prevent burning of the ensuing filter and polarizer. A 630-nm cuttoff filter (I) separated the pump and probe beams and a rotating film polarizer (J) adjusted the probe beam intensity to maximize the signal from the diode array without saturating the Reticon RL128G self-scanning linear photodiode array detector (K). The signal from the diode array was fed into a Processor Technology SOL computer (N) via 8-bit ADC's for storage purposes. The SOL was interfaced with an IBM personal computer which handled all numerical manipulations. The IBM plotted the beam profile (see Figure 2) and was programmed to fit a best Gaussian curve to the experimental data and to calculate the $(I_0 - I_\infty)/I_0$ values. A further modification to the initial system was to switch from a square cell to a cylindrical cell to decrease interferences due to solution convection (*14*).

**Reagents.** The formaldehyde stock solution was prepared by dissolving 4 4703 g of sodium formaldehyde bisulfite (Eastman Chemicals) in 1 L of deionized distilled water. This solution was standardized against iodine solutions with a starch indicator. Chromotropic acid (Fischer Chemicals)-formaldehyde solutions were prepared with doubly distilled $H_2SO_4$ (American Chemicals) following the NIOSH method (*15*).

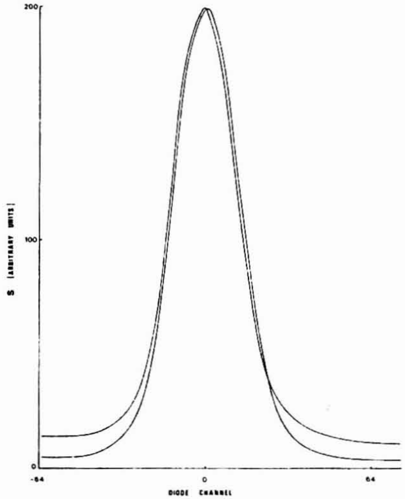

**Figure 2.** Diagram of the HeNe beam profile and the computer-fitted Gaussian profile as seen on the monitor. The signal axis is the scale of 0.256 of the A/D converter. The abscissa is the diode number referenced to the peak centre.

**Procedure.** All glassware was soaked in an $H_2SO_4$–$HNO_3$ acid bath overnight and then rinsed with deionized distilled water before use. The stock formaldehyde solutions were diluted successively to obtain the desired concentrations. Samples prepared following the NIOSH methodology were allowed to stand overnight to ensure full color development although it was noted that 1 h would have been sufficient (*15*). Before analyzing the samples and blanks using thermal lensing, a further 10-fold dilution was required to reduce the sulfuric acid concentration (vide infra).

All alignments and cell positions were optimized with a concentrated solution of formaldehyde ($\sim 10^{-5}$ M). For the simple system, the flat mirror (G) was adjusted until maximum intensity was observed on the oscilloscope screen. Then the cell was moved along the rail until the thermal lens effect was maximized. The two-laser system required alignment of the probe and pump beams which was performed before each day's run to accommodate any shift in the beams that might have occurred. This was accomplished by using the lens (D) which was on a horizontal and vertical adjustable mount to shift the pump beam in the appropriate direction to maximize the thermal lens signal observed on the monitor.

## RESULTS AND DISCUSSION

Dovichi and Harris (*16*) noted that the sensitivity enhancement that can be realized for a particular laser power is dependent on the thermooptical properties of the solvent in which the sample is dissolved. Solvents that exhibit high $dn/dt$ and low thermal conductivity are desirable for the thermal lens effect. In our experiments it was discovered early that the blank (a mixture of chromotropic acid, sulfuric acid, and water) created such a large lens that the pinhole detector was unable to differentiate between dark signal and the $I_\infty$ value. Since the blank solution was clear in color, it was assumed that the effect was due in part to absorption by the chromotropic acid and to a great deal of thermal convection in the sulfuric acid.

Preliminary experimentation showed that a 10-fold dilution of the blank was necessary to obtain a signal that was not seriously affected by thermal convection (*16*). Thus a 10-fold dilution of the color developed solutions of formaldehyde was added to the procedure.

To achieve the maximum sensitivity our system was capable of, the dye laser's most stable wavelength which was closely matched to the absorption maximum of the formaldehyde–chromotropic chromogen ($\lambda_{max} = 580$ nm) was chosen. The absorptivity of the chromogen at 600 nm was found to be $4.6 \times 10^3$ $M^{-1}$ $cm^{-1}$. A moderate power of 150 mW was found to be sufficient to pump the samples. Indeed for any greater power the convection problem would have reoccurred.

Our present two-laser system is modeled after the system of Ishibashi et al. (*13*) in that the HeNe probe laser is not focused before passing through the sample. Ishibashi et al. discuss Sheldon's abherent thermal lens model (*17*) and calculate enancement factors using his equations. They point out that both the parabolic and abherent models predict linear dependence at lower concentrations. The similarity of the two model's predictions for weak thermal lenses is further discussed by Harris and Carter (*18*). The analytical curve for formaldehyde from our data based on parabolic lens equations gave the better straight line.

A concentration range of $1.5 \times 10^{-7}$ M to $50 \times 10^{-7}$ M formaldehyde in water was studied using the single laser system. Triplicate scans of eight samples at each concentration were averaged, and the average values were used in determining the enhancement factor. The dual laser system was employed for analyzing a concentration range of $1.5 \times 10^{-8}$ to $50 \times 10^{-7}$ M. Triplicate scans of five samples at each concentration were averaged and used in the enhancement factor calculations. A detection limit of twice the standard deviation of the blank, where the blank is averaged over *all* runs with *all* sample concentrations, for each system was calculated to be $22 \times 10^{-7}$ M and $5.6 \times 10^{-7}$ M, respectively. This corresponds to absorptivity enhancement of 20.0 as defined in ref 10.

Although the standard deviation of the blank value as determined over *all runs* was quite large, the deviation of each day's blank was much smaller and it was felt that the detection limit reported above was not representative of the best performance achievable. There are several values that lie below the detection limit that appear to be significant. To determine whether these points could be considered to reflect real signals, they were compared to blanks prepared concurrently. At the lowest concentration of $1.5 \times 10^{-8}$ M a $t$ test indicated signal significance at the 99.9% level. Thus, it was apparent that higher sensitivity than quoted can be achieved with careful control of blanks and the extra effort implied. However, we have not been able to identify the specific chemical causes of the day to day blank variation. This is a problem which is not seen until the LTL technique is exploited because the conventional absorbance measures (*1*) do not emphasize small blank variations. Also, it should be pointed out that what can be small blank variations in absorption experiments are magnified by the enhancement factor, in our case 20-fold. A referee suggested that the variation is due to the variation in free formaldehyde in the lab environment entering the samples on a day to day basis. This is a very plausible explanation and we thank the referee.

Note that the addition of the second laser into our system proved to be beneficial. The reduction in noise in the probe beam allowed a large improvement in sensitivity.

As the system stands now, thermal lensing analysis of formaldehyde is an attractive alternative to GC an HPLC methods of analysis. GC and HPLC methods have been reported to use from 30 to 500 L of air per sample (*29, 30*) and/or sampling times from one (*6*) to several hours (*5*). Due to the fact that LTL can detect very low concentrations *in solution*, the amount of gas sample required to detect the same levels of formaldehyde is greatly reduced. With the $5.6 \times 10^{-7}$ M "detection limit", it would require only 8 L of gas sample at STP to detect formaldehyde in the 10 μg/L region assuming 95% collection efficiency in the NIOSH system (*1*). If one accepts the detection of $1.5 \times 10^{-8}$ M as the statistics have shown to be possible with extra effort in standardization, the volume of sample gas required is reduced to less than 1 L to detect less than 5 μg/L. This seems a practical target with improved signal processing.

**Registry No.** Formaldehyde, 50-00-0.

## LITERATURE CITED

(1) Perera, F.; Petito, C. *Science* **1982**, *216*, 18.
(2) Rybicky, J.; Horst, K.; Kambanis, S. M. *For. Prod. J.* **1983**, *33*, 1285.
(3) Van Der Wal, J. F. *Atmos. Environ.* **1982**, *16*, 2471–2478.
(4) Dumans, T. *J. Chromatogr.* **1982**, *247*, 289–295.
(5) Kennedy, E.; Hill, R., Jr. *Anal. Chem.* **1982**, *54*, 1739–1742.
(6) Grosjean, D. *Environ. Sci. Technol.* **1982**, *16*, 254–262.
(7) Miksch, R.; Anthon, D. W.; Fanning, L. Z.; Hollowell, C. D.; Reuzan, K.; Glanville, J. *Anal. Chem.* **1981**, *53*, 2118–2123.
(8) Georghiou, P.; Harlick, L.; Winsor, L.; Snow, D. *Anal. Chem.* **1982**, *54*, 567.
(9) Eckmann, A. D.; Dally, K. A.; Hankahan, L. P.; Anderson, H. A. *Environ. Int.* 1982, *8*, 156–166.
(10) Harris, J. M.; Dovichi, N. J. *Anal. Chem.* **1980**, *52*, 695A.
(11) Whinnery, J. R. *Acc. Chem. Res.* **1974**, *7*, 225.
(12) Fujiwara, K.; Lei, W.; Uchiki, H.; Shimokoshi, F.; Fuwa, K.; Kobayashi, T. *Anal. Chem.* **1982**, *54*, 2026–2029.
(13) Ishibashi, N.; Higashi, T.; Imasaka, T. *Anal. Chem.* **1983**, *55*, 1907–1910.
(14) Buffett, C. E.; Morris, M. D. *Appl. Spectrosc.* **1983**, *37*, 455–458.
(15) Tayloer, D. G., Ed. "NIOSH Manual of Analytical Methods P & Can 125"; National Institute for Occupational Safety and Health: Cincinnati, OH, 1977; DHHS (NIOSH) Publication No. 77-157A.
(16) Harris, J. M.; Dovichi, N. J. *Anal. Chem.* **1979**, *51*, 728.
(17) Sheldon, S. J.; Knight, L. V.; Thorne, J. M. *Appl. Opt.* **1982**, *21*, 1663–1669.
(18) Carter, C. A.; Harris, J. M. *Appl. Opt.* **1984**, *23*, 476–481.
(19) Sharma, D.; Villamagna, F.; Langford, C. H. *Can. J. Spectrosc.* **1983**, *29*, 6.

(20) Hu, C.; Whinnery, J. R. *Appl. Opt.* **1973**, *12*, 72–79.
(21) Haushalter, J. P. Morris, M. D. *Appl. Opt.* **1980**, *34*, 445.
(22) Swofford, R. L.; Morrell, J. M. *J. Appl. Phys.* **1978**, *49*, 3667.
(23) Ishibashi, N.; Mori, K.; Imaska, T. *Anal. Chem.* **1982**, *54*, 2039–2044.
(24) Ishibashi, N.; Mori, K.; Imaska, T. *Anal. Chem.* **1983**, *55*, 1075–1079.
(25) Long, M. E.; Swofford, R. L.; Albrecht, A. C. *Science* **1976**, 26.
(26) Gutzman, D. Co-op Workterm Report, Department of Chemistry, Concordia University, Montreal, 1983.
(27) Fang, H. L.; Swofford, R. L. *J. Appl. Phys.* **1979**, *50*, 6609.
(28) Crow, E. L.; Davis, F. A.; Maxfield, M. W. "Statistics Mannual"; Dover Publications Inc., New York, 1960.
(29) Tanner, R. L.; Meng, Z. *Environ. Sci. Technol.* **1984**, *18*, 723–726.
(30) Creech, G.; Johnson, R. T.; Stoffer, J. O. *J. Chromatogr. Sci.* **1982**, *20*, 69.

RECEIVED for review August 31, 1984. Accepted December 10, 1984.

---

# Determination of Structural Characteristics of Saturates from Diesel and Kerosene Fuels by Carbon-13 Nuclear Magnetic Resonance Spectrometry

**David J. Cookson and Brian E. Smith***

*The Broken Hill Proprietary Co., Ltd., Melbourne Research Laboratories, 245 Wellington Road, Mulgrave, Victoria, Australia 3170*

**Two saturated hydrocarbon fractions, one mainly consisting of *n*-alkanes and the other containing only branched plus cyclic saturates, have been separated from each of a variety of diesel fuels (approximate boiling range 230–320 °C) and kerosene fuels (approximately 190–230 °C) using silica chromatography and urea clathration. The *n*-alkane fractions have been simply characterized by using conventional $^{13}$C NMR spectrometry, yielding average carbon chain lengths. The branched plus cyclic saturates fractions have been characterized by using the gated spin echo (GASPE) $^{13}$C NMR technique, which yields individual $^{13}$C NMR subspectra for each $CH_n$ group type ($n = 0$ to 3) and allows the fractional abundances of $CH_n$ groups to be measured. These data have been employed in devising and calculating a number of novel average structure parameters which report on the extent of branching and occurrence of ring structures in the fractions investigated. Spectral data are also used to identify some specific submolecular structures.**

Achieving an understanding of the structural characteristics of fossil fuel products is usually a difficult task, primarily because such materials are generally complex mixtures of compounds. This is certainly the case for the diesel fuels (approximate boiling range 230–320 °C) and kerosene fuels (approximate boiling range 190–230 °C) studied in the present work. However, these fuels at least have the simplifying characteristic that they consist almost entirely of hydrocarbons. All of the samples examined here are also olefin free, such that component species can be described as saturated or aromatic. This article is concerned with the saturates class of compounds. Saturates have been isolated chromatographically from whole fuels, and have subsequently been separated into two fractions, one containing mainly *n*-alkanes and the other containing branched plus cyclic (naphthenic) saturates.

Although the composition of *n*-alkane fractions is relatively simple (see Figure 1, parts A and B) branched plus cyclic saturates fractions are complex mixtures (Figure 1C). This complexity derives from a number of factors. The boiling range of the source fuels allows for a range in the number of carbon atoms per molecule. For example, the diesel cuts studied typically include $C_{12}$ to $C_{19}$ *n*-alkanes. Also the empirical formulas of saturates components may take the form of $C_mH_{2m+2}$ for linear or branched saturates, or $C_mH_{2(m+1-x)}$ for cyclic saturates containing $x$ rings. Finally, species with the same molecular weight may be present in any of a number of isomeric forms.

It is obvious that the identification of each and every compound present in such a mixture would be an exceedingly difficult task, whatever techniques were applied. This is not the objective in the present work. Rather, the intention is to derive average structural information and to identify submolecular structures. Conventional $^{13}$C NMR spectrometry has previously been applied to fossil fuel saturates (see, for example, ref 1–7) but the structural inferences have been more limited than those derived here. This largely arises from the present application of selected multiplet subspectral $^{13}$C NMR analysis, using the gated spin echo (GASPE) technique (*8–10*). This procedure yields $^{13}$C NMR subspectra for each $CH_n$ ($n = 0$ to 3) group type. In a conventional $^{13}$C NMR spectrum of complex materials there is usually substantial overlap of resonances due to C, CH, $CH_2$, and $CH_3$ groups leading to spectral congestion. This problem is alleviated with the GASPE subspectral analysis. The accessibility of chemical shift information is consequently enhanced. Further, by identifying the $CH_n$ origin of individual resonances, the prospects for structure elucidation are improved. Also, since the method is quantitative the total abundances of $CH_n$ groups can be obtained and these data facilitate the derivation of average structure information.

From the outset it has been recognized that for average structure information to be credible, it is desirable that parameters devised should be as assumption-free as possible. Also, as far as is possible, average structure parameters should not derive from a concatenation of expressions, assumptions, and measurements, that might lead to unacceptable accumulated errors. These factors have been minimized in the present work and the credibility and reliability of structural interferences have been subjected to substantial scrutiny.

A total of nine diesel samples, six of which are petroleum derived and three of which are synfuels, have been studied,

0003-2700/85/0357-0864$01.50/0 © 1985 American Chemical Society

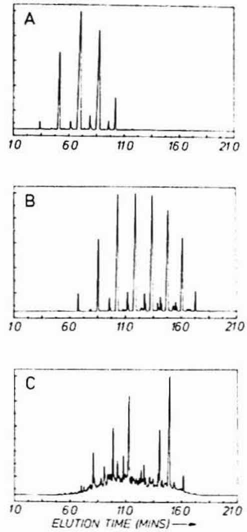

**Figure 1.** Gas chromatography traces of (A) urea adducted saturates from kerosene sample 10, (B) urea adducted saturates from diesel sample 1, and (C) branched plus cyclic saturates from diesel sample 1. The major peaks in traces (A) and (B) are due to $n$-alkanes. The minor peaks in traces (A) and (B) are due to branched alkanes, with 2-methyl and 3-methyl isomers being most abundant.

together with two kerosene samples, one each of petroleum and synfuel origins. This work is part of a larger program concerned with synfuels (i.e., fuels from nonpetroleum sources). It is of interest to understand the differences in compositions, structural characteristics, and properties of such fuels. Other work in this area, concerning the structural characteristics of diesel and kerosene aromatics, and the relationship between fuel composition and properties, will be published separately.

## EXPERIMENTAL SECTION

**Open Column Chromatography.** Saturates were separated from aromatics by elution with $n$-hexane on an open silica (Merck Silica Gel 90, predried overnight at 300 °C) column. Hexane was removed on a rotary evaporator. The procedure for separating $n$-alkanes from branched plus cyclic saturates using area adduction was based on that described in ref 11. Samples 9 and 11 (see "Sample Origins", below) were not treated with urea. $^{13}$C NMR of the total saturates fractions, together with other considerations, indicated that the $n$-alkane contents of these samples were very low.

**NMR Spectrometry.** All spectra were recorded on a Bruker WP-200 spectrometer (50.3 MHz $^{13}$C resonance frequency) at a temperature of 300 K. Chemical shifts are reported relative to internal tetramethylsilane. The gated spin echo (GASPE) $^{13}$C NMR method has been described previously (*8, 10*). It consists of a [relaxation delay]$-\pi/2-\tau-\pi-\tau-$[collect] $^{13}$C pulse sequence with $^1$H decoupling applied during the second $\tau$ period and during the data acquisition period. So-called conventional spin echo (CSE) data (*8*), obtained using the same pulse sequence but with $^1$H decoupling applied during both $\tau$ periods as well as the data acquisition period, were also recorded. GASPE data were collected for several $\tau$ values (*10*) assuming $J(CH) = 125$ Hz. These time domain data were combined to yield subspectra for each of C, CH, $CH_2$, $CH_3$, and CH + $CH_3$ groups in the sample, in the manner described in ref 10 rather than in the manner described in ref 8 and 9.

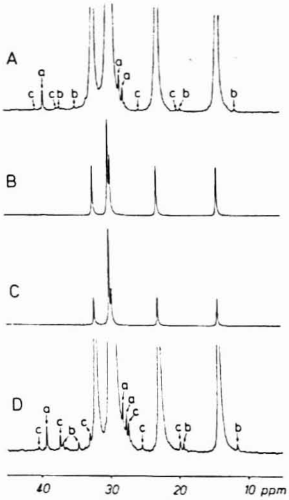

**Figure 2.** Inverse gated $^{13}$C NMR spectra of urea adducted saturates from kerosene sample 10 (A and B) and diesel sample 1 (C and D). A and D are vertical expansions of B and C, respectively. Peaks labeled "a", "b", and "c" are ascribed to 2-methyl, 3-methyl, and other alkane isomers, respectively.

Samples were made up to approximately 50 wt % in $CDCl_3$ solution and contained approximately 0.45 wt % of tris(acetylacetonato)chromium(III), $Cr(AcAc)_3$, relaxation reagent. A data acquisition time of 1.64 s was used in conjunction with a relaxation delay of 20 s. Under these conditions data are expected to be quantitative (*12*), free from distortions due to relaxation and nuclear Overhauser effects. Spectral integrations were carried out on C, $CH_2$, and CH + $CH_3$ GASPE subspectra, with the total integrated intensity closely approximating that found in the CSE spectrum. Where intensities of individual resonances or groups of resonances in a GASPE subspectrum were determined, areas were estimated from an expanded plotted integration curve rather than from peak print-out routines.

**Other Methods.** Gas chromatography was performed by the BHP Petroleum Laboratory using an in-house method for determining simulated distillation curves. A 12 m × 0.2 mm OV-101 fused silica WCOT column was employed with helium carrier gas and an oven temperature of 50–270 °C programmed at 8 °C min$^{-1}$, and detection was by FID. Hydrogen elemental microanalyses were performed by the Analytical Laboratories, Elbach, West Germany.

**Sample Origins.** Samples are given numerical designations (1 to 9 for diesels and 10 to 11 for kerosenes) in all tables. Samples 1 to 6 and sample 10 are straight run petroleum fuels, mostly of Australian origins, as follows: samples 1 and 10, Gippsland Basin; sample 2, Gippsland Basin/Indonesian crude blend; sample 3, Cooper Basin; sample 4, Perth Basin; sample 5, Surat Basin; sample 6, North West Shelf. Samples 7 to 9 and sample 11 are synfuels. Their origins are as follows: samples 9 and 11, anthracene oil (a black coal tar product); sample 7, a brown coal tar; sample 8, a shale oil. In all cases the synfuels were obtained by hydrotreating the above feedstocks, followed by distillation.

## RESULTS AND DISCUSSION

***n*-Alkanes.** The major features of the $^{13}$C NMR spectra of $n$-alkane fractions (Figure 2) are of trivial simplicity. Five resonances are observed due to $\alpha CH_3$ (14.3 ppm), $\beta CH_2$ (23.0 ppm), $\gamma CH_2$ (32.2 ppm), $\delta CH_2$ (29.7 ppm), and $\epsilon CH_2$ (30.0 ppm) corresponding to an $n$-alkane structure formalized as $(\alpha CH_3)_2(\beta CH_2)_2(\gamma CH_2)_2(\delta CH_2)_2(\epsilon CH_2)_y$, where the label $\epsilon$ refers

**Table I. Characteristics of Urea Adduct (*n*-Alkane) Fractions**

| sample | $N_C$ = average chain length | | | | % *n*-alkanes[b] | rel abundance of branched alkanes[c] | | |
|---|---|---|---|---|---|---|---|---|
| | $^{13}$C NMR | $^1$H NMR | GC[a] | av | | 2-methyl | 3-methyl | other |
| | | | | Diesels | | | | |
| 1 | 15.3 | 15.1 | 15.4 | 15.3 | 88 | 1.0 (1.0) | 0.4 (0.4) | 0.4 (0.4) |
| 2 | 15.7 | 15.5 | 16.0 | 15.7 | 91 | 1.0 (1.0) | 0.3 (0.4) | 0.7 (0.8) |
| 3 | 15.5 | 14.8 | 15.5 | 15.3 | 89 | 1.0 (1.0) | 0.5 (0.4) | 0.8 (0.7) |
| 4 | 14.6 | 15.0 | 15.3 | 15.0 | 90 | 1.0 (1.0) | 0.4 (0.5) | 0.9 (0.7) |
| 5 | 15.6 | 15.1 | 15.6 | 15.4 | 83 | 1.0 (1.0) | 0.4 (0.5) | 0.6 (0.7) |
| 6 | 15.5 | 15.5 | 15.0 | 15.3 | 91 | 1.0 (1.0) | 0.3 (0.4) | 0.6 (0.8) |
| 7 | 16.4 | 15.7 | 16.6 | 16.2 | 94 | 1.0 (1.0) | 0.2 (0.3) | 0.7 (0.7) |
| 8 | 15.0 | 14.8 | 15.9 | 15.2 | 84 | 1.0 (1.0) | 0.6 (0.7) | 2.1 (2.0) |
| | | | | Kerosene | | | | |
| 10 | 12.1 | 12.2 | 12.2 | 12.2 | 94 | 1.0 (1.0) | 0.2 (0.2) | 0.0[d] (0.0) |

[a] GC, gas chromatography. [b] From gas chromatograms. [c] From gas chromatograms or, in parentheses, from $^{13}$C NMR. [d] <0.1.

to $CH_2$ groups $\epsilon$ or further from the $\alpha CH_3$ group. Clearly the average *n*-alkane chain length, $N_C$, can be calculated from the formula

$$N_C = 8I(\alpha,\beta,\gamma,\delta,\epsilon)/I(\alpha,\beta,\gamma,\delta) \qquad (1)$$

where $I$ is the total $^{13}$C NMR intensity due to the groups in parentheses. Results are given in Table I and are compared with values calculated straightforwardly from gas chromatograms of total saturates fractions and from $^1$H NMR spectra of *n*-alkane fractions. The $^1$H NMR spectra of these fractions show a well-resolved triplet at 0.88 ppm due to terminal $CH_3$ groups and a low field peak centered at 1.27 ppm due to $CH_2$ groups. Thus, by use of symbols for intensity analogous to those in eq 1, it is readily appreciated that

$$N_C = \{3I(CH_2) + 2I(CH_3)\}/I(CH_3) \qquad (2)$$

All methods give similar results, showing average chain lengths of about 15–16 for diesels, and about 12 for the single kerosene examined.

Closer scrutiny of the $^{13}$C NMR spectra of the *n*-alkane fractions (Figure 2A,D) reveals the presence of very weak additional resonances. These are due to branched alkanes. Peaks labeled "a" (at 39.4, 28.2, and 27.7 ppm), "b" (at 36.9, 34.7, 19.4, and 11.5 ppm) and "c" (at 40.5, 37.4, 33.0, 27.4, 25.4, and 19.9 ppm) are mainly due to 2-methyl, 3-methyl, and other branched alkane isomers, respectively. These assignments follow from the discussion of branched alkanes to be given later.

The source of these branched "impurities" in the *n*-alkane fraction probably derives from the availability of straight-chain segments in these molecules, of sufficient length to allow stable urea clathrates to be formed (*13*). Gas chromatography (Figure 1) shows that branched species are usually present at about the 10 wt % level (Table I). The reason that the $^{13}$C NMR peaks labeled "a" to "c" in Figure 2 are so weak, is that most of the intensity associated with the straight chain portions of such molecules are occluded by the strong *n*-alkane intensity. If branched saturates in kerosene and diesel fuels are assumed to contain about 12 and 16 carbon atoms, respectively, on average, then the $^{13}$C NMR data predict weight percent abundances consistent with the gas chromatographic measurements. Relative abundances of branched isomers are reported in Table I.

**Branched Plus Cyclic Saturates.** *Selected Multiplet (GASPE) Subspectra.* An illustrative set of GASPE $^{13}$C NMR spectra for sample 3 is shown in Figure 3. It is common practice (*8–10*) to calculate five subspectra corresponding to C, $CH_2$, CH, $CH_3$, and CH + $CH_3$ groups and to compare these with the conventional spin echo spectrum, as shown in Figure 3. The latter is a close analogue of a conventional $^{13}$C NMR spectrum with inverse gated proton decoupling.

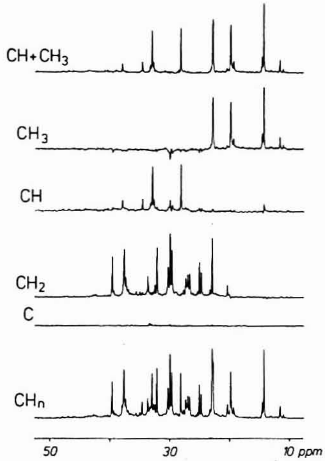

**Figure 3.** $^{13}$C NMR subspectra for the branched plus cyclic saturates from diesel sample 3. The conventional spin echo spectrum contains resonances from all $CH_n$ groups and is labeled "$CH_n$". The gated spin echo (GASPE) subspectra are labeled according to the component resonance types as "C", "$CH_2$", "CH", "$CH_3$", and "CH + $CH_3$".

While it has been noted that the GASPE method is more sensitive to variations in $J$(CH) coupling constant values than are some alternative subspectral methods for $CH_n$ group identification (*14, 15*), this is not a problem for samples of the sort studied in the present work, where $J$ values are uniformly close to 125 Hz. Indeed it is apparent from Figure 3 that excellent discrimination between $CH_n$ types is achieved and there is minimal cross contamination between subspectra. This is particularly obvious in the C subspectrum where all resonances except for two very weak peaks near 33 ppm, representing approximately 0.3% of total spectral intensity, are effectively nulled. These peaks are reliably attributed to quaternary carbons.

Individual CH and $CH_3$ subspectra are always of lower quality than other subspectra. They may contain weak artifacts arising from strong $CH_2$ intensity, which are often identifiable because they are of opposite sign in the two subspectra (see intensity near 30 ppm). It is for this reason that the higher quality CH + $CH_3$ subspectrum is calculated.

**Table II. Data for Branched Plus Cyclic Saturates Fractions**

| sample | % $^{13}$C NMR intensity as $CH_n$ C | CH | $CH_2$ | $CH_3$ | elemental % H content GASPE | microanalysis |
|---|---|---|---|---|---|---|
| | | | Diesels | | | |
| 1 | 0.2 | 15.9 | 59.4 | 24.5 | 14.9 | 14.3 |
| 2 | 0.3 | 16.8 | 58.9 | 24.0 | 14.8 | 14.4 |
| 3 | 0.3 | 15.0 | 62.6 | 22.1 | | |
| 4 | 0.0 | 14.7 | 63.3 | 22.0 | 14.8 | 14.4 |
| 5 | 0.3 | 14.6 | 63.0 | 22.1 | 14.8 | 14.3 |
| 6 | 0.5 | 21.0 | 58.1 | 20.4 | 14.3 | 14.1 |
| 7 | 0.4 | 19.1 | 59.7 | 20.8 | | |
| 8 | 0.0 | 21.3 | 61.0 | 17.7 | 14.2 | 13.9 |
| 9 | 0.0 | 22.6 | 71.9 | 5.5 | | |
| | | | Kerosenes | | | |
| 10 | 0.0 | 15.9 | 56.7 | 27.4 | 15.1 | 14.4 |
| 11 | 1.2 | 18.2 | 71.2 | 9.4 | 13.7 | 13.3 |

The individual CH and $CH_3$ data are used solely as a qualitative indicator of the $CH_n$ origin of intensity in the combined CH + $CH_3$ subspectrum, which is then used for integration. The $CH_n$ group distributions determined for the branched plus cyclic saturates samples are given in Table II.

*Initial Average Structure Parameters.* Concentration of stoichiometry leads to the following empirical formulas for saturated molecules, expressed in terms of $CH_n$ group abundances:

$$n\text{-alkane formula} \equiv [(CH_3)_2][CH_2]_m \tag{3}$$

$$\text{branched saturate formula} \equiv [(CH_3)_2][CH,CH_3]_a[C,(CH_3)_2]_b[CH_2]_m \tag{4}$$

$$a \text{ or } b > 0$$

$$\text{cyclic saturate formula} \equiv [CH]_x[C,CH_3]_y[C]_z[CH,CH_3]_a[C,(CH_3)_2]_b[CH_2]_m \tag{5}$$

$$a, b, x, y, z, > 0; x + y \text{ even integer}$$

In all cases $m \geq 0$ and $x$, $y$, $z$, $a$, $b$, and $m$ are integers. Stoichiometric constraints are implied for each term in brackets. For example, the first bracketed term in eq 4 implies that a branched alkane contains two $CH_3$ groups analogous to the terminal $CH_3$ groups in $n$-alkanes. Also, CH branching sites, each necessarily associated with an additional terminal $CH_3$ group, are allowed (second bracketed term), as are C branching sites, each associated with two additional terminal $CH_3$ groups (third bracketed term). Equation 5 can be related to eq 4 in that the formation of each saturated ring is associated with the loss of two hydrogen atoms. The presence of one ring is inferred from the absence of the $[(CH_3)_2]$ term. The presence of $(x + y)/2$ additional rings is implied by the first two terms in eq 5 and the presence of $z$ additional rings is implied by the third term. Formulas 4 and 5 lead directly to the expressions for the average structure parameters BS, $N_B$, and $N_R$

$$BS = N_C\{C + CH\} \tag{6}$$

$$N_B = N_C\{2C + CH\} \tag{7}$$

$$N_R = 0.5N_C\{2C + CH - CH_3\} + 1 \tag{8}$$

where $N_C$ is the average number of carbon atoms per molecule, BS is the average number of branching sites per molecule, $N_B$ is the average number of branches per molecule, $N_R$ is the average number of rings per molecule and C, CH, and $CH_3$ are the fractions of carbon atoms present as C, CH, and $CH_3$ groups, respectively. Equations 6 to 8 are valid for any mixture of saturates, each of which may have any number of branches of any length, any number of rings each of any number of carbons, with any kind of branching site or ring junction site. The meaning of these parameters can be appreciated by inspection of the examples in Figure 4.

To calculate average structure parameters from eq 6 to 8, it is first necessary to estimate $N_C$, the average number of carbons per molecule. In the present work this value is taken from the average $N_C$ calculated for $n$-alkanes (Table I) for samples 1–8 and sample 10. Although $n$-alkanes, branched saturates, and cyclic saturates may not have identical average numbers of carbon atoms per molecule, inspection of boiling point data (*16*) suggests that this is sufficiently close to being correct for the present purposes. For samples 9 and 11, for which an $n$-alkane fraction has not been isolated, $N_C$ values of 16 and 12, respectively, have been used as reasonable estimates. It will be seen from later discussion that samples 9 and 11 are structurally unique. Structural inferences are not sensitive to the $N_C$ values assumed. Calculated values of average structure parameters are given in Table III for all branched plus cyclic saturates samples studied.

*Substructural Assignment of Prominent Resonances.* It is apparent from Figure 3 that the $^{13}$C NMR spectrum for the branched plus cyclic saturates fraction of sample 3 is characterized by the existence of a moderate number of prominent

**Table III. Structural Parameters for Branched Plus Cyclic Saturates Fractions**

| sample | BS | $N_B$ | $N_R$ | $B/(B + C)$ | $C/(B + C)$ | $N_B$(B) eq 9 | $N_B$(B) eq 10 | $N_B$(C) | $N_R$(C) | $N_S$(C) |
|---|---|---|---|---|---|---|---|---|---|---|
| | | | | | Diesels | | | | | |
| 1 | 2.5 | 2.5 | 0.37 | 0.63 | 0.37 | 2.1 | 2.2 | 3.2 | 1.0 | 3.2 |
| 2 | 2.7 | 2.7 | 0.48 | 0.64 | 0.36 | 2.0 | 2.0 | 4.1 | 1.3 | 3.4 |
| 3 | 2.3 | 2.4 | 0.50 | 0.67 | 0.33 | 1.6 | 2.0 | 4.1 | 1.5 | 3.0 |
| 4 | 2.2 | 2.2 | 0.45 | 0.62 | 0.38 | 1.5 | 1.7 | 3.3 | 1.2 | 2.9 |
| 5 | 2.3 | 2.3 | 0.47 | 0.66 | 0.34 | 1.5 | 1.6 | 3.9 | 1.4 | 3.2 |
| 6 | 3.3 | 3.4 | 1.12 | 0.52 | 0.48 | 1.4 | 1.6 | 5.5 | 2.3 | 2.8 |
| 7 | 3.2 | 3.2 | 0.93 | 0.47 | 0.53 | 1.7 | 2.0 | 4.5 | 1.7 | 3.0 |
| 8 | 3.2 | 3.2 | 1.3 | 0.48 | 0.52 | 1.1 | 1.6 | 5.2 | 2.5 | 2.3 |
| 9 | 3.6 | 3.6 | 2.4 | | 1.0 | | | 3.6 | 2.4 | 0.8 |
| | | | | | Kerosenes | | | | | |
| 10 | 1.9 | 1.9 | 0.30 | 0.63 | 0.37 | 1.4 | 1.4 | 2.9 | 0.8 | 2.9[b] |
| 11 | 2.3 | 2.5 | 1.7 | | 1.0 | | | 2.5 | 1.7 | 1.1 |

[a] All parameters calculated using $CH_n$ abundances in Table II and average $N_C$ values in Table I. For samples 9 and 11, $N_C$ values of 16 and 12, respectively, were used. BS, number of branching sites per molecule; $N_B$, number of branches per molecule; $N_R$, number of rings per molecule; $B/(B + C)$, fraction of carbon atoms due to branched molecules; $C/(B + C)$, fraction of carbon atoms due to cyclic molecules; $N_B$(B), number of branches per branched molecule; $N_B$(C), number of branches per cyclic molecule; $N_R$(C), number of rings per cyclic molecule; $N_S$(C), number of side chains per cyclic molecule. [b] Assuming $N_R(C) = 1.0$.

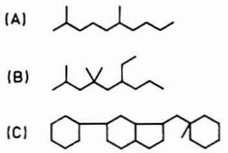

| | NUMBER OF CARBON ATOMS | BS | $N_B$ | $N_R$ |
|---|---|---|---|---|
| (A) | 12 | 2 | 2 | 0 |
| (B) | 14 | 3 | 4 | 0 |
| (C) | 23 | 6 | 7 | 4 |

**Figure 4.** Illustrative structures with average structural parameter values: BS, number of branching sites per molecule; $N_B$, number of branches per molecule; $N_R$, number of alicyclic rings per molecule. A quaternary carbon counts as two branches (for $N_B$) but only one branching site (for BS). Expressions for BS, $N_B$, and $N_R$ are given in eq 6–8.

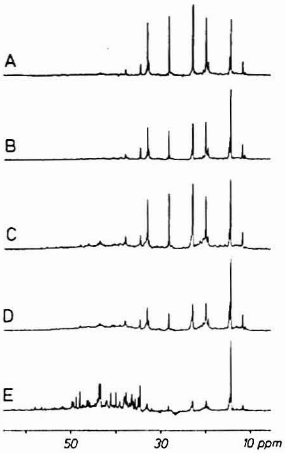

**Figure 5.** GASPE CH + $CH_3$ $^{13}C$ NMR subspectra for branched plus cyclic saturates from diesel samples 1 (A), 4 (B), 7 (C), 8 (D), and 9 (E).

peaks. Although it may not be obvious at the vertical scale amplification used in this figure, significant spectral intensity is also associated with a large number of weak resonances spread over the spectral width. These characteristics are common to samples 1 to 8 and sample 10. In the following discussion we are concerned only with the prominent peaks and will seek to identify their structural origins. Samples 9 and 11 are unique and will be discussed in the section concerned with "Reliability of Structural Inferences".

Were there no constraints on the isomeric forms present, these samples could contain a very large number of different compounds. For example, there are over 4000 conceivable $C_{15}$ (noncyclic) alkane isomers and over 360 000 isomers for $C_{20}$ alkanes (*17*). The relative simplicity of the prominent spectral patterns in Figures 3 and 5 is therefore striking and is indicative of a limited range of isomeric forms. The observed patterns are reminiscent of the spectra of isoprenoids like pristane and phytane, as has been noted previously for the conventional spectra of petroleum and shale oil saturates (*1*, *2*, *6*, *7*). It is necessary to examine the data more closely, however, before asserting the nature of branched alkanes present.

In the following discussion, the possibility that prominent spectral features are associated with isoprenoid branched alkanes is assessed by considering the compatability of observed and expected spectral characteristics. An isoprenoid branched alkane is taken as a molecule free of ring structures; in which only monomethyl (rather than dimethyl or ethyl etc.) branches are present, and where more than one branch is present, branching sites are separated by three carbons (as illustrated in Figure 4A). The number of carbon atoms per molecule is not necessarily a multiple of five.

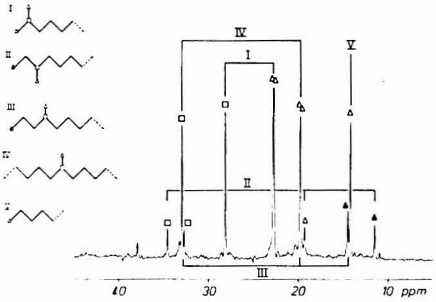

**Figure 6.** Assignment of major features in the CH + $CH_3$ GASPE $^{13}C$ NMR subspectrum of the branched plus cyclic saturates from diesel sample 1. Peaks are labeled with Roman numerals I–V and with symbols △ or ▲ for $CH_3$ groups and □ for CH groups, in accordance with the substructures shown to the left of the spectrum. Observed chemical shifts are as follows: substructure I, (△) 22.7, 22.8 ppm, (□) 28.1 ppm; substructure II, (▲) 11.5 ppm, (△) 19.3 ppm, (□) 34.6 ppm; substructure III, (▲) 14.5 ppm, (△) 19.8 ppm, (□) 32.7 ppm; substructure IV, (△) 19.8 ppm, (□) 33.0 ppm; substructure V, (△) 14.2 ppm.

The following spectral characteristics are utilized for spectral assignment in assessing the isoprenoid interpretation: (i) the $CH_n$ origin of resonances, as determined by the GASPE method; (ii) the observed chemical shifts, as compared with literature data for model compounds (*1*, *7*, *18*, *19*), and (iii) the intensity (peak area) relationships, as implied by the stoichiometry of inferred substructures.

Criteria (i) and (ii) readily lead to the assignments of CH + $CH_3$ subspectra in terms of just five substructural moieties (I to V) as illustrated in Figure 6. The following stoichiometric relationships for structures I to IV, have been tested, where the nomenclature identifies resonances according to substructure (viz., I to V), $CH_n$ type (in brackets) and chemical shift (ppm values).

$$\begin{array}{ccc} \mathrm{I(CH_3)} & = 2 \times & \mathrm{I(CH)} \\ 22.7\ \&\ 22.8\ \mathrm{ppm} & & 28.1\ \mathrm{ppm} \end{array}$$

$$\begin{array}{ccccc} \mathrm{II(CH_3)} & = & \mathrm{II(CH_3)} & = & \mathrm{II(CH)} \\ 11.5\ \mathrm{ppm} & & 19.3\ \mathrm{ppm} & & 34.6\ \mathrm{ppm} \end{array}$$

$$\begin{array}{ccc} \mathrm{III(CH_3)} & = & \mathrm{III(CH)} \\ 14.5\ \mathrm{ppm} & & 32.7\ \mathrm{ppm} \end{array}$$

$$\begin{array}{ccccccc} \mathrm{IV(CH_3)} & + & \mathrm{III(CH_3)} & - & \mathrm{III(CH_3)} & = & \mathrm{IV(CH)} \\ 19.8\ \mathrm{ppm} & & 19.8\ \mathrm{ppm} & & 14.5\ \mathrm{ppm} & & 33.0\ \mathrm{ppm} \end{array}$$

Observed intensities are satisfactorily consistent with expectations. The 14.5 ppm $CH_3$ peak associated with substructure III in Figure 6 is an exception. This is often of higher intensity than its partially resolved companion CH peak at 32.7 ppm (Figures 5 and 6) and must therefore often include intensity due to other substructures. With this exception, the assignments are considered to be well-founded.

The $CH_2$ subspectra are less easily treated. In Figure 7, eight chemical shift regions are denoted A to H and plausible substructures are illustrated. The relevant $CH_2$ group is

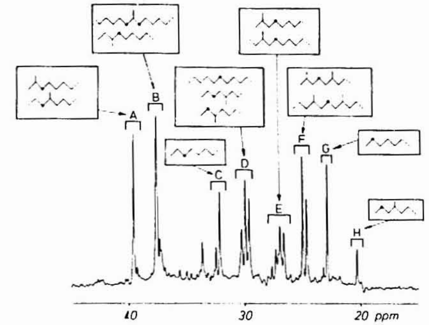

**Figure 7.** $CH_2$ GASPE $^{13}C$ NMR subspectrum of the branched plus cyclic saturates from diesel sample 1. Eight chemical shift regions are labeled as follows: A, 39.2 to 39.7 ppm; B, 36.7 to 37.6 ppm; C, 32.0 to 32.5 ppm; D, 29.6 to 30.3 ppm; E, 26.6 to 27.6 ppm; F, 24.6 to 25.0 ppm; G, 22.7 to 3.1 ppm; H, 19.4 to 20.4 ppm. Each region is associated with $CH_2$ groups marked by dots in the substructures illustrated. The chemical shift ranges for regions A to G are taken from literature data (*7*, *18*) for molecules containing the substructures illustrated. Peak positions observed in the present work also fall within the quoted ranges. The substructures illustrated are defined by carbon atom dispositions up to three carbons away from the $CH_2$ site in question. Possible structural variants involving differences four or more positions away from the $CH_2$ site in question are not necessarily illustrated.

highlighted by a dot in each of the substructures, and other carbon groups up to four carbons away are indicated by solid lines. Often the $CH_n$ type, plus the chemical shift observed, are not sufficient to delineate possible structural variants after the third carbon. The following stoichiometric requirements for $CH_2$ resonance intensities, particularly in relation to CH + $CH_3$ resonance intensities, have been tested:

$$\underset{39.5\text{–}39.7}{A(CH_2)} = \underset{28.1}{I(CH)} + \underset{32.7}{III(CH)}$$

$$\underset{37.3\text{–}37.6}{B(CH_2)} = \underset{34.6}{II(CH)} + \underset{32.7}{III(CH)} + 2 \times \underset{33.0}{IV(CH)}$$

$$\underset{32.1\text{–}32.5}{C(CH_2)} < \underset{22.9\text{–}23.1}{G(CH_2)} < \underset{14.2}{V(CH_3)}$$

$$\underset{24.6\text{ or }25.0}{F1(CH_2)} < \underset{28.1}{I(CH)}$$

$$\underset{19.9\text{–}20.4}{H(CH_2)} = \underset{32.7}{III(CH)}$$

The nomenclature is in the same format as that used for the CH + $CH_3$ subspectra above. Structure F1 is the upper structure in region F shown in Figure 7 and is probably associated with the 24.6-ppm peak, rather than that at 25.0 ppm (*7*). The above equalities and inequalities involve six of the eight $CH_2$ chemical shift regions. Observed intensities are satisfactorily consistent with expectations.

It is apparent that prominent spectral features can be interpreted in terms of substructures consistent with isoprenoids. It is inferred that branching is mainly of the monomethyl type and, where more than one branch is present in a structure, these are well separated. It is more difficult, however, to judge whether molecules with more than one branch follow the strict isoprenoid format, i.e., that branches are separated by three carbons as in Figure 4A. Resonances of carbons in only two of the substructures shown in Figures 6 and 7 report on the interrelationship between consecutive branches. These are the structures associated with region F in Figure 7. The $CH_2$ intensity in region F, denoted ($CH_2$,F), can be used as a test of the existence of a strict isoprenoid format in multiply branched saturates.

The number of branches per branched molecule, denoted $N_B(B)$, can be calculated from the prominent peak intensity identified in Figures 6 and 7 using the relationship

$$N_B(B) = N_C(CH^P)/\sum(CH_n^P) \qquad (9)$$

where superscript P denotes prominent peaks, and other symbols are as used in other equations. A molecule containing $N_B(B)$ isoprenoid branches must also contain $\{N_B(B) - 1\}$ of ($CH_2$,F) groups, such that

$$N_B(B) = N_C\{(CH_2,F)/\sum(CH_n^P)\} + 1 \qquad (10)$$

Thus if prominent intensity is solely due to isoprenoids, $N_B(B)$ values from eq 9 and 10 should be identical. Results given in Table III show that there is generally good agreement between these two calculations, suggesting the predominance of isoprenoid multiple branch interrelationships. It should be noted, however, that eq 9 and 10 require integrations of individual resonances in a complex spectrum. This procedure is considerably more error-prone than the whole subspectral integrations used to determine BS, $N_B$, and $N_R$. The ($CH^P$) and ($CH_2$,F) resonances are particularly weak for sample 8, such that the substantial discrepancy in the two calculated $N_B(B)$ values (1.1 and 1.6) observed for this sample, is regarded as insufficiently reliable to be interpreted.

*Assignment-Dependent Average Structure Parameters.* The proposition that prominent intensity can be largely ascribed to branched molecules requires further examination with regard to possible contributions from *n*-alkanes and cyclic saturates.

Prominent intensity is found in the spectra of branched plus cyclic saturates at chemical shifts within 0.1 ppm of shifts expected for *n*-alkanes (see Figure 3). However for diesel *n*-alkanes the peaks at 30.0, 32.2, 29.7, 23.0, and 14.3 ppm should be in the approximate ratio of 4:1:1:1:1 (Figure 2). Thus, even if the total intensity at 30.0 ppm in Figure 3 was assigned to *n*-alkanes, the contribution of *n*-alkanes to the other chemical shift regions would be low. Thus any *n*-alkane contribution to prominent spectral intensity is sufficiently low to be ignored.

It is anticipated that some of the spectral intensity in the vicinity of prominent peaks will be associated with cyclic structures, even if this only derives from minor accidental overlap. What is of concern here, however, is to judge whether a substantial proportion of prominent intensity is associated with cyclic molecules (plausibly deriving from branched side chains/substituents). A simple calculation indicates that this is improbable, at least for samples 1 to 5 and sample 10. For these samples the average number of rings per molecule, $N_R$, is calculated from the overall $CH_n$ group distribution to be between 0.30 and 0.50 (Table III). This implies that minimally (i.e., for the case where there is a single ring per cyclic molecule) between 70% and 50% of spectral intensity must be due to noncyclic molecules. The integrated intensity due to prominent peaks corresponds to between 62% and 67% of total intensity (see eq 11 for $B/(B + C)$ parameter). It is inferred that the assignment of prominent peaks to branched molecules is reasonable and this interpretation is also extended to samples 6 to 8. If it is also assumed that nonprominent spectral intensity is due to cyclic structures (see later), a range of additional average structure parameters can be devised.

Obviously the fractional abundance of branched molecules, $B/(B + C)$, is simply obtained by spectral integration of prominent peaks, according to

$$B/(B + C) = \sum(CH_n^P)/\sum(CH_n) \qquad (11)$$

The fractional abundance of cyclic molecules is obtained by difference

$$C/(B + C) = 1 - B/(B + C) \qquad (12)$$

The number of branches per branched molecule, $N_B(B)$, can be determined by using eq 9 or 10. Equation 9 is preferred because the CH intensity is in a less congested spectral region than is the ($CH_2$,F) intensity. The number of branches per cyclic molecule, $N_B(C)$, is calculated from

$$N_B(C) = \{(B + C)/C\}\{N_B - N_B(B)[B/(B + C)]\} \qquad (13)$$

The number of rings per cyclic molecule, $N_R(C)$ is given by

$$N_R(C) = N_R\{(B + C)/C\} \qquad (14)$$

The meaning of $N_B(B)$, $N_B(C)$, and $N_R(C)$ is self-evident from the earlier discussion of $N_B$ and $N_R$ (Figure 4). An additional parameter, the number of side chains per cyclic molecule, $N_S(C)$, can be calculated from

$$N_S(C) = N_B(C) - 2\{N_R(C) - 1\} \qquad (15)$$

This is simply a measure of the number of branches in cyclic molecules in excess of those associated with connections between rings. Thus $N_S(C)$ is unity for the structure in Figure 4C and would be equal to zero for decalin and two for dimethylcyclohexane. A summary of calculated parameters is given in Table III.

*Reliability of Structural Inferences.* The current approach to the elucidation of the structural features of branched and cyclic saturates is novel. Many average structure parameters have been introduced through a variety of expressions. It is therefore of particular importance to consider the reliability of structural inferences in some detail.

Various methods for the calculation of average structure parameters for fossil fuel products have long been in use (see, for example, ref 20–28). Such procedures invariably incorporate assumptions. Constraints on structural possibilities may be built into these approaches, or it may be necessary to assume that broad NMR chemical shift classifications are quantitatively valid. There are two types of average structure parameter devised in the present work. Equations 6–8 leading to BS, $N_B$, and $N_R$ for the total sample are virtually assumption free. The prime requirement is an accurate measurement of $CH_n$ abundances and the deduction of a suitable value of $N_C$, the average number of carbons per molecule. An approximate cross-check of $CH_n$ data can be gained by consideration of elemental hydrogen content. The weight percent hydrogen can obviously be calculated from $CH_n$ distributions. Results for eight samples are compared with microanalytical data in Table II. The NMR data suggest slightly higher hydrogen contents than the microanalytical data, though both methods are consistent to within 0.7 wt %. The total range of hydrogen contents deduced from GASPE NMR data for these eight samples is only 1.4 wt %. It is expected that microanalysis, though in reasonable agreement with NMR, is not an accurate test of deduced $CH_n$ distributions.

The second set of structural parameters devised, including $B/(B + C)$, $C/(B + C)$, $N_B(B)$, $N_B(C)$, $N_R(C)$, and $N_S(C)$, do depend on the assumption that spectral intensity can be subdivided into prominent and nonprominent features, largely due to branched and cyclic molecules, respectively. A number of observations support this spectral subdivision, though definitive evidence on the quantitative validity of the procedure is not available. (i) As shown in the previous section, assignment criteria are consistent with prominent intensity being largely due to branched molecules, though some contribution from cyclics cannot be excluded. (ii) It was also shown in the previous section that, for samples 1 to 5 and sample 10, the minimum cyclic saturates intensity required by $N_R$ was in reasonable accord with that deduced by $C/(B + C)$. Spectral subdivision is used to derive $C(B + C)$ but not $N_R$. (iii) Further, it is apparent from Table III that $C/(B + C)$ and $N_R$ values, for all samples, follow similar trends. (iv) Samples 9 and 11 consist almost entirely of cyclics (see below). These samples are characterized by a broad CH intensity distribution between about 27 and 60 ppm. The prominence of this spectral region for the samples studied (Figure 5) follows the same trends as do calculated $C/(B + C)$ values.

**Table IV. Comparison of Diesel Sample Groupings**[a]

| | range of parameter values | | | | |
|---|---|---|---|---|---|
| parameter | group I | | group II | | group III |
| BS | 2.2–2.7 | < | 3.2–3.3 | < | 3.6 |
| $N_B$ | 2.2–2.7 | < | 3.2–3.4 | < | 3.6 |
| $N_R$ | 0.37–0.50 | < | 0.93–1.3 | < | 2.4 |
| $C/(B + C)$ | 0.33–0.37 | < | 0.48–0.53 | < | 1.0 |
| $N_B(C)$ | 3.2–4.1 | < | 4.5–5.5 | > | 3.6 |
| $N_R(C)$ | 1.0–1.5 | < | 1.7–2.5 | ~ | 2.4 |
| $N_S(C)$ | 2.9–3.4 | ~ | 2.3–3.0 | > | 0.8 |
| $N_B(B)$ | 1.5–2.1 | | 1.1–1.7 | | |

[a] Group I, samples 1–5; group II, samples 6–8; group III, sample 9.

Having dealt with the question of assumptions, it is also of value to investigate the credibility of calculated structural parameter values. Molecular weight limitations demand that $1 < N_B(B) < 4$ for isoprenoids. All values calculated (Table III) are within this range. Also, by definition, $N_R(C)$ must be ≥1. This is so for all but sample 10, where the measured value of 0.8 is regarded as acceptable within experimental error. Samples 9 and 11 provide a unique opportunity to examine the credibility of structural parameter values, since their mode of production has been studied in detail (ref 29, and unpublished data). These samples were obtained by hydrotreating an anthracene oil which consisted mainly of two-ring aromatic and polynuclear aromatic species. The anthracene oil feedstock contained less than one $CH_3$ terminated side chain per 30 aromatic carbon atoms, and analysis of total hydrotreated products showed that $CH_3$ producing reactions were of minor significance. The calculated parameters $C/(B + C) \sim 1.0$, $N_R(C) = 2.4$ (sample 9) or 1.7 (sample 11), and $N_S(C) = 0.8$ (sample 9) or 1.1 (sample 11), therefore appear credible.

*Diesel Sample Comparisons.* Numerical investigations suggest that the average structure parameters devised in the present work are not unduly sensitive to plausible errors in raw data. Such considerations indicate that the set of nine diesel samples in Table III can be treated in terms of three groups. Group I consists of samples 1 to 5, group II consists of samples 6 to 8, and group III consists of sample 9. Comparisons between groups I, II, and III are summarized in Table IV. The values of BS, $N_B$, $N_R$, $C/(B + C)$, $N_B(C)$, and $N_R(C)$ are consistently larger for group II than for group I. Group II is therefore more branched, contains more cyclic molecules, and has more rings per cyclic molecule, than group I. Group III, as discussed in the previous section, largely consists of cyclic molecules, with 2.4 rings per molecule and 3.6 branches per molecule, on average.

$N_S(C)$ and $N_B(B)$ values do not follow such group trends. All group I and II samples show approximately three substituents per cyclic molecule, with the possible exception of sample 8. Sample 9 shows a distinctively low $N_S(C)$ value of 0.8. Most samples show 1.4 to 1.7 branches per branched molecule. Samples 1 and 2 yield slightly higher values (2.0, 2.1) and sample 8 shows a distinctively low value (1.1). All measurements indicate that $N_B(C) > N_B(B)$.

## CONCLUSIONS

It has been demonstrated that novel structural information can be derived for saturates from diesel and kerosene fuels using the GASPE $^{13}C$ NMR method. For the approach to be effective it is first necessary to isolate saturates from whole fuel samples. In principle the NMR analysis could be applied to a total saturates fraction. However, if *n*-alkanes are a major component, it is probable that the accuracy of parameters reflecting the presence and nature of branched and cyclic saturates would be reduced. It is for this reason that in the present work the major emphasis has been placed on a separate branched plus cyclic saturates fraction. Saturates differ in terms of branching and ring structures. It is believed that these characteristics can be sufficiently well-defined using the GASPE $^{13}$C NMR procedures to delineate clear differences in the composition of samples obtained from different sources.

## ACKNOWLEDGMENT

We thank C. J. Rix of the Royal Melbourne Institute of Technology and personnel of the BHP Petroleum Laboratory for assistance.

## LITERATURE CITED

(1) Bartle, K. D.; Jones, D. W.; Pakdel, H. "Molecular Spectroscopy"; West, A. R., Ed.; Heydon: London, 1976; Chapter 9.
(2) Netzel, D. A. "Synthetic Fuels from Oil Shale Symposium", Atlanta, GA, Dec 1979; p 271.
(3) O'Donnell, D. J.; Sigle, S. O.; Berlin, K. D.; Sturm, G. P.; Vogh, J. W. *Fuel* **1980**, *59*, 166.
(4) Takegami, Y.; Watanabe, Y.; Suzuki, T.; Mitsudo, T.; Itoh, M. *Fuel* **1980**, *59*, 253.
(5) Suzuki, T.; Itoh, M.; Watanabe, Y.; Mitsudo, T.; Takegami, Y. *J. Jpn. Pet. Inst.* **1981**, *24*, 151.
(6) Gillet, S.; Rubini, P.; Delpeuch, J.-J.; Escalier, J.-C.; Valentin, P. *Fuel* **1981**, *60*, 226.
(7) Netzel, D. A.; McKay, D. R.; Heppner, R. A.; Guffey, F. D.; Cooke, S. D.; Varie, D. L.; Linn, D. E. *Fuel* **1981**, *60*, 307.
(8) Cookson, D. J.; Smith, B. E. *Org. Magn. Reson.* **1981**, *16*, 111.
(9) Cookson, D. J.; Smith, B. E. *Fuel* **1983**, *62*, 34.
(10) Cookson, D. J.; Smith, B. E. *Fuel* **1983**, *62*, 986.
(11) Weiss, F. T. "Chemical Analysis"; "Determination of Organic Compounds: Methods and Procedures" Ewing, P. J., Kolthoff, I. M., Eds.; Wiley-Interscience: New York, 1970; Vol. 32 Chapter 1, p 14.
(12) Cookson, D. J.; Smith, B. E. *J. Magn. Reson.* **1984**, *57*, 355.
(13) Fetterly, L. C. "Non Stoichiometric Compounds"; Mandelcorn, L., Ed.; Academic Press: New York, 1964; Chapter 8.
(14) Bendall, M. R.; Pegg, D. T. *J. Magn. Reson.* **1983**, *53*, 272.
(15) Bildsoe, H.; Donstrup, S.; Jakobsen, H. J. *J. Magn. Reson.* **1983**, *53*, 154.
(16) "API Technical Data Book—Petroleum Refining"; American Petroleum Institute Division of Refining: Washington, DC, 1970; Vol. 1, Chapter 1.
(17) Henze, H. R.; Blair, C. M. *J. Am. Chem. Soc.* **1931**, *53*, 3077.
(18) Lindeman, L. P.; Adams, J. Q. *Anal. Chem.* **1971**, *43*, 1245.
(19) Grant, D. M.; Paul, E. G. *J. Am. Chem. Soc.* **1964**, *86*, 2984.
(20) Williams, R. B. *ASTM Spec. Tech. Publ.* **1958**, *No. 224*, 168.
(21) Brown, J. K.; Ladner, W. R. *Fuel* **1960**, *39*, 87.
(22) Clutter, D. R.; Petrakis, L.; Stenger, R. L.; Jensen, R. K. *Anal. Chem.* **1972**, *44*, 1395.
(23) Retcofsky, H. L. *Appl. Spectrosc.* **1977**, *31*, 116.
(24) Bartle, K. D.; Jones, D. W. "Analytical Methods for Coal and Coal Products"; Karr, C., Ed.; Academic Press: New York, 1978; Vol. 2, p 104.
(25) Bartle, K. D.; Ladner, W. R.; Martin, T. G.; Snape, C. E.; Williams, D. F. *Fuel* **1979**, *58*, 413.
(26) Yokoyama, S.; Uchino, H.; Katoh, T.; Sanada, Y.; Yoshida, T. *Fuel* **1981**, *60*, 254.
(27) Netzel, D. A.; Miknis, F. P. *Fuel* **1982**, *61*, 1101.
(28) Petrakis, L.; Allen, D. T.; Gavalas, G. R.; Gates, B. C. *Anal. Chem.* **1983**, *55*, 1557.
(29) Awadalla, A. A.; Cookson, D. J.; Smith, B. E. *Fuel*, in press.

RECEIVED for review August 21, 1984. Accepted December 10, 1984. Support for this work was provided under the National Energy Research Development and Demonstration Program, administered by the Australian Commonwealth Department of Resources and Energy.

---

# Comparison of Photoacoustic and Attentuated Total Reflectance Sampling Depths in the Infrared Region

**Daniel A. Saucy, Steven J. Simko, and Richard W. Linton***

*Kenan Laboratories of Chemistry, Department of Chemistry, University of North Carolina,*
*Chapel Hill, North Carolina 27514*

**Attentuated total reflectance (ATR) and photoacoustic spectroscopy (PAS) are surface-sensitive IR techniques. The maximum analytical depths for both techniques were compared for organic thin films by preparing polymers consisting of known thicknesses of polystyrene (PS) on poly(methyl methacrylate) (PMMA). Relative contributions of PS and PMMA to the spectra (1601 cm$^{-1}$, 1732 cm$^{-1}$, 3028 cm$^{-1}$ bands) suggest that ATR samples to a depth of <2 μm while the PAS analytical depth extends to 15–20 μm. These values are dependent upon optical and thermal properties of the sample and instrumental parameters. However, the general trends are expected to be applicable to organic thin films in the optically transparent, thermally thick category.**

Photoacoustic spectroscopy (PAS) is gaining acceptance as a technique for the chemical characterization of solids. Infrared spectrometry (IR) has long been employed to probe molecular structure. Combined IR/PAS is, thus, extending the types of molecular information which can be obtained directly from solid samples. The theory for photoacoustic spectroscopy has been reviewed by Rosencwaig and Gersho (*1, 2*) and experimental details have been discussed by Rosencwaig (*3, 4*). Both theory and experiment also have shown that PAS is sensitive to the near surface region of solids.

The more traditional IR techniques for surface studies are the various reflectance techniques, with attentuated total reflectance (ATR) and diffuse reflectance being the most common. However, both of these techniques suffer from restrictions on sample type. ATR is very dependent upon good and reproducible contact between the sample and the reflection element. Diffuse reflectance requires an optically thin, highly scattering sample. In these respects, PAS offers several advantages over ATR and diffuse reflectance techniques. The sample to be analyzed is placed directly into the sample cell. Thus sample morphology need not be altered in most cases, in contrast to ATR and diffuse reflectance, and spectra of the sample in its native state can be obtained nondestructively. In sum, PAS offers the potential for obtaining IR spectra of solid surfaces with a minimum of sample preparation and for a maximum of sample types.

Infrared surface studies have potential utility in a wide range of applications including adsorption, catalysis, and thin-film chemistry. Since both ATR and PAS are sensitive to a near-surface region of the sample, there exists a need to

0003-2700/85/0357-0871$01.50/0 © 1985 American Chemical Society

examine the relative surface sensitivities of these two techniques. This is especially true in light of differing conclusions reached in prior investigations (*4–6*), reflecting the influence of the optical and thermal properties of the solid. Krishnan (*4*) has stated that for samples of low thermal diffusivity, e.g., polystyrene, the depth of penetration for PAS is on the order of 10–100 μm for the modulation frequencies encountered in a standard FT-IR instrument. Harrick (*5*) gives an equation for the depth of penetration in ATR which yields a sampling depth of approximately 1 μm for polystyrene. Gardella et al. (*6*), however, report that for a polyurethane polymer containing polyether and poly(dimethylsiloxane), PAS samples less deeply than does ATR.

In this study, polymer samples consisting of known thickness films (0.5–19 μm) of polystyrene (PS) on poly(methyl methacrylate) (PMMA) were prepared. This enabled comparison of the effective sampling depths of ATR and PAS by examining the relative spectral contributions of the two polymers.

## EXPERIMENTAL METHODS

All IR spectra were obtained with a Digilab FTS-14 Fourier transform IR spectrometer. Spectra were transferred to a custom-designed Z-80 microprocessor based microcomputer (*7*) for analysis and data manipulation. All spectra were collected at 8 $cm^{-1}$ resolution, with a mirror velocity of 0.15 cm $s^{-1}$. PA spectra were obtained with a Princeton Applied Research Model 6003 photoacoustic cell and a PAR 6005 PA amplifier. The output from the PA amplifier was substituted for the deuterated triglycine sulfate (DTGS) detector signal when photoacoustic detection was desired. The Digilab acquisition software and hardware were modified so that either the PA or DTGS detector could be selected by the data system. Alternate PA and DTGS reference scans were obtained to correct for the effects of source intensity and residual $CO_2$ and $H_2O$ in the PA data. Detectors normally were switched every 20 scans. ATR spectra were acquired using a Harrick ATR accessory and a 45° KRS-5 reflection element at normal incidence. Photoacoustic spectra usually were acquired for 1000 scans vs. 300 for ATR spectra. All spectra were referenced to the DTGS spectrum acquired alternately as described above. ATR spectra then were ratioed to a blank KRS-5 crystal spectrum. PA peak intensities were determined by measuring the height of the peak above a base line drawn through the spectrum on either side of the peak of interest.

All samples were prepared by spin coating (Headway Research, Garland, TX, Model EC101) a PMMA film onto an 18 × 18 mm glass slide from a 40% (w/w) solution of PMMA (Aldrich) in toluene. The film was heated at 120 °C for approximately 5 min to remove all toluene. PS (Aldrich) then was spin coated onto the PMMA from a toluene solution ranging in concentration from 10 to 20% (w/w), depending on the PS film thickness desired. The thickness of the polystyrene film was determined with a profilometer (Tencor Instruments, Model Alpha Step 100). The accuracy of the thickness measurement depends upon the film thickness. The ATR sample thicknesses were estimated to be ±0.1 μm while the thicker PAS samples were ±0.5 μm. The variability in film thickness across the sample was found to be approximately twice these values.

The central portion of each square sample had the most uniform film thickness and was used to obtain the photoacoustic spectrum. ATR spectra were obtained from the sample cut in half and pressed against the KRS crystal. The PS thicknesses reported are those of the actual samples used in the spectroscopic studies.

## RESULTS AND DISCUSSION

**PS and PMMA Spectra.** Figure 1 shows the photoacoustic spectra of polystyrene and poly(methyl methacrylate) films. As expected from the polymer structures, there are clear differences between the spectra. PMMA has a sharp band at 1736 $cm^{-1}$ due to C=O stretching. This band will be used to quantify the PMMA contribution to the PA or ATR spectra of the PS-on-PMMA samples. The CH band at 841 $cm^{-1}$ could potentially be used for this purpose. However, it is much weaker than the C=O band and is detected in PS. A series of bands for PMMA also are present in the 1300–1100 $cm^{-1}$ region due to C–O stretching modes. Although these bands are more difficult to measure quantitatively because of spectral overlaps, they can be used to qualitatively judge the PMMA contribution to a spectrum. Polystyrene has several unique bands which can be used to judge the PS contribution to a PS-on-PMMA spectrum: the aromatic CH stretch (3028 $cm^{-1}$) and the aromatic C=C stretch (1601 $cm^{-1}$). Thus, the above spectral bands make it possible to determine if either PA or ATR is sampling through the surface PS layer and, thus, "seeing" the underlying PMMA. Because the parameters which influence PA ($\mu$, the thermal diffusion length) and ATR ($\lambda$, the IR wavelength, and $n$, the sample's index of refraction) sampling depths vary across the spectrum, the wavelengths of ratioed peaks should be as close together as possible. Thus, a suitable choice for the PS-on-PMMA system is the C=O stretch for PMMA and the aromatic C=C stretch for PS that are within 135 $cm^{-1}$ for each other. It should be noted that PA band intensities depend on modulation frequency which is related to spectral wavenumber ($f = 2V\nu$). Thus, the PA spectra to be discussed are not photometrically accurate. Teng and Royce (*8*) have presented a procedure, based on obtaining two PA spectra at different mirror velocities, to obtain photometrically accurate PA spectra. This procedure could not be applied here because of the spectrometer's fixed mirror velocity. The resulting lack of photometric accuracy will not deleteriously affect the interpretation of the PS-on-PMMA spectra to be presented. The PA intensity ratios of emission peaks will be used only to estimate maximum sampling depths, not to quantify the relative contributions of PMMA and PS to each of the various PA spectra.

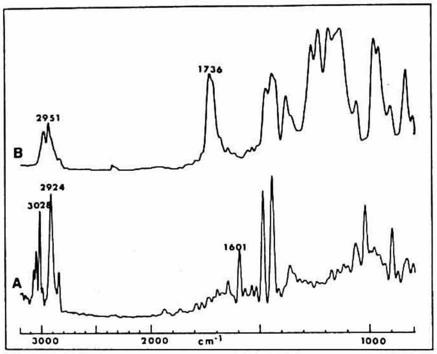

**Figure 1.** Photoacoustic spectra of pure (A) polystyrene, PS, and (B) poly(methyl methacrylate), PMMA, as free standing films. Spectra have been normalized to a DTGS detected reference spectrum.

**Sampling Depth—PAS.** The photoacoustic spectra for five different thicknesses of PS on PMMA are shown in Figure 2. As the thickness of the PS increases, an increase in polystyrene features relative to those of PMMA is clearly evident. The 3-μm sample exhibits only weak polystyrene features while the 19-μm sample shows the absence of PMMA's C=O stretch at 1732 $cm^{-1}$, yielding a spectrum virtually identical with that of pure PS (Figure 1). Table I shows the peak intensities for the aromatic CH stretch and aromatic C=C stretch bands of polystyrene ratioed to the C=O stretch of PMMA. These values reflect the increase in PS character of the spectra as the polystyrene film thickness increases. Since the C=O stretch band of PMMA disappears between the 16- and the 19-μm sample, the maximum depth

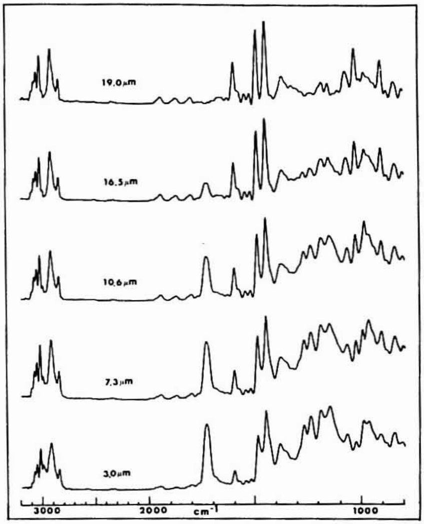

**Figure 2.** Photoacoustic spectra of five thicknesses of PS on PMMA. Spectra have been normalized to a DTGS detected reference spectrum.

**Table I. Peak Intensity Ratios for PA Spectra of Polystyrene (PS) on Poly(methyl methacrylate) (PMMA)**[a]

| PS film thickness, μm | $I$(3028 cm$^{-1}$/ 1732 cm$^{-1}$) | $I$(1601 cm$^{-1}$/ 1732 cm$^{-1}$) |
|---|---|---|
| 3 | 0.36 | 0.20 |
| 7.3 | 0.67 | 0.45 |
| 10.5 | 0.78 | 0.70 |
| 16.5 | 2.0 | 2.34 |
| 19.0 | >10 | >10 |

[a] 3028 cm$^{-1}$, aromatic CH stretch in PS; 1601 cm$^{-1}$, C=C stretch in PS; 1732 cm$^{-1}$ C=O stretch in PMMA.

sampled by PAS in this system is between 16 and 19 μm.

Sampling depth in PAS depends on both the thermal and optical properties of the sample. Samples can be classified as optically transparent or opaque and thermally thin or thick (*3, 4*) depending on the relation between sample thickness, thermal diffusion length, and optical path length. The absorption coefficients, $\beta$, for the major bands of PS (3025 cm$^{-1}$, 2927 cm$^{-1}$) were determined to be approximately 500 cm$^{-1}$ based on transmission spectra of known thickness PS films. The resulting optical path lengths for these bands, defined as the reciprocal of the absorption coefficient, are approximately 20 μm. Thus, all the polystyrene films examined in this study are classified as optically transparent since they are thinner than the optical path length. The thermal property of concern in this analysis is the thermal diffusivity, $\alpha$, which is the thermal conductivity divided by the product of sample density times specific heat. The thermal diffusion length, $\mu$, is calculated from $\alpha$ and the modulation frequency according to

$$\mu = \left(\frac{2\alpha}{w}\right)^{1/2} \tag{1}$$

where $w$ is the modulation frequency. In FT-IR, $w$ is equal to $4\pi\nu V$ where $\nu$ is the wavenumber (cm$^{-1}$) and $V$ is the mirror velocity (cm/s). By use of the value $1.3 \times 10^{-3}$ cm$^2$ s$^{-1}$ (*9*) for the thermal diffusivity of PS, the thermal diffusion lengths for the bands of interest in this study are 6.7 μm at 3028 cm$^{-1}$ and 9.3 μm at 1601 cm$^{-1}$.

Rosencwaig has divided possible samples into six classes which depend on the relative magnitudes of the thermal diffusion length and optical path length of the sample and its thickness. For the samples used in this study, once the PS film thickness is greater than the thermal diffusion length of polystyrene, the sample is classified as being thermally thick and optically transparent. For such a case, Rosencwaig (*3*) and Krishnan (*4*) state that only the radiation absorbed within the first thermal diffusion length contributes to the photoacoustic signal. Thus, features in the sample further than that distance from the surface should be photoacoustically "invisible". However, the data presented here clearly indicate that features as deep as at least twice the thermal diffusion length can be detected. This is evident in the 16-μm PS film sample, where the C=O stretch band of the PMMA substrate is still present.

A maximum sampling depth in excess of 1 thermal diffusion length may be understood by further examination of the thermal processes occurring in the solid. The thermal diffusion length, $\mu$, is a measure of the *average*, and not the maximum, distance that heat produced in the sample will move in one source modulation period. In discussing the temperature profile in the photoacoustic cell's fill gas as a result of the periodic heating of the sample surface, Rosencwaig (*3*) has shown that the time-dependent component of the temperature attentuates rapidly to zero with increasing distance from the sample surface. By a distance of $2\pi$ times the thermal diffusion length ($\mu$) in the gas, the ac component is fully damped out. This analysis for the gas also can be applied to the temperature variation within the sample itself. Thus, heat generated at a distance of more than $2\pi\mu$ in the solid should not reach the surface of the sample and thus will not contribute to the observed photoacoustic signal, as pointed out by McClelland and Kniseley (*10*). Examination of Rosencwaig's Figure 9.2 (*3*) for the temperature profile shows that substantial heating may occur at distances only up to about $\pi\mu$ from the heat source. This is very consistent with our observations for the PS films that indicate an estimated maximum sampling depth on the order of 2–3 thermal diffusion lengths. With the 16.5-μm PS film data (Table I), the estimated maximum sampling depth for the 3028-cm$^{-1}$ band is 16.5 μm/6.7 μm = 2.5 thermal diffusion lengths and for the 1601-cm$^{-1}$ band is 16.5 μm/9.3 μm = 1.8 thermal diffusion lengths.

**Sampling Depth—ATR.** The ATR spectra obtained from the 0.5-, 1.2-, 2.2-, and 3.9-μm PS-on-PMMA samples are shown in Figure 3. The figure demonstrates that the maximum analysis depth of ATR for this system is between 1.2 and 2.2 μm. The 1.2-μm sample has a weak but discernible C=O stretch band, which is completely absent in the 2.2-μm sample. Consistent with this much shallower sampling depth, the ATR spectrum of the 0.5-μm PS film exhibits all the major spectral bands of PS, in contrast to the PA spectrum, where the PS features are only barely visible (Figure 4).

Harrick (*5*) gives the following equation for the depth of penetration in ATR:

$$\text{penetration depth} = \frac{\lambda_1}{2\pi(\sin^2\theta - n_{21}{}^2)^{1/2}} \tag{2}$$

where $\lambda_1$ is the wavelength of light in the internal reflection element (IRE), $\theta$ is the angle of incidence, and $n_{21}$ is the refractive index ratio of sample and IRE. This equation neglects changes in the index of refraction of the sample as a function of absorbance and thus the true penetration depth

Table II. Expected Range of PA Sampling Depths for Organic Polymers and Compounds[a]

| sample | thermal diffusivity, cm$^2$/s | band, cm$^{-1}$ | mirror velocity, cm/s | max sampling depth, $\mu$m |
|---|---|---|---|---|
| polystyrene | $1.3 \times 10^{-3}$ | 1601 | 0.15 | 18.6 |
| range of polymers[b] | $(1.2–1.5) \times 10^{-3}$ | 1601 | 0.15 | 17.9–20.0 |
| range of compounds[c] | $(0.33–2.8) \times 10^{-3}$ | 1601 | 0.15 | 9.4–27 |
| polystyrene | $1.3 \times 10^{-3}$ | 4000–400 | 0.15 | 11.7–37 |
| range of polymers | $1.3 \times 10^{-3}$ (av) | 4000–400 | 0.15 | 11.7–37 |
| range of compounds | $1.4 \times 10^{-3}$ (av) | 4000–400 | 0.15 | 12.1–38.3 |
| polystyrene | $1.3 \times 10^{-3}$ | 1601 | 0.6–0.05 | 10.1–32 |
| range of polymers | $1.3 \times 10^{-3}$ (av) | 1601 | 0.6–0.05 | 10.1–32 |
| range of compounds | $1.4 \times 10^{-3}$ (av) | 1601 | 0.6–0.05 | 10.5–33 |

[a] Assume optically transparent, thermally thick case: film thickness $< 1/\beta$, film thickness $> \mu$, and maximum sampling depth $= 2\mu$. [b] Polymers included are nylon ($\alpha = 1.3 \times 10^{-3}$ cm$^2$/s), polyethylene ($\alpha = 1.3 \times 10^{-3}$), PMMA ($\alpha = 1.2 \times 10^{-3}$), polypropylene ($\alpha = 1.5 \times 10^{-3}$), and polystyrene ($\alpha = 1.3 \times 10^{-3}$). [c] Compounds included are glycerol, 1-octanol, anthracene, biphenyl, naphthalene, benzene, carbon tetrachloride, ethanol, and ethyl ether.

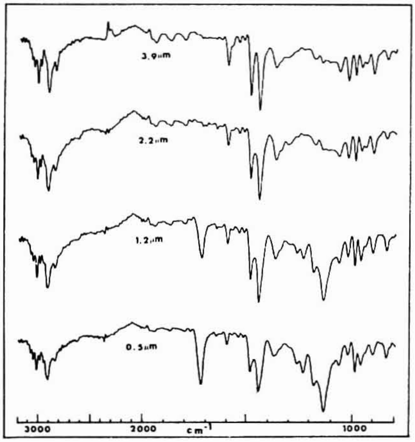

**Figure 3.** ATR spectra of four thicknesses of PS on PMMA. Spectra were obtained with a 45° KRS-5 crystal at normal incidence and were normalized to a blank crystal spectrum.

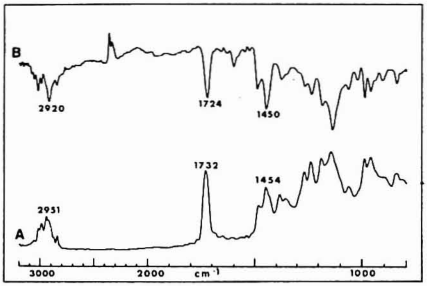

**Figure 4.** Comparison of (A) PA and (B) ATR spectra for a 0.5-$\mu$m PS-on-PMMA film.

may be slightly different from that calculated. For KRS-5 ($n = 2.37$) at $\theta = 45°$, eq 2 yields a penetration depth for the evanescent wave in PMMA ($n = 1.49$) at 1732 cm$^{-1}$ of 1.2 $\mu$m. This is the estimated depth at which the electric field has been attentuated to $1/e$ of its original value. Thus, the maximum ATR sampling depth should be greater than 1.2 $\mu$m. This conclusion is borne out by the results of Figure 3, where the 1.2-$\mu$m PS sample still exhibits a readily visible C═O stretch band due to PMMA. Beyond a depth of approximately 2.4 $\mu$m in polystyrene, the evanescent wave is expected to be reduced in intensity to less than 20% ($1/e^2$) of its initial value. No contribution from PMMA beyond this depth can be detected.

A comparison of Figures 2 and 3 suggests that PAS samples approximately an order of magnitude deeper than does ATR for the PS films using typical FT/IR operating conditions. However, some additional experimental control of relative sampling depths is possible in ATR by changing the angle of incidence, $\theta$, or changing the index of refraction of the IRE. The PAS sampling depth also can be varied by changing the mirror velocity and hence the thermal diffusion length, as has been mentioned by Vidrine (*11*). This procedure could not be tried since the mirror velocity of the FTS-14 spectrometer is fixed. A general overview of the influence of ATR and PA experimental variables on sampling depths is presented in the conclusions section.

**Sensitivity.** Figure 4 illustrates the relative surface specificity of ATR vs. PAS. ATR yields an identifiable PS spectrum from the smallest film thicknesses (0.5 $\mu$m) experimentally available. The photoacoustic experiment requires at least a 1.2-$\mu$m sample to show detectable PS features. Thin film samples on flat substrates are the ideal ATR samples but are far from the ideal PAS samples due to their low surface areas. A sensitivity advantage for PAS is realized when rough or even powdered samples are examined. For such cases, ATR often yields little or no spectral information.

## CONCLUSIONS

This study has shown that the maximum sampling depth of photoacoustic spectroscopy for PS-on-PMMA is approximately 20 $\mu$m. For polystyrene, whose thermal diffusivity is $1.3 \times 10^{-3}$ cm$^2$ s$^{-1}$, this depth corresponds to two to three thermal diffusion lengths. ATR, on the other hand, samples to an approximate depth of <2 $\mu$m (for KRS-5 and $n = 1.59$). Thus, in such circumstances the ATR sampling depth is considerably less than that for PAS and can be understood in terms of the thermal and optical properties of the sample. However, Gardella et al. (*6*) obtained ATR and PA spectra of Avcothane, a segmented poly(dimethylsiloxane)–polyether–polyurethane block copolymer, and concluded that PA samples less deeply than does ATR. As they point out, segregation of the siloxane component to the air–polymer interface is known to occur for Avcothane. However, studies by Thomas and O'Malley (*12*) have demonstrated that the surface structure which results from a copolymer of incompatible materials is composed of "isolated vertical domain

**Table III. Expected Range of ATR Sampling Depths for Organic Polymers and Compounds**

| sample | band, $\mathrm{cm}^{-1}$ | $\theta$, deg | $n_{\mathrm{IRE}}$ | $n_{\mathrm{sample}}$ | max sampling depth,[a] μm |
|---|---|---|---|---|---|
| polystyrene | 1601 | 45 | 2.37 | 1.59 | 2.8 |
| range of polymers[b] | 1601 | 45 | 2.37 | 1.49–1.59 | 1.9–2.8 |
| range of compounds[c] | 1601 | 45 | 2.37 | 1.35–1.65 | 1.5–5.1 |
| polystyrene | 4000–400 | 45 | 2.37 | 1.59 | 1.1–11 |
| range of polymers | 4000–400 | 45 | 2.37 | 1.52 (av) | 0.85–8.5 |
| range of compounds | 4000–400 | 45 | 2.37 | 1.43 (av) | 0.68–6.8 |
| polystyrene | 1601 | 75–45 | 2.37 | 1.59 | 0.90–2.8 |
| range of polymers | 1601 | 75–45 | 2.37 | 1.52 (av) | 0.87–2.1 |
| range of compounds | 1601 | 75–45 | 2.37 | 1.43 (av) | 0.83–1.7 |
| polystyrene | 1601 | 45 | 2.37–4.0 | 1.59 | 0.64–2.8 |
| range of polymers | 1601 | 45 | 2.37–4.0 | 1.52 (av) | 0.63–2.1 |
| range of compounds | 1601 | 45 | 2.37–4.0 | 1.43 (av) | 0.61–1.7 |

[a] Sampling depth = 1.5 × penetration depth. [b] Polymers included are nylon ($n$ = 1.5), polyethylene ($n$ = 1.51), PMMA ($n$ = 1.49), polypropylene (1.50), and polystyrene (1.59). [c] Compounds included are glycerol ($n$ = 1.475), 1-octanol (1.430), biphenyl (1.475), naphthalene (1.400), benzene (1.501), carbon tetrachloride (1.46), ethanol (1.361), and ethyl ether (1.353).

structures", leading to a laterally inhomogeneous surface where one component is raised somewhat above the other. The estimation of sampling depths from the copolymer surface is more prone to sampling artifacts than an estimation from a layered, smooth surfaced structure such as was used in the present study.

The results for PS-on-PMMA are expected to be applicable to a range of organic films. Table II shows the estimated maximum PAS sampling depths as a function of various experimental parameters for PS as well as a selected group of organic polymers and compounds. All the values in the table assume that the sample falls into the optically transparent, thermally thick class, i.e., sample thickness $<1/\beta$ and sample thickness $>\mu$. The first part of the table demonstrates the effect of thermal diffusivity on sampling depth. The latter portions examine the effect of band position and mirror velocity, respectively, over a typical range of values. The table shows that, indeed, PS is a representative compound in terms of its thermal properties. The range of predicted maximum sampling depths for frequently encountered experimental conditions is approximately 10–30 μm. Values at the lowest wavenumbers (approaching 400 $\mathrm{cm}^{-1}$) are somewhat higher.

Table III is a similar compilation of sampling depths for ATR. Again, the effects of various experimental parameters are examined. Polystyrene has a slightly higher than average index of refraction and thus the ATR sampling depths calculated for it are slightly larger than those for the averages in the polymer or organic compound categories. The sampling depth range estimated for the typical parameter values in an ATR experiment is approximately 0.6–3 μm. Values at the lowest wavenumbers (approaching 400 $\mathrm{cm}^{-1}$) are somewhat higher.

Comparing the ATR and PAS sampling depth ranges suggests that ATR consistently samples less deeply than does PAS, a conclusion supported by our experimental results. In addition, the variation in sampling depth over a given wavenumber range is greater for ATR than for PAS because of different proportionalities to the band wavenumber. Thus, PA and ATR spectra can exhibit differences in relative peak intensities even in a thick film sample.

The assumption of optical transparency made for the PAS calculations deserves some further discussion. The optical absorption coefficient, $\beta$, for the aromatic C–H stretch band in PS (1601 $\mathrm{cm}^{-1}$) is approximately 450 $\mathrm{cm}^{-1}$. For a very strongly absorbing band, such as the C=O stretch in PMMA, $\beta$ can be on the order of 2000 $\mathrm{cm}^{-1}$ (*4*), giving an optical absorption length of 5 μm. Thus, it is possible to have samples where a weakly absorbing band is classified as being optically transparent while a strong band is opaque. The effect that this situation will have on the spectrum depends on the relation between $1/\beta$ and $\mu$. As long as $\mu < 1/\beta$, regardless of the sample thickness, the PA signal will be proportional to $\beta$ and the band will be observed. If, on the other hand, $1/\beta < \mu <$ sample thickness, one has photoacoustic saturation and the PA signal becomes independent of $\beta$. As Krishnan (*4*) has noted, saturation can indeed occur in mid-IR/PA spectra and affects relative peak heights. Thus, the value of $\beta$ must be considered in analyzing PA spectra and sampling depths.

## ACKNOWLEDGMENT

The help of Ann Richard in understanding photoacoustic theory is gratefully acknowledged. Bruce Gay of U.S. EPA is thanked for the use of a globar IR source, and Royce Murray is thanked for access to the spin coater and profilometer.

## LITERATURE CITED

(1) Rosencwaig, A.; Gersho, A. *Science* **1975**, *190*, 556.
(2) Rosencwaig, A.; Gersho, A. *J. Appl. Phys.* **1976**, *47*, 64.
(3) Rosencwaig, A. "Photoacoustics and Photoacoustic Spectroscopy"; Wiley-Interscience: New York, 1980.
(4) Krishnan, K. *Appl. Spectrosc.* **1981**, *35*, 549.
(5) Harrick, N. J. "Internal Reflection Spectroscopy"; Wiley-Interscience: New York, 1967.
(6) Gardella, J. A., Jr.; Grobe, G. L., III; Hopson, W. L.; Eyring, E. M. *Anal. Chem.* **1984**, *56*, 1169.
(7) Woodard, F. E.; Woodward, W. S.; Reilley, C. N. *Anal. Chem.* **1981**, *53*, 1251A–1266A.
(8) Teng, Y. R.; Royce, B. S. H. *Appl. Opt.* **1982**, *21*, 77–80.
(9) "Thermophysical Properties of Matter"; Touloukian, Y. S., Ed.; IFI/Plenum: New York, 1973; Vol. 10.
(10) McClelland, J. F.; Kniseley, R. N. *Appl. Opt.* **1976**, *15*, 2658–2663.
(11) Vidrine, D. W. In "Fourier Transform Infrared Spectroscopy: Techniques in Fourier Transform Interferometry"; Ferraro, J. R., Basile, L., Eds.; Academic Press: New York, 1982; Vol. 3, Chapter 4.
(12) Thomas, H. R.; O'Malley, J. J. In "Photon, Electron and Ion Probes of Polymer Structure and Properties"; Dwight, Fabish, Thomas, Eds.; American Chemical Society: Washington, DC; 1981; pp 319–338.

RECEIVED for review August 24, 1984. Accepted December 26, 1984.

*Anal. Chem.* **1985**, *57*, 876–879

# Surface Reactivities of Polynuclear Aromatic Adsorbates on Alumina and Silica Particles Using Infrared Photoacoustic Spectroscopy

**Daniel A. Saucy, George E. Cabaniss,[1] and Richard W. Linton***

*Department of Chemistry, University of North Carolina, Chapel Hill, North Carolina 27514*

**Infrared photoacoustic spectra were obtained from organic films on inorganic particulate adsorbents. Under favorable conditions, including strong absorption bands and high surface area silica and alumina substrates, the detection sensitivity of photoacoustic spectroscopy is estimated to be 0.2 monolayers of an adsorbed organic compound. Because of the molecular information provided by IR spectroscopy, reactions of adsorbed organic compounds may be examined in situ. Examples shown involve photochemical reactions of sorbed polynuclear aromatic compounds that are potentially important in the atmospheric chemistry of combustion generated aerosols.**

The photoacoustic effect (*1*) recently has been adapted to photoacoustic spectroscopy (PAS) in the infrared (IR) region. Irradiation with an IR source produces temperature and pressure fluctuations in a closed sample cell resulting from the nonradiative decay of vibrationally excited molecules. A plot of pressure variation (photoacoustic emission) vs. IR frequency often yields a result directly analogous to an absorption spectrum. McClelland (*2*) has recently reviewed photoacoustic spectroscopy (PA) in detail.

The specific advantages that IR/PAS has over other IR techniques for the study of fine particulate specimens are as follows. Little or no sample preparation is necessary, in contrast to attentuated total reflectance (ATR) and diffuse reflectance. Thus, infrared spectra of the sample in its native state may be obtained nondestructively. In addition, PAS is not highly sensitive to light scattering effects. The range of accessible samples extends from pure powders to submonolayer films on particulate substrates. The amount of bulk sample required can be as little as 2–3 mg. Thus, the IR/PAS technique has potential utility in a wide range of particle science applications including adsorption, catalysis, and thin film chemistry.

This paper will examine the usefulness of the technique for infrared surface studies by focusing on the characterization of the reactivity of polynuclear aromatic hydrocarbons (PAH) adsorbed on fine particulate substrates. Many of the PAH compounds and their derivatives are potent mutagens and ubiquitous air pollutants (*3*). Pitts (*4*) and others (*5–8*) have shown that PAH can react photochemically and with $O_3$ and $NO_2$ to form oxygenated and nitrated derivatives with mutagenic properties significantly different from those of the original compound.

Since the PAH are usually found associated with airborne particulate matter and are presumably adsorbed on the particle surface, PAH reactions with $O_3$ and $NO_2$ as well as photochemical reactions will occur at the particle/atmosphere interface. Thus, the physicochemical characteristics of the particle's surface and the interaction of the PAH with it need to be examined in more detail. Photoacoustic spectroscopy is well suited to this application owing to its surface specificity and ability to accommodate particulate samples.

## EXPERIMENTAL METHODS

**Photoacoustic Spectroscopy.** All IR/PAS data were obtained with a Digilab FTS-14 Fourier transform IR spectrometer. Spectra were transferred to a custom designed, Z-80 microprocessor based microcomputer (*9*) for manipulation and data processing. All spectra were collected at 8 $cm^{-1}$ resolution, with a mirror velocity of 0.15 cm/s. A Princeton Applied Research Model 6003 photoacoustic cell was placed in the spectrometer's sample compartment to obtain spectra. The output from the PAR Model 6005 photoacoustic amplifier was substituted for the normal deuterated triglycine sulfate (DTGS) detector. Photoacoustic spectra normally were the result of 500–1000 scans. The spectrometer's acquisition software and hardware were modified to allow PA and DTGS spectra to be alternately collected (*10*). The DTGS spectrum was used as a reference to compensate the PAS spectrum for the effects of source intensity as well as residual $CO_2$ and $H_2O$ as suggested by Riseman (*11*) and Low (*12*). Unless stated otherwise, all PAS data have been so compensated.

**Sample Preparation.** The particulate adsorbents used in this study included a nonporous Cabosil M-5 fumed silica (Cabot Corp, Billerica, MA) with a B.E.T. determined surface area of 220 $m^2/g$ and particle size of a few tenths of a micrometer resulting from the aggregation of the nanometer diameter primary particles. Lichrosorb Si-60 silica (EM Laboratories, Elmsford, NY) with a surface area of 550 $m^2/g$ and mean particle diameter of 5 $\mu m$ and Spherisorb A5Y 5 $\mu m$ alumina (Phase-Sep, Happauge, NY) with a suface area of 93 $m^2/g$ also were used. Pore size distributions in the Lichrosorb and Spherisorb particles are not available.

The PAH compounds (Aldrich) were adsorbed by wetting ~200 mg of particles with 15 mL of an approximately $10^{-2}$ M $CH_2Cl_2$ solution of the PAH, followed by evaporation of the solvent at approximately 40 °C (*13*). Monolayer coverages of PAH were estimated assuming that one PAH molecule covers 50 Å$^2$ (*13*), that all PAH were deposited on the particle surface, and that all of the particle surface area was available for PAH adsorption.

The UV irradiation of particles was accomplished by dispersing a sample from a cyclohexane slurry onto a glass microscope slide. Only a small amount of nitroanthracene was extracted from the particles by the cyclohexane. The dispersed sample was exposed in ambient air to the light from a GE G8T5 germicidal lamp held 10 cm from the slide. Particles were scraped from the slide and used to obtain a photoacoustic spectrum. Subsequently, the sample was extracted with $CH_2Cl_2$ and the extract analyzed with a Hewlett-Packard 5880A gas chromatograph equipped with a 12-m methylsilicone fused silica capillary column and a flame ionization detector.

## RESULTS AND DISCUSSION

The ability of IR/PAS to examine submicrometer diameter particles is demonstrated in Figure 1. Spectrum A is the uncorrected PA emission spectrum from Cabosil fumed silica. The weak, sharp band at 3746 $cm^{-1}$ is due to the OH stretch of non-hydrogen-bonded (lone) silanol groups. The very strong, broad emission at approximately 1100 $cm^{-1}$ is due to siloxane (SiOSi) stretching, while the band at 1632 $cm^{-1}$ is the HOH bend of adsorbed water. Spectrum B is the same silica

---

[1] Present address: Department of Chemistry, Marshall University, Huntington, WV 25701.

0003-2700/85/0357-0876$01.50/0 © 1985 American Chemical Society

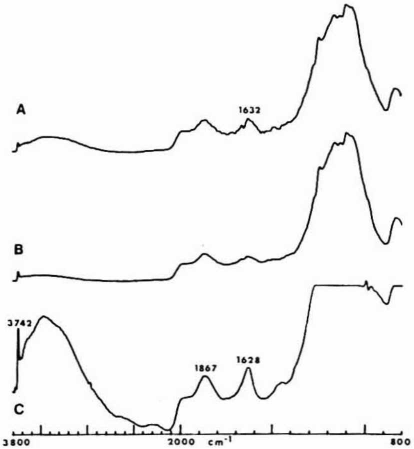

**Figure 1.** Spectra of Cabosil fumed silica: (A) photoacoustic spectrum of untreated silica; (B) photoacoustic spectrum after drying at 205 °C for 1 week; (C) transmission spectrum of untreated silica pressed pellet (plotted as absorbance).

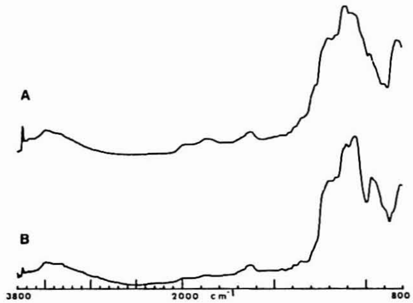

**Figure 2.** Comparative photoacoustic spectra of (A) Cabosil fumed silica and (B) Lichrosorb Si-60 silica.

after being dried at 205 °C for 1 week. The very broad band between 3700 and 3000 cm$^{-1}$, due to the OH stretch of adsorbed water, is expected to decrease after extensive drying. This decrease, viewed relative to the silanol band at 3746 cm$^{-1}$, is evident. For comparison, spectrum C shows the transmission spectrum obtained from a pressed pellet of pure Cabosil, plotted in absorbance units. The bands at 3742, 3464, 1867, and 1628 cm$^{-1}$ clearly correlate with those observed in the PA spectrum. Because of the very strong siloxane absorption below 1260 cm$^{-1}$, the transmission mode spectrum offers little structural information below this wavenumber. Cabosil silica also is a special case in that it readily forms clear pellets suitable for transmission analysis. Many particulate materials cannot easily be pressed into transmitting pellets and, thus, transmission mode spectra are difficult, if not impossible, to acquire. Furthermore, in the process of making a pellet, significant alteration of the sample may occur (*14*).

Subtle differences between two particulate adsorbents can be seen in Figure 2, showing comparative photoacoustic spectra of two different silicas. According to the manufacturer, the fumed silica (Cabosil) has a larger number of hydroxyl groups than does the Lichrosorb, and this is borne out by the

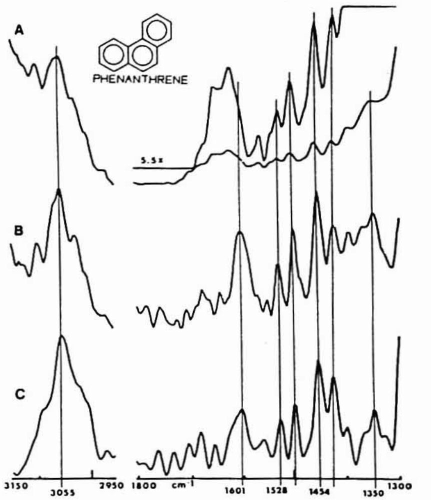

**Figure 3.** Photoacoustic spectra of phenanthrene adsorbed on Cabosil silica: (A) source compensated spectrum with inset at 5.5× vertical scale; (B) spectrum A after blank silica background substraction; (C) pure phenanthrene.

absence of a pronounced silanol band at 3742 cm$^{-1}$ in the latter's spectrum. Additional differences in the silica structures are suggested by the shape and position of the siloxane absorption at approximately 1100 cm$^{-1}$. Both silicas are seen to have a significant amount of adsorbed water.

The utility of PAS for the characterization of submonolayer organic films on particulate samples is demonstrated in Figure 3. Phenanthrene (0.95 monolayer, 124 mg/g) was adsorbed onto Cabosil silica. Spectrum A of Figure 3 is the source-compensated PA spectrum of this sample, with the inset showing a portion of the spectrum with the vertical axis expanded 5.5×. Comparison of this spectrum with that of pure phenanthrene (spectrum C) indicates that the phenanthrene bands at 3055, 1528, 1497, 1454, and 1423 cm$^{-1}$ are identifiable in the phenanthrene-on-silica spectrum. However, additional phenanthrene bands at 1601 and 1350 cm$^{-1}$ are not exhibited due to spectral overlap with silica features involving adsorbed water and siloxane band emissions. To more clearly show the phenanthrene features, it is possible to subtract a blank silica spectrum from the phenanthrene-on-silica spectrum. The result of performing such a background subtraction on spectrum A of Figure 3 is shown by spectrum B. As is evident, the removal of the silica features has enhanced the phenanthrene features. Even though they are present in the initial spectrum, the four phenanthrene bands between 1528 and 1423 cm$^{-1}$ more closely resemble the pure phenanthrene spectrum after silica background subtraction. The bands at 1601 and 1350 cm$^{-1}$ due to phenanthrene, which were not evident before background subtraction, also can be identified. Because of the adsorbed phenanthrene, it was not possible to fabricate a pellet of this sample suitable for obtaining a conventional transmission spectrum. An ATR spectrum revealed no features attributable to the PAH (*15*).

The quality of a PA spectrum also is very dependent on the surface area exposed to the incident radiation. The PA signal-to-noise ratio of surface sorbed molecules of a given monolayer coverage on a given particle size substrate usually will increase with the specific surface area available for ad-

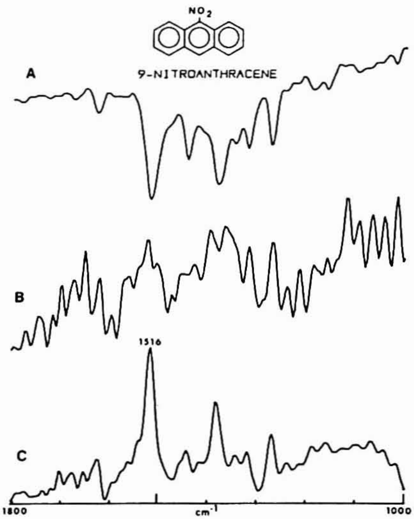

**Figure 4.** Transmission and photoacoustic spectra of 9-nitroanthracene in KBr: (A) transmission spectrum of pressed pellet; (B) photoacoustic spectrum of pressed pellet; (C) photoacoustic spectrum of ground pellet.

sorption. In other words, of two samples with the same monolayer level of coverage, the one with the higher surface area will have more adsorbate in the analytical volume and yield the stronger PA signal. Similarly, smaller particle sizes actually are advantageous in PAS due to their higher specific surface area to volume ratios. This surface area effect is demonstrated in Figure 4. An approximately 5% by weight nitroanthracene-in-KBr pellet was prepared and its transmission spectrum obtained (spectrum A). The pellet was then placed in the PA cell and its photoacoustic spectrum measured (spectrum B). Finally, the pellet was ground with a mortar and pestle to increase its effective surface area. The PAS data of the intact pellet show only very weak nitroanthracene features. After the pellet was ground, however, the spectrum (spectrum C) exhibits all of the nitroanthracene features evident in the transmission spectrum, clearly illustrating the increase in spectral quality gained when the sample surface area is increased.

Differences in the interactions of particle surfaces with an adsorbed organic molecule are exemplified in Figure 5, which compares 9-nitroanthracene adsorbed on Cabosil silica (A) and Spherisorb alumina (B). Changes are observed in the position of the antisymmetric NO stretch band. This band is at 1516 cm$^{-1}$ when the PAH is physically dispersed in KBr (shown previously in Figure 4), at 1520 cm$^{-1}$ when adsorbed on the silica and at 1528 cm$^{-1}$ when adsorbed on the alumina. These band positions were confirmed to ±4 cm$^{-1}$ by obtaining spectra from several samples. The observed lower $S/N$ of the alumina spectrum can be at least partly attributed to its lower surface area (93 vs. 220 m$^2$/g), since the difference in milligram-per-gram coverage (62 vs. 98) is smaller than the difference in observed $S/N$. The trend in band position is consistent with an increasing degree of hydrogen bonding interaction of the $NO_2$ group with either surface hydroxyl groups or adsorbed water as the substrate is changed from silica to alumina. In photodecomposition studies (*16*), nitroanthracene supported on alumina has been found to be slightly more stable to decomposition than when silica supported. One of the reasons for this difference in photochemical stability may be the strength of the nitroanthracene–sorbent surface interaction as manifested by the position of the antisymmetric NO stretch band in the PA spectrum. Hydrogen bonding alone would not be expected to affect the position of the antisymmetric stretch mode (*17*).

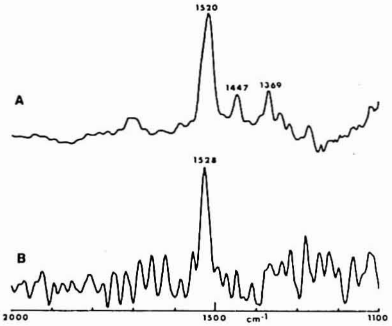

**Figure 5.** Photoacoustic spectra of 9-nitroanthracene adsorbed on (A) Cabosil silica (0.6 monolayer, 98 mg/g) and (B) Spherisorb alumina (0.9 monolayer, 62 mg/g).

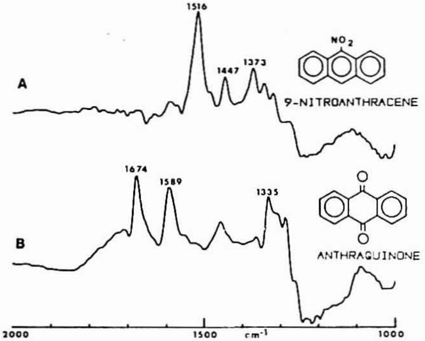

**Figure 6.** Photoacoustic spectra of ~1 monolayer 9-nitroanthracene-on-silica (A) before irradiation and (B) after 11 h of UV irradiation.

PAS, because of its nondestructive nature, also can be used for the in situ study of the reactions of adsorbed organic monolayers on particle substrates. Cabosil silica with about 1 monolayer (160 mg/g) of nitroanthracene was dispersed on a glass slide and exposed to UV radiation for 11 h. Approximately 2 mg of the irradiated sample was used to obtain a photoacoustic spectrum. Figure 6 shows the photoacoustic spectra of the sample, with a blank silica spectrum subtracted, before and after irradiation. Before exposure, the antisymmetric and symmetric NO stretches at 1516 and 1373 cm$^{-1}$, along with other nitroanthracene bands, are clearly evident (Figure 6A). The NO band can be detected at organic coverages as low as 0.2 monolayer (33 mg/g). Since the amount of sample necessary to obtain a spectrum from such a sample is approximately 2 mg, the minimum detectable total amount of nitroanthracene in the sample cell is approximately 65 μg. After UV irradiation, neither NO stretch band is detectable and new bands at 1674, 1589, and 1335 cm$^{-1}$ are evident after silica background subtraction (Figure 6B). These bands match

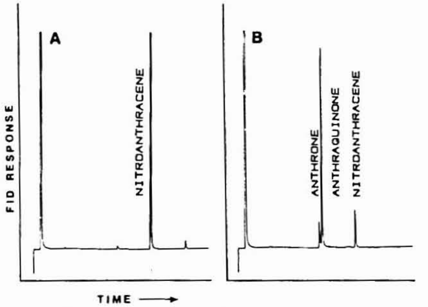

**Figure 7.** Gas chromatograms of $CH_2Cl_2$ extracts of UV irradiated sample: (A) before irradiation; (B) after 11 h of irradiation.

those of anthraquinone, which is the expected major photodecomposition product of nitroanthracene in the presence of oxygen (*18*). The presence of anthraquinone and disappearence of nitroanthracene are confirmed by GC analysis of a $CH_2Cl_2$ extract solution shown in Figure 7. Identification of the extract components is based on a comparison of retention times with those of authentic compounds. The major component (~70%) of the extract is, indeed, anthraquinone, with lesser (~15%) amounts of anthrone and unreacted nitroanthracene also present.

Unlike the GC experiment, IR/PAS allows for the in situ, nondestructive monitoring of surface reactions, including surface binding interactions that may alter the chemical state or photochemical stability of the sorbed PAH. Although several investigators have reported the use of PAS in the UV-visible range for the study of surface monolayers (*19–21*), this investigation establishes the utility of IR/PAS to characterize the reactions of submonolayers of organic molecules on high surface area particulate substrates.

## ACKNOWLEDGMENT

Helpful discussions with Mark Miller are gratefully acknowledged.

## LITERATURE CITED

(1) Bell, A. G. *Am. J. Sci.* **1880**, *20*, 305.
(2) McClelland, J. F. *Anal. Chem.* **1983**, *55*, 89A–105A.
(3) Pitts, J. N., Jr. *Philos. Trans. R. Soc. London, Ser. A* **1979**, *290*, 551–576.
(4) Pitts, J. N., Jr.; Van Cauwenberghe, K. A.; Grosjean, D.; Schmidt, J. P.; Fitch, D. R.; Belser, W. L.; Knudson, G. B.; Hynds, P. M. *Science* **1978**, *202*, 515–519.
(5) Korfmacher, W. A.; Natusch, D. F. S.; Taylor, D. R.; Mamantov, G.; Wehry, E. L. *Science* **1980**, *207*, 763–765.
(6) Tebbens, B. D.; Mukai, M.; Thomas, J. F. *Am. Ind. Hyg. Assoc. J.* **1971**, *32*, 365–372.
(7) Peters, J.; Seifert, B. *Atm. Environ.* **1980**, *14*, 117–119.
(8) Jaeger, T.; Hanus, V. *J. Hyg., Epidemiol., Microbiol., Immunol.* **1980**, *24*, 1–12.
(9) Woodard, F. E.; Woodward, W. S.; Reilley, C. N. *Anal. Chem.* **1981**, *53*, 1251A–1266A.
(10) Saucy, D. A.; Simko, S. J.; Linton, R. W. *Anal. Chem.* **1985**, *57*, 871–875.
(11) Riseman, S. M.; Eyring, E. M. *Spectrosc. Lett.* **1981**, *14*, 163–185.
(12) Low, M. J. D.; Parodi, G. A. *Spectrosc. Lett.* **1981**, *13*, 663–669.
(13) Cabaniss, G. E. Ph.D. dissertation, University of North Carolina, Chapel Hill, NC, 1984.
(14) Hair, M. L. "Infrared Spectroscopy in Surface Chemistry"; Marcel Dekker: New York, 1967; p 69.
(15) Saucy, D. A., unpublished results, University of North Carolina, 1984.
(16) Cabaniss, G. E.; Saucy, D. A.; Linton, R. W. In "Polynuclear Aromatic Hydrocarbons: Formation, Metabolism and Measurement"; Cooke, M., Dennis, A. J., Eds.; Battelle Press: Columbus, OH, 1983; pp 243–256.
(17) Bellamy, L. J. "The Infrared Spectra of Complex Molecules, Volume 2, Advances in Infrared Group Frequencies", 2nd ed., Chapman and Hall: London, 1980; pp 229–232.
(18) Chapman, O. L.; Heckert, D. C.; Reasoner, J. W.; Thackaberry, S. P. *J. Am. Chem. Soc.* **1966**, *88*, 5550–5554.
(19) Lochmüller, C. H.; Marshall, S. F.; Wilder, D. R. Anal. *Chem.* **1980**, *52*, 19–23.
(20) Castleden, S. L.; Elliot, C. M.; Kirkbright, G. F.; Spillane, D. E. M. *Anal. Chem.* **1979**, *51*, 2152–2153.
(21) Rosencwaig, A.; Hall, S. S. *Anal. Chem.* **1975**, *47*, 548–549.

RECEIVED for review November 2, 1984. Accepted December 26, 1984. This work was supported in part by Grant R-810773 from the U.S. EPA, Oak Ridge National Laboratories, and the University of North Carolina Research Council (No. 43645).

Anal. Chem. 1985, 57, 880-886

# Angular Distribution X-ray Photoelectron Spectroscopy Studies on Compacted Lead Ion Selective Membrane Powders

**Vaneica Young***[1] **and Paul C. McCaslin**[1]

*Department of Chemistry, Texas A&M University, College Station, Texas 77843*

**Changes in the distribution of species in the near surface region of compacted lead ion selective membrane powders, as revealed by angular distribution XPS, are reported. Scanning electron micrographs of pellets pressed at pressures ranging from a low of 7 lb/in.$^2$ to a high of 15 000 lb/in.$^2$ reveal surfaces of almost undistorted, compacted spheres with an average diameter of 0.25 $\mu$m. For untreated membranes, angular distribution XPS reveals the stratification of the "near surface" region of the surface layer of spheres. Scanning electron micrographs of EDTA and $HClO_4$ treated pellets show that an erosion of the surfaces occurs and angular distribution XPS analysis reveals the stratification of the "near surface" region of the new surfaces. Profilometry has been used to measure the surface topography of the pellets, and the data have been used to assess the effect of roughness on XPS intensity ratios.**

Lead ion sensors based on mixtures of lead sulfide and silver sulfide have been described in the literature (*1–11*). There are many variables present in the fabrication of lead ion selective electrodes from such membranes. The membrane powder may be formed by a variety of methods, e.g., coprecipitation of PbS and $Ag_2S$ by addition of a solution of $Na_2S$ to a solution of Pb(II) and Ag(I) (*2, 3*), coprecipitation of PbS and $Ag_2S$ by addition of a solution of Pb(II) and Ag(I) to $Na_2S$ solution (*5, 6*), coprecipitation of PbS and $Ag_2S$ using $H_2S$ (*1*), homogeneous coprecipitation of PbS and $Ag_2S$ using thiourea (*8*), and mechanical mixing of PbS and $Ag_2S$ powders (*7*). This list is by no means exhaustive. Secondly, the membrane may be cast by different methods, e.g., cold pressing (*2*) and pressure assisted sintering (*11*). Finally, the electrode can be geometrically constructed as an ionic contact membrane electrode or an all solid state electrode (*12*). There are discrepancies in the reported behavior of these electrodes which we feel can be ascribed to differences in the surface composition. We have previously reported the results of fixed angle X-ray photoelectron spectroscopy (XPS) studies on membranes cleaned by exposure to EDTA and $HClO_4$ solutions (*2*) and on membranes exposed to Cu(II) and Zn(II) solutions (*13*). Because previous studies (*14*) have shown that more than the surface monolayer is involved in interaction with external solutions, we have used angular distribution XPS (*15–17*) to investigate nondestructively the chemical speciation in the first 20 Å of compacted Pb ISE membrane powders. This has been done for untreated, EDTA treated, and $HClO_4$ treated membranes.

## EXPERIMENTAL SECTION

The powders were prepared by coprecipitation of PbS and $Ag_2S$ (1:1 mole ratio) from a solution containing $AgNO_3$ and $Pb(NO_3)_2$ by addition of a solution of $Na_2S$. The precipitate was filtered, washed, and dried at 110 °C overnight. The powders were compacted into 7 mm diameter pellets using a Quick Press. These pellets were exposed to 1 mL of 0.01 F ammoniacal EDTA or 0.1 F $HClO_4$ for 15 min, washed in a deionized water jet, and dried in nitrogen at room temperature. XPS spectra were recorded at takeoff angles of 18°, 38°, and 58° on a Hewlett-Packard 5950A ESCA spectrometer equipped with an angular distribution probe (Surface Science Model 259). In all cases, the takeoff angle is the angle of observation of photoemission relative to the sample surface. A computer system consisting of a memory upgraded HP 9825A computer, a HP 9885 disk drive, a HP 9872S graphics plotter, and a Teletype Model 43 teleprinter was used to control data collection and storage and for subsequent data reduction. All binding energies have been referenced to the ubiquitous hydrocarbon contamination peak at 285.0 eV. In addition, spectra were recorded for a number of standards. Argon ion etched galena crystals (Wards Natural Science Establishment, Inc.) were studied to assess the reliability of theoretical sulfur to lead cross section ratios. Spectra were also obtained for basic lead carbonate ($2PbCO_3 \cdot Pb(OH)_2$), lead carbonate, and lead sulfate. Pelletized reagent grade powders of these latter standards were used.

The present peak fitting subroutine allows us to choose from several different symmetrical line shapes (Gaussian, Lorentzian, secant, parametrized Lorentzian, and parametrized secant). For all data reported here, a Gaussian line shape function was used for curve resolving. Atom ratios have been calculated from time normalized intensity ratios. As shown previously, the exact equation has the form

$$\frac{N_{x,i}}{N_{y,j}} = \frac{I_{x,i}}{I_{y,j}} \frac{\sigma_{y,j}}{\sigma_{x,i}} \frac{\lambda_y(E_j)}{\lambda_x(E_i)} \frac{F(E_j,E_a)}{F(E_i,E_a)} \frac{T(E_j,E_a)}{T(E_i,E_a)} \tag{1}$$

where the subscripts x and y denote specific elements and the subscripts i and j denote specific levels in x and y, respectively. $E_i$ and $E_j$ are the respective kinetic energies of the photoelectron and $E_a$ is the analyzer pass energy, which is held constant in the HP5950A spectrometer. Each term is defined as follows: $N$ is the number of atoms, $I$ is the intensity, $\sigma$ is the asymmetry corrected photoionization cross section, $\lambda(E_i)$ is the inelastic mean escape depth, $F(E_i,E_a)$ is the electron-optical factor, and $T(E_i,E_a)$ is the analyzer transmission function. Equation 1 is derived from the exact expression for photoelectron intensity given in ref 18, where constant terms, such as the X-ray flux, cancel in the ratio. Recently, Elliott et al. (*19*) have calculated sensitivity factors for the HP5950 spectrometer. They have the form $S_{x,i} = \sigma_{x,i}F(E_i,E_a)T(E_i,E_a)$, so that eq 1 takes the form

$$\frac{N_{x,i}}{N_{y,i}} = \frac{I_{x,i}}{I_{y,i}} \frac{\lambda_y(E_j)}{\lambda_x(E_i)} \frac{S_{y,i}}{S_{x,i}} \tag{2}$$

In order to employ this equation, electron mean escape depths must be obtained from the literature or calculated by one of several published general equations. Experimental works prior to 1983 have shown that the product of $F(E_i,E_a)T(E_i,E_a)$ and $\lambda_x(E_i)$ cancel each other (*20*), so that eq 1 takes the simpler form

$$\frac{N_{x,i}}{N_{y,i}} = \frac{I_{x,i}}{I_{y,i}} \frac{\sigma_{y,i}}{\sigma_{x,i}} \tag{3}$$

Both eq 2 and 3 are applicable directly only if the spectra have been recorded with identical window widths. If not, the equations must incorporate the window width ($W$).

$$\frac{N_{x,i}}{N_{y,i}} = \frac{I_{x,i}}{I_{y,i}} \frac{\lambda_y(E_j)}{\lambda_x(E_i)} \frac{S_{y,j}}{S_{x,i}} \frac{W_x}{W_y} \tag{4}$$

$$\frac{N_{x,i}}{N_{y,i}} = \frac{I_{x,i}}{I_{y,i}} \frac{\sigma_{y,i}}{\sigma_{x,i}} \frac{W_x}{W_y} \tag{5}$$

Results obtained on the standard compounds will be used to

---

[1] Present address: Department of Chemistry, University of Florida, Gainesville, FL 32611.

0003-2700/85/0357-0880$01.50/0 © 1985 American Chemical Society

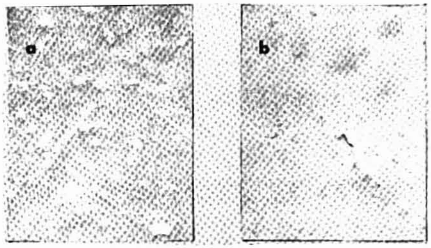

**Figure 1.** Scanning electron micrographs (450×) of Pb ISE membrane pellets pressed at (a) 7 lb/in.$^2$ and (b) 15 000 lb/in.$^2$.

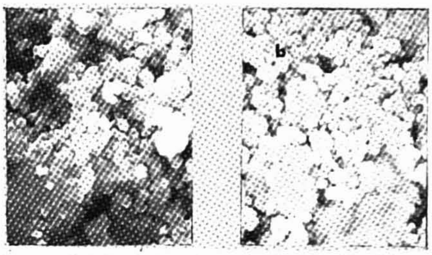

**Figure 2.** Scanning electron micrographs (20 000×) of Pb ISE membrane pellets pressed at (a) 7 lb/in.$^2$ and (b) 15 000 lb/in.$^2$.

determine whether eq 4 or eq 5 is used to analyze the data on the Pb ISE membrane pellets.

In addition, pellets compacted with a Quick Press (7 lb/in.$^2$) and pellets compacted at 1000, 2000, 5000, 10000, and 15000 lb/in.$^2$ using a 16 mm diameter KBr die (Beckman Model K-16) were examined with a JEOL JSM-25 S II scanning electron microscope. Pellets pressed at 7 lb/in.$^2$ and subsequently exposed to EDTA or $HClO_4$ for 15 min were also examined. Micrographs were recorded at magnifications of 450× and 20 000× and a particle size distribution for each untreated sample was determined by measuring the diameters of 27 particles. The topographies of these samples were also determined with an Alpha-step 100 profilometer (Tencor Instruments). The profilometer has an ultimate depth resolution of 100 Å and a lateral resolution of 50 Å.

## RESULTS AND DISCUSSION

In order to correctly interpret the XPS results, it is necessary that we know both the morphology and the topography of the surfaces of the pellets. The surface morphology has been investigated by use of scanning electron microscopy. In Figure 1, we show scanning electron micrographs of a pellet pressed at 15 000 lb/in.$^2$ and one pressed at 7 lb/in.$^2$ (450×). The pellet pressed at 7 lb/in.$^2$ shows a more pronounced local roughness than that pressed at 15 000 lb/in.$^2$ but the latter pellet contains more pores. This is even more evident at a magnification of 20 000× (Figure 2). These results can be understood as follows. In both compacting methods, the pressure is applied linearly, but this means that the packing is at least partially dependent on the eventual pellet density. Since the mass to eventual volume was greater for the 7 lb/in.$^2$ pellet than for the 15 000 lb/in.$^2$ pellet, the former is more densely packed. In both cases, 80% of the surfaces of the pellets consist of almost uniformly spherical particles. The particle size distributions are shown in Figure 3 and are quite similar for the two samples. The pellet pressed at 7 lb/in.$^2$ has an average particle diameter of 0.23 ± 0.04 μm, while that pressed at 15 000 lb/in.$^2$ has an average particle diameter of 0.25 ± 0.06 μm. These results show that even a pressure of 15 000 lb/in.$^2$ is not sufficient to cause large interparticle boundary regions at the surface. The main effect of increased pressure in the range studied is to cause some distortion of surface particles from spherical to ellipsoidal. Because the electron mean escape depth is only 20 Å (*2*), it is evident that any surface technique which does not employ ion etching will only reveal in part the composition of the surface layer of particles. Nevertheless, such studies are relevant because it is this layer of particles which is in intimate contact with the external environment.

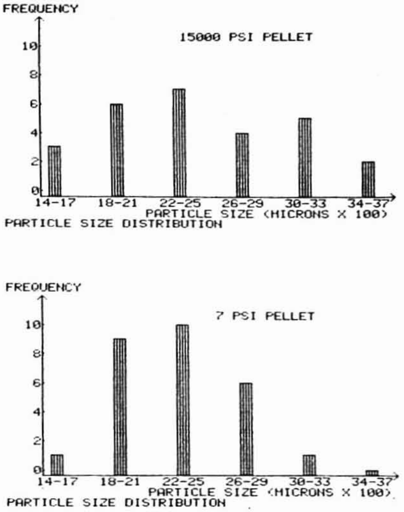

**Figure 3.** Particle size distribution for Pb ISE membrane pellets pressed at (a) 7 lb/in.$^2$ and (b) 15 000 lb/in.$^2$.

Since the SEM studies have revealed that the surfaces of the pellets are microscopically rough and since it has been shown that surface roughness influences XPS intensities (*15, 17*), it is important that we assess the effect of surface roughness on the intensity ratios to be employed in eq 4 or 5. For an atomically smooth surface with a fixed analyzer to sample geometry, an effective mean escape depth, $\lambda_e$, can be defined as

$$\lambda_e = \lambda \sin \theta \tag{6}$$

In this case, the photoelectron intensity signal is given by (*21–23*)

$$I\left(\frac{1}{\lambda_e}\right) = K'A \int_0^\infty X(z) \exp\left(\frac{-z}{\lambda_e}\right) dz \tag{7}$$

where $X(Z)$ is the depth dependent concentration, $A$ is the analyzed surface area, and $K'$ is a constant which includes all of the instrumental factors. If we take intensity ratios and perform an inverse LaPlace transform on the result, concentration ratios are obtained. The problems encountered when analyzing a rough surface are 2-fold. First of all, the area analyzed is no longer the irradiated area, due mainly to the effect of electron shading. Secondly, the angle of photoelectron escpae with respect to a surface tangent, $\theta'$, will vary across the effective area, $A_R$, which is also a function of $\theta$. In this case, the photoelectron intensity is given by

$$I_R(1/\lambda_e) = K' \int_0^\infty \int_{A_{R(\theta)}} x(z) \exp(-z/\lambda \sin \theta')\, dA_0\, dz \tag{8}$$

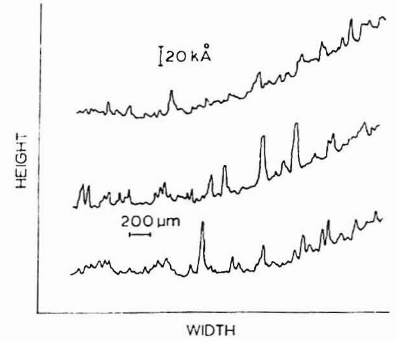

**Figure 4.** Profilometer topographs of a Pb ISE membrane pellet pressed at 7 lb/in.$^2$.

where $A_0$ is the effective aperture area of the spectrometer. From geometrical considerations, we find that

$$A_0 = A \sin\theta \qquad \text{(smooth surface)} \tag{9}$$

$$\mathrm{d}A_0 = \mathrm{d}A \sin\theta' \qquad \text{(rough surface)} \tag{10}$$

we then have

$$I_{\mathrm{R}}(1/\lambda_{\mathrm{e}}) = K'\int_0^{\infty}\int_{A_{R(\theta)}} x(z)\exp(-z/\lambda\sin\theta')\sin\theta'\,\mathrm{d}A\,\mathrm{d}z \tag{11}$$

If we assume that the depth profile is independent of the roughness (i.e., at any point on the surface, if we go perpendicular to a tangent at that point, we will obtain the same profile), we can move $x(z)$ outside of the inner integral

$$I_{\mathrm{R}}(1/\lambda_{\mathrm{e}}) = K'\int_0^{\infty} x(z)\int_{A_{R(\theta)}} \exp(-z/\lambda\sin\theta')\sin\theta'\,\mathrm{d}A\,\mathrm{d}z \tag{12}$$

In general, a polycrystalline material will exhibit different crystal facets at the surface and these facets may not interact with the environment at the same rate or even to give the same products. By analogy, one can infer that the packing arrangement of colloidal size particles can affect the depth profile at least at the very surface of the particles. The validity of the above assumption will depend on the functional form of the topography. One expects the assumption to be valid for smooth functions and to become increasing invalid as the number of step-function discontinuities increases.

How does $\sin\theta'$ vary with $A$ over $A_{\mathrm{R}}(\theta)$? To answer this question, we must actually know the functional form of the topography. In this paper, we show how profilometry can be used to generate an average functional form for the topography. In Figure 4, three 3 mm profilometer scans are shown for a pellet pressed at 7 lb/in.$^2$. As with any wave form, these data can be subjected to harmonic analysis and represented as a series of sine waves of varying amplitude and frequency. We have made the rough assumption (*15*) that this wave form can be represented as a single wave of amplitude and frequency derived from averaging the data. If we let $x$ measure distances parallel to the sinusoidal wave, then the depth, $z$, can be related to $x$ by the equation

$$z = \frac{a}{2}\sin\left[\frac{2\pi x}{\Lambda}\right] \tag{13}$$

where $a$ is the peak to peak amplitude and $\Lambda$ is the wavelength.

**Table I. Comparison of sin θ and ⟨sin θ′⟩ for Pellets Pressed at 7 lb/in.$^2$**

| $\theta$, deg | $\sin\theta$ | $\langle\sin\theta'\rangle$ |
|---|---|---|
| 18 | 0.3090 | 0.3089 |
| 38 | 0.6157 | 0.6155 |
| 58 | 0.8480 | 0.8478 |

In essence, we can think of the analyzed area as a rectangular "ruffled" potato chip with the $x$ direction going across the ridges and the $y$ direction remaining constant and independent of $\theta$. Our integral equation can then be written as

$$I_{\mathrm{R}}(1/\lambda_{\mathrm{e}}) = K'\int_0^{\infty} x(z)\langle\sin\theta'\exp(-z/\lambda\sin\theta')\rangle\,\mathrm{d}z \tag{14}$$

where

$$\langle\ \rangle = \frac{\int_{A_{R(\theta)}}\mathrm{d}A}{A_{R(\theta)}}\,\frac{\int\mathrm{d}x}{\Lambda}$$

In order to apply this equation, we must assume that we can calculate an average value for $\sin\theta'$. This can be done by numerical integration (Simpson's rule, Gaussian quadrature). For the 7 lb/in.$^2$ pellet, an average of the three 3 mm profilometer scans gives a peak-to-peak amplitude of 0.619 µm and a wavelength of 56.25 µm. In Table I, we compare $\sin\theta$ to the average value of $\sin\theta'$. It can be seen that the two values are virtually the same. The reason for this occurrence is the roughly 2 orders of magnitude difference between the amplitude and wavelength. This difference is so large that the surface appears to be smooth with respect to the angle of photoelectron escape, regardless of the complexity of the wave form. In such cases, the initial assumption is valid. Incidentally, for a sinusoidal surface, the shading parameters to be used as integration limits in the equation of the form

$$\int_{x_1}^{x_2} \ldots\,\mathrm{d}x \quad \text{(integrate over one wavelength)} \tag{15}$$

have been derived. By extensive geometrical considerations, we find that

$$x_1 = \frac{\Lambda}{2\pi}\cos^{-1}\left[\frac{\Lambda}{\pi a}\tan\theta\right] \tag{16}$$

$$\frac{a}{2}\tan\theta\sin\left(\frac{2\pi x_2}{\Lambda}\right) - x_2 = \frac{a}{2}\tan\theta\sin\left(\frac{2\pi x_1}{\Lambda}\right) - x_1 - \Lambda \tag{17}$$

Notice that photoelectron shading only occurs when

$$\frac{\Lambda}{\pi a}\tan\theta \le 1 \tag{18}$$

Thus experimental values of $\Lambda$ and $a$ can be used to find the corresponding $\theta$ cutoff values. In this particular case, no cutoff $\theta$ was found, indicating no shading. We conclude that roughness has a negligible effect on the intensity ratios for untreated membranes. In Figure 5, we show scanning electron micrographs for 7 lb/in.$^2$ pellets treated for 15 min with EDTA or $HClO_4$. At 450×, it is evident that "boulders", craters, and crevices are now present on surfaces whose local roughnesses are similar to that of the untreated pellet. Mathematically, the topography can be modeled by imposing jump discontinuities upon the sinusoidal topography of the untreated pellet. At the present time, we are not able to treat these systems by using profilometry because an entire surface topograph would have to be obtained; i.e., we need to know the

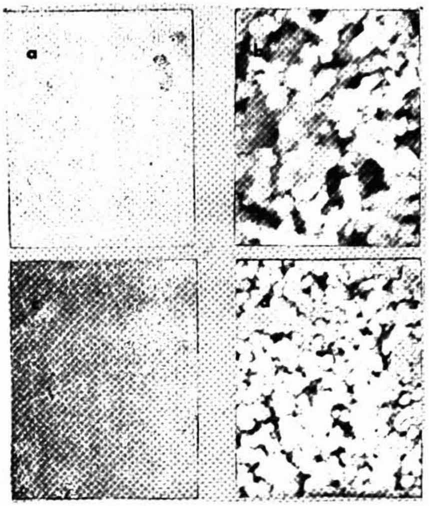

**Figure 5.** Scanning electron micrographs of EDTA treated Pb ISE membrane pellets at (a) 450× and (b) 20 000× and $HClO_4$ treated Pb ISE membrane pellets at (c) 450× and (d) 20 000×.

average "boulder" size, the average crater size, the average crevice size, and their respective densities. Qualitatively, we can say that the contents of "boulders" will occur with enhanced intensities and the contents of craters and crevices with diminished or even no intensity. Since the electron mean escape depth is so much smaller than the dimensions of these gross structures, the data at each angle will be affected to the same extent.

It is important to establish the uncertainty in the intensity ratios, because this will determine the uncertainty in the calculated atom ratios. One way to ascertain this uncertainty is to obtain standard spectra of some of the species to be encountered in the system studied. By comparing experimental cross section ratios, calculated from the intensities of the data assuming the bulk phase stoichiometry, with theoretical cross section ratios, we can assess both the reproducibility of the instrument and the uncertainty in the intensity ratios. Ratios based on eq 5 are compared in Table II. The theoretical ratios are calculated from the asymmetry corrected Scofield photoionization cross sections (*19*). The Scofield photoionization cross sections have a relative error of 0.1% (*24*), while the asymmetry parameters have a relative error of 1% (*25*). Thus the theoretical ratios are expected to have a relative error of ~1%. For the experimental values we see that the statistical uncertainty is small (three significant figures allowable). The reproducibility is a factor of 10 worse (two significant figures allowable). However, the agreement between experimental and theoretical ratios varies widely. For the most part, we can account for the large discrepancies. Because lead sulfate and the lead carbonate compounds are insulators, an electron flood must be used to neutralize their Volta potential. A much higher current (0.1 mA) must be used than when these same substances are present as a thin overlayer on a more conducting substrate. For example, galena (band gap = 0.37 ± 0.06 eV) containing a thin overlayer of lead sulfate and lead oxide does not charge. The high floodgun current can cause desorption of oxygen, carbon dioxide, and sulfur oxides.

**Table II. Experimental (Equation 5) and Theoretical Cross Section Ratios**

| ratio | experimental | theoretical |
|---|---|---|
| $\sigma_{S_{2p}}/\sigma_{Pb(4f_{7/2})}$ | 0.125 (±0.002)[a]<br>0.117 (±0.001)[b]<br>0.118 (±0.001)[c] | 0.135 |
| $\sigma_{S_{2p}}/\sigma_{S_{2s}}$ | 1.62 (±0.02)[a]<br>1.42 (±0.02)[c] | 1.04 |
| $\sigma_{Pb(4f_{7/2})}/\sigma_{Pb(4fd_{5/2})}$ | 1.15 (±0.01)[a]<br>1.19 (±0.01)[c]<br>1.32 (±0.05)[d]<br>1.32 (±0.04)[c] | 0.949 |
| $\sigma_{O_{1s}}/\sigma_{Pb(4f_{7/2})}$ | 0.196 (±0.002)[c]<br>0.190 (±0.001)[d]<br>0.194 (±0.001)[c] | 0.265 |
| $\sigma_{C_{1s}}/\sigma_{Pb(4f_{7/2})}$ | 0.077 (±0.001)[d]<br>0.0527 (±0.0005)[e] | 0.0906 |

[a] $Ar^+$ etched galena, $\theta = 38°$. [b] Galena polished and sonically washing in trichloroethylene, $\theta = 8°$ (contains carbon and oxygen contamination). [c] Lead sulfate. [d] Basic lead carbonate. [e] Lead carbonate.

**Table III. Experimental (Equation 4) and Theoretical HP 5950 Sensitivity Ratios for Lead Sulfate**

| ratio | experimental | theoretical |
|---|---|---|
| $\sigma_{S_{2p}}/\sigma_{Pb(4f_{7/2})}$ | 0.120 (±0.001)[a]<br>0.120 (±0.001)[b]<br>0.119 (±0.001)[c] | 0.136 |
| $\sigma_{S_{2p}}/\sigma_{S_{2s}}$ | 1.36 (±0.02)[a]<br>1.37 (±0.02)[b]<br>1.39 (±0.02)[c] | 1.01 |
| $\sigma_{Pb(4f_{7/2})}/\sigma_{Pb(4d_{5/2})}$ | 0.992 (±0.008)[a]<br>1.00 (±0.01)[b]<br>1.06 (±0.01)[c] | 0.829 |
| $\sigma_{O_{1s}}/\sigma_{Pb(4f_{7/2})}$ | 0.258 (±0.002)[a]<br>0.254 (±0.002)[b]<br>0.233 (±0.002)[c] | 0.329 |

[a] λ calculated by method of Penn. [b] λ calculated by method of Wagner. [c] λ calculated by method of Seah and Dench.

In Table III, we compare experimental sensitivity factor ratios calculated using eq 4 with theoretical sensitivity factors for lead sulfate. No experimental λ values can be found in the literature, so we have calculated λ ratios using three different methods; the method of Penn (*26*), the method of Wagner et al. (*27*) which gives a functional form equivalent to the approximate method of Szajman et al. (*28, 29*), and the method of Seah and Dench (*3*). The exact method of Szajman et al. is not easy to apply, because it requires a knowledge of the long wavelength dielectric response function, $\epsilon(w,0)$, and the band gap of the compound. The important conclusion which we can draw from Table III is that there is no improvement in the agreement between experimental and theoretical ratios for the compounds studied here. Therefore, we are justified in using the simpler equation to calculate atom ratios. In this paper, atom ratios involving the elements sulfur ($S_{2p}$), lead (Pb $4f_{7/2}$), and silver (Ag $3d_{5/2}$) are calculated. The results shown in Table II allow us to approximate a relative uncertainty of ~11% in the intensity ratios and hence the calculated atom ratios.

We were also interested in ascertaining the $C_{1s}$ binding energy for carbonate, since our previous assignment of the 288.1 eV $C_{1s}$ peak on Pb ISE membranes to basic lead carbonate (*2*) has been criticized as being too low. We find a $C_{1s}$ binding energy of 288.3 eV for basic lead carbonate and 288.6

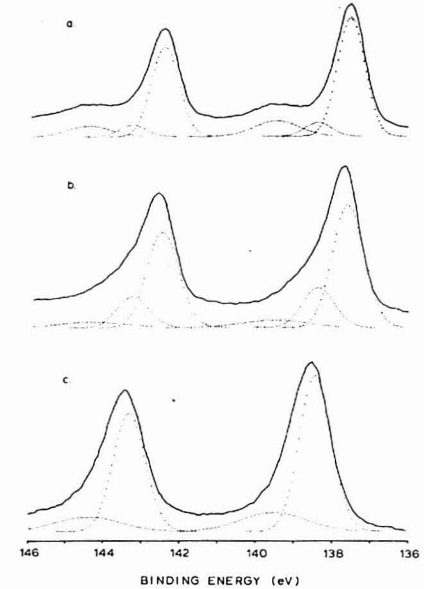

**Figure 6.** Pb 4f levels for (a) untreated Pb ISE membrane pellets, (b) EDTA treated Pb ISE membrane pellets, and (c) $HClO_4$ treated Pb ISE membrane pellets.

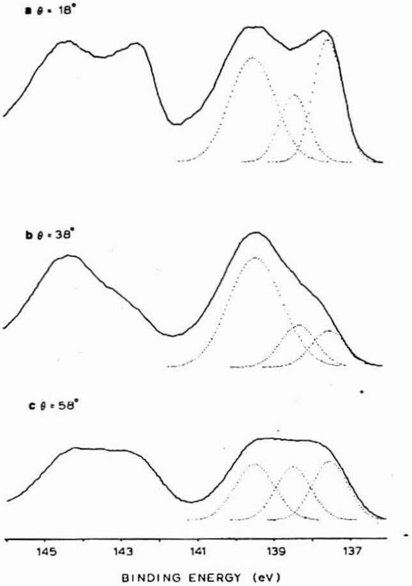

**Figure 7.** Pf 4f levels for $Cu^{2+}$ exchanged untreated Pb ISE membrane pellets.

**Table IV. Lead (137.6 eV) Plus One-Half Silver to Sulfide Atom Ratios for Pb ISE Membrane Pellets**

| treatment | 18° | 38° | 58° |
|---|---|---|---|
| none | 1.0 | 1.1 | 0.9 |
| EDTA | 0.9 | 1.0 | 1.0 |
| $HClO_4$ | 1.0 | 1.2 | 1.1 |

eV for lead carbonate. Such a high binding energy component in the $C_{1s}$ spectrum of lead sulfate is absent. Since all of the samples were prepared under identical conditions, it is unlikely that this peak can be ascribed to an oxygen-containing hydrocarbon contaminant. These values are considerably lower than the $C_{1s}$ binding energy observed for alkaline-earth carbonates (~289.6 eV) and probably reflect partial bond covalency in these compounds.

In this section, we present the angular distribution XPS results for the Pb ISE membrane pellets. The chemical speciation is the same as that reported previously (*2*). In that paper, the amount of Pb ox (this notation is used to designate PbO which has undergo $CO_2$ and $H_2O$ chemisorption) was determined indirectly by material balance calculations. In this paper, the Pb $4f_{7/2}$ level has been resolved into three peaks. Representative spectra are shown in Figure 6 where it is evident from the raw data that peaks are present at 137.6 eV and 139.5 eV. The inclusion of a third peak is justified as follows. The $C_{1s}$ level shows a high binding energy component at 288.2 ± 0.1 eV indicating the presence of carbonate. Since $Ag_2S$ has not been shown to undergo air oxidation, carbonate must be associated with lead. Our XPS results for the Pb $4f_{7/2}$ peak of lead carbonate and basic lead carbonate are 138.1 eV and 137.8 eV, respectively. Pederson (*31*) reported a Pb $4f_{7/2}$ binding energy of 138.2 eV for the latter. Thus we expect a lead peak somewhere in this binding energy region. Further evidence is based on the result obtained for copper ion exchange on these pellets as demonstrated in Figure 7. In Figure 7a, we began by obtaining the best two-peak fit to the Pb $4f_{7/2}$ level. The difference between the raw data and fit revealed a Gaussian peak with a maximum at 138.4 eV. In Figure 7c, it was not possible to generate the flat top shown using two Gaussian peaks with binding energy maxima of 137.6 eV and 139.5 eV, respectively. The three peak fits to each level gave lower $\chi^2$ values (a measure of the goodness of fit) than did any two-peak fits.

The peak at 137.6 eV corresponds to the binding energy of lead in PbS, PbO, and $Pb(OH)_2$ according to the literature (*32–41*). If this peak is due to PbS, then we would expect the ratio [Pb(137.6 eV) + Ag/2]/sulfide to be equal to unity. As shown in Table IV, this is observed to be true within experimental error for all the spectra. The fact that the observed ratio is constant within ±0.1 implies that sulfide ions are homogeneously distributed in the near surface region of the membranes. Therefore, we can investigate the distributions of the various species by ratioing them to sulfide. Each calculated ratio is divided by the corresponding value of the ratio shown in Table IV to correct for variations observed for [Pb(137.6 eV) + Ag/2]/S. The distributions are shown in Figure 8. The error bars reflect a relative uncertainty of 11%.

For the untreated pellets, the distribution plots present the average radial inhomogeneity at the "crust" of a surface layer of almost undistorted particles. Suppose we represent the diameter of the average particle by a line segment of 100 mm, then the depth probed into the surface of the particle by the present study could be represented by a line segment of length 0.9 mm. The present results show that lead segregation cannot be entirely attributed to the preferential segregation of lead sulfide oxidation products, because the intensity of the PbS component alone is greater than that expected for a 1:1 molar mixture of PbS and $Ag_2S$. This is a direct corroboration of

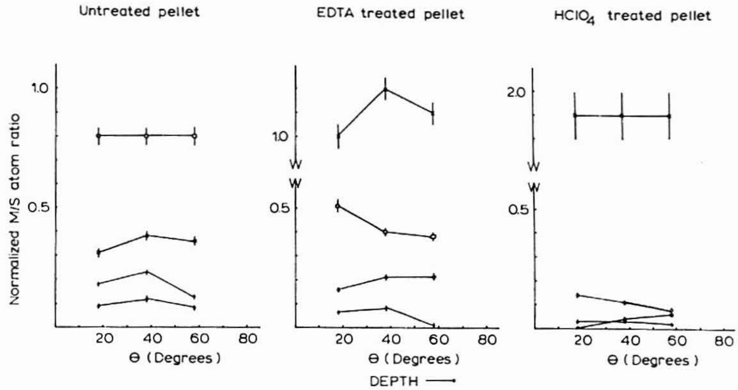

**Figure 8.** Distribution of metal species on (a) untreated, (b) EDTA treated, and (c) $HClO_4$ treated Pb ISE membrane pellets: (□) Pb 137.6 eV, (○) Pb 138.4 eV, (●) Pb 139.5 eV, (×) Ag.

the suggestion of Heijne et al. (*11*) that coprecipitation of lead and silver sulfides by the addition of $Na_2S$ to a solution of soluble lead and silver salts leads to radially inhomogeneous particles. The results also show that lead sulfate is richer in the surface than is Pb ox. An $O_{1s}$ peak appears at 533.6 eV; this may be attributed to either microporous or covalently bound water (*2, 42*). A comparison of the intensity of this peak at $\theta = 38°$ (this corresponds to the photoemission angle of the fixed geometry) to our previous results shows that the intensity has been reduced by only 5%. This indicates that the primary source of water is covalently bound water, since the pellet pressed at 15000 lb/in.$^2$, being more porous than that pressed at 7 lb/in.$^2$, would show a much larger 533.6-eV peak if the primary source of water were microporous. We believe that the water is primarily associated with Pb ox. In fact, it would be surprising if this did not occur since it has been demonstrated that along some crystal planes of a metal oxide, hydroxyl accommodation (chemisorbed water) is not sterically possible (*43, 44*). In these cases, coordination of the metal cation by adsorption of a water molecule as a $\sigma$-bonded ligand can occur. Furthermore, surface hydration of oxides can occur to a greater depth than the surface monolayer, as demonstrated for some hematites (*45–47*).

For the EDTA- and $HClO_4$-treated pellets, several important observations can be made. First of all, the high resolution SEM micrographs reveal that the surface is composed of many large, coalesced chunks of matter. This means that the original surface layers of almost undistorted spheres have been lost. This cannot occur by dissolution because $Ag_2S$ is not appreciably soluble in either solution. It is evident that the solutions destroy the small interparticle boundaries (composed predominately of lead species) and that the silver-rich cores adhere only weakly to the pellet and are lost by erosion. It is not possible to ascertain how many layers are lost by this mechanism. When a layer is reached where large interparticle boundaries are present, material is lost primarily by dissolution. In 0.01 F basic EDTA, the order of solubilities of the pure lead compounds in $PbSO_4 > 2PbCO_3{\cdot}Pb(OH)_2 > PbS$. Experimentally, we find that lead sulfate is significantly reduced and becomes essentially zero at $\theta = 58°$. However, Pb ox is slightly elevated whille lead sulfide is decreased. This may reflect differences in the rates of dissoution; both lead sulfate and lead sulfide are cubic crystals while basic lead carbonate, the major constituent in Pb ox, is hexagonal. In 0.1 F perchloric acid, the order of solubilities of the pure lead compounds is $2PbCO_3{\cdot}Pb(OH)_2 > PbSO_4 \sim PbS$. Experimentally, we find that all of the lead species are depressed relative to the untreated and EDTA treated pellets. No lead sulfide is observed at $\theta = 18°$; however lead sulfide increases with increasing $\theta$. Both Pb ox and lead sulfate decrease with increasing $\theta$. This suggests that under the right experimental conditions, the surface oxidation products can be completely removed with perchloric acid.

## CONCLUSIONS

Because of the particulate nature of Pb ISE membranes prepared by cold pressing at ≲15000 lb/in.$^2$, it is evident that the bulk membrane conductivity will depend on the contact between silver sulfide domains in the bulk particles. SEM results show large interparticle boundaries in this region, consistent with adequate bulk conductivity. These membranes function as ion sensors when ion interaction processes which can occur at the surfaces are coupled to conduction processes which can occur in the bulk. Under normal conditions of operation, ion interaction can only be coupled to ionic conductivity. However lead segregation in the particles coupled with small interparticle boundaries for the surface layer of particles does not allow for adequate contact between silver sulfide domains for the untreated membrane, hence the membrane cannot function in an electrode. The corrosion products do not prevent ion exchange at the surfaces because all of the lead species are exchangers for $Pb^{2+}$. The predominant species will merely define the theoretical lower detection limit for lead. It is evident that different treatments lead to different stratifications of the "crusts" of surface particles; however no general predictions can be made. For example, $HNO_3$ and $H_2SO_4$ are strong acids, so we might expect that they would be as effective as perchloric acid in removing surface lead. However, KarChaudhari and Cheng (*14*) found that with 0.1 F $HNO_3$, it took 12 h to remove 50% of the surface lead of a Pb ISE membrane and 1.0 F $H_2SO_4$ "showed no promising results". By contrast, 0.1 F perchloric acid is quite efficient in removing surface lead after only 15 min.

## ACKNOWLEDGMENT

The authors thank George Bettoney and the Dow Chemical Co. at Freeport, TX, for generously providing us with the software programs for the new data system.

**Registry No.** EDTA, 60-00-4; PbS, 1314-87-0; $Ag_2S$, 21548-73-2; $HClO_4$, 7601-90-3; $2PbCO_3{\cdot}Pb(OH)_2$, 1319-46-6; $PbCO_3$, 598-63-0; $PbSO_4$, 7446-14-2; galena, 12179-39-4.

## LITERATURE CITED

(1) Mascini, M.; Liberti, A. *Anal. Chim. Acta* **1972**, *60*, 405.
(2) KarCnaudhari, S. N.; Chang, F. C.; Cheng, K. L.; Young, V. Y. *Anal. Chem.* **1981**, *53*, 2048.
(3) Czaban, J. D.; Rechnitz, G. A. *Anal. Chem.* **1973**, *45*, 471.
(4) Koebel, M. *Anal. Chem.* **1974**, *46*, 1559.
(5) Hansen, E. H.; Ruzicka, J. *Anal. Chim. Acta* **1974**, *72*, 365.
(6) Ruzicka, J.; Lamm, C. G.; Tjell, J. Chr. *Anal. Chim. Acta* **1972**, *62*, 15.
(7) Ito, K.; Matsuda, N.; Maeda, T.; Ikeda, S.; Iida, T.; Nakagawa, G. *Denki Kagaku Oyobi Kogyo Butsuri Kagaru* **1979**, *47*, 220.
(8) Vlasov, Y. G.; Ermolenko, Y. E.; Iskhakova, O. A. *Zh. Anal. Khim.* **1979**, *34*, 1522.
(9) Semler, M.; Manek, B. In "Ion Selective Electrodes, Conference 1977"; Pungor, E., Buzas, I., Eds.; Elsevier: Amsterdam, 1978; pp 529–537.
(10) van de Leest, R. E. *Analyst (London)* **1977**, *102*, 509.
(11) Heijne, G. J. M.; van der Linden, W. E.; DenBoef, G. *Anal. Chim. Acta* **1978**, *100*, 193.
(12) Buck, R. P.; Shepard, V. R., Jr. *Anal. Chem.* **1974**, *46*, 2097.
(13) Young, V. Y.; KarChaudhari, S. N.; Cheng, K. L. *SIA, Surf. Interface Anal.* **1981**, *3*, 176.
(14) KarChaudhari, S. N.; Cheng, K. L. *Mikrochim. Acta* **1980**, II, 159.
(15) Fadley, C. S.; Baird, R. J.; Siekhaus, W.; Novakov, T.; Bergstrom, J. *J. Electron Spectrosc. Relat. Phenom.* **1974**, *4*, 93.
(16) Fadley, C. S. *J. Electron Spectrosc. Relat. Phenom.* **1974**, *5*, 725.
(17) Baird, R. J.; Fadley, C.; Kawamoto, S.; Mehta, M.; Alvarez, R.; Silva, J. *Anal. Chem.* **1976**, *48*, 843.
(18) Powell, C. J.; Larson, P. E. *Appl. Surf. Sci.* **1978**, *1*, 186.
(19) Elliott, I.; Doyle, C.; Andrade. J. D. *J. Electron Spectrosc. Relat. Phenom.* **1983**, *28*, 303.
(20) Kelly, M. A.; Scharpen, L. H., Surface Science Labs, Palo Alto, CA, private communication.
(21) Palmberg, P. W. *Anal. Chem.* **1973**, *45*, 549A.
(22) Seah, M. P. *Analusis* **1981**, *9*, 172.
(23) Hoffmann, S. *Analusis* **1981**, *9*, 181.
(24) Scofield, J. H. "Theoretical Photoionization Cross Sections from 1 to 1500 keV"; Livermore Laboratory Report UCRL-51326, 1973.
(25) Reilman, R. F.; Msezane, A.; Manson, S. T. *J. Electron Spectrosc. Relat. Phenom.* **1976**, *8*, 389.
(26) Penn, D. R. *J. Electron Spectrosc. Relat. Phenom.* **1976**, *9*, 29.
(27) Wagner, C. D.; Davis, L. E.; Riggs, W. M. *SIA, Surf. Interface Anal.* **1980**, *2*, 53.
(28) Szajman, J.; Leckey, R. C. G. *J. Electron Spectrosc. Relat. Phenom.* **1981**, *23*, 83.
(29) Szajman, J.; Liesegang, J.; Jenkin, J. G.; Leckey, R. C. G. *J. Electron Spectrosc. Relat. Phenom.* **1981**, *23*, 97.
(30) Seah, M. P.; Dench, W. A. *SIA, Surf. Interface Anal.* **1979**, *1*, 2.
(31) Pederson, L. R. *J. Electron Spectrosc. Relat. Phenom.* **1982**, *28*, 203.
(32) Wagner, C. D.; Riggs, W. M.; Davis, L. E.; Moulder, J. F.; Muilenberg, G. E. "Handbook of X-Ray Photoelectron Spectroscopy"; Perkin-Elmer Corporation: Eden Prairie, MN, 1979.
(33) Kim, K. S.; O'Leary, T. J.; Winograd, N. *Anal. Chem.* **1973**, *45*, 2214.
(34) Morgan, W. E.; Van Walzer, J. R. *J. Phys. Chem.* **1973**, *77*, 964.
(35) Thomas, J. M.; Tricker, M. J. *J. Chem. Soc., Faraday Trans 2* **1975**, *71*, 329.
(36) Zingg, D. S.; Hercules, D. M. *J. Phys. Chem.* **1978**, *82*, 1992.
(37) Pederson, L. R. *J. Electron Spectrosc. Relat. Phenom.* **1982**, *28*, 203.
(38) Shalvoy, R. B.; Fisher, G. B.; Stiles, P. J. *Phys. Rev. B* **1977**, *15*, 1680.
(39) Manocha, A. S.; Parks, R. L. *Appl. Surf. Sci.* **1977**, *1*, 129.
(40) Brion, D. *Appl. Surf. Sci.* **1980**, *5*, 133.
(41) Lichtman, D.; Craig, J. H., Jr.; Sailer, V.; Drinkwine, M. *Appl. Surf. Sci.* **1981**, *7*, 325.
(42) Young, V. *Carbon* **1982**, *20*, 35.
(43) Jones, P.; Hockey, J. A. *Trans. Faraday Soc.* **1971**, *67*, 2679.
(44) Munuera, G.; Stone, F. S. *Discuss. Faraday Soc.* **1971**, *52*, 205.
(45) Berubé, G.; Onoda, G. Y., Jr.; de Bruyn, P. L. *Surf. Sci.* **1967**, *8*, 448.
(46) Breeuwsma, A.; Lyklema, J. *Discuss. Faraday Soc.* **1971**, *52*, 324.
(47) Dumont, F.; Watillon, A. *Discuss. Faraday Soc.* **1971**, *52*, 352.

RECEIVED for review November 21, 1983. Resubmitted October 19, 1984. Accepted December 20, 1984. These results were reported in part at the 184th National Meeting of the American Chemical Society, Kansas City, MO, September 12–17, 1982. Partial support of the Robert A. Welch Foundation, Grant No. A-771, is gratefully acknowledged.

---

# Detection of Gaseous Organophosphorus Compounds Using Secondary Ion Mass Spectrometry

**Gary S. Groenewold and Peter J. Todd***

*Analytical Chemistry Division, Oak Ridge National Laboratory, Oak Ridge, Tennessee 37831*

**Molecular secondary ion mass spectrometry (SIMS) has been investigated for sensitivity and selectivity in the analysis of gaseous organophosphorus compounds. Abundant analyte ions were observed when the gaseous organophosphorus compounds were admitted into the secondary ion source, where a matrix was under primary ion bombardment. The best matrix for the detection of dimethyl methylphosphonate (DMMP), trimethyl phosphate (TMP), and diisopropyl methylphosphonate (DIMP) was determined to be polyphosphoric acid. The abundance of secondary analyte ions was observed to be linear with the introduction rate of gaseous analyte. The introduction rate necessary to produce a 3:1 signal-to-noise ratio in the intensity of secondary protonated molecular ions from DMMP was estimated to be $4 \times 10^{-11}$ mol $s^{-1}$. Substantially more analyte fragmentation is observed by using SIMS than by using methane chemical ionization mass spectrometry. Ten compounds representative of other compound classes were investigated in the same manner as the organic phosphonates; characteristic secondary protonated molecular ions were detected from amines only.**

The detection and identification of volatile organophosphonates and organophosphates is important because chemical warfare agents and insecticides belong to this class of compounds. Analytical methods for the detection of these compounds must be sensitive and selective because the compounds exhibit high toxicity at low levels and they are found in the environment as minor components of complex mixtures. In addition, analysis must be rapid, since these compounds hydrolyze quickly in the environment. Mass spectrometry analysis of this class of compounds has been performed using electron impact ionization (EI) and chemical ionization (CI) (*1–8*), and a review of this work has been published recently (*9*). Generally, electron ionization of organophosphorus compound leads to extensive fragmentation. In contrast, CI results in substantially less fragmentation, and picogram detection limits for organophosphorus compounds have been estimated based on the CI experiments (*1*). However, neither EI nor CI provides the selectivity required for the analysis of organophosphorus compounds; therefore, EI and CI mass spectrometry are usually used together with the slower technique of gas chromatography. When unknown gas chromatographic inseparable interferents are present, analysis is difficult if not impossible (*1*). Secondly, gas chromatography/mass spectrometry does not permit *continuous* analysis.

The goal of the present study is to develop a mass spectrometry ionization method that is selective for organophosphorus compounds and that would have sensitivity

0003-2700/85/0357-0886$01.50/0 © 1985 American Chemical Society

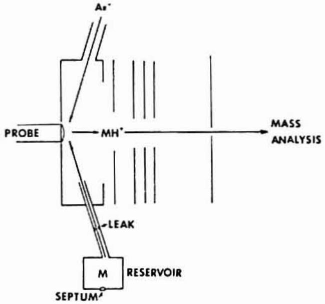

**Figure 1.** Schematic diagram of the introduction and ionization of gaseous compounds using a secondary ion mass spectrometry source. Analytes (M) are admitted to the source via molecular leak and are adsorbed onto the matrix, which is located on the end of the probe. Secondary ions ($MH^+$) are then sputtered into the gas phase by the 5-keV primary argon ion beam and subsequently mass analyzed.

comparable to CI. Molecular secondary ion mass spectrometry (SIMS) and fast atom bombardment mass spectrometry (FABMS) are techniques which have the capability for specificity because the abundances of secondary ions produced using these ionization techniques are known to be very sensitive to interactions which occur between the analyte and the matrix (*10–12*). Analyte introduction is a limitation of SIMS and FABMS, and it has prevented these methods from being used for dynamic (or real-time) analyses: typically, the analyte must be dissolved in a matrix prior to introduction into the source.

In spite of the sample introduction limitation, there is no a priori reason why SIMS or FABMS could not be used for a real-time analysis of gas-phase compounds. Volatile organics have been introduced into a SIMS ion source, but onto solid targets (*13*) or deposited onto metal targets at cryogenic temperatures prior to ion bombardment (*14*). In addition, gaseous oxygen introduced during ion bombardment of inorganic samples is known to enhance the abundances of certain metallic secondary ions (*15*). Therefore, gas-phase analyte–liquid matrix interaction is a reasonable expectation in molecular SIMS. In this report we describe experiments which demonstrate the sensitive and selective secondary ionization of volatile organophosphorus compounds which have been introduced to the SIMS source via a gas inlet system. Estimated limits of detection and the analyte fragmentation observed in the present secondary ionization experiments have been compared to chemical ionization results reported previously (*1*).

## EXPERIMENTAL SECTION

Compounds used in this study were all analytical reagent grade and were purchased from commercial sources, except for 10-crown-2, which was a gift from Wayne E. Zeller (University of Nebraska). The secondary ion mass spectrometer (*16, 17*) was operated at ambient temperature and 8-keV accelerating voltage. The energy of the primary argon ions was 5 keV. The primary ion beam current density was measured at 10 $\mu A/cm^2$ by using a Faraday cup mounted on the end of a probe. The mass spectrometer was fitted with an all-glass heated inlet system (R. J. Brunfeldt Co., Bartlesville, OK) which was operated at 200 °C. Gaseous analytes were admitted to the source via molecular leak. The analytes enter the source approximately 3 cm from the matrix (i.e., probe tip), as shown in Figure 1.

The inlet system was fitted with a capacitance manometer so that the molecular leak rate constant could be determined by monitoring the decrease in pressure with time for a known amount of material injected into the inlet system. Acetophenone was used for this determination because it does not condense on cold spots between the inlet system and the manometer and because it has a molecular weight that is similar to the organophosphorus compounds studied. A molecular leak rate constant of $3.5 \times 10^{-6}\ s^{-1}$ was determined with this procedure.

**Table I. Secondary Ion Mass Spectrum of Polyphosphoric Acid**[a]

| $m/z$ | rel abund, % | composition | $m/z$ | rel abund, % | composition |
|---|---|---|---|---|---|
| 31 | 22 | $P^+$ | 99 | 27 | $H_4PO_4^+$ |
| 32 | 2.6 | | 101 | 0.4 | |
| 47 | 100 | $PO^+$ | 115 | 0.3 | |
| 48 | 26 | $HPO^+$ | 127 | 0.6 | |
| 49 | 1.7 | | 128 | <0.2 | |
| 63 | 12 | $PO_2^+$ | 129 | <0.2 | |
| 64 | 4.2 | $HPO_2^+$ | 145 | 1.9 | $(HPO_3)H_2PO_2^+$ |
| 65 | 19 | $H_2PO_2^+$ | 161 | 2.2 | $(HPO_3)H_2PO_3^+$ |
| 80 | 0.7 | | 179 | 6.4 | $(HPO_3)H_4PO_4^+$ |
| 81 | 26 | $H_2PO_3^+$ | 207 | 0.2 | |
| 82 | 3.0 | | 225 | 0.3 | $(HPO_3)_2H_2PO_2^+$ |
| 83 | 0.5 | | 241 | 0.7 | $(HPO_3)_2H_2PO_3^+$ |
| 98 | 1.7 | | 259 | 0.9 | $(HPO_3)_2H_4PO_4^+$ |

[a] Ions with $m/z > 270$ are not reported.

## RESULTS AND DISCUSSION

Dimethyl methylphosphonate (DMMP), diisopropyl methylphosphonate (DIMP), and trimethyl phosphate (TMP)

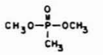

DMMP

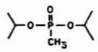

DIMP

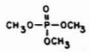

TMP

were chosen as analytes because these compounds are similar to chemical warfare agents, and because DMMP, DIMP, and TMP are not lethal. Samples were initially analyzed as 5% solutions (w/w) in three different matrices (glycerol, concentrated sulfuric acid, and polyphosphoric acid) to determine which matrix would produce the most abundant secondary ions. No secondary analyte ions were observed when 5% solutions of DMMP and TMP in glycerol were irradiated by the $Ar^+$ beam. In contrast, secondary analyte ions were observed from the DIMP/glycerol solution. Generally, the abundance of secondary organophosphorus ions increased as the matrix was changed from glycerol to sulfuric acid to polyphosphoric acid.

In addition to enhancing the abundances of secondary organophosphorus ions, polyphosphoric acid produces low background pressure in the mass spectrometer source (typically $2 \times 10^{-6}$ torr in our instrument, compared to $2 \times 10^{-5}$ torr for glycerol). As a consequence of its lower vapor pressure and lower evaporation rate, polyphosphoric acid persists on the probe tip even after 2 h of continuous primary ion bombardment. Polyphosphoric acid also has a lower mass spectral background than does glycerol, principally because polyphosphoric acid lacks a hydrocarbon backbone. The series of most abundant ions in the secondary ion mass spectrum of polyphosphoric acid is represented by structure a, where $n = 0, 1, 2, ...$ (Table I). Two other important ion series in

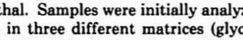

a

the spectrum arise from apparent loss of $H_2O$ and 2(OH) from ions a. Other abundant ions in the secondary ion mass spectrum correspond to $PO^+$ ($m/z$ 47) and $P^+$ ($m/z$ 31). We emphasize that an advantageous feature of polyphosphoric acid as a SIMS/FABMS matrix is the absence of intense peaks

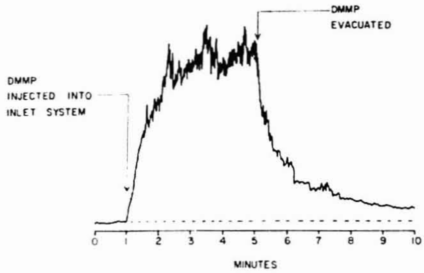

**Figure 2.** $(DMMP + H)^+$ ($m/x$ 125) abundance vs. time. DMMP was injected into inlet system at 1 min. DMMP was subsequently pumped out of inlet system at 5 min.

over large portions of the mass spectrum. Therefore, small quantities of analyte may be detected without interference from the matrix background. For these reasons, polyphosphoric acid was the matrix chosen for this work.

To test the efficacy of molecular SIMS for analysis of vapors, gaseous DMMP (mol wt 124) was admitted at a constant rate to the secondary ion source, where polyphosphoric acid was under primary ion bombardment (Figure 1). The abundance of $m/z$ 125 $(DMMP + H^+)$ increased to approximately half of its maximum value after only a few seconds (Figure 2). The rate of increase then slowed and the maximum ion abundance was recorded approximately 2 min following DMMP introduction. An analogous decay curve was observed when the DMMP was evacuated from the inlet system. The exponential profiles of the $(DMMP + H)^+$ abundance increase and decrease are due either to DMMP pressure equilibration in the inlet system or to DMMP adsorbing into the polyphosphoric acid. We cannot presently distinguish between these possibilities. Similar increase and decay profiles were observed for $(TMP + H)^+$. Dramatic increase and decay profiles were not recorded for $(DIMP + H)^+$ because the most abundant analyte ions were overlapped with matrix ion (vide infra). However, the response for DIMP is believed to be as rapid as for DMMP and TMP.

Gaseous DIMP was also detected by using glycerol as a matrix. However, polyphosphoric acid is preferred as a matrix in this case, because it has better matrix characteristics (vide supra). In contrast to DIMP, gaseous DMMP and TMP were not detected when using glycerol as a matrix.

A sensitive mass spectrometric analysis relies on detection of ions which can be used for analyte identification. These diagnostic ions will not be abundant if extensive analyte fragmentation occurs. Therefore, analyte ion $(M + H)^+$ fragmentation apparent in the SIMS spectrum was compared to fragmentation observed in the methane CI experiments of Sass and Fisher (Table II) (*1*). For DMMP and DIMP, less fragmentation is observed by using CIMS than by using SIMS, regardless of whether the analytes were introduced to the SIMS source as a gas or as a solution with the matrix. The increased fragmentation observed in SIMS may be the result of condensed phase solvolysis reactions occurring in the polyphosphoric acid. Side reactions between analyte and matrix (*12*) or target (*15*) are a general consequence of the use of a multicomponent solution for SIMS. Alternatively, the internal energy distribution characteristic of secondary ionization, which is presumably different from that characteristic of specific CI conditions (*1*), may give rise to more pronounced fragmentation (*18*).

Secondary ionization of DMMP and TMP introduced to the source as gases results in slightly more fragmentation than does secondary ionization of those compounds from homogeneous DMMP/polyphosphoric acid and TMP/polyphosphoric acid solutions. One rationalization of these results is that secondary ionization of an analyte introduced as a gas involves molecules which are not completely solvated, either because analyte surface concentration is too great or because the surface residence time is too short for equilibrium to be established. Reasonably, matrix–analyte interactions which enhance production of abundant secondary $(M + H)^+$ ions are reduced if analyte molecules are incompletely solvated. Reduction in analyte solvation may result in the production of secondary ions which have, on the average, more internal energy than secondary ions produced from solvated analytes. Consequently, more fragmentation would be expected from those secondary ions produced from only partially solvated analyte molecules (*18*).

**Table II. Relative Abundances (%) of Organophosphorus Ions Resulting from Secondary Ionization (SIMS) and Chemical Ionization (CIMS)**

Dimethyl Methylphosphonate (DMMP), mol wt 124

| $m/z$ | SIMS 5% DMMP PPA matrix$^b$ | SIMS Gaseous DMMP PPA matrix$^b$ | methane CIMS$^a$ gaseous DMMP |
|---|---|---|---|
| 125 | 100 | 86 | 100 |
| 95 | 4.9 | 9.0 | nr$^c$ |
| 94 | 12 | 19 | nr$^c$ |
| 93 | 75 | 100 | nr$^c$ |
| 79 | 42 | 67 | nr$^c$ |

Trimethyl Phosphate (TMP), mol wt 140

| $m/z$ | SIMS 5% TMP PPA matrix$^b$ | SIMS gaseous TMP PPA matrix$^b$ | methane CIMS gaseous TMP |
|---|---|---|---|
| 141 | 100 | 100 | na$^d$ |
| 109 | 34 | 41 | |
| 95 | 10 | 20 | |
| 93 | 8.8 | 14 | |
| 79 | 12 | 27 | |

Diisopropyl Methylphosphonate (DIMP), mol wt 180

| $m/z$ | SIMS 5% DIMP PPA matrix$^b$ | SIMS gaseous DIMP PPA matrix$^b$ | methane CIMS$^a$ gaseous DIMP |
|---|---|---|---|
| 181 | 0.85 | 1.5 | 75 |
| 139 | 0.85 | 4.7 | 100 |
| 125 | 0.66 | 2.3 | 48 |
| 97 | 7.7 | 100 | 85 |
| 43 | 100 | 30 | nr$^c$ |
| 41 | 65 | 16 | nr$^c$ |
| 39 | 53 | 13 | nr$^c$ |

$^a$ Data from ref 1. $^b$ PPA, polyphosphoric acid. $^c$ Abundance not reported and is probably low. $^d$ TMP not analyzed using methane CIMS.

In contrast to DMMP and TMP, few characteristic ion are observed from primary ion bombardment of the DIMP/polyphosphoric acid solution. These samples are characterized by abundant fragment ions at $m/z$ 43, 41, and 39, as shown in Table II. Ions which are characteristic of DIMP are more abundant in the secondary ion mass spectrum when DIMP is introduced as a gas. We believe that these observations are evidence for acid solvolysis of DIMP which occurs in the bulk of the polyphosphoric acid matrix.

The limits of detection were estimated for the three organophosphorus compounds in order to compare secondary ionization of gaseous analytes with other mass spectrometric ionization methods, specifically CI. The limits of detection were determined by injecting 1.0 μL of analyte into the inlet

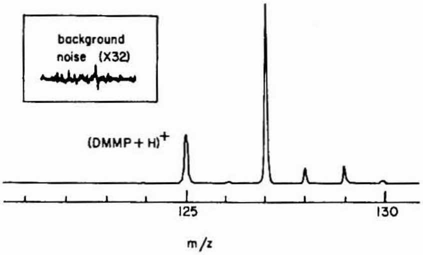

**Figure 3.** Partial secondary ion mass spectrum (1 scan) of gaseous DMMP, admitted to the mass spectrometer at a rate of $4.0 \times 10^{-9}$ g/sec. The peak *m/z* 125 corresponds to $(DMMP + H)^+$; m/z 127 is a background ion from the polyphosphoric acid matrix.

system and then acquiring a single mass spectrum. In these experiments, a small fraction of the analyte injected enters the secondary ion source at a constant rate. The constant introduction rate conditions were used to estimate detection limit because it was not possible to quickly admit small batches of analyte to the instrument used in this study.

Since it is impossible to introduce instantaneously a known quantity of sample, detection limits must be estimated based on the secondary ion intensity vs. the introduction rate. A signal-to-noise ($S/N$) value of 300 for the $(DMMP + H)^+$ peak was observed in the mass spectrum (Figure 3) following the injection of 1 $\mu$L of DMMP into the inlet system. A total of $1.6 \times 10^{-9}$ g of DMMP entered the secondary ion source while the $(DMMP + H)^+$ abundance was being measured. This amount was calculated as the product of the $(DMMP + H)^+$ peak width (typically 0.4 s), the amount of DMMP injected, and the molecular leak rate constant (see Experimental Section). We estimate the limit of detection to be $1.6 \times 10^{-11}$ g at a $S/N$ value of 3 assuming a linear relationship between secondary ion current and introduction rate (vide infra). This estimated detection limit is comparable to the $2.0 \times 10^{-11}$ limit estimated using methane CI (*1*). The detection limit for TMP was also estimated using this method at $2.2 \times 10^{-11}$ g.

The limit of detection estimated for DIMP was $2.9 \times 10^{-10}$ g. The peak at $m/z$ 97 was used in this determination, because it was 60 to 70 times more abundant than $(DIMP + H)^+$ (Table II). However, the use of $m/z$ 97 for the detection of DIMP has limitations, because a small background peak at this mass arises from the polyphosphoric acid matrix. Detection of $2.9 \times 10^{-10}$ g of DIMP was calculated to result in a $m/z$ 97 ion abundance which is 1.3 times greater than the abundance of the background $m/z$ 97. The background ion clearly acts to prevent the detection of smaller quantities of DIMP.

To test the suitability of secondary ionization for quantitative detection and to further evaluate the sensitivity, analyte ion abundance was plotted vs. the analyte introduction rate. The plots for DMMP and TMP are linear over 2 orders of magnitude, and they have approximately the same slope (Figure 4). Therfore, quantitation for TMP and DMMP should be possible by using secondary ionization. The DIMP plot was linear over only 1 order of magnitude; leak rates greater than 70 pmol/s did not cause the abundance of $m/z$ 97 to increase proportionally. The slope of the DIMP plot at leak rates less than 70 pmol/s was three times larger than the slopes of the DMMP and TMP plots. The unusual behavior of DIMP is not understood at this time. We speculate that the greater DIMP sensitivity observed at lower leak rates may be due to greater surface activity of DIMP compared to DMMP and TMP; this would be consistent with the leveling of the $m/z$ 97 abundance at higher DIMP introduction rates (*19*). Further, this lack of DIMP response at greater introduction rates may be due to saturation of the polyphosphoric acid surface by DIMP and/or solvolysis of DIMP in the bulk of the polyphosphoric acid matrix.

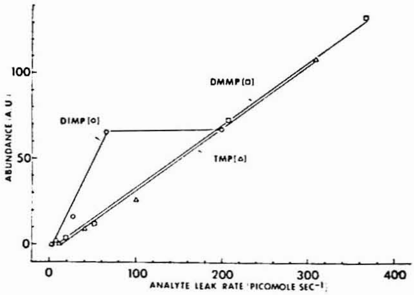

**Figure 4.** Secondary ion abundance vs. analyte leak rate. $(DMMP + H)^+$ (*m/z* 125) was monitored for DMMP, $(TMP + H)^+$ (*m/z* 141) was monitored for TMP, and $(DIMP + H - 2C_3H_6)^+$ (*m/z* 97) was monitored for DIMP.

Experiments were performed to identify other classes of compounds which could be ionized and therefore interfere with the analysis of the organophosphorus compounds. Benzyl alcohol, anisole, benzaldehyde, acetone, 10-crown-2, chlorobenzene, toluene, *n*-nitrotoluene, and benzonitrile were not detected and presumably were not ionized when admitted as gases to the secondary ion source. Low abundance protonated molecular ions were observed when acetophenone was admitted to the secondary ion source. Abundant protonated molecular ions were observed from both gaseous benzylamine and gaseous phenylpropylamine. It appears that gaseous amines are the only general class of compounds (besides the organophosphorus analytes) which can be analyzed by using SIMS with a polyphosphoric acid matrix. We conclude from this cursory study that secondary ionization of gaseous analytes has potential as a selective ionization technique if an appropriate matrix is used.

## CONCLUSIONS

Gaseous organophosphorus compounds may be preferentially ionized and sensitively analyzed by using SIMS with a polyphosphoric acid matrix. Limits of detection that were estimated by using SIMS were comparable to those estimated using CI (*1*). We believe that sensitivity of secondary ionization could be improved by moving the analyte source entrance closer to the matrix. The mechanism for the secondary ionization of these and other gaseous analytes is presently unknown. Analyte basicity, matrix acidity, analyte–matrix solubility, and analyte surface activity are factors which probably have an important bearing on secondary ion abundances. Experiments using matrices having different physical and chemical properties may help to elucidate the relative importance of these factors in secondary ionization. Although all possible interferents were not analyzed during the course of this work, these first experiments point to unusual selectivity for this ionization method.

## LITERATURE CITED

(1) Sass, S.; Fisher, T. L. *Org. Mass Spectrom.* **1979**, *14*, 257–264.
(2) Holtzclaw, J. R.; Campana, J. E. Paper presented at the 31st Annual Conference on Mass Spectrometry and Allied Topics, Boston, MA, May 8–13, **1983**.
(3) Hodges, R. V.; McDonnell, T. J.; Beauchamp, J. L. *J. Am. Chem. Soc.*, **1980**, *102*, 1327–1332.
(4) Busch, K. L.; Bursey, M. M., Hass, J. R.; Sovocool, G. W. *Appl. Spectrosc.* **1978**, *32*, 388–399.
(5) Cload, P. A.; Hutchinson, D. W. *Org. Mass Spectrom.* **1983**, *18*, 57–59.

(6) Meyerson, S.; Kuhn, E. S.; Ramirez, F.; Marecek, J. F.; Okazaki, H. *J. Am. Chem. Soc.* **1980**, *102*, 2398–2407.
(7) Meyerson, S.; Harvan, D. J.; Hass, J. R.; Ramirez, F.; Maracek, J. F. *J. Am. Chem. Soc.* **1984**, *106*, 6877–6883.
(8) Cairns, T.; Siegmund, E. G.; Bong, R. *Anal. Chem.* **1984**, *56*, 2547–2552.
(9) Chapman, J. R. *Organophosphorus Chem.* **1983**, *14*, 278–304.
(10) Barber, M.; Bordoli, R. S.; Elliot, G. J.; Sedgwick, R. D.; Tyler, A. N. *Anal. Chem.* **1982**, *54*, 645A–657A.
(11) Caprioli, R. M. *Anal. Chem.* **1983**, *55*, 2387–2391.
(12) Glish, G. L; Todd, P. J.; Busch, K. L.; Cooks, R. G. *Int. J. Mass Spectrom. Ion Proc.* **1984**, 177–192.
(13) Unger, S. E.; Cooks, R. G.; Steinmetz, B. J.; Delgas, W. N. *Surf. Sci.* **1982**, *116*, 211–217.
(14) Jonkman, H. T.; Michl, J.; King, R. N.; Andrade, J. D. *Anal. Chem.* **1978**, *50*, 2078–2082.
(15) Kloppel, K. D.; Seidel, W. *Int. J. Mass Spectrom. Ion Phys.* **1979**, *31*, 151–160.
(16) Todd, P. J.; Glish, G. L.; Christie, W. H. *Int. J. Mass Spectrom. Ion Proc.* **1984**, *61*, 215–230.
(17) Russell, D. H.; Smith, D. H.; Warmack, R. J.; Bertram, L. K. *Int. J. Mass Spectrom Ion. Phys.* **1980**, *35*, 381–391.
(18) Cook, K. D.; Chan, K. W. S. *Int. J. Mass Spectrom. Ion Phys.* **1983**, *54*, 135–149.
(19) Ligon, W. V.; Dorn, S. B. *Int. J. Mass Spectrom. Ion Proc.* **1984**, *57*, 75–90.

RECEIVED for review October 18, 1984. Accepted December 26, 1984. Research sponsored by the U.S. Department of Energy, Office of Basic Energy Sciences, under Contact DE-AC05-840R21400 with Martin Marietta Energy Systems, Inc., and by the U.S. Army, Aberdeen Providing Grounds, Aberdeen, MD. G. S. Groenewold acknowledges support from the U.S. Department of Energy Postgraduate Research Training Programs administered by Oak Ridge Associated Universities.

# Negative Gold Ion Gun for Liquid Secondary Ion Mass Spectrometry

**Charles N. McEwen***[1] **and J. Ronald Hass**

*Laboratory of Molecular Biophysics, National Institute of Environmental Health Sciences, Research Triangle Park, North Carolina 27709*

**A source-mounted ion gun which produces $Au^-$ ions as the primary bombarding particles in liquid SIMS is described. The $Au^-$ ion energy can be varied up to 20 keV utilizing the high voltage feedthroughs supplied with most high-performance magnetic instruments. Liquid SIMS results obtained with the gun are compared to results obtained using $Cs^+$ and $Xe^+$ ion bombardment.**

Liquid matrix secondary ion mass spectrometry (liquid SIMS) and fast atom bombardment (FAB) mass spectrometry are the methods of choice for the mass spectrometric analysis of compounds considered nonvolatile or thermally labile by electron impact or chemical ionization criteria. These methods involve the use of ion guns to produce kiloelectronvolt particles which bombard samples dissolved in liquid matrices. The sputtered ion species often contain a substantial fraction of intact molecular ions as well as diagnostic fragment ions.

A variety of ion guns are used, but the most common is the saddle field gun which is offered commercially by several manufacturers. This gun is too large to mount directly on the ion source and thus requires that a source housing inlet port be available with a line-of-sight to the sample probe.

The ion gun mounting problem was first overcome with a source mounted miniature capillaritron gun (*1*). Subsequently, source mounted cesium ion guns (*2, 3*) and a liquid metal ion gun (*4*) have been reported, which in addition to eliminating the necessity for a line-of-sight inlet port, also reduces the instrument gas load during liquid SIMS operations.

Improvements in liquid SIMS ion guns have been claimed for guns using more massive bombarding particles. For example, an order of magnitude increase in secondary ion signal is achieved by using singly charged mercury (*5*) or trimethylpentaphenyltrisiloxane ions (*6*) as the bombarding species instead of argon neutrals. However, the methods used to produce these primary ions are complex. In the extreme, 0.2–15 μm iron particles, accelerated using a van-de-Graaf accelerator, were used to produce SIMS spectra of organic materials (*7*).

A practical method of observing the effects of increasing the mass of the bombarding particles on secondary ion yield was recently described by Barofsky, et al. (*4*). These authors, using liquid metal ion guns, found that the $M + Na^+$ ion of stachyose increased in abundance with the increase of mass of the bombarding primary particle. For example, $Au^+$ ($m/z$ 197) gives ca. 5 times more signal than $Ga^+$ ($m/z$ 69). Additionally, the $M + Na^+$ signal from stachyose in glycerol bombarded with $Au^+$ ions from a liquid metal ion gun is ca. 50 times more intense than the $M + Na^+$ signal obtained using an $Ar^\circ$ beam from a saddle field gun.

The impressive results obtained with gold ion bombardment led us to consider simple and reliable ways of producing massive bombarding particles for liquid SIMS. Negatively charged particles were preferred because, for magnetic sector instruments operated in the positive ion mode, a wider energy range is available for the bombarding particle for any given feedthroughs or power supply. For example, with the ion source operating at + 8 kV and the ion gun at −12 kV, the negative primary ions will have 20-keV kinetic energy.

Sputter-type negative ion guns have been under development for a number of years (*9, 10*). The ion gun described here uses $Cs^+$ ion bombardment of a gold cone to sputter $Au^-$ primary ions and is based on work by Middleton and Adams (*11*). Higher intensity $Au^-$ sputter ion guns have been designed (*12*) but require additional complexity which was not considered necessary for this preliminary work.

This paper describes the construction of a source-mounted ion gun capable of producing 20-keV $Au^-$ ions. The gun's operating characterisitcs and a comparison of the results obtained during the sputtering of the polypeptide methionin-enkephalin from a glycerol matrix using $Au^-$, $Xe^+$, and

---

[1] Present address: Central Research and Development Department, E. I. du Pont de Nemours and Co., Experimental Station, Wilmington, DE 19898.

0003-2700/85/0357-0890$01.50/0 © 1985 American Chemical Society

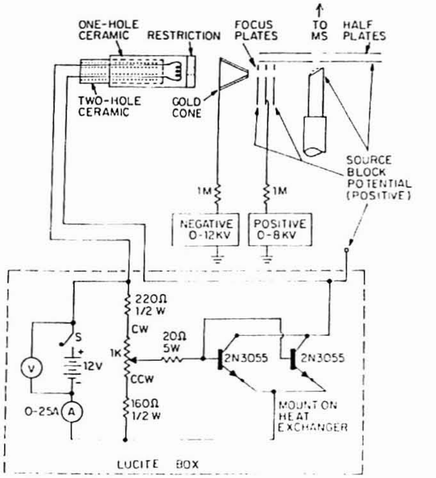

**Figure 1.** Schematic of $Au^-$ ion gun with focusing lens and $Cs^+$ ion gun filament control unit. Lucite is a registered Du Pont trademark.

$Cs^+$ ion bombardment are discussed. An indirect comparison is also made of $Au^-$ and $Au^+$ ion bombardment.

## EXPERIMENTAL SECTION

A cesium ion gun was mounted as described previously (*3*), except that it was moved about 1 cm further from the sample probe tip and was mounted in a Corning MACOR machinable glass ceramic holder (Corning Glass Works, Corning, NY). A gold cone ca. 5 mm diameter and 5 mm depth with a 1.5 mm hole in the bottom was inserted between the $Cs^+$ ion gun and the sample probe tip as shown (Figure 1). The ion source block (source walls) was removed and a three-element lens was installed. (For a description of the lens elements see ref 13). The $Cs^+$ ion gun, the gold cone, and the lens elements form a straight line path to the sample probe tip.

The $Cs^+$ ion gun (*4*) has been improved by using a 0.009 in. × 0.0045 in. rhenium ribbon (A. D. MacKay Metals, Darien, CT) instead of a tungsten filament, and by constricting the ion exit end to about 2 mm with a thin layer of Sauereisen No. 1 cement (Sauereisen Cements Co., Pittsburgh, PA). The schematic for the filament control unit is also shown in Figure 1.

In operation the $Cs^+$ ion gun is connected to ion source potential through a 100-kΩ resistor. The front and back plates of the lens assembly are connected directly to source potential, and the center lens element is connected to a variable voltage power supply (*13*). The gold cone floats at a negative potential with respect to the ion source and can be operated from ground potential up to a negative potential determined by the voltage characteristics of the feedthroughs or the power supply limit. A 1-MΩ resistor inserted between the power supply and the gold cone virtually eliminates arcing.

The gun assembly is attached to the ion source of a VG ZAB-2F mass spectrometer. Typical operating conditions are +6 kV source potential, +6.4 kV center lens element potential, and −10 kV gold cone potential. the $Cs^+$ ion gun filament typically operates between 1 and 2 A, which is sufficient to produce a 10–30 μA $Cs^+$ ion beam.

A 40 ng/μL methanol solution of methionin–enkephalin (United States Biochemicals, Cleveland, OH) was loaded in the desired amount onto a thin layer of glycerol containing oxalic acid on the sample insertion probe. A comparison was made of the $MH^+$ ion intensity of methionin–enkephalin scanning the magnetic sector between *m/z* 570 and *m/z* 580 using either a $Cs^+$ ion gun (*3*), a $Xe^+$ capillaritron ion gun (*1*) as modified in ref 13, or the $Au^-$ ion gun.

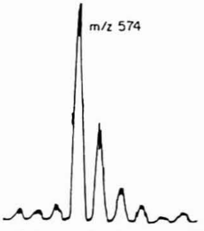

**Figure 2.** Molecular ion region for 40 ng of methionin–enkephalin in glycerol using $Au^-$ ion bombardment.

## RESULTS AND DISCUSSION

The $Au^-$ ion gun had an initial delay period in which the intensiy of the ion beam slowly increased as measured by the sputtering yield from glycerol. After an hour or so of operation, the ion intensity stabilized and the gun could be started with only the several second delay of the $Cs^+$ ion gun. The increase in $Au^-$ ion intensity is attributed to the time necessary to achieve a steady-state cesium concentration on the surface of the gold cone (*12*).

The ion current observed for the *m/z* 369 ion from glycerol when using the $Au^-$ ion gun is equivalent to the ion current obtained from the same *m/z* 369 ion when operating the focused $Xe^+$ capillaritron ion gun (*13*) under standard conditions of 3–5 μA primary beam current. Higher equivalent primary ion current can be obtained from the $Au^-$ gun, but with some instability due to arcing and at the expense of the long-term operation of the $Cs^+$ ion component of the gun.

The $Au^-$ ion gun was evaluated by using methionin–enkephalin in a glycerol matrix and comparing the results with those obtained by using focused $Cs^+$ and $Xe^+$ ion guns individually optimized and alternately mounted in the same position on the ion source (*13*). The mass spectrum of ca. 1 μg of methionin–enkephalin in glycerol is remarkably similar for all of the ion guns, except for small differences in ion intensities. These spectra compare closely with one obtained on a different ZAB-2F using Xe° as the primary beam (*1*). As expected, the charge of the bombarding particle had no obvious influence on the appearance of the spectrum.

To determine if the detection limit could be lowered using the more massive gold ion or the higher energy obtainable with the negative particle, successive dilutions of methionin–enkephalin in glycerol were placed on the probe. Figure 2 shows an example of the ion current obtained for the molecular ion region of methionin–enhephalin loaded at 40 ng (70 pmol) in glycerol and bombarded with 8-keV $Au^-$ ions. The results obtained with $Au^-$ primary ions compare quite closely to those obtained with the $Cs^+$ and $Xe^+$ ion guns. Thus, within experimental error (about a factor of 2) the minimum detectable limit is the same for the three guns. A previous rough comparison of $Cs^+$, $Xe^+$, and $Au^+$ (from a liquid metal ion gun (*4*)) without focusing lens showed less than a factor of 2 difference between the three guns in detection limit tests. Thus, one can expect in the kinds of tests conducted here to find little difference between $Au^+$ and $Au^-$ ion bombardment.

In each case the factor governing the minimum detection limit was the background chemical noise. Attempts to increase the ion signal also increased the intensity of the background peaks. In fact, operating at the lowest primary ion flux gives the best signal-to-background ratio. thus, in the mass range studied here, increasing the primary ion current beyond that necessary for the detection of the compound of interest is detrimental.

Increasing the $Au^-$ ion energy from 8 keV to 20 keV also resulted in a smaller signal-to-background ratio for the *m/z*

574 ion of methionin–enkephalin even though the total sample ion current increased. Because better extraction of the sputtered Au⁻ ions from the gold cone of the ion gun is expected at higher extraction voltages, some of the increase in background relative to signal may be due to the increased primary ion flux. these results can be rationalized by assuming the matrix signals resulted from nonspecific reactions of the degradation products occurring from the dissipation of the primary beam's kinetic energy. Therefore, an increase in either the primary beam energy or flux will result in increased background signal.

These results are disappointing in that they suggest that gains in detection of low and moderate molecular weight compounds will likely be offset by increased matrix signals; however at high mass, where matrix background is minimal and signal intensity important, high-mass high-energy primary ions may be useful in improving sensitivity. Thus, future studies are aimed at determining if high energy Au⁻ ion bombardment will lower the detection limit for high mass and difficult to analyze compounds.

## ACKNOWLEDGMENT

We thank D. F. Barofsky, Oregon Graduate Center, for the Au⁻ liquid metal ion gun, D. J. Harvan of N.I.E.H.S. for technical assistance, and C. A. Mitchell of the E. I. du Pont de Nemours & Co. for designing the cesium gun current regulator.

**Registry No.** Au⁻, 19498-55-6.

## LITERATURE CITED

(1) Rudat, M. A. *Anal. Chem.* **1982**, *54*, 1917.
(2) Aberth, W.; Straub, K. M.; Burlingame, A. L. *Anal. Chem.* **1982**, *54*, 2029.
(3) McEwen, C. N. *Anal. Chem.* **1983**, *55*, 967.
(4) Barofsky, D. F.; Giessmann, U.; Bell, A. E.; Swanson, L. W. *Anal. Chem.* **1983**, *55*, 1318.
(5) Stoll, R.; Schade, U.; Rollgen, F. W.; Giessmann, U.; Barofsky, D. F. *Int. J. Mass Spectrom. Ion Phys.* **1982**, *43*, 227.
(6) Wong, S. S.; Stoll, R.; Rollgen, F. W. *Z. Naturforsch. A* **1982**, *37A*, 718.
(7) Krueger, F. R.; Knabe, W. *Org. Mass Spectrom.* **1983**, *18*, 83.
(8) Dittner, P. F.; Datz, S. *J. Chem. Phys.* **1978**, *68* 2451.
(9) Alton, G. D. *IEEE Trans. Nucl. Sci.* **1983**, *NS-30*, 1480.
(10) Krohn, V. E. *J. Appl. Phys.* **1962**, *33*, 3523.
(11) Middleton, R.; Adams, C. T. *Nucl. Instrum. Methods* **1974**, *118*, 329.
(12) Alton, G. D.; Blazey, G. C. *Nucl. Instrum. Methods* **1979**, *166*, 105.
(13) Stoll, R.; Harvan, D. J.; Hass, J. R. *Int. J. Mass Spectrom. Ion Phys.* **1984**, *61*, 71.

Received for review November 2, 1984. Accepted January 4, 1985.

# Identification of Stereoisomers of Some Hexoses by Mass Spectrometry Using Fast Atom Bombardment and Mass Ion Kinetic Energy

**Germain Puzo,* Jean-Jacques Fournie, and Jean-Claude Prome**

*Centre de Recherche de Biochimie et de Génétique Cellulaires du C.N.R.S., 118 route de Narbonne,*
*31062 Toulouse Cedex, France*

**We present a method for the identification of underivatized aldohexose stereoisomers involving MIKE analysis of their solvated and cationized molecular ions (aldohexose–cat$^+$–matrix). These cluster ions have been generated by the FAB ionization mode using glycerol or diethanolamine as matrices. From their unimolecular dissociation spectra (MIKE), mainly two kinds of cationized ions (aldohexose–cat)$^+$ and (matrix–cat)$^+$ are generated. The abundances of these fragment ions are characteristic of all D-aldohexose stereoisomers.**

Identification of the various stereoisomers of aldohexoses by conventional mass spectrometry, EI/GC/MS, requires their chemical derivatization (*1*).

The use of soft ionization modes with the "in beam" technique have permitted the analysis by mass spectrometry of underivatized monosaccharides (*1*). Their mass spectra are characterized by a small amount of fragment ions and abundant pseudomolecular ions (M + O) (where M is the monosaccharide investigated and O represents H$^+$, $NH_4^+$, and alkali cations). These ionization modes, but more particularly FD, have been used for the purpose of molecular weight determination of sugars (*2*). To increase their ionization process and the abundance of their pseudomolecular ions, some authors have proposed, under FD conditions, the addition of an alkali salt to a sugar solution to form cationized molecular ions (M + cat)$^+$ by an attachment reaction between the monosaccharide and the alkali cation (*3, 4*).

More recently, Deutsch has shown that the use of $KH_2PO_4$ instead of KI or NaI under FD conditions enhances the thermal fragmentation for a given value of the emitter current permitting the identification of selected aldohexose isomers (*5*). Observed differences in the relative abundance of the fragmentation products were mainly attributed to the relative proportions of the pyranose and furanose forms (*5*). However, the use of this method as an analytical tool for monosaccharide isomer identification seems difficult on a routine basis due to the precision by which the temperature at the emitter surface is controlled. Variation in this temperature will result in lower reproducibility of the fragmentation abundances. An alternative approach for the identification of underivatized monosaccharides has been proposed by Rollgen et al. (*6*). They induce the decomposition of the cationized molecular ions (M + cat)$^+$, generated by FD by collision with a gas confined in a collision chamber located in the second field free area of a reversed geometry mass spectrometer, and analyze the fragmentations generated by scanning the electrostatic analyzer (MIKE/CID). Differentiation of some monosaccharides by this method is "in principle" possible; however the fluctuations in the abundance of the precursor ions during their analysis does not allow unequivocal differentiation.

0003-2700/85/0357-0892$01.50/0 © 1985 American Chemical Society

**Scheme I**

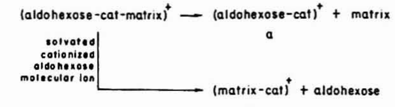
(aldohexose-cat-matrix)$^+$ → (aldohexose-cat)$^+$ + matrix
a
solvated cationized aldohexose molecular ion
(matrix-cat)$^+$ + aldohexose
b

matrices used: glycerol and diethanolamine (DEA)
alkali cations employed: Li$^+$, Na$^+$, K$^+$, and Rb$^+$

The production of ionic species from polar samples is more easily performed by use of the FAB ionization technique (*7, 8*).

The use of the liquid matrix increases the lifetime and the abundance of ion production allowing high reproducibility of MIKE/CID mass spectra. This ionization mode has been particularly successfully applied to the structural study of polysaccharides (*9*). We have shown that one process for the formation of cationized molecular disaccharide ions under FAB conditions involves a desolvatation reaction from the solvated cationized cluster ions (*10*). We have observed that this dissociation process is mainly governed by the relative cation affinity between the matrix and the sugar molecule (*10*).

In the present work, we have examined several aldohexose stereoisomers in an attempt to identify them from the unimolecular decomposition spectra of the corresponding cationized solvated cluster ions.

## EXPERIMENTAL SECTION

The FAB mass spectra and FAB/MIKE spectra were performed on a VG ZAB2F mass spectrometer. A 0.5-μL matrix (glycerol or diethanolamine) was deposited on the target with a Micropettor SMI Polylabo. To this was added 0.5 μL of a molar aqueous solution of aldohexose and 0.5 μL of 0.1 M of an aqueous solution of alkali iodide salt with 0.5-μL microcaps (Drummond).

MIKE spectra were recorded with a scan speed of 30 s over the energy range 8 kV, corresponding to the transmission of the main beam, and the energy value corresponding to the transmission of the ion b. In order to increase the peak height reproducibility, the scan speed was reduced by a factor of 10 several electronvolts before the energy corresponding to the transmission of ions a and b. Two MIKE's spectra were recorded for each sample loading on the target, the first after 10 s and the second after 60 s. The values presented in Figure 2 and Table I are the results of the average of these two measurements.

The above conditions were chosen because in the MIKE spectra of isobaric ions of the precursor ions (aldohexose-cat-matrix)$^+$, a signal may be observed at the same mass as the (aldohexose-cat)$^+$ in the absence of any aldohexose at the target surface. When glycerol is used as matrix, this signal corresponds to less than 3% compared to the signal corresponding to (aldohexose-cat)$^+$. However this percentage increases when DEA is used as matrix since the abundance of (aldohexose-cat)$^+$ decreases.

## RESULTS

The FAB mass spectra of the aldohexose stereoisomers in the presence of the alkali cations were quite similar for the matrices used (glycerol, diethanolamine). Mainly protonated (aldohexose + H)$^+$ and cationized (aldohexose + cat)$^+$ molecular ions and their solvated clusters (aldohexose + (H$^+$ or cat$^+$) + matrix) were formed. Fragment ions resulting from the successive expulsion of one and two molecules of water from the protonated species were also observed but in much lower abundance.

The competitive desolvation processes shown in Scheme I were investigated by examining the MIKE spectra of the cluster (hexose–cat$^+$–matrix) ions in order to differentiate the various aldohexose stereoisomers analyzed (for a preliminary communication, see ref 11). Figure 1 illustrates the principle of the method and shows the abundance of the ions a (allose–Na$^+$) and b (glycerol–Na$^+$) occurring from the unimolecular decomposition of the (allose–Na$^+$–glycerol) cluster ions. In the same way as the unimolecular dissociation of a proton-bound dimer (B$_1$–H–B$_2$)$^+$ allowed the measurement of the relative proton affinity of the B$_1$ and B$_2$ molecules (*12*), it could be expected that the relative abundance of the ions a and b reflected the relative cationic affinity of the hexose and the matrix, thus allowing a differentiation between the different hexose stereoisomers relative to their ability in complexing the alkali cation. The ratios a/b obtained by using glycerol as matrix and sodium or lithium as alkali cations for the different aldohexoses investigated are summarized in Figure 2. It may be observed that the ratio a/b for talose and galactose decreases going from Li$^+$ to Na$^+$. However, this ratio increases when sodium replaces lithium for all the other aldohexoses. Moreover this ratio may be seen to be characteristic of the stereoisomer. For instance, if we consider the solvated cluster (aldohexose–Li$^+$–glycerol), we observe a decreasing of the aldohexose–lithium affinity according to the following sequence: talose > idose > galactose = mannose > gulose > altrose > allose > glucose. Figure 2 also shows that this sequence is not affected by the nature of the alkali cation present. However the use of sodium allows a better differentiation between galactose and mannose, giving a more complete sequence to that given above: talose > idose > mannose > galactose > gulose > altrose > allose > glucose. For the purpose of determining the influence of the matrix in the aldohexose cationic affinity sequence previously established with glycerol, we have also used diethanolamine

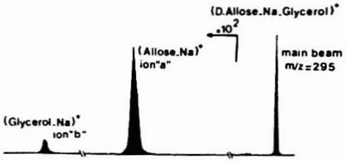

**Figure 1.** MIKE spectrum (allose–Na–glycerol)$^+$ cluster ion generated by FAB.

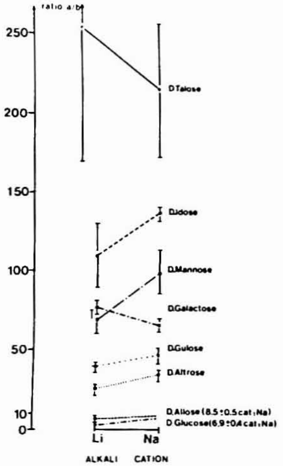

**Figure 2.** Values of the ratios a/b of the abundances of the ions a (aldohexose–cat)$^+$ and b (glycerol–cat)$^+$ resulting from the unimolecular dissociation of the (aldohexose–cat–glycerol)$^+$ cluster ions generated by the FAB ionization mode for all the D-aldohexose stereoisomers.

**Table I. Values of the Ratios a/b of the Abundances of the Ions a (aldohexose–cat)$^+$ and b (DEA–cat)$^+$ for cat = Na$^+$, K$^+$, and Rb$^+$ Occurring from the Unimolecular Dissociation of the (aldoxose–cat–DEA)$^+$ Cluster Ions Generated by the FAB Ionization Model for All the D-Aldohexose Stereoisomers**

| aldohexoses investigated | Na | K | Rb |
|---|---|---|---|
| D-talose | 2.1 ± 0.2 | 2.20 ± 0.03 | 2.0 ± 0.3 |
| D-idose | 0.55 ± 0.03 | 0.79 ± 0.02 | 0.9 ± 0.1 |
| D-mannose | 0.22 ± 0.03 | 0.60 ± 0.08 | 0.8 ± 0.1 |
| D-altrose | 0.21 ± 0.01 | 0.57 ± 0.04 | 0.8 ± 0.1 |
| D-galactose | 0.15 ± 0.03 | 0.42 ± 0.05 | 0.7 ± 0.1 |
| D-gulose | 0.10 ± 0.02 | 0.15 ± 0.03 | 0.1 ± 0.1 |
| D-glucose | 0.10 ± 0.02 | 0.14 ± 0.03 | 0.13 ± 0.05 |
| D-allose | 0.13 ± 0.02 | 0.13 ± 0.03 | 0.13 ± 0.03 |

(DEA) which has a higher basicity than glycerol. Table I summarizes the ratios a/b for the cationized ions a, (aldohexose–cat)$^+$ and b, (DEA–cat)$^+$ occurring from the unimolecular decomposition of the (aldohexose–cat–DEA)$^+$ cluster ion. The following alkali cations have been investigated: sodium (Na)$^+$, potassium (K)$^+$, and rubidium (Rb)$^+$. Lithium (Li)$^+$ has been excluded because it possesses a high affinity for the DEA matrix. In the same way, cesium, which gives a low amount of solvated cationized molecular ions, has not been used.

Table I shows a pronounced decrease in the ratios a/b when DEA is used instead of glycerol. For example when talose is analyzed, this ratio decreases by a factor of 100. A similar effect has been observed with a disaccharide (trehalose) and has been explained in terms of matrix basicity (*10*). We observe a similar alkali cation effect with DEA to that described for glycerol. This corresponds to an increase in the ratio a/b as the alkaline radii increases. However, for allose, glucose, and talose, the ratio a/b remains almost constant.

From Table I a relative cationic affinity sequence for sodium may be established: talose > idose > mannose = altrose > galactose > allose = gulose = glucose. As previously described, when glycerol is used as matrix, this sequence is not drastically affected by the nature of the alkali cation used.

From an analytical point of view and for complete identification of the aldohexose stereoisomers, the DEA possesses a too high cationic affinity compared to glycerol as a matrix. Hence, when the aldohexose stereoisomers are solvated with glycerol and cationized with sodium, their identification becomes unambiguous.

## DISCUSSION

From these results, it may be observed that which ever alkali cation is used (Li$^+$, Na$^+$, K$^+$, Rb$^+$) or which ever matrix is employed, glycerol or DEA, the aldohexoses talose and idose possess the highest cationic affinities. The fact that the cation affinity sequence for the aldohexoses is not drastically affected by the nature of the matrix could suggest that the conformation of the aldohexose in the (aldohexose–cat–matrix)$^+$ cluster ion is not drastically modified in the presence of the matrix. Consequently, a structure in which the alkali cation is solvated by the aldohexose and the matrix seems more likely compared to the following structures (matrix–aldohexose–cat)$^+$. However a pseudocyclic structure (aldohexose–cat–matrix)$^+$ is also a possibility and may be examined by the used of additional matrices of basicity intermediate to that of glycerol and DEA.

It should be important to establish a correlation between the cyclic ring forms (furanose, pyranose), the configuration of the anomer carbon of the different aldohexoses, and their ability to retain the alkali cation. Their equilibrium is affected by the temperature and the solvent. Thus, it is difficult to transpose the values observed in the literature to those expected at the target surface which is not temperature controlled. For example at 40 °C, talose, idose, and altrose possess the highest proportion of the furanose form (*13*). For talose and idose if a correlation exists between the proportion of furanose and pyranose forms and the ability to retain the alkali cation, it may be difficult to validate since mannose exists entirely in the pyranose form and has a cationic affinity higher than altrose. A possible solution to this could be obtained by examination of the aldohexose methyl glycoside in which the hydroxyl group linked to the anomeric carbon atom has been methylated permitting the above equilibrium to be blocked.

It has been postulated by Angyal et al. (*14*) that the ability to form a complex between an alkali cation and cyclitol is correlated to the presence on an axial–equatorial–axial sequence of the vicinil hydroxyls; this sequence is observed for talose, mannose, and allose. From an examination of the ratios a/b given in Figure 2 and Table I, it is apparent talose agrees with the assumption postulated above by Angyal et al.; however idose does not agree.

## CONCLUSION

The present work shows the mass spectrometry applicabilities for the identification of stereoisomers of aldohexoses. These compounds have previously been identified after their derivatization by GC/MS. The proposed approach in which hexose derivatization is avoid allows the identification of the eight stereoisomers of aldohexose. Also, the versatility of this method authorized its application to the determination of anomeric configurations of, for example, methyl glycosides.

In a purely scientific sense, it seems important to define the parameters which control the cation affinity of an aldohexose. The correlation between aldohexose forms and their ability to retain the alkali cation is not yet established. The examination of simplified analogue models should permit defining the arrangement of the hydroxyl groups which might explain their different ability to retain the alkali cation.

**Registry No.** DEA, 111-42-2; Na, 7440-23-5; K, 7440-09-7; Rb, 7440-17-7; D-talose, 2595-98-4; D-idose, 5978-95-0; D-mannose, 3458-28-4; D-altrose, 1990-29-0; D-galactose, 59-23-4; D-gulose, 4205-23-6; D-glucose, 50-99-7; D-allose, 2595-97-3; glycerol, 56-81-5.

## LITERATURE CITED

(1) Radford, T.; Dejongh, D. C. "Biochemical Applications of Mass Spectrometry"; Waller, G. R., Dermer, O. C., Eds.; Wiley: New York, 1980; pp 255–305.
(2) Wood, G. W. *Mass Spectrom. Rev.* **1982**, *1*, 63–98.
(3) Rollgen, F. W.; Schulten, H. R. *Org. Mass Spectrom.* **1975**, *10*, 660–668.
(4) Prome, J. C.; Puzo, G. *Org. Mass Spectrom.* **1977**, *12*, 28–32.
(5) Deutsch, J. *Org. Mass Spectrom.* **1980**, *15*, 240–243.
(6) Rollgen, F. W.; Giessmann, U.; Borchers, F.; Levsen, K. *Org. Mass Spectrom.* **1978**, *13*, 459–461.
(7) Devienne, F. M; Diebold, A.; Roustan, J. C. 4ème Symposium International sur les Jets Moléculaires, 1973, Cannes.
(8) Barber, M.; Bordoli, R. S.; Sedwick, R. D.; Tyler, A. N. *J. Chem. Soc., Chem. Commun.* **1981**, 325.
(9) Dell, A.; Ballou, C. E. *Biomed. Mass Spectrom.* **1983**, *10*, 50–56.
(10) Puzo, G.; Prome, J. C. *Org. Mass Spectrom.*, in press.
(11) Puzo, G.; Prome, J. C. *Spectrosc. Int. J.*, in press.
(12) Cooks, R. G.; Kruger, T. L. *J. Am. Chem. Soc.* **1977**, *99*, 1279–1281.
(13) Ferrier, R. J.; Collins, P. M. "Monosaccharide Chemistry"; Williams Clowes: London, 1972.
(14) Angyal, J.; Hickman, J. *Aust. J. Chem.* **1975**, *28*, 1279–1287.

RECEIVED for review October 15, 1984. Accepted December 10, 1984.

*Anal. Chem.* 1985, *57*, 895-899

# Laser Desorption Mass Spectrometry of Nonvolatiles under Shock Wave Conditions

**Buko Lindner and Ulrich Seydel***

*Forschungsinstitut Borstel, Parkallee 1-40, D-2061 Borstel, Federal Republic of Germany*

**For transmission-type laser desorption mass spectrometers, as the commercially available laser microprobe mass analyzer LAMMA 500, it is shown that a suitable combination of sample thickness and laser power density allows the reproducible selection of a defined desorption/ionization mode. The irradiance of thick samples ($\approx$20 $\mu$m) at high laser power densities ($\approx10^{11}$ W cm$^{-2}$), which does not lead to a perforation, offers extremely soft ionization conditions. For these conditions a model is described for the desorption mechanism of molecules from organic solids based on a nonthermal, shock wave driven process leading to the release of mainly intact molecules from the solid sample surface.**

Very soon after the laser had become available, the possibility of focusing its radiation to very small spot sizes and of achieving high power densities in short time intervals—yielding rapid heating of small sample volumes—called forth the interest of mass spectroscopists to use it as an desorption/ionization source. In the past 20 years, and with increasing tendency in the last 5 years, a large number of examples for the applicability of the laser desorption mass spectrometry LDMS—especially for the analysis of organic compounds—have been published (for review see ref 1 and 2). Mainly the construction of a modified laser focusing system by Hillenkamp et al. (*3*) brought considerable progress to the development of a laser microprobe mass analyzer, which became commercially available as LAMMA 500 (Leybold-Heraeus, Köln, FRG). Very soon the wide scope of this system—ranging from the sensitive tracing of elements and even organic molecules in biological specimens to the pure mass spectrometric application for the analysis of complex biomolecules—could be demonstrated in a large number of excellent papers (for review see ref 4 and 5). Considering the relatively long history of LDMS, it seems striking that there exists no unified model which would explain satisfactorily the physical processes leading to the desorption of intact molecules and fragments—or ions thereof—and with that of the structure of the mass spectra obtained from these particles.

However, considering the diversity of instrumentation and experimental design meanwhile used in laser desorption mass spectrometry ranging in laser wavelengths from 249 nm to 10.6 $\mu$m, in laser power density from 20 to $10^{12}$ W cm$^{-2}$, and in laser spot diameter at the sample surface from less than 1 $\mu$m to 4 mm (for review see Hillenkamp (*6*), the described situation becomes understandable, especially when taking furthermore into account the different laser–sample–detector geometries (transmission- and reflectance-type instruments). Even with the same instrument, the variation of just one parameter like the irradiance or the sample thickness may require different models for the description of the steps involved in ion formation, as will be discussed below. A question of major concern is whether the desorption process requires high temperatures at the sample surface or not. In other words, does the mechanism proceed thermally, that means here under direct influence of the temperature in the desorption region, or may other nonthermal mechanisms also lead to desorption.

But keeping in mind the above outlined situation concerning the diversity of instrumentation and sample handling, it is not to be expected that there will by the one model describing all experimental conditions. Kistemaker (*7–10*), Röllgen (*11*, *12*), Cotter (*13–17*), and Heresch (*18*) favor a thermal mode for their experimental conditions: sample on bulk substrates and irradiation with moderately focused laser beams at moderate laser power densities at the sample side. However, as is pointed out in some cases (*11*, *18*, *19*), thermal processes cannot explain sufficiently all observed phenomena. Hillenkamp distinguishes between two different processes occurring with different sample geometries (*20*). For bulk solids, examined in a way described above, he assumes a thermal mechanism. For thin films analyzed in a transmission-type instrument he suggests nonequilibrium processes. This might be backed by the measured energy spreads of the produced ions of up to 50 eV (*21*). Comparable values (up to 25 eV) have also been reported by Hardin and Vestal (*22*). Hercules proposed several processes occurring concurrently at different distances from the laser spot (*5*). We suggested a nonthermal shock-wave driven desorption process (*23*, *24*) to explain our findings that for a transmission-type instrument best results with respect to simplicity and reproducibility of spectra from complex organic compounds could be obtained at highest available laser power density ($\approx10^{11}$ W cm$^{-2}$) and relatively thick samples ($\approx$20 $\mu$m) not being perforated by the laser beam.

In this paper we try to corroborate these first findings experimentally. For this purpose we used various oligosaccharide samples to get information on the thermal stress exerted on the desorbed molecules. Oligosaccharides are known to be thermally labile—stachyose more than raffinose and sucrose—and have been used repeatedly for similar applications (*7–12*, *18*, *25*). We found direct evidence for the existence of at least two different desorption modes, thermal and nonthermal, depending on laser power density and sample thickness, which may even coexist under particular conditions. The successful application of the described soft desorption/ionization conditions is demonstrated for some oligo/polysaccharides containing up to 12 sugar units.

## EXPERIMENTAL SECTION

**Laser Desorption Mass Spectrometer.** The instrument used was the transmission-type laser microprobe mass analyzer LAMMA 500 (Leybold-Heraeus, Köln, FRG). The frequency quadrupled light of a Q-switched Nd-YAG laser (wavelength, 265 nm; pulse duration, 10 ns) is focused onto the front surface of the solid sample with a spot diameter down to approximately 1 $\mu$m at maximal power densities of $10^{11}$ W cm$^{-2}$ (adjustable over 3 orders of magnitude by neutral filters and laser amplifier setting). The ions produced on the opposite side (rear surface) of the freely suspended sample are registered by a TOF mass analyzer. The signals from the ion detector (SEM) were digitized by a Biomation 8100 transient recorder at a sampling time of 50 ns and transferred to a HP 1000 computer. A schematic of the experimental setup is given in Figure 1.

**Samples.** Sucrose, raffinose, stachyose, and $\gamma$-cyclodextrin were purchased from Sigma Chemicals (München, FRG), the

0003-2700/85/0357-0895$01.50/0 © 1985 American Chemical Society

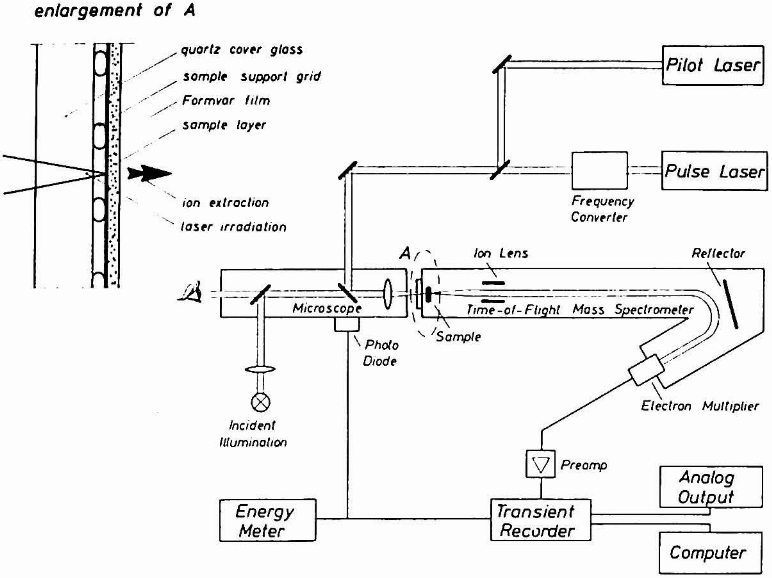
enlargement of A
quartz cover glass
sample support grid
Formvar film
sample layer
ion extraction
laser irradiation
Pilot Laser
Pulse Laser
Frequency Converter
A
Ion Lens
Reflector
Microscope
Time-of-Flight Mass Spectrometer
Sample
Photo Diode
Electron Multiplier
Incident Illumination
Preamp
Analog Output
Energy Meter
Transient Recorder
Computer

**Figure 1.** Schematic of the LAMMA 500 instrument.

highly purified octa- and dodecasaccharides isolated from bacteria (*Shigella flexneri*) (*26*) were a generous gift from A. Lindberg (University Hospital, Huddinge, Sweden).

Samples were prepared from aqueous solutions containing the sugar and NaI or KI at a molar ratio of approximately 5:1. Different amounts of these solutions were brought onto Formvar-coated copper grids (mesh width 100 $\mu$m) and dried to give thin layers homogeneous in thickness and consistency over the distance of several meshes. This way layers of different thickness could be achieved. The so prepared samples were mounted inside the TOF analyzer with the supporting grid facing the laser (see Figure 1, inlay).

**Measurements.** From sucrose, raffinose, and stachyose, layers of thicknesses $d_1 \approx 1$ $\mu$m and $d_2 \approx 20$ $\mu$m were mass analyzed at the laser irradiances of $p_1 \approx 10^8$ W cm$^{-2}$ and $p_2 \approx 10^{11}$ W cm$^{-2}$ (32× objective, diameter of the spot of direct laser–sample interaction $\approx 3$ $\mu$m). To account for the limited reproducibility of the fragmentation patterns (mainly caused by variations in laser performance and focusing) as well as of total ion intensities of the spectra produced by each single laser pulse, 25 single spectra were registered and averaged for each combination of sample thickness and laser power density. With the sampling time of 50 ns the quasi-molecular peaks could only be registered if a suitable delay time was chosen. For this reason the spectra do not comprise the low mass region, which in each case showed mainly high cation signals.

## RESULTS AND DISCUSSION

Figure 2 gives the averaged positive ion LD mass spectra of stachyose obtained under different experimental conditions. Clearly, under the aspect of getting low-level fragment intensity, i.e., the "softest" desorption/ionization, the most favorable conditions are realized in spectrum 2a obtained from a thick sample layer at highest laser power density and without perforating the sample. The spectrum comprises only the abundant quasi-molecular peak $[M + Na]^+$ at $m/z$ 689 and one low-intensity fragment peak $C_{18}H_{32}O_{16}Na^+$ at $m/z$ 527, originating from unimolecular decomposition by cleavage of a glycosidic bond and hydrogen transfer. It should be pointed out that similar spectra were observed under these conditions also when the laser beam was focused onto the supporting Cu grid, resulting in an indirect energy input.

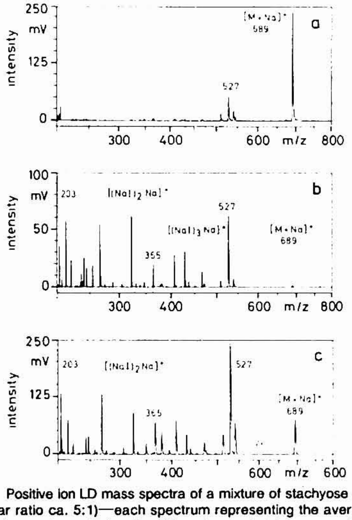

**Figure 2.** Positive ion LD mass spectra of a mixture of stachyose and NaI (molar ratio ca. 5:1)—each spectrum representing the average of 25 single spectra—obtained for different sample thicknesses *d* and laser power densities *p*: (a) $d \approx 20$ $\mu$m, $p \approx 10^{11}$ W cm$^{-2}$, no perforation of sample; (b) $d \approx 1$ $\mu$m, $p \approx 10^8$ W cm$^{-2}$, perforation of sample; (c) $d \approx 1$ $\mu$m, $p \approx 10^{11}$ W cm$^{-2}$, perforation of sample.

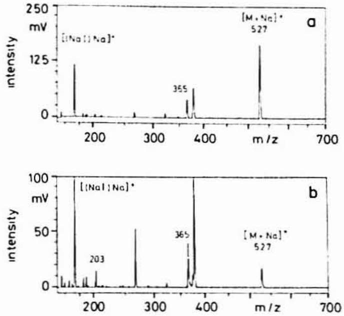

**Figure 3.** Positive ion LD mass spectra of a mixture of raffinose and NaI (molar ratio ca. 5:1)—each spectrum representing the average of 25 single spectra—obtained for different sample thicknesses $d$ and laser power densities $p$: (a) $d \approx 20$ μm, $p \approx 10^{11}$ W cm$^{-2}$, no perforation of sample; (b) $d \approx 1$ μm, $p \approx 10^{8}$ W cm$^{-2}$, perforation of sample.

Spectrum 2b demonstrates the other extreme—low laser power density and a thin sample layer—showing a high level of fragmentation with peaks at $m/z$ 527 ($C_{18}H_{32}O_{16}Na^+$), $m/z$ 365 ($C_{12}H_{22}O_{11}Na^+$), and $m/z$ 203 ($C_6H_{12}O_6Na^+$), which again stem from glycosidic bond ruptures. The quasi-molecular peak, in this case, is reduced nearly to zero intensity, and additional fragment peaks can be observed beside intensive NaI-cluster peaks.

Spectrum 2c (Figure 2c) resembles the pattern of spectrum 2b in respect to the intensive fragments at $m/z$ 203, 365, and 527 and the NaI cluster peaks. However, the intensity of the quasi-molecular peak at $m/z$ 689 is higher. This spectrum seems to represent an overlap of the physical processes responsible for the patterns shown in Figure 2a,b. The application of low laser power density to thick sample layers did not lead to a detectable ion yield. Only in some cases weak cation signals were registered.

A similar influence of the experimental conditions on the fragmentation patterns as described for stachyose were observed also for raffinose and sucrose (Figure 3, Figure4). Beside the fragment ion peak at $m/z$ 365 both spectra of raffinose (Figure 3) exhibit additional intense mass peaks at $m/z$ 379 which could be shown to originate from ion formation by alkali attachment. (The admixture of CsI instead of NaI led to a corresponding shift of these peaks by 110 mass units). Presently we cannot offer a verified explanation of the underlying ion building processes. This is particularly difficult because impurities of the raffinose could be definitely excluded (applying extensive chemical analytical techniques), and for the other sugars respective peaks—if at all—were observed only at negligible intensities. The obviously little influence of the experimental conditions on the patterns of the sucrose spectra (Figure 4)—even for a thin sample excited by low laser irradiance (Figure 4b) an intense quasi-molecular peak is observed—may be explained by the comparably high thermal stability.

Figure 5 shows the average of 45 positive ion LD mass spectra of γ-cyclodextrin obtained under the same experimental conditions as those in Figures 2a, 3a, and 4a. This spectrum does not comprise any fragment ion peaks.

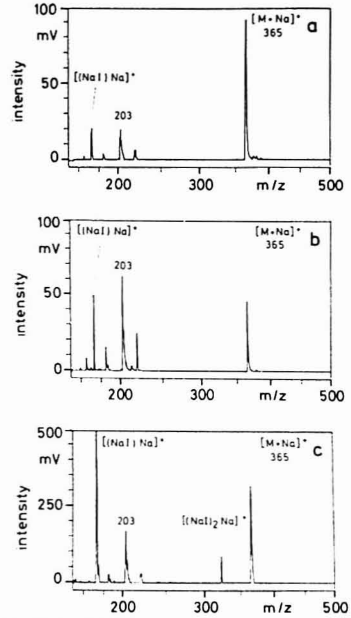

**Figure 4.** Positive ion LD mass spectra of a mixture of sucrose and NaI (molar ratio ca. 5:1)—each spectrum representing the average of 25 single spectra—obtained for different sample thicknesses $d$ and laser power densities, $p$: (a) $d \approx 20$ μm, $p \approx 10^{11}$ W cm$^{-2}$, no perforation of sample; (b) $d \approx 1$ μm, $p \approx 10^{8}$ W cm$^{-2}$, perforation of sample; (c) $d \approx 1$ μm, $p \approx 10^{11}$ W cm$^{-2}$, perforation of sample.

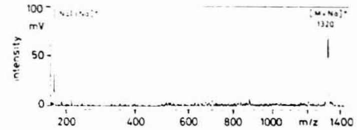

**Figure 5.** Positive ion LD mass spectrum of a mixture of γ-cyclodextrin and NaI (molar ratio ca. 5:1), representing the average of 45 single spectra (sample thickness $d \approx 20$ μm, laser power density $p \approx 10^{11}$ W cm$^{-2}$, no perforation of sample).

If spectra of thermally labile substances like the investigated sugar do not exhibit considerable fragmentation, a direct influence of temperature can be excluded. This holds for the spectra depicted in Figures 2a, 3a, and 4a which were obtained from thick sample layers irradiated at the highest laser power density without producing perforations. The desorption/ionization must proceed at a locus spatially separated from the locus of direct laser–sample interaction. Since there is experimental and theoretical evidence that the impact of a laser beam as used in our experiments on a solid sample leads to a temperature rise of up to some thousand degrees at the surface within the laser pulse duration (*8, 27–30*), yielding heating rates of approximately $10^{11}$ K s$^{-1}$ for a laser pulse width of 10 ns. A direct influence of this high temperature would inevitably lead to drastic fragmentation. In other words, the desorption process as depicted in Figures 2a, 3a, and 4a must be nonthermal. We have therefore postulated a process triggered by a laser-driven shock wave (*23, 24*). The high heating rate of $\approx 10^{11}$ K s$^{-1}$ within the thin surface layer of direct laser–sample interaction well exceeds the limit of approximately $10^9$ K s$^{-1}$ above which an explosive vaporization ("phase explosion") should occur (*31*), which may be accompanied by plasma generation. This thermal ablation produces a shock wave which traverses the solid under energy dissi-

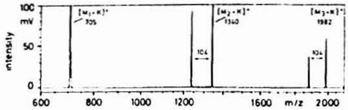

**Figure 6.** Positive ion LD mass spectrum of a mixture of approximately equal molar amounts of stachyose $M_1$, an octasaccharide $M_2$, and a dodecasaccharide $M_3$ (both isolated from the bacterial species *Shigella flexneri* (*30*) and of KI (sample thickness $d \approx 20$ μm, laser power density $p \approx 10^{11}$ W cm$^{-2}$, no perforation of sample).

pation. The principles of the thermodynamics governing this vaporization are described in detail for metals in ref 32. It must be emphasized, however, that quantitative calculations for the organic substances under investigation can hardly be done at present because of the lack of thermophysical data. At the rear surface the shock wave leads to the desorption of intact molecules (and possibly fragments) and of alkali ions via vibrational disturbance of the binding potentials. The latter stem from impurities or from alkali salts added to enhance the quasi-molecular ion yield. In experiments with relatively thick metal foils and organic layers ($d \approx 30$ μm) which were covered on the back side with alkali salts, it could be shown that the shock wave mode also leads to the desorption of alkali ions from a solid, not perforated sample. Gas-phase reactions between the neutral molecules and the codesorbed alkali ions should lead to the formation of these quasi-molecular ions (*18, 33–35*).

In contrast to the spectra produced by shock-wave-driven non-thermal desorption, the patterns of the spectra in Figures 2b, 3b, and 4b, which were obtained from thin samples with the laser beam perforating the layer at low irradiance, show considerable fragmentation. A possible explanation for this fragmentation is the thermal stress which is exerted on the molecules being desorbed at the locus of direct laser–sample interaction. However, other processes like fast collisional dissociation, which might put additional stress on the molecules (*36*), cannot be fully excluded.

The spectra described so far represent the extremes in the experimental conditions: thick sample layers, high laser power density and thin sample layers low laser power density, respectively. A combination of these parameters (thin sample layer, high laser power density) obviously leads to patterns comprising features of both extremes (Figure 2c). From this it may be concluded that under such conditions a combination of the above described desorption modes may occur with varying contributions to the overall ion yield. It seems reasonable to assume that the two processes occur within the same time scale but are laterally separated.

The shock-wave-driven desorption mode from organic solids is favorable, especially for molecular weight determination. This is clearly demonstrated with γ-cyclodextrin in Figure 5, which does not show any fragmentation in contrast to the results of Cotter who observed a sequence of fragmentation peaks (*37*)—besides the quasi-molecular peak—under his bulk analysis conditions. Such a high degree of fragmentation was not obtained in our experiments even under the conditions of high thermal stress.

Another example for this application is given in Figure 6. Here, estimations of the molecular weight, based on biochemical data, of a dodecasaccharide isolated from a bacterial species (*S. flexneri*) were to be confirmed. For internal mass scale calibration the unknown compound was mixed with approximately equal molar amounts of stachyose and an octasaccharide of *S. flexneri* of already known structure and with KI. The spectrum shows a very simple pattern with intense quasi-molecular ion peaks of the three sugars at $m/z$ 705, 1340, and 1982 and two peaks each 104 mass units lower than the respective quasi-molecular ions also showing alkali attachment. At the moment it cannot be decided whether these peaks are due to laser-induced fragmentation or, more likely, originate from the chemical pretreatment.

After statements of Denoyer et al. (*4*) Heinen (*19*), Cotter (*37*), and Simons (*38*), soft desorption/ionization should be achieved for organic solids from thin samples under as low a laser irradiance as possible for observation of ions. The above examples, however, may serve as an experimental proof that under the controlled conditions of high laser power density and thick homogeneous sample layers in a transition geometry a very soft desorption/ionization is realized.

## ACKNOWLEDGMENT

We thank F. W. Röllgen, University of Bonn, FRG, for many stimulating and fruitful discussions. We also gratefully acknowledge the skillful technical assistance of H. Lüthje.

**Registry No.** NaI, 7681-82-5; KI, 7681-11-0; stachyose, 470-55-3; raffinose, 512-69-6; sucrose, 57-50-1; γ-cyclodextrin, 17465-86-0.

## LITERATURE CITED

(1) Conzemius, R. J.; Capellen, J. M. *Int. J. Mass Spectrom. Ion Phys*. **1980**, *34*, 197.
(2) Conzemius, R. J.; Simons, D. S.; Byrd, G. D. "Microbeam Analysis"; Gooley, R., Ed.; San Francisco Press: San Francisco, CA, 1983; p 301.
(3) Hillenkamp, F.; Kaufman, R.; Nitsche, R.; Unsöld, E. *Appl. Phys*. **1975**, *8*, 381.
(4) Denoyer, E.; Van Grieken, R.; Adams, F.; Natusch, D. F. S. *Anal. Chem*. **1982**, *54*, 26.
(5) Hercules, D. M.; Day, R. J.; Balasanumgam, K.; Dang, P. A.; Li, C._P. *Anal. Chem*. *1982*, *54*, 280.
(6) Hillenkamp, F. "Ion Formation from Organic Solids"; Benninghoven, A., Ed.; Springer-Verlag: Berlin, Heidelberg, New York, Tokyo, 1983; Springer Series in Chemical Physics, Vol. 25, p 190.
(7) Kistemaker, P. G.; van der Peyl, G. J. Q.; Haverkamp, J. "Soft Ionization Biological Mass Spectrometry"; Morris, H. R., Ed.; Heyden & Son: London, Philadelphia, Rheine, 1981; p 120.
(8) Van der Peyl, G. J. Q.; Haverkamp, J.; Kistemaker, P. G. *Int. J. Mass Spectrom. Ion Phys*. **1982**, *42*, 125.
(9) Van der Peyl, G. J. Q.; Isa, K. Haverkamp, J.; Kistemaker, P. G. *Int. J. Mass Spectrom. Ion Phys*. **1983**, *47*, 11.
(10) Van der Peyl, G. J. Q.; van der Zonde, W. J.; Bederski, K.; Boerboom, A. J. H.; Kistemaker, P. G. *Int. J. Mass Spectrom. Ion Phys*. *1983*, *47*, 7.
(11) Stoll, R.; Röllgen, F. W. *Org. Mass Spectrom*. **1979**, *14*, 642.
(12) Stoll, R.; Röllgen, F. W. *Org. Mass Spectrom*. **1981**, *16*, 72.
(13) Cotter, R. J. *Anal. Chem*. **1980**, *52*, 1767.
(14) Cotter, R. J. *Anal. Chem*. **1981**, *53*, 719.
(15) Van Breemen, R. B.; Snow, M.; Cotter, R. J. *Int. J. Mass Spectrom. Ion Phys*. **1983**, *49*, 35.
(16) Cotter, R. J; Tabet, J.-C. *Int. J. Mass Spectrom. Ion Phys*. **1983**, *53*, 151.
(17) Tabet, J.-C.; Cotter, R. J. *Anal. Chem*. **1984**, *56*, 1662.
(18) Heresch, F. "Ion Formation from Organic Solids"; Benninghoven, A., Ed.; Springer-Verlag: Berlin, Heidelberg, New York, Tokyo, 1983; Spinger Series in Chemical Physics, Vol. 25, p 217.
(19) Heinen, H. J. *Int. J. Mass Spectrom. Ion Phys*. **1981**, *38*, 309.
(20) Hillenkamp, F. *Int. J. mass Spectrom. Ion Phys*. **1983**, *45*, 305.
(21) Nitsche, R.; Kaufmann, R.; Hillenkamp, F.; Unsöld, E; Vogt, H.; Wechsung, R. *Isr. J. Chem*. **1978**, *17*, 181.
(22) Hardin, E. D.; Vestal, M. L. *Anal. Chem*. **1981**, *53*, 1492.
(23) Seydel, U.; Lindner, B. "Ion Formation from Organic Solids"; Benninghoven, A., Ed.; Springer-Verlag: Berlin, Heidelberg, New York, Tokyo, 1983; Springer Series in Chemical Physics, Vol. 25, p 240.
(24) Lindner, B.; Seydel, U. "Secondary Ion Mass Spectrometry"; Benninghoven, A., et al., Eds.; Spinger-Verlag: Berlin, Heidelberg, New York, Tokyo, 1984; Springer Series in Chemical Physics, Vol. 36, p 370.
(25) Heinen, H. J.; Meier, S.; Vogt, H.; Wechsung, R. *Adv. Mass Spectrom*. **1980**, *8*, 342.
(26) Carlin, N. I. A.; Lindberg, A. A.; Bock, K.; Bundle, D. R. *Eur. J. Biochem*. **1984**, *139*, 189.
(27) Ready, J. F. "Effects of High Power Irradiation"; Academic Press: New York, 1971.
(28) Burns, A. R. *Soc. Photo-Opt. Instrum. Eng. Proc*. **1983**, *380*, 224.
(29) Magill, J.; Bloem, J.; Ohse, R. W. *J. Chem. Phys*. **1982**, *76*, 622.
(30) Cotter, R. J.; Tabet, J.-C. *Am. Biotechnol. Lab*. **1984**, March, 10.
(31) Martynyuk, M. M. *Sov. Phys.—Tech. Phys*. (*Engl. Transl*.) **1976**, *21*, 430.
(32) Seydel, U.; Fucke, F.; Wadle, H. "Bestimmung thermophysikalischer Daten flüssiger hochschmelzender Metalle mit schnellen Pulsaufheizexperimenten"; Verlag P. Mannhold: Düsseldorf, 1980.
(33) Van der Peyl, G. J. Q.; Isa, K.; Haverkamp, J.; Kistemaker, P. G. *Nucl. Instrum. Methods* **1982**, *198*, 125.
(34) Stoll, R.; Röllgen, F. W. *Z. Naturforsch*. **1982**, *37A*, 9.
(35) Cotter, R. J.; Snow, M.; Colvin, M. "Ion Formation from Organic Solids"; Benninghoven, A., Ed.; Springer-Verlag: Berlin, Heidelberg,

New York, Tokyo, 1983; Springer Series in Chemical Physics, Vol. 25, p 206.
(36) Röllgen, F. W., private communication and Proceedings of the 2nd LAMMA Workshop, D-2061 Borstel, FRG, 1983, p 57.
(37) Cotter, R. J. *Anal. Chem.* **1984**, *56*, 485.
(38) Simons, D. S. "Ion Formation from Organic Solids"; Benninghoven, A., Ed.; Springer-Verlag: Berlin, Heidelberg, New York, Tokyo, 1983; Springer Series in Chemical Physics, Vol. 25, p 158.

RECEIVED for review September 17, 1984. Accepted December 20, 1984.

---

# Reliability Ranking and Scaling Improvements to the Probability Based Matching System for Unknown Mass Spectra

**Barbara L. Atwater, Douglas B. Stauffer, and Fred W. McLafferty***
*Chemistry Department, Cornell University, Ithaca, New York 14853*

**David W. Peterson**
*Scientific Instrument Division, Hewlett-Packard, 1501 California Avenue, Palo Alto, California 94304*

**Statistical evaluations of the effects of five matching parameters on the probability of retrieving a correct answer with the probability based matching (PBM) system have been made. Combining the resulting values found in matching an unknown spectrum makes it possible to rank retrieved reference spectra according to the predicted match reliability. This ranking substantially improves the performance of PBM, and the reliability value is especially helpful in avoiding the assumption that the best matching spectrum represents the correct compound when its spectrum is actually not in the reference file. Quadratic scaling of the abundance values of the unknown compensates for spectral differences caused by instrumental variations, a critical problem in matching reference spectra. Other improvements include a more effective "flagging" technique to remove spurious reference peaks. Extensive applications with a commercial GC/MS system have demonstrated the increased effectiveness made possible by these PBM modifications.**

Thousands of gas chromatograph/mass spectrometers (GC/MS) are now used daily worldwide (*1*). A major application is the identification of unknown compounds, which in many laboratories results in the production of hundreds of unknown mass spectra per day, making obvious the need for computerized identification systems (*2–16*). For samples representing complex mixtures, incomplete GC separation is unavoidable (*17, 18*); for the resulting spectra which represent more than one component reverse searching (only requiring the peaks of the reference to be in the unknown) improves retrieval performance (*4–7*). By far the most widely used retrieval algorithm of this type appears to be probability based matching (PBM) (*4, 7*). Although other search systems (*3, 10–12*) are valuable, when evaluated under various conditions (*7, 10, 12*) none appears clearly superior to PBM. In the last decade PBM has been used extensively by individual implementation (*16*), through computer networks (Cornell Computer Services, Uris Hall, Ithaca, NY 14853) (*19*), and on a commercial GC/MS systems, resulting in a variety of helpful criticisms.

A major problem to many users, which appears to be common to all retrieval algorithms, is that the match ranking factors such as the "similarity index" (*3*) or "confidence (*K*) value" (*4, 7*) give only a qualitative indication of the probability that the retrieved compound represents a correct answer. For example, although a *K* value of 150 implies a higher match confidence than a value of 100, it does not directly indicate whether the probability of a correct identification is 50% or 95%. This deficiency can cause a particularly serious problem when the unknown compound is not represented in the reference file, as almost always the algorithm retrieves a "best", even though a poor, match. We show here that the effect of a variety of matching indicators can be evaluated statistically, so that a combination of these can serve as a *quantitative* measure of the predicted reliability of the match.

A second serious problem for mass spectral matching systems utilizing a comprehensive reference file is the variation in peak abundances caused by mass discrimination and change in sample concentration during the spectrum scan. As suggested independently by Dromey (*8*), various methods of tilting and scaling the unknown spectrum to compensate for such spectral differences are investigated here. The PBM algorithm has also been modified to improve the "peak flagging" which discards anomalous peaks in the reference spectrum.

## EXPERIMENTAL SECTION

Computers used include a DEC PDP-11/45 containing 56 kilobyte memory and 64 megabyte random-access disk storage, an IBM 370/168 multiuser system, and the H/P-1000 computer of the H/P 5985 GC/MS system. The data base was the expanded Registry of Mass Spectral Data (Electronic Data Div., Wiley, 605 Third Ave., New York, NY 10158) containing 41 429 different spectra of 32 403 different compounds, from which 2091 isotopically labeled spectra were excluded. From those compounds in the file represented by more than one spectrum (measured under other experimental conditions) 900 were selected at random, with the restriction that all spectra of the compound must have a quality index (QI) ≥ 0.5 (*20*). For each of these compounds the spectrum of highest QI value was used to make up the list of unknown spectra, which were excluded from the data base in testing. Every odd-numbered spectrum of this list was used to make up a second "odd" list of 450. The performances of these two lists and of the PBM program versions were evaluated by using recall/reliability plots (*21, 22*), which show the proportion of correct answers which are retrieved as a function of the proportion of retrieved answers which are correct. For the "odd" list poor PBM retrievals were used to correct obvious errors and delete

0003-2700/85/0357-0899$01.50/0 © 1985 American Chemical Society

**Table I. Predicted Reliability Values (%) for *K* Categories**

| | molecular ion present | | | | molecular ion absent | | | |
|---|---|---|---|---|---|---|---|---|
| *K* | 0 flags | 1 flag | 2 flags | 3 flags | 0 flags | 1 flag | 2 flags | 3 flags |
| 150 | 99.5 | 99.4 | 98.7 | 96.7 | 95.0 | 94.5 | 89.5 | 81.0 |
| 140 | 99.3 | 99.0 | 97.8 | 95.9 | 94.0 | 92.0 | 84.3 | 76.5 |
| 130 | 99.0 | 98.5 | 96.4 | 94.0 | 92.0 | 87.5 | 77.8 | 70.5 |
| 120 | 98.7 | 97.8 | 94.3 | 90.0 | 89.5 | 84.3 | 72.0 | 56.3 |
| 110 | 98.2 | 96.6 | 91.5 | 83.5 | 86.5 | 79.8 | 62.0 | 40.5 |
| 100 | 97.5 | 94.5 | 86.3 | 76.5 | 83.0 | 68.5 | 40.5 | 30.0 |
| 90 | 96.4 | 91.5 | 80.5 | 69.5 | 77.8 | 62.0 | 37.0 | 27.7 |
| 80 | 94.3 | 86.3 | 74.0 | 59.3 | 72.0 | 45.8 | 30.7 | 23.3 |
| 70 | 91.0 | 80.5 | 64.8 | 49.0 | 45.5 | 33.0 | 22.7 | 18.7 |
| 60 | 83.0 | 69.5 | 50.3 | 37.5 | 40.0 | 27.7 | 20.3 | 17.3 |
| 50 | 73.0 | 44.3 | 33.5 | 22.0 | 30.3 | 18.5 | 16.5 | 13.0 |
| 40 | 54.0 | 22.0 | 19.3 | 15.5 | 21.3 | 13.5 | 12.0 | 9.0 |
| 30 | 21.0 | 15.5 | 14.0 | 12.3 | 16.0 | 9.0 | 8.3 | 6.0 |
| 20 | 14.0 | 12.3 | 11.0 | 9.5 | 8.3 | 6.0 | 5.0 | 4.3 |

**Table II. Predicted Reliability Values (%) for $\Delta K$ Categories**

| | molecular ion present | | | | molecular ion absent | | | |
|---|---|---|---|---|---|---|---|---|
| $\Delta K$ | 0 flags | 1 flag | 2 flags | 3 flags | 0 flags | 1 flag | 2 flags | 3 flags |
| 0 | 97.5 | 97.0 | 94.5 | 91.0 | 91.0 | 89.5 | 80.7 | 75.0 |
| 10 | 96.5 | 85.8 | 91.0 | 87.0 | 88.7 | 85.3 | 75.0 | 68.7 |
| 20 | 91.0 | 83.8 | 76.3 | 70.7 | 75.0 | 64.3 | 56.0 | 50.0 |
| 30 | 78.7 | 68.5 | 62.3 | 55.3 | 59.5 | 45.7 | 38.3 | 32.0 |
| 40 | 68.5 | 52.0 | 48.0 | 32.7 | 47.3 | 29.7 | 26.8 | 19.7 |
| 50 | 58.0 | 40.3 | 32.3 | 24.3 | 34.5 | 23.0 | 19.5 | 15.0 |
| ≥60 | 45.0 | 30.5 | 24.3 | 21.3 | 25.5 | 18.7 | 15.0 | 11.5 |

the worst spectra; the final set contained 431 unknown spectra. The matches were classified (*7*) as: (a) the identical compound or a stereoisomer, designated as "class I", and (b) a compound which should give a very similar mass spectrum because its structure is closely related to that of the unknown ("class IV"). From these compounds were selected the 392 unknowns for the current Wiley/NBS file of 80 000 spectra; the list of unknowns and their class IV matches and mismatches is available from Cornell for comparative evaluations.

The basic PBM matching algorithm (*7*) was modified with tighter window tolerances, using ±37% and ±20% for peaks of <9% and ≥9% abundance, respectively. To reduce the number of low abundance artifact peaks used in the condensed spectrum, the molecular ion isotopic peak of highest mass previously included was removed and peaks of a specific value of $U + A$ (log base 2 "uniqueness" and "abundance" values) (*7*) having abundances <1% were chosen after higher abundance peaks. The correlation (*20*) between the number of atoms in a molecule ($N$) and the number of peaks in its mass spectrum was tried to determine the number of peaks ($p$) in the condensed spectrum (*13*); neither $p = N/3 + 5$ nor $N/2 + 5$ showed any improvement over the original method (*7*).

**Abundance Based Flagging.** For the reference peak of mass $j$ of the condensed reference spectrum, the rho value $\rho_j$ is the ratio of the abundance of that peak in the unknown to its abundance in the reference. The first PBM calculation of the confidence ($K_1$) value uses the abundance window based on the minimum rho ($\rho_{\min}$) value (*7*). The second, third, and fourth confidence values ($K_2$, $K_3$, $K_4$) are calculated by using as $\rho_{\min}$ the lowest $\rho_j$ value of any peak for which the unknown has an abundance of ≥1% for $K_2$, ≥9% for $K_3$, and ≥38% for $K_4$ (*13*). Replacing this, now for the $K_2$–$K_4$ calculations the new $\rho$ value must be incremented by a minimum amount. If $\rho < 0.65$, the new $\rho$ must be >50% (relative) larger; if $\rho \geq 0.65$, the new $\rho$ must be 0.15 (absolute) larger.

**Spectrum Tilting and Scaling.** If a reference spectrum matches with $K \geq 10$, the abundances of the unknown are adjusted by "tilting" or "scaling" (recommended), and the resulting spectrum is rematched against the reference. "Tilt" is a geometrical skewing function $2^{n\Delta m/200}$, for which $n$ can have positive or negative values from 1 through 4 and $\Delta m$ is the mass difference between the peak in question and the peak of lowest mass in the unknown spectrum. Thus for $n = +1$ the abundance for $\Delta m = 50$ would be multiplied by $2^{0.25}$, or 1.19.

"Scaling" optimizes the matching of peak abundances by adjusting those of the reference spectrum as a function of mass with a quadratic polynominal to minimize the sum-of-squares difference $D$ between them and the corresponding abundances of the unknown (eq 1), where $X_i$ and $R_i$ are the abundances of the $i$th peaks

$$D = \sum_i [X_i - (a + bm_i + cm_i^2)R_i]^2 \tag{1}$$

common to the unknown and reference spectra, respectively, and $m$ is the $m/z$ value. To minimize $D$ ($\partial D/\partial a = \partial D/\partial b = \partial D/\partial c = 0$), eq 1 yields the linear system of eq 2, which is solved by

$$\begin{bmatrix} \sum_i m_i^2 R_i^2 & \sum_i m_i^3 R_i^2 & \sum_i m_i^4 R_i^2 \\ \sum_i m_i R_i^2 & \sum_i m_i^2 R_i^2 & \sum_i m_i^3 R_i^2 \\ \sum_i R_i^2 & \sum_i m_i R_i^2 & \sum_i m_i^2 R_i^2 \end{bmatrix} \begin{bmatrix} a \\ b \\ c \end{bmatrix} = \begin{bmatrix} \sum_i m_i^2 X_i R_i \\ \sum_i m_i X_i R_i \\ \sum_i X_i R_i \end{bmatrix} \tag{2}$$

Gaussian elimination. To minimize the effect of contamination of a peak by another component of the unknown, each reference is scaled 5 times. On the $n$th scaling the $n - 1$ peaks of highest contamination, as previously defined (*7*), are not used in computing $a$, $b$, and $c$. In addition, the first flagged peak (if any) of the nonscaled match is ignored for $n = 1$–$4$ and the first two for $n = 5$ (however, the abundances of such contaminated or flagged peaks are still scaled for matching). Scaling is limited to reference spectra matching with a predicted reliability value (vide infra) of ≥15% (also >30% of the fifth highest reliability value already retrieved); for further scaling, the first must have increased the predicted reliability by >10% absolute.

**Reliability Ranking.** The algorithm was modified to predict the probability that a retrieved reference is a correct match. This reliability value, RL, is dependent on the values of $K$, $\Delta K$ (the difference between the $K$ value for a perfect match with the unknown and the $K$ value found), number of peak flagging operations (0–3), whether the reference molecular ion was or was not used in matching, and the tilt ($n$) factor. The collective effect of these separate values on RL using the class IV definition was determined statistically (*13*) with the 431 unknowns (Tables I and II). For example, a smoothed plot of reliability vs. $K$ value showed 9.2% of matches with $K = 98$–$102$ and zero flags to be incorrect, while matches of $K = 98$–$102$ with no molecular ion were

Table III. Adjustments (%) Made to Predicted Reliability Values of Scaled Spectra

| $S^a$ | | $V^b$ | | $m_0{}^c$ | $RL_{40}$ | $RL_{80}$ | std dev | no. of spectra |
|---|---|---|---|---|---|---|---|---|
| without scaling | | | | | 29.0 | 67.5 | 6.1 | 1376 |
| 0 | 1.0 | $1.5 \times 10^{-3}$ | 0.22 | all | 42.7 | 66.3 | 7.7 | 479 |
| 0 | 1.0 | $5.5 \times 10^{-4}$ | $1.5 \times 10^{-3}$ | all | 34.2 | 58.3 | 5.1 | 565 |
| −150 | <0 | $1.5 \times 10^{-3}$ | 0.22 | all | 25.5 | 55.0 | 2.7 | 994 |
| 0 | 1.0 | $6.8 \times 10^{-8}$ | $5.5 \times 10^{-4}$ | <80 | | | | |
| −150 | <0 | $5.5 \times 10^{-4}$ | $1.5 \times 10^{-3}$ | all | 30.7 | 41.5 | 2.6 | 2087 |
| −150 | <0 | $6.8 \times 10^{-8}$ | $5.5 \times 10^{-4}$ | 40–<80 | | | | |
| 0 | 1.0 | $6.8 \times 10^{-8}$ | $5.5 \times 10^{-4}$ | >80 | | | | |
| 1.0 | 55 | $6.8 \times 10^{-8}$ | $5.5 \times 10^{-4}$ | 80–<120 | | | | |
| 1.0 | 55 | $5.5 \times 10^{-4}$ | 0.22 | all | | | | |
| −150 | <0 | $6.8 \times 10^{-8}$ | $5.5 \times 10^{-4}$ | >120 | 17.5 | 43.6 | 2.9 | 556 |
| 1.0 | 55 | $6.8 \times 10^{-8}$ | $5.5 \times 10^{-4}$ | <80 | | | | |
| −150 | <0 | $6.8 \times 10^{-8}$ | $5.5 \times 10^{-4}$ | 80–<120 | 22.2 | 27.2 | 6.4 | 480 |
| 1.0 | 55 | $6.8 \times 10^{-8}$ | $5.5 \times 10^{-4}$ | >120 | | | | |

[a] Number of spectra giving maximum predicted reliability values for scale ($S$) values: −150 to −2.7, 1179; −2.7 to <0, 1401; zero, 1029; >0 to 1.0, 530; 1 to 55, 1028. [b] For curve ($V$) values: $6.8 \times 10^{-8}$ to $2.0 \times 10^{-4}$, 1290; $2.0 \times 10^{-4}$ to $5.5 \times 10^{-4}$, 1106; $5.5 \times 10^{-4}$ to $1.5 \times 10^{-3}$, 1307; $1.5 \times 10^{-3}$ to 0.22, 1464. [c] For minimum/maximum mass ($m_0$) values: <40, 777; 40 to 79, 1666; 80 to 119, 1229; ≥120, 1495.

incorrect 85% more often than the average of all matches of this $K$ value, resulting in a predicted RL value of 83% for $K = 100$, no flags, and no molecular ion. Matching a specific reference spectrum gives a separate predicted RL value from $K$ and $\Delta K$, the higher of which is used, up to a maximum value 10 units above that from $K$. This value is adjusted for tilt by subtracting from the predicted RL value the following absolute values: $K$, negative tilt, 10 if $K \geq 80$, 20 if $K < 80$; $K$, positive tilt, 8; $\Delta K$, negative tilt, 7, positive tilt, 3.

The recommended PBM system now uses quadratic scaling (*14*) rather than tilting. The predicted RL value was found to relate to the actual reliability found for the 431 unknowns as follows: RL (%) = 0–5, 0; 40, $RL_{40}$; 80, $RL_{80}$; and 100, 100; intermediate points are interpolated linearly. The values of $RL_{40}$ and $RL_{80}$ depend (Table III) on the degree of scaling, which is described by three factors: scale ($S$, eq 3), where $U_i$ is the $U$ value of the $i$th reference peak

$$S = \sum_i (U_i - U_{av}) \Delta A_i \tag{3}$$

$U_{av}$ is the average $U$ value of all reference peaks and $\Delta A_i$ is the change caused by scaling in the $A$ value of the $i$th reference peak; curvative ($V$), described by eq 4, which when combined with eq 1 yields eq 5; and $m_0$, the mass of the minimum or maximum of the quadratic function.

$$V = |d^2y/dx^2| / [1 + (dy/dx)^2]^{3/2} \tag{4}$$

$$V = |2c| / (4c^2m^2 + 4cbm + b^2 + 1)^{3/2} \tag{5}$$

## RESULTS AND DISCUSSION

**PBM Performance before Modification.** The recall/reliability performance of the subset of 450 "odd" unknowns agreed within ±2%, on average, of that of the full set of 900 unknowns using $K$ values and class I matching criteria (*13*), justifying the use of the smaller subset of unknowns for testing further modifications. The recall/reliability performance found by Pesyna (*7*) using the same PBM algorithm with a data base only 57% as large, but using unknowns selected by average molecular weight, gave recall values which were on average 8% higher (*13*). Correcting errors, which reduced the 450 to 431 spectra, approximately halved this discrepancy in recall values. There also should be a larger possibility of error caused by increasing the proportion of wrong answers in the data base (*15*). The class I performance at low recall values was much lower with the larger data base, reflecting (*13*) an increased number of reference structures closely related to those of the unknowns. Class IV matching criteria are designed to be less sensitive to such deficiencies of mass spectrometry, and so are used here to be more sensitive to the performance of the retrieval algorithm itself.

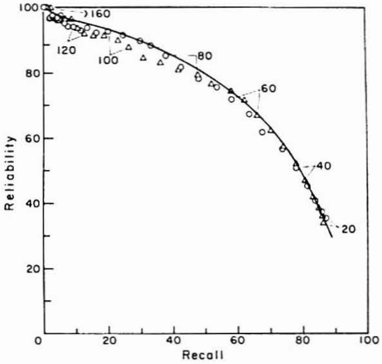

**Figure 1.** Effect of abundance based flagging on PBM performance (class IV, $K$ values, class I recall): Δ, results with original PBM (*7*); O, with abundance based flagging; —, with a minimum increment of $\rho_{min}$ in each flagging (actually based on the difference between these and the previous conditions run with slightly modified parameters) (*14*). The separate data point values 20, 40, ..., 160 represent the minimum $K$ values included in determining the recall/reliability values.

**Abundance-Based Flagging.** Examination of condensed spectra of correct answers not retrieved using the original algorithm (*7*) showed some contained more than three artifact peaks of low abundance which had been included in the condensed spectrum because they had high $U$ values. An artifact peak produces an unusually low (or zero) value of $\rho_{min}$; if after three flagging operations all artifact peaks are not eliminated, the resulting low $\rho_{min}$ value prevents the match of other reference peaks of higher abundance. The new method removes all low $\rho$ value peaks of <1% abundance in the first flagging operation, those of <9% in the second, and those of <37% in the last flagging. This yields a significant improvement (Figure 1) in reliability at low recall values. This is further increased (solid line in Figure 1) by instead forcing $\rho_{min}$ to increase by 50% relative or, if ≥0.65, by 0.15 absolute in each flagging operation.

**Optimum $\rho$ Value.** An alternative method for setting the level of the abundance window used in matching was unsuccessful (*14*). The $\rho$ value of each peak was used as $\rho_{min}$ in

Table IV. Class IV Retrieved Spectra[a] of Highest $K$ Value vs. Tilt Category

| | without tilting | with tilting (tilt factors, $n$) | | | | | | | | | |
|---|---|---|---|---|---|---|---|---|---|---|---|
| | | overall | 0 | +1 | +2 | +3 | +4 | −1 | −2 | −3 | −4 |
| match | 2301 | 2353 | 707 | 346 | 192 | 146 | 113 | 301 | 259 | 136 | 153 |
| mismatch | 4208 | 4967 | 1077 | 469 | 310 | 219 | 218 | 693 | 665 | 691 | 625 |
| reliability | 35% | 32% | 40% | 42% | 38% | 40% | 34% | 30% | 28% | 16% | 20% |

[a] All spectra retrieved in each tilt category for which $K > 20$ and % contamination < 70.

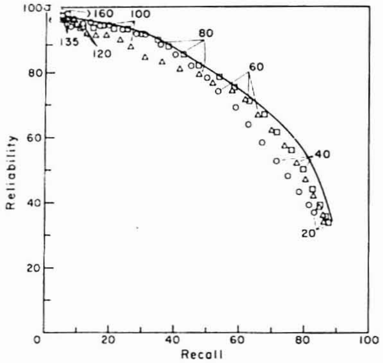

Figure 2. Effect of tighter window tolerances and spectrum tilting or scaling (class IV, $K$ values, class I recall): △, results with original PBM (*7*); ○, with tighter window tolerances; □, with tilting and tighter window tolerances; —, with scaling and tighter window tolerances on basis described in Figure 1 legend.

separate calculations to find the highest matching value. For spectra of pure unknowns this lowered performance by a few percent at >50% recall. Apparently this system allows artifically high $\rho_{\min}$ values which can improve the match of an incorrect spectrum; this should be a more serious problem with the spectra of mixtures.

**Tighter Window Tolerances.** Cleij, van't Klooster, and van Houwelingen (*12*) show that basing abundance tolerances used in matching on data reproducibility yields improved performance. Figure 2 shows that the tighter window tolerances gave an improvement in reliability at low recall, but the opposite effect at high recall values. At low recall values, for which high $K$ values are required, tighter window tolerances exclude peaks from wrong answers more often than from correct ones. On the other hand, at high recall values where only a few peaks must be within the window tolerance, reference spectra which are correct answers must already be badly skewed, so that tightening the window tolerances eliminates their peaks as often as those of incorrect spectra. Thus methods to compensate for skewing were sought.

**Spectrum Tilting.** The relative abundances in a spectrum can be skewed as a function of mass through instrumental mass discrimination and through changing sample pressure during the spectrum scan, a common problem in GC/MS. Dromey (*13*) has independently suggested a procedure for optimizing the degree of match for spectra of pure compounds, but his method was not tested on a statistically large data set. Similar approaches, tilting and scaling, are described here. In the first the peak abundances in the unknown mass spectrum were tilted by a factor of $2^n$ every 200 mass units ($n = \pm 1$–4). For the best matches (highest $K$ value) found for any value of $n$, the zero and positive tilts show a somewhat improved reliability except for $n = +4$, but the negative tilts show substantially decreased reliabilities. This appears to be due to the greater importance which such negative tilting gives to the low mass peaks, which are well-known (*23*) to provide less specific structure information; other data (*13*) show that the more specific high-mass peaks are preferentially removed by flagging with negative tilting. A recall improvement of ~5% at higher recall values (Figure 2) was achieved by allowing only tilting functions $n = 0$–3, no peak flagging for tilted spectra, and tighter window tolerances. Note that changing the unknown peak abundances by a factor of 16 every 200 mass units gives the best match for a surprising number (6%) of correct answers, comparable to those for a factor of 8.

**Quadratic Scaling.** The quadratic skewing function, which allows a minimum or maximum, produces an additional improvement in recall of several percent (Figure 2) at >65% recall, and so is used in the current PBM algorithm in place of tilting. To compare the number of spectra giving the highest RL values for different values of scale and curve (footnote, Table III) with the corresponding tilt data (Table IV), $n = 1$ tilt corresponds to $V = 2.4 \times 10^{-5}$ and $S = 1$ or 2 (highly spectrum dependent). As found for tilting, both positive and negative scale values over a wide range were effective for a substantial proportion of spectra. The minimum or maximum mass ($m_0$) of the scaling functions found most effective were centered around $m/z$ 70 (*14*); this is consistent with the maximum in relative abundance often shown by quadrupole spectra as compared to spectra from magnetic instruments. Maximum curvatures ($V$ values) much higher than achieved by the exponential tilting function were surprisingly effective and appear to be the main reason for the improved performance of scaling. Many values are much larger than expected from differences in instrumental mass discrimination and are more likely caused by scanning a spectrum during a GC/MS run while going over the top of the GC peak. This could also be caused by amplifier saturation or even errors in transcribing sensitivity factors.

**Reliability Ranking.** The effect of the values of $K$, $\Delta K$, matching of the molecular ion, number of flagging operations, and tilting on the actual reliability of the match was determined statistically with the 431 unknowns (Tables I and II). Evaluating the degree of match with the resulting predicted reliability (RL) value gave a very significant improvement in PBM performance, especially at lower recall values (Figure 3). For example, the proportion of class I wrong answers at 20% recall has been reduced from 32% to 21%, while the class IV wrong answers have been reduced from 9% to 2%; this last value was achieved previously only at 3%, not 20%, recall. Comparison of the predicted reliability values (numbers next to data points in Figure 3) and the actual reliability values ($Y$ axis position) for class IV matches also demonstrates this reliability improvement (e.g., predicted reliability of 90% is actually 96% correct); the predicted reliability values in the final algorithm have been adjusted for this. An important part of the improvement at low recall values is the incorporation of ranking by $\Delta K$ values, which were shown originally (*7*) to give much better predictions than $K$ values at low recall. In general the improvement results from better data weighting, an accepted primary criterion of retrieval system performance (*22*). At the highest recall values the reliability ranking makes no difference in performance because exactly the same spectra,

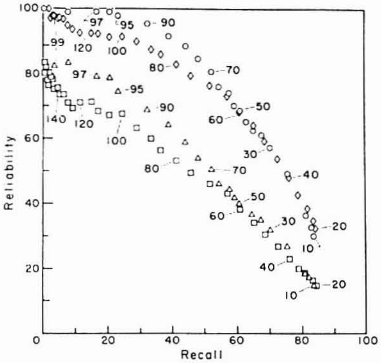

**Figure 3.** Effect of ranking retrieved spectrum by predicted reliability values (classes I and IV, respectively, both with class I recall): □, ◊, results with *K* value ranking with spectrum tilting (see Figure 2); △, ○, with reliability ranking. Algorithm did *not* include the minimum increment of $\rho_{min}$ (Figure 1) and used tilting, *not* scaling (Figure 2).

and thus the same number of correct and incorrect answers, were saved in both cases as both used a threshold value of $K = 20$. This threshold has been changed to >10% RL in the current PBM system. The original study (*7*) showed a substantial effect of the unknown's molecular weight on PBM performance; this should also be incorporated into the reliability ranking.

The effect of reliability ranking can be illustrated by the results from an actual unknown supplied by D. Henneberg as part of a test of different retrieval systems (*10*). Although the unknown spectrum was that of 1-dodecene, the first references retrieved by PBM without reliability ranking were those of undecanol and 1-tridecene, $K = 99$ (Table V). Their predicted class IV reliabilities are only 41% and 32%, lowered by the failure to match the molecular ion and by the three flagging operations. However, the unknown has a peak corresponding to the molecular ions of the 1-dodecene reference spectra, and for three of these fewer flagging operations were necessary. Thus the five best answers by reliability ranking are now correct.

**Two-Level PBM.** An extensive effort was made to use further data of the reference spectrum, not in the PBM condensed spectrum, to improve the ranking of the best matching compounds found in the original PBM search. A variety of ways of assigning new uniqueness values to the peaks of this small subset of spectra, followed by further PBM-type matching, were unsuccessful in improving the PBM performance; the additional structurally significant peaks were accompanied by an offsetting number of artifacts or misleading peaks (*14*).

**Applicability of Reliability Ranking.** These PBM improvements (except scaling) have been available for over 2 years on a commercial GC/MS system used in hundreds of laboratories. Experienced users have generally recognized these improvements as significant; some of their suggestions have resulted in further improvements to be reported separately. This concept has also been extended to the prediction of the presence of specific substructures out of a list of 600 from unknown mass spectra using the "self-training interpretive and retrieval system" (*24*). For other types of libraries retrieval systems having several parameters indicating the degree of match should also benefit by combining these into a single value to provide a quantitative indication of the probability that the retrieved file actually represents the unknown.

**Table V. *K* Value and Reliability Ranking for PBM Matching of an Unknown Mass Spectrum of 1-Dodecene (*10*)**

| retrieved compds, ranking by *K* values[a] | confidence | | class IV reliability, % | rank by RL value |
|---|---|---|---|---|
| | $K$[b] | $\Delta K$ | | |
| undecanol | 99*** | 21 | 41 | 9 |
| 1-tridecene | 99*** | 29 | 32 | 10 |
| *1-dodecene* | 90**+ | 23 | 87 | *2* |
| *1-dodecene* | 90**+ | 23 | 87 | *3* |
| *1-dodecene* | 87***+ | 20 | 73 | *4* |
| *1-dodecene* | 87+ | 16 | 94 | *1* |
| 5,6-methylenedecane | 84* | 23 | 55 | 6 |
| 6-methylheptanol | 81*** | 26 | 28 | 11 |
| methylundecanethiol | 80* | 40 | 52 | 7 |
| 1-pentadecene | 78** | 42 | 42 | 8 |
| *1-dodecene* | 77***+ | 21 | 64 | *5* |

[a] The correct answer is in italics. The data base has 11 different $C_{12}H_{24}$ compounds. [b] The number of asterisks (*) indicates the number of flagging operations; plus (+) indicates that the molecular ion was matched.

## ACKNOWLEDGMENT

We are grateful for stimulating discussions with R. G. Dromey, R. G. Ellis, K. S. Haraki, I. K. Mun, J. W. Serum, and R. Venkataraghavan and to PBM users, too numerous to be named here, for valuable suggestions.

## LITERATURE CITED

(1) Burlingame, A. L.; Whitney, J. O.; Russell, D. H. *Anal. Chem.* **1984**, *56*, 417R.
(2) Smith, D. H. "Computer-Assisted Structure Elucidation"; American Chemical Society: Washington, DC, 1977.
(3) Hertz, H. S.; Hites, R. A.; Biemann, K. *Anal. Chem.* **1971**, *43*, 681.
(4) McLafferty, F. W.; Hertel, R. H.; Villwock, R. D. *Org. Mass Spectrom.* **1974**, *9*, 690.
(5) Abramson, F. P. *Anal. Chem.* **1975**, *47*, 45.
(6) Gronneberg, T. O.; Gray, N. A. B.; Eglinton, G. *Anal. Chem.* **1975**, *47*, 415.
(7) Pesyna, G. M.; Venkataraghavan, R.; Dayringer, H. G.; McLafferty, F. W. *Anal. Chem.* **1976**, *48*, 1362.
(8) Dromey, R. G. *Anal. Chim. Acta* **1979**, *112*, 133.
(9) Atwater, B. L.; McLafferty, F. W. *Anal. Chem.* **1979**, *51*, 1945.
(10) Henneberg, D. *Adv. Mass Spectrom.* **1980**, *8b*, 1511.
(11) Domokos, L.; Henneberg, D.; Wiemann, B. *Anal. Chim. Acta* **1983**, *150*, 37.
(12) Cleij, P.; van't Klooster, H. A.; van Houwelingen, J. C. *Anal. Chim. Acta* **1983**, *150*, 23.
(13) Atwater, B. L. Ph.D. Thesis, Cornell University, 1980.
(14) Stauffer, D. B. Ph.D. Thesis, Cornell University, 1984.
(15) McLafferty, F. W.; Stauffer, D. B. *Int. J. Mass Spectrom. Ion Proc.* **1984**, *58*, 139.
(16) Shackelford, W. M.; Kline, D. M.; Faas, L.; Kurth, G. *Anal. Chim. Acta* **1983**, *146*, 15.
(17) Rosenthal, D. *Anal. Chem.* **1982**, *54*, 63.
(18) Davis, J. M.; Giddings, J. C. *Anal. Chem.* **1983**, *55*, 418.
(19) Milne, G. W. A.; Heller, S. R. *J. Chem. Inf. Comput. Sci.* **1980**, *20*, 204.
(20) Speck, D. D.; Venkataraghavan, R.; McLafferty, F. W. *Org. Mass Spectrom.* **1978**, *13*, 209–213.
(21) McLafferty, F. W. *Anal. Chem.* **1977**, *49*, 1441–1443.
(22) Salton, G. "Automatic Information Organization and Retrieval"; McGraw-Hill: New York, 1968.
(23) McLafferty, F. W. "Interpretation of Mass Spectra"; 3rd ed.; University Science Books: Mill Valley, CA, 1980; pp 79–84.
(24) Haraki, K. S.; Venkataraghavan, R.; McLafferty, F. W. *Anal. Chem.* **1981**, *53*, 386–392.

RECEIVED for review August 8, 1984. Accepted December 26, 1984. This work was supported by the Industry/University Cooperative Research Program of the National Science Foundation, Grants CHE-7910400 and -8303340.

# Multicomponent Mixture Analysis Using Room-Temperature Phosphorimetry

**Ebenezer B. Asafu-Adjaye, Jung Im Yun, and Syang Y. Su***

*Department of Chemistry, Virginia Commonwealth University, Richmond, Virginia 23284*

**A multicomponent mixture analysis without separation using the room-temperature phosphorescence technique is described. Mixtures prepared from four or five analytical reference standards of toxic substances obtained from the Environmental Protection Agency were used for this study. The room-temperature phosphorescence characteristics of each of these compounds are reported as well as the results of analyses of these synthetic mixtures. The method of calibration curves/subtraction was used to determine two spectroscopically overlapping compounds in mixtures.**

Several approaches have been extensively studied for the analyses of multicomponent mixtures without separation using fluoresecence detection. The approaches of line narrowing (*1*), matrix isolation (*2*), and Shpol'skii solvent effect (*3*) have been used to improve spectral resolution for mixture analyses. The synchronous wavelength (*4*) and energy (*5*) scanning techniques have been demonstrated to have improved selectivity and minimized interference from scattering or other analytes in the mixture. Multicomponent mixture analyses have also been accomplished by the excitation-emission-matrix (EEM) and rank annihilation or least-squares methods (*6*, *7*). Other methods such as the selective modulation (*8*) and the selective excitation (*9*) approaches and the use of diode arrays (*10*) and image detectors (*11*) have also been described. In addition, total room-temperature fluorescence and phosphorescence (*12*) have recently been applied to mixture analysis. Most of the above approaches have employed polynuclear aromatic hydrocarbons as the model compounds in mixture analyses.

However, phosphorescence has not become a popular method due to the need for cryogenic equipment and optics, the irreproducibility of the formation of the cooled matrix, and the inconvenience of the sampling process (*13*, *14*). The introduction and development of room-temperature phosphorescence (RTP) avoids the liabilities associated with low-temperature measurements. RTP also provides better selectivity than low-temperature phosphorescence (LTP). Progress in the development and application of RTP has been reviewed in two recent monographs (*15*, *16*). However, RTP is less sensitive compared to LTP. The RTP intensity of a compound was found to be related to the strength of interaction between the compound and its environment such as ionic and hydrogen bonding between phosphors and substrates (*14*, *17*). A few compounds have been shown to interact with substrates strongly enough to induce RTP. The nature of the phosphor–substrate interactions that give rise to RTP are, however, not yet fully understood. Factors other than ionic and hydrogen bondings may also contribute to the RTP inducement (*14*). Nonetheless, the differences in the RTP inducing interactions between individual phosphors and different substrates provide a means of achieving selectivity. This paper describes a study that seeks to use this effect to improve RTP selectivity for application to mixture analyses without separation.

Room-temperature phosphorimetry (RTP) has been demonstrated to be a technique of choice for assaying single-component mixtures (*15*, *16*, *18*). There have been few instances of qualitative analyses of multicomponent mixtures using RTP. They include the use of synchronous scanning (*16*), selective external heavy atom perturbation (*16*), and the combination of substrate and heavy atom effects (*19*).

It is difficult to determine a multicomponent mixture due to the broad nature of RTP spectra. Thus far, only one report has applied RTP to quantitative multicomponent mixture analyses (*12*). In this study, overlapping RTP spectra are resolved by optimizing the conditions of added heavy atoms and different sample substrates so that only one component in a mixture then exhibits RTP. In an earlier study of the analysis of naphthaleneacetic acid (NAA) in a mixture of six pesticides all on P-81 (cationic exchange paper), only NAA exhibited RTP (*19*). All seven compounds exhibited RTP when placed on DE-81 (anionic exchanger paper). By selection of different sample substrates and different added heavy atoms, it is plausible that one component can be observed by RTP in the presence of potentially interfering compounds.

Room-temperature phosphorescence of mixtures of four or five model compounds were studied without separation. A nonphosphorescent compound was included to detect if there is any quenching effect present in mixture analyses. The structures of two of the five compounds studied are very similar, namely, 1-naphthoic acid and 2-naphthoic acid. The salt of 1-naphthoic acid, sodium 1-naphthoate, has been studied in detail (*20*). Substrate and heavy atom effects were used to resolve the RTP responses of the components in the mixture. The method of signal subtraction using calibration curves was also used for the analysis of two compounds whose RTP responses overlapped (*12*). The RTP responses of the five compounds and the results of the analyses of several synthetic mixtures are also described.

## EXPERIMENTAL SECTION

**Apparatus.** A Turner Model 430 spectrofluorometer (Sequoia-Turner Co., Mountain View, CA) and an improved version of a luminescence sampling system (*19*) were used. Spectral band-passes of excitation and emission monochromators were both set at 60 nm. The sampling system had 20 circular depressions, each 6.4 mm in diameter, on a copper disk to hold and position the paper sample disks. A microdispenser (Drummond Scientific Co., Broomall, PA) was used to deliver 2 μL of sample or heavy atom solutions onto the paper sample disks. The same phosphoroscope controller and chopper were used as previously described (*19*).

**Reagents.** The analytical reference standard samples of pesticides (see Table I) were obtained from the Environmental Protection Agency (EPA) (Research Triangle Park, NC) and used without further purification in preparing both individual and mixture solutions for the study. Potassium iodide, potassium chloride (Fisher Scientific Co., Fair Lawn, NJ), and lead acetate (Mallinckrodt, St. Louis, MO) were of ACS analytical reagent grade. Absolute ethyl alcohol was purchased from U.S. Industrial Chemicals Co., New York. The pesticide and heavy atom solutions were prepared in 1:1 ethyl alcohol/Nanopure deionized water (Barnstead, Sybron Co., Boston, MA). Ion exchange chromatographic papers, DE-81 (anion) and P-81 (cation) (Whatman

0003-2700/85/0357-0904$01.50/0 © 1985 American Chemical Society

**Table I. Room-Temperature Phosphorescence Characteristics of Five Toxic Substances**

| compounds[a] | structures | $\lambda_{ex}/\lambda_{em}$, nm | substrates | heavy atoms[b] | LOD,[c] ng | LDR[d] (slope) |
|---|---|---|---|---|---|---|
| naphthaleneacetamide (4880) | 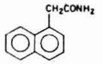 | 299/504 | DE-81 | $I^-$ | 0.26 | 400 (0.92) |
| | | 299/504 | P-81 | $Pb^{2+}$ | | |
| 2-naphthoic acid (P772) | 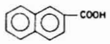 | 298/509 | DE-81 | $I^-$ | 2.06 | 390 (0.97) |
| | | 298/509 | P-81 | $Pb^{2+}$ | | |
| 1-naphthoic acid (P771) | 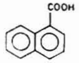 | 304/514 | DE-81 | $I^-$ | 1.66 | 380 (0.94) |
| | | 312/520 | P-81 | $Pb^{2+}$ | 12.6 | |
| 3,4-dimethoxybenzaldehyde (P358) | 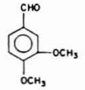 | 325/480 | DE-81 | $I^-$ | *e* | |
| | | 335/480 | P-81 | $Cl^-$ | 25.6 | 400 (1.11) |
| 1,2-diphenylhydrazine (P453) | 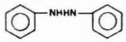 | (no RTP) | DE-81 | $I^-$ | | |
| | | (no RTP) | P-81 | $Pb^{2+}$ | | |

[a] EPA code numbers of the analytical reference standards included in this study are listed in parantheses. [b] The concentrations of both $I^-$ and $Pb^{2+}$ heavy atoms are 1 M. [c] Signal/noise = 3 is used for the limit of detection (LOD) calculation. [d] Linear dynamic range is calculated by dividing the upper linear range concentration by the LOD of that compound. [e] Very weak.

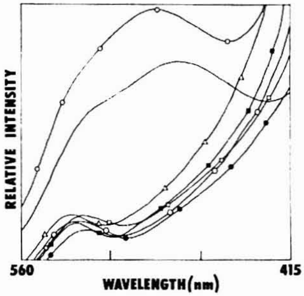

**Figure 1.** Spectra of mixture 4 and its pure components with curve identification symbols and amounts studied, excitation wavelength 335 nm, on P-81 substrate using $Cl^-$ as heavy atom: ○, 3,4-dimethoxybenzaldehyde (428 ng); —, mixture 4; △, 1-naphthoic acid (100 ng); □, 2-naphthoic acid (105 ng); ○, naphthaleneacetamide (87 ng); ■, 1,2-diphenylhydrazine (102 ng); ●, blank (2 μL of 0.5 M KCl in 50% ethanol).

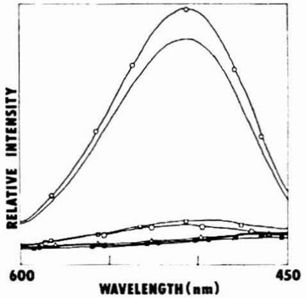

**Figure 2.** Spectra of mixture 1 and its pure components with curve identification symbols and amounts studied, excitation wavelength 299 nm, on P-81 substrate using $I^-$ heavy atom: ○, naphthaleneacetamide (348 ng); —, mixture 1; □, 2-naphthoic acid (105 ng); ○, 1-naphthoic acid (100 ng); ■, 1,2-diphenylhydrazine (102 ng); △, 3,4-dimethoxybenzaldehyde (107 ng); ●, blank (2 μL of 0.5 M KI in 50% ethanol).

Chemical Separation Inc., Clifton, NJ), were used to prepare the 6.4 mm diameter paper sample disks.

**Procedure.** The procedure for obtaining phosphorescence spectra was the same as previously described (*19*). The compositions of various mixtures used in this study are given in Table II.

## RESULTS AND DISCUSSION

**Room-Temperature Phosphorescence Characteristics.** Table I gives the room-temperature phosphorescence characteristics of the five compounds studied. All of the compounds, except 1,2-diphenylhydrazine, phosphoresced utilizing some combination of solid substrate and heavy atom. Among the other compounds, 3,4-dimethoxybenzaldehyde was the only one that exhibited very weak RTP on DE-81 in the presence of $I^-$. However, its phosphorescence was more intense on P-81 substrate in the presence of $Cl^-$ than the responses observed for the other compounds and systems studied as shown in Figure 1. The limits of detection and linear dynamic ranges of the three organic compounds that exhibited useful RTP signals for single-component mixture analyses using the DE-81 and $I^-$ combination are reported. However, different combinations of P-81 and heavy atoms provided different degrees of selectivity for these three compounds as exemplified by different shifts in excitation–emission wavelengths of some of the substances. In addition to these wavelength shifts, there was also a drastic decrease in signal intensities for some compounds as shown in Figure 2. With the same sensitivity range, the RTP intensities of all the compounds except naphthaleneacetamide were reduced drastically when P-81 substrate and $I^-$ heavy atom were employed. Similar behavior is shown in Figure 3, where signal intensities were virtually the same as that of the blank except for those due to 1-naphthoic acid and 3,4-dimethoxybenzaldehyde. It is this selectivity, provided by different combinations of substrates and heavy atoms, that was used for mixture analyses of the

**Table II. Concentrations of Various Compounds in the Mixtures**

| mixture | naphthalene-acetamide, μg/mL | 1-naphthoic acid, μg/mL | 2-naphthoic acid, μg/mL | 3,4-dimethoxy-benzaldehyde, μg/mL | 1,2-diphenyl-hydrazine, μg/mL |
|---|---|---|---|---|---|
| 1 | 174.0 | 50.0 | 52.5 | 53.5 | 51.0 |
| 2 | 87.0 | 50.0 | 52.5 | 53.5 | 51.0 |
| 3 | 43.5 | 50.0 | 52.5 | 53.5 | 51.0 |
| 4 | 43.5 | 50.0 | 52.5 | 214.0 | 51.0 |
| 5 | 75.0 | 156.0 | 79.0 | 80.0 | 0.0 |
| 6 | 75.0 | 78.0 | 79.0 | 80.0 | 0.0 |

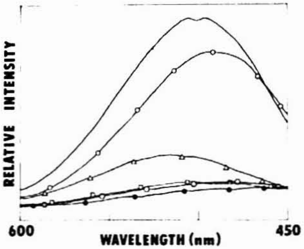

**Figure 3.** Spectra of mixture 5 and its pure components with curve identification symbols and amounts studied, excitation wavelength 312 nm, on P-81 substrate using $Pb^{2+}$ as heavy atom: —, mixture 5; O, 3,4-dimethoxybenzaldehyde (160 ng); Δ, 1-naphthoic acid (312 ng); □, 2-naphthoic acid (158 ng); O, naphthaleneacetamide (150 ng); ●, blank (2 μL of saturated aqueous lead acetate).

components without separation.

**Mixture Analyses.** A study of the room-temperature phosphorescence characteristics of various pesticides on different solid substrates and heavy atoms was carried out. It was observed that RTP signal intensities were extremely low or not different from the blank for all the substances except naphthaleneacetamide, when P-81 and $I^-$ and excitation/emission wavelengths of naphthaleneacetamide were used. Hence, this combination of substrate and heavy atom made it feasible to determine naphthaleneacetamide in the presence of the other components in the mixture without any need for separation. Several synthetic mixtures were prepared for this study, and their compositions are given in Table II. Results of the determination of naphthaleneacetamide are shown in Table III. Signal intensities obtained for the mixtures compared favorably with those of the pure naphthaleneacetamide of the same concentration as in the mixture. At concentrations of naphthaleneacetamide of below ca. 50 μg/mL, the error increased as the signal-to-noise ratio decreased. The standard deviations also given in Table III were calculated from eight data points acquired from different aliquots of the sample on different sample disks. The magnitude of the standard deviations reported in Tables III, IV, and V for individual mixtures is partly due to experimental constraints that required using sample paper disks with an area larger than the cross-sectional area of the excitation beam in the present work (*21*). Other sources of error include sample spotting error, sample alignment problems, and variations in the time when observations were made. It was also observed that there was not any quenching effect arising from the nonphosphorescent compound, 1,2-diphenylhydrazine, on the mixture analyses. Mixtures 5 and 6, however, are exceptional and need a further study.

In the 3,4-dimethoxybenzaldehyde determination in mixtures 3 and 4, a similar trend as described above was observed. The determinations were made using P-81 as the substrate and $Cl^-$ as the heavy atom. Signal observation was made at the characteristic wavelengths of 3,4-dimethoxybenzaldehyde. The results are shown in Table IV.

**Table III. Determination of Naphthaleneacetamide in Mixtures**

| sample[a] | amt of naphthaleneacetamide, ng: prepared | amt of naphthaleneacetamide, ng: exptl[b] | rel error,[c] % | rel std dev,[d] % |
|---|---|---|---|---|
| mixture 1 | 348 | 341.8 | 1.8 | 13.1 |
| mixture 2 | 174 | 186.6 | 7.2 | 3.2 |
| mixture 3 | 87.0 | 101.4 | 16.6 | 14.8 |

[a] The determinations were carried out using P-81 as substrate and 0.5 M $I^-$ as heavy atom at excitation/emission wavelengths of 299/504 nm, respectively. [b] Amounts calculated from calibration curve of pure naphthaleneacetamide and represent average of eight data points from eight different sample aliquots. [c] Relative error = (difference between experimental and prepared amounts/prepared amount) × 100%. [d] Relative standard deviations (RSD) were calculated using eight data points for each sample in this table.

**Table IV. Determination of 3,4-Dimethoxybenzaldehyde in Mixtures**

| sample[a] | amt of 3,4-dimethoxybenzaldehyde, ng: prepared | amt of 3,4-dimethoxybenzaldehyde, ng: exptl[b] | rel error,[c] % | rel std dev,[d] % |
|---|---|---|---|---|
| mixture 3 | 107 | 100.2 | 6.4 | 14.9 |
| mixture 4 | 428 | 399.1 | 6.8 | 17.2 |

[a] The determinations were carried out using P-81 substrate and 0.5 M $Cl^-$ as heavy atom, at excitation/emission wavelengths of 335/480 nm, respectively. [b] Amount calculated from calibration curve of pure 3,4-dimethoxybenzaldehyde and represents average of eight data points from eight different sample aliquots. [c] Relative error = (the difference between prepared and experimental amounts/prepared amount) × 100. [d] Relative standard deviations (RSD) were calculated using eight data points for each sample in this table.

Attempts to determine 1- and 2-naphthoic acids in mixtures in a similar manner as above failed because of significant contributions to the RTP signal by some of the other components in the mixture. This was true even at higher concentrations of these two compounds. However, on using $Pb^{2+}$ as the heavy atom with P-81 as the substrate, 1-naphthoic acid was found to phosphoresce appreciably at the excitation/emission wavelength maxima of 312/520 nm with a significant contribution from only 3,4-dimethoxybenzaldehyde. A signal subtraction method was therefore employed to obtain the results shown in Table V. The method involved the acquisition of calibration curves for both 1-naphthoic acid and 3,4-dimethoxybenzaldehyde at the same excitation and emission wavelengths of 312 and 520 nm, respectively. The concentrations of 3,4-dimethoxybenzaldehyde in the mixtures were determined using P-81 and $Cl^-$ at 335/480 nm as mentioned previously. The RTP signal intensities at 312/520 nm corresponding to these concentrations were obtained from its

**Table V. Determination of 1-Naphthoic Acid in Mixtures**

| samples[a] | amt of 1-naphthoic acid, ng |  | rel error,[c] % | rel std dev,[b] % |
|---|---|---|---|---|
|  | prepared | exptl[b] |  |  |
| mixture 5 | 312 | 337.8 | 8.31 | 11.7 |
| mixture 6 | 156 | 132.2 | 15.3 | 6.1 |

[a] Amounts of 3,4-dimethoxybenzaldehyde in mixtures were first obtained using the calibration curve of the compound with P-81/$Cl^-$ as described in Table IV. Their corresponding RTP intensities with P-81/$Pb^{2+}$, at 312/520 nm, were subsequently obtained. These were subtracted from the combined RTP signals of mixtures. The net signals and calibration curves of 1-naphthoic acid on P-81/$Pb^{2+}$, at 312/520 nm, were used to calculate the amounts of the acid in this table. [b] These were calculated using four data points from four sample aliquots. [c] Relative error = (difference between prepared and experimental amounts/prepared amount) × 100%.

calibration curve. These signal intensities were subtracted from the appropriate total signals of the mixtures to obtain the signal due only to 1-naphthoic acid. The concentration of 1-naphthoic acid was then determined from its calibration curve. As can be discerned from Table V, there was a close correspondence between the calculated and true concentrations of 1-naphthoic acid. The differences observed may be attributed to the fact that the calibration curve for 3,4-dimethoxybenzaldehyde at those particular wavelengths (312/520 nm) was not linear over the range of concentrations used. This is not surprising since the excitation/emission wavelengths for 3,4-dimethoxybenzaldehyde occurs at 335/480 nm where a wider linear dynamic range is obtained.

The results of this study showed that RTP of components in mixtures can be used for determinations by utilizing appropriate substrates and heavy atoms at their individual maximum wavelengths. Spectral deconvolution can often be avoided in this instance although partial overlap still occurs in some cases. Using this approach, one can obtain wider linear dynamic ranges (LDR) and lower limits of detection (LOD) of analyses by observing at their maximal excitation/emission wavelengths. There are many solid substrates and heavy atoms that can be used for this purpose. Cationic, anionic, and neutral paper substrates, polymer-salt substrates, and inorganic compound crystal, powder, and plate substrates, as well as anionic and cationic heavy atoms are among the list (*16*). The drawbacks of this approach include that only phosphorescent compounds in a mixture can be determined and those components which still are overlapped spectroscopically will present difficulties. The results presented here, together with an earlier report (*19*), indicate that by using an appropriate combination of substrate and heavy atom, it is possible to assay multicomponent mixtures without prior separation.

## ACKNOWLEDGMENT

The authors thank the Environmental Protection Agency for providing the reference standard pesticides and toxic organic substances used in the study. They also thank F. M. Hawkridge for his constructive comments on this work.

**Registry No.** $I^-$, 20461-54-5; $Cl^-$, 16887-00-6; naphthaleneacetamide, 31093-43-3; 3,4-dimethoxybenzaldehyde, 120-14-9; 1-naphthoic acid, 86-55-5; 2-naphthoic acid, 93-09-4; 1,2-diphenylhydrazine, 122-66-7.

## LITERATURE CITED

(1) Chiang, I.; Hayes, J. M.; Small, G. J. *Anal. Chem.* **1982**, *54*, 318.
(2) Maple, J. R.; Wehry, E. L.; Mamantov, G. *Anal. Chem.* **1980**, *52*, 920.
(3) D'Silva, A. P.; Fassel, V. A. *Anal. Chem.* **1984**, *56*, 985A.
(4) Vo-Dinh, T.; Gammage, R. B.; Martinez, P. R. *Anal. Chem.* **1981**, *53*, 253.
(5) Inman, E. L., Jr.; Winefordner, J. D. *Anal. Chem.* **1982**, *54*, 2018.
(6) Warner, I. M.; Davidson, E. R.; Christian, G. D. *Anal. Chem.* **1977**, *49*, 2155.
(7) Ho, C.-N.; Christian, G. D.; Davidson, E. R. *Anal. Chem.* **1981**, *53*, 92.
(8) O'Haver, T. C.; Parks, W. M. *Anal. Chem.* **1974**, *46*, 1886.
(9) Boto, K. G.; Bunt, J. S. *Anal. Chem.* **1978**, *50*, 392.
(10) Milano, M. J.; Kim, K. Y. *Anal. Chem.* **1977**, *49*, 555.
(11) Talmi, Y.; Baker, D. C.; Jadamec, J. R.; Saner, W. A. *Anal. Chem.* **1978**, *50*, 936A.
(12) Senthilnathan, V. P.; Hurtubise, R. J. *Anal. Chem.* **1984**, *56*, 913.
(13) Ward, J. L.; Walden, G. L.; Winefordner, J. D. *Talanta* **1981**, *28*, 201.
(14) Parker, R. T.; Freedlander, R. S.; Dunlap, R. B. *Anal. Chim. Acta* **1980**, *119*, 189.
(15) Hurtubise, R. J. "Solid Surface Luminescence Analysis: Theory, Instrumentation, Applications"; Marcel Dekker: New York, 1981.
(16) Vo-Dinh, T. In "Chemical Analysis"; Elving, P. J., Winefordner, J. D., Eds.; Wiley: New York, 1984; Vol. 68.
(17) Dalterio, R. A.; Hurtubise, R. J. *Anal. Chem.* **1984**, *56*, 336.
(18) Vannelli, J. J.; Schulman, E. M. *Anal. Chem.* **1984**, *56*, 1030.
(19) Su, S. Y.; Asafu-Adjaye, E. B.; Ocak, S. *Analyst (London)* **1984**, *109*, 1019.
(20) Schulman, E. M.; Walling, C. *J. Phys. Chem.* **1973**, *77*, 902.
(21) McAleese, D. L.; Dunlap, R. B. *Anal. Chem.* **1984**, *56*, 836.

RECEIVED for review August 16, 1984. Resubmitted January 7, 1985. Accepted January 7, 1985.

Anal. Chem. 1985, 57, 908–917

# Background Detection and Correction in Multicomponent Analysis

**D. W. Osten and B. R. Kowalski***

*Laboratory for Chemometrics, Department of Chemistry, University of Washington, Seattle, Washington 98195*

**The multicomponent linear additive model is frequently used in analytical chemistry for the analysis of several components in a single sample. The pressure of unsuspected components in the mixture, which affect the measured response, results in a volume dependent sample background. A method has been developed to test for the presence of a background interferent during the quantitation step of a multicomponent analysis. If a background is detected, quantitative estimates of the desired analyte concentrations can be obtained by applying several chemically and physically meaningful constraints. Two distinct quantitation methods, which are known as the perpendicular projection and the extreme vertex projection techniques, have been proposed.**

The multicomponent linear additive model is often used by analytical chemists in the analysis of mixture samples. In applying this model to the analysis of a complex mixture, the analyst must make the assumption that the measured response, for example, the absorbance spectrum of a mixture sample, is a function of only the known components in the sample. This requires knowledge of not only the desired analytes but also all potential interferents.

Least-squares regression is perhaps the most frequently used method of estimating the concentrations of several components in a mixture sample. This method will yield the best estimates, in terms of smallest squared errors, of the analyte concentrations provided calibration spectra for all the sample components are included in the analysis. Warner and co-workers (*1*) observed that least squares fitting techniques can be strongly affected by not accounting for all the sample components. They proposed nonnegative least squares and linear programming as alternative methods if some of the components are not known. Leggett (*2*) used nonnegative least squares and simplex optimization to overcome the problem of negative molar absorptivities or concentrations. Gayle and Bennett (*3*) concluded that if the incorrect model was used, for example, necessary calibration spectra were missing during the quantitation step, conventional least squares, nonnegative least squares, and linear programming will all yield incorrect results. Haaland and Easterling (*4*) approached the problem of unknown components in a mixture sample by selecting only the spectral regions which provided the best agreement to the available calibration spectra.

The method of self-modeling curve resolution proposed by Lawton and Sylvestre (*5*) and the similar approach of Martens and co-workers (*6, 7*) are based on the chemically meaningful assumptions that both response measurements and analyte concentrations must be nonnegative. This approach has the advantage of not requiring that the analyst know the pure component spectra nor the actual number of components which influence the measured mixture response. However, applying curve resolution directly to the problem of quantitating several known analytes in the presence of unsuspected interferents does not make use of the known calibration spectra of the desired analytes. A hybrid approach combining these different techniques has been developed and is the subject of the remainder of this work. This approach assumes all but one of the pure component spectra are known by the analyst. The one unknown spectrum is the spectrum of the composite sample background, and includes all of the sample components not identified by the analyst.

## THEORY

The mathematical model used with this hybrid approach is the multicomponent linear additive model. The response of the mixture is measured at $P$ different sensors, e.g., wavelengths. At each sensor, the response can be expressed as

$$r_l = \sum_{i=1}^{N} c_i k_{il} + \sum_{j=1}^{T} c_j k_{jl} \qquad (1)$$

$$\text{for all } l = 1, ..., P$$

where $r_l$ is the response of the $l$th sensor due to the $N$ known analytes present at concentrations, $c_i$, and $T$ interferents present at concentrations, $c_j$, with sensitivity coefficients, $k_{il}$ and $k_{jl}$, respectively. Neither the concentrations nor the spectra, equivalently the $p$ sensitivity coefficients, of the $T$ interferents are known. However, their composite effect on the response of the $l$th sensor can be defined as

$$f_l = \sum_{j=1}^{T} c_j k_{jl} \qquad (2)$$

$$\text{for all } l = 1, ..., P$$

By a simple substitution, eq 1 can be written as

$$r_l = \sum_{i=1}^{N} c_i k_{il} + f_l \qquad (3)$$

$$\text{for all } l = 1, ... P$$

where $f_l$ is the sample or volume dependent background. The model may also be expressed in vector notation as

$$\mathbf{r}' = \mathbf{c}'\mathbf{K} + \mathbf{f}' \qquad (4)$$

where $\mathbf{r}$ is a column vector with length $P$ containing the measured mixture response, $\mathbf{c}$ is a column vector with length $N$ of unknown analyte concentrations, $\mathbf{f}$ is a column vector of length $P$ containing the background contribution, and $\mathbf{K}$ is the $N \times P$ matrix of sensitivity coefficients. The only assumptions made with this model are that each sensor responds linearly to all of the components over the concentration range of interest and that no constant or instrumental background is present.

The approach to be described is a quantitation method only. It does not address the question of calibration. It is assumed the matrix **K** has been obtained by an acceptable method. In general, if matrix effects are absent, then any of the approaches suggested by Kaiser (*8*) will be satisfactory. If matrix effects are present, then standard additions or the GSAM (*9*) approach should be used. It should be noted that if a sample background is present during the calibration step, then the correct **K** matrix will be obtained if a method based on dif-

0003-2700/85/0357-0908$01.50/0 © 1985 American Chemical Society

ferential responses, i.e., standard additions, is used. In order to statistically test for the presence of interferents in the mixture spectrum, it is further assumed that the uncertainities in each of the sensitivity coefficients are known. This assumption places no limitation upon the analysis aside from requiring the analyst to perform replication during the calibration step.

An attempt to solve eq 4 by direct application of least-squares regression is destined to fail. The required solution for the concentration vector **c** will yield

$$\mathbf{c}' = (\mathbf{r}' - \mathbf{f}')\mathbf{K}'(\mathbf{K}\mathbf{K}')^{-1} \qquad (5)$$

Since the vector of background responses, **f**, is unknown, an infinite number of solutions for the concentration vector, **c**, are obtained. Only if all elements of **f** are known or they are all identically equal to zero does a unique solution for **c** exist. Assuming **f** is exactly the null vector is equivalent to assuming a sample background does not exist.

In the present model, each pure component spectrum and mixture spectrum can be considered as a single point in a $P$-dimensional measurement space, where each axis in this space represents the response measured with a single sensor. Assuming that all calibration and mixture spectra are normalized to constant area, any mixture spectrum composed of only the $N$ desired analytes is a linear combination of the $N$ pure component spectra, and since any $N$ noncollinear points are sufficient to define an $(N - 1)$-dimensional hyperplane, all mixtures composed of only these analytes must lie on the same $(N - 1)$-dimensional hyperplane. Additionally, since the $N$ pure spectra are linear combinations of themselves, they must also lie on this hyperplane. A mixture spectrum which is composed of some or all of the $N$ desired analytes plus one or more interfering components will normally not fall on this $(N - 1)$-dimensional hyperplane. The exception occurs if the composite response due to the interferents can be expressed as a linear combination of the desired analytes. Therefore, the problem of identifying if interferences are present is equivalent to determining if the point representing the measured response of the mixture lies on or off the $(N - 1)$-dimensional hyperplane defined by the pure analyte spectra.

In actual practice, all experimental measurements, both those made during the calibration step and those made when obtaining the spectrum of the mixture, will be effected by noise. The noise causes a degree of "thickness" to the $(N - 1)$-dimensional model. The problem of determining if a particular mixture spectrum contains unsuspected interferents is ultimately a statistical question. This problem can be stated as: Given a mixture point, whose location is known with some uncertainty, and a $(N - 1)$-dimensional hyperplane, whose location is also somewhat uncertain, is the distance from the mixture point to the hyperplane defined by the pure component spectra statistically significant?

**Test for Unsuspected Components.** Assume that the calibration matrix, **K**, has been obtained and the analyst wishes to quantitate a measured mixture spectrum, **r**, but is unwilling to assume that a sample background is absent. Each row of the **K** matrix is in effect the spectrum, composed of $P$ points, of a single analyte. Define a new matrix **X**, such that the first $N$ rows of **X** are exactly the elements of the matrix **K** and the $N + 1$ row of **X** contains the measured response of the mixture. Next, define an analogous matrix **U**, such that each element, $u_{ij}$, of **U** contains a measure, e.g., one standard deviation, of the uncertainty in the corresponding element, $x_{ij}$, of the matrix **X**. The first $N$ rows are simply the uncertainties in the sensitivity coefficients, i.e., the $P$ point spectra, and the $N + 1$ row contains the uncertainties in the measured mixture response. The dimensions of **X** and **U** are $N + 1$ by $P$ columns.

The first step is to normalize **X**, such that each spectrum, i.e., each row, has the same area. Since the elements of **X** represent responses, e.g., absorbances, of a chemical component, all elements in **X** are by definition equal to or greater than zero. Normalization of the response and uncertainty matrices is accomplished such that the sum of the responses in each spectrum is equal to one.

$$a_i = \sum_{j=1}^{P} x_{ij} \qquad (6)$$

$$\text{for all } i = 1, ..., N + 1$$

$$x_{ij} = x_{ij}/a_i \qquad (7)$$

$$\text{for all } i, j \text{ (computer division)}$$

The uncertainty matrix must be normalized by using the same factor to prevent altering the relative uncertainty of the spectra in the $P$-dimensional measurement space.

$$u_{ij} = u_{ij}/a_i \qquad (8)$$

$$\text{for all } i, j$$

Next, the data matrix is centered by subtraction of the mean response of each sensor for the $N$ desired analytes.

$$\bar{x}_j = (1/N)\sum_{i=1}^{N} x_{ij} \qquad (9)$$

$$\text{for all } j = 1, ..., P$$

$$x_{ij} = x_{ij} - \bar{x}_j \qquad (10)$$

$$\text{for all } i, j$$

Since mean centering represents a translation in the $P$-dimensional measurement space, it is not necessary to perform this operation on the uncertainty matrix.

The second moment matrix, $\mathbf{X'X}/N$, is then calculated using only the first $N$ rows of the scaled, centered data matrix, **X**. Since the centering was based on only the pure component spectra and the second moment matrix was calculated using only these spectra, the rank of this moment matrix cannot be greater than $N - 1$. Diagonalization of this moment matrix gives rise to the matrices **E** and **V**, such that

$$(\mathbf{X'X}/N)\mathbf{V} = \mathbf{EV} \qquad (11)$$

where **V** is a $P \times P$ matrix containing the eigenvectors of the moment matrix and **E** is a diagonal matrix containing the $P$ eigenvalues. This modified moment matrix results in $N - 1$ nonzero eigenvectors, which are sufficient to exactly reproduce the $N$ pure component spectra.

The scaled and centered mixture spectrum, $\mathbf{x}_{N+1}$, is projected by

$$\mathbf{s}_{N+1}' = \mathbf{x}_{N+1}'\mathbf{V} \qquad (12)$$

where **V** is the $P \times (N - 1)$ matrix of eigenvectors of the modified moment matrix. The mixture spectrum is then predicted from the $N - 1$ eigenvectors and the just calculated factor scores by

$$\hat{\mathbf{x}}_{N+1} = \mathbf{V}\mathbf{s}_{N+1} \qquad (13)$$

The difference between the predicted and actual mixture representations in the $P$-dimensional measurement space is calculated as

$$\mathbf{h} = \mathbf{x}_{N+1} - \hat{\mathbf{x}}_{N+1} \qquad (14)$$

where **h** is the vector of residual differences observed. The sums of the squared elements of the original mixture spectrum and the residuals are calculated as

$$s_{\mathrm{m}} = \sum_{j=1}^{P} x_{N+1,j}^{\,2} \qquad (15)$$

$$s_r = \sum_{j=1}^{P} h_{N+1,j}^{\;2} \tag{16}$$

These values are compared and if the residual vector is found to contain more than $1 \times 10^{-3}\%$ of the original variance present in the mixture spectrum, then the residual vector, **h**, is normalized to a length of one and augmented onto the projection matrix, **V**, as

$$v_{jN} = h_j / s_r^{1/2} \tag{17}$$

$$\text{for all } i = 1, ..., P$$

where $v_{jN}$ represents the $j$th element in the $N$th column of **V**. This threshold may be adjusted. Its purpose is to avoid selecting a residual vector arising solely from computational round off error as the final rotation vector. If the residual vector is smaller than this test value, then the mixture spectrum must be a linear combination of the $N$ pure component spectra, hence the sample background is absent. The matrix **V** is no longer a matrix of eigenvectors. However, the columns of **V** are still orthogonal and **V** may be used as a rotation matrix. The $P \times N$ rotation matrix **V** is then used to project the entire scaled, centered data matrix, **X**, from the $P$-dimensional measurement space into a $N$-dimensional feature space. If **S** is defined to be the coordinates of **X** in the projected space, then **S** is given by

$$\mathbf{S} = \mathbf{XV} \tag{18}$$

where **X** and **V** are the data matrix and the adjusted eigenvector matrix defined above. The first $N$ rows of **S** contain the factor scores representing the pure component spectra in the $N$-dimensional feature space. The $N + 1$ row of **S** is the rotated representation of the mixture spectrum. The uncertainty in the factor scores can be obtained by an identical rotation performed on the matrix **U**, which yields

$$\mathbf{W} = \mathbf{UV} \tag{19}$$

where **W** is the uncertainty matrix in the $N$-dimensional eigenvector space. The problem of measuring the distance from the mixture spectrum to the $(N - 1)$-dimensional hyperplane containing all mixtures composed of the $N$ desired analytes has been reduced from a geometrical problem in $P$ space to a somewhat simpler problem in the smaller dimensional $N$ space.

The statistical problem of determining if the distance from the ideal mixture model, defined by the hyperplane, to the measured mixture response is significant requires evaluation of the uncertainty in the various measurements. The advantage of using this particular rotation is apparent when the background test is attempted. The $(N - 1)$-dimensional hyperplane defined by the $N$ pure component spectra is now also defined by the first $N - 1$ vectors of the rotation matrix. The projection axis for the orthogonal projection of the mixture spectrum onto the hyperplane defined by the calibration standards is simply the $N$th vector in the rotation matrix, **V**. The distance from the mixture spectrum to its projected image is obtained directly from the factor score for the mixture spectrum on the $N$th projection vector, which is simply the $N$th element in the $N + 1$ row of the matrix **S**. Since the distance from the mixture to the ideal model along each of the original $P$ measurement axes contributes positively to the observed distance along the final rotation vector in the $N$ dimensional feature space, it is necessary to scale the observed distance by the square root of the number of sensors employed. The scaled distance is observed distance divided by the square root of $P$.

In this situation, the scaled distance between the mixture point and the hyperplane is the difference to be tested with respect to the uncertainty in the location of the mixture point and the uncertainty in the hyperplane directed along the measurement axis. In order to use a $t$ test for the comparison of two mean values, the analyst must know the difference between the mean values, the standard deviations of the means, and the number of measurements which have been made. In the current problem, careful consideration of the available degrees of freedom leads to the conclusion that the number of degrees of freedom associated with each spectrum is approximately proportional to the number of sensors employed. Making measurements with a large number of sensors allows the normal distribution, instead of the $t$ distribution, to be used without causing the introduction of a large error into the statistical background test. The two-sided Normal test for comparison of two mean values is given by Nattrella (*10*). The test statistic, $u$, is calculated as

$$u = z_{1-(\alpha/2)}((\sigma_A^{\,2}/n_A) + (\sigma_B^{\,2}/n_B))^{1/2} \tag{20}$$

where $z_{1-(\alpha/2)}$ is the value of the Normal distribution for a selected probability, $\alpha$, $\sigma_A$, and $\sigma_B$ are the uncertainties in the locations of the mixture point and the model, i.e., the projected image of the mixture, and $n_A$ and $n_B$ are the number of mixture and calibration spectra measured, respectively. The test statistic, $u$, is calculated based on an assumption that the noise is randomly distributed. However, the rotation operator which has been described will always select the final rotation vector to maximize the correlation between the vector and the residual response of the mixture not fitted by the calibration spectra. If the observed mixture spectrum contained only the desired analytes and random noise, a randomly selected final rotation vector would be expected to span all of the residual variance for a few sensors, some of the residual variance for most of the sensors, and none of the residual variance for some of the sensors. Overall, this vector would span only a portion of the residual variance of the mixture arising from random noise in the analytical measurement. On the average, half of the residual variance would be explained by a randomly selected final rotation vector. The rotation method used maximized the correlation between the final rotation vector and the residual variance. Therefore, this vector accounts for all of the residual variance in the mixture spectrum. This causes the scaled distance used in the background test to be twice as large as would be expected. If the scaled distance between the mixture point and the model, defined by the hyperplane, is greater than two times $u$, then the mixture is significantly different than the model, i.e., a sample background is present.

**Quantitation.** Assuming that an unsuspected spectral background has been uncovered by this approach, the question then arises of selecting the best method for obtaining estimates of the desired analyte concentrations. It was shown earlier that if the background spectrum is not known, then direct quantitation is not possible.

The general problem of quantitating an $N$-component mixture sample, which has been shown to contain an unidentified background component or composite background, can be most easily understood by first considering the simpler problem of quantitating a three-component mixture, e.g. two analytes plus background. In this case, the two pure analyte spectra are initially present in the calibration matrix, **K**. Therefore, when the data matrix **X** is formed, it will have three rows and $P$ columns. After normalizing each row to constant area and mean centering, the three spectra are projected from the $P$-dimensional measurement space into a two-dimensional feature space. The orthogonal rotation method which has been described will result in a matrix **S** of the form

$$\mathbf{s} = \begin{vmatrix} s_{11} & 0 \\ s_{21} & 0 \\ s_{31} & s_{32} \end{vmatrix} \tag{21}$$

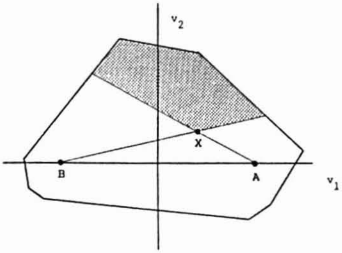

**Figure 1.** The positions of the two pure spectra, A and B, the mixture spectrum, X, and the constraint lines defining the nonnegative response region for the analysis of a hypothetical two analyte plus background mixture. The shaded region indicates the allowed region within which the pure spectra of the background component must lie.

where $s_{11} = -s_{21}$. The points $(s_{11}, 0)$ and $(s_{21}, 0)$ are the locations of the two scaled pure analyte spectra. Proper quantitation of the two desired analytes in the mixture spectrum requires that an estimate of the location of the background spectrum be made. Two additional constraints derived from the methods used for multicomponent resolution can be applied (*5*). These assumptions are: first, only nonnegative responses are allowed; and second, only nonnegative quantities of each component are permitted.

The first constraint, nonnegative responses, can be used to form a bounded region within which any physically meaningful spectrum, including the pure background, must be located. Since each spectrum has been centered prior to being projected, the nonnegativity constraint requires $\epsilon_1$ and $\epsilon_2$ be selected such that

$$\bar{x}_j + \epsilon_1 v_{1j} + \epsilon_2 v_{2j} \geq 0 \quad (22)$$

$$\text{for all } j = 1, ..., P$$

where $\epsilon_1$ and $\epsilon_2$ are the scalars which define the location of an arbitary allowed spectrum in the two-dimensional space. The shape of the entire feasible region can be obtained by recognizing that eq 22 actually provides $P$ separate inequality relationships, each of which defines an allowed half plane. The intersection of these $P$ half planes is the allowed region within which any nonnegative spectrum must fall.

The second constraint obtained from multicomponent resolution, nonnegative quantities of each component, requires that the observed mixture spectrum be a linear combination of the pure analyte and background spectra. Since each of the spectra have been normalized to constant area, this restriction implies that the mixture spectrum must lie inside the triangle defined by the two analyte spectra and the background spectrum. The region of the two-dimensional feature space which satisfies both of these constraints is shown in Figure 1.

Quantitative resolution of the mixture spectrum into the response due to each of the pure analytes and the response due to the background can be accomplished by an extension of the method described by Sharaf and Kowalski (*11*, *12*) for quantitating two component curve resolution mixtures. The matrix **S** contains the locations of the two pure analytes and the mixture points in 2-space. If these points are labeled as A, B, and X for analyte 1, analyte 2, and the mixture point, respectively, then A = $(s_{11}, 0)$, B = $(s_{21}, 0)$, and X = $(s_{31}, s_{32})$. Assume the true spectrum of the background is at point C, where C = $(s_{01}, s_{02})$. Now, define X′ as the image of X projected onto the line segment AB along axis XC, as shown in Figure 2. The projected image, X′, is located at $((s_{31}s_{02} - s_{32}s_{01})/(s_{02} - s_{32}), 0)$. For a given normalized spectrum, $\mathbf{x}_i$, the

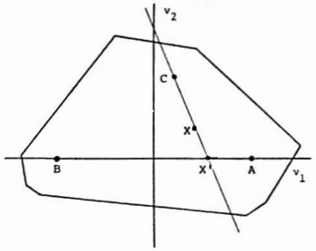

**Figure 2.** The image X′ of the mixture point is obtained by projection of the rotated mixture point, X, along the axis drawn from the pure background spectrum, C, onto the line segment AB connecting the two pure analytes.

coordinates, $(s_{i1}, s_{i2})$, of the point representing the mixture spectrum are given by

$$s_{i1} = (\mathbf{x}_i - \bar{\mathbf{x}})\mathbf{V}_1 \quad (23)$$

$$s_{i2} = (\mathbf{x}_i - \bar{\mathbf{x}})\mathbf{V}_2 \quad (24)$$

Since the two pure spectra, the background spectrum, and the mixture spectrum have all been normalized to constant area, the mixture spectrum can be expressed as a linear combination of the pure component and background spectra. If $\alpha$, $\beta$, and $\gamma$ are defined as the fraction of the mixture spectrum due to the background, analyte 1, and analyte 2, respectively, then the following relationships must hold:

$$\mathbf{x}_3 = \alpha\mathbf{x}_0 + \beta\mathbf{x}_1 + \gamma\mathbf{x}_2 \quad (25)$$

$$\alpha + \beta + \gamma = 1 \quad (26)$$

where $\mathbf{x}_0$ is the spectrum of the pure background. Additionally, any spectrum must also satisfy

$$\mathbf{x}_i = \bar{\mathbf{x}} + s_{i1}\mathbf{V}_1 + s_{i2}\mathbf{V}_2 \quad (27)$$

Rearrangement of eq 25, 26, and 27 results in

$$s_{31}\mathbf{V}_1 + s_{32}\mathbf{V}_2 = (\alpha s_{01} + \beta s_{11} + \gamma s_{21})\mathbf{V}_1 + (\alpha s_{02} + \beta s_{12} + \gamma s_{22})\mathbf{V}_2 \quad (28)$$

This vector equation implies that these relationships must also hold

$$s_{31} = \alpha s_{01} + \beta s_{11} + \gamma s_{21} \quad (29)$$

and

$$s_{32} = \alpha s_{02} + \beta s_{12} + \gamma s_{22} \quad (30)$$

Equation 27 placed no restrictions on the location of the points representing the pure component spectra. Recall that the rotation matrix employed resulted in the matrix **S** having a form such that $s_{21} = -s_{11}$ and $s_{12} = s_{22} = 0$. This allows eq 29 and 30 to be rewritten as

$$s_{31} = \alpha s_{01} + \beta s_{11} - \gamma s_{11} \quad (31)$$

and

$$s_{32} = \alpha s_{02} \quad (32)$$

From eq 32, it is immediately apparent that $\alpha$, the fraction of the mixture response due to the background component, is simply given as

$$\alpha = s_{32}/s_{02} \quad (33)$$

Solution of the system of three equations in three unknowns represented by eq 26, 31, and 32, results in

$$\beta = \frac{s_{02}(s_{11} + s_{31}) - s_{32}(s_{01} + s_{11})}{2s_{02}s_{11}} \quad (34)$$

$$\gamma = \frac{s_{02}(s_{11} - s_{31}) - s_{32}(s_{01} - s_{11})}{2s_{02}s_{11}} \qquad (35)$$

A modified approach may also be used for calculating the fractional responses. Since the points X, X′, and C are collinear, it can easily be shown that

$$\alpha = \frac{\langle \mathrm{X},\mathrm{X}' \rangle}{\langle \mathrm{C},\mathrm{X}' \rangle} \qquad (36)$$

where $\langle i,j \rangle$ represents the Euclidean distance between the points $i$ and $j$. Any point, including X′, which lies along the line segment AB in Figure 2 can be considered as two-component mixtures composed of only the analytes 1 and 2. Sharaf and Kowalski (*14*) proved the fraction of the mixture response due to a single component was related to the relative positions of the mixture and the two pure component spectra. In this situation, a portion of the mixture response has already been found to be caused by the background component: therefore the line segment AB represents the fraction of the remaining response due to the two desired analytes A and B. If X′ is selected by the method described above, then assume

$$\beta = (1 - \alpha)\frac{\langle \mathrm{B},\mathrm{X}' \rangle}{\langle \mathrm{A},\mathrm{B} \rangle} \qquad (37)$$

where $1 - \alpha$ is the fraction of the mixture response not due to the background component. After substitution of eq 33 or 36 into this relationship, calculation of the distances based on the known positions of A, B, and X′ yields

$$\beta = \frac{s_{02}(s_{11} + s_{31}) - s_{32}(s_{01} + s_{11})}{2s_{02}s_{11}} \qquad (38)$$

This is exactly the value obtained for $\beta$ by the original derivation. Quantitative resolution can now be accomplished. The concentration of analyte 1, expressed relative to the concentration of the calibration standard and corrected for the background interferent, is given by

$$\text{fraction analyte 1} = \frac{\beta a_{N+1}}{a_1} \qquad (39)$$

where $a_1$ and $a_{N+1}$ are the original areas of the calibration spectrum of analyte 1 and the area of the mixture spectrum, respectively. The concentration of analyte 2 is found by an analogous relationship

$$\text{fraction analyte 2} = \frac{\gamma a_{N+1}}{a_2} \qquad (40)$$

The quantitation described assumed that the location of the true background spectrum, C, was known. As is the case with other forms of multicomponent resolution, the exact location of C is not known, only a bounded region which must contain C is available. Conceivably, the location of the pure background spectrum might be the same as the location of the mixture spectrum: this situation would imply that the observed mixture was composed of entirely background and all of the desired analytes were absent. At the other extreme, the background spectrum might be as far from the mixture spectrum as possible. In the absence of any further information regarding the background, two different projection methods have been developed: perpendicular projection and extreme vertex projection. Neither of these projection methods will totally correct for the effects of the background components; however, they do provide a method of estimating the magnitude of the background response. These projection methods are illustrated in Figure 3.

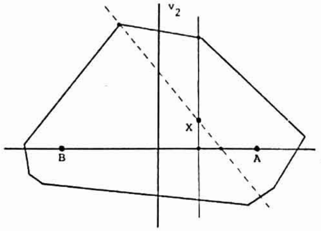

**Figure 3.** The perpendicular (solid line) and extreme vertex (dashed line) projections for the estimation of the fraction of the mixture response due to the background component.

The perpendicular projection method is based on an assumption that the spectrum of the background is approximately equally similar to both of the pure component spectra. This method will minimize the distance between the point representing the mixture spectrum and its projected image. The point used as an estimate of the pure background spectrum is obtained from the intersection of the perpendicular projection axis and the outer bound, i.e., the nonnegative response constraint.

The extreme vertex projection method is based on an assumption that the spectrum of the mixture is primarily due to the desired analytes. This projection minimizes the estimate of the fraction of the mixture response resulting from the background component. The point used as an estimate of the pure background is selected to minimize the $\alpha$ calculated by eq 36. It can easily be shown that this point must occur at a vertex of the constraint polygon. The term, extreme vertex projection, selected when this method was first developed, is not precisely correct since the most distance vertex from the mixture point is frequently but not necessarily always the vertex which minimizes $\alpha$.

The two methods discussed for estimating the fraction of the mixture response due to the background have been described in detail for the case of a two analyte plus background mixture. The algorithms may be directly extended into higher dimensions. The perpendicular projection and extreme vertex projection methods retain the same physical interpretations in higher dimensional situations. After estimation of the location of the background spectrum, the quantitation of an $N$ component mixture can be accomplished by an extension of the geometrical approach described in eq 36 and 37.

## EXPERIMENTAL SECTION

The absorption of visible or ultraviolet radiation, as described by the Beer–Lambert law, is a common analytical application of the multicomponent linear additive model. Two separate experimental systems were investigated. All computations and simulated mixture experiments were performed on the Department of Chemistry VAX 11/780 computer.

**Metal Ions in Aqueous Solution.** Visible absorption spectra of four calibration and eight mixture samples were recorded every 2.0 nm from 350 to 850 nm with a Kontron UVIKON Model 820 UV/visible spectrophotometer equipped with a Kontron Model 48 thermoprinter. All subsequent data analysis was accomplished by using a subset of 20 wavelengths selected every 24 nm from 850 to 394 nm. Stock solutions were prepared by dissolving the appropriate metal salt in 4% nitric acid. Calibration standards and synthetic mixture samples were prepared by dilution of the stock solutions. The metal salts used and the concentrations of the corresponding calibration standards, in grams of salt per milliliter of solution, were as follows: $Cr_2(SO_4)_3{\cdot}nH_2O$, $6.275 \times 10^{-3}$ g/mL; $Ni(NO_3)_2{\cdot}6H_2O$, $4.391 \times 10^{-2}$ g/mL; $Co(NO_3)_2{\cdot}6H_2O$, $4.384 \times 10^{-2}$ g/mL; and $Cu(NO_3)_2{\cdot}2^1/_2H_2O$, $8.757 \times 10^{-2}$ g/mL. The compositions of the mixture samples are given in Table I. Each synthetic mixture contained equal amounts of chromium and nickle with varying amounts of cobalt and/or copper added to simulate the background component.

**Table I. Concentration of Individual Metal Ions, Expressed in Terms of Amounts Relative to the Corresponding Calibration Sample, in Eight Mixture Samples Used for Visible Absorption Spectrophotometry**

| mixture | Cr | Ni | Co | Cu |
|---|---|---|---|---|
| 1 | 1.00 | 0.50 | 0.00 | 0.00 |
| 2 | 1.00 | 0.50 | 0.10 | 0.00 |
| 3 | 1.00 | 0.50 | 0.20 | 0.00 |
| 4 | 1.00 | 0.50 | 0.40 | 0.00 |
| 5 | 1.00 | 0.50 | 0.00 | 0.10 |
| 6 | 1.00 | 0.50 | 0.00 | 0.20 |
| 7 | 1.00 | 0.50 | 0.10 | 0.20 |
| 8 | 1.00 | 0.50 | 0.20 | 0.10 |

**Table II. Six Groups Comprising the Second Simulated RNA Mixture Data Set**

| group | analyte 1 | analyte 2 | background |
|---|---|---|---|
| A | adenylic | guanylic | cytidylic |
| B | adenylic | cytidylic | guanylic |
| C | cytidylic | guanylic | adenylic |
| D | adenylic | guanylic | uridylic |
| E | adenylic | uridylic | guanylic |
| F | cytidylic | guanylic | uridylic |

**Simulated Mixtures of RNA Constituents.** Two different sets of RNA mixture absorption spectra were simulated by using 18 analytical wavelengths spaced every 4 nm from 220 to 288 nm. The first data set, used for evaluation of noise and replication effects, consisted of 120 mixture samples. Each mixture was composed of equal amounts of adenylic and cytidylic acid, to which was added a selected amount of guanylic acid as a simulated background component. The background component was added so that the fraction of the mixture response due to the background ranged from zero to 8.0% at ten selected levels: 0.0, 0.2, 0.5, 1.0, 1.5, 2.0, 3.0, 4.0, 6.0, and 8.0%. The calibration spectra and the mixture spectrum were obtained by averaging either 5, 10, or 20 simulated replicate measurements. Each individual measurement was perturbed by adding random noise at one of four selected levels. The noise was modeled as a normal distribution with a mean of zero and relative standard deviation of 0.5, 1.0, 2.0, or 4.0% RSD. The standard deviation calculated from the simulated replicate experimental measurements was used to estimate the experimental measurement uncertainty. A second data set, used to evaluate the effects of varying the relative amounts of each analyte and the amount and identity of the interfering background constituent, consisted of 210 mixture samples. All of the calibration and mixture spectra in the second data set were the average of five replicate measurements to which 1.0% RSD noise was added. The 210 mixture samples were further subdivided into six groups of 35 samples each, which varied in the identity of the two components included as desired analytes and the component selected to act as the background component. The compounds comprising these six groups are shown in Table II. Within each group of 35 mixtures, the two analytes were present in seven different quantities relative to each other. These levels ranged from ten units of analyte one per unit of analyte two, to one unit of analyte one per ten units of analyte two: 10:1, 5:1, 2:1, 1:1, 1:2, 1:5, and 1:10. At each of these levels the fraction of the response due to the background component was varied in five steps: 0.5, 1.0, 2.0, 4.0, and 8.0%. Each of the 330 simulated experiments was repeated 20 times. The results for the 20 sets of estimated analyte concentrations were averaged.

## RESULTS AND DISCUSSION

The objective of the aqueous metal ion experiment was 2-fold: first, to determine if the presence of a simulated background component could be detected; and second, to evaluate the performance of the two projection methods in correcting for the background response. The spectra of the calibration solutions and the mixture samples are shown in Figures 4 and 5. Each mixture spectrum, except mixture number 1, is dependent not only on the chromium and nickel analytes but also on the added background constituent. It would be difficult if not impossible for the analyst to determine which mixtures were not adequately represented by the two-component model by observing the mixture spectrum alone. The eight mixture samples were then quantitated by three methods: ordinary least-squares regression, and rotation from a 20-dimensional measurement space to a two-dimensional feature space followed by the perpendicular projection and extreme vertex projection techniques. The results obtained are summarized in Table III. As expected, ordinary least-squares regression gives no indication of the presence of the background component and results in estimated concentrations which are significantly in error. Comparing the ordinary least-squares results for successive mixtures indicates that the errors in the concentration estimates appear to be correlated. Additionally, the errors appear to be dependent on the identity, consequently also the spectrum, of the background interferent. In mixtures 2–4, where cobalt is the background component, the chromium estimate is always high and the nickel estimate is always low. When copper was added as an interferent, e.g., mixtures 5 and 6, the reverse occurs, the chromium estimate is low, and the nickel is biased high. In mixture 8, in which both copper and cobalt were added, the estimates for both expected analytes are too high indicating that the ordinary least-squares method may overestimate both analytes due to its inability to assign a portion of the total response to the background component. There was some improvement in the results obtained when the two projection methods were used. The perpendicular projection method performed best for mixtures 7 and 8. In these mixtures, which contained both added cobalt and copper, the background response affected almost the entire spectral region. Quantitation of mixtures 2–4 and 5–6, which contained either

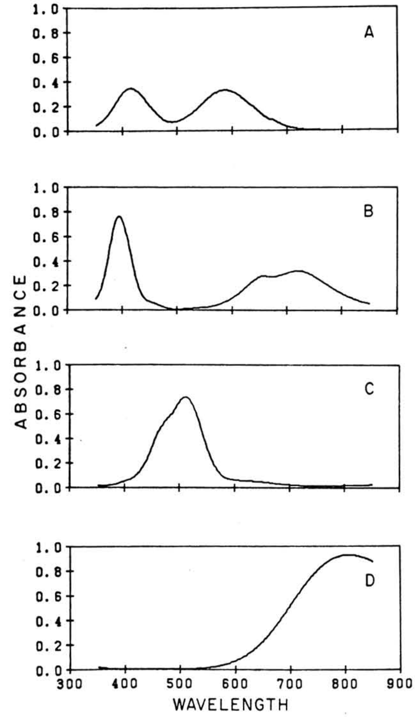

**Figure 4.** Pure spectra of aqueous metal ion calibration solutions: (a) chromium ion, (b) nickel ion, (c) cobalt ion, and (d) copper ion.

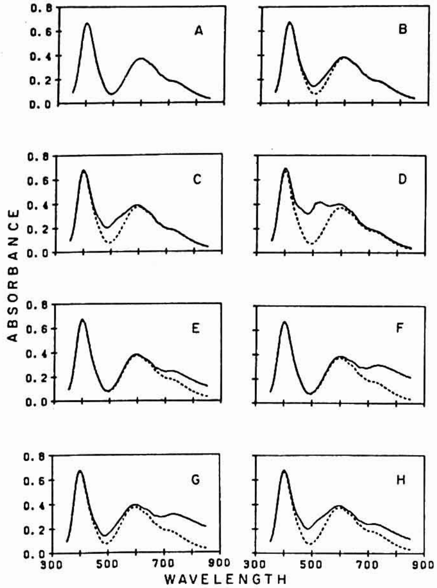

**Figure 5.** Absorption spectra of mixtures 1–8 (labeled A to H, respectively) for the metal ion samples described in Table II. In mixtures 2–8, containing an added background, the dotted line indicates the response which would be observed for the same mixture in the absence of the background component.

**Table III. Amounts of Chromium and Nickel Found in the Mixture Samples by Quantitation Using Ordinary Least Squares (OLS), Perpendicular Projection (PP), and the Extreme Vertex Projection (EVP) Methods**[a]

| mixture | | OLS | PP | EVP |
|---|---|---|---|---|
| 1 | Cr | 1.000 | 0.992 | 0.995 |
| | Ni | 0.504 | 0.500 | 0.501 |
| 2 | Cr | 1.098 | 1.039 | 1.023 |
| | Ni | 0.482 | 0.463 | 0.501 |
| 3 | Cr | 1.192 | 1.069 | 1.035 |
| | Ni | 0.458 | 0.425 | 0.504 |
| 4 | Cr | 1.398 | 1.138 | 1.078 |
| | Ni | 0.410 | 0.367 | 0.506 |
| 5 | Cr | 0.930 | 0.831 | 1.017 |
| | Ni | 0.640 | 0.568 | 0.503 |
| 6 | Cr | 0.834 | 0.695 | 1.004 |
| | Ni | 0.778 | 0.612 | 0.504 |
| 7 | Cr | 0.928 | 0.776 | 1.041 |
| | Ni | 0.743 | 0.591 | 0.495 |
| 8 | Cr | 1.109 | 0.977 | 1.055 |
| | Ni | 0.582 | 0.524 | 0.497 |

[a] In all cases the correct amounts of chromium and nickel are 1.000 and 0.500 units, respectively.

added cobalt or added copper, was not as accurate. This was postulated to be caused by the fact that the spectral background was affecting only a portion of the mixture spectrum, hence the assumption underlying the perpendicular projection method that the background is about equally similar to both analytes is in error. The extreme vertex projection appeared to perform well for all eight mixture samples. This can be explained by recognizing that the pure spectra of these four metal ions are fairly unique. For each metal there is a spectral region in which that metal ion has the dominant effect on the response. Because of these unique spectral regions the two-dimensional representations of the metal ion spectra are found close to the outer bound.

Zscheile and co-workers (*13*) used four RNA constituents to evaluate the instability of the solution obtained for three- and four-component mixtures by ordinary least-squares regression. More recently, Kalivas (*14*) performed simulated GSAM experiments using these four compounds. Zscheile et al. observed that the quantitative results obtained for a three-component mixture of adenylic, cytidylic, and guanylic acids were markedly better than the results obtained for a four-component mixture composed of the three above compounds and uridylic acid. They postulated that this improvement was due to the close linear relationship between the absorption spectra of adenylic and uridylic acids. Simulated experiments were performed with these compounds in order to: first, determine the effects of the measurement noise and measurement replication on the detectability of a simulated background component; second, evaluate the effect of the uniqueness of the background response on its detectability; and third, evaluate the successfulness of the perpendicular and extreme vertex projection methods over a wide range of mixture samples.

**Simulated Data Set 1.** Figure 6 illustrates the distance in the two-dimensional feature space from the point representing the mixture spectrum to the line segment drawn between the two pure analyte spectra, representing the ideal two-component model, as a function of the percent added background. The measured distance, e.g., average score of the mixture on the second rotation vector, was found to be related to the amount of background present. When the percentage of the response due to the background component was greater than approximately twice the measurement noise, this distance was linearly related to the amount of background present. At background levels below about half of the measurement noise, the distance appeared to be virtually independent of the added background. The background level at which the departure from linearity was observed depended not only on the measurement noise but also on the number of simulated replicate measurements. In all 120 mixtures, the uncertainty in the position of the ideal two-component model, calculated from the estimated uncertainties in the calibration spectra, along the axis of the second rotation vector was found to depend on both the measurement noise and the number of replicate measurements. For simulated mixtures obtained from five replicate measurements, the added background is not detected until the percentage of the response due to the background is greater than two times the noise level. Simulated mixtures of 10 replicate measurements allow detection of the noise at twice the noise level. If 20 replicate measurements are made, a background component with a response as low as half of the noise level may be successfully detected.

**Simulated Data Set 2.** The average errors in the estimated quantities of analytes 1 and 2 for the entire set of 210 simulation mixtures and three subsets, by compound group, by relative amounts of analytes, and by amount of background added, are summarized in Table IV. Over all 210 mixtures the perpendicular projection method provided the lowest average error: the next best results were obtained using the extreme vertex projection technique; and the poorest results were obtained from ordinary least-squares regression. No underlying relationship could be distinguished which related the magnitude of the errors in the analyte estimates to the

**Table IV. Average Percentage Error in Analytes 1 and 2 When Quantitation Is Performed by Ordinary Least-Squares Regression, Perpendicular Projection, and Extreme Vertex Projection Methods**

| | OLS | | PP | | EVP | |
|---|---|---|---|---|---|---|
| | anal. 1 | anal. 2 | anal. 1 | anal. 2 | anal. 1 | anal. 2 |
| all 210 | 2.10 | 9.56 | 0.11 | 7.47 | 2.04 | 8.05 |
| compd group | | | | | | |
| A | −10.99 | 21.52 | −13.34 | 19.22 | −6.49 | 16.01 |
| B | 7.90 | 3.83 | 5.96 | 2.03 | 3.46 | 6.60 |
| C | −3.86 | 15.33 | −5.73 | 12.93 | −3.31 | 13.08 |
| D | 11.13 | 1.04 | 9.36 | −0.53 | 9.65 | 0.56 |
| E | 10.87 | 1.48 | 9.11 | −0.22 | 10.43 | 0.74 |
| F | −2.48 | 14.17 | −4.68 | 11.37 | −1.53 | 11.18 |
| rel amt | | | | | | |
| 10:1 | −0.65 | 28.53 | −1.66 | 25.83 | −1.33 | 29.48 |
| 5:1 | 0.71 | 15.56 | −1.41 | 13.25 | −1.17 | 14.65 |
| 2:1 | 0.88 | 7.74 | −1.00 | 5.97 | −0.70 | 5.95 |
| 1:1 | 1.16 | 5.20 | −0.70 | 3.31 | −0.07 | 3.16 |
| 1:2 | 1.65 | 3.93 | −0.19 | 2.05 | 1.10 | 1.78 |
| 1:5 | 3.45 | 3.11 | 1.51 | 1.15 | 5.01 | 0.78 |
| 1:10 | 6.18 | 2.86 | 4.24 | 0.88 | 11.42 | 0.51 |
| background | | | | | | |
| 0.5% | 0.36 | 1.43 | −0.70 | 0.41 | −0.13 | 0.38 |
| 1.0% | 0.64 | 2.94 | −0.54 | 1.83 | −0.29 | 1.85 |
| 2.0% | 1.30 | 5.91 | −0.19 | 4.50 | 1.07 | 4.72 |
| 4.0% | 2.68 | 12.18 | 0.40 | 9.87 | 2.97 | 10.70 |
| 8.0% | 5.51 | 25.35 | 1.58 | 20.71 | 6.16 | 22.59 |

**Table V. Summed Absolute Values of the Percentage Error for 36 Simulated Mixtures (20 Averaged Replicate Measurements) from Data Set**

| | measurement noise | | | | | | | |
|---|---|---|---|---|---|---|---|---|
| | 0.5% | | 1.0% | | 2.0% | | 4.0% | |
| background | PP | EVP | PP | EVP | PP | EVP | PP | EVP |
| 0.2% | 0.12 | 0.05 | 0.60 | 0.47 | 1.36 | 1.20 | 3.88 | 3.21 |
| 0.5% | 0.35 | 0.45 | 0.43 | 0.25 | 0.86 | 0.69 | 3.52 | 2.79 |
| 1.0% | 0.95 | 1.19 | 0.69 | 0.90 | 0.53 | 0.42 | 1.96 | 1.48 |
| 1.5% | 1.70 | 2.00 | 1.40 | 1.65 | 1.07 | 0.87 | 1.02 | 0.68 |
| 2.0% | 2.08 | 2.65 | 2.10 | 2.46 | 1.38 | 1.62 | 1.89 | 0.26 |
| 3.0% | 3.44 | 4.22 | 3.30 | 3.96 | 2.67 | 3.13 | 1.95 | 1.67 |
| 4.0% | 4.66 | 5.65 | 4.68 | 5.63 | 3.91 | 4.68 | 3.02 | 3.47 |
| 6.0% | 7.31 | 8.67 | 7.13 | 8.60 | 6.65 | 8.01 | 6.02 | 7.08 |
| 8.0% | 9.87 | 11.78 | 9.82 | 11.67 | 9.45 | 11.28 | 8.60 | 10.12 |

correlation between the two-analyte spectra or to correlation between the analyte and background spectra; i.e., no clear compound group effect was evident for the six analyte–background combinations attempted. It was noted, however, the relative performance of the three quantitation methods was consistent. For example, compound group B, which yielded the best results by ordinary least-squares regression, also yielded the best results for the two projection methods. The poorest results for all three methods occurred with compound group A. For all three quantitation methods, the summed percentage error for the two analytes was larger for the mixtures of unequal amounts of analytes, e.g., 10:1 or 1:10, than for mixtures of near equal amounts. In mixtures composed of unequal amounts of analytes, the larger percentage error generally corresponded to the analyte present in the smaller amount. For all levels of added background, the errors obtained from ordinary least-squares regression were larger and more biased high than the corresponding perpendicular or extreme vertex projections. This was expected since the two projection methods subtract a portion of the initial response prior to quantitation of the two analytes. While in many cases the improvement was easily observed, the overall errors with the perpendicular projection or the extreme vertex projection are smaller but still significant. The perpendicular projection method provided better results than the extreme vertex projection method if more than 1.0% background was present. For mixtures containing 0.5 or 1.0% background, extreme vertex projection gave slightly better results. Since the noise level in the second data set was fixed at 1% for all of the mixtures, the first data set, which contained four different noise levels, was reexamined in order to determine whether the shift in the projection method providing the most accurate results was related to the noise level. Table V shows the results for the same nine mixtures taken from the first data set at four different noise levels. These data substantiate the conclusion that the perpendicular projection method is more accurate if the percentage of the response due to the background is greater than the percent measurement noise. The extreme vertex projection method provides more accurate results if the percent background response is less than the noise level. This occurs because in cases where the background is less than the noise, the distance from the mixture point to the ideal model, as shown in Figure 6, is independent of the background response and either projection method is overcorrecting for the background response. The extreme vertex projection method is designed to minimize the fraction of the total response due to the background component, hence in this situation it overcorrects by the least amount and provides slightly better results.

The initial objectives of this investigation were 2-fold. First, to develop a method which would provide the analyst with a means of detecting the presence of unsuspected interferents

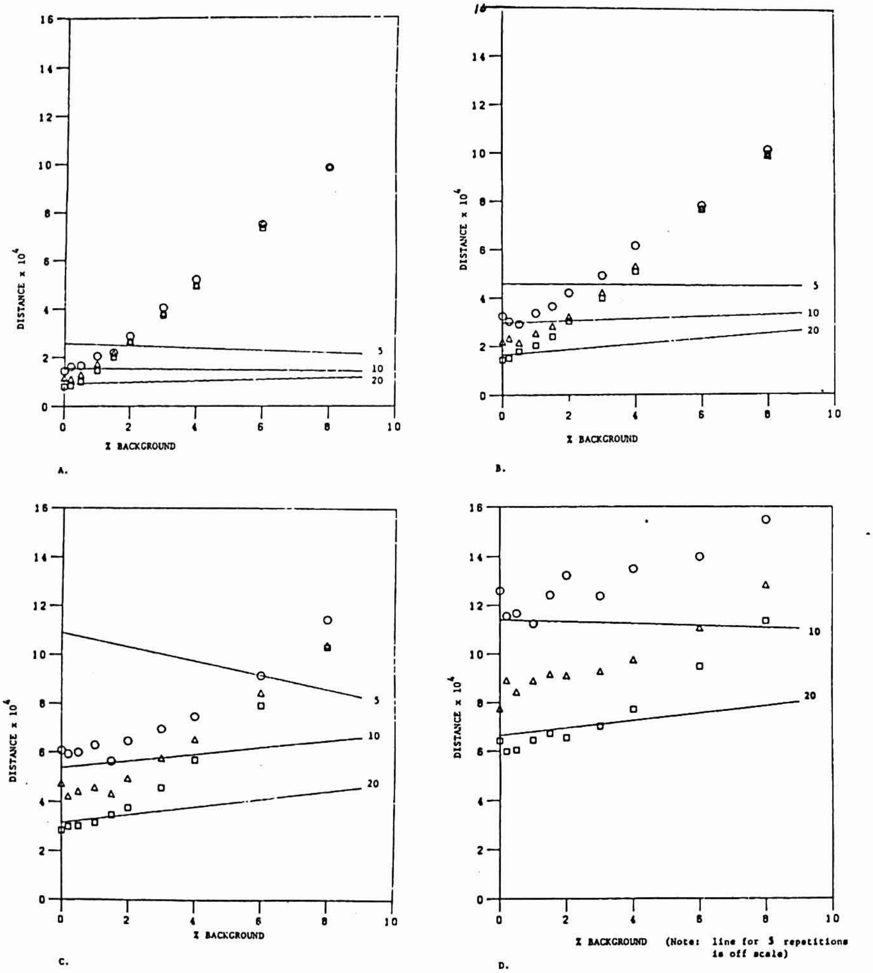

**Figure 6.** Scaled distance from the observed mixture spectrum to the ideal model as a function of the background added (○, 5 replicate measurements; △, 10 replicate measurements; □, 20 replicate measurements). The solid lines represent the threshold, 2*$u$, above which a background can be detected. The RSD of the noise in the simulated mixture is (A) 0.5%, (B) 1.0%, (C) 2.0%, and (D) 4.0%.

during a multicomponent analysis. Second, to provide a means of obtaining estimates of the desired analyte concentrations if an unsuspected interferent was found. The methods which have been proposed have combined approaches based on multicomponent calibration, quantitation, and resolution methods.

The simulated experimental data collected for mixtures of RNA constituents indicate that a background test based on estimating the model uncertainty from the measurement error can be used to test for the presence of unsuspected interferents during a multicomponent analysis. Figure 6 suggests an overall limit to the detectability of background interferents. These results imply that the level at which a background response can be detected depends on the noise and the number of replicate measurements. Simulations performed with higher levels of noise, e.g., 2.0 and 4.0% RSD, illustrate the problems caused by a small number of replicate measurements. The model uncertainty in the two-dimensional feature space decreases noticeably when the number of replicate measurements is increased from 5 to 10 and finally to 20 repetitions.

Over a wide range of samples the perpendicular projection method provided more accurate results than ordinary least-squares regression. The extreme vertex projection method also gave improved results, but unless the background components possessed unique spectral features this method did not perform as well as the perpendicular projection approach. Recalling that the perpendicular projection method was based on the assumption that the background was approximately equally similar to each of the desired analyte spectra may allow a further improvement in this method. The individual sensor loadings into the perpendicular projection axis, equivalently the final rotation vector, indicates the sensors which are the most highly correlated with those features of the mixture not fitted by the calibration spectra. If the analysis is overdetermined with respect to the number of sensors employed, then elimination of those sensors which load most strongly into the final rotation vector may result in decreasing the overall effect of the background components on the mixture response. This suggests an additional criteria which might be useful for optimizing the sensor selection in a multicomponent analysis. While both of these two quantitation approaches provided improved results, significant errors may still occur. The problem of background detection increases as more known analytes are present due to the increased likelihood that the background can be modeled as a linear combination of the analytes. These difficulties imply that identification of all sample components, both desired analytes and interferents, affecting the measured response is still a worthwhile goal for obtaining the most accurate analytical results.

## LITERATURE CITED

(1) Warner, I. M.; Davidson, E. R.; Christian, G. D. *Anal. Chem.* **1977**, *49*, 2155-2159.
(2) Leggett, D. J. *Anal. Chem.* **1977**, *49*, 276-281.
(3) Gayle, J. B.; Bennett, H. D. *Anal. Chem.* **1978**, *50*, 2085-2089.
(4) Haaland, D. M.; Easterling, R. G. *Appl. Spectrosc.* **1982**, *36*, 665-673.
(5) Lawton, W. H.; Sylvestre, E. A. *Technometrics* **1971**, *13*, 617-633.
(6) Martens, H. *Anal. Chim. Acta* **1979**, *112*, 423-442.
(7) Spjøtvoll, E.; Martens, H.; Volden, R. *Technometrics* **1982**, *24*, 173-180.
(8) Kaiser, H. *Pure Appl. Chem.* **1973**, *34*, 35-61.
(9) Saxberg, B. E. H.; Kowalski, B. R. *Anal. Chem.* **1979**, *51*, 1031-1038.
(10) Nattrella, M. G. "Experimental Statistics"; Government Printing Office: Washington, DC, 1963; National Bureau of Standards Handbook 91; Chapter 5.
(11) Sharaf, M. A.; Kowalski, B. R. *Anal. Chem.* **1981**, *53*, 518-522.
(12) Sharaf, M. A.; Kowalski, B. R. *Anal. Chem.* **1982**, *54*, 1291-1296.
(13) Zscheile, F. P.; Murray, H. C.; Baker, G. A.; Peddicord, R. G. *Anal. Chem.* **1962**, *34*, 1776-1780.
(14) Kalivas, J. H. *Anal. Chem.* **1983**, *55*, 565-567.

RECEIVED for review June 18, 1984. Resubmitted November 27, 1984. Accepted November 27, 1984. This work was supported in part by the Office of Naval Research.

# Automated Fluorometric Method for Hydrogen Peroxide in Atmospheric Precipitation

**Allan L. Lazrus,* Gregory L. Kok, Sonia N. Gitlin, and John A. Lind**
*National Center for Atmospheric Research, P.O. Box 3000, Boulder, Colorado 80307*

**Scott E. McLaren**
*Atmospheric Science Research Center, 1400 Washington Avenue, Albany, New York 12222*

**An automated analytical technique for the determination of hydrogen peroxide ($H_2O_2$) in the liquid phase has been developed. The chemistry of this technique is based on the reaction of $H_2O_2$ with horseradish peroxidase and *p*-hydroxyphenylacetic acid (POPHA). The resulting reaction forms the fluorescent dimer of POPHA. By use of conventional fluorescence detection techniques a detection limit of 1.2 × $10^{-8}$ M (0.4 ppbm) $H_2O_2$ is obtained for a 1.5-mL aqueous sample. The coefficient of variation is 0.66% at 1.6 × $10^{-6}$ M (53 ppbm). The analytical chemical reaction responds stoichiometrically to both $H_2O_2$ and organic hydroperoxides. To discriminate $H_2O_2$ from organic hydroperoxides, a novel dual-channel chemical flow system has been devised to separately determine total hydroperoxides and organic hydroperoxides. The concentration of $H_2O_2$ is determined by the difference between these two measurements. The system has been tested extensively for potential interferences commonly found in environmental aqueous samples, and none has been observed.**

Hydrogen peroxide rapidly oxidizes bisulfite ion in water at pH values below 4.5, and therefore is currently believed to contribute significantly to the generation of sulfuric acid in atmospheric precipitation (*1*, *2*).

Studies on $H_2O_2$ in precipitation samples have been limited by the availability of sensitive analytical techniques. Early studies on $H_2O_2$ in precipitation were conducted using iodometric techniques (*3*, *4*). The luminol chemiluminescence analytical method for $H_2O_2$ (*5*, *6*) provided the first approach for determining $H_2O_2$ at the 10 nM level in precipitation. The luminol technique has been modified by adapting hemin as a catalyst (*7*). Recently a scopoletin based enzyme technique has been used for the determination of $H_2O_2$ in precipitation samples (*8*).

Interferences were observed in the luminol technique applied to atmospheric precipitation samples collected during autumn in Boulder, CO. The interference was detected by the persistence of a positive signal for $H_2O_2$, even though the sample had been treated with the enzyme catalase. The selective decomposition of $H_2O_2$ by catalase has been used earlier to identify $H_2O_2$ in atmospheric samples (*9*)

$$2H_2O_2 \xrightarrow{\text{catalase}} 2H_2O + O_2 \qquad (1)$$

Peroxidase is another enzyme characterized by selectivity toward hydroperoxides. In the presence of a hydrogen donor molecule such as *p*-hydroxyphenylacetic acid (POPHA) the enzyme peroxidase catalyzes the reduction of $H_2O_2$ via the following reaction (*10*):

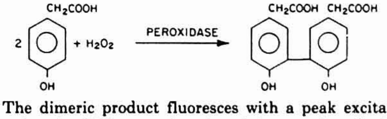

(2)

The dimeric product fluoresces with a peak excitation wavelength of 320 nm and peak emission wavelength of 400 nm (*10*). The stoichiometry of reaction 2 indicates that for every hydroperoxide (-O-O-H) bond broken, one dimer is formed. The fluorescence of this dimer is therefore directly

© 1985 American Chemical Society

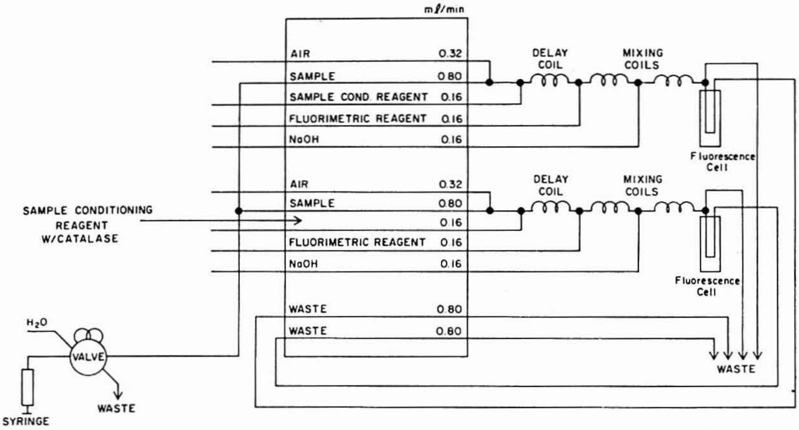

**Figure 1.** Technicon AutoAnalyzer pump manifold and flow system.

proportional to the peroxide concentration.

An automated analytical technique based on the selectivity of the two enzymes, catalase and peroxidase, has been developed in order to provide a highly specific method for atmospheric samples. In addition, comparative analyses of $H_2O_2$ in cloud water were conducted between the luminol method and the present technique at Whiteface Mountain, NY.

The technique utilizes a dual channel flow system and dual cell fluorometer which provides simultaneously the fluorescent signal resulting from the peroxidase reaction (eq 2) and an analytical blank derived from the catalase reaction (eq 1). The chemical reagents are identical in both channels, except for the addition of catalase to the second channel which destroys the $H_2O_2$ before the addition of POPHA.

The catalase analytical blank is provided for two reasons: first, the reaction of some organic hydroperoxides and POPHA will also be catalyzed by peroxidase; second, fluorescent organic substances could conceivably occur in polluted rain which might interfere with the fluorescence signal of the POPHA dimer.

It should be pointed out that only insignificant catalase blank signals (e.g., less than 1% of the $H_2O_2$ signal) have been observed in precipitation samples collected at Boulder and Denver, CO, or in cloud water samples collected at Whiteface Mountain, NY. The Henry's law coefficients of both methylhydroperoxide and peroxoacetic acid are so much lower than that of $H_2O_2$ that significant scavenging of these organic substances from air by cloud droplets or rain is not likely (*11*).

## EXPERIMENTAL SECTION

A detailed description of the reagents is given in Table I. The flow system is operated with a Technicon AutoAnalyzer peristaltic pump. The pump manifold is comprised of standard AutoAnalyzer pump tubes and components (Figure 1). Since reagent addition and timing are critical, the use of Technicon flow-certified pump tubes is advisable.

The sample (1.5 mL) is loaded, using a glass syringe with a Teflon plunger, into a sample injection valve and split equally between the two channels. The sample channel is initially segmented with air bubbles in order to maintain sharp concentration gradients along the stream.

The sample conditioning reagent (Table I) is then added. Potassium hydrogen phthalate buffer adjusted to pH 5.5 maintains the sample in the appropriate pH range for both the catalase and peroxidase reactions. The buffered reagent also contains EDTA to prevent possible interferences by metal ions.

**Table I. Reagent Concentrations Used**

Sample Conditioning Reagent
0.35 M KHPhthalate[a], adjusted to pH 5.5
$8.4 \times 10^{-4}$ M tetrasodium EDTA[b]

Sample Conditioning Reagent with Catalase
0.35 M KHPhthalate, adjusted to pH 5.5
$8.4 \times 10^{-4}$ M tetrasodium EDTA
490 $\sigma$ units of catalase/mL[c] of reagent

Fluorescence Reagent
0.35 M KHPhthalate, adjusted to pH 5.5
$8.0 \times 10^{-3}$ M *p*-hydroxyphenylacetic acid[d]
8 purpurogallin units of peroxidase[e]/mL reagent

Base
0.4 M NaOH[f]

[a] Potassium hydrogen phthalate, Fischer Scientific Co. P-243. Adjust pH using 10 N NaOH. [b] Sigma Chemical Co., ED 4SS. [c] Sigma Chemical Co., Stock C-100. [d] Kodak (Eastman Kodak Co.), Lot No. C8B. [e] Sigma Chemical Co., Stock P8375, Type VI. [f] J.T. Baker Co.

The fluorescence reagent (Table I) next joins the sample stream. The POPHA must be purified before use by recrystallizing from aqueous solution. Activated charcoal is used in the recrystallization to remove impurities. All other reagents can be used as received. The fluorescence reagent can be kept for several days and should be discarded when either the base line becomes unsteady or significant degradation of the linearity of response is observed.

NaOH (Table I) is then added to the sample stream. The fluorescence quantum yield of the POPHA dimer diminishes below pH 9.0 but remains at a maximum above pH 10.0. The addition of NaOH maintains the reaction stream at pH 10.0 or higher permitting analysis of samples as acidic as pH 2.0 without measurement artifact.

The reaction stream passes through a five-turn, 2 mm i.d. glass mixing coil after the addition of each reagent.

The second sample channel is identical with the first, except that the sample conditioning reagent contains catalase in addition to the other constituents. The catalase used was obtained from Sigma Chemical Co. This material, obtained from bovine liver, is doubly crystallized and suspended in water containing 0.1% thymol with an indicated activity of 35 300 Sigma units per mg of protein. One Sigma unit of catalase activity will decompose $1.0 \times 10^{-6}$ mol of $H_2O_2$/min at pH 7.0 at 25 °C, while the concentration of $H_2O_2$ falls from $10.3 \times 10^{-6}$ to $9.2 \times 10^{-6}$ mol/mL of reaction mixture.

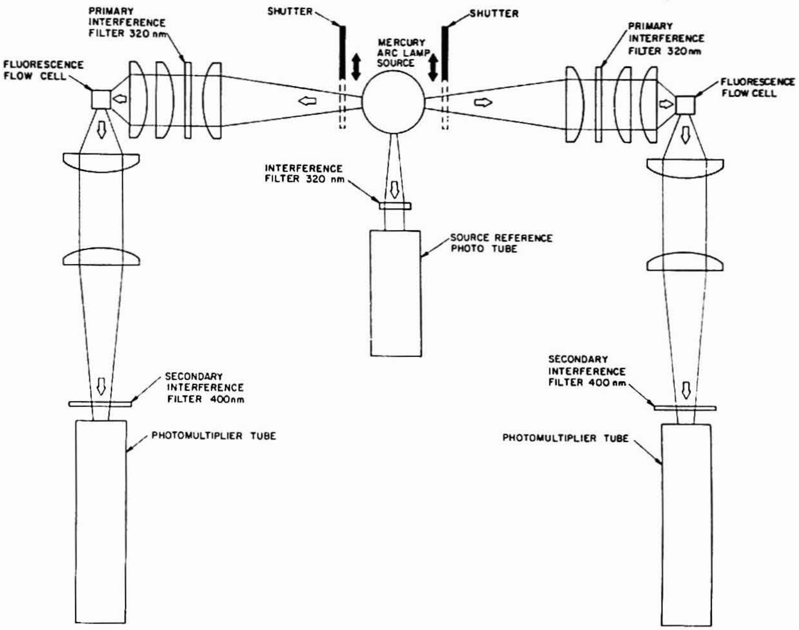
PRIMARY INTERFERENCE FILTER 320 nm
SHUTTER
MERCURY ARC LAMP SOURCE
SHUTTER
PRIMARY INTERFERENCE FILTER 320nm
FLUORESCENCE FLOW CELL
FLUORESCENCE FLOW CELL
INTERFERENCE FILTER 320 nm
SOURCE REFERENCE PHOTO TUBE
SECONDARY INTERFERENCE FILTER 400nm
SECONDARY INTERFERENCE FILTER 400 nm
PHOTOMULTIPLIER TUBE
PHOTOMULTIPLIER TUBE

**Figure 2.** Optical diagram for the dual beam fluorometer.

$H_2O_2$ standards were prepared by serial dilution of a stock $H_2O_2$ standard. The $H_2O_2$ concentration of the stock standard is determined by titration with $KMnO_4$. A 1% $H_2O_2$ standard is prepared by dilution of commercially available 30% $H_2O_2$. The 1% standard is preserved by the addition of $5 \times 10^{-5}$ M sodium stannate. Stock $H_2O_2$ solutions prepared in this manner are found to decay at a rate of about 1% per month. Working standards are prepared daily. Glassware to be used for the first time in preparing $H_2O_2$ standards should be washed with soap, rinsed, and allowed to soak in deionized water for several days with frequent water changes.

To calibrate the catalase channel all traces of catalase must be removed from the system. This is accomplished by replacing the catalase reagent with 0.1 N HCl and running the flow system for a few minutes. The strong acid will denature the catalase instantly. After the removal of the catalase, water is set in place of the catalase reagent and the channel calibrated with $H_2O_2$ in the regular manner.

In analytical work with $H_2O_2$ it is important that all solutions be prepared from water that is free of bacteria as well as ionic impurities. In these studies, solutions were prepared from water purified by a cartridge deionization and organic removal system (Millipore Corp). The resistance of the final water was greater than $1.8 \times 10^7$ Ω. Bacteria may be present in cartridge deionization systems which rapidly decompose $H_2O_2$. It is important that a filter to remove bacteria be present on the outlet of the cartridge system and that the system be cleaned frequently.

Methyl hydroperoxide, ethyl hydroperoxide, and *n*-propyl hydroperoxide used to test the method were synthesized by the procedure of Riche and Hitz (*14*). These peroxides were purified through repeated extractions and washings with water. Technical grade *tert*-butyl hydroperoxide was obtained from Mallinkrodt. Peroxoacetic acid, 40%, was purchased from FMC Corp, Buffalo, NY. Methyl hydroperoxide and peroxoacetic acid were individually assayed by using iodometric techniques (*15*).

To use the instrument for the quantitative determination of methyl hydroperoxide and peroxoacetic acid up to concentrations of about $3 \times 10^{-5}$ M, it is sufficient to calibrate with $H_2O_2$. For higher concentrations, or for organic hydroperoxides of higher molecular weight, calibrations with the specific compounds are necessary. Except in the case of peroxoacetic acid the rate of the peroxidase-catalyzed reaction is slower for these compounds and at higher concentrations under the described conditions of the automated test incomplete reaction may lead to nonlinearities.

An optical diagram of the dual-beam fluorometer is shown in Figure 2. The instrument is comprised of two fluorometer units with a common excitation source. Both beams are identical in terms of the optical and electronic components.

The fluorometer is designed using an H85A3/UV mercury arc lamp as the excitation source and Hamamatsu R268 photomultiplier tube for fluorescence detection. Since the optical system is designed to be used specifically with the peroxidase/POPHA reagent system, interference filters rather than monochromators are used to isolate the excitation and emissions wavelengths, 320 and 400 nm, respectively. The optical system is rigidly mounted on an aluminum base plate.

The instrument is designed for use on an aircraft in measuring cloud water composition. The unit can be mounted into a standard electronic rack panel. The weight of the instrument is 22 lbs, and its dimensions are 18 × 10 × 15 in. It requires 120 W at 115 V. For the complete fluorometer unit two chassis are required: one contains the fluorometer and the reagent flow system while the second contains the signal processing electronics and the readout unit.

The electronics system, shown in Figure 3, is comprised of two identical high voltage/electrometer units for detection and amplification of the fluorescence signals, and a common system monitor to track the high voltage power supplies and the excitation lamp output.

The sensitivity of the two optical channels is adjusted by changing the high voltage applied to the photomultiplier tubes. In this manner the signal output from each detector can be adjusted to be equivalent for a given peroxide concentration. The high voltage applied can be read out at the system monitor.

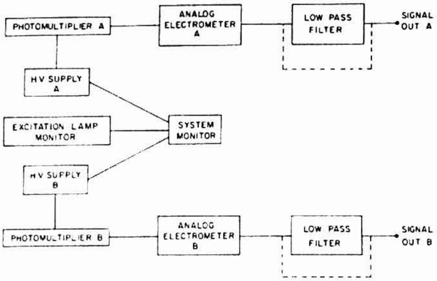

**Figure 3.** Signal processing system for the dual beam fluorometer.

The photocurrent representing the fluorescence signal is amplified with an analog electrometer. Current suppression from $10^{-9}$ to $10^{-4}$ A is provided if suppression of high background signals is necessary. To reduce the noise in the signal output, a low pass filter, 0.1 Hz frequency cutoff, can be switched into the circuit following the electrometer. At low signal levels or high suppression currents this filter will reduce the high frequency noise in the output. At higher signal levels the filter can be switched out for improved response times. The signal output is 0–1 V full scale. Further details on fabrication of the fluorometer are available from the authors.

## RESULTS AND DISCUSSION

By use of the reagent concentrations given above, the detection limit is 0.4 ppbm. At $1.56 \times 10^{-6}$ M $H_2O_2$ the standard deviation is $1.02 \times 10^{-8}$ M, equivalent to a coefficient of variation of 0.7%.

Plots of peak height vs. concentration are linear with concentration up to about $1.8 \times 10^{-5}$ M or 0.6 ppm $H_2O_2$. Most values we have measured at Boulder, CO, or Whiteface Mountain, NY, are below this concentration. Above this value the curve becomes slightly nonlinear.

We have adjusted the concentration of reagents to accommodate $H_2O_2$ concentrations from $1.1 \times 10^{-8}$ M (0.4 ppbm) to $1.5 \times 10^{-4}$ M (5000 ppbm) in order to eliminate the need to dilute samples during field measurements. At concentrations above 0.6 ppm, the calibration points have been readily fitted by a quadratic regression equation with a correlation coefficient of 0.9998.

A considerable effort was made to discover the cause of the nonlinearity at higher concentrations. A likely cause in the case of fluorometry is the attenuation of exciting radiation in the path of the beam as a result of absorption by higher concentrations of absorbing molecules. However, dilution of the solutions of the dimer of POPHA by a factor of 10 did not alleviate the nonlinearity. Another possibility is a decreasing yield of dimer from the higher concentrations of $H_2O_2$. However, no improvement was observed after increasing the concentrations of POPHA or peroxidase, changing the pH, or increasing reaction time. The possibility that the buffer, present in relatively high concentration, interferes chemically with the reaction was disproved since using Tris, glycine, ammonia, or borax buffers in lieu of potassium biphthalate gives a similar effect. Reaction involving enzymes frequently become nonlinear after the initial stages. However, reducing the reaction time in the automated test by a factor of 4 did not ameliorate the problem. Given the fact that the analytical precision did not decrease at the higher $H_2O_2$ concentrations in spite of the slight nonlinearity, no further efforts were made.

The peroxidase channel will yield a signal for organic hydroperoxides as well as for $H_2O_2$. Dialkyl peroxides do not give a signal. Since catalase does react slowly with some organic hydroperoxides, it is necessary to establish the conditions under which the $H_2O_2$ is completely removed by the catalase while organic hydroperoxides are left unreacted to provide an accurate analytical blank.

Methyl hydroperoxide, ethyl hydroperoxide, *n*-propyl hydroperoxide, *tert*-butyl hydroperoxide, and peroxoacetic acid were investigated. Only methyl hydroperoxide exhibited an appreciable reaction with catalase under the conditions of the automated test. If MeOOH is destroyed by too much catalase, the background signal is too low, and the difference between the signals of the two channels would indicate a spuriously high $H_2O_2$ value. On the other hand, incomplete destruction of the $H_2O_2$ by too little catalase would yield too high a background signal, and a final $H_2O_2$ value which is spuriously low. To investigate the effect of these two compensating errors, the rates of conversion of MeOOH and $H_2O_2$ by catalse under the recommended instrumental conditions were studied. At 22 °C and a constant 40-s reaction time, the rates of loss of MeOOH and $H_2O_2$ were studied as a function of catalase concentration. The following expressions describe the rates occurring specifically under the conditions of the automated instrument:

$$\ln \frac{(H_2O_2)_{\text{final}}}{(H_2O_2)_{\text{initial}}} = [-(1.7 \pm 0.1) \times 10^{-6}](\text{catalase})(\Delta t)$$

$$\ln \frac{(\text{MeOOH})_{\text{final}}}{(\text{MeOOH})_{\text{initial}}} = [-(0.072 \pm 0.008) \times 10^{-6}](\text{catalase})(\Delta t)$$

where (catalase) is activity of catalase as Sigma units per liter and $\Delta t$ is time as seconds.

Catalase reacts 24 times faster with $H_2O_2$ than with MeOOH under the conditions of the automated methods. To minimize errors introduced by MeOOH, we use a concentration of 2 ppm catalase protein in the reaction mixture. The catalase in the reagent reservoir is 8 times more concentrated to compensate for the dilution factor, indicated in Figure 1, to a final activity of 70600 Sigma units per liter.

The application of the above empirical rate expressions yield the following errors in $H_2O_2$ determination for the worst case in which the organic peroxide is entirely MeOOH and is present at the indicated percentages of total hydroperoxide:

| % MeOOH | 0% | 5% | 10% | 20% |
|---|---|---|---|---|
| % $H_2O_2$ error | −0.82% | +0.13% | +1.2% | +3.5% |

These small errors represent maximum errors to be expected from this source, since in actual practice the background signal in atmospheric samples will probably not represent MeOOH exclusively. MeOOH is the only organic peroxide likely to be present in atmospheric samples with sufficient reactivity with catalase to cause a problem.

When operated at higher pH values, e.g., using Tris buffer adjusted to pH 8.6, the test is affected by the adduct of formaldehyde and bisulfite ion (hydroxymethanesulfonic acid). Normally, bisulfite ion will not coexist with $H_2O_2$ in precipitation samples. However, the adduct of formaldehyde and bisulfite ion can coexist with $H_2O_2$ at pH 5 (*12*). The hydrolysis rate increases with pH (*13*) and when the adduct encounters the buffer at pH 8.6 it releases sufficient bisulfite to interfere with the formation of the dimer. The adduct at $5 \times 10^{-6}$ M reduces the signal of $H_2O_2$ ($5.6 \times 10^{-6}$ M) by 6%. This interference was eliminated by first adding formaldehyde ($1 \times 10^{-2}$ M) to the sample stream through a 0.16 mL min$^{-1}$ pump manifold tube. With formaldehyde present, the adduct at 1.5 M × $10^{-5}$ causes no interference in the measurement of $H_2O_2$ at either $1.5 \times 10^{-6}$ or $1.5 \times 10^{-7}$ M $H_2O_2$. Running the test at pH 5.5, as described in the Experimental Section, eliminates the interference by hydroxymethanesulfonic acid and therefore the need to introduce formaldehyde reagent.

Table II. Sample Deterioration Tests

| date | pH | $[H_2O_2]$, μM | decay/hours | % loss per h |
|---|---|---|---|---|
| 4/7/82 | 5.3 | 2.90 | −80%/48 | 1.7 |
| 5/4/82 | 5.9 | 25.7 | −26%/5 | 5.2 |
| 2nd Determination | | | −100%/5 | 20 |
| 5/11/82 | 5.5 | 3.20 | −52%/5 | 10.4 |
| 5/12/82 | 5.4 | | −30%/24 | 1.3 |
| 7/27/82 | 5.5 | 24.7 | −80%/16 | 5.0 |
| 2nd Determination | | | −100%/24 | 4.2 |
| 7/28/82 | 5.5 | 3.1 | −27%/16 | 1.7 |
| 7/29/82 | | 12.6 | −22%/16 | 1.4 |
| 8/4/82 | | 28.8 | −100%/16 | 6.3 |
| 6/9/83 | | 3.1 | −21%/0.75 | 28.0 |
| 2nd Determination | | | −34%/1.2 | 28.0 |
| 6/14/83 | | 3.5 | −7%/1.8 | 3.9 |
| 2nd Determination | | | −10%/2.1 | 4.8 |
| average[a] | | | | 5.6 ± 8.1 |

[a] Not including replicate determinations.

There is no significant change in sensitivity at the lower pH.

Both negative and positive interferences were tested by adding known quantities of substances to standard solutions of $H_2O_2$. We have not found interfrences by commonly occurring atmospheric trace constituents. Ferrous ion and hydroquinone tend to eliminate the $H_2O_2$ signal by reaction with $H_2O_2$. Ammonium, potassium, sodium, ferric, and manganous ions had no effect. Iodide, bromide, chloride, phosphate, nitrate, and benzoate ions had no effect. Formaldehyde, methanol, glyoxal, acetone, methylamine, dimethylamine, methyl ethyl ketone, toluene, benzene and peroxyacetylnitrate had no effect.

Nitrite in neutral solution shows neither a positive nor negative interference. However, below pH 3.0, nitrite ion chemically reduces $H_2O_2$ (*17*). Bisulfite ion below pH 4.6 also rapidly reacts with $H_2O_2$ in the sample.

By far the greatest source of error is loss of $H_2O_2$ with time in collected samples. We have found that glass and Teflon containers, though superior to other types, still do not prevent significant loss of $H_2O_2$. The addition of common preservatives for $H_2O_2$ such as sodium stannate and acetanilide to samples of precipitation does not prevent appreciable loss. Refrigeration of samples does appear to have a beneficial effect, but by no means eliminates the problem.

Sample deterioration clearly is a major problem. Data indicating the problem for samples collected at Boulder and then refrigerated are given in Table II. Since the duration of precipitation events may be several hours or more, a technique for fixing $H_2O_2$ concentrations is badly needed. Similarly, the collection of cloud water samples by aircraft with subsequent analysis at laboratories several hours later can introduce a large loss of $H_2O_2$. Since the dimer of *p*-hydroxyphenylacetic acid formed in this test is stable for several days, we have been exploring the possibility of forming the dimer by immediately reacting the $H_2O_2$ with reagent stored in the sample collection vessel. At the present time, this approach appears successful and will be discussed in a later paper.

In standard addition studies it is necessary to work rapidly and to measure the $H_2O_2$ concentration in the original sample immediately before each addition. In ambient precipitation samples $H_2O_2$ can decay rapidly. If the data are not corrected for this $H_2O_2$ decomposition, a false bias in the standard addition data will appear. Matrix effects have not been observed in samples at Boulder or Denver, CO. However, it is impossible to evaluate the peroxidase $H_2O_2$ analytical technique for all of the differing sample matrix conditions which may be encountered. It is recommended that the standard addition be conducted on a portion of the precipitation samples collected in each sampling program.

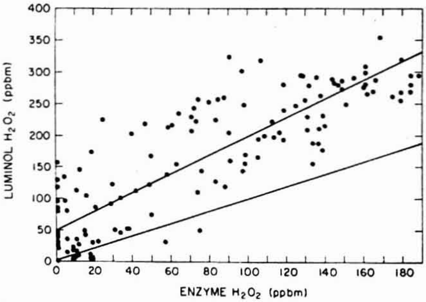

**Figure 4.** Intercomparison between the luminol method and the peroxidase enzyme technique on cloud water samples collected at Whiteface Mountain, NY. Upper line represents least-squares regression fit; lower line represents perfect agreement between tests. The ordinate equals luminol results (ppbm) and the abscissa equals enzyme results (ppbm). Concentration range is zero to the median $H_2O_2$ value.

As part of testing this technique, measurements of $H_2O_2$ in 284 cloud water samples at the peak of Whiteface Mountain were made simultaneously using the luminol and enzyme systems. The data indicated that the percentage difference between the luminol and enzyme methods is a function of peroxide concentration and that at values below $1.5 \times 10^{-5}$ M $H_2O_2$ (0.5 ppm) the discrepancies can be quite large. The median concentration of $H_2O_2$ by the enzyme method was $5.4 \times 10^{-6}$ M (0.18 ppm).

A paired sample *t* test applied to the 284 comparisons indicated that the two techniques are statistically different at a significance level less than 0.001. Including all data pairs (maximum observed $H_2O_2$ = 3815 ppbm) the regression equation relating the two data sets is

$$\text{luminol } (H_2O_2) = 1.01 \text{ enzyme } (H_2O_2) + 71.05 \quad (3)$$

with a correlation coefficient of 0.98. Clearly the correlation using the entire concentration range was reasonably good.

The median value of $H_2O_2$ by the enzyme technique was 183 ppbm. By use of only data points below the median value, the regression equation becomes

$$\text{luminol } (H_2O_2) = 1.5 \text{ enzyme } (H_2O_2) + 48.58 \quad (4)$$

with a correlation coefficient of 0.86. The 95% confidence limits of the correlation coefficient were 0.81 and 0.90 using the Fisher Z transformation. The lower line in Figure 4 indicates the plot anticipated for perfect agreement between the two methods, and the upper line shows the actual linear regression represented by eq 4. The data show a tendency for the luminol signal to be higher than the enzyme signal. Catalase was added to samples to destroy $H_2O_2$ prior to testing by the luminol method. However, only a portion of the signal was eliminated. The residual signals were comparable to the differences between the $H_2O_2$ concentrations indicated by the two analytical tests, suggesting a positive interference in the luminol method.

## ACKNOWLEDGMENT

Very valuable and appreciated contributions were made by Paul Sperry and Bruce Gandrud.

## LITERATURE CITED

(1) Penkett, S. A.; Jones, B. M. R.; Brice, K. A.; Eggleton, A. E. J. *Atmos. Environ.* **1979**, *13*, 123–137.

(2) Möller, D. *Atmos. Environ.* **1980**, *14*, 1067–1076.
(3) Schöne, E. *Z. Anal. Chem.* **1984**, *33*, 127.
(4) Matsui, H. *J. Meteorol. Soc. Jpn.* **1949**, *2*, 380–381.
(5) Kok, G. L.; Darnall, K. R.; Winer, A. M.; Pitts, J. N., Jr.; Gay, B. W., Jr. *Environ. Sci. Technol.* **1978**, *12*, 1077.
(6) Kok, G. L. *Atmos. Environ.* **1980**, *14*, 656.
(7) Yoshizumi, K.; Aokikazuyuki, I. N.; Toshichi, O.; Toshimi, K.; Shujkamakura; Tajima, M. *Atmos. Environ.* **1984**, *18*, 395–401.
(8) Zika, R.; Saltzman, E.; Chameides, W. L.; Davis, D. D. *J. Geophys. Res.* **1982**, *87*, 5015–5017.
(9) Heikes, B. G.; Lazrus, A. L.; Kok, G. L.; Kunen, S. M.; Gandrud, B. W.; Gitlin, S. N.; Sperry, P. D. *J. Geophys. Res.* **1982**, *87*, 3045.
(10) Guilbault, G. G.; Brignac, P.; Juneau, M. *Anal. Chem.* **1968**, *40*, 1256.
(11) Lind, J.; Kok, G. L., submitted for publication.
(12) Richards, L. W.; Anderson, J. A.; Blumenthal, D. L.; McDonalds, J. A.; Kok, G. L.; Lazrus, A. L. *Atmos. Environ.* **1983**, *17*, 911.
(13) Kok, G. L.; Gitlin, S. N.; Lazrus, A. L., submitted for publication.
(14) Rieche, A.; Hitz, F. *Ber. Dtsch. Chem. Ges.* **1920**, *62*, 2458.
(15) Johnson, R. M.; Siddigu, I. W. "The Determination of Organic Peroxides"; Pergammon Press: London, 1970.
(16) Aubar, M.; Taube, H. *J. Am. Chem. Soc.* **1954**, *76*, 6243–6247.
(17) Bhattacharyya, P. K.; Veeraraghavan, R. *J. Chem. Kinetics* **1977**, *60*, 629–640.

RECEIVED for review October 15, 1984. Accepted December 26, 1984. The development of the analytical method was funded by the Electric Power Research Institute under Contract 1630-12. The intercomparison between the peroxidase and luminol methods was funded by the Environmental Protection Agency. Although the research described in this report has been funded in part by the United States Environmental Protection Agency through interagency agreement EPA-AD49F2A182 to the National Science Foundation, it has not been subjected to the agency's required peer and policy review and therefore does not necessarily reflect the views of the agency, nor does mention of trade names or commercial products constitute endorsement or recommendation for use. The National Center for Atmospheric Research is sponsored by the National Science Foundation.

# Determination of Acidity Constants by Solvent Extraction/Flow Injection Analysis Using a Dual-Membrane Phase Separator

**Lynette Fossey and Frederick F. Cantwell***

*Department of Chemistry, University of Alberta, Edmonton, Alberta, Canada T6G 2G2*

**The absorbances of both the organic and aqueous phases in a solvent extraction/flow injection analysis system are simultaneously monitored. Acidity constants are determined from straight line plots relating the ratio of peak areas in the aqueous and organic phases, $A_a/A_o$, to the hydrogen ion activity of the aqueous phase. Theoretical equations describing this relationship for both HA and $BH^+$ charge type acids are derived and verified experimentally using 3,5-dimethylphenol ($pK_a = 10.09 \pm 0.01$) and *p*-toluidinium ion ($pK_a = 5.28 \pm 0.01$). The distribution coefficient of the neutral conjugate species is also obtained during the experiment. Some distinct practical advantages to using the dual-membrane device over the single-membrane device are discussed.**

The use of solvent extraction for determining acid–base dissociation constants (*1–7*) is particularly attractive for compounds that have low solubility in water and whose two conjugate species have the same absorption spectrum. For such compounds, the low solubility precludes accurate $pK_a$ determinations by potentiometric titration in water, and the similarity of spectra precludes the use of the spectrophotometric technique. However, the labor and time involved diminish the attractiveness of batchwise solvent extraction for this purpose.

Continuous extraction systems employing rapid phase separation make it possible to perform solvent extraction measurements much more rapidly and conveniently and therefore make $pK_a$ determination by solvent extraction more attractive (*8*). Solvent extraction/flow injection analysis (FIA) employing either one or two porous membranes as phase separators has been shown to give precise, accurate, and very rapid analytical determinations of drugs in pharmaceutical tablets (*9, 10*). In the present paper we use a solvent extraction/FIA technique employing two membrane phase separators which allows simultaneous spectrophotometric monitoring of concentration in both the aqueous and organic phases. Equations are derived which relate peak areas in the organic and aqueous phases to hydrogen ion activities in the aqueous phase and which permit the determination of acidity constants of both HA and $BH^+$ charge type acids. Validity of the equations is experimentally demonstrated using 3,5-dimethylphenol and *p*-toluidinium ion as test acids.

## THEORY

The relationship between sample peak area in the organic phase $A_0$, and the hydrogen ion concentration in a solvent extraction/FIA system has been derived for a $BH^+$ type acid in earlier papers from this laboratory (*9, 10*). In the present paper, we are concerned with determining a "mixed" acidity constant which incorporates the concentrations of the protonated and deprotonated sample species and the activity of the hydrogen ion.

The equation relating peak areas in the organic phase with hydrogen ion activity in the aqueous phase can be written as

$$A_0 = \frac{bfn\epsilon_{B,o}K_BK_a}{F_aa_H + F_aK_a + F_oK_bK_a} \tag{1}$$

Here $b$ is the path length of the spectrophotometer flow cell, $f$ is a response factor which relates the absorbance from the detector to a count rate on the integrator, $n$ is the moles of sample injected, $\epsilon_{B,o}$ is the molar absorptivity of the sample in the organic phase, $K_B$ is the distribution coefficient of the conjugate base B, $K_a$ is the acidity constant of $BH^+$, $F_a$ and $F_o$ are flow rates of the aqueous and organic phases, respectively, and $a_H$ is the hydrogen ion activity in the aqueous phase. This equation is similar to eq 4 in ref 10 if the "system constant" in that paper is defined as $K = fb\epsilon_{B,o}$.

0003-2700/85/0357-0922$01.50/0 © 1985 American Chemical Society

A similar expression can be derived for sample peak area in the aqueous phase, $A_a$, taking into account both absorbing species, B and $BH^+$

$$A_a = \frac{b'f'n(\epsilon_{B,a}K_a + \epsilon_{BH^+,a}a_H)}{F_a a_H + F_a K_a + F_o K_B K_a} \tag{2}$$

where $b'$ is the path length of the flow cell in the spectrophotometer used to monitor the aqueous phase, $f'$ is the response factor for the aqueous phase detector and integrator, and $\epsilon_{B,a}$ and $\epsilon_{BH^+,a}$ are the molar absorptivities for the neutral and protonated sample species, respectively, in the aqueous phase.

The denominators of eq 1 and 2 are the same so that dividing eq 2 by eq 1, yields the following simple expression:

$$\frac{A_a}{A_o} = \frac{b'f'\epsilon_{B,a}}{bf\epsilon_{B,o}K_B} + a_H\frac{b'f'\epsilon_{BH^+,a}}{bf\epsilon_{B,o}K_a K_B} \tag{3}$$

When the sample is injected into reagent buffers of various pH, and peak areas are simultaneously measured in the organic and aqueous pahses, a plot of $A_a/A_o$ vs. $a_H$ should yield a straight line. It is then possible to determine the acidity constant for $BH^+$ from the slope, $S_1$, and intercept, $I_1$, of the plot as well as the molar absorptivity ratio of the protonated and deprotonated sample species in the aqueous phase

$$K_a = \frac{I_1}{S_1}\frac{\epsilon_{BH^+,a}}{\epsilon_{B,a}} \tag{4}$$

The distribution coefficient of the neutral conjugate species B can also be calculated by using $K_a$ and the data collected for the organic phase. As discussed previously *(10)*, eq 1 can be linearized by taking the reciprocal of both sides so that a plot of $1/A_o$ vs. $a_H$ should be linear. The distribution coefficient $K_B$ can be calculated from the following expression:

$$K_B = \frac{I_2F_a - S_2F_aK_a}{S_2F_oK_a} \tag{5}$$

where $I_2$ and $S_2$ represent the intercept and slope, respectively, of the plot of $1/A_o$ vs. $a_H$.

An equation can be derived also for an HA type acid which relates sample peak area in the organic phase, $A_o$, to the aqueous phase pH, assuming that HA is the only extractable species

$$A_o = \frac{bfn\epsilon_{HA,o}K_{HA}a_H}{F_a a_H + F_a K_a + F_o K_{HA} a_H} \tag{6}$$

where $\epsilon_{HA,o}$ is the molar absorptivity for the neutral form of the sample species in the organic phase and $K_{HA}$ is the distribution coefficient of the neutral species HA. Likewise for the aqueous phase

$$A_a = \frac{b'f'n(\epsilon_{HA,a}a_H + \epsilon_{A^-,a}K_a)}{F_a a_H + F_a K_a + F_o K_{HA} a_H} \tag{7}$$

where $\epsilon_{HA,a}$ and $\epsilon_{A^-,a}$ are the molar absorptivities of the protonated and deprotonated sample species, respectively, in the aqueous phase. Dividing eq 7 by eq 6 yields the following:

$$\frac{A_a}{A_o} = \frac{b'f'\epsilon_{HA,a}}{bf\epsilon_{HA,o}K_{HA}} + \frac{1}{a_H}\frac{b'f'\epsilon_{A^-,a}K_a}{bf\epsilon_{HA,o}K_{HA}} \tag{8}$$

A plot of $A_a/A_o$ vs. $1/a_H$ should yield a straight line from which can be calculated the acidity constant, $K_a$

$$K_a = \frac{S_3}{I_3}\frac{\epsilon_{HA,a}}{\epsilon_{A^-,a}} \tag{9}$$

where $S_3$ and $I_3$ represent the slope and $y$ intercept, respectively, of the plot of $A_a/A_o$ vs. $1/a_H$. Finally, to measure $K_{HA}$, eq 6 can be linearized by taking the reciprocal of both sides, viz.

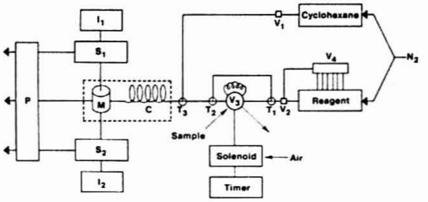

**Figure 1.** Diagram of the solvent extraction/FIA instrument used for p$K_a$ determinations; see text for details.

$$\frac{1}{A_0} = \frac{F_a + F_oK_{HA}}{bfn\epsilon_{HA,o}K_{HA}} + \frac{1}{a_H}\frac{F_aK_a}{bfn\epsilon_{HA,o}K_{HA}} \tag{10}$$

A plot of $1/A_o$ vs. $1/a_H$ should yield a stright line with slope, $S_4$, and $y$ intercept, $I_4$, from which the distribution coefficient can be calculated using the expression

$$K_{HA} = \frac{I_4F_aK_a - S_4F_a}{S_4F_o} \tag{11}$$

## EXPERIMENTAL SECTION

**Apparatus.** A diagram of the solvent extraction/FIA system used in the p$K_a$ determination is shown in Figure 1. Its design is similar to that of a previously described instrument *(10)* with the main difference being that there is only one aqueous solvent. Solvent flows are maintained via constant $N_2$ pressure pumping. The organic phase is cyclohexane which is contained in a glass bottle inside an aluminum pressure cylinder. The six reagent buffers and water are held in seven glass containers inside a multireagent aluminum pressure cylinder described previously *(10)*.

Valve $V_4$ is a six-port rotary valve (part no. R6031V6, Laboratory Data Control) used to select any one of six reagent buffers. Valve $V_2$ is a three-port slider valve (part no. CAV 3031, LDC) which allows selection of either buffer or a water wash. All tubing is made of Teflon, whith 0.3 mm i.d. tubing used whenever it is desirable to minimize sample band broadening or to provide increased resistance to flow and 0.8 mm i.d. tubing used in the rest of the system.

The sample is injected via an automatic sample injection valve $V_3$ (part no. SVA-8031, LDC) into the reagent stream, which is a buffer of known pH. This injection valve contains a "dummy" loop of equal size to the injection loop, so that the flow rate of aqueous reagent is the same in both the load and inject positions. The reagent stream is split at $T_1$ into two parallel branches which are reunited at $T_2$ to facilitate mixing between the sample and the buffer and to reduce refractive index effects (see Results and Discussion). The aqueous phase joins the cyclohexane stream at tee-fitting $T_3$ (part no. CJ-3031, LDC) and the resulting two-phase flow passes through the extraction coil, C.

The aqueous phase is separated from the organic phase at the end of the extraction coil via a dual-membrane phase separator as described in a previous paper *(10)*. The extraction coil and phase separator are immersed in a constant temperature bath, shown as dashed lines in Figure 1. The absorbance of the organic phase is monitored with spectrophotometer $S_1$ (Spectroflow Monitor 757, Kratos Analytical Instruments) while the absorbance of the aqueous phase is monitored with spectrophotometer $S_2$ (Varichrom photometric detector, Varian). The signals from S1 and S2 are fed to two channels of a digital integrator (VISTA CDS 401, Varian) to obtain peak areas. The signals are also monitored as peaks on recorders (not shown). A peristaltic pump, P (Gilson Instruments, Ville-Belle, France), is used on the outlet lines to ensure accurate flow control *(9, 10)*.

The apparatus was modified for determination of molar absorptivity ratios of the protonated and deprotonated sample species in the aqueous phase by disconnecting $T_2$ from $T_3$ and disconnecting the membrane phase separator, M, from the aqueous phase detector, $S_2$, and then directly connecting $T_2$ to $S_2$.

All pH measurements were made with a glass and calomel electrode pair using an Accumet Model 525 pH meter (Fisher Scientific Co.).

**Reagents.** Water was demineralized, distilled, and finally distilled from alkaline permanganate. Analytical grade cyclohexane was purified by passage through a silica gel column containing a sintered glass frit at the outlet. Reagent buffers of pH 9.60, 9.70, 9.80, 9.90, 10.00, and 10.11 and ionic strength 0.10 were prepared by adding enough $NH_4Cl$ to yield a final concentration of 0.10 M and enough concentrated aqueous ammonia to yield the desired pH in a final volume of 1000 mL. Reagent buffers of pH 4.61, 4.78, 5.02, 5.22, 5.42, and 5.63 and ionic strength of 0.10 were prepared by adding enough sodium acetate to yield a final concentration of 0.10 M and enough glacial acetic acid to yield the desired pH in a final volume of 500 mL. 3,5-Dimethylphenol (Aldrich Chemical Co.) and *p*-toluidine (B.D.H. Chemicals) were both 99+% pure as reported by the manufacturers. Sample solutions of 3,5-dimethylphenol and *p*-toluidine contained 0.10 M NaCl.

For the determination of molar absorptivity ratios, reagent buffers of pH 2.0, 12.0, and 12.6 were prepared by appropriate dilution of a solution of concentrated HCl or NaOH with $H_2O$ until the desired pH was reached.

**Molar Absorptivity Determination.** Molar absorptivity ratios for the protonated and deprotonated sample species in the aqueous phase were measured with the same spectrophotometer and wavelength setting as those used for the acidity constant determination.

The molar absorptivity ratio, $\epsilon_{HA,a}/\epsilon_{A^-,a}$ for 3,5-dimethylphenol was determined by preparing two sample solutions, both $3.0 \times 10^{-4}$ M in 3,5-dimethylphenol but one adjusted to pH 2.0 with HCl and the other adjusted to pH 12.6 with NaOH. These samples were injected into an HCl or NaOH reagent of the same pH and peak areas were measured for six replicate injections. Important instrument parameters were as follows: flow rate, 0.7 mL/min; wavelength, 281 nm; volume injected, 44 μL; sampling frequency, one injection per minute; $N_2$ pressure, 20 psig. The flow rates differed slightly (0.01 mL/min) for the two reagents so that peak areas were corrected to a constant flow rate of 0.690 mL/min as previously described (*9*).

The molar absorptivity ratio, $\epsilon_{BH^+,a}/\epsilon_{B,a}$, for *p*-toluidine was determined similarly by using $5.0 \times 10^{-4}$ M *p*-toluidine sample solutions—one adjusted to pH 2.0 with HCl and the other adjusted to pH 12.0 with NaOH. Changes in the instrumental parameters were as follows: flow rate, 0.5 mL/min; wavelength, 260 nm. Here too a small correction was made to peak areas as a result of slightly different flow rates of the two reagents (*9*).

**Calibration Curves.** These were measured with the apparatus shown in Figure 1. Samples were all 0.10 M in NaCl to reduce refractive index effects (see Results and Discussion). Calibration curves for 3,5-dimethylphenol were obtained at a wavelength of 281 nm by injecting samples ranging in concentration from $8 \times 10^{-5}$ M to $8 \times 10^{-4}$ M into an ionic strength 0.10, pH 9.80 $NH_3/NH_4Cl$ buffer. Calibration curves for *p*-toluidine were obtained at a wavelength of 260 nm by injecting samples ranging in concentration from $4 \times 10^{-4}$ M to $1.4 \times 10^{-3}$ M into an ionic strength 0.10, pH 5.11 acetic acid/sodium acetate buffer. The organic and aqueous phases were monitored simultaneously and peak areas were measured for each sample injected.

**Acidity Constant Determination.** The acidity constant of 3,5-dimethylphenol was determined by injecting a sample solution that was $4.0 \times 10^{-4}$ M in 3,5-dimethylphenol and 0.10 M in NaCl into reagent buffers of various pH. The reagents were ionic strength 0.10 $NH_3/NH_4Cl$ buffers that ranged in 0.1 increments of pH from pH 9.6 to pH 10.1. Additionally, a sample that was 0.10 M in NaCl was injected into each reagent buffer to serve as a blank. The extraction coil was made long enough to ensure that extraction equilibrium was attained, and the extraction coil and phase separator were thermostated to 25.0 ± 0.1 °C. Both the organic and aqueous phases were monitored simultaneously, and peak areas were measured for each sample injected. The pH of the aqueous effluent was measured for each buffer used to ensure that no change in pH occurred during the extraction/FIA procedure.

Important instrument parameters for the acidity constant determination of 3,5-dimethylphenol were as follows: wavelength for both detectors, 281 nm; extraction coil, 200 cm; volume injected, 44 μL; sampling frequency, one injection per minute; $N_2$ pressure, 40 psig; total cyclohexane flow rate, $F_o$, 2.5 mL/min; total aqueous flow rate, $F_a$, 2.2 mL/min; cyclohexane flow through the membrane, $F_{m,o}$, 0.9 mL/min; aqueous flow through the membrane, $F_{m,a}$, 1.1 mL/min.

The acidity constant of the *p*-toluidinium ion was determined in a similar manner using a sample solution that was $1.0 \times 10^{-3}$ M in *p*-toluidine and 0.10 M in NaCl. The reagents were ionic strength 0.10 acetic acid/sodium acetate buffers that ranged in 0.2 pH increments from pH 4.6 to pH 5.6. The phase separator and extraction coil were thermostated at 20.0 ± 0.1 °C. Instrument parameters that differed from those listed above for 3,5-dimethylphenol were as follows: wavelength for both detectors, 260 nm; $F_a$, 2.1 mL/min; $F_{m,a}$, 1.0 mL/min.

## RESULTS AND DISCUSSION

Two compounds, 3,5-dimethylphenol and *p*-toluidine, were chosen to test the method for HA and $BH^+$ charge type acids, respectively. Although our discussion will pertain mainly to the use of a dual-membrane phase separator to monitor both the organic and aqueous phases, two single-membrane phase separators each designed as previously (*9*) and placed in series could be used instead.

**Experimental Conditions.** In the design of the experiment for the determination of the acidity constant of a particular compound, several factors should be taken into account. The first is the choice of the organic solvent. In order to accurately measure peak areas in both the organic and aqueous phases, for reagent pHs in the vicinity of the expected $pK_a$ of the sample, it is necessary that the distribution coefficient for the sample be neither too large nor too small. The value of $K_{HA}$ or $K_B$ should be between approximately 1 and 10, although this will depend on the molar absorptivities of the sample species in the two phases.

The derivation presented in the theory section assumes that dimerization of the sample in the organic phase and ion-pair extraction of the sample with components present in the buffer are negligible. If they are not, the equations must be modified to take them into account. Dimerization of the sample in the organic phase is more likely to be encountered at higher concentrations and when the sample is polar and the organic phase is nonpolar. This problem may be avoided by keeping the sample concentration low. In the present case a preliminary check for dimerization was made via Beer's law plots for 3,5-dimethylphenol and *p*-toluidine in cyclohexane using the Cary 118 spectrophotometer over the concentration ranges of interest. For the former compound a plot of absorbance at 281 nm vs. concentrations from $4 \times 10^{-5}$ M to $8 \times 10^{-4}$ M was linear with a zero intercept. For the latter compound a plot over the concentration range $4 \times 10^{-5}$ M to $1 \times 10^{-3}$ M made at 287 nm was linear with zero intercept.

The absence of ion-pair extraction of 3,5-dimethylphenolate ($A^-$) and of *p*-toluidinium ($BH^+$) was checked by seeing if detectable concentrations of these are extracted into cyclohexane from 0.10 M NaCl solutions adjusted to pHs where either $A^-$ or $BH^+$ were the only species present in significant amounts. In batch extractions, with absorbances of the cyclohexane phases measured on the Cary 118 spectrophotometer, no detectable 3,5-dinitrophenol was extracted from an aqueous phase at pH 12.6 and no detectable *p*-toluidine was extracted from an aqueous phase at pH 2.0.

When mutual solubility of the aqueous and organic solvents is significant, the phases should be preequilibrated before they are used in the solvent extraction/FIA system. Preequilibration of the phases will not affect the value of the acidity constant determined but may affect the value of the measured

Table I. Acidity Constant Determination by Solvent Extraction/FIA

| compound | trial no. | slope (±% RSD)[a] | *y* intercept[b] | $pK_a'$ |
|---|---|---|---|---|
| 3,5-dimethylphenol | 1 | $4.49 \times 10^{-10}$ (±1.3%) | 2.71 ± 0.10 | $10.08 \pm 0.01_4$[c] |
|  | 2 | $4.49 \times 10^{-10}$ (±1.1%) | 2.84 ± 0.08 | $10.10 \pm 0.01_3$[c] |
| *p*-toluidinium | 1 | $4.31 \times 10^{5}$ (±0.73%) | 6.17 ± 0.08 | $5.30 \pm 0.01_3$[d] |
|  | 2 | $4.10 \times 10^{5}$ (±0.77%) | 6.16 ± 0.09 | $5.27 \pm 0.01_3$[d] |

[a] Percent relative standard deviation. [b] Uncertainties are 95% confidence limits. [c] Temperature = 25.0 ± 0.1 °C and ionic strength = 0.10. [d] Temperature = 20.0 ± 0.1 °C and ionic strength = 0.10. [e] Uncertainties are one standard deviation.

Table II. Distribution Coefficient Determination by Solvent Extraction/FIA

| compound | trial no. | slope (±% RSD)[a] | *y* intercept[b] | $F_o$, mL/min | $F_a$, mL/min | distribution coefficient[e] |
|---|---|---|---|---|---|---|
| 3,5-dimethylphenol | 1 | $4.75 \times 10^{-16}$ (±2.1%) | $(2.14 \pm 0.02) \times 10^{-5}$ | 2.50 | 2.18 | 2.4 ± 0.2[c] |
|  | 2 | $4.60 \times 10^{-16}$ (±4.3%) | $(2.16 \pm 0.03) \times 10^{-5}$ | 2.49 | 2.22 | 2.4 ± 0.2[c] |
|  | 3 | $4.94 \times 10^{-16}$ (±2.2%) | $(2.16 \pm 0.02) \times 10^{-5}$ | 2.57 | 2.26 | 2.2 ± 0.2[c] |
| *p*-toluidine | 1 | 0.700 (±0.47%) | $(1.669 \pm 0.009) \times 10^{-5}$ | 2.50 | 2.12 | 3.2 ± 0.2[d] |
|  | 2 | 0.648 (±0.63%) | $(1.72 \pm 0.01) \times 10^{-5}$ | 2.60 | 2.12 | 3.3 ± 0.2[d] |

[a] Percent relative standard deviation. [b] Uncertainties are 95% confidence limits. [c] Temperature = 25.0 ± 0.1 °C and ionic strength = 0.10. [d] Temperature = 20.0 ± 0.1 °C and ionic strength = 0.10. [e] Uncertainties are one standard deviation.

distribution coefficient (*11*). In the present case the phases were not preequilibrated since the solubility of cyclohexane in water is only 0.006% at 25 °C and the solubility of water in cyclohexane is 0.01% at 20 °C (*12*).

Salt was added to the sample solutions injected for two reasons. Most importantly, an inert electrolyte is added to ensure constant ionic strength throughout the concentration profile of the sample zone and to match the ionic strength of the sample zone to the surrounding buffer. It additionally served to reduce refractive index effects, as discussed in the next section.

Unlike a spectrophotometric determination of acidity constants, it is not necessary that the molar absorptivities of the protonated and deprotonated sample species in the aqueous phase be different at the wavelength chosen. It is, of course, also not necessary to have both spectrophotometers set to the same wavelength.

It is desirable to choose the pH of the buffers to be in the vicinity of the inflection point of the peak area vs. reagent pH plot for the sample (*10*). For distribution coefficients in the suggested range of 1 to 10, this inflection point will occur within about one pH unit of the sample $pK_a$.

**Refractive Index Peaks.** Peaks can occur in flow injection analysis as a consequence of a difference in refractive index between the sample plug injected and the surrounding reagent stream. The effect is characterized by adjacent positive and negative peaks as the sample passes through the flow cell. The refractive index peak is superimposed upon the absorbance peak for the sample and may affect peak heights and shapes, especially for samples of low absorbance. Various authors have noted this effect (*13–15*) and Betteridge et al. (*15*) have given a detailed analysis of the phenomenon as it pertains to flow injection analysis.

In the present study refractive index peaks occurred in the aqueous phase. It was found, in general that the area of the positive portion of the refractive index peak is equal to the area of the negative portion. Thus, there is no net contribution to the peak area for the absorbance peak of the sample. If, however, the sample absorbance peak is small compared to the refractive index peak, the observed peak shape will be distorted, preventing proper integration by an electronic integrator. This imposes a limit on sample detection.

One way to get around this problem is to match the refractive index of the sample and reagent carrier stream. In the present case, the *ionic strength* of the sample solution was matched to that of the reagent stream by adding salt (NaCl) to the sample. While this did not completely match the refractive indexes, it brought them much closer together and greatly reduced the size of the refractive index peaks. The size and shape of the refractive index peaks were routinely monitored by injecting 0.10 M NaCl into each reagent, in place of the sample. Their small size and the fact that the positive and negative portions were of equal area resulted in no problems in measuring sample peak areas for the sample concentrations employed.

**Molar Absorptivities.** Accurate ratios for the molar absorptivities of the two conjugate species in the aqueous phase are required in eq 4 and 9. These were measured by a flow-injection technique, without solvent extraction, as described earlier, in which the ratio of peak areas obtained at low pH and at high pH is equal to the ratio of molar absorptivities. For 3,5-dimethylphenol $\epsilon_{HA,a}/\epsilon_{A^-,a}$ at 281 nm was 0.500 ± 0.005, while for *p*-toluidine $\epsilon_{BH^+,a}/\epsilon_{B,a}$ at 260 nm was 0.353 ± 0.006.

**Calibration Curves.** Equations 1 through 11 assume a linear relationship between integrator signal and concentration. This was checked for 3,5-dimethylphenol and *p*-toluidine for both the organic and aqueous phases using the solvent extraction/FIA system. The plot of peak area for the organic phase vs. concentration of 3,5-dimethylphenol injected was linear with relative standard deviation (RSD) for the slope of 0.28%. The *y* intercept and its 95% confidence limits were 64.0 ± 64.8 in arbitrary integration units. A similar plot for the aqueous phase was linear also with a RSD for the slope of 0.46%. The *y* intercept and its 95% confidence limits were −3038.0 ± 4218.6.

The plot of peak area for the organic phase vs. concentration of *p*-toluidine injected was linear with a RSD for the slope of 0.74%. The *y* intercept and its 95% confidence limits were 9.4 ± 881.4 in arbitrary integration units. The corresponding plot for the aqueous phase was a straight line with a RSD for the slope of 1.2%. The *y* intercept and its 95% confidence limits were 1556.8 ± 6631.5.

The zero *y* intercepts of the calibration plots for both compounds in the aqueous phase shows that the underlying refractive index peaks do not have a net effect on sample peak areas.

**Acidity Constants.** The acidity constant for 3,5-dimethylphenol was determined from plots of $A_a/A_o$ vs. $1/a_H$. The experiment was run twice and peak areas obtained were based on an average of six replicate injections of sample into each buffer. The slope and *y* intercept values of the plots along with the calculated $pK_a$'s and computed errors are reported in Table I. The linearity of the plots is evidence for the validity of the equations for HA charge type acids. The average value of the p$K_a$ for 3,5-dimethylphenol at an ionic strength of 0.10 and temperature of 25 °C was $10.09 \pm 0.01_4$. The stated uncertainty is one standard deviation and includes the computed error in determining the slope, *y* intercept, and molar absorptivity ratio as well as an estimated error due to the calibration of the pH meter used to measure the pHs of the reagent buffer solutions. Literature values for the acidity constant of 3,5-dimethylphenol at 25.0 °C determined spectrophotometrically and corrected for activity coefficient effects to zero ionic strength are 10.20 (*16*) and 10.19 (*17*). For comparison purposes if we correct our p$K_a$ value to zero ionic strength by calculating the activity coefficient via the Davies equation (*18*), we obtain a p$K_a°$ value of 10.20.

The acidity constant for the *p*-toluidinium ion was determined from duplicate plots of $A_a/A_o$ vs. $a_H$. The results are reported in Table I. The linearity of the plots is proof of the validity of the equations for $BH^+$ charge type acids. The average value of the p$K_a$ for the *p*-toluidinium ion at an ionic strength of 0.10 and a temperature of 20.0 °C was $5.28 \pm 0.01_3$. Literature values determined at 20 °C and an ionic strength of 0.1 are 5.44 (*19*), 5.21 (*20*), and 5.159 (*21*). Since the literature values show considerable variation, we can only say that our value is well within the range of reported values.

**Distribution Coefficients.** The distribution coefficients for B and HA between cyclohexane and the aqueous buffers can be calculated from eq 5 and 11, respectively. However, since the experiment was optimized for determination of acidity constants, the pH region examined is not the best for accurate measurement of $K_B$ and $K_{HA}$. The slopes and *y* intercepts of the plots, the total flow rates of the aqueous and organic phases, and the calculated distribution coefficients and computed errors are reported in Table II for replicate trials. The uncertainties are one standard deviation and they include the error in the slope and *y* intercept, in the acidity constant, in the total flow rates of the organic and aqueous phases, and in the calibration of the pH meter.

**Comments.** Although this discussion has dealt with the determination of acidity constants using data collected from both the organic and aqueous phases, it is possible to determine them by monitoring peak areas in only the organic phase. Equation 10 indicates that for an HA acid, a plot of $1/A_0$ vs. $1/a_H$ should give a straight line. If the system constant, $\epsilon_{HA,o}bf$, is measured in a separate experiment and accurate values are obtained for $F_a$, $F_o$, and $n$, a value for $K_{HA}$ can be calculated from the intercept and $K_a$ can be calculated from the slope of that plot. The system constant is determined by using a single phase FIA system by injecting a sample of known concentration (dissolved in the organic phase) into a stream of the same organic phase. The injection valve is placed close to the detector of interest to minimize band broadening, and peak areas are measured for each sample injected. It is of course important to use the same detector and integrator settings as for the acidity constant determination. The system constant is determined from the relation $A = nK/F_0$ (*9*).

Similarly for a B base, eq 1 can be rearranged to describe a linear relationship between $1/A_o$ and $a_H$ (*10*). The product $K_BK_a$ can be calculated from the intercept and $K_a$ from the slope of that plot, if accurate values are measured for $\epsilon_{B,o}bf$, $F_a$, $F_o$, and $n$.

The disadvantage of the two-membrane method described in this paper, compared to the one membrane method is that two spectrophotometric detectors are necessary in the former. However there are some *distinct advantages* to measuring peak areas in both phases. It is not necessary to know the flow rates, the number of moles of sample injected, the extraction constant, or the system constant. It is also not necessary that the phases be preequilibrated or that the flow rates be constant from one injection to the next. These conclusions become evident upon examination of eq 3, 4, 8, and 9 in which none of the above appears, either explicitly or implicitly. The net effect is that very accurate values for acidity constants can be obtained. Work is presently under way to allow both the aqueous and organic phases to be monitored using the reference and sample channels of a single spectrophotometric detector.

## LITERATURE CITED

(1) Sekine, T.; Hasegawa, Y.; Ihara, N. *J. Inorg. Nucl. Chem.* **1973**, *35*, 3968–3970.

(2) Golumbic, C.; Goldbach, G. *J. Am. Chem. Soc.* **1951**, *73*, 3966–3967.

(3) Golumbic, C.; Orchin, M.; Weller, S. *J. Am. Chem. Soc.* **1949**, *71*, 2624–2627.

(4) Golumbic, C.; Orchin, M. *J. Am. Chem. Soc.* **1950**, *72*, 4145–4147.

(5) Ezumi, K.; Kubota, T. *Chem. Pharm. Bull.* **1980**, *28*, 85–91.

(6) Kubota, T.; Ezumi, K. *Chem. Pharm. Bull.* **1980**, *28*, 3673–3678.

(7) Xie, T. M.; Dryssen, D. *Anal. Chim. Acta* **1984**, *160*, 21–30.

(8) Kinkel, J. F. M.; Tomlinson, E. *Int. J. Pharm.* **1980**, *6*, 261–275.

(9) Fossey, L.; Cantwell, F. F. *Anal. Chem.* **1982**, *54*, 1693–1697.

(10) Fossey, L.; Cantwell, F. F. *Anal. Chem.* **1983**, *55*, 1882–1885.

(11) Carmicheal, M.; Cantwell, F. F. *Can. J. Chem.* **1982**, *60*, 1286–1290.

(12) "High-Purity Solvent Guide"; Burdick & Jackson Laboratories Inc.: Muskegon, MI, 1980.

(13) Ham, G. *Anal. Proc.* **1981**, *18*, 69–70.

(14) Anderson, L. *Anal. Chim. Acta* **1979**, *110*, 123–128.

(15) Betteridge, D.; Dagless, E. L.; Fields, B.; Graves, N. F. *Analyst (London)* **1978**, *103*, 897–908.

(16) Chen, D. T. Y.; Laidler, K. J. *Trans. Faraday Soc.* **1962**, *58*, 480–489.

(17) Herington, E. F. G.; Kynaston, W. *Trans. Faraday Soc.* **1957**, *53*, 138–142.

(18) Davies, C. W. *J. Chem. Soc.* **1938**, 2093–2092.

(19) Bolton, P. D.; Hall, F. M. *Aust. J. Chem.* **1967**, *20*, 1797–1804.

(20) Willi, A. V.; Meir, H. *Helv. Chim. Acta* **1956**, *39*, 318–322.

(21) Bernasconi, C.; Koch, W.; Zollinger, Hch. *Helv. Chim. Acta* **1963**, *46*, 1184–1190.

RECEIVED for review October 19, 1984. Accepted December 19, 1984. This work was supported by an Alberta Heritage Foundation for Medical Research Studentship to L.F., by the Natural Sciences and Engineering Research Council of Canada, and by the University of Alberta.

Anal. Chem. 1985, 57, 927-933

# Electrochemistry and Reverse Pulse Polarographic Determination of 1,2-Dibromo-2,4-dicyanobutane

**Marek Wojciechowski**[1] **and Janet Osteryoung***

*Department of Chemistry, State University of New York at Buffalo, Buffalo, New York 14214*

**The electrochemical reduction of the antibacterial agent 1,2-dibromo-2,4-dicyanobutane (DBDCB, Tektamar) at mercury electrodes in actonitrile is investigated by a variety of techniques. Reverse pulse voltammetry shows that the stoichlometry of this two-electron reduction requires the liberation of two bromide ions and an organic product of composition $C_6N_2H_6$ per molecule of reactant. An electroanalytical method for the determination of DBDCB based on reverse pulse polarography is described and used to determine the solubility of DBDCB in water. The solubility of DBDCB in water calculated from five analyses is 0.164% (standard deviation 0.010%) for a 5-ms pulse time or 0.158% (standard deviation 0.004%) for a 50-ms pulse time.**

The subject of electroreduction of halogenated organic molecules is as old as modern electrochemistry. The first report on the electrochemical cleavage of the carbon–halogen bond was published in 1938 by Plump and Hammett (*1*). It was followed by numerous mechanistic studies which have been summarized in several review articles (*2–9*).

In general, organic halides undergo irreversible cathodic reduction with formation of halide ions and, often more than one, organic products. The mechanism of the process, as well as the structure of intermediates and products, depends on the molecular structure of the reacting compounds and the reduction conditions, i.e., the nature of the solvent and electrolyte, the electrode material and potential, and the time scale of the experiment. It has been shown by several groups of investigators that mercury electrodes (*4, 6–16*), or other metallic electrodes, e.g., lead or tin (*4, 17–19*), often participate in reduction of organic halides. In many studies involving mercury electrodes, organomercury species have been detected among the intermediate or final products. The lower the energy of the carbon–halogen bond and the greater the energy of the metal–carbon bond, the greater is the probability of formation of organometallic compounds. Yields of organometallic products usually decrease if the electrolysis potential is changed to more negative values.

When alkyl halides are considered, reduction is easier if fewer carbons are in the chain, if chlorine is replaced by bromine or bromine is replaced by iodine, or if the molecule contains an electron-withdrawing group (β-substituents have the strongest effect). Moreover, the reactivity of halogenated hydrocarbons increases when more than one halogen atom is substituted on a single carbon or on adjacent carbons. Vicinal dihalides are more easily reduced than comparable geminal halides. In contrast with geminal halides which are reduced stepwise, molecules having two halogens on vicinal carbons lose both halogens in a single two-electron step which leads to the formation of an olefin. Further reduction of the olefin requires higher energy and often is not possible in an electrochemical experiment.

The cyanide group is known in organic chemistry as a very strong electron-withdrawing functional group. Thus, halogenated alkyl nitriles are reduced at more positive potentials than corresponding alkyl halides. Electrochemical behavior of monohalogenopropionitriles on mercury electrodes in aqueous solutions has been investigated by Feoktistov and Zhdanov (*20*). The compound β-chloropropionitrile did not reduce at the dropping mercury electrode, whereas β-bromopropionitrile exhibited a two-electron wave. On the other hand, β-iodopropionitrile exhibited two one-electron waves. The first wave was attributed to formation of a radical undergoing fast dimerization to yield an electroinactive dimer. The second, more negative wave generated propionitrile. A different mechanism involving formation of stable organomercury intermediates has been postulated by Rifi (*6*). Jura and Gaul presented results of polarographic and coulometric studies of polychlorinated propionitrile and derivatives in $EtOH/H_2O$ solutions (*21*).

In this publication we report on electrochemical reduction of 1,2-dibromo-2,4-dicyanobutane (DBDCB) at mercury electrodes in acetonitrile. DBDCB is an example of a vicinal dihalide in which the carbon–halogen bond is highly activated by adjacent nitrile groups. This makes DBDCB a very strong oxidant. In 1982 DBDCB was introduced by Merck & Co., under the trade name Tektamer, as an antibacterial agent (biocide, slimicide). Its activity as a preservative of aqueous systems is comparable with the activity of organomercury compounds, but its lower toxicity makes it more suitable for the food industry (*22, 23*). DBDCB attracted us for two reasons. Firstly, we expected very high electrochemical activity of DBDCB, particularly on mercury electrodes. Secondly, we were interested in developing an electrochemical method of determination of DBDCB which could compete with the gas chromatographic method, the only method recommended for DBDCB by its manufacturer. Recently we published the results of our studies of electrooxidation of mercury in the presence of halide ions in acetonitrile (*24–27*). It was suggested there that the mercury–halide ion processes could play an important role in mechanistic studies of electroreduction of halogenated organics, and, moreover, they could be applied in analysis of these compounds. This work emphasizes both aspects. Knowledge of the mercury oxidation reactions helped us in better understanding the processes involved in cathodic reduction of DBDCB in acetonitrile (this solvent was chosen because of poor solubility of DBDCB in water). With respect to describing the reduction process, our central aim was to establish quantitatively the stoichiometry of the cathodic reaction by using reverse pulse voltammetry. An analytical method for determination of this compound, based on reverse pulse polarography, is proposed.

## EXPERIMENTAL SECTION

The compound 1,2-dibromo-2,4-dicyanobutane (DBDCB) was obtained from Merck (98% purity; trade name Tektamer 38) and was used without further purification. Tetraethylammonium perchlorate (TEAP), tetraethylammonium bromide (TEAB), and mercuric bromide were purified and solutions prepared and standardized as described previously (25). Acetonitrile (AN) was

---

[1] Present Address: Department of Chemistry, University of Maryland Baltimore County, Catonsville, MD 21228.

0003-2700/85/0357-0927$01.50/0 © 1985 American Chemical Society

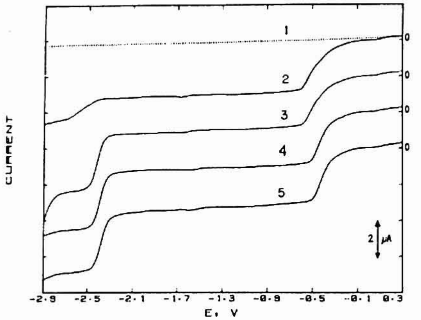

**Figure 1.** Dc polarograms for 0.5 mM solution of DBDCB in acetonitrile: curve 3, after addition of 0.2 M phenol; curve 4, AN containing 10% EtOH; curve 5, AN containing 10% MeOH. The supporting electrolyte was 0.09 M TEAP. Drop time was 0.5 s. Dotted line 1 is the background.

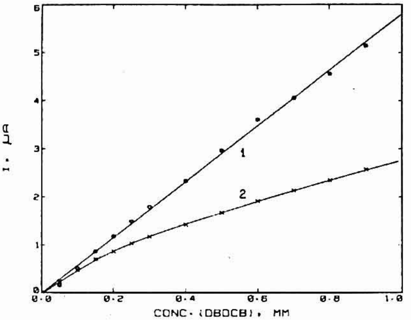

**Figure 2.** Concentration dependence on the height of the first and the second wave shown in Figure 1 (curve 2): curve 1, current measured between 0.00 V and −0.78 V; curve 2, current measured between −2.14 V and −2.78 V. Drop time was 1.0 s. DBDCB was present in 0.1 M TEAP/AN solution.

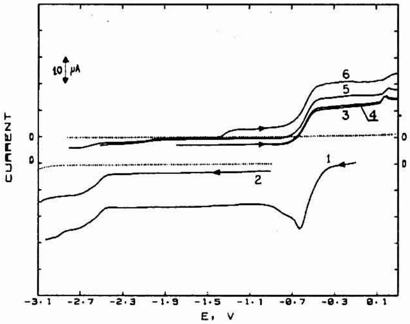

**Figure 3.** NPP and RPP polarograms obtained in 0.5 mM solution of DBDCB in 0.1 M TEAP/AN: delay time, 0.5 s; 5 ms pulse duration; $E_{in}$ −0.1 V (1), −0.9 V (2, 3), −1.8 V (4), −2.52 V (5), or −2.82 V (6). Dotted lines were obtained in a solution without DBDCB.

from Burdick & Jackson (UV grade). Water was distilled and repurified with a Millipore Milli-Q System. All other chemicals were at least ACS grade. Unless specified otherwise all voltammetric experiments were performed with a computer-controlled pulse-voltammetric instrument based upon a Digital Equipment Corp. PDP-8/e minicomputer and homemade interface. The system has been described elsewhere (28). A dropping mercury electrode (DME) had the following characteristic: natural drop time 7.85 s (measured in AN at the OCP and 84 cm height of the mercury column); flow rate, 0.813 mg $s^{-1}$. Drop time of the DME was controlled by an EG&G PARC Model 172 drop knocker controlled by the computer. Experiments with a static mercury electrode were carried out with an EG&G PARC Model 303 static mercury drop electrode (SMDE). The medium drop size (0.0182 $cm^2$ area) was used. All potentials were measured and are reported against an $Ag/Ag^+$ electrode (Ag/0.01 M $AgNO_3$ and 0.1 M TEAP in AN||0.1 M TEAP||solution). The supporting electrolyte used in this work was TEAP (0.1 M in AN) unless otherwise specified. Solutions were deoxygenated with argon (repurified to remove traces of oxygen and saturated with AN). Experiments were carried out at 25.0 °C.

Cyclic staircase voltammetry (CSCV) of DBDCB in AN was performed in an argon atmosphere containing <2 ppm $H_2O$ and <1 ppm $O_2$ (Vacuum Atmospheres drybox with a MO-40-1H dry-train control system). A hanging mercury drop electrode (HMDE) (Metrohm Model E-410; 0.022 $cm^2$ area) or a glassy-carbon disk electrode (GCDE) (IBM; 5 mm in diameter) was used for CSCV.

Constant potential coulometry of DBDCB on mercury (a mercury pool electrode; ca. 8 $cm^2$) was carried out as described before (27). Dc polarography was used in situ to monitor changes in composition of the solution during the course of electrolysis.

All voltammetric curves shown in this work are displayed with the current scale increasing upward and with the potential scale increasing to the right. Therefore anodic waves appear above the zero-current line and grow from the left to the right.

## RESULTS AND DISCUSSION

**Dc Polarography.** Dc polarography experiments in AN showed that the reduction of DBDCB on mercury occurs in two main steps. As shown in Figure 1 (curve 2) the first step produces a complex, poorly shaped wave. The limiting current of this wave, measured at −0.78 V, increased proportionally to the concentration of DBDCB (Figure 2, curve 1) and was not affected by proton donors. The second step gave two overlapping waves beginning at −2.4 V. The total limiting current was not proportional to the concentration (Figure 2, curve 2). Increase of the concentration of DBDCB caused larger separation and variation of the height ratios of the overlapping waves. The addition of protic substances to the solution substantially changed the process. In the presence of phenol, ethanol, or methanol only a single, well-shaped wave was obtained, with $E_{1/2}$ −2.43 V, −2.40 V, or −2.39 V, respectively. (The more positive of the overlapping waves in acetonitrile had $E_{1/2}$ at −2.50 V.) The height of this wave is almost the same as the total height of the wave at −0.5 V. All these facts suggest the participation of protons in the mechanism of the second process. The rate of the process is controlled by availability of protons in the solvent. In the presence of a sufficient concentration of a proton donor the process becomes diffusion controlled.

The first reduction step is not affected by proton donors. Although the $E_{1/2}$ of the corresponding wave shifts toward more positive potentials with addition of these substances, this is caused by a change of the reference potential rather than involvement of protons in the process. (Note the similar changes in the $E_{1/2}$ value of the more negative wave in Figure 1.)

**Normal and Reverse Pulse Polarography.** Figure 3 shows the normal pulse polarographic (NPP) and reverse pulse polarographic (RPP) curves obtained in an acetonitrile solution of DBDCB (0.5 mM). The NPP curve (curve 1) exhibits a reduction wave deformed by a maximum and another poorly defined wave at −2.4 V. The shape, position, and height of the second wave is not changed if the initial potential ($E_{in}$)

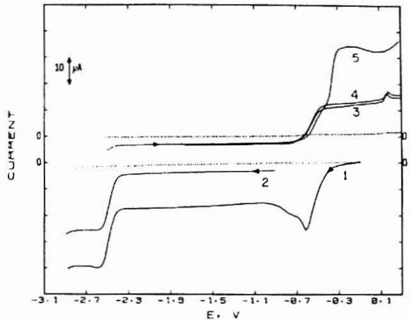

**Figure 4.** NPP and RPP polarograms obtained in 0.5 mM solution of DBDCB in 0.1 M TEAP + 0.02 M phenol/AN. All the experimental conditions were the same as shown in Figure 3.

is set at −0.9 V, which corresponds to the plateau of the first reduction wave (curve 2). This indicates that products of the electrolysis at −0.9 V do not adsorb on the electrode surface and do not undergo any chemical transformation which could alter the second process. The same was observed in the solution containing phenol (Figure 4, curves 1 and 2). The presence of phenol affects the second process as in dc polarography.

The RPP curves recorded in acetonitrile (Figure 3, curves 3–5) show a single anodic wave with $E_{1/2}$ equal to −0.60 V. The shape, position, and height of this wave remains constant when $E_{in}$ is shifted from the limiting plateau of the first wave to the limiting plateau of the second wave. This clearly indicates that the only electroactive product of the reduction of DBDCB was generated in the first step, i.e., on the limiting plateau of the more positive reduction wave.

On the basis of the literature summarized above on the cathodic reduction of halogenated organic compounds, we assumed that free bromide ions had to be among products of the reduction of DBDCB and that the reduction could not be reversible. On the other hand, we knew that free bromide ions cause anodic oxidation of mercury at the potentials where the RPP wave was observed for DBDCB. And indeed, pulse polarographic experiments with solutions containing $Br^-$ (1 mM) or $HgBr_2$ (0.5 mM) gave exactly the results we expected, namely, voltammograms identical with those of Figure 3 for the more positive process (see, e.g., Figures 6 and 7 of ref 25). Moreover, comparison of the RPP wave obtained in DBDCB solutions with and without phenol (Figures 3 and 4, curves 3 and 4) rules out any participation of protons in the first reduction process.

The above results suggest the reduction of DBDCB in the potential range corresponding to the plateau between the first and the second wave follows the reaction

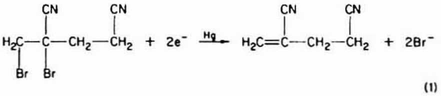

$$H_2\underset{Br}{C}-\overset{CN}{\underset{Br}{C}}-CH_2-\overset{CN}{CH_2} + 2e^- \xrightarrow{Hg} H_2C=\overset{CN}{C}-CH_2-\overset{CN}{CH_2} + 2Br^- \qquad (1)$$

Furthermore the RPP wave at $E_{1/2} = -0.60$ V corresponds to the reaction (cf. ref 25)

$$Hg + 3Br^- \rightarrow HgBr_3^- + 2e^- \qquad (2)$$

Our main interest in reaction 1 was to determine accurately the stoichiometry with respect to electrons and bromide ions. We did not attempt to identify specifically the suggested organic product 2,4-dicyano-1-butene. It should be noted that establishing the stoichiometry does specify the composition of the organic product as $C_6N_2H_6$. According to reactions 1 and 2 the ratio of the limiting currents of the NPP and RPP waves should be 3:2 (assuming no significant difference in diffusion coefficients of DBDCB and $Br^-$). For Figure 3, curve 1, the current at −1.1 V, measured with respect to the background line, is 15 μA, and for curve 3 the current at −0.4 V, measured vs. the background line, is 10 μA. Thus the experimental ratio is exactly that predicted.

The height of the RPP wave was proportional to $t_p^{-1/2}$ (pulse time) at constant $t_d$ (delay time at $E_{in}$), and to $t_d^{1/6}$ at constant $t_p$, as well as to concentration of DBDCB. This unequivocally proves that reaction 1 is controlled by diffusion of DBDCB.

In the presence of proton donors the limiting current of the second wave DBDCB is diffusion controlled and corresponds to a second two-electron step (cf. curves 3, 4, and 5 in Figure 1 and curve 1 in Figure 4).

The NPP wave obtained when $E_{in}$ was placed at the plateau of the first reduction wave (Figure 4, curve 2) corresponds to a two-electron reduction of the organic product of reaction 1. By analogy with other systems the second wave in the presence of protons probably corresponds to reduction of the double bond of the first product in a two-electron, two-proton process.

The RPP polarograms with $E_{in}$ at the plateau of the second reduction wave exhibited an additional anodic wave (Figure 4, curve 5) with $E_{1/2}$ of −0.35 V. This wave is caused by anodic oxidation of mercury in the presence of phenoxide ions formed from phenol molecules as a result of the proton abstraction by reaction at $E_{in}$. Similar anodic waves, although at different potentials, were observed on RPP polarograms obtained in DBDCB solutions containing ethanol or methanol. In this case anodic depolarization of mercury was caused by ethoxide and methoxide ions. Karabinas et al. (*29*) have reported on an analogous anodic process involving $CH_3O^-$ ions formed during the electroreduction of some organic compounds on mercury in methanol.

Without an addition of proton donor (according to specifications of the manufacturer, the solvent used in this study contains only ca. 0.01 M water), the second reduction step of DBDCB has a more complicated mechanism (cf. curve 2 in Figure 1 and curves 1 and 2 in Figure 3). RPP experiments with $E_{in} = -2.82$ V produced a small anodic wave with $E_{1/2} = -1.33$ V (Figure 3, curve 6). We believe that this wave is due to the anodic oxidation of mercury in the presence of hydroxide ions generated at $E_{in}$. Kolthoff and Coetzee (*30*) reported on the anodic oxidation of mercury with $OH^-$ ions in acetonitrile. They gave the $E_{1/2}$ value as −0.9 V vs. SCE. This would correspond with the potential ca. −1.20 V vs. the $Ag/Ag^+$ electrode used in our work. From our experience we know that hydroxide ions are very unstable in acetonitrile and the position of the anodic wave is strongly affected by the concentration of water in the solvent. Considering these facts our conclusion regarding the RPP wave with $E_{1/2} = -1.33$ V seems to be reasonable. Moreover, this wave can be observed only at very short pulse times (for example, in a 0.5 mM solution of DBDCB the wave is not present for pulse times 50 ms and longer). The formation of hydroxide ions at −2.82 V indicates that the trace water present in the solvent serves as a proton donor in the second reduction stage of DBDCB. Detailed further investigation of the mechanism of the second reduction process of DBDCB in dry acetonitrile was beyond the scope of this work.

Although reaction 1 is responsible for the current measured at the plateau of the first wave, the question remained of what reactions occur at more positive potentials. During the course of this work we discovered that mercury reacted chemically

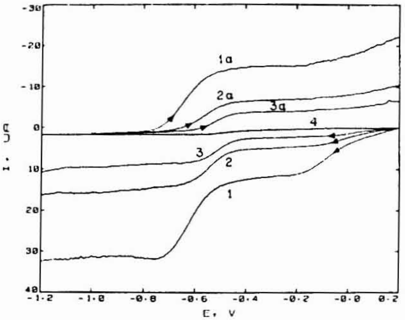

**Figure 5.** NPP and RPP polarograms of the first reduction step of DBDCB (0.2 mM) in acetonitrile (0.1 M TEAP solution). SMDE was used with a 2 s delay before pulse was applied. Pulse times were 5 (1, 1a), 20 (2, 2a), or 50 ms (3, 3a). Dc polarogram for the same delay time is shown as curve 4. $E_{in}$ was 0.2 V (curves 1–3) or −1.0 V (curves 1a–3a).

with DBDCB with formation of a gray precipitate covering the mercury surface (cf. discussion below on constant potential coulometric experiments). Moreover, the results of cyclic voltammetry on a glassy carbon electrode (cf. cyclic voltammetry section below) proved that mercury was involved in the first step of DBDCB reduction. Examining, for example, the shape of the first wave on curve 2, Figure 1, provides additional indications about adsorption involved in the process. It can be seen that the reduction is initiated at a potential of ca. 0.2 V and a trace wave and the main wave with a very poorly shaped foot are obtained. It was clear that NPP experiments with $E_{in}$ in the range 0.1 to −0.3 V (see the maximum on curve 1, Figure 3) were reflecting electrochemistry of the products generated on the electrode surface rather than the electrochemistry of DBDCB itself.

In further investigation of this process we used a static mercury drop electrode (SMDE), which better suited studies involving surface reactions or adsorption than a DME electrode with growing surface area. Using double potential step chronocoulometry in a 0.2 mM DBDCB/AN solution, we found that neither chemical reaction nor charge transfer was occurring at 0.2 V. Therefore we chose this potential for $E_{in}$ in the NPP experiments on the SMDE. The NPP curves obtained in the same solution are displayed in Figure 5 (curves 1–3). It is obvious now, that the first reduction process of DBDCB contains actually two major steps. The more negative wave ($E_{1/2}$ = −0.62 V for 5 ms pulse) corresponds exactly with the anodic wave present on the RPP curve (curves 1a–3a). This reduction wave arises from the final reduction of DBDCB to the unsaturated dinitrile and free bromide ions (cf. reaction 1). The height of this wave decays as $t_p^{-1/2}$, as expected for a diffusion controlled process.

We know from our earlier studies (*25*) that free bromide ions cannot exist on the mercury electrode surface at potentials more positive than −0.4 V. In this range mercury is oxidized and the products are adsorbed. Thus, it seems reasonable that at the plateau between the two NPP waves (Figure 5) the following reaction takes place:

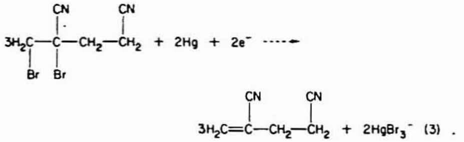

$$3H_2\underset{Br}{C}-\overset{CN}{\underset{Br}{C}}-CH_2-\overset{CN}{CH_2} + 2Hg + 2e^- \dashrightarrow 3H_2C{=}\overset{CN}{C}-CH_2-\overset{CN}{CH_2} + 2HgBr_3^- \quad (3)$$

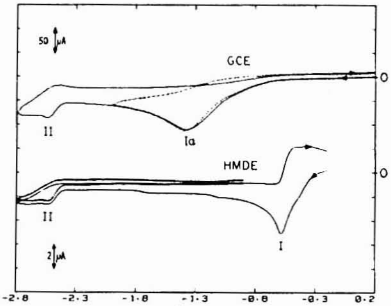

**Figure 6.** Cyclic voltammetry of DBDCB on glassy carbon electrode (GCE) and on hanging mercury dropping electrode (HMDE) in acetonitrile. The solution was 0.5 mM in DBDCB and 0.1 M in TEAP. The scan rate was 0.63 V $s^{-1}$.

This reaction was inhibited by adsorption of $HgBr_3^-$ on the electrode surface (e.g., the height of the first wave decayed with increasing pulse time much faster than expected for a diffusion controlled process).

Double potential step chronocoulometric (DPSCC) experiments with DBDCB showed unequivocally that $HgBr_3^-$ (formed at −0.3 V) adsorbed on mercury up to a monolayer completely stopping reaction 3.

In the potential range positive of −0.1 V, where in the presence of bromide ions mercury is oxidized to $Hg_2Br_2$, reaction 4 must be considered.

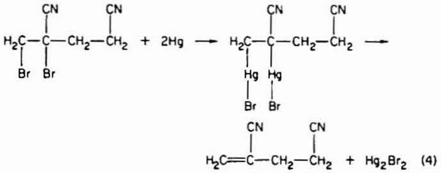

$$H_2\underset{Br}{C}-\overset{CN}{\underset{Br}{C}}-CH_2-\overset{CN}{CH_2} + 2Hg \rightarrow H_2\underset{\substack{Hg\\Br}}{C}-\overset{CN}{\underset{\substack{Hg\\Br}}{C}}-CH_2-\overset{CN}{CH_2} \rightarrow H_2C{=}\overset{CN}{C}-CH_2-\overset{CN}{CH_2} + Hg_2Br_2 \quad (4)$$

Using DPSCC we observed two facts. Firstly, there was no significant charge transferred if the mercury drop was extruded at −0.05 V. Secondly, reduction of $Hg_2Br_2$ accumulated on the surface was detected if the potential was stepped to −1.0 V. Analysis of the DPSCC data for different times (0.5 s to 12 s) spent at −0.05 V gave the rate of the chemical reaction of DBDCB on mercury surface equal to $5.2 \times 10^{-11}$ mol $s^{-1}$ $cm^{-2}$ (in moles of DBDCB per unit surface area of mercury). The rate of a similar reaction between $HgBr_2$ (in solution) and mercury at −0.05 V ($Hg_2Br_2$ was also formed) was $2.9 \times 10^{-10}$ mol $s^{-1}$ $cm^{-2}$ (in moles of $HgBr_2$), which appears to be more than 5 times larger than that for DBDCB. Neither of these two chemical processes was controlled by diffusion of reactant. This seems reasonable considering the fact that the $Hg_2Br_2$ layer on mercury was constantly growing.

Finally it should be stated explicitly that although we were not able to detect experimentally organomercury intermediates, they cannot be ruled out from the mechanism of the cathodic reduction of DBDCB on mercury electrodes. The chemical reaction of DBDCB with mercury is discussed below.

**Cyclic Voltammetry.** Cyclic voltammograms obtained in a DBDCB solution with a glassy carbon electrode (GCE) or with a hanging mercury drop electrode (HMDE) are shown in Figure 6. The curves feature a striking difference in the position and shape of the first, more positive, reduction peak.

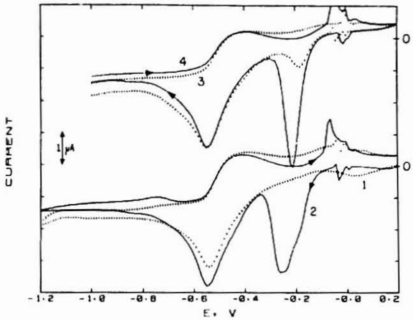

**Figure 7.** Comparison of CV voltammograms obtained in 0.2 mM DBDCB (dotted lines) and in 0.2 mM $HgBr_2$ solutions in 0.1 M TEAP/AN. The electrode was SMDE. The initial potential was 0.2 V for curves 1 and 2 or −1.0 V for curves 3 and 4. A 2 s delay at initial potential was used and the scan rate was 0.25 V $s^{-1}$.

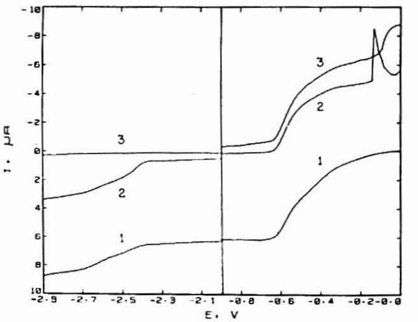

**Figure 8.** Dc polarograms (DME, 1.0 s drop time) during the electrolysis of 1.0 mM DBDCB solution at mercury pool electrode: curves 1, before the electrolysis; curves 2, after the electrolysis at −0.9 V; curves 3, after the electrolysis at −2.82 V.

On GCE the broad, irreversible reduction peak ($I_a$) has $E_p = -1.38$ V whereas on HMDE the first peak has $E_p = -0.58$ V. This huge difference proves the catalytic effect of mercury on the first reduction process of DBDCB. The second reduction process was not affected by the electrode material. In the absence of proton donors this process gave rise to two overlapping peaks with $E_p = -2.54$ V and −2.67 V. The same two peaks were obtained in solutions after the chemical reduction of DBDCB with mercury, or after the electrolysis of DBDCB at a mercury electrode at −0.9 V. The peak observed at GCE at −1.38 V was not present under these conditions. It proves the same product, i.e., unsaturated dinitrile, is produced in the first reduction step on both GCE and mercury electrodes, as well as in the chemical reduction with mercury. If water or other proton donor was added to acetonitrile, only one two-electron irreversible wave was observed at $E_p = -2.50$ V.

Comparison of the CV experiments carried out in solutions containing DBDCB or $HgBr_2$ at the same concentration is shown in Figure 7. In both cases the curves in the potential range below −0.35 V are very similar. This proves the formation of two bromide ions per molecule of DBDCB. The anodic peaks correspond to the oxidation of mercury in the presence of released $Br^-$ ions. There was no evidence for electrochemical regeneration of DBDCB. The difference between the reduction of $HgBr_2$ and DBDCB can be observed at potentials above −0.35 V. At potential +0.2 V, $HgBr_2$ reacts with mercury with deposition of $Hg_2Br_2$ on the surface of the electrode (note the stripping peak for $Hg_2Br_2$ at −0.2 to −0.3 V). The same potential prevents, however, mercury from reacting with DBDCB. The small reduction peak ($E_p$ ca. 0.0 V) on curve 1 can be attributed to reduction of organomercury product of reaction between mercury and DBDCB at +0.2 V, that adsorbed on the electrode, inhibiting further reaction. Larger scan rates caused a significant increase of this peak together with shift toward more negative potentials. This is in good agreement with results of pulse polarographic experiments discussed in the previous part.

**Constant Potential Coulometry.** During preparation for coulometric experiments we observed that mercury was easily (chemically) oxidized by DBDCB. In quiescent solutions a darkish precipitate covered the surface of the mercury pool inhibiting further reaction. If the precipitate was mechanically removed from the surface by means of vigorous stirring or ultrasonic vibration (under open circuit potential conditions) DBDCB was completely converted into unsaturated dinitrile and insoluble $Hg_2Br_2$ (darkening of the precipitate was caused by slow disproportionation with formation of metallic mercury on $Hg_2Br_2$ particles). This conclusion is based on the fact that after the reaction the more positive polarographic wave of DBDCB was absent and the waves at −2.47 V and −2.62 V remained almost unchanged. Thus, reaction 4 above appears to be responsible for the chemical reduction of DBDCB by mercury. Although it was practically impossible to reduce the suspension electrochemically, addition of bromide ions caused immediate solubilization of $Hg_2Br_2$ according to the reaction

$$Hg_2Br_2 + Br^- \rightleftharpoons HgBr_3^- + Hg \qquad (5)$$

Reduction of $HgBr_3^-$ generated in the above reaction was detected polarographically. After the reaction with mercury in the absence of $Br^-$ ions there was no polarographic wave present in the potential range more positive than −0.7 V.

Because of the passivation of the mercury pool electrode, electrolysis of DBDCB solutions required the following procedure. A 30-mL portion of 0.1 M TEAP/AN (supporting electrolyte) was introduced into the cell containing the Hg pool. After deaeration a −0.90 V potential was applied to the Hg pool electrode and a sample of the DBDCB solution was injected into the cell through the opening in the cell top (during the injection only an insignificant amount of the air entered the cell). The solution was constantly bubbled with argon and the Hg pool electrode was intensively stirred with a magnetic stirring bar. The electrolysis of 32.0 μmol of DBDCB at −0.90 V required 5.76 C of charge. This corresponds to 93.3% of the charge calculated for two-electron reduction. During the entire electrolysis no precipitation was observed. Free $Br^-$ ions were detected with the DME (oxidation of mercury, Figure 8). Except for a current offset the more negative reduction waves were not changed by the electrolysis. Almost the same electrolysis yield for reduction of DBDCB at −0.90 V (94.6%) was obtained in a solution initially containing $Br^-$ ions (TEAB). As was expected, electrolysis at −2.82 V of the product of electrolysis at −0.90 V gave $n$ lower than 2 (0.8 to 1). This suggests that the complete reduction was not possible under the conditions of limited availability of protons in the solvent.

**Reverse Pulse Polarographic Method for Determination of DBDCB.** We have shown above that under the conditions of a dc polarographic experiment the limiting current of the first reduction wave is controlled by diffusion of DBDCB. The reduction process produced two bromide ions per molecule of DBDCB, and there was no indication of ad-

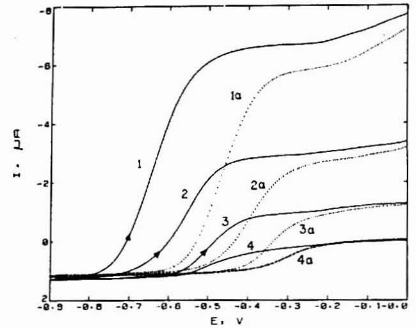

**Figure 9.** RPP and Dc polarograms of DBDCB in acetonitrile or in acetonitrile containing 9% water (dotted lines). A 1.0 s delay time was used for the DME electrode. $E_{in}$ was −0.9 V; pulse time was 5 (1, 1a), 20 (2, 2a), or 50 ms (3, 3a). Curves 4 and 4a represent the dc experiment.

sorption of the final products. However, due to adsorption of the intermediates and kinetic complications of their reduction, the current signal could not be enhanced by using normal pulse voltammetry. The normal pulse voltammorgrams ($E_{in}$ = −0.1 V, potential pulses changing to more negative potentials) exhibited maxima and therefore could not be used analytically. Also the dc polarographic curves were poorly shaped. Our study proved that the reduction of DBDCB on mercury is completely irreversible and none of the products can be reoxidized. On the other hand, bromide ions produced at the limiting plateau were suitable for sensitive and quantitative detection.

The mercury electrode can be anodically oxidized in the presence of free bromide ions. In acetonitrile this process is diffusion controlled and can be monitored with the pulse polarographic technique (*25*). Thus, if a mercury electrode is held at a potential where DBDCB is reduced, and the bromide ions are generated with the rate controlled by diffusion, and if potential is pulsed in the positive direction, the resulting anodic current should be proportional to the bulk concentration of DBDCB. Typical anodic curves (obtained for different pulse times) in this reverse pulse polarographic experiment are shown in Figure 9. Additions of water (up to 10 vol %) caused significant shift of the wave toward more positive potentials. This, however, did not affect the shape of the wave, although a slight decrease of the height caused by smaller diffusion coefficient was observed. Calibration curves for 5 and 50 ms pulse durations are plotted in Figure 10.

As expected, they are linear in a wide range of concentration (0.01–1.0 mM). The linearity of calibration curves was not changed when water (up to 10%) was present in acetonitrile. Also the presence of dissolved oxygen did not interfere with the reverse pulse wave if the initial potential was more positive than the potential of the reduction of oxygen. The value $E_{in}$ = −0.8 V was the optimum for this purpose.

We applied this method for determination of the solubility of DBDCB in water. A saturated aqueous solution of DBDCB was filtered, and a 25, 50, or 75 μL sample was diluted with a 5-mL portion of 0.1 M TEAP in acetonitrile containing 10% $H_2O$. Quantitation was done by using the standard addition method with the 0.05 M solution of DBDCB in acetonitrile serving as a standard. The reverse pulse polarographic (DME) scan was run from $E_{in}$ = −0.77 V with pulse duration of 5 or 50 ms. The solubility of DBDCB in water calculated from the results of five analyses was 0.164% or 0.158% for 5 ms or 50 ms pulse time, respectively. The standard deviation was 0.010% or 0.004%, respectively.

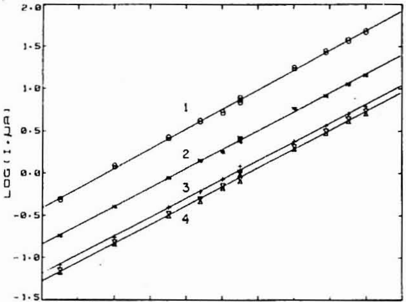

**Figure 10.** log RPP and dc limiting current (DME) vs. concentration. DBDCB solutions were prepared in 0.1 M TEAP/AN. Lines 1 and 2 are from RPP experiments (delay time, 1.0 s; $E_{in}$ = −0.9 V; pulse time was 5 ms (1) or 50 ms (2)). Drop time in the dc experiments was 1.0 s (3) or 0.5 s (4).

These results show the very good precision and sensitivity of the method.

## ACKNOWLEDGMENT

Appreciation is expressed to the Merck-Calgon Corp. for providing a sample of 1,2-dibromo-2,4-dicyanobutane. The authors wish to thank Marek Lipsztajn and Zenon Karpinski for valuable discussions.

**Registry No.** DBDCB, 35691-65-7.

## LITERATURE CITED

(1) Plump, R. E.; Hammett, L. P. *J. Electrochem. Soc.* **1938**, *73*, 523–538.
(2) Elving, P. J.; Pullman, B. In "Advances in Chemical Physics"; Prigogine, I., Ed.; Wiley-Interscience: New York, 1961; Vol. 1, Chapter 1.
(3) Perrin, C. L. *Prog. Phys. Org. Chem.* **1965**, *3*, 165.
(4) Feoktistov, L. G.; Tomilov, A. P.; Smirnov, Yu. D.; Goldin, M. M. *Sov. Electrochem.* (*Engl. Transl.*) **1965**, *1*, 791–796.
(5) Mann, C. K.; Barnes, K. K. "Electrochemical Reactions in Nonaqueous Systems"; Marcel Dekker: New York, 1970; Chapter 1.
(6) Rifi, M. R. "Organic Electrochemistry"; Baizer, M. M., Ed.; Marcel Dekker: New York, 1973; Chapter 6.
(7) Feoktistov, L. G. In "Organic Electrochemistry", 2nd ed.; Baizer, M. M., Lund, H., Eds.; Marcel Dekker: New York, 1983; Chapter 7.
(8) Howley, M. D. In "Encyclopedia of Electrochemistry of the Elements"; Bard, A. J., Lund, H., Eds.; Marcel Dekker: New York, 1980; Vol. XIV.
(9) Becker, J. Y. In "The Chemistry of Functional Groups, Supplement D, The Chemistry of Halides, Pseudo Halides and Azides"; Patai, S., Rappoport, Z., Eds.; Wiley: New York, 1983; Part 1, Chapter 6.
(10) Hush, N. S.; Oldham, K. B. *J. Electroanal. Chem.* **1963**, *6*, 34–45.
(11) Ershler, A. B.; Teodoradse, G. A.; Fakhimi, M.; Butin, K. P. *Sov. Electrochem.* (*Engl. Transl.*) **1966**, *2*, 295–302.
(12) Mann, C. K.; Webb, J. L.; Walborsky, H. M. *Tetrahedron Lett.* **1966**, *20*, 2249–2255.
(13) Rogers, L. B.; Diefenderfer, A. N. *J. Electrochem. Soc.* **1967**, *114*, 942.
(14) Brown, O. R.; Taylor, K. *J. Electroanal. Chem.* **1974**, *50*, 211–220.
(15) La Perriere, D. M.; Carroll, W. F., Jr.; Willett, B. C.; Torp, E. C.; Peters, D. G. *J. Am. Chem. Soc.* **1979**, *101*, 7561–7568.
(16) Mbarak, M. S.; Peters, D. G. *J. Org. Chem.* **1982**, *47*, 3397–3403.
(17) Ulery, H. E. *J. Electrochem. Soc.* **1969**, *116*, 1201–1205.
(18) Brown, O. R.; Taylor, K.; Thirsk, H. R. *J. Electroanal. Chem.* **1974**, *53*, 261–269.
(19) Ulery, H. E. *J. Electrochem. Soc.* **1972**, *119*, 1474–1478.
(20) Feoktistov, L. G.; Zhdanov, S. I. *Electrochim. Acta* **1965**, *10*, 657–662.
(21) Jura, W. H.; Gaul, R. J. *J. Am. Chem. Soc.* **1958**, *80*, 5402–5409.
(22) *Fed. Regist.* **1981**, *46* (134, BK.1) 36129–36130.
(23) *Fed. Regist.* **1981**, *46* (149), 39589.
(24) Wojciechowski, Marek; Osteryoung, Janet *Anal. Chem.* **1982**, *54*, 1713–1719.
(25) Wojciechowski, Marek; Osteryoung, Janet *Anal. Chem.* **1984**, *56*, 1884–1890.
(26) Wojciechowski, Marek; O'Dea, J. J.; Osteryoung, Janet *J. Phys. Chem.* **1983**, *87*, 4725–4730.

(27) Wojciechowski, Marek; Osteryoung, Janet *J. Phys. Chem.* **1984**, *88*, 5245–5251.
(28) Brumleve, T. R.; O'Dea, J. J.; Osteryoung, R. A.; Osteryoung, Janet *Anal. Chem.* **1981**, *53*, 702–706.
(29) Karabinas, P.; Kokkinidis, G.; Jannakoudakis, D. *J. Electroanal. Chem.* **1979**, *98*, 141–148.
(30) Kolthoff, I. M.; Coetzee, J. F. *J. Am. Chem. Soc.* **1957**, *79*, 1852–1858.

RECEIVED for review August 27, 1984. Accepted December 17, 1984. This work was supported by the National Science Foundation under Grant No. CHE 8305748.

# Distribution of Electrochemical Activity on Graphite–Epoxy Surfaces

**Royce C. Engstrom,* Michael Weber, and Jane Werth**[1]

*Department of Chemistry, University of South Dakota, Vermillion, South Dakota 57069*

**The technique of iontophoresis was used to spatially resolve the distribution of electrochemical activity on electrodes prepared from approximately 1:1 mixtures of graphite powder and nonconducting epoxy. Electrochemical activity was found to reside in irregularly shaped areas having dimensions measured in tens of micrometers. Active regions were separated from one another by regions of low activity having similar dimensions. The electrochemical activity was found to be associated with microscopically observed gray areas on the graphite–epoxy surface, which appear to be aggregates of graphite particles.**

A number of carbon-based composite materials have been used to prepare solid electrodes for voltammetry. Carbon-paste electrodes have been in use for years, prepared by mixing graphite powder with Nujol oil or some other organic binder (*1, 2*). Rigid, polishable composite electrode surfaces have been prepared from a mixture of graphite and Kel-F (*3–5*) or graphite and epoxy (*6–9*). In these composite preparations, a heterogeneous electrode surface must result, consisting of regions of electrochemically active graphite and regions of inactive binder. Heterogeneous electrodes show peculiar electrochemical behavior attributable to nonlinear diffusion toward active regions (*10–14*). Using the theory of Gueshi et al. (*10*), Weisshaar and Tallman estimated the dimensions of active regions on Kel-F–graphite surfaces to be 2–15 μm (*5*). Landsberg and Thiele estimated that their carbon-paste electrodes had active regions with diameters of 11–38 μm (*11*). A detailed description of the distribution of electrochemical activity on the electrode surface would be beneficial in the interpretation of results obtained with composite electrodes. Furthermore, composite electrodes have been used to preconcentrate analytes prior to electrochemical detection by a mechanism that may involve the binder material (*15, 16*). Knowledge of the spatial relationship between regions of binder material and regions of electrochemical activity may help in the design and optimization of such preconcentration schemes.

We have reported on the use of iontophoresis for mapping electrochemical activity on surfaces with a spatial resolution in the micrometer range (*17*). By use of model heterogeneous electrodes prepared from small-diameter platinum wires or epoxy-impregnated reticulated vitreous carbon (RVC-epoxy), it was demonstrated that regions of electrochemical activity as small as 10 μm could be detected and that the size and shape of an individual active region could be defined with a resolution of 10 μm. Briefly, the technique of iontophoresis involves electrophoretic ejection of an electroactive species from a micropipet onto a microscopic area of an electrode surface. The electrode, poised at a potential capable of electrolyzing the ejected species, generates a faradaic current whose amplitude is taken as a measure of the electrode activity in the immediate vicinity of the micropipet tip. By moving the micropipet with a micropositioner, we can record the faradaic response as a function of position on the electrode surface, thereby generating a "map" of surface activity.

In the present work, the technique of iontophoresis has been applied to the study of graphite–epoxy electrode surfaces. The distribution, size, and geometries of electroactive regions on the surface have been elucidated and related to microscopic surface structure.

## EXPERIMENTAL SECTION

**Apparatus.** The instrumentation system for iontophoretic characterization of electrode surface heterogeneity has been described previously (*17*). The system provides for controlling the potential of the working electrode, positioning the micropipet over the electrode surface with an accuracy of approximately 2 μm, ejecting the electroactive species from the micropipet onto the electrode surface, measuring the transient faradaic response current, and transferring the data to a recorder. Micropipets with tip diameters of under 1 μm were filled with a solution of 0.5 M potassium ferrocyanide, and ferrocyanide ions were ejected by selecting the appropriate polarity of ejection current. The working electrodes were held at 0.5 V vs. the saturated calomel electrode so that ferrocyanide ions were oxidized upon being ejected onto the electrode surface.

Graphite–epoxy electrodes were prepared by mixing graphite powder (~1 μm particle size) with a nonconducting epoxy (Epotek 320, Epoxy Technology, Billerica, MA) resulting in a thick paste that was 45–50% graphite by weight. After the paste was thoroughly mixed, a length of 7 mm diameter glass rod was packed to a depth of about 1 cm with the graphite–epoxy mixture, and a length of copper wire was inserted into the mixture for the purpose of making electrical contact. After the mixture was cured for 2 h at 80 °C, the graphite–epoxy surface was sanded flat and then polished on successively finer emery papers followed by a slurry of 0.3 μm alumina (Fisher Scientific, St. Louis, MO). The electrode was fitted into the cell which was designed to be held in the stage of a microscope, so that positioning of the micropipet over the electrode surface could be observed under the microscope.

For purposes of comparison, a glassy carbon electrode was prepared from Tokai glassy carbon, grade 30s (International

---

[1] Present address: School of Medicine, University of South Dakota, Vermillion, SD 57069.

0003-2700/85/0357-0933$01.50/0 © 1985 American Chemical Society

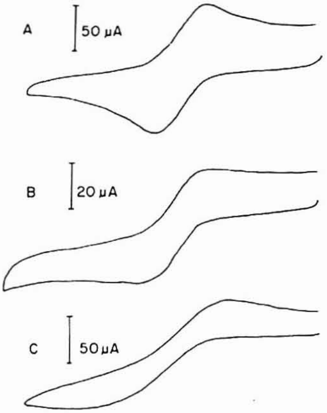

Figure 1. Cyclic voltammograms of 5 mM potassium ferrocyanide in 1 M potassium chloride at (A) glassy carbon, (B) RVC-epoxy, and (C) graphite–epoxy electrodes: cathodic limit, −0.2 V; anodic limit, 0.6 V; scan rate, 50 mV/s.

Minerals and Chemical Corp., New York). An epoxy-impregnated RVC electrode was prepared as previously described (*17, 18*). Both of these electrodes were polished with the same procedure as used for the graphite–epoxy electrodes. The reference electrode was a saturated calomel electrode and the auxiliary electrode was a platinum wire. Cyclic voltammograms were taken with a Model CV-1B (Bioanalytical Systems, West Lafayette, IN) and an X-Y recorder (Model 2000, Houston Instruments, Austin, TX).

**Reagents.** The micropipet filling solution (0.5 M potassium ferrocyanide) and the supporting electrolyte (0.10 M potassium nitrate) were prepared with reagent grade chemicals and distilled, deionized water.

**Procedure.** The working electrode was placed into the electrochemical cell, the cell was filled with supporting electrolyte, and a potential of 0.5 V was applied to the working electrode. With the aid of the micropositioner and the microscope, a micropipet was moved to within a few micrometers of the electrode surface. Final vertical positioning of the micropipet was done by occasionally applying an ejection current pulse and monitoring the resultant faradaic transient until a response of sufficient amplitude was obtained. It is estimated that the micropipet can be placed within 3–5 µm of the surface in this manner. Once the micropipet was in position, an ejection was made (typically 1000 nA for 300 ms), the faradaic transient recorded, and the coordinates of the micropipet position noted. The position was then incremented along the electrode surface, repeating the ejection and recording the faradaic response. By plotting the amplitude of the faradaic response against micropipet position, we developed a map of electrode surface activity. Both one-dimensional maps (a single straight-line pass over a section of the electrode) and two-dimensional maps (multiple passes back and forth over the surface, incrementing in both the X and Y dimension) were obtained.

## RESULTS AND DISCUSSION

**Cyclic Voltammetry.** Figure 1 shows cyclic voltammograms taken in a solution of 5 mM potassium ferrocyanide and 1 M potassium chloride at glassy carbon, RVC-epoxy, and graphite–epoxy electrodes. The glassy carbon electrode exhibited the peak-shaped anodic and cathodic currents expected for a smooth, uniformily active electrode of ordinary dimensions. In contrast, the RVC-epoxy electrode, with its array of well-defined, but irregularly shaped active regions, showed currents that more closely resemble plateaus than peaks. As described by Sleszynski and Osteryoung (*18*), the RVC-epoxy electrodes behave as ensembles of individual electrodes of very small dimensions, so that nonlinear diffusion toward active regions gives rise to increased mass transport, resulting in "steady-state" currents. The graphite–epoxy electrodes gave voltammograms that were qualitatively similar to the RVC-epoxy electrodes, indicating the heterogeneous nature of the graphite–epoxy electrodes. (The graphite–epoxy electrodes did give noticeably less reversible voltammograms.) The following results characterize the heterogeneity of the graphite–epoxy surfaces.

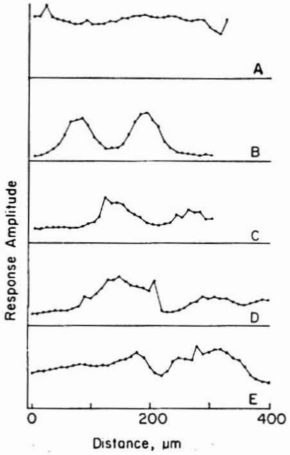

Figure 2. Faradaic response amplitudes for the one-dimensional iontophoresis of (A) glassy carbon, (B) RVC-epoxy, and (C–E) various regions on graphite–epoxy electrodes: applied potential, 0.5 V. Each data point represents a 10-µm interval.

**Iontophoresis.** The distribution of electrochemical activity on the three types of electrodes was studied by performing one-dimensional iontophoretic mappings of the surfaces. Figure 2 shows the plots of faradaic response amplitude as a function of micropositioner setting at (A) glassy carbon, (B) RVC-epoxy, and (C) several regions on graphite–epoxy electrodes. The glassy carbon profile shows a relatively uniform activity as expected, the response showing no significant trends over the 350-µm distance examined. A similar-sized region on the RVC-epoxy surface showed two distinct regions of activity with widths of approximately 50 µm each. The boundaries between active and inactive regions were well-defined, just as they are under microscopic examination. The profiles of the graphite–epoxy surfaces showed definite spatial variation of electrochemical activity, but the variations were not as clearly delineated as those on the RVC-epoxy electrodes. On the graphite–epoxy surfaces, the regions of increased activity had dimensions ranging from 80 µm to 130 µm, and the regions of activity were separated from one another by distances of 50 µm to 150 µm. Transitions from regions of high activity to regions of lower activity were not as abrupt as those on RVC-epoxy, and the regions of activity did not all exhibit the same level of faradaic response. It is likely that the regions of activity on the graphite–epoxy surface possess varying degrees of microscopic roughness due to the granular nature of the graphite that comprises the graphite–epoxy substrate.

The geometries of active regions on the graphite–epoxy surfaces were determined by developing two-dimensional maps of faradaic response. Several areas on the electrode surface were chosen at random for characterization. The resulting

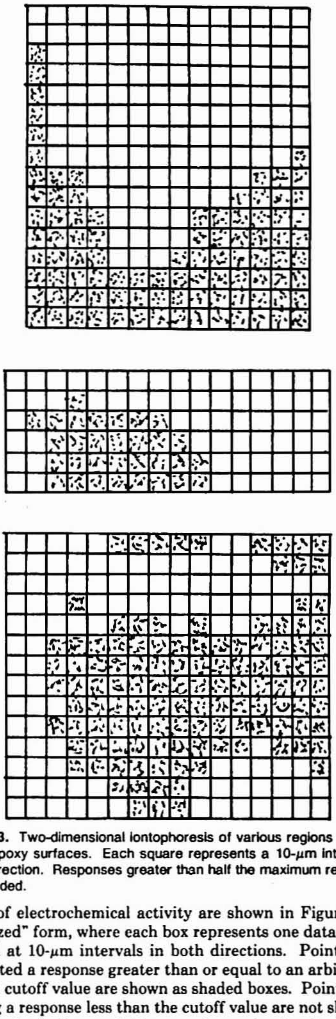

**Figure 3.** Two-dimensional iontophoresis of various regions on graphite–epoxy surfaces. Each square represents a 10-μm interval in each direction. Responses greater than half the maximum response are shaded.

maps of electrochemical activity are shown in Figure 3 in "digitized" form, where each box represents one data point, spaced at 10-μm intervals in both directions. Points that generated a response greater than or equal to an arbitrarily chosen cutoff value are shown as shaded boxes. Points generating a response less than the cutoff value are not shaded. This method of presentation permits ready visualization of the shapes of the active regions. The plots show that the regions are irregularly shaped, with dimensions measured in tens of micrometers in all directions.

**Activity–Structure Relationship.** Under microscopic examination, the graphite–epoxy surface exhibits gray regions and black regions, with boundaries between the regions showing up with varying degrees of clarity. In an effort to define which were the electrochemically active regions, the micropipet was made to traverse across the boundaries between gray and black regions. Near each boundary, several iontophoretic ejections were made over the gray area and then over the adjacent black area. The regions chosen for this experiment were ones whose boundaries were particularly well-defined, so that a clear decision could be made as to whether the micropipet tip was over a gray or black region. Consequently, the results, which are summarized in Table I, indicate a higher degree of reproducibility was observed in Figure 2. For each of the three boundary regions studied, the gray areas generated significantly higher responses to iontophoretic ejections than did the black areas.

**Table I. Responses Generated at Gray and Black Regions of Electrode Surface**

| | response, arbitrary units | |
|---|---|---|
| | black region | gray region |
| region 1 | 31 (2)[a] | 49 (3) |
| region 2 | 10 (2) | 25 (3) |
| region 3 | 38 (2) | 47 (1) |

[a] Value in parentheses is the standard deviation obtained from three to five measurements.

To ensure that the higher responses from gray regions did not arise simply because gray regions might be physically elevated over black regions, and therefore closer to the micropipet tip, the flatness of the surface was determined. The distance between micropipet tip and electrode surface could not be directly measured by microscopic examination. However, it was possible to note the vertical micropositioner setting at that point where the micropipet tip touched the surface, because the tip would bend slightly as it dragged on the surface. The elevations of black and gray regions, respectively, in units of micrometers with the standard deviations in parentheses ($n = 3$), were 351 (1) and 349 (2) for region 1, 376 (2) and 374 (1) for region 2, and 345 (1) and 351 (2) for region 3. At the 95% confidence level, there was no significant difference in the elevation of black and gray regions.

## CONCLUSIONS

In the mixing of graphite and epoxy, it appears that the graphite particles clump together, resulting in an electrode surface with a heterogeneous distribution of electrochemical activity, similar to the model that has been proposed for Kel-F–graphite electrodes (5). Regions having a high density of graphite appear gray and exhibit a relatively high level of electrochemical activity, while regions having a low density of graphite appear black, the color of the epoxy binder, and exhibit low or no electrochemical activity. The dimensions of both types of regions are of the order of tens of micrometers and therefore are of dimensions that affect diffusional patterns during cyclic voltammetry experiments. The response profiles shown here suggest that approximately half of the geometric area of the graphite–epoxy surface is electrochemically active.

**Registry No.** C, 7440-44-0; graphite, 7782-42-5.

## LITERATURE CITED

(1) Adams, R. N. "Electrochemistry at Solid Electrodes"; Marcel Dekker: New York, 1969; pp 26, 280.
(2) Adams, R. N. *Anal. Chem.* **1958**, *30*, 1576.
(3) Anderson, J. E.; Tallman, D. E.; Chesney, D. J.; Anderson, J. L. *Anal. Chem.* **1978**, *50*, 1051.
(4) Weisshaar, D. E.; Tallman, D. E.; Anderson, J. L. *Anal. Chem.* **1981**, *53*, 1809.
(5) Weisshaar, D. E.; Tallman, D. E. *Anal. Chem.* **1983**, *55*, 1146.
(6) Swofford, H. S.; Carman, R. L. *Anal. Chem.* **1966**, *38*, 966.
(7) Anderson, J. E.; Tallman, D. E. *Anal. Chem.* **1976**, *48*, 209.
(8) Cheng, H. Y.; Falat, L. *Anal. Chem.* **1982**, *54*, 2111.
(9) Cheng, H. Y.; Falat, L. *J. Electroanal. Chem.* **1983**, *157*, 393.
(10) Gueshi, T.; Tokuda, K.; Matsuda, H. *J. Electroanal. Chem.* **1978**, *89*, 247.
(11) Landsberg, R.; Thiele, R. *Electrochim. Acta* **1966**, *11*, 1243.
(12) Scheller, F.; Muller, S.; Landsberg, R.; Spitzer, H. J. *J. Electroanal. Chem.* **1968**, *19*, 187.
(13) Gueshi, T.; Tokuda, K.; Matsuda, H. *J. Electroanal. Chem.* **1979**, *101*, 29.
(14) Reller, H.; Kirowa-Eisner, E.; Gileadi, E. *J. Electroanal. Chem.* **1982**, *138*, 65.
(15) Cheng, H. Y.; Falat, L.; Li, R. L. *Anal. Chem.* **1982**, *54*, 1384.
(16) Wang, J.; Freiha, B. A. *Anal. Chim. Acta* **1983**, *148*, 79.

(17) Engstrom, R. C. *Anal. Chem.* **1984**, *56*, 890.
(18) Sleszynski, N.; Osteryoung, J.; Carter, M. *Anal. Chem.* **1984**, *56*, 130.

RECEIVED for review October 29, 1984. Accepted December 26, 1984. Acknowledgment is made to the donors of the Petroleum Research Fund, administered by the American Chemical Society, and to the National Science Foundation, Grant No. CHE-8411000, for partial support of this work.

# Flow Injection and Liquid Chromatography Detector for Amino Acids Based on a Postcolumn Reaction with Luminol

**Allan MacDonald**[1] **and Timothy A. Nieman***

*Department of Chemistry, University of Illinois, 1209 West California Street, Urbana, Illinois 61801*

**A detector for amino acids is based on suppression of chemiluminescence (CL) in the Co(II)–luminol–peroxide system. The scheme involves two successive postcolumn reactions, complexation followed by CL. Following the column, Co(II) is added to the effluent. The stream then enters a microporous membrane cell where an alkaline luminol/peroxide solution is added. The CL emission is proportional to the free Co(II) concentration. When an amino acid elutes, it complexes Co(II) and reduces the free Co(II) concentration; the CL intensity then drops and a peak results. Detection limits depend upon the magnitude of the complex formation constants, and range from 0.004 to 20 nmol in flow injection mode. Precision is 1–4%. Compared to the classical ninhydrin reaction, this method is faster, can be run at room temperature, can determine secondary amino acids without varying the reaction or instrument, has simpler instrumentation, and, in favorable cases, has lower detection limits.**

As evidenced by recent reviews (*1–7*), there is much interest in developing chemiluminescent (CL) techniques for detection in order to take advantage of the sensitivity the method can provide. As a lack of selectivity has been the major limitation of CL based determination, it has naturally been suggested that CL be applied for detection of separated species. A few examples exist for the use of the luminol (3-aminophthalhydrazide) reaction as a detector for metals separated as their chloro complexes on a strong anion exchange column (*8–11*). One of these approaches measured Zn and Cd by suppression of the Co(II)-enhanced luminol reaction (*11*).

There are also a few examples of solution CL as an HPLC detector for organic species (*12–21*). Direct reaction with lucigenin has been used for detection of ascorbic acid and dehydroascorbic acid (*12*). Energy transfer from peroxyoxalate CL reactions to fluorescent analytes has been the basis for several other detection schemes (*13–19*). An early example of this method is the detection of dansylated amino acids using bis(2,4,6-trichlorophenyl) oxalate and $H_2O_2$ as the fluorescent excitation reaction (*13*). Another detector (*20*) was a spray detector based on energy transfer from $O_2(^1\Delta g)$ generated by reaction of hypochlorite with hydrogen peroxide at pH 10. In addition to liquid-phase detection, gas-phase chemiluminescent reactions have been employed for detection of HPLC or GC separated species (*22–28*).

Our interest has been to develop a CL detector for amino acids in flowing streams such as in an HPLC detector. Metal ion chelators such as citrate and EDTA are known to cause suppression of metal ion enhanced luminol CL (*29*). Also, amino acids have been detected in a static system by suppression of Cu(II)-enhanced luminol CL (*30, 31*). Our system monitors the CL from a steady flow of Co(II) reacting with luminol and hydrogen peroxide in a alkaline solution. If an amino acid is injected into the Co(II) stream, some of the Co(II) is complexed and decreased CL light intensity results. The injected slug of amino acid analyte then results in a negative peak, and the analyte concentration may be determined from the size of that peak.

## EXPERIMENTAL SECTION

**Instrumental Methods.** Figure 1 shows a schematic of the flow system used for HPLC detection. The flow system used for flow injection analysis was identical with the system in Figure 1 with the exception of the column being removed. The mobile phase was pumped by an Altex 110 pump, equipped with a pulse dampener (Anspec H1302), followed by a Rheodyne 7010 injector with a 20-μL sample loop. The mobile phase was then mixed in a tee-mixer with a Co(II) solution which was delivered from a pressurized reservoir (ca. 5 psi). A short delay loop followed before the solution was mixed with the precombined luminol/$H_2O_2$/KOH solution in the flow cell. The luminol/$H_2O_2$/KOH reagent solution was also delivered from a pressurized reservoir (Ominfit glass reagent reservoir bottles). The light intensity produced was monitored by a Hamamatsu R372 photomultiplier tube. Flow of reagent solutions was controlled with Nupro metering valves and was monitored using flowmeters (Fisher and Porter or Manostat).

The flow cells used in the course of these studies were microporous membrane flow cells developed previously in this group (*32, 33*).

Separations were performed on a Whatman Partisil 10 SCX column using a mobile phase of 0.01 M acetic acid/sodium acetate buffer at pH 5.5 with a flow rate of 1.0 mL/min.

**Reagents and Solutions.** Luminol (Aldrich), amino acids (ICN pharmaceuticals, National Biochemical, Mallinckrodt, or Sigma), and all other reagents (Analytical Reagent Grade) were used without further purification.

The luminol/$H_2O_2$/KOH reagent solution composition was 10 mM luminol, 20 mM $H_2O_2$, 35 mM KOH, and 1 μM EDTA. This solution was stable for about 1 week. Solutions of Co(II) were prepared by serial dilution from a stock solution of $10^{-3}$ M $Co(NO_3)_2\cdot 6H_2O$. Solutions of KOH were prepared from Acculute solutions (Anachemia).

Water purified by a Continental Millipore Milli-Q system was used for all solutions.

## RESULTS AND DISCUSSION

Figure 2 illustrates the theory of the mechanism of the response of this detector. If only uncomplexed Co(II) enhances the luminol reaction, then the emission intensity would vary as the concentration of uncomplexed Co(II). In the presence of a chelating ligand the fraction of free Co(II) is given by the ligand concentration and the complex formation constants,

---

[1] Present address: Clorox Technical Center, P.O. Box 493, Pleasanton, CA 94566.

0003-2700/85/0357-0936$01.50/0 © 1985 American Chemical Society

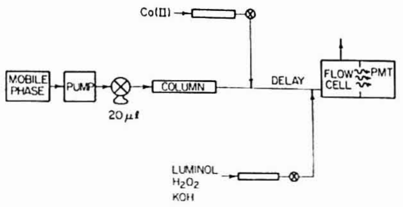

**Figure 1.** Block diagram of flow system.

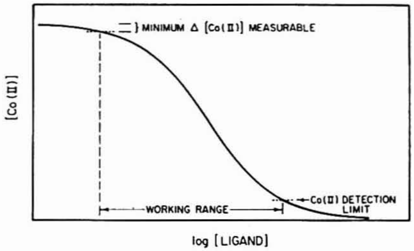

**Figure 2.** Hypothetical plot of free Co(II) concentration as a function of ligand concentration.

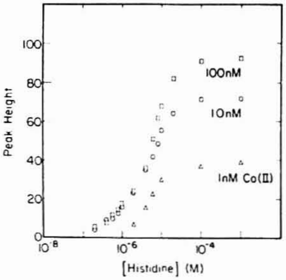

**Figure 3.** Effect of stock Co(II) concentration on histidine working curve.

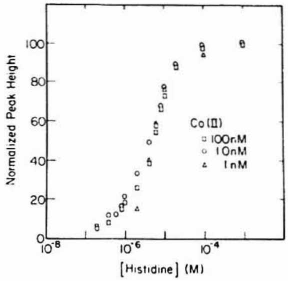

**Figure 4.** Normalized histidine working curves for several stock Co(II) concentrations.

regardless of the initial concentration of Co(II). In terms of light intensity, a negative peak from the background intensity is observed due to the complexation of some of the Co(II) by the analyte. For the purpose of this discussion, the peak is discussed in positive terms in that measurements are described as peak height or peak area. The maximum ligand concentration which can be measured by peak height is that ligand concentration which causes the free Co(II) concentration at the center of the analyte band to drop below the detection limit for Co(II) under these conditions. As the ligand concentration is lowered, the working curve should follow the curve defined by a plot of fraction of Co(II) remaining vs. ligand concentration. This curve is nonlinear; it is sigmoidal if the ligand concentration axis is logarithmic. The ligand detection limit is determined by the smallest change in free Co(II) concentration which is measurable.

**Reagent Optimization and Composition.** Figure 3 shows the effect of the stock concentration on the working curve for histidine. As the stock concentration of Co(II) is increased from 1 nM to 100 nM, the working range, measured by peak height, increases. The detection limit is about the same using 10 nM and 100 nM Co(II). The data for histidine concentrations below $2 \times 10^{-6}$ M using 1 nM Co(II) are not shown as they were indistinguishable from the noise in the background intensity.

These data can be explained in terms of the theory described above. The maximum measurable concentration (by peak height) should decrease with decreases in stock Co(II) concentration. As the stock Co(II) concentration is decreased, the fraction of this concentration which represents the detection limit of Co(II) increases; therefore, the ligand concentration at which the maximum peak height is reached is lowered.

If the noise in the background light intensity were proportional to this intensity and the Co(II) working curve were linear, the minimum detectable change in Co(II) concentration would be independent of the stock Co(II) concentration. By use of 10 and 100 nM Co(II) these conditions are apparently upheld because the observed detection limit for histidine was approximately the same. With 1 nM Co(II) the noise in the background intensity was proportionately larger, causing a degraded detection limit. To summarize, the ligand working curve should have a wider working range but similar detection limits with increasing Co(II) concentration. This theory agrees with the data in Figure 3.

Three other matters related to the stock Co(II) concentration should be noted. First, the peaks are wider for lower stock Co(II) concentrations at high ligand concentration. This behavior is predicted by our model in that, as mentioned above, the detection limit for Co(II) is a larger fraction of the lower stock concentration and therefore a wider portion of the analyte peak will cause maximum suppression. Second, the absolute level of the residual light, or that light remaining after virtually all (99.9%) of the Co(II) is complexed, is constant because it is due to a combination of stray light and the CL emission due to reagent impurities and the leaching of the flow system components by the reagents. As the stock Co(II) concentration decreases, the absolute level of the signal decreases, and therefore the residual light level becomes larger *relative* to the signal. Third, if the free Co(II) concentration controls the CL intensity and if the fraction of free Co(II) is dependent on ligand concentration, then the relative peak height (relative to the maximum observed at high ligand concentration) should be independent of stock Co(II) concentration. Figure 4 shows the data of Figure 3 replotted as relative peak height. It can be seen that this hypothesis is supported.

Figure 5 shows a plot of the ratio of [$H_2O_2$] to [luminol] vs. the peak CL intensity observed using 1 nM Co(II). This experiment was performed on a four-channel stopped flow instrument which automatically prepared dilutions of stock solutions (*34*). The results show that, although there is a slight dependence on the absolute concentrations of luminol and

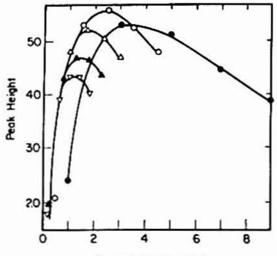

**Figure 5.** Optimization of $[H_2O_2]/[luminol]$ ratio: luminol concentration is (●) 1, (○) 2, (△) 3, (▲) 4, and (×) 5 mM.

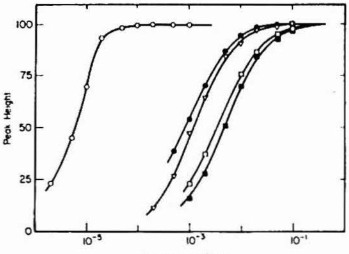

**Figure 6.** Working curves for five amino acids: (○) histidine, (●) glycine, (×) α-alanine, (□) β-alanine, (■) glutamic acid.

hydrogen peroxide, the ratio of the two concentrations is more important in obtaining maximum CL. Optimizing the background light intensity is important as the sensitivity of the method increases with background intensity if the Co(II) flow is held constant. Therefore the $H_2O_2$:luminol ratio in the stock solution was 20 mM:10 mM. The absolute concentrations chosen were higher than those shown in Figure 5 as the stock solution would be diluted by the other reagents and the mobile phase. The optimal KOH concentration or flow rate was found empirically.

**Delay Length.** The effect of the length of the delay between the point where the eluent and the cobalt are mixed to the point where these are mixed with the CL reagent solution was observed. Two competing effects were anticipated. The first effect was that band broadening would increase with delay time, thus diluting the sample. The second effect was that mixing of the analyte and the cobalt would be improved by increasing the delay length and that these solutions would have a longer time to react with each other before reacting with the reagent solution. Working curves for five amino acids were prepared using delay times ranging from 1.4 to 6.5 s. The results for these experiments showed a slight decrease in analytical signal at the longest delay time. At the shorter delay times no discernible pattern was present. With delays below 1 s, the signal decreases. With no delay (just the 0.05 s in the mixer and connector to the flow cell) the signal is only one-third of that obtained with a 1 s or longer delay.

**Relative Response of Amino Acids.** As further assurance that a complexation mechanism was in effect, the relative responses of a series of amino acids were measured. The amino acids chosen and the logarithm of the highest order formation constant with cobalt were as follows: β-alanine, 3.58; glutamic acid, 8.46; α-alanine, 8.48; glycine, 11.0; and histidine, 11.9 (*35*). Figure 6 shows the results. In general, detection of the amino acids follow their formation constants. The only exception was that detection of glutamic acid was worse than would be predicted from its formation constant, especially compared to α-alanine. However, glutamic acid is much more acidic than α-alanine. Samples of $10^{-3}$ M α-alanine and $10^{-3}$ M glutamic acid were adjusted to pH 7 and tested. The results were then the same for both amino acids. Detection of histidine is much more sensitive than the other amino acids, even considerably better than glycine which has a similar formation constant with Co(II). However, histidine is a tridentate ligand which could give it a kinetic advantage over the other amino acids tested which were bidentate ligands. This result agrees nicely with results obtained by Haapakka (*36*) when he examined the effect of denticity of ligands on the inhibition of cobalt enhanced electrogenerated chemiluminescence of luminol. He found inhibition in the order EDTA > iminodiacetic acid > glycine.

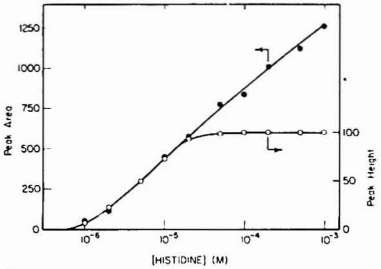

**Figure 7.** Comparison of peak height (○) and peak area (●) working curves.

**Peak Height vs. Peak Area.** The working curves shown above were nonlinear with a limited pseudolinear working range. Figure 7 compares the working curve for histidine obtained using peak area with the curve obtained using peak height. As we have previously mentioned, there is a fundamental limitation of the working curve due to the fact that there is a detection limit for Co(II). The dramatic increase in linear working range using peak area is probably somewhat due to increased diffusional band broadening. However, even in the absence of band broadening, the portion of the peak width for which the free Co(II) concentration is below the detection limit increases at high analyte concentrations, and results in a wider peak with a flat top. From these data it can be seen that the increase in dynamic range from about 1 order of magnitude to over 3 orders of magnitude more than outweighs any difficulty in obtaining peak areas when quantitative results are required.

**Selection of Chromatographic Mobile Phase.** As with all postcolumn reaction schemes, the selection of a mobile phase which is compatible with the detection reaction is a critical step in the development of the method. The constraints that the Co(II)–luminol reaction system for detection of amino acids imposes upon the selection of the mobile phase are that a noncomplexing buffer of low buffer capacity should be used. A standard method for separation of amino acids is to elute them from a strong cation exchange column using citrate buffers, pH, and ionic strength appropriate for specific applications (*37*). Citrate buffers are incompatible with CL detection for two reasons. First, citrate complexes Co(II) (log $k_f$ = 25.3) (*35*), thus competing with the amino acid complexation of Co(II). Second, the buffer is acidic while the CL reaction of luminol is optimized at a pH closer to 11 or 12. Although a polymeric column is often used in ion exchange separation of amino acids (*38*, *39*), a silica-based Partisil column was available in the lab so it was used in this case.

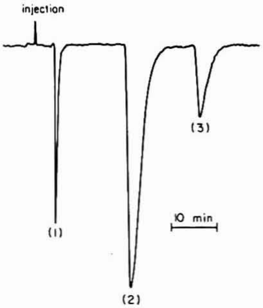

**Figure 8.** Sample chromatogram: (1) glycine, 10 nmol, (2) histidine, 2 nmol, (3) arginine, 10 nmol; mobile phase, 0.01 M acetic acid/acetate buffer at pH 5.5, 1.0 mL/min.

**Table I. Detection Limits for Amino Acids by Chemiluminescence**

| amino acid | detection limit, nmol |
|---|---|
| Acidic | |
| hydroxyproline | 1 |
| aspartic acid | 20 |
| glutamic acid | 1 |
| Neutral | |
| glycine | 0.4 |
| α-alanine | 0.4 |
| β-alanine | 2 |
| cystine | 0.01 |
| valine | 1 |
| phenylalanine | 2 |
| Basic | |
| lysine | 0.4 |
| histidine | 0.004 |
| arginine | 0.04 |

In order to use the Partisil 10 SCX column, it is necessary to use an acidic mobile phase as aqueous solutions of pH >7.5 will dissolve the silica. An acetate buffer is acceptable for this CL detection scheme because log $K_f$ for a Co(II)–acetate complex is only 1.9 (*35*).

Figure 8 shows a test chromatogram of glycine, histidine, and arginine. The conditions used are described in the figure caption. Of the amino acids tested, only histidine and arginine were retained under these conditions. Table I gives detection limits for a number of amino acids by this detection method; all values were measured without the chromatographic column. As illustrated earlier in Figure 7, the working range is about 1 order of magnitude if peak heights are used and over 3 orders of magnitude if peak areas are used. The precision is $^1/_2$% at large peak heights, $2^1/_2$% at midrange peak heights, and $4^1/_2$% at low peak heights.

**Flow Cell Considerations.** The choice of a flow cell for CL detectors involves a trade-off. In order to obtain a measurable amount of light, a large volume of reacting solution must be viewed by the photomultiplier tube. Consequently, the flow cell dead volume is relatively large. However, the larger the dead volume is, the greater is the dilution of sample due to band broadening.

The microporous membrane cell had been developed in our group for chemiluminescence detection in flowing streams and applied to determination of metal ions (*32*), glucose (*33, 40*), and cholesterol (*41*). The cell offers several advantages for this present work. First, a stable pH gradient could be maintained across the membrane (*33*); there is a large pH change from the mobile phase to the reaction zone. Second, the reagent flow rate would be regulated by the membrane so that the flow rate would be more stable than that regulation which could be obtained using the needle valves alone. Third, the reagent flow rate could be made very small (0.1 mL/min) to minimize both sample dilution and reagent consumption. The microporous membrane cell used in the work described was about 0.12 × 1.48 × 1.59 cm and was measured to contain about 85 μL. On the basis of resolution considerations a smaller cell would be desirable. A new cell was constructed with dimensions about 0.12 × 0.12 × 1.59 cm and was measured to contain about 20 μL. To accommodate the smaller cell the pressure on the reagent reservoir was increased from 10 psi to about 18 psi. Even at this pressure, the flow of reagent through the microporous membrane was reduced.

Use of the smaller volume cell results in lower CL emission intensities, but on a relative basis the peak heights are virtually unchanged. Lower intensities would be predicted due to the smaller volume of emitting solution viewed by the detector. Exact predictions of expected signal levels are complicated by different reagent flow rates and residence times between the two cells. The reduced cell volume had no effect on the working range.

## CONCLUSIONS

Compared to ninhydrin detection, this chemiluminescence detection approach is faster and takes place at room temperature without thermostating. Since detection is based on complexation, secondary amino acids are detectable without modification of the detection reaction or instrumentation, as is necessary with both the ninhydrin and *o*-phthalaldehyde schemes (*39*). The instrumentation is simple as no light source or wavelength discrimination device is required.

As the detection limit for amino acids by this method is fundamentally determined by the magnitude of the formation constant of the amino acid with Co(II), changing the metal ion used to produce CL could alter detection limits. Both Cu(II) and Ni(II) enhance luminol CL and have larger formation constants with amino acids (*35*); the detection limit for Co(II) is lower than those for either Cu(II) or Ni(II), however. One could also consider using this CL detection scheme with a metal ion like Fe(III) which has higher formation constants with oxygen containing ligands than does Co(II); one then should be able to detemine species like carboxylic acids, ketones, or phenols.

**Registry No.** $Co(NO_3)_2$, 10141-05-6; hydroxyproline, 51-35-4; aspartic acid, 56-84-8; glutamic acid, 56-86-0; glycine, 56-40-6; α-alanine, 56-41-7; β-alanine, 107-95-9; cystine, 56-89-3; valine, 72-18-4; phenylalanine, 63-91-2; lysine, 56-87-1; histidine, 71-00-1; arginine, 74-79-3; luminol, 521-31-3.

## LITERATURE CITED

(1) Seitz, W. R. *CRC Crit. Rev. Anal. Chem.* **1981**, *13*, 1–58.
(2) Wehry, E. L. *Anal. Chem.* **1982**, *54*, 131R–150R.
(3) Mottola, H. A.; Mark, H. B. *Anal. Chem.* **1982**, *54*, 62R–83R.
(4) Wehry, E. L. *Anal. Chem.* **1984**, *56*, 156R–173R.
(5) Mottola, H. A.; Mark, H. B. *Anal. Chem.* **1984**, *56*, 96R–112R.
(6) Majors, R. E.; Barth, H. G.; Löchmuller, C. H. *Anal. Chem.* **1984**, *56*, 300R–349R.
(7) Miller, J. N. *Analyst (London)* **1984**, *109*, 191–198.
(8) Hartkopf, A. V.; Delumyea, R. *Anal. Lett.* **1974**, *7*, 79–88.
(9) Neary, M. P.; Seitz, W. R.; Hercules, D. M. *Anal. Lett.* **1974**, *7*, 583–590.
(10) Delumyea, R.; Hartkopf, A. V. *Anal. Chem.* **1976**, *48*, 1402–1405.
(11) Burguera, J. L.; Burguera, M.; Townshend, A. *Anal. Chim. Acta* **1981**, *127*, 199–201.
(12) Veazey, R. L.; Nieman, T. A. *J. Chromatogr.* **1980**, *200*, 153–162.
(13) Kobayashi, S.; Imai, K. *Anal. Chem.* **1980**, *52*, 424–427.
(14) Melbin, G. *J. Liq. Chromatogr.* **1983**, *6*, 1603–1616.
(15) Sigvardson, K. W.; Birks, J. W. *Anal. Chem.* **1983**, *55*, 432–435.
(16) Kobayashi, S.; Sekino, J.; Honda, K.; Imai, K. *Anal. Biochem.* **1981**, *112*, 99–104.
(17) Honda, K.; Sekino, J.; Imai, K. *Anal. Chem.* **1983**, *55*, 940–943.
(18) DeJong, G. J.; Lammers, N.; Spruit, F. J.; Brinkman, U. A.; Frei, R. W. *Chromatographia* **1984**, *18*, 129–133.

*Anal. Chem.* **1985**, *57*, 940–945

(19) Weinberger, R.; Mannan, C. A.; Cerchio, M.; Grayeski, M. L. *J. Chromatogr*. **1984**, *288*, 445–450.
(20) Shoemaker, B.; Birks, J. W. *J. Chromatogr*. **1980**, *209*, 251–263.
(21) Hill, E. A.; Nelson, J. K.; Birks, J. W. *Anal. Chem*. **1982**, *54*, 541–546.
(22) Birks, J. W.; Kuge, M. C. *Anal. Chem*. **1980**, *52*, 897–901.
(23) Getty, R. H.; Birks, J. W. *Anal. Lett*. **1979**, *12* (A5), 469–476.
(24) Nelson, J. K.; Getty, R. H.; Birks, J. W. *Anal. Chem*. **1983**, *55*, 1767–1770.
(25) Bruening, W.; Concha, F. J. M. *J. Chromatogr*. **1977**, *142*, 191–201.
(26) Massey, R. C.; Crews, C.; McWeeny, D. J.; Knowles, M. E. *J. Chromatogr*. **1982**, *236*, 527–529.
(27) Nord, P. J. *Diss. Abstr. Int. B* **1982**, *43*, 419.
(28) Yu, W. C.; Goff, E. U. *Anal. Chem*. **1983**, *55*, 29–32.
(29) Burdo, T. G.; Seitz, W. R. *Anal. Chem*. **1975**, *47*, 1639–1643.
(30) Pantel, S.; Weisz, H. *Anal. Chim. Acta* **1975**, *74*, 275–280.
(31) Pablvanets, B. I.; Ryabov, A. K.; Shnaiderman, E. M. *Zh. Anal. Khim*. **1975**, *30*, 2439–2443.
(32) Nau, V. J.; Nieman, T. A. *Anal. Chem*. **1979**, *51*, 424–428.
(33) Pilosof, D.; Nieman, T. A. *Anal. Chem*. **1982**, *54*, 1698–1701.
(34) Stieg, S.; Nieman, T. A. *Anal. Chem*. **1980**, *52*, 796–800.
(35) Inczedy, J. "Analytical Applications of Complex Equilibria"; Halsted Press: London, 1976; pp 317–368.
(36) Haapakka, K. E. *Anal. Chim. Acta* **1982**, *139*, 229–236.
(37) Niederwieser, A. In "Chromatography: A Lab Handbook of Chromatographic and Electrophoretic Methods", 3rd ed.; Heftmann, E., Ed.; Van Nostrand-Reinhold, New York, 1975.
(38) Lee, D. P. *LC, Liq. Chromatogr. HPLC Mag*. **1984**, *2*, 828–832.
(39) Dong, M. W.; DiCesare, J. L. *LC, Liq. Chromatogr. HPLC Mag*. **1983**, *1*, 222–228.
(40) Malavolti, N. L.; Pilosof, D.; Nieman, T. A. *Anal. Chem*. **1984**, *56*, 2191–2195.
(41) Malavolti, N. L.; Pilosof, D.; Nieman, T. A. *Anal. Chim. Acta*, in press.

RECEIVED for review August 20, 1984. Accepted January 7, 1985. This research was supported in part by the National Science Foundation (CHE-81-08816).

# Laser-Induced Fluorescence Spectrometry of Aromatic Hydrocarbon Derivatives in Vapor-Deposited Parent Molecule Matrices

**Charles F. Pace and Jon R. Maple***

*Department of Chemistry, University of New Mexico, Albuquerque, New Mexico 87131*

**The analytical utility of a low-temperature parent molecule matrix for the characterization of mixtures of aromatic hydrocarbon derivatives by fluorescence detection has been assessed, using a prototype system consisting of chloronaphthalenes in a naphthalene matrix. By vapor deposition of the samples and the naphthalene matrix, it has been demonstrated that good precision, low detection limits, and high-resolution excitation and fluorescence spectra can be obtained. Chloronaphthalenes can be detected at low nanogram levels from a two-photon excitation spectrum, while the two-photon excitation bandwidths are about 1 cm$^{-1}$ (fwhm) and are virtually independent of the position of substitution when the parent molecule matrix is used. With UV (single photon) excitation subpicogram detection limits have been reported and each chloronaphthalene in a 10-component mixture can be selectively excited without fluorescence interference from the other components of the mixture. The 9% precision of the quantitative measurements is limited only by the stability of the laser excitation source.**

There is a considerable interest in developing highly selective analytical methodologies which are capable of precisely characterizing the composition of environmentally hazardous materials which contain a complex variety of aromatic hydrocarbon derivatives (AHDs). The interest in individual AHDs is due in large part to the fact that the carcinogenic or mutagenic nature of an aromatic compound is strongly affected by the number, position, and identity of substituents on the parent molecule (*1–3*). Since there is an enormous number of possible derivatives for each aromatic hydrocarbon and since trace concentrations of AHDs are often highly toxic, carcinogenic, or mutagenic, a suitable analytical methodology must be highly selective and sensitive.

Fluorescence methods which utilize the Shpol'skii effect are particularly attractive because of the high-resolution fluorescence spectra that result from preparing many aromatic hydrocarbons in low-temperature Shpol'skii (i.e., $n$-alkane) frozen solutions (*4*). The fluorescence peaks are sharp enough to distinguish individual AHDs, such as methyl derivatives of phenanthrene, chrysene, pyrene, benz[*a*]anthracene, benzo[*a*]pyrene, and benzo[*h*]quinoline (*5–8*). Moreover, the high selectivity of laser excited Shpol'skii spectrometry (LESS) minimizes the need for fractionation of complex samples and retains the high sensitivity associated with fluorescence detection (*4, 7–9*). Nevertheless, there are many examples of situations in which the Shpol'skii effect does not occur and the excitation and emission bands of individual AHDs in complex samples cannot be resolved. This is often the case when a substituent on a parent compound is highly polar, as in the case of monohydroxyl derivatives of naphthalene (*10*) and pyrene (*11*) or carboxyl derivatives of benzo[*a*]pyrene (*12*), for example. Furthermore, there are no reports in the literature of observations of the Shpol'skii effect for many environmentally hazardous AHDs, including hydroxyl, chloro, and bromo derivatives of naphthalene, biphenyl, dibenzofuran, and dibenzo-*p*-dioxin. Thus, it is highly desirable to find low-temperature matrix materials in which these and many other AHDs exhibit high-resolution excitation and emission spectra so that the high selectivity and sensitivity advantages of LESS can be retained.

We have recently advocated the usage of aromatic hydrocarbon crystals for the analysis of AHDs in situations where a suitable Shpol'skii matrix cannot be found (*13, 14*). By the choice of an aromatic hydrocarbon matrix material with a molecular size matched to the AHDs of interest, the AHDs can be incorporated into well-defined sites or vacancies in the crystal, thereby minimizing inhomogeneous broadening. For example, methylnaphthalene (MN) derivatives prepared by normal freezing in durene crystals exhibit high-resolution excitation and emission lines at low temperatures (*13, 14*). Moreover, even though the MN 0–0 transition energies are closely spaced, each MN in a complex mixture can be identified from a two-photon excitation (TPE) spectrum (*14*). Both the TPE and the selective excitation methods are highly sensitive and have resulted in subpicogram detection limits

0003-2700/85/0357-0940$01.50/0 © 1985 American Chemical Society

for MNs. In addition, both methods have been demonstrated to be suitable for the identification of individual MNs in a raw shale oil prepared in a durene crystal without utilizing any preseparations.

An important problem limiting the analytical applications of cryogenic fluorometry is that there is no known matrix material which results in sharp spectral features for many AHDs of interest. We suggest that the parent molecule is a good matrix choice for AHDs. We will test this hypothesis by using a naphthalene matrix for chloronaphthalene (CN) derivatives, which are wide-spread pollutants of our environment and which have chemical and physical properties similar to PCBs (*15*). One reason that the parent molecule may be expected to be a suitable matrix material is that it is approximately the same size and shape as its derivatives, as required for minimizing inhomogeneous broadening. Another advantage of the parent molecule is that the $S_1$ state is generally more energetic than for its derivatives. As a result the derivatives can be selectively excited without introducing matrix fluorescence interference. An additional advantage of the parent molecule is that it is generally available from commercial sources. Finally, it is possible that the parent molecule will be a suitable matrix for a wide variety of its derivatives, in contrast to a durene matrix which is apparently suitable only for methylated (and possibly fluorinated) naphthalenes.

Besides finding a suitable low-temperature aromatic matrix material, there are several other problems that limit the analytical usefulness of aromatic matrices. For example, we have previously observed a wide range of up to 6 orders of magnitude in the limits of detection for MNs prepared by normal freezing in durene (*14*). The formation of analyte microcrystals and limited solubility of analyte in the host material can also be problematic. In an attempt to solve or limit these problems, the usefulness of vapor deposition (i.e., matrix isolation) sample preparation procedures will be explored. The matrix isolation procedure involves codepositing a vaporized mixture of sample and matrix onto a cold surface and, in the case of rare gas and *n*-alkane matrices, is characterized by a wide linear dynamic range and good precision (*9, 16*). Solubility problems are of course entirely circumvented.

In order to characterize the usefulness of a parent molecule matrix, several different spectrometric procedures could be used. Two of these are selective excitation of fluorescence from the analyte and TPE. A comparison of these two methods for CNs in a naphthalene matrix will be useful, since the only comparison of these two procedures made to date is the MN in durene results (*14*). An alternative spectrometric procedure involves taking advantage of the X-trap emission which occurs when guests (i.e., analytes) are placed in lattice positions in an aromatic host. For example, when 2-chloronaphthalene (2-CN) is placed in a naphthalene crystal, phosphorescence is observed from an X-trap, which is a naphthalene molecule which has been displaced or misoriented by a neighboring 2-CN molecule (*17*). The X-trap phosphorescence peaks are very narrow and the emission wavelengths are sensitive to the identity of the guests incorporated in the crystal. Although we have observed X-trap emission from vapor deposited CNs, no attempt has been made to utilize this phenomenon. However, the exciting possibility of using X-trap emission to identify nonfluorescing molecules (e.g., bromonaphthalenes, nitronaphthalenes, halogenated dibenzo-*p*-dioxins, etc.) by high-resolution phosphorescence spectrometry will be evaluated elsewhere.

## EXPERIMENTAL SECTION

**Reagents.** Naphthalene, 1-fluoronaphthalene (1-FN), and 1-CN were purchased from Aldrich, while 2-FN was obtained from Pfaltz and Bauer, and 2-CN and all disubstituted CNs were purchased from Ultra Scientific. All chemicals were used as received, except for naphthalene, which was zone refined with an apparatus built in our laboratory. A description of this apparatus and the zone refining procedures is given elsewhere (*14, 18*). HPLC grade acetone (Fisher Scientific) was the solvent for all stock solutions.

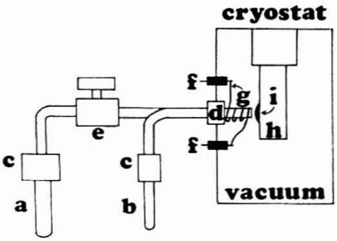

Figure 1. Deposition apparatus used to vapor deposit chloronaphthalenes in a naphthalene matrix. See text for description.

**Sample Preparation.** A few of the samples have been prepared by normal freezing. The sample and 50 mg of naphthalene were placed in a capillary tube which was then sealed. The sample was melted and lowered by a motor out of an oven at a rate of 1 cm/h. The crystal was removed from the capillary tube and glued to the copper cold finger of a closed cycle refrigerator (Air Products, Model CSA-202A).

Unless specifically stated otherwise, all samples have been prepared by vapor deposition, using a modification of the matrix isolation procedures (*8, 9, 16*) utilized for aromatic hydrocarbons placed in rare gas or Shpol'skii matrices. The deposition apparatus is diagramed in Figure 1 and the parts are labeled with letters. The naphthalene matrix material is placed in a 0.25 in. o.d. glass tube (part a) that is attached to an ultratorr male connector (part c, made by Cajon Co., Macedonia, OH). The vaporized naphthalene passes through 0.125 in. o.d. stainless steel tubing, a shutoff valve (part e), and then more stainless steel tubing before being deposited on the cold finger (part h) of the refrigerator at the spot marked with an i. In order to slide the stainless steel tubing through the ultratorr union (part d, Cajon Co.), the inside of this union was widened by drilling. The O-rings inside the ultratorr union prevent leakage of air into the vacuum area inside the refrigerator shroud. The sample is placed in a 0.125 in. o.d. glass tube (part b). Before the sample and matrix material are vaporized, all parts (except for parts a and b) of the apparatus are heated to 60 °C by heating tape. The stainless steel tubing inside the vacuum area is electrically heated with insulated nichrome wire (part g). A small ac voltage is applied to this nichrome wire via the electrical feedthroughs (part f). The apparatus may be moved in and out of the ultratorr union and the tip (of the stainless steel tubing) is placed about 1 mm from the copper cold finger.

The first step in preparing a deposit was to heat the apparatus and to inject 30 $\mu$L of a 0.1 mg/$\mu$L naphthalene solution into the matrix tube (a) and the sample solution into the sample tube (b). The acetone solvent in the sample tube was carefully evaporated, while no attempt was made to remove the solvent in the matrix tube. Both the sample and matrix tubes were frozen by liquid nitrogen prior to applying a vacuum to remove air. The next step was to place the matrix tube in a water bath held at 32 °C (although any temperature in the range 30–35 °C works well). This temperature was sufficient to maintain a naphthalene vapor flow rate which was high enough to prevent the aggregation of solute molecules because of too low of a matrix to solute ratio. When the cold finger temperature was lowered to 240 K, the valve (part e) was opened and the naphthalene vapor immediately started sticking to the cold finger. The acetone solvent would not freeze at 240 K and was evacuated from the refrigerator. After about 1 min the naphthalene matrix formed a spot a few millimeters in diameter and almost 1 mm thick. At this time the liquid nitrogen trap was removed, and the ambient temperature of the atmosphere warmed the sample tube to near room temperature in less than a minute. Then, the sample tube was rapidly heated

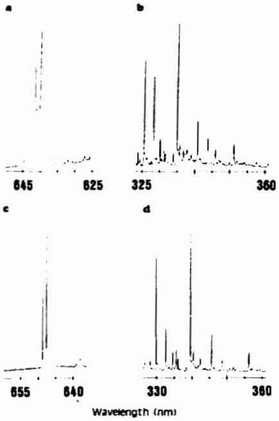

**Figure 2.** (a) Two-photon excitation and (b) laser-induced fluorescence ($\lambda_{ex}$ = 320.1 nm) spectra of 2-chloronaphthalene vapor deposited in *n*-pentane. (c) Two-photon excitation and (d) laser-induced fluorescence ($\lambda_{ex}$ = 324.4 nm) spectra of 2-chloronaphthalene vapor deposited in naphthalene. DCM laser dye dissolved in methanol was used to obtain the two-photon excitation spectra.

to evaporate any of the CN sample still in the tube. The vaporized sample and naphthalene mixed in about 5 cm of tubing before freezing onto the opaque deposit. The total deposition time for the matrix and sample was 2 min and the sample was located in an area (about 1 mm × 1 mm) on the tip of the deposit. The temperature of the deposit was lowered to 10 K prior to spectroscopic observations.

In order to prepare CNs in a Shpol'skii matrix, the matrix tube of the apparatus was replaced by an assembly (*8, 9*) that allows *n*-alkane vapor to flow at a controlled rate. The sample deposition procedure was exactly the same as when a naphthalene matrix was used, except that the copper cold finger was maintained at 100 K for the deposit. This deposition temperature resulted in the minimum amount of inhomogeneous broadening of the CN absorption bands.

**Instrumentation.** The excitation source was an excimer laser (Lumonics TE-861T) pumped dye laser (Quanta Ray PDL-1E). Laser output in the 620–660 nm and 640–680 nm wavelength ranges was obtained with DCM laser dye dissolved in methanol and $Me_2SO$, respectively. One photon, UV excitation was achieved by frequency doubling the dye laser output with an angle-tuned KDP crystal. The dye laser induced fluorescence was dispersed by a 0.64-m grating monochromator (Instruments SA HR-640), which was set at a band-pass of about 0.1 nm. The fluorescence was detected by an RCA 8850 photomultiplier tube and the signal was processed by a gated integrator prior to collection and storage by a PDP-11/23 laboratory computer. TPE spectra were obtained by scanning the dye laser wavelengths with the photomultiplier tube placed directly in front of the sample. Filters which passed light in the 315–400 nm wavelength range were placed on the tube. With this experimental configuration all CN fluorescence wavelengths were simultaneously detected by the tube. TPE spectra were not corrected for the effect of decreasing laser power near the ends of the dye tuning range. Further information concerning the instrumentation and data collection is given elsewhere (*13, 14, 18*).

## RESULTS AND DISCUSSION

We have investigated the usefulness of Shpol'skii matrices for the analysis of CNs, since the literature concerning the spectroscopy of chlorinated AHDs in Shpol'skii matrices is very limited. In the TPE spectrum in Figure 2a the inhomogeneous broadening of 2-CN in *n*-pentane is evident. The two sharp peaks at 640.3 nm and 641.8 nm correspond to the TPE 0–0 wavelengths for 2-CN molecules residing in two distinctly different environments in the *n*-alkane polycrystalline lattice. The broad hump underneath the two sharp peaks is due to two-photon 0–0 transitions of 2-CN molecules residing in a multitude of other sites in the matrix. This interpretation of this spectrum is substantiated from spectra similar to the LIF spectrum of 2-CN in Figure 2b. The 320.1-nm excitation wavelength that was used for this spectrum corresponds to (one photon) excitation of the 2-CN molecules residing in the site giving rise to the sharp two-photon peak at 640.3 nm in Figure 2a. LIF spectra obtained at other wavelengths within the inhomogeneously broadened 0–0 absorption band resulted in spectra similar to the one in Figure 2b, but the peaks were shifted in energy by an amount equal to the transition energy difference. The extent of inhomogeneous broadening manifested by the TPE spectrum of 2-CN in Figure 2a is similar to that observed for 1-CN but is far in excess of the amount of inhomogeneous broadening observed for 1-methylnaphthalene and 2-methylnaphthalene, which are virtually the same size and shape as 1-CN and 2-CN, respectively.

Although energy selected spectra, such as the one in Figure 2b, exhibit well-resolved fluorescence peaks, it is not generally possible to selectively excite a single CN (in a multicomponent sample) because the inhomogeneously broadened absorption bands of the CNs extensively overlap. Furthermore, it is not possible to obtain sharp energy selected LIF spectra for each CN in the same *n*-alkane matrix. Evidently, the extent of homogeneous broadening in a Shpol'skii matrix is very sensitive to the position of the chloro substituents. A similar observation has been made for chloroanthracenes (*19*). Thus, because of extensive inhomogeneous and homogeneous broadening, we have concluded that a Shpol'skii matrix is of very limited usefulness for the multicomponent analysis of chlorinated AHDs.

The TPE spectrum in Figure 2c of 2-CN in a vapor-deposited naphthalene matrix indicates that inhomogeneous broadening has been minimized and that it is possible for vapor deposited aromatic matrices to result in high-resolution spectra comparable to the results that can be obtained by conventional methods (i.e., normal freezing) for preparing guest molecules in a crystalline aromatic host. The two peaks at 647.7 nm and 648.8 nm are the 0–0 peaks for 2-CN molecules residing in the two possible positions in a naphthalene lattice (*17*). Both peaks have a bandwidth of 1.1 $cm^{-1}$ and the peak wavelengths are identical with the peak wavelengths of 2-CN prepared by normal freezing in a naphthalene crystal. The only significant difference between the TPE spectra of 2-CN in matrices prepared by normal freezing and vapor deposition is the site distribution. For example, the peak height ratio of the TPE peaks at 647.7 nm and 648.8 nm is about 1.9 in Figure 2c, while the same ratio is about 0.17 when the normal freezing sample preparation method is employed. This indicates that the sample preparation method can affect the tendency of a CN molecule to occupy the two possible lattice positions.

The sharp TPE and laser-induced fluorescence (LIF) spectra shown in Figure 2, parts c and d, respectively, can only be obtained when the deposition temperature (i.e., the temperature of the surface upon which the sample is deposited) exceeds 230 K. Lower deposition temperatures result in an amorphous solid and the TPE and LIF spectra of CN guests and the naphthalene matrix are excessively broadened. In contrast, Shpol'skii matrices are usually deposited at the lowest possible temperature and then are annealed (*8, 9*). Annealing does not produce spectral sharpening for vapor deposited naphthalene or CN guests, regardless of the de-

**Table I. $S_1$ Origins for Chloronaphthalenes**

| compound | 0–0 wavelength, nm |
|---|---|
| 1-fluoronaphthalene | 318.6 |
| 2-fluoronaphthalene | 319.1, 320.1 |
| 1-chloronaphthalene | 322.0 |
| 2-chloronaphthalene | 323.9, 324.4 |
| 1,2-dichloronaphthalene | 328.7 |
| 1,4-dichloronaphthalene | 327.9 |
| 1,5-dichloronaphthalene | 332.6 |
| 1,8-dichloronaphthalene | 329.6, 332.9 |
| 2,3-dichloronaphthalene | 327.5 |
| 2,7-dichloronaphthalene | 327.9 |

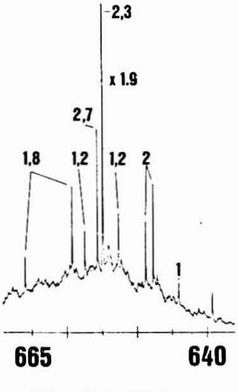

**Figure 3.** Two-photon excitation spectrum (obtained with DCM in $Me_2SO$ solvent) of ten-component mixture consisting of 10 ng of each substance listed in Table I: 1, 1-chloronaphthalene (1-CN); 2, 2-CN; 1,2, 1,2-dichloronaphthalene (1,2-DCN); 1,8, 1,8-DCN; 2,3, 2,3-DCN; 2,7, 2,7-DCN. The 2,3-DCN peak has been attenuated by a factor of 1.9.

position or annealing temperature. Apparently, naphthalene molecules are frozen at random orientations when the deposition temperature is below 230 K and the molecules are unable to reorient into favorable lattice positions when the temperature is raised. The difference in annealing effects upon *n*-alkane and aromatic matrices is presumably due to the structural rigidity of aromatic hydrocarbons.

A ten-component mixture containing 10 ng of each compound listed in Table I was deposited in a naphthalene matrix. The TPE spectrum of this mixture is depicted in Figure 3. The broad band emission underneath the TPE peaks is mainly due to background emission from the matrix and drops in intensity at the long and short wavelength ends of the spectrum because of the declining dye laser power. The 0–0 TPE peaks occur at exactly twice the (one photon) 0–0 wavelengths tabulated in Table I and are all highly resolved (ca. 1 $cm^{-1}$ fwhm bandwidth). This indicates that the extent of both homogeneous and inhomogeneous broadening is relatively insensitive to the position of the chloro substituents on the parent molecule when the parent molecule matrix is utilized, in contrast to the situation with a Shpol'skii matrix. This is clearly a very important advantage in using a parent molecule matrix for AHDs.

Four compounds cannot be detected from the TPE spectrum in Figure 3. Both 1-FN and 2-FN can be detected by TPE at the 10-ng level when DCM laser dye is dissolved in methanol but cannot be distinguished in Figure 3 because of the low laser power below 641 nm. 1,4-Dichloronaphthalene (1,4-DCN) has an anomalously large (one and two photon) detection limit, presumably due to an unusually low quantum yield of fluorescence. Because a naphthalene crystalline solid has $C_i$ site symmetry, the $S_0 \rightarrow S_1$ two-photon transition will be forbidden by parity selection rules for all centrosymmetric naphthalene derivatives (*14*). This is the reason why the TPE 0–0 band for 1,5-DCN cannot be seen in this spectrum and this is an example of a disadvantage in using a parent molecule matrix when employing excitation scans to characterize a sample. A high energy vibronic band would have to be used to identify a molecule with a symmetry forbidden 0–0 transition, but the high energy vibronic band would often be obscured by the intense excitation peaks of the parent molecule matrix.

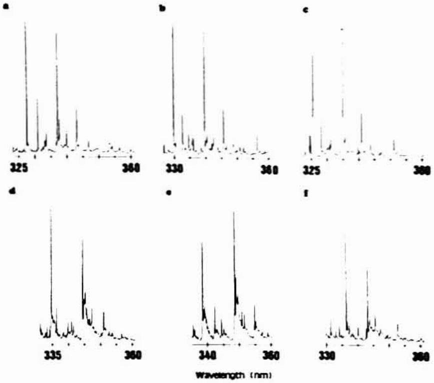

**Figure 4.** Laser-induced fluorescence spectra of ten-component mixture consisting of 10 ng of each substance listed in Table I. Selective excitation wavelength for (a) 1-chloronaphthalene ($\lambda_{ex}$ = 322.0 nm), (b) 2-chloronaphthalene ($\lambda_{ex}$ = 324.4 nm), (c) 2-fluoronaphthalene ($\lambda_{ex}$ = 320.1 nm), (d) 1,2-dichloronaphthalene ($\lambda_{ex}$ = 328.7 nm), (e) 1,5-dichloronaphthalene ($\lambda_{ex}$ = 332.6 nm), and (f) 2,3-dichloronaphthalene ($\lambda_{ex}$ = 327.5 nm).

Each of the 10 components in the mixture (used to obtain the TPE spectrum in Figure 3) was selectively excited by (one photon) excitation of a 0–0 wavelength. Six examples of these LIF spectra are displayed in Figure 4. In each case the component which was selectively excited could be readily identified and peaks due to fluorescence from other components could not be discerned. For example, compare the pure compound and selectively excited fluorescence spectra of 2-CN in Figures 2d and 4b, respectively. Of all of these 10 components, 1-FN, 2-FN, 1-CN, and 2-CN would be expected to be the most difficult to selectively excite, since the 0–0 absorption bands for these compounds might overlap with vibronic absorption bands of the disubstituted CNs, which have lower energy 0–0 transitions. From the example of Figure 4a–c (for 1-CN, 2-CN, and 2-FN), it can be seen that there was no significant overlap of the absorption bands. The relative strength of the phonon wings for some of the disubstituted CNs can be seen in the selectively excited LIF spectra of 1,2-DCN and 1,5-DCN in Figure 4d,e and are characteristic of the DCNs in which at least one chloro substituent was located on the transverse axis of the naphthalene molecule. The phonon wings in the LIF spectra of DCNs with both substituents on the longitudinal axis (e.g., 2,3-DCN and 2,7-DCN) were significantly less intense, as can be seen in the selectively excited fluorescence spectra of 2,3-DCN in Figure 4f.

**Quantitative Results.** The TPE detection limit was defined as the amount of substance needed to obtain a 0–0 peak height equal to two times the standard deviation of the noise. The 330-pg TPE detection limit measured for 2,3-DCN was far greater than the subpicogram TPE detection limits obtained for some MNs prepared by normal freezing in durene (*14*). The reason for such a large difference is the significantly greater amount of trap emission (*20*) occurring from the vapor deposited matrix. The TPE detection limits for the other CNs were not determined but can be estimated from comparisons of the peak heights in the TPE spectrum in Figure 3. As this spectrum indicates, the TPE detection limits do not in general vary by much more than an order of magnitude. This is in contrast to the MN results, which were obtained by using normal freezing sample preparations and which resulted in TPE detection limits ranging from less than 0.1 pg to 100 ng. The elimination of a wide range in detection limits is an important analytical advantage in using vapor deposition techniques. Although the detection limits for CN samples prepared by normal freezing in naphthalene crystals have not been determined, we have noticed that large amounts (i.e., micrograms) of CNs must be used to detect TPE peaks in these crystals and the detection limits are probably at least 3 orders of magnitude higher than those that can be obtained by vapor deposition. This clearly is another very important advantage for using the vapor deposition procedure. However, this may not always be an advantage since there are some guest–host systems, such as the MNs in durene, in which lower detection limits may be achieved by normal freezing.

The LIF detection limits obtained by UV excitation have not been determined, but we note that the 339.7-nm 2-CN peak had a $S/N$ ratio of 40 when 1 pg of 2-CN was deposited. This indicates that the CN LIF detection limits are 3 to 5 orders of magnitude lower than the TPE detection limits, in contrast to the 1 to 2 orders of magnitude difference reported for the MNs in durene crystals. The reason for such a large discrepancy is probably due to the greater amount of trap emission from the vapor deposited matrix. This background trap emission is structureless and extends to wavelengths as long as ca. 420 nm. Since the monochromator discriminates against this background emission, while the TPE technique does not, trap emission may be largely responsible for the large differences in TPE and LIF detection limits.

In order to assess the linear dynamic range that can be obtained for CNs in a vapor-deposited naphthalene matrix, varying amounts of 2-CN were deposited along with 2 ng of 2-FN, which was used as an internal standard. Laser excitation at 324.4 and 320.1 nm was used for 2-CN and 2-FN, respectively, and the fluorescence peak heights at 330.0 and 325.6 nm, respectively, were measured. A log–log plot of the weight of 2-CN vs. the fluorescence intensity ratio (2-CN/2-FN) is shown in Figure 5. This plot is linear from 10 pg to 100 ng of 2-CN and has a correlation coefficient of 0.998. A nonlinearity was observed below 10 pg, but this turned out to be due to the presence of 2-CN impurity in the 2-FN internal standard. Since the slope is 0.52, the 2-CN fluorescence intensity does not vary linearly with the weight that was deposited. Analogous nonlinear intensity behavior has been observed for metal ions placed in inorganic crystals (*21*). The reason for this nonlinearity may be due to an energy transfer process wherein the electronic energy of excited 2-CN molecules is transferred to neighboring X-traps. Additional experiments will be required to further elucidate the observed 2-CN fluorescence intensity dependence.

Various factors which can affect the precision of our measurements have been studied. For these precision studies 30 ng of 2-CN was deposited six times along with 10 ng of 2,3-DCN, which was used as an internal standard. Laser excitation at 324.4 nm and 327.5 nm was employed for 2-CN and 2,3-DCN, respectively. In all cases the peak heights that were used in calculations were the average of four measurements. The greatest source of error appears to be caused by variations in the relative fluorescence peak intensities. For example, the ratio of the 2-CN to 2,3-DCN peak heights (at 330.0 and 336.2 nm, respectively) exhibited a relative standard deviation of 18% for the six deposits. In contrast, when the sum of the two 2-CN peak heights at 330.0 and 339.7 nm was divided by the 336.2-nm 2,3-DCN peak height, the relative standard deviation was 13%. Variations in the relative peak heights of 2-CN could be caused by fluorescence polarization effects. That is, the 2-CN molecules may be frozen into preferred orientations that are not reproducible from deposit to deposit. Variations in the site distribution of 2-CN molecules could not be detected. For example, the sum of the two 0–0 TPE peak heights of 2-CN was divided by the 2,3-DCN 0–0 TPE peak height and the relative standard deviation of 9% for six deposits was exactly the same as the corresponding precision when only one of the 2-CN 0–0 peak heights was used. The 9% precision that was measured is the same as the average relative standard deviation for multiple measurements of a given peak and is limited by a drifting laser power. The good precision of our measurements is comparable to the results obtained by matrix isolation when rare gas and Shpol'skii matrices are employed (*8, 9, 16*).

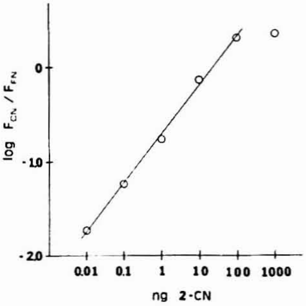

**Figure 5.** Analytical calibration curve for 2-chloronaphthalene vapor deposited in a naphthalene matrix. The internal standard is 2-fluoronaphthalene.

We have tested a new strategy for characterizing complex mixtures of AHDs. By use of a low-temperature matrix consisting of aromatic hydrocarbons with a molecular size and shape which is matched to the AHDs of interest, spectral broadening is minimized and the peak absorptivity and emissivity are maximized. This minimizes or entirely eliminates the need for complex fractionation procedures while at the same time allowing the discrimination of very similar AHDs. An important advantage of a parent molecule matrix is that its usage results in very sharp spectral features for its derivatives and the sharpness is virtually independent of the position of substitution. Furthermore, as will be demonstrated elsewhere, high resolution emission and excitation spectra can be obtained for a wide variety of substituent species (including polar substituents) when the parent molecule matrix is used. As previously mentioned, nonfluorescing AHDs can also be identified by observing X-trap emission, rather than analyte fluorescence. We are currently investigating this application of aromatic hydrocarbon matrices since it could significantly increase the applicability of emission spectrometry to AHDs. Another important advantage of a parent molecule matrix is that it is potentially applicable to a number of environmentally hazardous AHDs in which high resolution emission or excitation spectra have never been reported. In particular, this would include hydroxyl, chloro, and bromo derivatives of naphthalene, biphenyl, dibenzofuran, and dibenzo-*p*-dioxin. Of course, the general applicability of a parent molecule has not been proven, but the preliminary results reported here for CNs are highly encouraging. Finally, we note the demonstration herein that AHDs can be prepared by vapor deposition in an aromatic matrix without sacrificing the resolution of emission and excitation peaks is very important, because it allows the analytical chemist to bypass critical thermodynamic problems, such as insolubility and unfavorable distribution coefficients, which are encountered in conventional preparations of aromatic crystals. With vapor deposition of the sample, good precision, high resolution, and low detection limits can simultaneously be obtained.

**Registry No.** 2-Chloronaphthalene, 91-58-7; 1-fluoronaphthalene, 321-38-0; 2-fluoronaphthalene, 323-09-1; 1-chloronaphthalene, 90-13-1; 1,2-dichloronaphthalene, 2050-69-3; 1,4-dichloronaphthalene, 1825-31-6; 1,5-dichloronaphthalene, 1825-30-5; 1,8-dichloronaphthalene, 2050-74-0; 2,3-dichloronaphthalene, 2050-75-1; 2,7-dichloronaphthalene, 2198-77-8; naphthalene, 91-20-3.

## LITERATURE CITED

(1) Cairns, T.; Siegmund, E. G. *Anal. Chem.* **1981**, *53*, 1183A–1193A.
(2) Karasek, F. W.; Onuska, F. I. *Anal. Chem.* **1982**, *54*, 309A–324A.
(3) Schmeltz, I.; Tosk, J.; Hilfrich, J.; Hirota, N.; Hoffmann, D.; Wynder, E. L. In "Carcinogenesis: Polynuclear Aromatic Hydrocarbons"; Jones, P. W., Freundenthal, R. I., Eds.; Raven Press: New York, 1978; Vol. 3, pp 47–60.
(4) D'Silva, A. P.; Fassel, V. A. *Anal. Chem.* **1984**, *56*, 985A–1000A.
(5) Garrigues, P.; Ewald, M. *Anal. Chem.* **1983**, *55*, 2155–2159.
(6) Garrigues, P.; De Vazelhes, R.; Ewald, M.; Juossot-Dubien, J.; Schmitter, J.-M.; Guiochon, G. *Anal. Chem.* **1983**, *55*, 138–140.
(7) Yang, Y.; D'Silva, A. P.; Fassel, V. A. *Anal. Chem.* **1981**, *53*, 894–899.
(8) Conrad, V. B.; Wehry, E. L. *Appl. Spectrosc.* **1983**, *37*, 46–50.
(9) Maple, J. R.; Wehry, E. L.; Mamantov, G. *Anal. Chem.* **1980**, *52*, 920–924.
(10) Maple, J. R.; Wehry, E. L. *Anal. Chem.* **1981**, *53*, 266–271.
(11) Colmsjo, A. L.; Zebuhr, U. Y.; Ostman, L. E. *Chem. Scr.* **1982**, *20*, 123–126.
(12) Conrad, V. B. Ph.D. Dissertation, University of Tennessee, 1983.
(13) Thornberg, S. M.; Maple, J. R. *Anal. Chem.* **1984**, *56*, 1542–1544.
(14) Thornberg, S. M.; Maple, J. R. *Anal. Chem.* **1985**, *57*, 436–439.
(15) Brinkman, U. A. T.; Reymer, H. G. M. *J. Chromatogr.* **1976**, *127*, 203–243.
(16) Wehry, E. L.; Mamantov, G. *Anal. Chem.* **1979**, *51*, 643A–656A.
(17) Wolf, H. C.; Port, H. *J. Lumin.* **1976**, *12/13*, 33–46.
(18) Thornberg, S. M. Ph.D. Dissertation, University of New Mexico, 1984.
(19) Carter, T. P.; Gillispie, G. D. *J. Chem. Phys.* **1982**, *86*, 2691–2695.
(20) Karl, N. In "Crystals: Growth, Properties, and Applications"; Freyhardt, H. C., Ed.; Springer-Verlag: New York, 1980; pp 1–90.
(21) Johnston, M. V.; Wright, J. C. *Anal. Chem.* **1982**, *54*, 2503–2507.

RECEIVED for review December 4, 1984. Accepted January 14, 1985. Acknowledgment is made to the Sandia UNM Research Program and to the donors of the Petroleum Research Fund, administered by the American Chemical Society, for the partial support of this research.

---

# CORRESPONDENCE

## Optimized Field-Flow Fractionation System Based on Dual Stream Splitters

*Sir:* The cardinal rule for increasing separation speed (as well as resolution) in field-flow fractionation (FFF) is to reduce as far as possible the mean thickness $l$ of the cloud of particles compressed against the accumulation wall of the FFF channel. This rule, known since 1973 (*1*), can be deduced from the following limiting equation for the time, $t_p$, needed to generate one theoretical plate

$$t_p = 4l^2/D \qquad (1)$$

where $D$ is the particle diffusion coefficient. A separation requiring $N$ plates for adequate resolution therefore requires a time of $Nt_p$, which equals

$$t = 4Nl^2/D \qquad (2)$$

showing a quadratic dependence of $t$ on $l$ and demonstrating the desirability of minimizing $l$ (*1*, *2*).

In response to this conclusion, experimental FFF is often operated with $l$ values in the range 1–10 μm. For typical channels of about 0.25 mm (250 μm) thickness, this means that the sample layer is very thin compared to the channel, and that the sample therefore occupies only a small fraction of channel cross section, as illustrated in Figure 1.

In order to avoid a substantial degradation of resolution, the total experimental time for a run usually includes, along with the above time $Nt_p$ (see eq 2) for separation, a period in which flow is halted to allow for sample relaxation at the beginning of the run (*3*). This *stop-flow* time is governed by the *relaxation time* $\tau$, which can be expressed as the longest distance (usually channel thickness $w$) the particles must traverse to form the steady-state cloud divided by the field-induced velocity $U$

$$\tau = w/U \qquad (3)$$

However, since $l = D/U$, $U$ can be replaced by $D/l$, giving

$$\tau = lw/D \qquad (4)$$

showing that $\tau$ is also reduced by minimal $l$ values, again emphasizing the importance of reducing $l$.

With the help of eq 1, we find

$$\frac{\tau}{t_p} = \frac{w}{4l} = \frac{1}{4\lambda} \qquad (5)$$

where $\lambda = l/w$. This equation shows that waiting without flow time $\tau$ for relaxation consumes the same amount of time as that required for generating $(1/4\lambda)$ plates. For example, if the retention parameter $\lambda \sim 10^{-2}$, $\tau$ is ~25 times longer than $t_p$. Since FFF is highly selective, adequate separation power may be provided by anywhere from 20 to 1000 plates, depending on the resolution required. This is seen by noting that with $N$ plates, unit resolution can be gained between species whose relative difference $\Delta M/M$ in molecular weight is given by (*4*)

$$\frac{\Delta M}{M} = \frac{4}{N^{1/2}S} \qquad (6)$$

where the selectivity $S$ approaches unity for sedimentation FFF and values somewhat lower for most other FFF tech-

0003-2700/85/0357-0945$01.50/0 © 1985 American Chemical Society

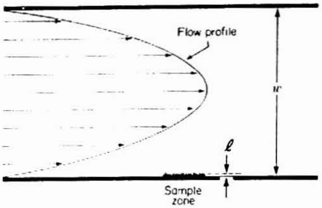

**Figure 1.** Approximate scale model demonstrating the extreme thinness of a desirable sample cloud (in this case with $l = 4$ μm) compared to channel thickness $w$ (here 240 μm). For these dimensions, the sample is carried downstream one-tenth as fast as the average carrier velocity, $R = 0.1$.

niques. Thus when low resolution (large $\Delta M/M$) is adequate, the stop-flow time needed for relaxation may be about as long as the actual separation time.

For clarification, we point out that the minimal-$l$ rule may seem anomalous because the velocity $\mathcal{V}$ of a particle zone is approximately proportional to $l$ as shown by the limiting equation (5)

$$\mathcal{V} = \frac{6l}{w}\langle v \rangle = 6\lambda \langle v \rangle \tag{7}$$

where $\langle v \rangle$ is the average carrier velocity and $w$ the channel thickness. This equation suggests that small $l$'s spawn small $\mathcal{V}$'s and thus retard elution through the FFF channel. However, under optimized conditions, the reduction in $l$ (say 2-fold) will be accompanied by a large (8-fold) increase in $\langle v \rangle$, and thus, by eq 7, a substantial (4-fold) increase in zone velocity $\mathcal{V}$ and a corresponding (4-fold) reduction in separation time $t$, in agreement with eq 2. (These conclusions stem from the fact that $N = LwD/24l^3\langle v \rangle$; with a fixed $N$ needed for separation, we observe that $\langle v \rangle$ will change in proportion to $l^{-3}$.)

The minimal-$l$ rule can be implemented by increasing the field strength $S$. (Quantity $S$ can be equated to centrifugal acceleration in sedimentation FFF, temperature gradient in thermal FFF, etc.). However, carried to the extreme, increasing $S$ and decreasing $l$ values lead to several complications, including increasing particle-wall interactions, and, as $l$ approaches the particle diameter, the onset of steric effects (*6*). We also encounter concentration problems as we attempt to crowd sufficient particles for detectability into increasingly thin clouds. Thus, in fact, there is an optimum working range for $l$ that replaces the absolute goal of minimal $l$. However, this range can be forced toward the smallest possible values by a judicious choice of experimental conditions.

While the cardinal rule of seeking small $l$ values must underlie any serious effort to gain maximum speed, the rule needs modification, interpretation, and extension to account for the various complicating factors as noted above and for the fact that many samples consist of particles having a wide size distribution.

With respect to the latter problem, different particles in a sample may have $l$ values differing by several orders of magnitude; not all of these $l$'s can simultaneously lie in the optimal range. Various programming methods have been proposed to partially offset this problem (*7, 8*). For example, with field programming, one ideally starts with an $S$ value sufficiently high to optimally separate the small particles. The value of $S$ is then lowered so that successively larger particles come into the optimal range, each size effectively taking its turn at optimal migration. One problem with field programming is that in the course of each particle's wait, during which it has a suboptimal $l$, it may migrate anomalously due to steric effects or possibly adsorb on the wall (*8*). Another problem is that when the field strength is changed rapidly to get quickly through the particle size range, particles are unable to diffuse rapidly enough to maintain the steady-state value of $l$. While corrections for this secondary relaxation have been developed recently (9), they cannot be readily applied to complex samples having particles of various densities and shapes.

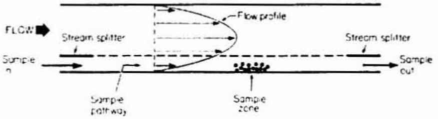

**Figure 2.** Schematic diagram of FFF channel with stream splitter at both inlet and outlet.

An alternative to field programming is flow programming (*10*), in which the field is held constant while the flow is increased. With this program, small particles with large $l$'s that take a long time, $t_p$, to generate a plate (see eq 1) are displaced through the channel slowly to gain adequate plates. Larger particles with small $l$'s, which move very slowly at first due to both small $l$ and small $\langle v \rangle$ (see eq 7), are, in their turn, eluted rapidly by the increasing $\langle v \rangle$. However, if the largest particles have $l$'s too small for normal migration, anomalous results will be found. In other words, flow programming promises to work well over a given range of $l$ values, but the practical magnitude of that range is probably limited.

It has been suggested that a combination of field and flow programming might be most effective to avoid the above problems (*8*). However, the use of any degree of flow programming leads to another complication: variable flow tends to destabilize the detector signal.

A number of the above difficulties can be ameliorated by using a system having stream splitters. First of all, we focus on the use of a channel with a split outlet. The split outlet system is one (see Figure 2) in which the carrier near the accumulation wall carrying the particle cloud is split away from the larger particle-free stream occupying the remainder of the channel (*11*). With this system, the sample is greatly concentrated in the outlet stream and more easily detected, relieving one of the above problems: the delicate balance between detectability and sample concentration.

It is furthermore proposed that the substream containing the sample be withdrawn at a constant flow level using an "unpump" (*12*) for flow control. In this way, flow programming can be utilized such that the flow variability shows up only in the waste stream, hindering detectability in the sample substream.

It is additionally proposed that the system have a "stream splitter" at the inlet. This "splitter" would have the same basic structure as the outlet splitter, but with flow entering instead of leaving, it would serve to merge two streams into one. The lower stream would contain the sample, and the upper stream would provide a sheath of pure carrier to confine the sample; with streamlined convergence the sample would be held in a thin layer near the accumulation wall, requiring little time for relaxation. Thus, if the sample-containing stream carried the fraction $\alpha$ of the total flow, the sample would emerge into the channel contained in a thin lamina of thickness $\alpha w$. This thickness would replace $w$ in eq 3 and 4, giving

$$\tau = \frac{\alpha w}{U} = \frac{\alpha l w}{D} \tag{8}$$

Thus, if only one-tenth ($\alpha = 0.1$) of the total flow entered through the sample inlet stream, $\tau$ would be reduced to one-tenth of its previous value, and the stop-flow procedure used to accommodate relaxation would only take one-tenth as long. Furthermore, with decreasing $\alpha$, it would become increasingly feasible to bypass the stop-flow procedure entirely;

not only does $\tau$ reduce in proportion to $\alpha$, but the severity of the distortion resulting when relaxation is coupled to ongoing flow (*3*) would be lessened by the reduced velocity of the wall-hugging lamina containing the sample. With the stop-flow eliminated, the procedure would be faster and much simpler and would be readily automated for repetitive sampling. (Instead of requiring the coordination of injection with the stopping and restarting of flow at the beginning of each cycle, one would only need repetitive injection into the steady sampling stream.)

In addition, the inlet splitter could be used to shorten the time needed to establish gradients across the channel in hyperlayer FFF (*13*). For example, in sedimentation hyperlayer FFF, the density modifier (and possibly the sample) could be introduced through the lower (outer) stream, thus greatly reducing the time necessary to establish a steady-state density gradient and to realize normal sample migration.

In summary, the dual stream splitter system proposed here should reduce the duration of, or eliminate the need for, stop flow with any of the subtechniques of FFF. At the same time, with proper flow control applied to the sample substream at the outlet, the system should readily accommodate any combination or sequence of nonprogrammed and programmed operation including both field and flow programming, thus giving much better control over optimization. Along with these advantages, the system would provide a means for concentrating the sample to improve detectability and to reduce sample load requirements. These concurrent advantages should make the dual stream splitter system useful for streamlining, simplifying, and speeding up most applications of FFF. The system should be especially advantageous for samples requiring maximum speed and frequent repetition.

## LITERATURE CITED

(1) Giddings, J. C. *Sep. Sci.* **1973**, *8*, 567.
(2) Giddings, J. C.; Martin, M.; Myers, M. N. *J. Chromatogr.* **1978**, *158*, 419.
(3) Yang, F. J.; Myers, M. N.; Giddings, J. C. *Anal. Chem.* **1977**, *49*, 659.
(4) Giddings, J. C. *Pure Appl. Chem.* **1979**, *51*, 1459–1471.
(5) Giddings, J. C.; Myers, M. N.; Caldwell, K. D.; Fisher, S. R. "Methods of Biochemical Analysis"; Glick, D., Ed.; Wiley: New York, 1980; p 79.
(6) Myers, M. N.; Giddings, J. C. *Anal. Chem.* **1982**, *54*, 2284.
(7) Yang, F. J. F.; Myers, M. N.; Giddings, J. C. *Anal. Chem.* **1974**, 46, 1924.
(8) Giddings, J. C.; Caldwell, K. D. *Anal. Chem.* **1984**, *56*, 2093.
(9) Yau, W. W.; Kirkland, J. J. *Anal. Chem.* **1984**, *56*, 1461.
(10) Giddings, J. C.; Caldwell, K. D.; Joellmer, J. F.; Dickinson, T. H.; Myers, M. N.; Martin, M. *Anal. Chem.* **1979**, *51*, 30.
(11) Giddings, J. C.; Lin, H. C.; Caldwell, K. D.; Myers, M. N. *Sep. Sci.* **1983**, *18*, 293.
(12) Brimhall, S. L.; Myers, M. N.; Caldwell, K. D.; Giddings, J. C. *J. Polym. Sci.* **1984**, *22*, 339–345.
(13) Giddings, J. C. *Sep. Sci.* **1983**, *18*, 765–773.

**J. Calvin Giddings**

Department of Chemistry
University of Utah
Salt Lake City, Utah 84112

RECEIVED for review September 14, 1984. Accepted December 26, 1984. This project was supported by Public Health Service Grant GM 10851-27 from the National Institutes of Health.

---

# Pulsed Semiconductor Laser Fluorometry for Lifetime Measurements

*Sir:* Laser fluorometry is quite useful for ultratrace analysis and for characterization of the sample molecule. However, the expense of the laser and the complexity of its operation limit practical applications. A recently developed semiconductor laser has the advantage of being much smaller and less expensive, and it may readily be installed in a commercial spectrometer. Photoacoustic spectrometry (*1*), conventional spectrophotometry (*2–4*), fluorometry (*5*), and thermal lens spectrophotometry (*6*) have been demonstrated using a continuous wave semiconductor laser. A semiconductor laser can be operated in a pulsed mode (*7*), but it has not yet been used for the purpose of spectrometry. When short electric pulses are applied to the semiconductor laser, picosecond laser pulses can be obtained although the peak power is low. This laser can be pulsed rapidly, so that it may be advantageous as a light source for time-correlated photon counting fluorometry.

Most molecular fluorescence studies are carried out in the ultraviolet and visible regions. A short-chained polymethine dye has strong absorption and emission bands in the visible region and has been used for characterization of a micelle (*8*) and of a liposome (*9*) by measuring the fluorescence lifetime and quantum yield. Extending the double-bond conjugation by increasing the number of methylene groups in the chain results in a polymethine dye which has a very strong absorption band in the near-infrared region (800–900 nm). To the best of our knowledge, no study has been reported using time-resolved fluorometry in the near-infrared region. This is apparently due to the lack of a good light source and photodetector for use in this wavelength region.

In this study, we present the lifetime measurement of a polymethine dye in various solvents utilizing a novel pulsed semiconductor laser in a time-correlated photon counting system. A relationship between the fluorescence lifetime and solvent polarity is reported and its potentiality for use in evaluation of microenvironmental hydrophobicity is discussed.

## EXPERIMENTAL SECTION

**Apparatus.** A block diagram of the laser fluorometer is shown in Figure 1. The light source is a pulsed semiconductor laser (Hamamatsu Photonics, Picosec Light Pulser, C1308), which has a pulse width of 136 ps and a peak output power of 1.3 W. The laser was usually operated at a repetition rate of 10 kHz. Laser emission (wavelength 823 nm, bandwidth 3 nm) was directed to a conventional quartz sample cuvette with an optical fiber and a lens (focal length (FL), 7 mm; 10 mm i.d.). The fluorescence emission was collected with a lens (FL 31 mm, 28 mm i.d.) and then passed through an interference filter (Ditric 15-20785, 19 mm i.d., transmission maximum 850 nm, transmission at 830 nm 0.3%), and a color filter (Toshiba V-R63, 630 nm cutoff). The fluorescence signal is finally focused by a lens (FL 60 mm, 28 mm i.d.) onto the photocathode of a red-sensitive photomultiplier (Hamamatsu R 928, 185–930 nm), which was typically operated at 1500 V. The output signal was fed sequentially to a constant fraction discriminator (Ortec 583), a time-to-amplitude converter (Ortec 457), and a multichannel analyzer (Norland Ino-tec IT-5300). The synchronous output signal (4 V, 100 ns) from the semiconductor laser was delayed and inverted by using a pulse generator (Hewlett-Packard 8013B) and fed to a constant fraction discriminator (Ortec 473A). The fluorescence lifetime was calculated by a microcomputer (Sord M223 Mark III).

**Reagents.** The polymethine dye 3,3′-diethyl-2,2′-(4,5:4′,5′-dibenzo)dithiatricarbocyanine iodide (NK 427) was obtained from Nippon Kanko-Shikiso Kenkyusho and was used without further purification. Guaranteed grade organic solvents were obtained from Kishida Chemical Co. and were used as received. The water was doubly distilled and deionized.

## RESULTS AND DISCUSSION

**Time Resolution.** The time profile of the laser pulse as

0003-2700/85/0357-0947$01.50/0 © 1985 American Chemical Society

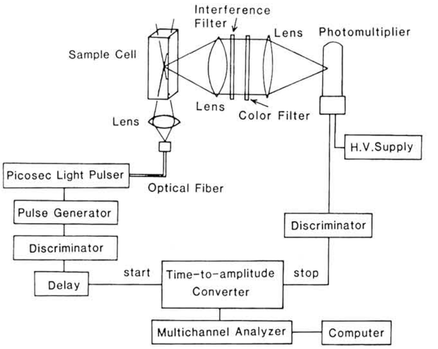

**Figure 1.** Block diagram of experimental apparatus for measurement of fluorescence lifetime.

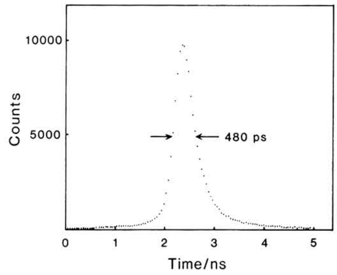

**Figure 2.** Excitation time profile of laser pulse recorded by present fluorometric system.

measured by the present laser fluorometer is shown in Figure 2. The full width at the half maximum (fwhm) is 480 ps. Since pulse width of the semiconductor laser is 136 ps and the time resolution of the electronics is even shorter, the observed time resolution is assumed to be limited by the transit time spread (TTS) of the photomultiplier. Further optimization of the experimental conditions might improve the resolution to 200 ps (*10*). For example, a microchannel plate photomultiplier has shorter TTS (*11*), but a transmission type photocathode is not available for this type (the available range is 300–840 nm). A cross-field photomultiplier (TTS = 30 ps (*12*)) may be more advantageous due to better time resolution (228 ps (*13*)) and high sensitivity in the near-infrared region (300–900 nm) but is rather expensive. An avalanche photodiode operated in a single photon counting mode has very short TTS and is sensitive out to 1100 nm (silicone diode) or 1570 nm (germanium diode). A time resolution of 70 ps has already been achieved by using the avalanche photodiode (*14*). A passively mode-locked semiconductor laser is reported to have a very short pulse width of 5.1 ps (*15*). We believe that a laser fluorometric system consisting of a mode-locked semiconductor laser and an avalanche photodiode incorporated into a time-correlation photon counting system would be quite attractive for the measurement of picosecond fluorescence decay.

**Fluorescence Lifetime of Polymethine Dye.** The fluorescence decay curve and the fluorescence intensity were measured for NK 427 without deaeration of the sample solutions; deaeration caused little effect in these parameters. Since the time resolution of the fluorometer was not necessarily sufficient, the fluorescence lifetime ($\tau$) was estimated by using the simple equation ($\Delta_1^2 + \tau^2 = \Delta_0^2$) where $\Delta_1$ is the decay time obtained from the profile of the laser pulse ($\Delta_1$ = 320 ps) and $\Delta_0$ is the observed lifetime for the sample. By this procedure the fluorescence lifetime was corrected about 10% for the sample with the shortest lifetime in this study. A deconvolution procedure would be necessary in order to obtain rigorously quantitative results. The error in data fitting to a single exponential decay curve was about 7% in the worst case and less than 1% in the best case. The fluorescence quantum yield was calculated by dividing the integrated fluorescence intensity by the absorbance of the sample solution. As depicted in Figure 3A, the fluorescence lifetime decreases with increasing dielectric constants of those solvents which contain an OH group. A correlation coefficient in fitting to a linear curve was −0.987. Acetone deviates from the line, possibly due to the relatively small hydrogen-bonding interaction of the dye and solvent molecules. The fluorescence quantum yield (Figure 3B), shows a similar dependence upon dielectric constant. However, a correlation coefficient was −0.730, and it was difficult to fit the data to the line. The deviation observed when ethylene glycol was the solvent is due to rapid decomposition of NK 427, which is not stable in this solvent. Fluorescence lifetime as measured by time-correlated photon counting fluorometry is not affected by gradual sample decomposition, which is a serious problem in the time-gated signal measurement of the decay curve, and is therefore preferable to quantum yield for the evaluation of fluorescence characteristics of the sample molecule. The present results show that fluorescence quenching increases with increasing solvent polarity, as the solute–solvent interaction increases. This result suggests that a polymethine dye could possibly be used as a hydrophobic probe, although NK 427 itself could not be directly combined with biochemical polymers such as proteins. The NK 427 dye was selected initially since it is strongly fluorescent and has been previously used as a laser dye. More than 2000 dyes in this group are commercially available (*16*), so that a suitable dye for biochemical polymer studies should be identifiable by screening of this class of dye molecules. A few polymethine dyes have already been used as molecular probes in order to elucidate the characteristics of protein, but all of these studies have been performed by using excitation in the visible region (*17*). We expect that a similar approach should be possible in the near-infrared region. The fluorometry system developed and presented above would provide a powerful analytical technique for obtaining information about the microenvironmental hydrophobicity of proteins.

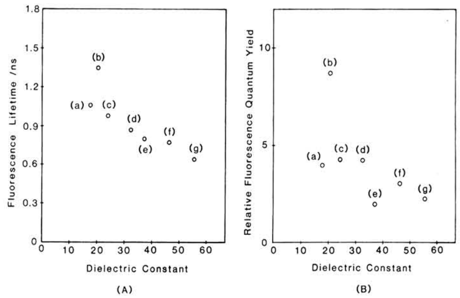

**Figure 3.** Fluorescence characteristics of polymethine dye: (A) fluorescence lifetime, (B) fluorescence quantum yield; (a) 2-methyl-1-propanol, (b) acetone, (c) ethanol, (d) methanol, (e) ethylene glycol, (f) water:methanol 3:7, (g) water:methanol 1:1. The lifetime measurement was carried out at 30 °C.

**Registry No.** NK 427, 20682-18-2.

## LITERATURE CITED

(1) Kawabata, Y.; Kamikubo, T.; Imasaka, T.; Ishibashi, N. *Anal. Chem.* **1983**, *55*, 1419–1420.
(2) Imasaka, T.; Kamikubo, T.; Kawabata, Y.; Ishibashi, N. *Anal. Chim. Acta* **1983**, *153*, 261–263.

(3) Ohtsu, M.; Kotani, H.; Tagawa, H. *Jpn. J. Appl. Phys.* **1983**, *22*, 1553-1557.
(4) Chan, K.; Ito, H.; Inaba, H. *Appl. Opt.* **1983**, *22*, 3802-3804.
(5) Imasaka, T.; Yoshitake, A.; Ishibashi, N. *Anal. Chem.* **1984**, *56*, 1077-1079.
(6) Nakanishi, K.; Imasaka, T.; Ishibashi, N., unpublished results, Faculty of Engineering, Kyushu University, 1984.
(7) Tsuchiya, Y.; Takeshima, A.; Hosoda, M. *Rev. Sci. Instrum.* **1981**, *52*, 579-581.
(8) Sato, H.; Kawasaki, M.; Kasatani, K.; Nakashima, N.; Yoshihara, K. *Bull. Chem. Soc. Jpn.* **1983**, *56*, 3588-3594.
(9) Handa, T.; Komatsu, H.; Matsuzaki, K.; Nakagaki, M. *Nippon Kagaku Kaishi* **1984**, 8-13.
(10) Kinoshita, S.; Kushida, T. *Rev. Sci. Instrum.* **1982**, *53*, 469-472.
(11) Murao, T.; Yamazaki, I.; Yoshihara, K. *Appl. Opt.* **1982**, *21*, 2297-2298.
(12) Abshire, J. B.; Rowe, H. E. *NASA Tech. Memo.* **1977**, *NASA TM-X-78028*.
(13) Koester, V. J. *Anal. Chem.* **1979**, *51*, 458-459.
(14) Cova, S.; Longoni, A.; Andreoni, A.; Cubeddu, R. *IEEE J. Quantum. Electron.* **1983**, *QE-19*, 630-634.
(15) Ippen, E. P.; Eilenberger, D. J.; Dixon, R. W. *Appl. Phys. Lett.* **1980**, *37*, 267-269.
(16) "Organic Chemicals List"; Nippon Kanko-Shikiso Kenkyusho: Okayama, 1969 (supplement 1974).
(17) Ohkuma, S.; Moriyama, Y.; Takano, T. *J. Biochem.* **1983**, *94*, 1935-1943.

**Totaro Imasaka**
**Akinori Yoshitake**
**Kaoru Hirata**
**Yuji Kawabata**
**Nobuhiko Ishibashi***

Faculty of Engineering
Kyushu University
Hakozaki, Fukuoka 812, Japan

RECEIVED for review August 16, 1984. Accepted December 31, 1984. This research is supported by a Grant-in-Aid for Scientific Research from the Ministry of Education of Japan and by a Kajima Foundation Research Grant.

# Laser Photodissociation/Tandem Mass Spectrometry of Synthetic Porphyrins: A Structural Probe

*Sir:* Structural determination of peripherally modified porphyrins generally requires confirmation from several instrumental methods—mass spectrometry, NMR, and absorption spectrometries. Electron ionization mass spectrometry provides molecular weight and structural information unless the porphyrin is intractable or it contains labile side chains or "tails". Field desorption mass spectrometry can provide molecular weight information on such troublesome species, but it usually does not yield structural information. Recently, we reported the usefulness of the desorption ionization mass spectrometry methods—fast-atom bombardment (FAB), desorption chemical ionization, and "in-beam" electron ionization for molecular weight and side-chain determinations of intractable synthetic prophyrins (*1, 2*). Generally, FAB gave the most significant structural and molecular weight information for the various synthetic compounds studied, relative to the other two desorption ionization methods. Although FAB yielded molecular weight information, other abundant molecular adduct ions resulting from sample reactions with the thioglycerol matrix and sample/matrix impurities were observed in the spectra of the porphyrins. These adduct ions could confuse the identification of a compound.

Tandem mass spectrometry methods (*3, 4*) could be used to dissociate each of the various suspected molecular parents ions, which would include adduct ions, etc., in order to confirm the authenticity of the actual molecular ion. Collisional activation of the mass-selected ions results in the deposition of a range of internal energies, where the average excitation energy is dependent on the collision energy (*5*) and the number of collisions (*6*). This nondiscrete energy deposition may result in nonselective fragmentation of the ions of interest. Furthermore, collision-induced dissociation of mass-selected ions at the same nominal mass-to-charge ratio (low-resolution tandem mass spectrometry) could confuse the interpretation of the resulting composite daughter ion mass spectrum.

Photodissociation of mass-selected ions results in an additional degree of selectivity (*6–8*). A discrete energy or range of energies can be deposited into the mass-selected ion by photoexcitation. This discrete excitation results in both molecular-specific and bond-selective photodissociation especially when the molecular ions are produced with low internal energies. FAB has been shown to produce ions with relatively low internal energy (*9*), and the low degree of fragmentation observed in FAB spectra is indicative of such low internal-energy ions.

This paper reports preliminary mass spectrometry/mass spectrometry (MS/MS) results on the photodissociation of a series of synthetic porphyrin molecular ions produced by FAB. The photodissociation mass spectra of one series of "tailed" porphyrins yielded information on the structure of the "tail". The photofragment spectra of a series of meso-substituted tetraphenylporphines gave information on the meso substituent. Adduct ions of the porphyrin molecules did not yield significant photofragment mass spectra. One example is given of photodissociation of a porphyrin molecular ion isobaric with an interfering glycerol cluster ion, which illustrates the selectivity of the method over collisional-activation techniques.

## EXPERIMENTAL SECTION

A reverse-geometry, double-focusing mass spectrometer (ZAB-2F, VG Analytical, Ltd., Manchester U.K.) was used as a mass-analyzed ion kinetic energy spectrometer (*10*). The instrument was modified to allow coaxial ion/photon beam overlap in the second field-free region of the mass spectrometer, similar to that reported elsewhere (*11*). An argon ion laser (Spectra Physics Model 171-18) was operated at 10 or 20 W ($\sim$2-mm beam diameter) in the multiline mode (457.9-514.5 nm; 2.7-2.4 eV), and phase-sensitive detection was accomplished by mechanically chopping the laser beam (2.5 kHz) and detecting the signal with a lock-in amplifier.

The residence time of the fast ion beam in the photodissociation region is on the order of several microseconds resulting in a very low photon fluence ($10^{-3}$ J/cm$^2$), which is much less than that generally required for multiphoton processes (1 J/cm$^2$). Therefore, the photodissociation processes reported here are single-photon processes. A discussion of multiphoton events can be found elsewhere (*12, 13*).

Mass-analyzed ion kinetic energy spectrometry (MIKES) photofragment spectra of the porphyrin molecular ion ($[M + H]^+$ and $M^{+}\cdot$) were averaged by using a multichannel analyzer with 16 to 64 spectra depending on the signal-to-noise ratio. Repetitive

This article not subject to U.S. Copyright. Published 1985 by the American Chemical Society

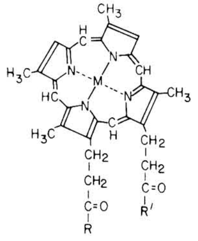

COMPOUNDS 1 - 6

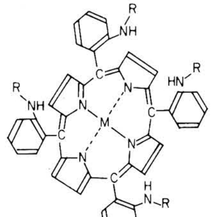

COMPOUNDS 7 - 10

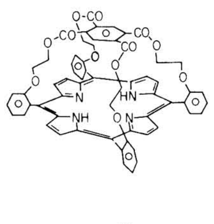

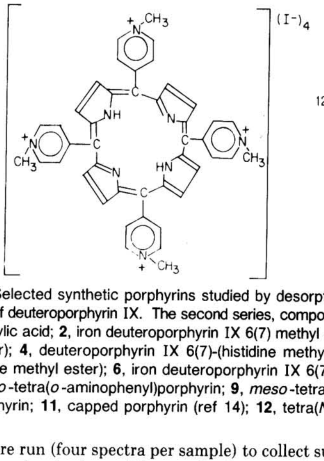

| COMPOUND NO. | M | R | R′ | MW | EMPIRICAL FORMULA |
|---|---|---|---|---|---|
| 1. | Zn | OH | OH | 572 | $C_{30}H_{28}O_4N_4Zn$ |
| 2. | Fe(III) | $OCH_3$ | 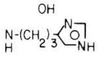 | 685 | $C_{37}H_{39}O_3N_7Fe$ |
| 3. | H,H | $OCH_3$ | 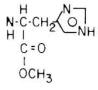 | 675 | $C_{38}H_{41}O_5N_7$ |
| 4. | H,H | R′ | 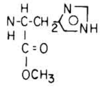 | 812 | $C_{44}H_{48}O_6N_{10}$ |
| 5. | Zn(II) | $OCH_3$ | 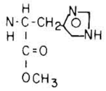 | 737 | $C_{38}H_{39}O_5N_7Zn$ |
| 6. | Fe(III) | $OCH_3$ | 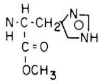 | 729 | $C_{38}H_{39}O_5N_7Fe$ |
| 7. | H,H | H | | 674 | $C_{44}H_{34}N_8$ |
| 8. | Zn(II) | H | | 736 | $C_{44}H_{32}N_8Zn$ |
| 9. | H,H | $\underset{\underset{O}{\|}}{C}\text{-}C(CH_3)_3$ | | 1010 | $C_{64}H_{66}N_8O_4$ |
| 10. | Fe(III) | $\underset{\underset{O}{\|}}{C}\text{-}C(CH_3)_3$ | | 1064 | $C_{64}H_{64}N_8O_4Fe$ |
| 11. | H,H | | | 1036 | $C_{62}H_{44}N_4O_{12}$ |
| 12. | | | | 1186<br>(678) | $C_{44}H_{38}N_8\cdot 4I$<br>$C_{44}H_{38}N_8$ |

**Figure 1.** Selected synthetic porphyrins studied by desorption ionization mass spectrometry. The first series, compounds **1–6**, are functional derivatives of deuteroporphyrin IX. The second series, compounds **7–12**, are meso-substituted pseudo-tetraphenylporphines: **1**, zinc deuteroporphyrin IX dicarboxylic acid; **2**, iron deuteroporphyrin IX 6(7) methyl ester (3) imidazolepropylamide; **3**, deuteroporphyrin IX 6(7) methyl ester 7(6)-(histidine methyl ester); **4**, deuteroporphyrin IX 6(7)-(histidine methyl ester) 7(6)-(histidine methyl ester); **5**, zinc deuteroporphyrin IX 6(7) methyl ester 7(6)-(histidine methyl ester); **6**, iron deuteroporphyrin IX 6(7) methyl ester 7(6)-(histidine methyl ester); **7**, *meso*-tetra(*o*-aminophenyl)porphyrin; **8**, zinc *meso*-tetra(*o*-aminophenyl)porphyrin; **9**, *meso*-tetra(α,α,α,α-*o*-pivalaminophenyl)porphyrin; **10**, iron *meso*-tetra(α,α,α,α-*o*-pivalaminophenyl)porphyrin; **11**, capped porphyrin (ref 14); **12**, tetra(*N*-methylpyridinium iodide)porphyrin.

samples were run (four spectra per sample) to collect sufficient data. The molecular ions of the porphyrins were obtained by fast-atom bombardment using a thioglycerol matrix as described previously (*1*, *2*).

The synthetic porphyrins (Figure 1) were surplus from an earlier study (*1*, *2*), and they were prepared as described therein. Only those photodissociation product ions that dominated the daughter ion spectra (>10% of the base peak) will be discussed. All losses reported are with respect to the molecular ion, and α, β, and γ cleavages are with respect to the carbonyl group on the "tails"

(R or R′ as specified).

## RESULTS AND DISCUSSION

**Porphyrin Photodissociation Mass Spectra.** *Deuteroporphyrin IX Derivatives.* The base peak in the photodissociation mass spectrum of this series of "tailed" porphyrins (Compounds 1–6, Figure 1) was a result of photoinduced β-cleavage to the carbonyl group containing the R′ functionality (loss of $CH_2COR'$). Generally, the major fragmentations were similar to those reported for the FAB spectra (2). The first compound, zinc deuteroporphyrin IX dicarboxylic acid, also gave an abundant fragment (27%) resulting from a γ-cleavage (R equals R′), and the second compound, iron(III) deuteroporphyrin IX 6(7) methyl ester (3) imidazolepropylamide, likewise gave an abundant (70%) β-cleavage (loss of $CH_2COR$). Compound 2 was the only one out of the five compounds containing an imidazole terminus (compounds 2–6) where a fragment ion corresponding to the loss of the imidazole terminus (20%) was observed.

Compounds 3, 4, 5, and 6, which form a pseudohomologous series, showed various α, β, and γ cleavages in rather low abundances (20–30%). The spectrum of the iron-containing member of the series (compound 6) was obtained at 10 W laser power, while the metal-free and zinc-containing members required a higher power (20 W) to detect photodissociation products. Compound 3, deuteroporphyrin IX 6(7) methyl ester, 7(6)-(histidine methyl ester) has been observed to undergo disproportionation and recombination in the matrix (*1*) resulting in the abundant deuteroporphyrin IX 6(7)-(histidine methyl ester) 7(6)-(histidine methyl ester) species (compound 4). The photodissociation mass spectrum of this species (10 W laser power) resulted in two abundant (100%) product ions from β and γ cleavages of the R′ "tail". All three compounds gave the loss of the R′ moiety.

*Meso-Substituted Tetraphenylporphine Derivatives.* The loss of one meso-substituent (anilino group) dominated the photodissociation mass spectra of compounds 7 and 8, and the loss of ammonia (85% and 25%) also was observed. The "picket-fence" porphyrins (compounds 9 and 10) of this pseudohomologous series (compounds 7, 8, 9, and 10) both yielded the loss of the "pickets" (R groups) as the base peak. A single R group loss dominated for the metal-free porphyrin, and the losses of both one and two R groups were the base peaks for the iron-containing porphyrin. The loss of a *tert*-butyl group was observed in high abundance (60%) for compound 9. The iron *meso*-tetra(α,α,α,α-*o*-pivalaminophenyl)porphyrin required high laser power (20 W) to obtain the photodissociation mass spectrum. This compound 10 also gave the fragments $[M - R - t\text{-Bu}]^+$ and $[M - NHR]^+$, which were not observed in the FAB mass spectrum (2). In contrast, the $[M - t\text{-Bu}]^+$ species was the most abundant ion in the FAB mass spectrum.

The capped porphyrin (compound 11) gave a weak photodissociation mass spectrum with three intense (~100%) fragments that corresponded to the loss of OH, CO, and $CO_2$ from the molecular ion.

The tetra(*N*-methylpyridinium iodide)porphyrin (tetraquarternary ammonium salt), compound 12, gave a molecular parent ion at *m/z* 678, corresponding to $[M - 4I]^+$ (2). The photodissociation mass spectrum of this species was the most intense of all the porphyrins studied. The two observed photofragments corresponded to $[M - CH_3]^+$ and $[M - NHCH_3]^+$.

**Photoselectivity—Mixture Analysis.** Our earlier study on the FAB of synthetic porphyrins demonstrated the ability of FAB to give abundant molecular ions from these intractable species (*1*, *2*); however, very abundant adduct ions were also observed. These adduct ions in the molecular ion region, some of which could not be identified, could confound the identification of an unknown species or the verification of a synthetic product. The photodissociation mass spectrum of each of the suspect ions in the molecular ion region will yield characteristic spectral information, which establishes the identity of the true molecular ion. As a first example, an interference ion in the FAB spectrum of compound 4, 14 mass units above the molecular ion, which could correspond to a homologue of compound 4, did not yield photofragments. Clearly, based on the expected photo β-cleavages from the tailed porphyrins (established in the previous section), this $[M + 14]^+$ species is unrelated to the synthetic porphyrin of interest. (This does not rule out the possibility that the $[M + 14]^+$ is some porphyrin reaction product or adduct ion.) Also, the unidentified adduct ion observed in the FAB spectrum of compound 7, corresponding to $[M + 149]^+$ gave a photofragment at $[M - 44]^+$, which is not structurally indicative of a compound 7 porphyrin-related species, similar to the previous examples. These two results illustrate how the photodissociation technique combined with FAB can be used to confirm the identity of the true molecular ion.

Ions that are isobaric with an ion of interest also can interfere in a mass spectrometry/mass spectrometry experiment especially with low-resolving power spectrometers (triple quadrupole or MIKE spectrometers). For example, the protonated molecule of compound 8, zinc *meso*-tetra(*o*-aminophenyl)porphyrin, has the same nominal mass as the glycerol cluster ion $[(C_3H_8O_3)_8H]^+$. The collision-induced dissociation (CID) MIKES spectrum of compound 8 gives abundant fragment ions from the loss of the $NH_2$ species (40%), the loss of one (100%) and two (25%) anilino groups ($C_6H_4NH_2$), and the loss of an anilino and $NH_2$ species (25%) (see Figure 2A). The $n = 8$ glycerol cluster gives a series of daughter ions due to the loss of $(C_3H_8O)_n$ for $n = 1–7$. The loss of $(C_3H_8O)_{1,2}$ from the $n = 8$ glycerol cluster ion gives fragment ions that coincide with the nominal mass of the anilino loss fragments of compound 8, $[M - (C_6H_4NH_2)_{1,2}]^+$. A CID/MIKES spectrum of a porphyrin/glycerol mixture (glycerol >> porphyrin/thioglycerol is shown in Figure 2B. The presence of the glycerol cluster ion fragments ($n = 5$, 6, and 7) dominates this spectrum. The kinetic energy release of the glycerol fragment ions ($n = 6$ and 7) are must less than the isobaric porphyrin product ions. This can be seen by comparing the peak widths of the fragment ions in Figure 2A,B. The porphyrin is only a minor component of the mixture used to obtain the CID/MIKES spectrum shown in Figure 2B. Figure 2C,D shows the photodissociation MIKES spectra of the porphyrin and porphyrin/glycerol mixture. Glycerol photofragments were not observed in a separate experiment on the photodissociation of the glycerol cluster isobaric ion, because the glycerol cluster ion does not photodissociate at the wavelengths used in our experiments. Although the photodissociation mass spectrum of the mixture (Figure 2D) is weak, the major features of the spectrum obtained from the pure compound are observed; for example, the similar kinetic-energy release of the porphyrin photofragments. The signal-to-noise ratio could be improved by signal averaging for a longer period of time. This rather simple, but practical example encountered in our studies demonstrates the potential for selective dissociation by photon/ion interactions. Also, the combined technique of FAB/photodissociation/MS/MS will allow the study of the gas-phase ion spectroscopy and energetics of such intractable compounds.

As a point of contrast it is worth commenting on the similarity of the CID and photodissociation MIKES spectra of the porphyrin discussed with respect to Figure 2. The average collisional excitation energy has been determined to be approximately 2.4 eV (6). This collisional energy is at the low end of the range of (multiline) photoexcitation energies

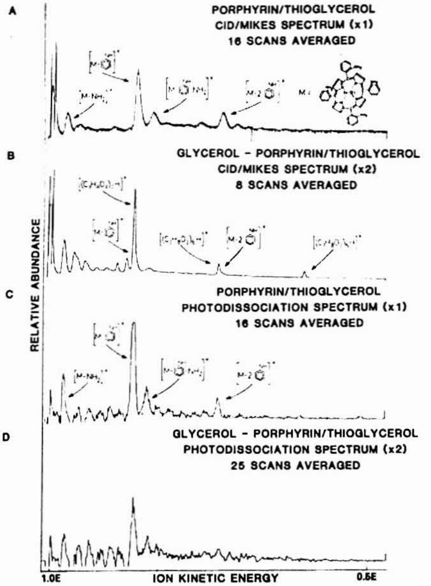

**Figure 2.** The CID/MIKES and photodissociation/MIKES spectra of the molecular ion ($m/z$ 737) of compound **8**, zinc *meso*-tetra(*o*-aminophenyl)porphyrin, in thioglycerol and of the $m/z$ 737 species in a glycerol/thioglycerol mixture: (A) CID/MIKES spectrum of the porphyrin in a thioglycerol matrix; (B) CID/MIKES spectrum of the $m/z$ 737 species. A small percentage of the porphyrin/thioglycerol sample was admixed with glycerol. The glycerol $[(C_3H_8)_8H]^+$ ($m/z$ 737) cluster ion is isobaric with the porphyrin molecular ion. The glycerol cluster daughter ions are also isobaric with some of the porphyrin daughter ions, which could confuse interpretation of the mass spectrum; (C) Photodissociation/MIKES spectrum of the porphyrin in a thioglycerol matrix; (D) Photodissociation/MIKES spectrum of the $m/z$ 737 species from the glycerol–porphyrin/thioglycerol mixture, which is due only to the photodissociation of the porphyrin. (In a separate experiment, we were not able to detect any ionic photofragments from the glycerol cluster ion at $m/z$ 737).

(2.41–2.71 eV) used in these studies. Therefore, similar daughter ions and kinetic energy releases from the porphyrin in the CID and photodissociation spectra are observed. However, the collisional activation energy can exceed the 2.71-eV photoexcitation maximum, which implies that the onset for the fragmentation of the glycerol cluster ion lies above 2.7 eV.

## CONCLUSIONS

This rather spectroscopically limited laser/mass spectrometric study demonstrates the concept and potential of ion photodissociation to characterize selectively complex and intractable molecules of biological importance ionized by the new desorption ionization techniques. The use of a tunable photon source will enhance selectivity and sensitivity because the photodissociation can be performed at a wavelength specific for the compound of interest and having an optimal photon absorption cross section, thus leading to enhanced photofragmentation. Further investigation of the ion photodissociation spectra of the porphyrins over a continuous range of wavelengths would allow the direct comparison of the ion spectra and the electronic absorption spectra. This would provide insight into the ion structure and the dynamics of ion/photon interactions and the electronic structure of the molecular ions.

## ACKNOWLEDGMENT

The authors thank Michael L. Gross (University of Nebraska) for suggesting the porphyrins for study, Leon Kurlansik (Naval Medical Research Institute) for providing the novel synthetic porphyrins, and Steven Schneider for technical assistance.

**Registry No.** **1**, 32407-78-6; **2**, 94636-67-6; **3**, 85771-00-2; **4**, 94905-12-1; **5**, 94636-66-5; **6**, 94643-17-1; **7**, 52199-35-6; **8**, 67595-98-6; **9**, 55253-62-8; **10**, 83198-46-3; **11**, 55022-76-9; **12**, 36674-90-5.

## LITERATURE CITED

(1) Kurlansik, L.; Williams, T. J.; Campana, J. E.; Green, B. N.; Anderson, L. W.; Strong, J. M. *Biochem. Biophys. Res. Commun.* **1983**, *111*, 478–483.
(2) Kurlansik, L.; Williams, T. J.; Strong, J. M.; Anderson, L. W.; Campana, J. E. *Biomed. Mass Spectrom.* **1984**, *11*, 475–481.
(3) McLafferty, F. W., Ed. "Tandem Mass Spectrometry"; Wiley: New York, 1983.
(4) Cooks, R. G., Ed. "Collision Spectroscopy"; Plenum Press: New York, 1978.
(5) Kim, M. S.; McLafferty, F. W. *J. Am. Chem. Soc.* **1978**, *100*, 3279–3282.
(6) Griffiths, I. W.; Mukhtar, E. S.; March, R. E.; Harris, F. M.; Beynon, J. H. *Int. J. Mass Spectrom. Ion Phys.* **1981**, *39*, 125–132.
(7) Mukhtar, E. S.; Griffiths, I. W.; Harris, F. M.; Beynon, J. H. *Org. Mass Spectrom.* **1981**, *16*, 51.
(8) Kim, M. S.; Morgan, T. G.; Kingston, E. E.; Harris, F. M. *Org. Mass Spectrom.* **1983**, *18*, 582–586.
(9) Cook, K. D.; Chan, K. W. S. *Int. J. Mass Spectrom. Ion Proc.* **1983**, *54*, 135–149.
(10) Morgan, R. P.; Beynon, J. H.; Bateman, R. H.; Green, B. N. *Int. J. Mass Spectrom. Ion Phys.* **1979**, *28*, 171–191.
(11) Mukhtar, E. S.; Griffiths, I. W.; Harris, F. M.; Beynon, J. H. *Int. J. Mass Spectrom. Ion Phys.* **1981**, *37*, 159–166.
(12) Pantell, R. H.; Puthoff, H. E. "Fundamentals of Quantum Electronics"; Wiley: New York, 1969.
(13) Bowers, M. T., Ed. "Gas-Phase Ion Chemistry, Vol. 3, Ions and Light"; Academic Press: New York, 1984.
(14) Almog, J.; Baldwin, J. E.; Dyer, R. L.; Peters, M. *J. Am. Chem. Soc.* **1975**, *97*, 226–227.

[1] Present address: Celanese Research Co., Summit, NJ 07901.

**Elaine K. Fukuda**[1]
**Joseph E. Campana***

Naval Research Laboratory
Chemistry Division
Washington, D.C. 20375-5000

Received for review September 21, 1984. Accepted January 4, 1985. This work was supported by the Office of Naval Research. E.K.F. thanks the National Research Council for support as an NRC/NRL Cooperative Research Associate.

---

# Unbiased Generalized Standard Addition Method

*Sir:* During the last decade there has been a lot of interest in the quantitative analysis of multicomponent data. This is due to our increased ability to collect multiwavelength data and to handle the required matrix transformations on computers which are now interfaced to analytical instruments. Recently, a method for multicomponent analysis using standard additions of more than one analyte, component of interest, was developed. This method is called the generalized

0003-2700/85/0357-0952$01.50/0 © 1985 American Chemical Society

standard addition method (GSAM) (*1–4*), which is able to detect and correct for spectral interferences, matrix effects, and drift.

The computational procedure of the GSAM is composed of two steps. A matrix of linear response constants showing the contribution of analytes to sensor responses is computed at the first step. To compute this matrix, the initial response of the unknown sample is subtracted from the response data matrix. The determined matrix is used at the second step to compute the concentrations in the sample. Unfortunately, the subtraction of initial response from the response matrix results in biased estimates of the concentrations in the unknown sample. This point is well illustrated by referring to the quantitation of an unknown, using one-dimensional (regular) standard addition. To estimate the unknown concentration, the response of the analytical sensor is plotted against the number of moles added to the unknown. The best straight line is fitted to these points and extended back to intersect the abscissa. The point where the intersection occurs is the initial number of moles of unknown. The best straight line fit to measured responses will yield the "best linear unbiased estimate" (BLUE) of the unknown. Unlike the one-dimensional standard addition, the multidimensional GSAM's quantitation results are not BLUE. This follows from the subtraction of initial response from the response matrix. In the one-dimensional method, this is equal to enforcing the straight lint to pass through the initial sample response. In the rest of this note, this argument will be clarified and a technique that allows the achievement of BLUE for the multidimensional GSAM is presented.

## THEORY

**Probem Formulation and Notation.** Boldface capital letters are used for matrices, e.g., $\mathbf{X}$, superscript T for transposed matrices, e.g., $\mathbf{X}^T$, boldface small characters for vectors, e.g., $\mathbf{x}$, and $\mathbf{x}_0$, and italic lower case characters for scalers, e.g., $x$. Superscript + denotes the pseudoinverse, e.g., $\mathbf{X}^+$. The symbol $(\mathbf{x}|\mathbf{X})$ designates a partitioned matrix.

There are $m$ ($i = 1, ..., m$) sensors, $n$ ($j = 1, ..., n$) standard additions, and $p$ ($k = 1, ..., p$) analytes. The matrix $\mathbf{Q}$ which is of the order $m \times (n + 1)$ is the matrix of instrumental responses multiplied by the total volume. $\mathbf{C}$ is the matrix of number of moles of analytes and is of order $p \times (n + 1)$. The matrix $\mathbf{A}$ of order $m \times p$ connects the two matrices by

$$\begin{pmatrix} q_{1,0} & q_{1,1} & \cdots & q_{1,n} \\ q_{2,0} & q_{2,1} & \cdots & q_{2,n} \\ \vdots & & & \\ q_{m,0} & q_{m,1} & \cdots & q_{m,n} \end{pmatrix} = \begin{pmatrix} a_{1,1} & a_{1,2} & \cdots & a_{1,p} \\ a_{2,1} & a_{2,2} & \cdots & a_{2,p} \\ \vdots & & & \\ a_{m,1} & a_{m,2} & \cdots & a_{m,p} \end{pmatrix} \times \begin{pmatrix} c_{1,0} & c_{1,1} & \cdots & c_{1,n} \\ c_{2,0} & c_{2,1} & \cdots & c_{2,n} \\ \vdots & & & \\ c_{p,0} & c_{p,1} & \cdots & c_{p,n} \end{pmatrix} \quad (1)$$

or

$$\mathbf{Q} = \mathbf{AC}$$

The first columns $\mathbf{q}_0$ and $\mathbf{c}_0$ are the vectors of initial sample concentration and response. The matrix $\mathbf{C}$ may be written as $\mathbf{C} = \Delta\mathbf{C} + \mathbf{c}_0\mathbf{j}^T$ where $\mathbf{j}$ is a vector with $n + 1$ elements all of which are units. $\Delta\mathbf{C}$ is the added concentrations matrix. Now eq 1 is read as

$$\mathbf{Q} = \mathbf{A}(\Delta\mathbf{C} + \mathbf{c}_0\mathbf{j}^T) \quad (2)$$

which is a nonlinear equation (because of the multiple, $\mathbf{Ac}_0$, of two unknown quantities) and its solution requires the use of iterative methods. In order to overcome this difficulty, Saxberg and Kowalski (*1*), in their formulation of the GSAM, suggested separating the matrix $\mathbf{Q}$ into two terms, as follows: $\mathbf{Q} = \Delta\mathbf{Q} + \mathbf{q}_0\mathbf{j}^T$. In doing this separation, one presupposes that $\mathbf{q}_0$ is equal to $\hat{\mathbf{q}}_0$ which is the BLUE of the vector of initial sample response.

When this assumption is made, eq 2 may be separated into two equations

$$\Delta\mathbf{Q} = \mathbf{A}\ \Delta\mathbf{C} \quad (3a)$$

$$\mathbf{q}_0 = \mathbf{Ac}_0 \quad (3b)$$

Equation 3a is solved first to find $\mathbf{A}$ which in turn is used by eq 3b to quantify the unknown number of moles. It is obvious that both $\mathbf{A}$ and $\mathbf{c}_0$ are biased due to the assumption $\hat{\mathbf{q}}_0 = \mathbf{q}_0$.

**Solution of the Unbiased GSAM.** In order to get a BLUE and yet avoid the time-consuming solution of a nonlinear matrix equation, it is suggested here to use a nonzero intercept model. The matrices involved will be redefined as $\mathbf{A}^* = (\mathbf{a}_0|\mathbf{A})$, $\mathbf{C}^* = (\mathbf{j}|\Delta\mathbf{C}^T)^T$, and the matrix $\mathbf{Q}$ remains unaltered. Now, eq 1 may bae rewritten as

$$\mathbf{Q} = \begin{pmatrix} a_{1,0} & a_{1,1} & \cdots & a_{1,p} \\ a_{2,0} & a_{2,1} & \cdots & a_{2,p} \\ \vdots & & & \\ a_{m,0} & a_{m,1} & \cdots & a_{m,p} \end{pmatrix} \times \begin{pmatrix} 1 & 1 & \cdots\cdots & 1 \\ 0 & \Delta c_{1,1} & \cdots & \Delta c_{1,n} \\ \vdots & & & \\ 0 & \Delta c_{p,1} & \cdots & \Delta c_{p,n} \end{pmatrix} \quad (4)$$

or

$$\mathbf{Q} = \mathbf{A}^*\mathbf{C}^*$$

The benefit of using the nonzero intercept model is removing $\mathbf{c}_0$ from eq 4 which allows quantitation of $\mathbf{A}$ by linear methods. It is also obvious that $\mathbf{a}_0$ is equal to $\hat{\mathbf{q}}_0$ which is now inserted into

$$\hat{\mathbf{q}}_0 = \mathbf{a}_0 = \mathbf{Ac}_0 \quad (5)$$

to obtain a BLUE of the analyte amounts.

It may be noted that the solution of a nonzero intercept model does not require a solution of matrices of order greater by one than the zero intercept model, and thus an additional sensor is needed (in contrast to what is claimed in ref 5). Rather, a transformation that allows the solution of matrices with the same order as the zero intercept model can be used (*6*). The solution of eq 5 is presented in the Appendix.

Frank et al. (*2*) applied the partial least-squares method (PLS) to the GSAM. They found that the results obtained by PLS were superior in terms of noise rejection to those obtained by conventional least squares. The superiority of quantifying by the PLS is well explained by the fact that in the PLS method the initial responses are also used in estimating the constants matrix.

Jochum et al. (*3*) and Moran and Kowalski (*4*) derived expressions to describe the effect of random experimental error on the GSAM. The derivation of the error estimates was complicated by the fact that the original computation is made by two steps. By use of the unbiased GSAM this difficulty is avoided as the second step does not introduce error. Thus error estimate by either of the methods (condition number (*3*) or variance matrix (*4*)) is much simpler.

## APPENDIX

**Solution of the Unbiased GSAM.** According to the least-squares approach, eq 4 is right multiplied by $(\mathbf{j}|\Delta\mathbf{C}^T)$ to obtain the normal equation

$$\mathbf{Q}(\mathbf{j}|\Delta\mathbf{C}^T) = (\mathbf{a}_0|\mathbf{A})\begin{pmatrix} \mathbf{j}^T \\ \Delta\mathbf{C} \end{pmatrix}(\mathbf{j}|\Delta\mathbf{C}^T) \quad (6)$$

After the multiplications are performed, eq 6 results in two matrix equations

$$\mathbf{Qj} = \mathbf{a}_0(n + 1) + \mathbf{A}\ \Delta\mathbf{Cj} \quad (7)$$

$$\mathbf{Q} = \mathbf{a}_0\mathbf{j}^{\mathrm{T}} + \mathbf{A}\,\Delta\mathbf{C} \tag{8}$$

The mean of the responses for each sensor is defined by

$$\bar{q}_i = \sum_{j=1}^{n+1} q_{ij}$$

Thus, the vector of mean responses, $\bar{\mathbf{q}}$, is computed by

$$\bar{\mathbf{q}} = \frac{\mathbf{Qj}}{n+1} \tag{9}$$

The mean $\bar{\mathbf{c}}$ of added analyte concentrations is also given by

$$\bar{\mathbf{c}} = \frac{\Delta\mathbf{C}\ \mathbf{j}}{n+1} \tag{10}$$

Now, it is observed that eq 7 may be written as

$$\mathbf{a}_0 = \bar{\mathbf{q}} - \mathbf{A}\bar{\mathbf{c}} \tag{11}$$

When this value of $\mathbf{a}_0$ is inserted into eq 8, the following equation is obtained:

$$\mathbf{Q} - \bar{\mathbf{q}}\mathbf{j}^{\mathrm{T}} = \mathbf{A}(\Delta\mathbf{C} - \bar{\mathbf{c}}\mathbf{j}^{\mathrm{T}}) \tag{12}$$

Defining $\tilde{\mathbf{Q}} = \mathbf{Q} - \bar{\mathbf{q}}\mathbf{j}^{\mathrm{T}}$ and $\Delta\tilde{\mathbf{C}} = \Delta\mathbf{C} - \bar{\mathbf{c}}\mathbf{j}^{\mathrm{T}}$ which are zero mean matrices of responses and concentrations, respectively, eq 12 is now written

$$\tilde{\mathbf{Q}} = \mathbf{A}\,\Delta\tilde{\mathbf{C}} \tag{13}$$

whose solution is

$$\mathbf{A} = \tilde{\mathbf{Q}}\,\Delta\tilde{\mathbf{C}}^{+} \tag{14}$$

Quantification of the sample is performed by

$$\hat{\mathbf{q}}_0 = \mathbf{A}\mathbf{c}_0 \tag{15}$$

Since $\hat{\mathbf{q}}_0 = \mathbf{a}_0$, the value of $\mathbf{a}_0$ from eq 11 is inserted into eq 15, to get

$$\bar{\mathbf{q}} = \mathbf{A}(\mathbf{c}_0 + \bar{\mathbf{c}}) \tag{16}$$

and finally

$$\mathbf{c}_0 = \mathbf{A}^{+}\bar{\mathbf{q}} - \bar{\mathbf{c}} \tag{17}$$

## LITERATURE CITED

(1) Saxberg, B. E. H.; Kowalski, B. R. *Anal. Chem.* **1979**, *51*, 1031.
(2) Frank, I. E.; Kalivas, J. H.; Kowalski, B. R. *Anal. Chem.* **1983**, *55*, 1800.
(3) Jochum, C.; Jochum, P.; Kowalski, B. R. *Anal. Chem.* **1981**, *53*, 85.
(4) Moran, M. G.; Kowalski, B. R. *Anal. Chem.* **1984**, *56*, 562.
(5) Brown, C. W.; Lynch, P. F.; Obremski, R. J.; Lavery, D. S. *Anal. Chem.* **1982**, *54*, 1472.
(6) Campbell, S. L.; Meyer, C. D. "Generalized Inverses of Linear Transformations"; Pitman: London, 1979; pp 32–41.

**Avraham Lorber**

Nuclear Research Centre—Negev
P.O. Box 9001
Beer-Sheva 84190, Israel

RECEIVED for review November 2, 1984. Accepted January 2, 1985.

---

# Square Wave Voltammetry at Electrodes Having a Small Dimension

*Sir:* Square wave voltammetry is a large amplitude differential technique in which a wave form composed of a square wave superimposed on a staircase is applied to the working electrode (*1*, *2*). Current measurements are made near the end of the pulse in each square wave half cycle; the difference of these two currents, when plotted vs. staircase potential, yields a symmetrical, peak-shaped net current voltammogram. The simplicity and fidelity of this net current response as an indicator of analyte properties under conditions which complicate conventional voltammetric methods are the subjects of this paper.

The trend towards smaller sample sizes, in situ analysis, and detection in flowing streams makes it harder to use analytical voltammetry under the customary boundary conditions of planar semiinfinite diffusion. This in turn severely limits the ability of traditional voltammetric techniques (i.e., differential pulse and cyclic voltammetry) of electroanalysis to quantitate and characterize analytes. The time scale of differential pulse voltammetry (minutes) makes it impractical for many applications, especially those which require contemporaneous, rather than retrospective information. Cyclic voltammetry is limited at low analyte concentrations by charging currents, and the shape of the voltammogram depends on the mode of diffusion. Under conditions of nonplanar diffusion the well-known peaked response tends toward an S-shaped wave (*3*) while for restricted diffusion it tends toward a symmetrical peak (*4*). Ideally what is desired is a method which preserves quantitative information in a simple peak-shaped response invarient in shape regardless of the electrode geometry, time scale of the experiment, or mechanism of mass transport. Our experiences with pulse methods in a variety of experimental situations suggest that square wave voltammetry possesses these attributes and hence will be very useful in many modern applications of voltammetry to quantitative analysis.

Figure 1 shows a direct comparison of cyclic staircase and square wave voltammetry used at identical scan rates with a planar reticulated vitreous carbon electrode and a reversible redox couple. The results for staircase voltammetry are very nearly the same as those for cyclic voltammetry and become identical as the staircase amplitude approaches zero at constant scan rate. Nonplanar diffusion is known to make a significant contribution to the total current measured under these conditions with this type of electrode (*5*). Note that the staircase voltammogram is severely distorted from the reversible shape afforded by ordinary linear diffusion and offers no easily quantifiable features (*6*). On the other hand the square wave voltammogram offers a prominent symmetrical peak with a characteristic position, width, and height. Unlike the result for staircase voltammetry, the peak shape is independent of the quantity $r/(Dt)^{1/2}$ where $r$ is a characteristic dimension of the electrode, $D$ is the diffusion coefficient of the reacting species, and $t$ is a characteristic time of the experiment. (When $r/(Dt)^{1/2} >> 1$ only planar semiinfinite diffusion is observed.) For practical purposes the peak potential coincides with the half wave potential of the redox couple, the peak width indicates the effective number of electrons transferred, and the peak height is a measure of analyte concentration. Hence, voltammetric analyses and measurements are greatly simplified by the use of the square wave wave form. Its usefulness for rapid surveys of electrochemical properties should also be obvious.

Many other types of electrodes which exhibit nonplanar or restricted diffusion on the time scale of the experiment yield simple peak-shaped voltammograms. Included in this group are an embedded thin wire cross section (microdisk), exposed

0003-2700/85/0357-0954$01.50/0 © 1985 American Chemical Society

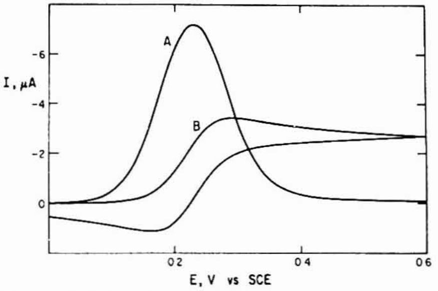

**Figure 1.** Reticulated vitreous carbon electrode (Normar Industries, 4 × 1, 100; cf. ref 5), 45 μm equivalent radius, 1.0 M KCl, 0.5 mM potassium ferrocyanide, pH 2.68: (A) square wave voltammogram, 10 Hz, 10 mV step height, 50 mV amplitude ($r/(Dt)^{1/2} = 0.7$); (B) cyclic staircase voltammogram, 10 Hz, 10 mV step height ($r/(Dt)^{1/2} = 0.5$).

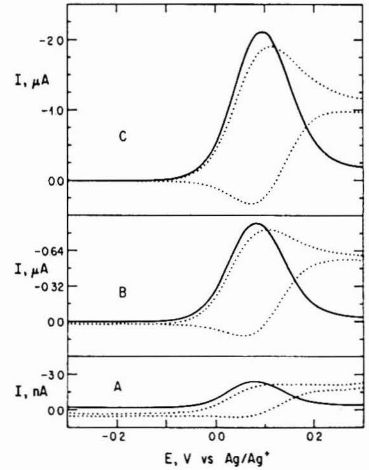

**Figure 2.** Square wave voltammograms obtained with various microelectrode geometries: (A) graphite microdisk (8 μm diameter, 50 Hz, $r/(Dt)^{1/2} = 0.8$); (B) exposed graphite fiber (8 μm diameter, 900 μm length, 50 Hz, $r/(Dt)^{1/2} = 0.8$); (C) exposed gold wire (50 μm diameter, 1800 μm length, 60 Hz, $r/(Dt)^{1/2} = 5.6$). The step height was 5 mV and the square wave amplitude was 50 mV. The reference electrode was Ag/0.01 M $AgNO_3$, 0.1 M $LiClO_4$ in acetonitrile. The analyte was 1.0 (A, B) or 0.5 (C) mM ferrocene in 0.1 M $LiClO_4$ acetonitrile solution. Dotted lines denote forward and reverse currents.

thin wire (circular cross section), exposed graphite fiber (bilobal cross section), embedded thin foil cross section (line), mercury thin film on planar glassy carbon, and an LED electrode. The LED electrode is an extreme example of a poorly defined microgeometry. It was prepared by drilling a small hole through a common light emitting diode (LED) indicating lamp and using the cross section of the severed chip connector wire as the working electrode. Detailed theoretical and experimental investigations of the first five geometries listed above are presently in progress in our laboratories.

Some typical experimental results are shown in Figure 2. In spite of the skewed form of the forward and reverse currents (dotted lines), the symmetry of the net current peak is retained in each case. The amount of skewness of the forward and reverse currents is a complex function of wave form and diffusion field and is beyond the scope of this paper. The difference in peak height between curves A and B (a factor of 400) is due largely to using as an electrode the surface area of a cylinder instead of its relatively small cross section. Enhanced peak currents are also observed when thin metallic wires (curve C) are employed as electrodes instead of graphite fibers. Hence, the use of simple exposed fibers or wires with square wave voltammetry appears to be an attractive alternative to use of multielement arrays of microdisks with cyclic voltammetry.

These results suggest that the shape of the net current voltammogram is insensitive to the curvature and boundaries of the diffusion field around the electrode. This is an especially useful feature of square wave voltammetry since the diffusion fields around many practical microelectrodes frequently cannot be precisely controlled or reproduced. Also, some easily constructed and economical electrodes, 25 μm diameter platinum wires, for example, are much more effectively used with square wave than with cyclic staircase voltammetry. A peak-shaped response is always obtained regardless of the length or shape of the wire. For these reasons we expect that the use of microelectrodes with square wave voltammetry will lead to improved electrode designs and increased experimentation on the microdimensional scale.

## ACKNOWLEDGMENT

The authors wish to thank Neal Sleszynski, David Whelan, Mary Schreiner, and Prasanna Sekhar for their contributions to this work.

## LITERATURE CITED

(1) Ramaley, L., Krause, M. S. *Anal. Chem.* **1969**, *41*, 1362.
(2) Christie, J. H.; Turner, J. A.; Osteryoung, R. A. *Anal. Chem.* **1977**, *49*, 1899–1903.
(3) Wightman, R. M. *Anal. Chem.* **1981**, *53*, 1125A–1134A.
(4) Hubbard, A. T.; Anson, F. C. In "Electroanalytical Chemistry"; Bard, A. J., Ed.; Marcel Dekker: New York, 1970; Vol. IV, pp 129–214.
(5) Sleszynski, Neal; Carter, J. M.; Osteryoung, Janet *Anal. Chem.* **1984**, *56*, 130–135.
(6) Aoki, K.; Akimoto, K.; Takuda, K.; Matsuda, H.; Osteryoung, Janet *J. Electroanal. Chem.*, in press.

**John O'Dea**
**Marek Wojciechowski**
**Janet Osteryoung***

Department of Chemistry
State University of New York at Buffalo
Buffalo, New York 14214

**Koichi Aoki**

Department of Electronic Chemistry
Tokyo Institute of Technology
Nagatsuta, Midori-ku, Yokohama 227, Japan

RECEIVED for review July 26, 1984. Resubmitted December 20, 1984. Accepted December 20, 1984. This work was supported by the National Science Foundation under Grant No. CHE8305748 and by the Office of Naval Research.

*Anal. Chem.* **1985**, *57*, 956-957

# AIDS FOR ANALYTICAL CHEMISTS

## Constrained Calibration Curves: A Novel Application of Lagrange Multipliers in Analytical Chemistry

**J. J. Leary* and E. B. Messick**[1]

*Department of Chemistry, James Madison University, Harrisonburg, Virginia 22807*

The generation and use of calibration curves have always been important aspects of analytical chemistry, and numerous papers have appeared in this journal concerning various least-squares curve fitting techniques and their applications. However, no reference has been made to a general approach for fitting equations to data when the physical reality of the situation dictates that the curve pass through one or more given points. Calibration curves, for example, often are known to pass through points such as (0, 0), (100, 100), (100, 1), or (1, 1). The special case of a curve passing through the origin is often treated by constructing the mathematical model without the inclusion of a constant term that would provide an estimate of the $y$ intercept. The general case of forcing an equation to pass through a specific point or points is conveniently treated via the use of one or more Lagrange multipliers (*1*). The use of Lagrange multipliers to simplify constrained maximization or minimization problems in physics and physical chemistry is well documented (*2–5*); however, the application of this very powerful and easy to use technique has, to date, not been applied to problems within the realm of analytical chemistry. The main goal of this manuscript is to illustrate how the use of Lagrange multipliers can supplement the more traditional least-squares curve fitting procedures. The concept of degrees of freedom when describing the variability of data around a calibration curve is also discussed.

The approach to be used is general, but it will be illustrated with reference to a specific example. Table I provides a set of data that was obtained in an experiment designed to determine the volume percent ethanol in ethanol–water mixtures using a gas chromatograph equipped with a thermal conductivity detector (*6*). The independent variable is volume percent ethanol, and the experimentally determined response is the ratio (area ethanol/(area ethanol + area water)) × 100. The data are definitely nonlinear, but because the slope is changing slowly and no inflection points are apparent, the goal will be to fit a second-order polynomial through the data without using weighting factors. Furthermore, the curve is to be constrained to pass through the points (0, 0) and (100, 100), pure water and pure ethanol, respectively.

The general second-order polynomial is given by eq 1, and eq 2 summarizes the function that would normally be minimized via the method of least squares. The importance of

$$y = a_0 + a_1x + a_2x^2 \qquad (1)$$

$$Q = \sum_{i=1}^{N} w_i[y_i(\text{data}) - y_i(\text{curve})]^2$$

$$Q = \sum_{i=1}^{N} w_i[y_i - (a_0 + a_1x_i + a_2x_i^2)]^2 \qquad (2)$$

incorporating the $w_i$'s (weighting factors) into least-squares problems has been discussed (*7, 8*). To proceed from eq 2, it would be necessary to obtain or to calculate the weighting factors. However, the procedure for the least-squares minimization of $Q$ is essentially the same irrespective of the values of the $w_i$'s; therefore, all points will be given $w_i$ values equal to one. This simplification allows maximum attention to be focused on the use of Lagrange multipliers, and eq 2 simplifies to eq 2a.

**Table I**

| vol. % ethanol | area % for ethanol peak | vol. % ethanol | area % for ethanol peak |
|---|---|---|---|
| 10 | 8.16 | 60 | 49.4 |
| 20 | 15.9 | 70 | 59.7 |
| 30 | 22.7 | 80 | 70.6 |
| 40 | 31.5 | 90 | 83.6 |
| 50 | 39.8 | | |

$$Q = \sum[y_i - (a_0 + a_1x_i + a_2x_i^2)]^2 \qquad (2a)$$

C1 and C2 summarize the constraints that are to be imposed.

$$\text{C1} = 0 = a_0 + a_1 \times 0 + a_2 \times 0^2 \qquad (3)$$

$$\text{C2} = 100 = a_0 + a_1 \times 100 + a_2 \times 100^2 \qquad (4)$$

A new function ($F$) is constructed from eq 2a–4 by using the Lagrange multipliers $\alpha$ and $\beta$.

$$F = \alpha \times \text{C1} + \beta \times \text{C2} + Q \qquad (5)$$

The minimum of the function $F$ is determined by taking partial derivatives with respect to the parameters $a_0$, $a_1$, and $a_2$, and setting the resulting equations (6–8) equal to zero.

$$\partial F/\partial a_0 = 0.5\alpha + 0.5\beta + a_0N + a_1\sum x + a_2\sum x^2 - \sum y = 0 \qquad (6)$$

$$\partial F/\partial a_1 = 0\alpha + 50\beta + a_0\sum x + a_1\sum x^2 + a_2\sum x^3 - \sum xy = 0 \qquad (7)$$

$$\partial F/\partial a_2 = 0\alpha + 5000\beta + a_0\sum x^2 + a_1\sum x^3 + a_2\sum x^4 - \sum x^2y = 0 \qquad (8)$$

Equations 6–8 and the constraining eq 3 and 4 are solved simultaneously. Matrix methods are probably the simplest approach for solving such systems of linear equations; however, many other methods are possible. Depending upon the method used to solve the set of equations, the Lagrange multipliers may remain undetermined. It is for the latter reason that they are sometimes called undetermined multipliers. The previously mentioned five equations are solved simultaneously using the data in Table I, and the $a_0$, $a_1$, and $a_2$ values obtained are recorded in Table II. The corresponding values of the Lagrange multipliers are $\alpha = 7.79$ and $\beta = -9.11$.

The treatment used in this paper assumes that all of the uncertainty appears in the experimentally determined response and that there is no uncertainty associated with the independent variable. This is normally a valid assumption for calibration curves generated by using carefully prepared

---

[1] Present address: Merck, Sharp and Dohme, Elkton, VA 22827.

0003-2700/85/0357-0956$01.50/0 © 1985 American Chemical Society

**Table II**

| data used | constraints | $a_0$ | $10a_1$ | $10^3a_2$ | $N$ | d.f. | SD |
|---|---|---|---|---|---|---|---|
| [a] | none | 2.72 | 5.57 | 3.73 | 9 | 6 | 0.508 |
| [b] | none | 1.69 | 5.61 | 4.00 | 11 | 8 | 1.39 |
| [a] | [c] | 0.00 | 5.88 | 4.12 | 9 | 8 | 1.99 |

[a] All data taken from Table I. [b] Data from Table I plus the points (0, 0) and (100, 100). [c] Equation forced through points (0, 0) and (100, 100).

standards. In such cases the standard error of estimate is given by

$$\mathrm{SD} = \left( \frac{[y_i(\mathrm{data}) - y_i(\mathrm{curve})]^2}{\mathrm{d.f.}} \right)^{1/2} \tag{9}$$

The numerator of eq 9 is normally accepted; however, controversies arise when attempting to specify the number of degrees of freedom (d.f.). In any statistic designed to quantitate the degree of variability in a set of data, the number of degrees of freedom will equal the number of data points that can be thought of as being independent (*9, 10*). For example, this definition accounts for the use of $N - 1$ degrees of freedom in the calculation of the variance of a data set if the experimentally determined mean has been used as the measure of the central tendency, while $N$ degrees of freedom are used in the calculation of variance if the population mean is available and is used. Equation 10 can be used to determine the number of degrees of freedom in eq 9.

$$\mathrm{d.f.} = N - P + C \tag{10}$$

where $N$ is the number of data points, $P$ is the number of parameters being determined, and $C$ is the number of constraints ($C \leq P$). The validity of eq 10 is best illustrated by using two extreme cases. First, if there are no constrains, the degrees of freedom will equal the number of data points minus the number of parameters being determined. This is true because it can be shown that once the parameters are known, the $y$ values of any $P$ data points can be calculated using (1) the corresponding $x$ values, (2) the equations for the partial derivatives of the function with respect to the parameters (which have been set equal to zero), and (3) the $x$ and $y$ coordinates of the remaining $N - P$ data points. Therefore, once the parameters are known, only $N - P$ of the data points remain independent, and thus, there will be only $N - P$ degrees of freedom. The second case is one in which the number of constraints ($C$) equals the number of parameters ($P$); the constraining equations can be used by themselves to calculate the parameters. Therefore, because none of the data need be used to determine the calibration curve parameters, all $N$ data points remain independent, giving $N$ degrees of freedom.

A single Lagrange multiplier can be used to force a straight line to pass through the origin. Equation 10 shows that there will be $N - 1$ degrees of freedom associated with statistics designed to quantitate the variability of experimental data around such a curve. The degrees of freedom associated with this special case were mistakenly listed as $N - 2$ by Strong in a recent publication (*11*), and although Ellerton (*12*) noted the correct value of $N - 1$, he did not discuss the reason for specifying this number of degrees of freedom.

Table II summarizes the polynomial coefficients and some statistics associated with three of the many possible calibration curves that can be generated employing the data in Table I and, in the second case, the points (0, 0) and (100, 100). For each curve the degrees of freedom have been calculated using eq 10, and the standard errors of estimate have been calculated using eq 9. A real data set, as opposed to a simulated one, was used because it illustrates a third and final point of this paper. Namely, it is dangerous to attempt to use any single statistic as a measure of the correctness of a mathematical model. Comparison of the standard error of estimate values recorded in Table II might lead to the conclusion that the unconstrained calibration curve is the best model, and the doubly constrained curve is the worst. Normally the best mathematical models are those based upon well-established theories (e.g., Beer's law). In the special case where the correct mathematical model is known to be a polynomial but the order of the polynomial is unknown, statistical tests exist that provide information concerning the order of the polynomial (*13*). In the absence of adequate theory upon which to base a model, the best approach probably involves the use of common sense followed by a careful examination of the individual residual values $[y_i(\mathrm{data}) - y_i(\mathrm{curve})]$ (*14*). Examination of the residuals associated with all three examples included in Table II indicates that there are systematic errors associated with each of the models (many positive residuals followed by a series of negative residuals), meaning that better models could almost certainly be constructed. However, since the standard error of estimate is less than 2%, approximately the precision inherent in the data set given in Table I, any of the models might be adequate. Although the doubly constrained model has the largest standard error of estimate, it is the only one of the three that reflects the conditions that must be satisfied at the two points that are known a priori.

The example used to illustrate the use of Lagrange multipliers for constraining calibration curves involved only a single independent variable. However, the method is general, and any number of Lagrange multipliers can be used to constrain equations in any number of independent variables as long as the number of constraints being imposed does not exceed the number of parameters being determined.

## ACKNOWLEDGMENT

The authors wish to thank H. E. Donley of the JMU Mathematics and Computer Science Department for his help and advice throughout this project.

## LITERATURE CITED

(1) Meyer, S. L. "Data Analysis for Scientists and Engineers"; Wiley: New York, 1975; Chapter 33.
(2) Atkins, P. W. "Physical Chemistry", 2nd ed.; W. H. Freeman: San Francisco, CA, 1982.
(3) Mortimer, R. G. "Mathematics for Physical Chemistry"; MacMillan Publishing Co.: New York, 1981.
(4) Dence, J. B. "Mathematical Techniques in Chemistry"; Wiley-Interscience: New York, 1975.
(5) Boas, M. L. "Mathematical Methods in the Physical Sciences"; Wiley: New York, 1966.
(6) Leary, J. J. *J. Chem. Educ.* **1983**, *60*, 675.
(7) Jurs, P. C. *Anal. Chem.* **1970**, *42*, 747–750.
(8) Sands, D. E. *J. Chem. Educ.* **1974**, *51*, 473–474.
(9) Youden, W. J. "Statistical Methods for Chemists"; Wiley: New York, 1951.
(10) Laitinen, H. A.; Harris, W. E. "Chemical Analysis"; McGraw-Hill: New York, 1975.
(11) Strong, F. C. *Anal. Chem.* **1979**, *51*, 298–299.
(12) Ellerton, R. R. W. *Anal. Chem.* **1980**, *52*, 1152–1153.
(13) Gerald, C. F. "Applied Numerical Analysis", 2nd ed.; Addison-Wesley: New York, 1978; Chapter 10.
(14) Box, G. E. P.; Hunter, W. G.; Hunter, J. S. "Statistics for Experimenters—An Introduction to Design, Data Analysis and Model Building"; Wiley: New York, 1978.

RECEIVED for review October 5, 1984. Accepted December 11, 1984.

958 *Anal. Chem.* 1985, *57*, 958–959

# Microdetermination of Nitrogen in Organic Compounds by the Sodium Fusion–Spectrophotometric Method

**Ernest J. Breda**

*E. I. du Pont de Nemours & Company, Inc., Beaumont Works, P.O. Box 3269, Beaumont, Texas 77704*

In the absence of the preferred Dumas nitrogen apparatus or the more sophisticated nitrogen analyzers, a micro-Parr bomb can serve to determine microquantities of nitrogen in organic compounds.

The sample or compound, either solid or nonaqueous liquid, is decomposed by fusing with metallic sodium in a sealed nickel bomb (*1*). The nitrogen is converted to sodium cyanide. The excess sodium is decomposed with absolute ethanol. The solution is adjusted to pH 7.1–7.2 with dilute hydrochloric acid and analyzed for cyanide by the Chloramine-T and mixed pyridine/pyrazolone reagent method (*2, 3*). The absorbance of the blue color formed is measured with a spectrophotometer at 615 nm. The amount of cyanide found is converted to the equivalent nitrogen in the compound.

Sodium fusion is used in classical chemistry for the qualitative identification of nitrogen in organic compounds. Of course some stable compounds are incompletely decomposed by this technique. With a micro-Parr bomb on hand and in the interest of expedience, the sodium fusion technique was tried for quantitative nitrogen estimation in some research compounds. Surprisingly, some fairly decent results were obtained on some known compounds by this means.

The method is not as rapid as desired but it is handy, simple, and economical. As with any micro or semimicro method, this procedure is sensitive to technique. Compounds must contain carbon and be essentially free of moisture.

## EXPERIMENTAL SECTION

**Apparatus.** The sodium fusion bomb was the same as described by Lohr, Bonstein, and Frauenfelder (*1*), except that the collar was made of Type 304 stainless steel. Other details were the same. The bomb was tested and utilized as described in the reference. It was held in a cast iron clamp behind a safety shield. The bomb was heated with a Tirrell gas burner.

A semimicro or five-place balance was used to weigh approximately 100 mg of sample containing small amounts of nitrogen or a microbalance to weigh 4 to 6 mg of pure compounds.

A Beckman Model DU spectrophotometer with 1-cm and 10-cm matched cells was used for absorbance measurements. However, any equivalent instrument will suffice.

A pH meter equipped with a thin combination glass and calomel electrode was used to measure pH.

**Reagents.** All reagent solutions were prepared from reagent grade chemicals and distilled water and stored in glass or polyethylene bottles.

Other materials were as follows: sodium spheres, $^1/_{16}$ to $^1/_4$ in. diameters (Matheson, Coleman and Bell No. CB 1035), stored under kerosene; ethyl alcohol, absolute; hydrochloric acid/water, 1/3 by volume; hydrochloric acid, 0.1 N; sodium hydroxide, 0.1 N; Chloramine-T solution, 1% aqueous; pyridine, 1-phenyl-3-methyl-5-pyrazolone solution, prepared as in ref 2; bis(pyrazolone), Eastman No. 6969; mixed pyridine/pyrazolone solution, prepared as in ref 2; stock potassium cyanide solution, prepared as in ref 2, 1 mL = 1 mg of $CN^-$ (approximately), analyzed by the Liebig titration method against silver nitrate (*4*), solution loses strength gradually and must be rechecked every week; standard potassium cyanide solution, dilute 10 mL of the stock KCN solution to 1 L with water, 1 mL = 10 $\mu$g of $CN^-$ (approximately); working standard KCN solution, dilute 10 mL of standard KCN solution to 100 mL with water, 1.00 mL = 1.0 $\mu$g of $CN^-$ or equivalent to 0.54 $\mu$g of N (approximately), prepare daily; standard silver nitrate solution, 0.0192 N, prepared and standardized as in ref 2.

**Calibration.** From a pipet 1- to 6-mL amounts of working KCN standard solution were transferred to separate 25-mL volumetric flasks and diluted to 15 mL with deionized water. Then 0.2 mL of Chloramine-T solution was added to each flask and stoppered. The mixture was swirled several times and allowed to stand 1 to 2 min. From a pipet, 5 mL of mixed pyridine/pyrazalone solution was added and diluted to 25 mL with water, stoppered, and mixed by inverting several times. The solution color was allowed to develop for 25–30 min and the absorbance measured at 615 nm in 1-cm cells. The absorbance was plotted on the ordinate vs. micrograms of nitrogen in 25 mL on the abscissa of natural coordinate paper. Lower concentrations of cyanide were measured in longer path cells.

**Preparation of Sample.** Weigh by difference on a semimicro balance approximately 0.1 g of sample in a long stemmed glass weighing tube or weighing boat and place the sample into the bomb cylinder. Dry a pellet of sodium between pieces of filter paper and place the pellet on top of the sample in the bomb and seal the bomb. Tighten the plug with a wrench while holding the bomb in a vise. Place the sealed bomb in the cast iron clamp and hold it at an angle of approximately 45° from the horizontal. Heat the bomb over a Tirrill burner for 15 min. During 10 min of the heating time, the lower 1- to 2-cm portion of the bomb cylinder should be at a cherry red heat. *CAUTION*: The heating of the bomb should be conducted behind a safety shield. Conduct the sodium elimination and pH adjustment in a hood. After heating, allow the bomb to cool under a jet of air. Remove the bomb from the clamp and wash with distilled water. Dry off with a filter paper and discard the paper and washings.

Open the bomb carefully and remove the gasket. Any material adhering to the gasket is washed with distilled water into a 100-mL beaker containing 5 mL of absolute ethyl alcohol. Add absolute ethyl alcohol dropwise to the bomb cylinder to destroy the excess sodium as indicated by the evolution of gas. When no further evolution of gas is visible, carefully pour the contents of the bomb into the beaker containing the ethanol and the washings from the gasket and wash off the edges of the bomb cylinder with dropwise addition of ethanol. Again, add alcohol to the bomb cylinder to destroy any residue of sodium. Repeat the operation if necessary until all sodium is destroyed. Finally, wash out the bomb and the sides of the bomb with a fine spray of water from a wash bottle. The volume of the solution in the beaker should be approximately 20–25 mL. Place the beaker in a dish containing ice water. Carefully neutralize the solution in the beaker with 1/3 hydrochloric acid/water to near a pH between 7.1 and 7.2 using a pH meter. Approach the pH 7.1–7.2 region from the high side using 0.1 N hydrochloric acid to make small adjustments in pH. Should the pH drop below 7, readjust with 0.1 N sodium hydroxide. Use a glass rod for stirring the solution during pH adjustment. Transfer the solution including any unburned carbon into a 50- or 100-mL volumetric flask depending on the level of nitrogen content present. Dilute the solution to the mark with water. Allow the carbon to settle in the flask before sampling.

**Determination of Nitrogen as Cyanide.** Transfer a suitable aliquot (usually 5 or 10 mL) of the sample solution to a 25-mL volumetric flask and treat as in the preparation of the calibration curve. From the calibration curve read the nitrogen content in 25 mL corresponding to the observed absorbance of the solution at 615 nm in the appropriate cell. Calculate the parts per million of nitrogen content of the sample.

**Analysis of Pure Nitrogen Compounds.** In a glass weighing tube, accurately weigh 4 to 6 mg of sample by difference. Place the sample into the bomb cylinder and treat as above under Preparation of Sample. After adjustment of pH to 7.1–7.2, transfer the solution to a 1-L volumetric flask. Dilute to 1 L with distilled water. Analyze a 5- or 10-mL aliquot of the solution the same as in the Determination of Nitrogen as Cyanide. Calculate the percent nitrogen.

$$\%\ \text{N} = \frac{\mu\text{g of N from graph} \times \text{aliquot factor}}{10 \times \text{mg of sample}}$$

0003-2700/85/0357-0958$01.50/0 © 1985 American Chemical Society

Table I. Analyses of Pure Nitrogen Compounds

| compound | % nitrogen | | deviation | type of N linkage |
|---|---|---|---|---|
| | calcd | found | | |
| acetanilide,[a] $C_8H_9NO$ | 10.36 | 10.33 | −0.03 | amide |
| | | 10.22 | −0.14 | |
| | | 10.48 | +0.12 | |
| | | 10.45 | +0.09 | |
| | | 10.20 | −0.16 | |
| | | 10.12 | −0.24 | |
| *p*-carbomethoxybenzamide, $C_9H_9NO_3$ | 7.82[b] | 7.80 | −0.02 | amide |
| | | 7.70 | −0.12 | |
| | | 7.69 | −0.13 | |
| tris(hydroxymethyl)methylamine,[c] $C_4H_{11}NO_3$ | 11.44[d] | 9.84 | −1.72 | amine |
| | | 9.88 | −1.68 | |
| *p*-nitroaniline,[e] $C_6H_6N_2O_2$ | 19.88[d] | 20.12 | +0.24 | amine and nitro |
| | | 20.08 | +0.20 | |
| dimethylglyoxime,[e] $C_4H_4N_2O_2$ | 24.13 | 23.82 | −0.31 | oxime |
| | | 23.92 | −0.21 | |
| disodium ethylenediaminetetraacetate dihydrate,[f] $Na_2C_{10}H_{14}N_2O_8 \cdot 2H_2O$ | 7.45[d] | 7.50 | +0.05 | amine |
| | | 7.35 | −0.10 | |
| | | 7.30 | −0.15 | |
| methyl *p*-cyanobenzoate,[f] $C_9H_7NO_2$ | 8.60[d] | 8.65 | +0.05 | nitrile |
| | | 8.73 | +0.13 | |
| | | 8.45 | −0.15 | |
| methyl *p*-nitrobenzoate[f] | 7.65[d] | 7.52 | −0.13 | nitro |
| | | 7.40 | −0.25 | |
| potassium nitrate,[g] $KNO_3$ | 13.86 | 0.05 | | potassium salt |
| | | 0.08 | | |
| $KNO_3$ + benzoic acid[e] | 13.86 | 1.37 | | |
| | | 1.50 | | |
| sodium nitrate,[h] $NaNO_3$ | 16.48 | 0.05 | | sodium salt |
| | | 0.05 | | |
| $NaNO_3$ + benzoic acid[e] | 16.48 | 2.65 | | |
| | | 3.00 | | |

[a] Reference standard, Eastman Kodak. [b] Theoretical. [c] Eastman Kodak, reagent grade. [d] Calculated from purity. [e] Eastman Kodak, ACS reagent. [f] Aldrich Chemical, reagent grade. [g] Fisher Certified standard. [h] Fisher Certified ACS reagent.

## RESULTS AND DISCUSSION

Table I shows data on the recoveries of nitrogen as cyanide when essentially pure compounds were analyzed. The essential requirement for this analysis is that the sample must contain carbon to form the cyanide. In the analysis of non-carbon compounds, a substance such as benzoic acid or other easily decomposable non-nitrogen carbon compound must be added to make the analysis work. Since a truly non-carbon organic type compound was not available or found, the chemistry was not studied as to what happens in the absence of carbon. One can only speculate on a possibility being the formation of free nitrogen which we know will not analyze like cyanide. Several organic nitrogen compounds with different N linkages were analyzed on a high spot basis. With one exception all the tested compounds gave good recoveries of nitrogen.

Tris(hydroxymethyl)methylamine, $C_{14}H_{11}O_3N_7$, gave rather poor recovery (see data). The reason for this is not known at present without more detailed study. It is possible that this compound did not decompose completely at the conditions of the test. It may also be that some species other than cyanide formed or something that affected the color formation in the Chloramine-T/pyridine/pyrazolone test. A remote possibility may be that the compound was not as pure as represented. No separate purity analysis was made on any of the compounds tested since they were represented to be essentially of reagent grade quality. The melting points were determined and found to be at or approximately those reported for the pure compounds. Purities were accepted as represented and nitrogen contents calculated on the purity basis. The known compunds were all dried before analysis. Those with melting points above 100 °C were dried at 100–102 °C in an oven for 1 h and then kept in a $P_2O_5$ desiccator. Compounds with melting points below 100 °C like methyl *p*-nitrobenzoate, mp 94–96 °C, were dried over $P_2O_5$ in a vacuum desiccator at 35 °C for 24 h.

Two inorganic compounds, potassium nitrate and sodium nitrate, were fused and analyzed. As expected, no cyanide formed. The brucine method for nitrates (5) showed nearly all the nitrate present in either case. Fusing the same nitrate compounds with benzoic acid present showed about 10–16% of the nitrate converted to cyanide. The rest of the nitrogen remained intact as the nitrate. This behavior raised the question of what happens if an organic nitrate compound is fused with sodium, but this was not tested.

In one case—acetanilide—the repeatability of the analysis was tested. The variation of the results was approximately that of the pyridine/pyrazalone method for cyanide or about 2 parts in 100 parts.

A note of caution should be observed. Both sodium and cyanide are extremely hazardous substances. The analyst must wear appropriate safety equipment. The hands should be covered with surgical or thin PVC gloves in handling the cyanide solutions. Exercise care when working with metallic sodium, it should not come in contact with an aqueous wet sample nor should excess bits and pieces of sodium be discarded indiscriminately. Pieces of sodium must be returned to the kerosene layered storage bottle. Alternately destroy unusable pieces of sodium carefully by placing them in absolute ethanol, 1-propanol, or 1-butanol until all evolution of gas ceases, then flush away with water.

**Registry No.** Na, 7440-23-5; acetanilide, 103-84-4; *p*-carbomethoxybenzamide, 6757-31-9; tris(hydroxymethyl)methylamine, 77-86-1; *p*-nitroaniline, 100-01-6; dimethylglyoxime, 95-45-4; disodium ethylenediaminetetraacetate dihydrate, 6381-92-6; methyl *p*-cyanobenzoate, 1129-35-7; methyl *p*-nitrobenzoate, 619-50-1; nitrogen, 7727-37-9; chloramine T, 127-65-1; pyridine, 110-86-1; pyrazolone, 39455-90-8.

## LITERATURE CITED

(1) Lohr, L. J.; Bonstein, T. E.; Frauenfelder, L. J. *Anal. Chem.* **1953**, *25*, 1115–1117.
(2) "Standard Methods for the Examination of Water and Wastewate", 13th ed.; American Public Health Association: New York, 1971; pp 402–403, 404–406.
(3) Epstein, J. *Ind. Eng. Chem., Anal. Ed.* **1947**, *19*, 272–274.
(4) Kolthoff, I. M.; Sandell, E. B. "Textbook of Quantitative Inorganic Analysis", revised ed.; MacMillan: New York, 1943.
(5) "Standard Methods for the Examinatio. of Water and Waste Water", 13th ed.; American Public Health Association: New York, 1971; pp 461–464.

RECEIVED for review November 16, 1984. Accepted January 10, 1985.

Anal. Chem. 1985, 57, 960

# Vacuum-Actuated High-Vacuum Glass Valve

**C. A. M. Brenninkmeijer**[*1] **and M. L. Louwers**

*Louwers Hapert, Hapert, The Netherlands*

Glass has once been the major construction material for vacuum systems. In the course of time, metal has replaced glass in the construction of larger vacuum systems. Nonetheless, for smaller vacuum systems glass use is frequently up-to-date, mainly because of its low cost, inertness, and transparency. In certain instances, such as the manipulation of corrosive gases, the application of glass is required. However, because of the recent trend toward automation, the nonavailability of automatic glass stopcocks or valves may exclude some present and future applications of glass.

A wide range of glass valves, from the greased stopcock type to modern O-ring valves is presenty available. As has been discussed (*1*) operation of these valves with motors or pneumatic cylinders is not straightforward except for certain types of O-ring valves. The vacuum seals in these O-ring valves are based on the slight compression of Viton O-rings and little friction is involved. Consequently, these valves could be fitted with a small pneumatic cylinder, enabling remote control and automation (*2*). Although this solution proves satisfactory, a simple concept has led to a new type of automatic glass valve with additional advantages.

The new automatic glass valve is shown in Figure 1. When the chamber in the knob of the valve is evacuated to 0.1 bar or less, air entering through the vent indicated will push the butyl rubber membrane upward, thus moving the plunger to the opened position. When air is readmitted to the chamber, spring action will force the plunger into the closed position. The chamber is vacuum sealed by means of the membrane itself, and will hold vacuum for several hours. The outer edge of the membrane is squeezed tight between the two sections of the knob. The inner seal of the membrane with the glass plunger is obtained by its tight fit in the 1 mm diameter hole in the membrane. The plastic ring on the plunger also promotes a tight seal at this place. The main function of the plastic ring, however, is to prevent the membrane from snapping over the flange of the plunger. Because of the 20 mm diameter ring a force of at least 30 N is exerted on the plunger upon applying vacuum in the closed position. The counter-acting springload in this position is 10 N and after subtracting also the force exerted on the plunger when the side opening of the valve is at vacuum, 14 N or more results, which is sufficient to always open the valve. During the withdrawal of the plunger the force of the spring increases to 20 N. However, the diameter of the membrane of 28 mm, combined with a thickness of 0.7 mm, ensures a complete opening of the valve. The chamber in the knob is connected by a thin silicone rubber tube via a three-way solenoid valve to a suitable vacuum supply. This vacuum of 0.1 bar or less can either by supplied by a volume of several liters, which is evacuated repeatedly, or any small vacuum pump. Water jet pumps are unsuitable because of the risk of corroding the spring.

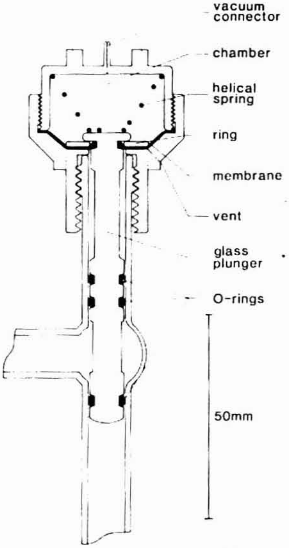

**Figure 1.** Cross section of O-ring glass tap with vacuum actuator. Materials used were Delrin or PVC for knob and ring, butyl rubber for membrane, and 1 mm steel for the spring.

The vacuum actuated glass valve has some additional convenient properties. First of all, besides the described mode of operating, manual operation remains possible by turning the knob. Another feature is that the valve closes upon loss of power. Moreover, the actuator is small and lightweight. The vacuum actuated glass valves have proven to operate satisfactorily over many thousands of cycles.

## LITERATURE CITED

(1) Brenninkmeijer, C. A. M. *Int. J. Appl. Radiat. Isot.* **1981**, *32*, 679-680.
(2) Van Wershoven, J.; Vervest, J. *Polytech. Tijdschr.* [*Ed.*]: *Werktuigbouw* **1974**, *29*, 2-5.

Received for review November 13, 1984. Accepted January 8, 1985.

---

[1] Present address: Institute of Nuclear Sciences, DSIR, Lower Hutt, New Zealand.

0003-2700/85/0357-0960$01.50/0 © 1985 American Chemical Society

# AUTHOR INDEX

Alfheim, J. A., 861
Almgren, M., 817
Ando, T., 834
Aoki, K., 954
Asafu-Adjaye, E. B., 904
Atwater, B. L., 899
Avery, M. J., 790

Breda, E. J., 958
Brenninkmeijer, C. A. M., 960
Brinkman, U. A. T., 806

Cabaniss, G. E., 876
Campana, J. E., 949
Cantwell, F. F., 922
Carr, P. W., 793
Caruso, J. A., 846
Conroy, C. M., 822
Cookson, D. J., 864

Eldan, M., 851
Engstrom, R. C., 933

Fossey, L., 922
Fournie, J.-J., 892
Frei, R. W., 806
Fukuda, E. K., 949

Giddings, J. C., 945
Gitlin, S. N., 917
Goldbart, Z., 851
Griffiths, P. R., 822
Groenewold, G. S., 886

Haas, D. L., 846
Hara, L. Y., 841
Hartwick, R. A., 811
Hass, J. R., 890
Hirata, K., 947
Hussam, A., 793

Imasaka, T., 947
Ishibashi, N., 947

Jinno, K., 822
Junk, G. A., 790

Kawabata, Y., 947
Kok, G. L., 917
Kowalski, B. R., 908
Kuwamoto, T., 829

Langford, C. H., 861
Lazrus, A. L., 917
Leary, J. J., 956
Lind, J. A., 917
Lindner, B., 895
Linton, R. W., 871, 876
Lorber, A., 851, 952
Louwers, M. L., 960

MacDonald, A., 936
Maple, J. R., 940
McCaslin, P. C., 880
McEwen, C. N., 890
McLafferty, F. W., 899
McLaren, S. E., 917
Messick, E. B., 956
Munson, B., 786

Nielen, M. W. F., 806
Nieman, T. A., 936

O'Dea, J., 954
Okada, T., 829
Onuska, F. I., 801
Osten, D. W., 908
Osteryoung, J., 927, 954
Otsuka, K., 834

Pace, C. F., 940
Parsons, M. L., 841
Peterson, D. W., 899
Prome, J.-C., 892
Puzo, G., 892

Rudewicz, P., 786

Saucy, D. A., 871, 876
Seydel, U., 895
Simko, S. J., 871
Smith, B. E., 864
Ståhlberg, J., 817
Stauffer, D. B., 899
Su, S. Y., 904

Terabe, S., 834
Terry, K. A., 801
Todd, P. J., 886
Tomellini, S. A., 811

Underhill, D. W., 826

Weber, M., 933
Werth, J., 933
Wojciechowski, M., 927, 954
Woodruff, H. B., 811

Xiao-quan, S., 857

Yoshitake, A., 947
Young, V., 880
Yun, J. I., 904

Zhe-ming, N., 857
Zhi-neng, Y., 857

## Future Articles

**Sample Preparation and System Calibration for Proton-Induced X-ray Emission Analysis of Hair from Occupationally Exposed Workers**

Eric Clayton and K. K. Wooller

**Three-Component Curve Resolution in Liquid Chromatography with Multiwavelength Diode Array Detection**

Bernard Vandeginste, Raymond Essers, Theo Bosman, Joost Reijnen, and Gerrit Kateman

**Quantitative Determination of Boron and Phosphorus in Borophosphosilicate Glass by Secondary Ion Mass Spectrometry**

Paul K. Chu and Stephen L. Grube

**Assessment of Adsorption/Solvent Extraction with Polyurethane Foam and Adsorption/Thermal Desorption with Tenax-GC for the Collection and Analysis of Ambient Organic Vapors**

Mary P. Ligocki and James F. Pankow

**Analysis of Paraffin Wax Oxidates by Differential Infrared Spectrometry**

Muhammad Nazir

**Temperature Dependence of the Voltammetric Response of Thin Electroactive Polymer Films**

James Q. Chambers and György Inzelt

**Analysis of Binary and Ternary Mixtures of Titanium, Zirconium, and Hafnium by Derivative Sinchronous Fluorescence Spectrometry**

Soledad Rubio, Agustina Gómez-Hens, and Miguel Valcárcel

**Probability-Based-Matching Algorithm with Forward Searching Capabilities for Matching Unknown Mass Spectra of Mixtures**

Douglas B. Stauffer, Fred W. McLafferty, Robert D. Ellis, and David W. Peterson

**Quantitative Analysis of Aqueous Species Using Raman Spectrometry and Equilibrium Model Calculations**

J. A. Sorensen, L. C. Thompson, and G. E. Glass

**Accurate Mass Measurement in the Absence of Calibrant for Capillary Column Gas Chromatography/Fourier Transform Mass Spectrometry**

Carolyn L. Johlman, David A. Laude, Jr., and Charles L. Wilkins

**Photomultiplier Gating for Improved Detection in Laser-Excited Atomic Fluorescence Spectrometry**

M. D. Seltzer, Martha Schulz Hendrick, and R. G. Michel

**Application of a Nested Loop System for the Flow Injection Analysis of Trace Aqueous Peroxides**

Purnendu K. Dasgupta and Hoon Kwang

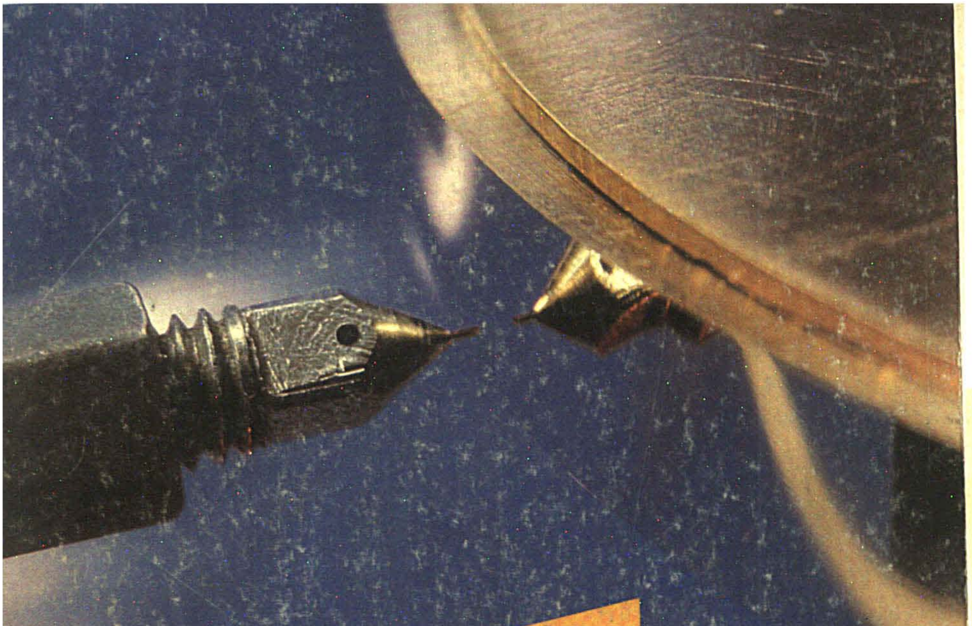

CRYOLECT. SUB-NANOGRAM GC/IR.

Mattson's Cryolect offers 100x the sensitivity of conventional GC/IR.

There's no light pipe; the Cryolect freezes up to five hours of chromatography in an argon matrix on a gold collector disk.

The Cryolect offers

- capillary GC sensitivity
- full GC flexibility
- full IR flexibility
- sharp, intense bands

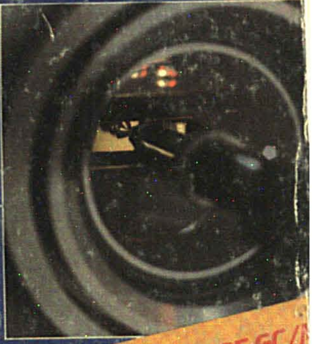

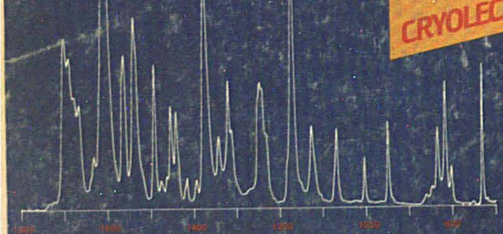

20 ng p-DIMETHYLAMINOBENZALDEHYDE

CRYOLECT. GC/IR WITH THE SENSITIVITY OF GC/

**Mattson Instruments,**

6333 ODANA ROAD
MADISON, WI 53719
(608) 273-2370

TELEX 262006

CIRCLE 139 ON READER SERVICE CARD